Stall Detection and Control in Industrial Fans

Edited by Geoff Sheard

Permissions Acknowledgements

Contents

List of Figures

List of Tables

Foreword

Engineers responsible for both a product's design and its application make every effort to ensure they do not fail in service. However, either from human error or a lack of fundamental understanding, failures do occur. The inevitable question is, 'Did it break, or did you break it?'

In an increasingly competitive world, product designers are under pressure to innovate in order to differentiate their product from the competition. With innovation comes improvement, but also risk. If we set aside avoidable errors that occur as a consequence of inexperience or a lack of care, this risk manifests itself as an in-service failure. When we study these failures, we learn that whilst designers strive to create the best possible product, in the process they may inadvertently overlook certain issues or from time to time some failure reveals wholly new phenomena. Consequently, a latent design error is responsible for the in-service failure.

In the same competitive environment system designers are subject to the same pressure imposed on product designers. System specifications are becoming more demanding and consequently, products that have performed well in the past may no longer be fit for purpose. Therefore, a more demanding system specification can result in a product inadvertently operating beyond its design limit. Thus, the system design is responsible for the in-service failure.

An in-service failure invariably results in different perspectives on the part of those responsible for both the product and system design. Is it really so surprising that they seldom agree? From the system designer's point of view the product designer hides behind codes and standards which product manufacturers write to protect their own interests. From the product designer's point of view the system designer simply does not comprehend the system's complexity for which they are responsible, or the implications of the decisions he or she makes when designing the system.

Despite the difficulty of establishing why products fail in-service, even in the most difficult of circumstances it is possible to identify patterns amongst failures. From those patterns we may begin to elucidate the underlying failure mechanisms. Those involved must find a way to work together to identify the underlying causes, adapting both product and system design in response to that new knowledge.

The collection of papers in this volume illustrates how a pattern of in-service failures can inform a research effort that goes on to facilitate developing new products that are better able to operate in the environments within which they are applied. In collecting and editing these papers, Geoff Sheard has provided an important record which is an essential source of information to those who wish to understand how we can apply research to ensure that the resulting products are relevant in a changing world. All readers will be interested to follow the path described in this volume and will learn much in the process.

Norman Rhodes
Senior Vice President
Parsons Brinckerhoff
15 July 2014

Acknowledgements

About the Editor

Wearing many hats, Geoff Sheard is the Fläkt Woods Group Vice President of Fan Technology, a leading global supplier of energy-efficient solutions operating in both the air climate for buildings and air movement for the infrastructure and industry markets. He is a director of Fläkt Woods Limited, Solyvent Fläkt Woods Limited and Fläkt Woods Fans (Australia) Pty Limited.

Geoff is an Honorary Professor at the Aston University Department of Engineering and Applied Science, a Visiting Professor at *Sapienza* University of Rome *Dipartimento di Ingegneria Meccanica e Aerospaziale* and a Visiting Professor at the University of Northampton Business School.

Geoff is President of the Air Movement & Control Association (AMCA), member of the AMCA Executive Board and Chairman of the European Air Movement & Control Association Board of Directors. He is also a member of the International Gas Turbine Institute (IGTI) Board of Directors and Vice Chairman of the Institution of Mechanical Engineers (IMechE) Fluid Machinery Group.

Geoff has doctorate degrees from the University of Oxford in turbomachinery aerodynamics and from the University of Northampton in leadership and team development. He also holds a master's degree in business administration from Cranfield University and a bachelor's degree in mechanical engineering from Liverpool University.

A chartered engineer, a Liveryman of the Worshipful Company of Engineers, a fellow of the Institution of Mechanical Engineers, a fellow of the Royal Aeronautical Society, a fellow of the American Society of Mechanical Engineers, and a fellow of the Chartered Institute of Building Service Engineers, Geoff has published widely in both technical and management areas. His publication list extends to 236 publications including 10 books, two monographs plus over 60 journal articles and patents. Geoff is editor of the *Journal of Management Development*, a member of the *Journal of Power and Energy* and *African Journal of Engineering* editorial boards, and the *Leadership and Organisational Development Journal* editorial review board.

Introduction:
Stall Detection and Control

Geoff Sheard

"To understand is to perceive patterns"[1] said Isaiah Berlin, British social and political theorist, philosopher and historian. It is not necessary to accept events as either inevitable or irresistible. It is possible to discover patterns by classifying and correlating. Above all, it is possible to predict.

This volume of collected papers documents research undertaken in response to a need — the majority of industrial fan in-service failures occur as a consequence of inadvertently operating them in an aerodynamically stalled condition. The volume arises from discussions around 11 papers and two patents that collectively comprise the chapters and appendices. Each makes a contribution that collectively characterise the stall phenomena in industrial fans. They provide industrial fan designers with the necessary knowledge to predict the imminent onset of stall, and if unavoidable, manage its effect.

The chapters relate to one of three separate, but complementary aspects of the reported research that collectively comprised a single fundamental research and applied development effort:

(1)   stall phenomena in industrial fans;
(2)   stall detection; and,
(3)   stall resistant blade concepts.

Since the early 1950s, stall phenomena have been the subject of wide-spread study within the aerospace community. Engineers have improved systematically the stability limit of both the fans and compressors intended for aerospace application over the decades. The result has been both more highly loaded aerodynamic designs and an improved understanding of those designs' stability limit. In contrast, the industrial fan community is still largely developing new products using empirical techniques. Industrial fan designers have become skilled at applying empirical techniques. However, their ability to predict the stability limit of industrial fans is constrained by their lack of insight into the physical flow mechanisms at play within industrial fan blading. The physical flow mechanisms associated with the stall phenomena in aerospace fans and compressors are similar to those in industrial fans, but not identical. It

---

[1] Berlin, I. (1997), "Historical Inevitability", in Hardy, H., and Hausheer, R. (Eds), *The Proper Study of Mankind: An Anthology of Essays*, Chatto & Windus, London, UK.

is therefore necessary for engineers within the industrial fan community to adopt aerospace style experimental methods to characterise the stall phenomena.

Characterising the stall phenomena in industrial fans is an essential first step towards detecting the precursors that signal the imminent on-set of stall. Historically, researchers have associated the majority of industrial fan in-service failures with inadvertently operating the fan in an aerodynamically stalled condition. This has classically resulted because of an error in control system logic, or a damper's mechanical failure. Consequently, the industrial fan community has tended to regard in-service failures as a commercial opportunity. However, during the 2000s control system error or damper failure could no longer explain an increasing proportion of industrial fan in-service mechanical failures. Although there is still some debate within the industrial fan community, a consensus has emerged as to why an increasing proportion of industrial fans are failing in service. First, the applications into which industrial fans are installed are becoming more likely to inadvertently drive them into stall. Second, more highly loaded aerodynamic designs result in smaller fans for a given duty point. A smaller fan has a lower cost, but a more highly loaded fan will suffer a more severe stall. A conclusion is that commercial pressure to design lower cost fans in combination with applications more likely to inadvertently drive a fan into stall is responsible for the increase in 'unexplainable' in-service failures.

If we accept that the majority of industrial fan in-service failures occur as a consequence of inadvertently operating the fan in an aerodynamically stalled condition, we must ask ourselves how the industrial fan community should respond. A response is to develop a stall-warning system tailored to the stall phenomena typical of industrial fans. A complementary response is to develop design methods that will facilitate the design of intrinsically more 'stall tolerant' industrial fans. As has previously been noted, the industrial fan community is still developing new products using empirical techniques. However, the advent of open-source computational methods has resulted in those methods now becoming available within an industrial context. Therefore, industrial fan designers can now pick up and apply the same tools and techniques that the aerospace community has historically used. Applying aerospace style computational methods to industrial fan design is challenging. Industrial fans include intrinsically non-aerodynamic features such as electric motors from which the flow will inevitably separate. Despite the challenge, applying computational methods to industrial fan design can provide insight into the flow-field physics. Therefore, they offer industrial fan designers the opportunity to develop more stall tolerant fan designs.

Chapter 1: Literature Review

The adopted research philosophy was first, to characterise the stall phenomena in industrial fans and second, to complement the characterisation with developing both a stall detection system and intrinsically stall tolerant blades. Engineers required insight into the stall phenomenon in industrial fans before they could develop either an industrial fan specific stall detection system or stall tolerant blades. However, researchers did not undertake characterisation of the stall phenomena in

industrial fans in a vacuum. Other scholars' findings working in both the aerospace and industrial fan community informed the research.

Chapter 1 presents a review of stall detection and control techniques. The authors wrote this paper to place the work and reported research in the other papers that form the edited volume into context. The review identifies the key challenges that those within the aerospace fan, aerospace compressor and industrial fan communities are addressing. The review's specific focus is on identifying those aspects of aerospace technology that one can most likely apply successfully to industrial fans. Thus, the review provides a road map for researchers who are both developing stall control technology and attempting to apply that technology to industrial fans.

Chapters 2, 3 and 4: Stall Phenomena in Industrial Fans

Scholars and engineers within the aerospace fan community have studied the detection and analysis of different forms of aerodynamic instability for several decades. Some have studied the phenomenon of rotating stall in both single and multi-stage axial flow compressors in their attempts to describe the mechanism underlying rotating stall. Rotating stall is a flow mechanism by which the rotor adapts to a reduced flow rate and results in a non-uniform flow pattern rotating in the annulus. However, research conducted on high-speed aerospace fans and compressors is not directly applicable to industrial fans. Although the physical flow mechanisms are similar, there is a need to characterise the stall phenomena in industrial fans. Consequently, the three chapters that follow focus on characterising industrial fan stall pre-cursors and the stall recovery process. Each provides a different perspective on the stall phenomena in industrial fans. Collectively they provide the necessary insight to facilitate developing a stall detection system that can identify incipient stall.

Chapter 2 presents an experimental study of the mechanical impact of aerodynamic stall. Metro and railway tunnel ventilation fans are routinely driven transiently into stall. Stall occurs when the fans are both operated at part speed and subjected to a pressure pulse as a train passes. The reported research establishes the increase in peak blade unsteady stress level at full and part speed operation in stall. The objective was to evaluate the reduction in the fan blade's mechanical safety factor. We may calculate the mechanical safety factor from a combination of direct stress induced by the fan's rotation and unsteady stress induced by aerodynamic forces. As one reduces, the other may increase and still maintain a constant mechanical safety factor. The reported research was able to identify the maximum safe speed at which the studied fan could operate at an aerodynamically stalled condition without risking mechanical failure. The chapter concludes by presenting three strategies for tunnel ventilation fan selection in applications where the selected fan will most likely stall. The chapter closes by considering the advantages and disadvantages of each selection strategy and concludes by briefly assessing the strengths and weaknesses of each.

Chapter 3 reports a research programme aimed at establishing the nature of both rotating stall pre-cursors and the physical flow phenomena that characterise rotating stall recovery for an industrial fan. Scholars within the aerospace community

have characterised the performance of both fans and compressors intended for aerospace application. However, the research reported in this chapter is the first published study on rotating stall inception and recovery in an industrial fan by varying fan blade pitch angle at constant speed. The authors investigated both the nature of the stall condition and the incipient stall precursors' characteristics as the fan was driven from stable operation into rotating stall. An analysis of unsteady pressure measurements indicated that a low frequency tone was associated with establishing the first rotating stall cell. The cell became established, and then collapsed after approximately one second. As it collapsed rather than developed, it constituted a rotating stall precursor. Traditional stall-warning systems alert operators when the fan or compressor has stalled. A stall warning system that could identify the presence of a rotating stall cell before it collapsed has the potential to alert operators that stall is incipient, but has not yet occurred.

Chapter 4 presents the results of a research programme that utilised two strategies to study rotating stall recovery patterns. The reported research is the first published study on a fan's rotating stall recovery in the same experimental facility using two independent recovery strategies. The authors were able to recover a fan from rotating stall either by varying blade pitch at constant speed, or by varying speed at constant blade pitch. They studied the physical flow phenomena associated with rotating stall recovery. The transient fluid flow behaviour associated with rotating stall recovery by varying blade pitch was indicative of both a mild and progressive transition. In contrast, rotating stall recovery by varying fan speed occurred more suddenly. In comparison with the variable pitch transition, the variable speed transition was more indicative of recovery from mild surge. From this the authors concluded that rotating stall recovery via variable speed resulted in significantly higher unsteady mechanical stress induced in fan rotating components than recovery via variable pitch.

Chapters 5, 6 and 7: Stall Detection

The research reported in Chapters 2, 3 and 4 collectively clarify the stall precursors that characterise incipient stall in industrial fans. A rotating stall cell emerges and collapses within one second, and is characterised by a low frequency tone. In Chapters 5, 6 and 7, the authors develop a stall detection methodology that is capable of identifying stall precursors and therefore is able to provide a warning when stall is incipient. In Chapter 5 the authors utilise a symmetrised dot pattern (SDP) technique to transform an unsteady pressure measurement into a visual image. The resulting images for stable operation, incipient stall and rotating stall were distinctly different, and therefore provided a basis for differentiating between operating conditions. In Chapter 6 the authors went on to evaluate the viability of making unsteady pressure measurements in the fans inlet plenum, as opposed to over the fan blades. The success of the symmetrised dot pattern technique at differentiating between operating conditions using unsteady pressure measurements made in the inlet

plenum encouraged the authors to continue their research. Chapter 7 presents a developed form of the symmetrised dot pattern technique that can differentiate between operating conditions using a far-field acoustic measurement made in the fan's general vicinity. As the acoustic stall warning method does not require mounting sensors in the fan casing, it has proven particularly suitable for application with those fans that have already commenced in-service operation.

The research reported in Chapter 3 established the nature of industrial fan aerodynamic instabilities associated with incipient and rotating stall. Chapter 5 complements this work, presenting research programme results to characterise the aerodynamic instabilities of interest. This was to facilitate identifying a shift in an industrial fan's operating condition from stable operation to incipient stall or rotating stall. Researchers have historically based stall-detection methods on analysing pressure or vibration signals in either the time or frequency domain. However, the signals that researchers associate with stall precursors are often low compared to the background noise. Therefore, they require significant computational effort to extract. This makes conventional methods of stall-detection difficult to apply in active stall control systems. The research reported in Chapter 5 presents a stall-detection method based on analysing symmetrised dot patterns. Symmetrised dot patterns represent an input signal on polar coordinates, and changes in the input signal frequency content manifest themselves as changes in the resultant symmetrised dot patterns. Engineers can use the generation of symmetrised dot patterns in real time as the basis of an 'incipient' stall detection method that is able to identify stall pre-cursors. Thus, the authors were able to demonstrate that the symmetrised dot pattern technique is able to identify that an industrial fan is likely to stall before it actually has.

The research presented in Chapter 5 establishes that the symmetrised dot pattern technique can differentiate between stable operation, incipient stall and rotating stall conditions. The authors made this characterisation using the output of unsteady pressure transducers mounted directly over a fan's blades. Researchers have historically based stall-detection methods on analysing near-field signals. In contrast, Chapter 6 presents a research programme focused on establishing an industrial fan operating state using sensors mounted in both the near-field on the fan casing over the blades and in the far-field in the inlet plenum upstream of the fan rotor. The results demonstrated that the symmetrised dot pattern technique is able to differentiate between stable operation, incipient stall and rotating stall conditions through an analysis of far-field data. The far-field data analysis was successful in differentiating between operating conditions despite a low signal-to-noise ratio. Although the signal-to-noise ratio was low, the authors were able to demonstrate that the proposed diagnostic approach could differentiate between operating conditions using data recorded over a time period of as little as half a rotor revolution. This data acquisition period is shorter than the time-scales associated with establishing and collapsing the first rotating stall cell that constitutes the stall precursor in an industrial fan. In combination with using sensors in the far-field, the short data acquisition time establishes the potential of the symmetrised dot pattern technique. It can therefore form a key component within an active stall control system.

Having established the viability of the symmetrised dot pattern technique as the basis of an incipient stall detection method, the authors of Chapter 7 considered how engineers might apply the method in an industrial fan context. Industrial fans are typically installed as a part of a wider process. Consequently, shutting them down to fit sensors in the casing over the blades or in the inlet plenum upstream of the fan rotor requires engineers to shut down the entire process. The research presented in Chapter 7 demonstrates the viability of the symmetrised dot pattern technique to differentiate between stable operation, incipient stall and rotating stall conditions using acoustic measurements. The authors made these measurements with a microphone external to both the fan and the duct system within which it was installed. The reported research presents a systematic analysis of the microphone position's influence on the ability of the symmetrised dot pattern technique to generate identifiably different symmetrised dot patterns.

The authors were able to demonstrate that engineers may use the symmetrised dot pattern technique in combination with acoustic measurements in the fan's near vicinity as the basis of an incipient stall detection method. A microphone in the fan's near vicinity or the near vicinity of the duct system within which it is installed is sufficient to provide an input signal from which engineers may create distinctly different symmetrised dot patterns in different fan operating conditions. Therefore, one may 'install' the resultant stall detection system simply by placing a microphone close to the fan that requires monitoring. Thus, a stall detection system based on the symmetrised dot pattern technique facilitates the monitoring of industrial fans that are already installed and operational without requiring operators to shut them, or the process of which they are a part, down.

Chapters 8, 9, 10 and 11: Stall Resistant Blade Concepts

Chapters 5, 6 and 7 present the symmetrised dot pattern technique which provides operators with an incipient stall detection method that they can apply to operational industrial fans. Consequently, the operator can monitor any in-service industrial fan that he or she considers at risk. The ability to warn an operator when stall becomes incipient enables him or her to take remedial action to avoid stall, but does not guarantee that an industrial fan will never stall. As industrial fan applications become more demanding, the risk that they will inadvertently drive into stall increases. Although an effective incipient stall warning method is helpful, there remains a need to develop more 'stall tolerant' blade concepts.

In Chapter 8 the authors explore the use of blade sweep to extend an industrial fan's stall-free operating range. Using blade sweep is well established within the aerospace fan community, but has yet to find wide-spread application within the industrial fan community. Chapters 9 and 10 are more radical in their approach, taking inspiration from the humpback whales' pectoral fins. These fins incorporate tubercles along the leading edge that enable these sea mammals to perform sharp turns when hunting. An ability to turn more quickly than other whales suggests that the tubercles have not evolved accidentally or randomly. They have a beneficial effect on

the pectoral fin's hydrodynamic performance. When applied to an industrial fan blade the tubercles delay the onset of stall, and reduce the stall's severity when it does occur. Chapter 11 complements the work reported in Chapters 8, 9 and 10 on blade design by characterising an anti-stall ring's performance, fitted to a fan casing over the fan blades' leading edge.

Chapter 8 presents a research programme that characterised the influence of blade forward sweep on an industrial fan blade's aerodynamic performance. Experimental studies on fan blades designed for aerospace application found that a forward swept bladed rotor featured a wider stall-free operational range, with higher efficiency and total pressure peak. The computational analysis that the authors present in Chapter 8 demonstrate that when applied to an industrial fan blade, the forward swept stacking line induces a vorticity component in the blade leading edge's near vicinity. The sweep also attenuated span-wise secondary flow features, reducing the boundary layer fluid's centrifugal migration. A reduced migration lessened the accumulation of low-energy fluid in the blade-tip region. Additionally, sweep reduced the peak velocity in the blade-tip region, which in turn reduced the pressure difference across the blade tip-to-casing gap. Thus, sweep reduced the blade-tip leakage flow, and consequently, the blade-tip leakage vortex's intensity. The net result on the blade-to-blade flow-field was a reduction in both radial flow and the intensity of secondary flow features that resulted in improved fan stability limit. The authors concluded that forward sweep can improve the fan's performance in industrial as well as aerospace application.

We may regard the research that the authors report in Chapter 8 as a classical application of technology developed for aerospace application into an industrial context. It is natural that the industrial fan community should look to the aerospace community for inspiration as it has successfully developed a wide range of technical solutions that are potentially applicable in an industrial context. However, there are other potential sources of inspiration. One possible source comes from biomimicry, the study of nature, its models and processes, with insight providing the inspiration for man-made applications of that which occurs naturally in nature. In Chapter 9 the authors study a humpback whale's pectoral fins that incorporate tubercles along the leading edge. Other researchers have concluded that it is the presence of these tubercles that enables humpback whales to perform sharp turns when hunting. Taking its inspiration from this sea mammal, the authors of Chapter 9 report the results of a numerical study into the effect of a sinusoidal leading edge modelled on humpback whale tubercles on both symmetrical and cambered aerofoil performance. The research was primarily concerned with elucidating the fluid flow mechanisms associated with the presence of a sinusoidal leading edge, and the impact of those mechanisms on profile performance. The authors found that a sinusoidal leading edge influenced aerofoil lift. It exhibited an early recovery post-stall for the symmetric profile and both an early recovery post-stall and a gain in lift post-stall for the cambered profiles. The authors concluded that applying a sinusoidal leading edge had the potential to result in a more 'stall tolerant' industrial fan blade design.

The research reported in Chapter 9 established the physical flow mechanisms induced in the flow-field by the presence of a sinusoidal leading edge, and its beneficial

effect. The authors undertook the computational analysis as a 'numerical laboratory' using a three-dimensional computational analysis to model two-dimensional cascades of aerofoils. This computational approach was effective at elucidating the underlying physical flow mechanisms, but does not constitute a blade design methodology. Chapter 10 presents a design methodology for applying sinusoidal leading edge blade profiles to finite span aerofoils. The authors demonstrate that when applied to a three-dimensional industrial fan blade, a sinusoidal leading edge presence improved the blade's stall resistance. The design methodology is focused on optimising the sinusoidal leading edge blade profile in order to induce the desired vorticity distribution at the blade trailing edge. The authors identified three variables: the number of sinusoids from the blade tip, sinusoid wavelength in the span-wise direction and sinusoid amplitude in the chord-wise direction. They utilised the developed methodology to optimise the three variables, adapting a blade from a baseline design to create a 'whale-fan' incorporating a sinusoidal leading edge blade profile. The authors concluded that the sinusoidal leading edge blade profile resulted in a whale fan that is inherently more aerodynamically resistant to the effect of stall than the baseline design.

The research in Chapters 8, 9 and 10 is focused on developing intrinsically stall-tolerant blade designs. This is an approach to developing industrial fans that can better tolerate the effect of operating in an aerodynamically stalled condition. However, it is not the approach that the industrial fan community traditionally favours. Historically, the industrial fan community has embraced using 'anti-stall' stabilisation rings with industrial fans intended for applications where operation in an aerodynamically stalled condition is likely. The research that the authors present in Chapter 2 evaluates the impact of a stabilisation ring. The authors concluded that rotating stall resulted in unsteady mechanical stress in fan blades increasing by a factor of five without a fitted stabilisation ring and only a factor of two with a fitted stabilisation ring. This reduction in unsteady mechanical stress in fan blades represented a significant improvement in the studied fans' 'stall tolerance'. However, a negative consequence of the stabilisation ring was reduced fan efficiency. Current and forthcoming legislation dictating minimum allowable fan and motor efficiency grades has effectively rendered the stabilisation ring obsolete as a consequence of its negative impact on fan efficiency.

In Chapter 11 the authors present a research programme aimed at characterising the flow-field within a stabilisation ring. This was to establish why a stabilisation ring reduces fan efficiency, with the objective of identifying how engineers might avoid this reduction. The authors concluded that the stabilisation ring's effect on the studied fan's blade-to-blade flow-field at its peak efficiency and peak pressure operating points is minimal. However, at a deep stall operating point, the stabilisation ring has a significant impact on the blade-to-blade flow-field. Most significantly, the stabilisation ring's presence results in control of a hub separation, indicating that the stabilisation ring affects the blade-to-blade flow-field over the entire blade span. The authors also observed that at the fan's peak efficiency operating point the presence of a stabilisation ring reduced fan efficiency by 2.4 per cent. They concluded that flow within the stabilisation ring was highly separated. This separated flow constitutes an

aerodynamic loss mechanism that reduces fan efficiency. The authors concluded that if one could optimise vane design within the stabilisation ring to eliminate separated flow at the peak efficiency operating point, this would eliminate the loss mechanism and thus increase fan efficiency. In combination with intrinsically stall tolerant blade designs, an optimised stabilisation ring has the potential to result in a stall tolerant industrial fan, capable of operating in those application where occasional operation in an aerodynamically stalled condition is unavoidable.

Summary of Chapters

Geoff Sheard

This chapter-by-chapter summary of technical contribution provides the reader with a detailed description of the work in each chapter. It clarifies each chapter's content and summarises its contribution to knowledge. Thus it augments the discussion presented in the introduction. The introduction clarified why the authors undertook the work and linked each chapter, making explicit their collective contribution to knowledge. Together the introduction and summary of chapters clarify the rationale for undertaking the research, and the logic underpinning the move from one reported research programme to the next.

The papers comprising each chapter constitute selected publications from the published scholarly work relating to the development of stall detection and control technology. The Editor selected them for inclusion based on the degree to which the content contributed towards the creation of a coherent body of knowledge.

Chapter 1 A Critical Review of Stall Control Techniques in Industrial Fans

The authors specifically wrote the paper that forms the basis of Chapter 1 to be the first chapter of this edited volume. It reviews modelling and interpretation advances of industrial fan stall phenomena, related stall detection methods and control technologies. Competing theories have helped engineers refine fan stability and control technology. With the development of these theories, three major issues have emerged. The authors first consider the interplay between aerodynamic perturbations and instability inception. An understanding of the key physical phenomena that occurs with stall inception is critical to alleviate stall by design or through active or passive control methods. The authors then review the use of passive and active control strategies to improve fan stability. Whilst historically compressor design engineers have used passive control techniques, recent technologies have prompted them to install high-response stall detection and control systems that provide industrial fan designers with new insight into how they may detect and control stall. Finally, the chapter reviews the methods and prospects for early stall detection to complement control systems with a warning capability. Engineers may use an effective real-time stall warning system to extend a fan's operating range by allowing it to operate safely at a reduced stall margin. This may also enable the fan to operate in service at a more efficient point on its characteristic.

In their review, the authors provide an overview of stall control technologies for industrial fans. These control technologies play an important role in many industrial

applications. The authors examined the stall phenomenon and paid particular attention to fluid dynamics, stall inception and mechanical failure that may occur when operating industrial fans. The authors then introduced the technologies that exist today for stall identification and control, distinguishing between active and passive technologies. Engineers can use passive technologies to prevent the worst stall consequence: mechanical failures. Industrial fan manufacturers primarily use passive control technologies in service.

Although innovation in passive technology is possible, passive technologies generally reduce fan efficiency. Researchers, therefore, focus on active stall control technologies in an ongoing effort to develop effective stall detection systems. Active stall control technologies include those that are still the subject of both fundamental research and applied development and therefore, at the time of writing, are still immature. Despite the need for further research and development of active stall control systems, and their associated stall detection systems, they offer the greatest potential for medium-term improvement. We can most readily realise the potential for medium-term improvement in industrial fan applications, as industrial fans are relatively low-speed machines in comparison to compressors. Consequently, active stall control systems based upon stall detection have the potential for practical application in industrial fans first, with the experience gaining in industrial fan application informing the development of higher speed systems that engineers can then use in compressor applications.

Chapter 2 The Mechanical Impact of Aerodynamic Stall on Tunnel Ventilation Fans

Chapter 2 presents a research programme aimed at establishing the ability of an industrial fan to operate without risk of mechanical failure in the event of aerodynamic stall. The research establishes the aerodynamic characteristics of a typical industrial fan intended for tunnel ventilation application when operated in both stable and stalled aerodynamic conditions, with and without an 'anti-stall' stabilisation ring, with and without a 'non-stalling' blade angle and at full, half and one-quarter design speeds. It also measures the fan blades' peak unsteady stress, thus facilitating an analysis of the implications of the experimental results for mechanical design methodology.

The measured peak unsteady stress for a fan with a fitted stabilisation ring during aerodynamic stall resulted in alternating stress increasing, and consequently, the fan blade mechanical safety factor reducing. The reduction in mechanical safety factor is significant, as it indicates that although the stabilisation ring provides some mechanical protection in the event of aerodynamic stall, it does not provide complete protection. The authors concluded that some industrial fan designers assume that a stabilisation ring provides complete mechanical protection in the event of aerodynamic stall, an incorrect assumption that may have been the root cause of previously 'unexplained' in-service failures in tunnel ventilation fans. Engineers associate the tunnel ventilation application with pressure pulses as trains pass the

ventilation shafts within which the fans are situated. Researchers know that these pressure pulses can transiently drive ventilation fans into aerodynamic stall.

The authors conclude by presenting three different strategies for tunnel ventilation fan selection in applications where the selected fan will most likely stall. The first strategy selects a fan with a low blade angle that is non-stalling. The second strategy selects a fan with a high pressure developing capability. The third strategy selects a fan with a fitted stabilisation ring. The authors concluded that the three fan selection strategies that tunnel ventilation system designers classically use each have specific advantages and disadvantages. The optimum fan selection strategy in a specific application will, therefore, depend on the impact of fan diameter on plant room cost, and the relative importance of both the fan's initial and operating cost.

The authors also consider the implication for tunnel ventilation fans that engineers correctly select to operate within the stable part of their characteristic at full design speed that they then operate at part-speed. A fan that will not stall when subjected to a pressure pulse at full design speed will likely drive into stall if one operates it at half design speed and certainly drive into stall if one operates it at quarter design speed. The authors were able to demonstrate that for a tunnel ventilation fan with a stalling blade angle, without a fitted stabilisation ring, operating at full design speed, the mechanical factor of safety during stable operation is lower than at half design speed during stalled operation. As such, they concluded that one could operate the studied fan at half design speed in an aerodynamically stalled condition without risk of mechanical failure.

Chapter 3 Stall Inception, Evolution and Control in a Low-speed Axial Fan with Variable Pitch in Motion

Chapter 3 reports the base research that established the viability of differentiating between industrial fan operating conditions. The research comprised an experimental study to investigate stall precursors at different blade stagger-angle settings. The authors systematically drove the studied fan from stable operating to an incipient stall condition and then into rotating stall. They established the studied fan's characteristics by visually inspecting unsteady pressure signals from two circumferentially off-set pressure transducers. This enabled the authors to establish the characteristic features that constituted the studied fan's stall precursors that characterised incipient stall.

The authors commenced their analysis with a visual inspection of unsteady pressure data. This enabled them to characterise the studied fan's stall precursors, identifying that as blade angle increased, the fan transitioned from stable operation into rotating stall in less than ten rotor revolutions. Emerging stall cells rotating at a range of speeds that corresponded to different fractions of full fan design speed characterised the incipient stall condition.

The authors fitted the studied fan with two pressure transducers over the fan blades, with a 60 degree azimuthal offset. They performed a Fourier transformation of a cross-correlation of the two pressure signals to provide further insight into the

physical flow phenomena at play within the studied fan's blading. The spectral analysis of cross-correlated data when stall was incipient revealed a low-frequency tone that the authors associated with a rotating stall cell presence. There were also harmonics present in the spectra. These harmonics occurred as a consequence of interaction between weak pressure instabilities that emerged as stall became incipient. The authors concluded that the low-frequency tone and its harmonics characterised incipient stall for the studied fan.

The presence of identifiable features in the unsteady pressure data associated with incipient stall indicates that it is theoretically possible to identify that stall is incipient. However, traditional fan and compressor stall warning systems are unable to utilise the spectrum of a pressure signal, or the spectrum of the correlation between two circumferentially offset pressure transducers. The required sampling time is long compared to the time scales that researchers associate with stall precursors. Consequently, traditional fan and compressor stall warning systems are able to identify rotating stall, but not incipient stall.

Identifying that a fan or compressor has transitioned from stable operation to rotating stall is useful, as it alerts operators to the need for corrective action. However, operation in rotating stall results in damage to the fan or compressor. A technique that enables the identification of stall precursors would facilitate generating a warning that a fan or compressor was about to stall. This has the potential to enable operators to take action before rotating stall has become established, and therefore, before any mechanical damage.

Chapter 4 The Role of Variable Pitch in Motion Blades and Variable Rotational Speed in an Industrial Fan Stall

Chapter 4 presents an experimental programme that utilised two strategies to study rotating stall recovery patterns in an industrial fan. The authors' primary research objective was to characterise the physical flow phenomena that occur with the transition from stalled to stable operation.

The authors' experimental facility incorporated a fan with both variable pitch in motion blades and a variable speed drive. The facility enabled the authors first, to study the evolution of unsteady pressure signals on the fan casing whilst varying fan blade pitch and then to examine varying fan rotational speed. Consequently, they were able to recover a fan from stall either by varying blade pitch at constant speed, or by varying speed at constant blade pitch. They also studied the physical flow phenomena that occurs with stall recovery by cross-correlating signals from circumferentially offset high-frequency response pressure transducers and then analysed the cross-spectra. This enabled the authors to gain insight into the transient fluid flow behaviour that occurs with stall recovery in the studied industrial fan class.

The authors' analysed pressure signals via a Fourier transformation of cross-correlated pressure signals from two azimuthal positions 60 degrees offset. They conducted the analysis on data that they obtained during the transition from stalled to stable operation for recovery from stall via both varying blade pitch at constant fan

speed, and varying fan speed with constant blade pitch. A qualitative inspection of the pressure signals and cross-spectrum for the stall recovery transition via each of the two methods highlighted differences in both the unsteady pressure and cross-spectrum between the variable pitch in motion and variable speed recovery transients.

An analysis of the variable pitch in motion data from the recovery transient from stalled to stable operation indicates that a rotating stall cell breaks down into a series of weak rotating instabilities that constitute a recovery bubble. In contrast, an analysis of the variable speed data from the recovery transient from stalled to stable operation indicates that the rotating stall cell contains more energy and breaks down very late in the stall recovery process.

The authors calculated the spectra of the pressure data that they took during the recovery transient. The spectra indicated the presence of a low-frequency tonal component that researchers associate with incipient stall recovery. The analysis also identified tone-band modulations in the measured unsteady pressure that the authors characterised as harmonics that occur as a consequence of interaction between weak rotating instabilities that occur during the stall recovery process.

A conclusion of the reported research is that the transient fluid flow behaviour that occurs with stall recovery by varying blade pitch was indicative of both a mild and progressive transition. In contrast, stall recovery by varying fan speed occurred more suddenly. In comparison with the variable pitch transition, the variable speed transition was more indicative of recovery from mild surge, from which we may conclude that stall recovery via variable speed resulted in significantly higher unsteady mechanical stress induced in fan rotating components than recovery via variable pitch.

Chapter 5 Stall Warning in a Low-speed Axial Fan by Sound Signal Visualisation

In Chapter 5 the authors present the base research underpinning development of a novel stall-detection method for application with industrial fans. The developed method utilises a symmetrised dot pattern (SDP) technique that is capable of differentiating between fan operating conditions. The authors' present an analysis of measured acoustic and structural data across nine fan operating conditions represented in a three-by-three matrix. The matrix is a combination of (i) three speeds (full-, half- and quarter-speed) and (ii) three operational states (stable operation, incipient stall and rotating stall). They use the symmetrised dot pattern matrix and structural data to differentiate critical stall conditions (those that will lead to the fan's mechanical failure) from non-critical ones (those that will not result in mechanical failure), thus providing a basis for an intelligent stall-warning methodology.

The authors' research aim was to develop a signal processing technique that is capable of detecting presence of the aerodynamic instabilities that constitute stall precursors. The objective was to initiate action to prevent the onset of rotating stall.

Researchers have historically based stall-detection methods on an analysis of pressure or vibration signals in either the time or frequency domain. However, the signals that researchers associate with stall precursors are often low compared to the background noise. They require significant computational effort to extract, and significant time to gather sufficient data to make extraction possible at all. Therefore, conventional methods of stall-detection are typically able to identify that a fan or compressor is operating in rotating stall, but not that stall is incipient.

The symmetrised dot pattern technique has proven successful in real-time speech recognition systems, differentiating between rapidly changing input signals. Therefore, the authors considered that the technique had the potential to identify the aerodynamic instabilities that occur with incipient stall. Symmetrised dot patterns represent an input signal on polar coordinates, and thus changes in the input signal frequency content manifest themselves as changes in the resultant symmetrised dot patterns.

The authors were able to demonstrate that one may generate symmetrised dot patterns with data recorded during one revolution of the studied fan. As stall precursors typically occur over a time scale similar to that of one revolution, the authors were able to generate symmetrised dot patterns fast enough to capture them. This enabled the authors to use these patterns as the basis of an 'incipient' stall detection method. Thus, a symmetrised dot pattern technique based stall detection system is able to identify that a fan is likely to stall before it actually has.

The authors' analysis extended to a matrix of nine operating condition and speed combinations. The resultant symmetrised dot patterns were distinctly different. In combination with a structural analysis, the authors were able to correlate symmetrised dot patterns associated with conditions that did, and did not constitute a risk of mechanical failure. Thus, they offered the possibility of an intelligent diagnostic system.

Chapter 6 Demonstration of a Stall Detection System for Induced-draft Fans

The need to monitor the operating condition of induced draft fans used in coal fired power stations inspired the authors' research in Chapter 6. Over time fan blade erosion degrades the blades' pressure developing capability, and can result in a gradual transition from stable operation into a condition where stall is incipient and finally a condition where rotating stall is established fully. The presence of erosive material in the gas-path results in sensors fitted over the fan blades becoming unreliable in service and prone to failure. Consequently, the reported research focuses on establishing the studied fan's operating condition using data from a sensor mounted in the fan's inlet plenum.

The authors characterised the studied fan's performance by establishing its stability limit over a range of blade stagger angles. They made time-resolved pressure measurements with pressure transducers fitted into both the fan casing over the fan blades (the near-field) and the inlet plenum one fan diameter upstream of the fan rotor (the far-field). They then studied data from near- and far-field pressure

transducers, and used the symmetrised dot pattern technique to generate symmetrised dot patterns from both.

The authors generated symmetrised dot patterns for the studied fan's stable operation, when stall was incipient and during rotating stall. They focused on the evolution of the measured near- and far-field pressure signals as the blade stagger angle increased. The symmetrised dot pattern technique was able to generate distinctly different symmetrised dot patterns during the studied fan's stable operation, when stall was incipient and during rotating stall. The far-field pressure data had a significantly lower signal-to-noise ratio than the near-field pressure data. Despite the low signal-to-noise ratio, the symmetrised dot pattern technique still was able to generate distinctly different symmetrised dot patterns using data from the far-field pressure transducer. Differentiating the symmetrised dot patterns proved possible, even when the authors collected data over a time period equivalent to as little as half a rotor revolution.

The authors concluded that the symmetrised dot pattern technique was remarkably effective. An ability to generate symmetrised dot patterns using data that they collected over half a rotor revolution facilitated the identification of incipient stall. The aerodynamic instabilities that constitute stall precursors typically form and collapse in a time scale equivalent to one rotor revolution. Therefore, identifying incipient stall requires an analysis technique to function with data that the authors collected over a similar time scale. The authors judged the symmetrised dot pattern technique's effectiveness as remarkable as it was not only able to generate identifiably different symmetrised dot patterns using data collected over half a rotor revolution, but could do so with low signal-to-noise ratio data collected in the far-field.

The authors concluded that the symmetrised dot pattern technique successfully demonstrated the ability to work with data collected over a short time scale in combination with low signal-to-noise level data. This combination validated the technique as a viable incipient stall detection method for in-service monitoring of industrial fan operating conditions.

Chapter 7 Experiments on the Use of Signal Visualisation Techniques for In-service Stall Detection in Industrial Fans

Chapter 7 extends the research programme from Chapter 6 as the authors present a stall detection method based on acoustic measurements. In Chapter 6 the authors presented a research programme aimed at establishing the fan's operating condition using far-field, as opposed to near-field data. The motivation for the research was a need to avoid fitting pressure sensors in induced draft fan casings over the blades (the near-field), instead using data from a pressure transducer fitted in the fan inlet plenum (the far-field). The success of this research programme encouraged the authors to consider the possibility of applying the signal processing techniques to acoustic data measured in the fan's near vicinity.

The authors explore the symmetrised dot pattern technique's capability to differentiate between fan operating conditions using acoustic data from a number of

locations around the fan and its associated duct system. Critically, the use of a microphone in the near vicinity of the fan or its associated duct system does not require fitting a sensor in either the fan casing over the blades or in the fan inlet plenum. Engineers associate the most challenging industrial fan applications with erosive particles in the gas path, high-temperature gas passing through the fan or a combination of both. Therefore, sensors fitted in the gas path are prone to be unreliable in service. Consequently, any stall detection method has a significant advantage if it can differentiate between fan operating conditions using data from a microphone placed external to the fan or the duct system within which it is fitted.

The authors evaluated the symmetrised dot pattern technique's effectiveness to differentiate between fan operating conditions using data from a microphone that they placed in different locations around the fan and the duct system within which it was fitted. Low signal-to-noise ratio signals characterised all locations. However, the symmetrised dot pattern technique was able to produce distinctly different symmetrised dot patterns for stable operation, incipient stall and rotating stall operating conditions, irrespective of the microphone location.

The authors concluded that the symmetrised dot pattern technique is able to identify incipient stall using data from a microphone external to the fan or its duct system. The symmetrised dot pattern technique had proven particularly effective at differentiating between fan operating conditions with low signal-to-noise level signals. As such, the symmetrised dot pattern technique constitutes a viable basis for an incipient stall detection method. The use of a microphone external to the fan or the duct system within which it was fitted also facilitated using the incipient stall detection method in applications where sensors would be unreliable in service if fitted within the fan casing over the blades or in the fan's inlet plenum. Further, with no requirement to fit sensors in the fan casing or inlet plenum, the authors could utilise the incipient stall detection method in conjunction with operational fans. As the incipient stall detection method requires only a microphone placed in the near vicinity of the fan or its duct system, there is no need to shut down either the fan or the process of which it is a part.

Chapter 8 Using Sweep to Extend Stall-free Operational Range in Axial Fan Rotors

Chapter 8 presents a research programme that established the viability of using blade forward sweep as a strategy to improve an industrial fan's stability limit. Former experimental studies by other scholars working in the aerospace community have concluded that the forward swept bladed rotor featured a wider stall-free operational range, with higher efficiency and total pressure peak. The authors undertook a numerical investigation of two highly loaded industrial fan blades of forced-vortex design. The fans had a design point flow and pressure typical of an industrial fan. The authors designed the two blades with identical nominal design parameters and, respectively, with a 35 degree forward-swept blade and an un-swept blade.

The authors assessed the pay-off derived from the sweep technology with respect to the improved operating range. They analysed the flow structure which

developed through the blade passages and downstream of the rotors, as well as loss distributions at design and near-peak pressure operating conditions. The three-dimensional flow structure analyses showed that sweeping the blade forward attenuates the forced-vortex span-wise secondary flows. Moreover, the swept rotor features a reduced sensitivity to leakage flow effects. Consequently, it operates more efficiently when it approaches its stability limit and therefore stalls later.

The authors concluded that the forward swept stacking line induces a vorticity component in the blade leading edge's vicinity which is in opposition to that forced by the blade's forced-vortex design concept. Turning the incoming end wall boundary layer achieves this. The attenuation of span-wise secondary flows occurred as a consequence of the induced vorticity component. Reducing secondary flows resulted in rearranging the axial velocity profile with the forward-swept blading. This rearrangement resulted in reducing the centrifugal migration of near-surface fluid on the swept blade suction side. This reduction prevented the accumulation of low-energy fluid near the blade-tip region.

The net effect of a forward-swept stacking line in the blade-tip region is a reduction of the leading edge peak velocity which in turn reduces the peak blade tip-to-casing pressure difference. A 35 degree forward sweep of the blade stacking line therefore proved effective at limiting blade over-tip leakage. The net result was an improvement in the fans stability limit. Therefore, the authors concluded that forward sweep can improve the fan's performance in industrial as well as aerospace application.

Chapter 9 On the Role of Leading Edge Bumps in the Control of Stall Onset in Axial Fan Blades

The research in Chapter 9 takes its inspiration from humpback whale pectoral fins that are characterised by a series of tubercules that result in a sinusoidal-like leading edge. This is an example of biomimicry, the study of nature, its models and processes, with insight providing the inspiration for man-made applications of that which occurs naturally in nature. Other researchers have concluded that it is the presence of these tubercles that enables humpback whales to perform sharp turns when hunting.

Taking its inspiration from this sea mammal, the authors report the results of a numerical study into the effect of a sinusoidal leading edge modelled on humpback whale tubercles on both symmetrical and cambered aerofoil performance. The authors used the computational analysis as a 'numerical laboratory', using three-dimensional computational models to study the performance of two-dimensional aerofoil cascades. The authors adopted this approach as their primary objective was to elucidate the effects of the modified leading edge on lift-to-drag performance and the influence of camber on lift and drag.

The authors found that a sinusoidal leading edge influenced aerofoil lift. They computed turbulent flow around the aerofoils with and without a sinusoidal leading edge at different angles of attack. They calculated the lift and drag of both cambered and un-cambered aerofoils. They also calculated the lift and drag of the same

cambered and un-cambered aerofoils with a sinusoidal leading edge. Both cambered and un-cambered aerofoil lift coefficients changed as a consequence of introducing a sinusoidal leading edge. The cambered profile with a sinusoidal leading edge exhibited a 30 per cent increase in post-stall lift compared to the same profile without a sinusoidal leading edge.

The authors observed that the increase in cambered profile post-stall lift induced by the sinusoidal leading edge's presence occurs because the leading edge geometry impacts the profile's velocity and vorticity fields. A sinusoidal leading edge introduces peaks and troughs along a profile's leading edge that induce vortex pairs. These vortices migrate from leading to trailing edge and supress suction side separated flow regions that develop at the trailing edge as a profile approaches stall. The separated flow is suppressed because it is confined to trailing edge regions down-stream of a leading edge trough. By confining the separated flow at the trailing edge, a sinusoidal leading edge is able to minimise the extent of separated flow regions and thus improve profile post-stall lift. Therefore, the authors were able to conclude that applying a sinusoidal leading edge had the potential to result in a more 'stall tolerant' industrial fan blade design.

Chapter 10 The Application of Sinusoidal Blade Leading Edges in a Fan Design Methodology to Improve Stall Resistance

Chapter 10 extends the research in Chapter 9, reporting a programme of work to design a 'whale-fan' that incorporates a sinusoidal leading edge blade profile that mimics the tubercles on the humpback whale's pectoral fins. In Chapter 9 the authors used two-dimensional aerofoil cascades to study the effects of a sinusoidal profile on aerofoil lift and drag performance. The research was concerned with elucidating the fluid flow mechanisms induced by the sinusoidal profile, and the impact of those mechanisms on aerofoil performance.

The reported research in Chapter 10 focuses on applying the research in Chapter 9 to designing and optimising a finite-span aerofoil. The chapter presents the assumptions when developing a three-dimensional aerofoil design methodology that correlates the blade leading edge's sinusoidal profile with the desired vorticity distribution at the trailing edge. The authors apply the developed methodology to the design of a fan blade's tip region to control separation at the trailing edge. The authors' present numerically derived whale-fan performance characteristics, and compare them with both the baseline fan's numerically and experimentally derived performance characteristics.

The authors established that when applied to a three-dimensional blade, a sinusoidal leading edge presence also improved the blade's stall resistance. The research focuses on assumptions when developing the design methodology. The design methodology objective was to optimise the sinusoidal leading edge blade profile in order to induce the desired vorticity distribution at the blade trailing edge. The authors identified three variables: number of sinusoids from the blade tip, sinusoid wavelength in the span-wise direction and, sinusoid amplitude in the chord-wise direction.

The authors utilised the developed methodology to optimise the three variables. They adapted a blade from a baseline fan to create a 'whale-fan' blade. The final whale-fan blade design has a blade with a sinusoidal leading edge blade profile with three per cent blade chord amplitude, five per cent blade span wavelength and four and a half sinusoids from the blade tip.

The authors carried out numerical computations on both the baseline fan and the whale-fan. The numerical computations for the baseline fan were within the combined uncertainty of experimental measurements and assumptions when accounting for the effect of compressibility and the fan stator. The agreement between the two gave confidence in the computational results. The authors then compared the numerical computations for the baseline fan quantitatively with those for the whale-fan. They analysed and compared the difference between the two sets of results with those of previous researchers. The analysis confirmed that the choice of amplitude, wavelength and number of sinusoids resulted in similar flow-field features to those that had resulted in an improvement in the infinite span aerofoils' post stall lift recovery. Thus, the authors concluded that the sinusoidal leading edge blade profile resulted in a whale-fan that is inherently more aerodynamically resistant to the effect of stall than the baseline fan.

Chapter 11 Investigation on Anti-stall Ring Aerodynamic Performance in an Axial Flow Fan

Chapter 11 reports the results of a research programme to characterise the performance of an anti-stall 'stabilisation' ring. A stabilisation ring consists of an annular chamber that is incorporated into the fan casing over the fan blade's leading edge. As a tip-limited axial fan approaches stall, boundary layer fluid centrifuges up the blade. The fan stalls at the point when flow inside the annulus reverses direction in the blade tip region. The stabilisation ring provides an annular chamber into which this fluid may flow. It incorporates a set of vanes that redirect the reverse flow into an axial direction, and then reintroduce it into the main-stream flow up-stream of the fan blade leading edge. Although effective in stabilising the fan's characteristic, stabilisation rings typically reduce fan efficiency by three per cent, and consequently are becoming progressively less acceptable as required minimum fan efficiencies increase.

The authors combine experimental measurements of overall fan performance with and without a fitted stabilisation ring and a numerical analysis of the flow-field within the stabilisation ring. The stabilisation ring's effect is to stabilise the fan characteristic, such that it rises continuously back to zero flow. Results from the computational analysis at peak efficiency, peak pressure and deep stall operating points provide an insight into the stabilisation ring's effect on the fan blade-to-blade flow-field. At the peak efficiency and peak pressure operating points the stabilisation ring's effect is minimal. However, at the deep stall operating point, the stabilisation ring has a significant impact on the blade-to-blade flow-field. Most significantly, the stabilisation ring's presence results in controlling a hub separation, indicating that the stabilisation ring affects the blade-to-blade flow-field over the entire blade span.

The experimentally measured fan efficiency with a fitted stabilisation ring at the peak pressure operating point was 0.6 per cent lower than the efficiency when the authors measured it without a fitted stabilisation ring. The computational analysis indicated that the flow within the stabilisation ring is attached to the stabilisation ring vanes at the peak pressure operating point. From this we may conclude that when the flow within the stabilisation ring remains attached to the vanes, fitting a stabilisation ring reduces fan efficiency by 0.6 per cent. In contrast, the experimentally measured fan efficiency with a fitted stabilisation ring at the peak efficiency operating point was 2.4 per cent lower than the efficiency when the authors measured without a fitted stabilisation ring. The computational analysis indicated that the flow within the stabilisation ring is separated from the stabilisation ring vanes at the peak efficiency operating point. From this we may conclude that the separated flow through the stabilisation ring constitutes an aerodynamic loss mechanism that reduces fan efficiency by 1.8 per cent.

Operators do not run industrial fans at their peak pressure point. They typically operate them at or close to their peak efficiency operating point. The conclusion that at the peak efficiency operating point flow within the stabilisation ring is highly separated provides an insight into how industrial fan designers may improve fan efficiency. If one could optimise vane design within the stabilisation ring to eliminate separated flow at the peak efficiency operating point, this would eliminate the loss mechanism and increase fan efficiency.

Appendix 1 A Method of Detecting Stall in an Axial Fan

The two appendices in this volume are each a developed form of a patent. Patents are written in a formal style that is difficult for those unfamiliar to penetrate. As such, we tend not to read or reference patents. To overlook patents, however, is to overlook a significant source of intellectual property. The two patents included in this volume each document one aspect of intellectual property originated by the inventors. This intellectual property was originated as part of the research documented in the papers that form the basis of the chapters of this edited volume. We have edited each into a more readable form, in an effort to make its content more accessible to the reader.

The patent that we have converted into this appendix's text supports the research reported in Chapter 5. It was the research that the authors presented in Chapter 5 that originated the concept of a stall detection method based on using the symmetrised dot pattern technique. This proved to be a suitable subject for a patent as it is particularly advantageous in detecting incipient stall. Detecting incipient stall has many practical as well as cost advantages. Taking corrective action to avoid stall extends a fan's service life. It also enables one to operate a fan closer to its peak efficiency operating point that is invariably at a lower stall margin than operators historically would have considered acceptable.

There are four primary reasons for the effectiveness of the symmetrised dot pattern technique. First, generating symmetrised dot patterns is quite light on the

signal processing requirement, so it is easier to conduct the signal processing in real time, and therefore identify incipient stall, as opposed to stall that has already happened. Second, the technique is effective when working with low signal-to-noise ratio signals. Third, the technique is effective with signals from a microphone placed in any location. Known techniques for stall detection need a pressure measurement over the blade. As such, the symmetrised dot pattern technique, in combination with an acoustic measurement, is able to create a visual pattern that one can use to detect incipient stall in any location, not just with a pressure transducer over the blade itself. Fourth, because of its low processing power requirements and its speed of processing the acoustic signals, the symmetrised dot pattern technique is able to produce the acoustic signal's visual representation that incorporates features that are linked to the approach of stall.

Chapter 5 and the patent that forms the basis of this appendix document the process by which the intellectual property underpinning the symmetrised dot pattern technique incipient stall detection method is based. The authors undertook the development of that intellectual property into a product through establishing a *Sapienza* University of Rome spin-off company. The spin-off company was successful in bidding for European Union funding, winning a €100,000 grant to develop the intellectual property into a viable product that the inventors could use to monitor an industrial fan's operating condition in real time. Although not suitable as a subject of an academic paper, the development effort has been successful, with manufacturers applying the resulting incipient stall detection product into a wide range of rotating equipment monitoring applications.

Appendix 2 Axial Air Movement Fans

The patent that the authors have converted into the text for this appendix supports the research in Chapters 8, 9, 10 and 11 by providing an insight into a complementary method of damping very large fan blades, making them less susceptible to the effects of operation in an aerodynamically stalled condition.

Very large fan blades are classically used in wind tunnel applications. For over a hundred years, engineers have relied on wind tunnels to design new aircraft. The Wright brothers used a wind tunnel whilst developing their ground breaking Wright Flyer in 1901. Investment in such wind tunnels reached a peak between the late 1920s and early 1940s in the rush to develop new aircraft. Despite the phenomenal advance in computer technology during the post-war years, wind tunnels remain the definitive method of establishing an object's aerodynamic performance. Wind tunnels are here to stay; however, the World War II era wind tunnels are reaching the end of their working life. Now, the industrial fan community faces the challenge of refurbishing and replacing critical components, thus revisiting the work of early wind tunnel pioneers.

Refanning any wind tunnel is challenging, invariably involving a unique set of demands and constraints. Very occasionally, however, an engineering team encounters a 'once in a career' challenge that cannot call on previous experience.

The Office National d'Etudes et de Recherches Aérospatiales (ONERA) at Modane in the French Alps are owners of a vast and venerable transonic wind tunnel. They approached the inventors of the patent that forms the basis of this appendix to evaluate the feasibility of designing a replacement fan.

The inventors challenge was to replace a 15 metre diameter wind tunnel fan with a power consumption of 88 MW at full speed. It was immense, a true leviathan and unlike anything the inventors had previously seen. They had to evaluate the practicality of not only replacing the original fan, but also had to address issues with the original design that were reducing wind tunnel productivity. After a year of preparatory work, the inventors' engineering team embarked upon a four-year project to design, validate, manufacture, install and commission a new fan. The project culminated in the wind tunnel re-entering commercial service on 7 October, 2008.

The patent itself relates to one aspect of the inventors' research, a need to increase axial fan blade damping. An axial fan comprises a hub fitted with blades extending outwardly. The intellectual property that is the subject of the patent is the inclusion of at least one damping mass within the blade. The mass can oscillate relative to the blade in response to oscillatory flexing the blade at its first bending frequency, thus damping the flexing. The development effort was not suitable as a subject for an academic paper. A practical embodiment of the invention that did not result in the damping mass suffering a fatigue failure constitutes a source of competitive advantage that the authors could not report in the open literature.

A Critical Review of Stall Control Techniques in Industrial Fans

S. Bianchi, A. Corsini, A.G. Sheard and C. Tortora

ABSTRACT

This chapter reviews modelling and interpretation advances of industrial fan stall phenomena, related stall detection methods and control technologies. Competing theories have helped researchers refine fan stability and control technology. With the development of these theories, three major issues have emerged. In this chapter we first consider the interplay between aerodynamic perturbations and instability inception. An understanding of the key physical phenomena that occur with stall inception is critical to alleviate stall by design or through active or passive control methods. We then review the use of passive and active control strategies to improve fan stability. Whilst historically compressor design engineers have used passive control techniques, recent technologies have prompted them to install high-response stall detection and control systems that provide industrial fan designers with new insight into how they may detect and control stall. Finally, the chapter reviews the methods and prospects for early stall detection to complement control systems with a warning capability. Engineers may use an effective real-time stall warning system to extend a fan's operating range by allowing it to operate safely at a reduced stall margin. This may also enable the fan to operate in service at a more efficient point on its characteristic.

INTRODUCTION

When a single fan operates in isolation the unstable aerodynamic condition, which we refer to as 'stall', occurs at low flow rates. This type of stall varies according to fan type, but is most severe in axial fans, forward-curved centrifugal fans and

backward-inclined centrifugal fans (de Jager, 1995). Fan stall occurs as the fan reaches its stable operating range limit. This happens when the pressure rise across a fan increases to the fan's pressure developing limit and the flow velocity through the fan reduces to the point at which it first falls to zero, and then reverses. As the flow through a fan reverses, it separates from the fan blades with the turbulence that occurs with the separated flow buffeting the fan blades. This aerodynamic buffeting induces an increase in unsteady stress within the blades that can result in mechanical failure.

As a fan approaches stall, the separated flow initially occurs within one blade passage. Stall in one blade passage increases the aerodynamic blade loading on the adjacent blade passage, with a consequence that the 'stall cell' moves to the next blade passage. This results in a cascading effect as a stall cell jumps from blade passage to blade passage. The shape of and distance between fan blades affect how the stall impacts fan performance with more highly aerodynamic loaded blade designs suffering a more severe reduction in performance during stall than lightly loaded designs. Centrifugal fans with radial blades show little change in performance in the event of stall. Radial-blade centrifugal fans do not rely on air passing through the fan perpendicular to the centrifugal force which fan impeller rotation induces. As a result, stall is less of an issue in centrifugal fans generally than it is in axial fans.

Axial fans are particularly vulnerable to stall. Industrial fan manufacturers do not recommend axial fans for use in applications that require widely varying flow requirements unless a means of keeping flow rates above the stall point is available. Industrial fan manufacturers use proprietary anti-stall devices to control the flow in the axial fans' tip region. These anti-stall devices have the effect of stabilising the fan's performance. This eliminates the drop in fan performance at the point where it would have stalled without the anti-stall device, with the fan exhibiting a continuously rising pressure characteristic back to zero flow. This fan stabilisation is at the expense of fan efficiency, which typically reduces between two and five per cent with the presence of an anti-stall device. With an increasing focus on energy efficiency, anti-stall devices are becoming progressively less acceptable as industrial fan manufacturers strive to meet increasingly demanding minimum efficiency targets.

Historically, manufacturers have utilised anti-stall devices where a fan operates in conditions that may result in the fan stalling. However, application in which engineers do not expect the fan to stall can still result in stall. A fan can stall as a result of fan blade erosion or fouling, or a significant increase in system pressure as a consequence of filters clogging. Additionally, a classical cause of industrial fans stalling is running them in parallel. When in parallel operation, one fan starting or stopping as others operate will inevitably result in the fan stalling during its starting and stopping transient. Consequently, poor fan maintenance, the blockage of filters within the system, or inappropriate control system programming can all result in fan stall.

A practice that engineers habitually employ in an attempt to avoid fan stall is over-sizing of industrial fans for their application. System design engineers classically apply a safety factor to a fan's operating point when specifying industrial fans. Each engineer involved in the system's design adds his or her own safety factor. The

result is that when finally installed, a fan operates on its characteristic far to the left of its optimum operating point. This lowers operating efficiency, with fans capable of achieving 80 per cent efficiency at their optimum operating point and frequently achieving less than 60 per cent when installed.

The European Union Regulation 327 became legally binding on 1 January, 2013. This set the minimum Fan and Motor Efficiency Grades (FMEGs) for industrial fans. The 2013 minimum fan and motor efficiency grades have resulted in approximately 33 per cent of fans sold before 1 January, 2013, now being illegal within Europe as a consequence of not meeting the minimum fan and motor efficiency grade for their application. The European Union will raise minimum fan and motor efficiency grades on 1 January, 2015. In the USA, the Department of Energy has been monitoring activity within the European Union. On 1 February, 2013, the US federal government published a framework document in the *Federal Register*. This outlined the intended approach to fan regulation that aims to eliminate inefficient fans within the USA by 2019. The industrial fan community widely anticipates that the Department of Energy will adopt the same approach as the European Union, increasing the minimum allowable fan and motor efficiency within three years of introducing the initial 2019 targets. In practice, Asian countries take their lead on industry regulation from either Europe or the USA and with both now regulating, or declaring intent to do so, it is likely that Asian countries will do the same. Consequently, we may expect that over the next decade minimum fan or fan and motor efficiencies worldwide will first become mandatory and second, increase over time.

Given today's regulatory environment it is reasonable to assume that the pressure on design engineers will increase to develop fans with high peak efficiency. The practice of oversizing fans and fitting anti-stall devices will become progressively less acceptable as a consequence of the negative impact on fan efficiency. The result of specifying a fan such that it operates closer to its peak efficiency point when installed will increase the probability that the fan may stall. The peak efficiency operating point is invariably close to the fan's stability limits, and consequently erosion, fouling or filter clogging are more likely to result in stall. Therefore, the design of inherently 'stall tolerant' fans, and development of a stall detection system for in-service use, are becoming a rising priority for the industrial fan community.

Researchers have not systematically studied industrial fan in-service performance. However, advanced instrumentation and field testing can play a role in establishing where industrial fans actually operate on their characteristic and in those applications where a fan is prone to stall, assist in the verification and refinement of stall control techniques. Thus, it is not enough to focus on the development of improved design-point performance. Researchers must develop a more complete picture of the challenges that occur with different industrial fan applications if they are to gain an insight into how they may improve fan efficiency without inadvertently producing fan designs more likely to stall in real-world applications. This chapter describes some of the competing perspectives on the physics that underpin fan aerodynamic stability, and how knowledge of that physics can facilitate new industrial fan technology development.

STALL AND SURGE DYNAMICS IN
AXIAL COMPRESSORS AND FANS

Predicting the conditions under which an aerodynamic instability will occur should be a standard part of the industrial fan design process. Over decades researchers have studied different forms of aerodynamic instability. Many studies have clarified the problem of axial flow compressor rotating stall, focusing on multi-stage machines (Day and Cumpsty, 1978; Greitzer, 1980; Moore, 1984). Emmons *et al*.'s (1955) earlier work was one of the first attempts to describe the mechanism underlying stall propagation. In general, two primary aerodynamic instabilities occur in decelerating rotors: (i) 'rotating stall' in which regions of reversed flow occur locally; and (ii) 'surge' in which periodic backflow over the entire annulus results in violent oscillations in the compression system (Gravdahl and Egeland, 1999). Both forms of aerodynamic instability place mechanical stress on the rotors which can eventually lead to mechanical failure.

Those researchers who have studied the subject report that strain gauge measurements on axial compressors indicate that bending stress in blades exceeds those measured during stable operation by a factor of five under rotating stall conditions (Sheard and Corsini, 2012). Increasing bending stresses by a factor of five results in blade fatigue and consequently blade failure. The blade failure may occur whilst the fan operates under rotating stall conditions, but more usually does not. Typically, the fan's operation under rotating stall conditions results in initiating a fatigue crack. Once initiated, a fatigue crack may propagate under the influence of the bending stresses induced in the fan blades by normal operation. Consequently, a fan may fail due to fatigue days, weeks or even months after operating under rotating stall conditions. In contrast, a surge can lead to the bending stress that increases to a magnitude at which mechanical failure occurs during the surge event itself.

Rotating stall is a progressive phenomenon that does not necessarily result in the breakdown of a fan's pressure developing capability. Rotating stall, at least for axial machines (Funk *et al*., 1992), constitutes inception of the more severe flow instability, surge. Surge is a self-excited cyclic phenomenon, which affects the compression system as a whole. Large amplitude pressure rise and annulus averaged mass flow fluctuations characterise surge. It develops where a compressor's constant speed pressure rise-volume flow characteristic line has an abrupt change in slope (Funk *et al*., 1992). In Wo and Bons (1994), the authors studied compressor performance, and reported experimental results that enabled them to conclude that a compressor's pressure rise-flow characteristic includes a region with positive slope. This indicates stall occurrence. Consequently, surge onset is dependent on both the compressor's characteristic and the system's characteristics into which it discharges.

Although we may regard rotating stall as a precursor to surge, the two constitute different aerodynamic phenomena. The average flow during rotating stall is steady in time, but is circumferentially non-uniform. During a surge the flow is unsteady, but circumferentially uniform. It is as a consequence of a steady average flow with time that rotating stall may be localised within one or more of a compressor's stages. This has little or no effect on the system within which a manufacturer installs it. In con-

trast, the unsteady flow associated with surge impacts not only on the compressor, but the entire compression system.

Rotating stall and surge are distinctly different aerodynamic phenomenon, but do share a common characteristic. We may regard both as the compression system's natural oscillatory modes (Pinsley *et al*., 1991; Rodgers, 1991; Simon and Valavani, 1991; Paduano *et al*., 1993a, 1993b, 1994; Simon *et al*., 1993). Researchers are still debating whether rotating stall can result in centrifugal and single-stage axial compressor mechanical failure, or if only surge can result in mechanical damage in these classes of rotating machines. The debate is inconclusive, and within the community that has studied rotating stall in centrifugal and single-stage axial compressors there is disagreement as to the importance of rotating stall. This chapter focuses on industrial fan technology rather than compressor technology, where researchers agree that rotating stall does result in mechanical damage and ultimately failure. Although a review of the effect of rotating stall in centrifugal and single-stage axial compressors is beyond the scope of this chapter, we review the extant literature within the context of its applicability to industrial fans. Our aim is to apply to the study of industrial fans the research from those academics and practitioners who focus on centrifugal and single-stage axial compressors.

THE AERODYNAMICS OF STALL

For multi-stage axial compressors, rotating stall occurs at low shaft speeds and surge occurs at high speeds (Greitzer and Moore, 1986; Epstein *et al*., 1989; Ffowcs Williams and Huang, 1989; Eveker and Nett, 1991, 1993; Gysling *et al*., 1991; Funk *et al*., 1992; Ffowcs Williams *et al*., 1993; Day, 1994; Eisenlohr and Chladek, 1994; Goto, 1994; Eveker *et al*., 1995). The distinction between low and high shaft speeds is a distinction between the ratio of pressure forces and flow momentum, which increase with increasing rotor speed. Recovering a multi-stage axial compressor from rotating stall is more difficult than recovery from surge (Copenhaver and Okiishi, 1993). Rotating stall is not a single phenomenon, but rather two distinctly different phenomena (Day, 1993):

- part-span, where there is only a restricted blade passage region;
- full-span, the blade passage region is even smaller than in the case of part-span;
- small scale, where a small part of the annular flow path is blocked; and
- large scale, where a large part of the annular flow path is blocked.

Surge has a more complex typology than rotating stall. We can distinguish at least four different surge categories with respect to flow and pressure fluctuations (Funk *et al*., 1992; Day, 1994; Kim and Fleeter, 1994).

- Mild surge: a phenomenon associated with small pressure fluctuations and a periodicity governed by the Helmholtz resonance frequency. Flow reversal does not occur.

- Classic surge: a phenomenon associated with larger oscillations at a lower frequency than mild surge, also with no flow reversal. High frequency oscillations may also be present as the surge dynamics are nonlinear and introduce higher harmonics.
- Modified surge: a phenomenon associated with the entire annulus flow fluctuating in the axial direction, with rotating stall superimposed. This results in unsteady and non-axisymmetric flow. Modified surge is a mix of rotating stall and classic surge.
- Deep surge: a phenomenon associated with a more severe version of classic surge, where flow reversal occurs over the entire annulus.

When we consider an industrial fan's characteristics, we see that for a fixed blade angle and fan speed, as pressure across the fan reduces, flow increases. Bianchi *et al.* (2010) studied the characteristics of an industrial fan, identifying the stable region over which reducing pressure results in increasing flow. In addition to the fan characteristic's stable region Bianchi *et al.* (2010) characterised the fans unstable region, Figure 1.1.
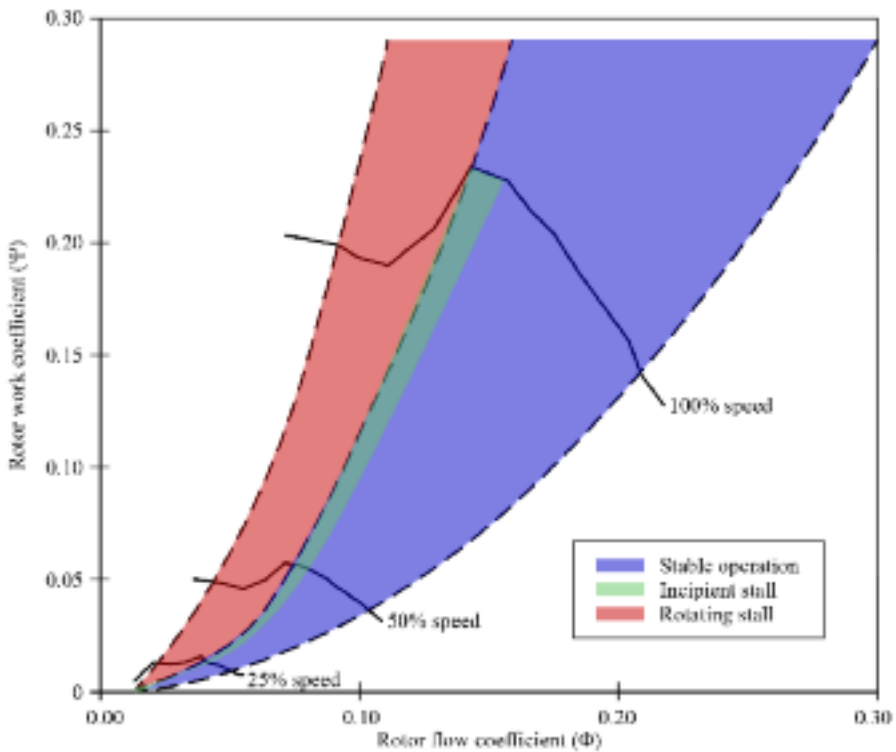
FIGURE 1.1. Regions of stable operation, incipient stall and rotating stall identified by Sheard *et al.* (2011) for an axial tunnel ventilation fan operating at full, half and quarter design speed.

The resistance of an aerodynamic system increases with the square of the flow velocity through the system. Generating velocity, fan pressure increases with the square of velocity. If the required pressure is beyond the fan's peak pressure developing capability, the fan moves from the stable to unstable region. As a fan moves into the unstable region, both pressure and flow reduce. As the flow reduces, the required pressure to drive the flow through the system falls with the square root of velocity. This results in the fan moving back into the stable region. As the fan operation stabilises, it generates additional flow and correspondingly, increasing system pressure until it drives into the unstable region again. This cyclic behaviour results in a hunting action that generates a characteristic sound similar to breathing.

An industrial fan's cyclic behaviour may occur as a consequence of poor system design or leakage within the system. Classically, the systems into which engineers apply industrial fans include multiple branches with dampers fitted to enable flow to be directed down different branches at various times. If a branch in the system includes a damper that becomes stuck open, then this branch may result in the system becoming unbalanced, with a consequence that the fan may drive itself into an unstable region. In cases where the fan is operating primarily within the stable region with only occasional excursions into the unstable region, the fan can operate for extended periods of time without mechanical failure. In severe cases the fan motor will overload and overheat, and if the cyclic behaviour continues, fan blade mechanical failure will occur.

Stall inception

The first challenge in attempting to identify appropriate approaches to stall control in industrial fans is to develop a fundamental understanding of the key physical phenomena which drive stall. The focus of any characterisation must be the stall inception process, as opposed to the characterisation of fully developed stall. Many researchers have characterised fully developed stall, with the research in the extant literature primarily focused on axial compressors. For a comprehensive review see Day and Cumpsty (1978). When considering the key physical phenomenon that drive stall in industrial fans, it is helpful to consider an industrial fans' tendency to exhibit cyclic behaviour as it moves from the stable to unstable region. A functional description of the processes at play during this cycle behaviour can provide the necessary insight to conceptualise, specify and design a stall detection system.

Studying a subset of the published research scholars have conducted on industrial fans and in compressor research facilities the identification of key processes at play as an industrial fan moves from the stable to unstable region of its characteristic. Results that researchers have obtained in compressor research facilities reproduce the physical phenomena at play within full scale compressors. A review of the results obtained in low-speed fan and scaled compressor facilities indicates that there is a hierarchy of possible stall inception mechanisms, starting with those that occur with low-speed compressors and moving on to those that occur with multi-stage high-speed compressors.

When we study the literature on low-speed fan and scaled compressor facilities, it is apparent that two competing perspectives dominate the debate on stall inception and the physical mechanisms at play within rotating machinery. The first perspective focuses on long wavelength processes, or waves which span at least several blade pitches circumferentially. These waves constitute the primary physical process that determines compressor stability. The competing perspective focuses on short length scale events that are localised within one to four blade passages. Researchers consider these short length scale events as primarily responsible for stall inception. Although physical explanations of short length scale event significance dates back to Emmons, the concept that they may occur with stall inception is relatively new (Emmons *et al.*, 1955).

Several studies have suggested that some tip flow features in both compressors, low- and high-speed axial fans are directly responsible for generating short wavelength disturbances. The researchers studying short wavelength disturbances refer to them as 'spikes' or 'pips' that are responsible for localised part-span stall cells (Bright *et al.*, 1998; Camp and Day, 1998; Deppe *et al.*, 2005; Vo *et al.*, 2005). The stall cell's spike-like inception in a single stage is clearly evident in data that researchers obtained from a model fan (Bianchi *et al.*, 2012). We can see the spike-like inception at 28.5 seconds, Figure 1.2, with the flow then returning to its steady state condition for half a second before becoming unsteady at 29 seconds. Researchers
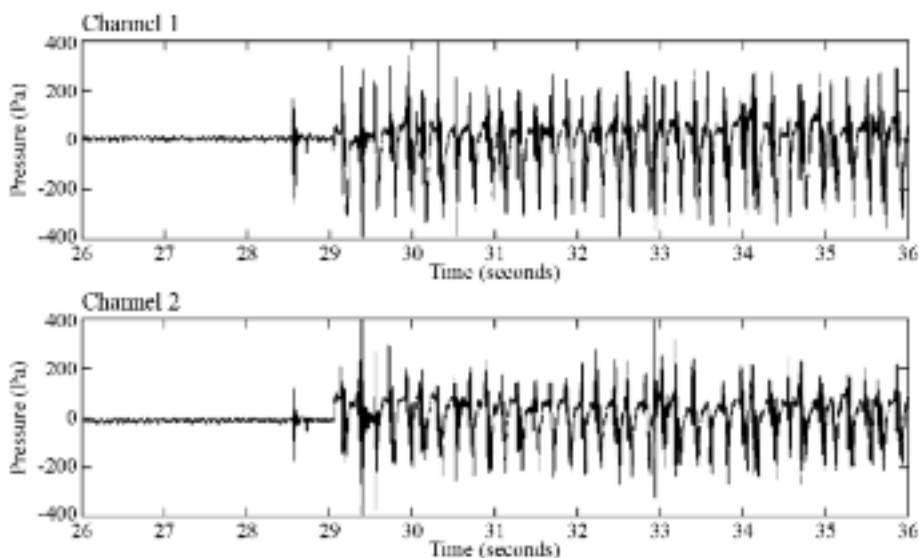
FIGURE 1.2. Data recorded from a pair of circumferentially offset high frequency response pressure transducers located over the blades of a 1250 mm diameter model of a variable pitch in motion induced draft fan. From 26 to 28.5 seconds the fan is operating in the stable region of its characteristic. We can observe a spike-like feature at 28.5 seconds that is characteristic of stall inception. From 29 to 36 seconds the variation in pressure is associated with the fan operating in a rotating stall operating condition (Bianchi *et al.*, 2012).

studying stall inception mechanisms in industrial fans have correlated the spike-like inceptions with a change in fan acoustic emissions (Cumpsty, 1989). Other scholars studying the link between stall inception and acoustic emissions have utilised arrays of azimuthally distributed probes in an attempt to link the rotating unsteady pressure signals that they have measured in centrifugal pumps and compressors to their acoustic signatures (Okada, 1987; Mongeau *et al.*, 1995). Kameier and Neise (1997), Bianchi *et al.* (2010) and Sheard *et al.* (2011) also studied the link between stall inception and acoustic emissions by establishing a link between tip-clearance noise and associated blade-tip flow instabilities in axial turbomachinery.

Stall development

There is a general consensus among researchers that stall is an instability phenomenon, local to the fan stage or rotor, in which a circumferentially non-uniform flow pattern ultimately results in completely blocking the annulus. As the fan blades become progressively more highly loaded, the stall commences with a 'spike like' event and evolves into a rotating stall. The rotating stall classically evolves into a full stall or surge if there is a high enough system back-pressure. A local stagnant flow region appears when the flow stalls. The region propagates in the same direction as the blade rotation. This results in the stall region rotating around the annular flow path at a fraction of the rotor speed. The speed with which the stall rotates is typically between 20 and 50 per cent of the rotor speed for fully developed stall. Initially, rotating stall cells rotate faster (Day, 1993).

In reviewing rotating stall evolution, Cumpsty (1989) noted that the drop in overall performance can occur as a so-called 'progressive stall' or an 'abrupt stall'. Engineers usually associate the former with a part-span stall, which results in a small performance drop; whereas, they associate the latter with a full-span stall and a large drop in performance. Notably, the part-span rotating stall occurs typically in single blade rows (Cumpsty, 1989) and usually leads to more complex disturbances in single-rotor or stage machines than in multi-stage compressors (Moore, 1984).

Mechanical failure

Engineers have used strain gauges' on axial compressors (Rippl, 1995) to measure bending stress in blades that exceed stable operation by a factor of five under 'rotating stall' conditions. Figure 1.3 illustrates an example of an industrial fan blade's mechanical failure that occurs with the unsteady mechanical loading that resulted from the fan stalling. In this example, stall resulted in a blade fatigue failure after operating approximately ten hours in a stalled condition. If this fan had been able to generate a back-pressure high enough to result in surge, the bending stress's heightening magnitude would have been enough to cause a mechanical failure during the surge event itself.

FIGURE 1.3. An example of a fan blade with a blade mechanical failure at the root aerofoil interface. This fan operated for approximately ten hours in rotating stall before the mechanical failure (Sheard and Corsini, 2011).

An additional issue that industrial fan designers face is new legislation that governs the design of industrial fans that are intended for duel use. In this context, duel use refers to a fan used to both ventilate a tunnel or building during normal operation, and clear smoke from escape routes in the event of a fire. Within the European Union it is a legal requirement to supply fans that are certified in accordance with EN 12101-3 requirements (EN12101-3, 2002; Sheard and Jones, 2012), and outside the European Union the same requirements defined in EN 12101-3 are embodied within ISO 21927-3 (ISO 21927-3, 2006; Sheard and Jones, 2008). When extracting hot gas and smoke, an industrial fan's aluminium blades will grow thermally at a faster rate than the steel casing within which they rotate. Consequently, if the blades are not to touch the casing in the event of a fire the ambient blade tip-to-casing gap must be larger than would be the case if the fan were for ambient use only (Sheard and Jones, 2012). A consequence of increasing the blade tip-to-casing gap is typically a 20 per cent reduction in the fan's pressure developing capability. Fan designers frequently underestimate the impact of increasing the blade tip-to-casing gap on an industrial fan's pressure developing capability. A result of underestimating this reduction is that fans intended for dual-use operation are typically more prone to stall in service (Sheard and Corsini, 2011).

A particular feature of the environment within which industrial fans in tunnel ventilation applications operate is the pressure pulses that occur with trains moving through a tunnel. Pressure pulses can be up to ±50 per cent of the overall tunnel ventilation fan's work coefficient. Such pressure pulses drive the tunnel ventilation fan first up, and then down its characteristic operating range (Cardillo *et al.*, 2014). To ensure that the tunnel ventilation fan continues to operate in an aerodynamically stable manner during this pressure transient, the tunnel ventilation system designer must incorporate sufficient margin to ensure that the tunnel ventilation fan does not stall due to the pressure pulses that occur with a train approaching and then moving away from a ventilation shaft.

A tunnel ventilation fan's propensity to stall under the influence of a pressure pulse is compounded when one operates at part speed. It is increasingly common to operate tunnel ventilation fans at part speed. Typically, the need for tunnel ventilation reduces at night, and therefore, one can achieve adequate cooling at a lower fan speed, and consequently at a lower operating cost. Although one may operate the tunnel ventilation fans at a lower speed, the speed of trains travelling within the tunnel remains constant, and therefore the pressure pulse magnitudes to which tunnel ventilation fans are subjected also remains constant. When a tunnel ventilation fan operates at half design speed, its pressure developing capability reduces by a factor of four. Consequently, a pressure pulse that could be accommodated at full speed will almost certainly drive the same tunnel ventilation fan into stall at half design speed.

As tunnel ventilation fan speed reduces, with a constant pressure pulse associated with trains passing the ventilation shaft within which the fan is located, there will be a critical speed at which a fan operating in supply mode stalls as the train approaches, or if the fan is operating in extract mode stalls as the train departs. Aerodynamic stall results in a significant increase in the unsteady forces applied to the fan blades. However, as the pressure pulse is transient the fan is not operated in a stalled

condition for an extended period of time. Consequently the unsteady aerodynamic forces do not result in an immediate mechanical failure. However as a tunnel ventilation fan may be subjected to many pressure pulses each day, over time the cumulative effect of driving transiently into stall is to initiate a fatigue crack in one blade that then goes on to grow during stable operation until the blade mechanically fails.

We may conceptualise the impact of both positive and negative pressure pulses on a tunnel ventilation fan's operating point by referring to Figure 1.4. This provides an insight into how a fan adapts to a pressure pulse, with the duty point shifting up and down the fan characteristic under the influence of a +1,000 Pa and −1,000 Pa pressure pulse. It is custom and practice within the industrial fan community to assume that a pressure pulse may be modeled by shifting the system curve up and down by the magnitude of the pressure pulse. In Figure 1.4 the + and −1,000 Pa pressure pulse system curves are generated by shifting the system curve up and down 1,000 Pa respectively. Under the influence of a positive pressure pulse the fan operating point is assumed to shift from the fan duty point (Point A, Figure 1.4) to the point where the fan characteristic intersections the +1,000 system curve. Under the influence of a negative pressure pulse the fan operating point is assumed
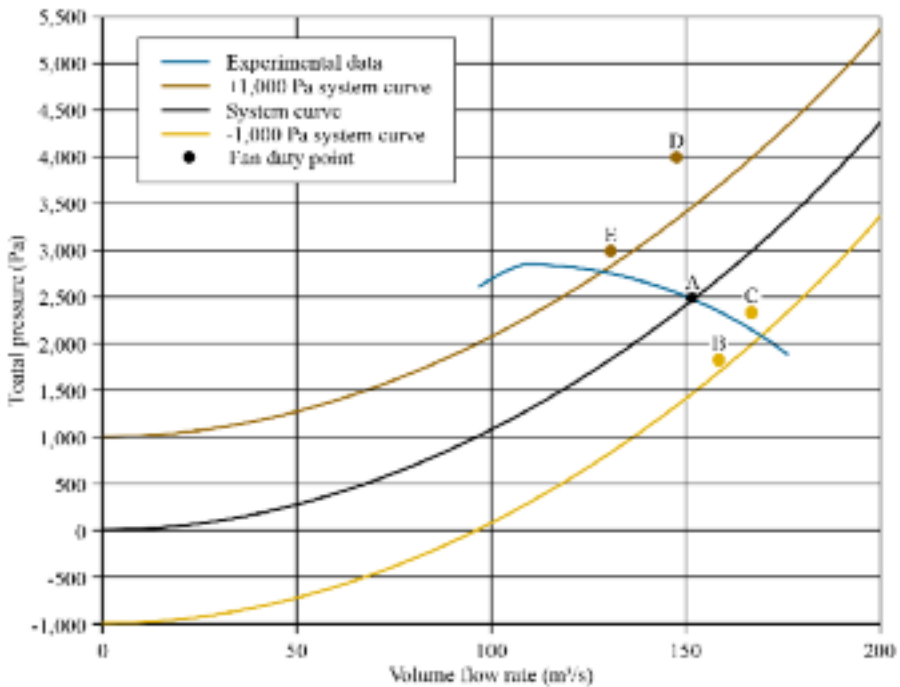
FIGURE 1.4. The effect of a pressure pulse on a tunnel ventilation fan. Industrial fan designers have historically assumed that a fan runs up and down its characteristic in the presence of a pressure pulse. Unsteady computational results for both a positive and negative pressure pulse indicate that the fan's operating point departs from its steady state characteristic during the transient associated with a pressure pulse (brown and yellow symbols). This departure results in unsteady aerodynamic forces increasing by a factor of two compared to those associated with operation of the fan at its duty point (Cardillo *et al.*, 2014).

to shift from the fan duty point to the point where the fan characteristic intersects the –1,000 system curve. In so doing the fan is assumed to respond to a pressure pulse as if the change in pressure associated with the pressure pulse is slow in comparison to the reaction time of the fan.

Recent research (Cardillo *et al*., 2014) suggests that tunnel ventilation fans do not respond to a pressure pulse as if the change in pressure associated with the pressure pulse is slow in comparison to the reaction time of the fan. The interaction between changing pressure in a tunnel and the flow-field around fan blades is both transient and complex. When a pressure pulse within a tunnel is studied, it may be conceptualised as a change in volume flow rate through the fan. Unsteady computational results for a tunnel ventilation fan operating in extract mode (Cardillo *et al*., 2014) indicate that the impact of a train approaching the ventilation shaft within which a tunnel ventilation fan is situated is to unload the fan. The result is that the fan duty point shifts almost instantaneously to a lower pressure (Point C, Figure 1.4). As a train passes the ventilation shaft with the tunnel ventilation fan operating in extract mode, the fan is over loaded. The result is that the fan operating point shifts almost instantaneously to a higher pressure (Point E, Figure 1.4).

When we consider shift in a fan's operating point from Point A to Point C and from Point A to Point E, Figure 1.4, they are reasonably close to the point at which the negative and positive pressure pulse system curves cross the fan's characteristic. This indicates that the general assumptions within the industrial fan community do apply. However, they do not apply during the transitional experience of shifting from Point A to Point C which is via Point B, or from Point A to Point E which is via Point D. The data point of primary concern is the negative pressure pulse that transiently increases the pressure across the fan instantaneously shifting the fans operating point to Point D, Figure 1.4. The instantaneous pressure across, and flow rate through the fan takes Point D beyond the fan's peak pressure developing capability. Under steady state operating conditions, attempting to operate the studied fan at Point D would result in the fan stalling. Significantly the time scales of this shift in operating point are so rapid that the fan does not stall (Cardillo *et al*., 2014).

Despite the fan not stalling, unsteady forces on fan blades were shown to double at Point D in comparison to those associated with stable operation at Point A, the fan's duty point (Cardillo *et al*., 2014). This doubling of unsteady blade forces is significant. Within the industrial fan community designers generally believe that as long as a pressure pulse can be accommodated within the fan's pressure developing capability, as is the case in the example given in Figure 1.4, there is no mechanical consequence associated with pressure pulses. This is not the case and consequently, if blade designs are to avoid in-service mechanical failure, engineers must design them to accommodate the elevated aerodynamic forces that occur with pressure pulses.

STALL CONTROL TECHNIQUES

We typically derive flow control methodologies from an understanding of the relevant mechanisms or processes (Gad-el-Hak, 2000) and we can categorise them according to how one utilises flow control (Joslin *et al*., 2005). This can be:

- active, entailing flow control; or
- passive, entailing a flow management.

Engineers have successfully applied passive and active stall control techniques into both industrial fan and compressor applications. However, passive stall control techniques are the norm in industrial fan applications, and were the norm in compressor applications in the 1950s and 1960s. The drive to improve stability margin has been most intense within the compressor industry, and consequently, that is where the majority of active stall control research effort has taken place over the last two decades.

Active control systems

Active control systems monitor the event and its physics by relying on adequate warning or detection schemes in order to achieve the control objective. In contrast, passive control systems modify the flow dynamics in an effort to prevent the stall inception or to reduce the stall. Researchers have traditionally based the passive or preventive control concepts around blade or casing geometry modifications.

Active: blade pitch control

Rotor pitch control is a technique that engineers mostly use in open rotors such as propellers or wind turbines to reduce the power when the air speed is above an allowable limit. With regards to axial fans, changing the angle formed by the blade's chord perpendicular to the axis direction constitutes a way to recover from stall. Lowering the pitch angle reduces the incidence angle onto the blade and reduces the blade loading. When we consider a variable pitch in motion (VPIM) fan's characteristic, it is apparent as the pitch angle reduces the fan's operating point migrates from the unstable to the stable region of the fan's characteristic, Figure 1.5. It is the movement from the unstable to stable region that allows a reduction in blade angle to constitute a method by which a stall control system may recover a fan from stall. Bianchi *et al.* (2012) studied experimental data from a variable pitch in motion fan as pitch angle reduced, observing that the pressure stabilised after 89 seconds, Figure 1.6, with reducing pitch angle. Consequently, a fan that was stalling with a 70° pitch angle no longer stalls when the pitch angle reduces to 50°.

Active: rotational frequency control

A change in fan rotational speed does not result in a recovery from stall. Assuming that a fan is installed in a system with characteristics that obey the fan laws, a fan that is operating in the unstable region of its characteristic at full design speed will also be operating in the unstable region of its characteristic at reduced speeds. Therefore, reducing fan speed does not constitute a stall control method. Despite this reservation, reducing fan speed can protect a fan from the mechanical effects associated with operating in the unstable region of its characteristic. The direct mechanical
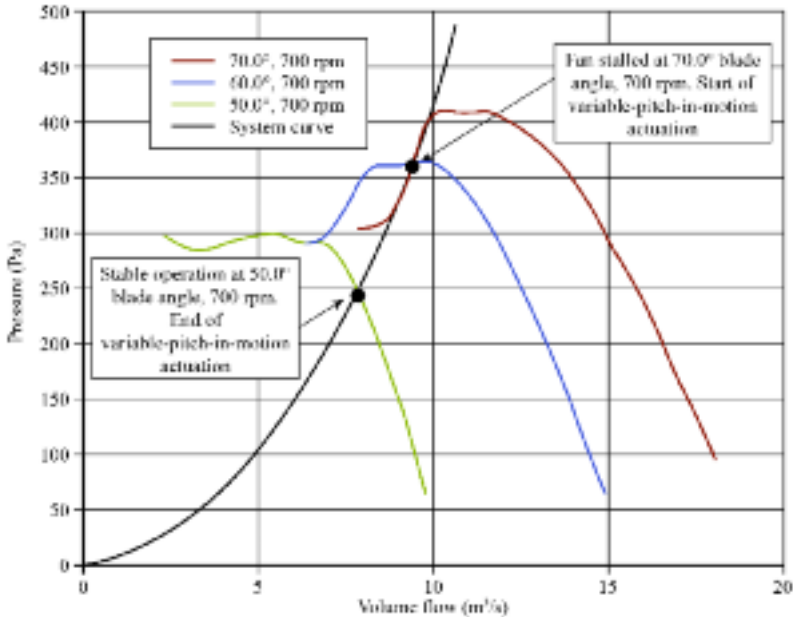
FIGURE 1.5. Stall recovery using variable pitch in motion (VPIM) blades. Operating points at 70°, 60° and 50° pitch angle with all data taken at a rotational frequency of 700 rpm. At 70° the fan is operating in a stalled condition, to the left of the characteristic's peak pressure. At 60° the fan remains stalled, with the fan operating just to the left of the peak in its characteristic. At 50° the fan is operating in the stable part of its characteristic, to the right of the characteristic's peak pressure (Bianchi *et al*., 2012).

stress in rotating components reduces with the square of speed. Consequently, reducing from full to half design speed will reduce the direct mechanical stress in rotating components by a factor of four. However, operating a fan in the unstable region of its characteristic results in an increase in alternating stress induced in the fan blades as a consequence of the aerodynamic buffeting associated with stall.

Sheard and Corsini (2012) studied the effect of operating a fan in the unstable region of its characteristic at full and part speed. They were faced with a particular problem with the fans supplied for an extension of the Athens Metro. Although the fans met their specification, during the summer when residents close to metro ventilation shaft portals were trying to sleep with their windows open, the noise from portals was loud enough to be problematic. The Athens Metro was asked to reduce night time portal noise emissions. A study of ventilation fan installations indicated that adding additional silencers was not practical. As there were multiple fans installed in each ventilation shaft, with only one required to run at night to supply the required flow of ventilation air, an option was to run multiple fans at reduced speed. Running a fan at reduced speed will reduce fan noise, but reduce the flow of ventilation air. Running multiple fans will increase the volume of ventilation air, but as there are now multiple sound sources, the noise generated increases. Critically, the increase in noise associated with multiple sources will be less than the reduction associated with running multiple fans at reduced speed. Consequently, running multiple fans at part speed reduces overall portal noise emissions.
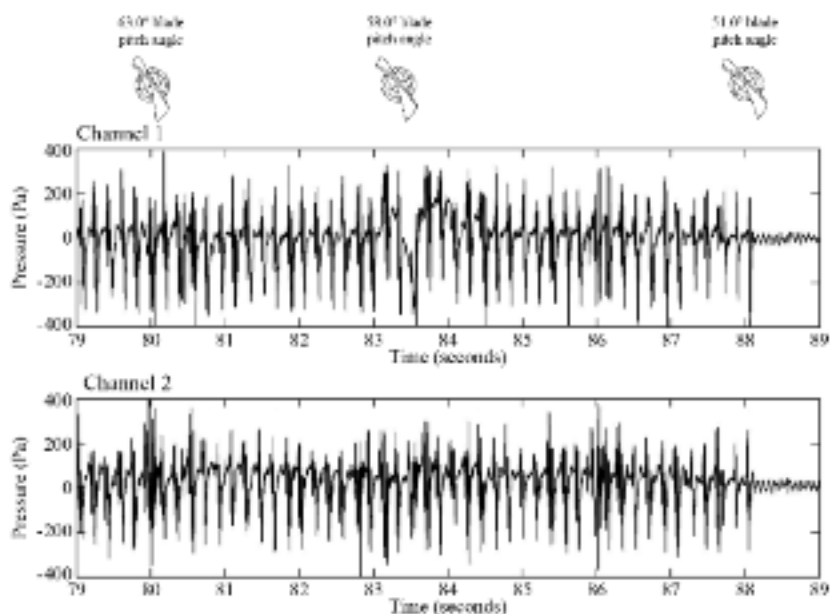
FIGURE 1.6. Data recorded from a pair of circumferentially offset high frequency response pressure transducers located over the blades of a 1,250 mm diameter model of a variable pitch in motion induced draft fan. Blade angle reduces with increasing time, with the fan finally transitioning from stalled operation to stable operation at 89 seconds, at which time blade angle had reduced from an initial 70° to 51° at 89 seconds (Bianchi *et al.*, 2012).

However, the reduction in fan pressure developing capability associated with part-speed operation was potentially problematic. The ventilation fans were subjected to a 500 Pa pressure pulse each time a train passed the ventilation shaft within which they were installed. When running at part-speed this pressure pulse would result in the ventilation fans driving from the fan characteristic's stable to unstable region each time a train passed the ventilation shaft. Although the ventilation fans would only drive into the unstable region of their characteristic transiently, with hundreds of trains passing each ventilation shaft each day, the cumulative effect would be the development of a fatigue crack in a blade followed by a mechanical failure.

Sheard and Corsini (2012) studied the tunnel ventilation fan's mechanical performance. They fitted strain gauges to the blades, measuring the unsteady stress associated with operating the fan in both the fan characteristic's stable and unstable region at full, half and quarter design speed. In combination with the calculated direct stress in the fan blades at each speed, Sheard and Corsini (2012) were able to derive a mechanical safety factor, Table 1.1. The results indicated that the tested fan may operate at full design speed in the stable region of its characteristic with a mechanical safety factor of 2.3. The same fan may also operate at half design speed in the unstable region of its characteristic with a mechanical safety factor of 2.5. As the safety factor 2.5 is larger than the safety factor 2.3, we may conclude that one may operate this fan at half design speed in the unstable region of its characteristic with less risk of mechanical failure than at full design speed in the characteristic's stable

Table 1.1. *Safety factors derived from strain gauge data for a fan at full and part speed (Sheard and Corsini, 2012).*

Fan type	Per cent design speed	Normal operating safety factor	Stalled operating safety factor
Plane casing, stalling blade angle	100	2.3	0.3
Plane casing, stalling blade angle	50	10.0	2.5
Plane casing, stalling blade angle	25	106.0	7.3

region. Consequently, reducing fan speed from full to half design speed does not constitute a method of controlling stall, but does constitute a method of protecting the fan from mechanical failure in the event that operating in the fan characteristic's unstable part is unavoidable.

Sheard and Corsini (2012) extended their analysis, scaling the studied fans' characteristics from full to 90 per cent design speed. They observed that by doing so the fans' pressure developing capability reduced to a point where the 500 Pa pressure pulses to which this fan was subjected in practical application would take the fan to within 5 per cent of the fans' peak pressure developing capability. When Sheard and Corsini (2012) scaled the studied fans' characteristics from half to 55 per cent design speed they concluded that a 500 Pa pressure pulse would still drive the fan from the stable to unstable region of its characteristic. However the increase in speed resulted in the mechanical safety factor reducing from 2.5 at half design speed to 2.0 at 55 per cent design speed. From the above, Sheard and Corsini (2012) concluded that the tested fan could operate at up to 55 per cent design speed in the unstable region of its characteristic, and down to 90 per cent design speed whilst remaining in the characteristic's stable region. The speed range between 55 and 90 per cent design speed was blocked in the fans' variable speed drive, and ensured that the fan only operated at speeds that did not put the fan at risk of mechanical failure under the influence of the pressure pulses.

Industrial fan manufacturers also utilise rotational frequency control to protect ventilation fans from the effect of unforeseen changes in system resistance. As the change in system resistance is unforeseen, it is not possible to predict the time when the change will occur. Bianchi *et al.* (2010) studied a tunnel ventilation fan's stall characteristics using four unsteady pressure probes that they mounted on the fan casing whilst driving the studied fan into stall at full, half and quarter of its nominal design speed. This allowed Bianchi *et al.* (2010) to study the unsteady pressure signals that occurred with the fan's stable operation when instability was incipient and during stalled operation, Figure 1.7. Analysing the unsteady pressure signals enabled Bianchi *et al.* (2010) to characterise the fan and identify the fan characteristic's stable and unstable regions at different fan speeds. From this, we may use an unsteady pressure measurement on the fan casing, in combination with the 'blocked' speed range, 55 per cent to 90 per cent of design speed for the fan that Sheard and Corsini studied (2012), as input for a control algorithm that establishes if a fan is mechanically at risk or may continue to operate without risk of mechanical failure.
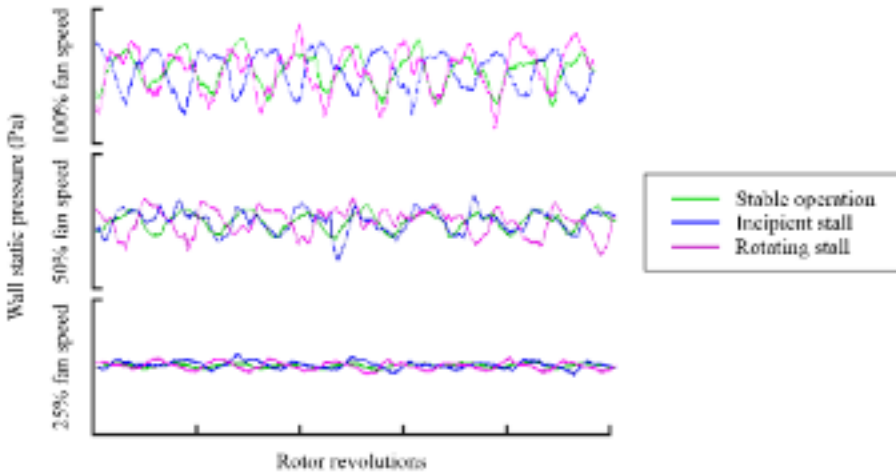
FIGURE 1.7. Low-pass filtered data (20 kHz) from a high frequency response pressure transducer located over the blades of a tunnel ventilation fan. The authors recorded the data during stable operation (green), when stall was incipient (blue) and with the fan operating in rotating stall (red) at full, half and quarter design speed (Bianchi *et al.*, 2010).

Active: air injection

Researchers typically associate spike-like pressure pulses with stall inception in single rotor or stage industrial fans and compressors. A stall control technique that is effective in suppressing the spike-like pressure pulses is air injection. Air injection involves injecting high-speed jets of air into the blade tip region that induces a transfer of momentum from the jet to the slower moving mainstream flow. The effectiveness of the high-speed jets in suppressing the onset of stall is linked to the jets' influence on the tip clearance vortex's evolution and other flow features that occur with the over-tip blade flow.

Researchers have extensively studied air injection. Suder *et al.* (2001) proposed a discrete tip injection technique, and Nie *et al.* (2002) and Lin *et al.* (2011) based their proposal on micro-air injection. Whilst requiring significant power to drive the associated control system actuation, these control techniques result in 5 to 10 per cent improvement in compressor stall margin. More recently, researchers have studied the underlying flow physics that occur with flow-field excitation in the blade tip-to-casing region using a spatially distributed actuation system to control the blade tip leakage vortex's evolution (Weigl *et al.*, 1997). The researchers' hypothesis is that controlling the blade tip leakage vortex's evolution will promote the tip vortices' dissipation and therefore will suppress a part of the flow structure involved in spike formation.

A potential advantage of a spatially distributed actuation system to control the blade tip leakage vortex evolution is the low power requirement that occurs with control system actuators. The necessary power requirement to drive a control

system's actuators constitutes a loss of efficiency for the industrial fan or compressor to which the control system is fitted. In an effort to minimise the power requirement, Vo *et al.* (2008) proposed the use of acoustic actuation and Corke and Post (2005) proposed magnetic actuators. Interest remains high in air injection within the compressor community, with Vo (2007) proposing a method to suppress rotating stall inception in multi-stage compressors around the compressor's full circumference, Figure 1.8. At the time of writing the use of air injection is limited to compressor applications as a consequence of the complexity and cost of the technology. The industrial fan community continues to monitor the compressor community's progress, but currently there is no active research aimed at transferring this technology to industrial fans.
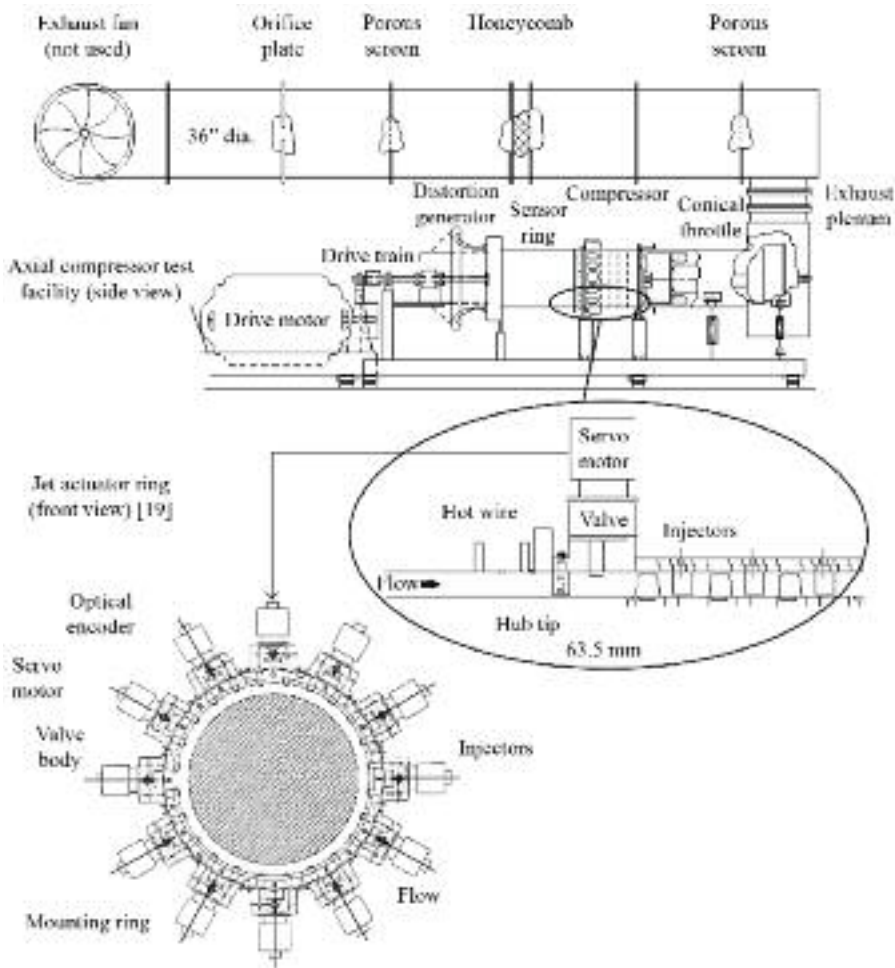
FIGURE 1.8. The Massachusetts Institute of Technology (MIT) low-speed three-stage axial compressor test facility with jet actuation (Vo, 2007).

Active: bleed valves

Researchers have tested stall control with bleed valve actuation on a small scale with compressors at low speed (Yeung and Murray, 1997; Prasad *et al.*, 1999). The bleed valve opens to suppress the onset of stall. The technique aims to maintain the average flow through a compressor above the compressor's critical flow, below which the compressor blades will stall. The operator maintains average flow using bleed air from the compressor discharge that increases the flow through the compressor's lower pressure stages.

Prasad *et al.* (1999) have presented two schemes for using bleed valve actuation: bleed air back into the compressor inlet and bleed air back into a recirculation plenum-inlet. In the former, the bleed air does not affect the flow through the inlet; however, the bleed does decrease the flow to the combustor. In the latter, the flow into the combustor is equal to the inlet flow with the recirculated air reducing the compressor load. The second scheme is more effective as bleed recirculation delays the onset of rotating stall and the delay increases with the magnitude of recirculation. Recirculation reduces flow into the combustor by altering the compressor's operating point and consequently, an operator should not use recirculation continuously, but only when stall is imminent.

Passive control systems

Researchers base passive approaches to stall control on techniques that modify the flow-field in the blade tip-to-casing region. Passive approaches date back to the 1950s, when researchers first utilised casing treatments in axial compressors. Skewed slots and grooves cut into the casing above the rotor improved stall-margin, with grooves both improving stall-margin and having the lowest impact on compressor efficiency (Tan *et al.*, 2010). The relatively low cost of passive approaches has resulted in industrial fan manufacturers historically favouring them. Consequently, whilst the compressor community today utilises primarily active control approaches, industrial fan manufacturers are still developing and refining passive approaches.

Passive: stabilisation rings

Industrial fan manufacturers have historically favoured the stabilisation ring, fitted to the fan casing, as the preferred anti-stall device. As an axial fan approaches stall, the flow velocity through the fan reduces and the axial fan blades increasingly act as a centrifugal fan impeller. Although anti-stall devices have evolved, their most common present day embodiment consists of a stabilisation ring placed around a fan casing immediately upstream of the fan blades' leading edge, Figure 1.9. As an axial fan approaches stall, the flow velocity through the fan reduces and the flow progressively centrifuges towards the blade tips. At a critical pressure across the fan, the flow velocity falls to zero, and the flow in the blade tip region reverses. The stabili-
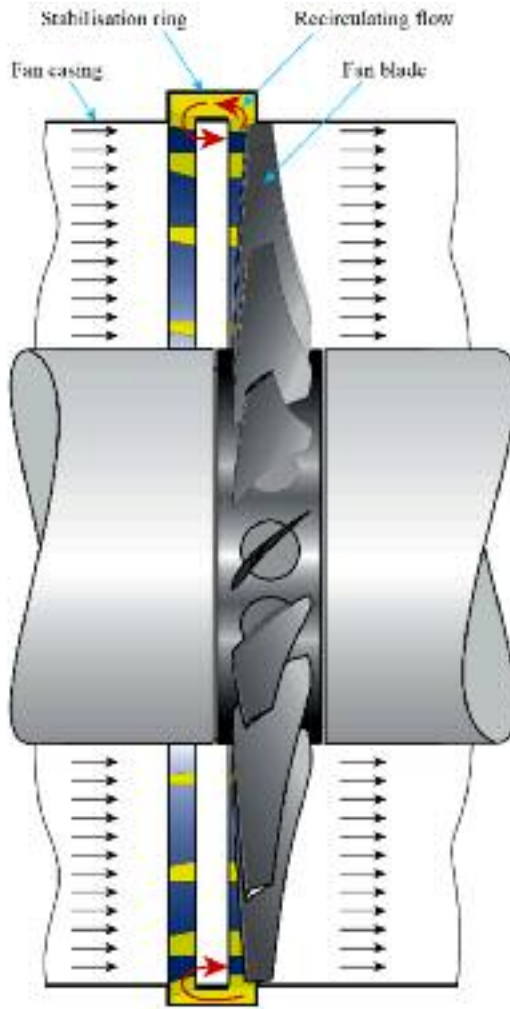
FIGURE 1.9. An axial flow fan fitted with a stabilisation ring. The stabilisation ring comprises an extension to the fan casing just over and upstream of the blades. The stabilisation ring incorporates static vanes, shown in yellow. As a fan approaches stall the flow through the fan is centrifuged up the blades, and stalls as the flow spills out of the fan inlet. The stabilisation ring vanes redirect the flow in an axial direction, and reintroduce it upstream. This process of straightening and reintroducing the flow stabilises the fan's performance, eliminating the drop in pressure developing capability classically associated with stall (Eurovent, 2007).

sation ring is able to stabilise fan performance as it contains a set of static vanes. These static vanes redirect the reverse flow into an axial direction, and then reintroduce it into the mainstream flow upstream of the blades, Figure 1.10. This stabilises the fan's characteristic, with the fan now exhibiting a pressure characteristic that rises continuously back to zero flow.
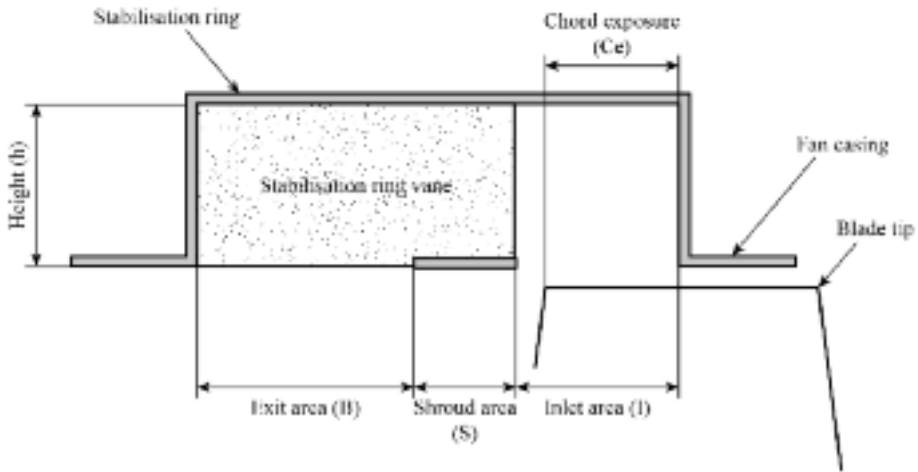
FIGURE 1.10. The proposed 'stabilisation ring' arrangement adapted from Karlsson and Holmkvist (1986) by Bard (1984).

In 1965, Ivanov patented the first stabilisation ring (1965); however, the use of a full set of guide vanes upstream of the fan was difficult to apply in practical applications. Later Karlsson and Holmkvist (1986) developed the stabilisation ring concept that incorporated the static vanes into a ring fitted around the fan casing. Despite the effectiveness of Karlsson and Holmkvist's stabilisation ring concept, it does have one unintended negative consequence. A fan fitted with a stabilisation ring will lose between 2 and 5 per cent efficiency as a direct consequence of the stabilisation ring (Sheard and Corsini, 2011; Corsini *et al.*, 2014).

The advent of the Energy using Product (EuP) Directive within the European Union has resulted in a mandatory minimum Fan and Motor Efficiency Grades (FMEGs) that became legally binding on 1 January, 2013. The minimum FMEGs will increase on 1 January, 2015. The industrial fan community widely expects that at some point in the future minimum allowable FMEGs will effectively render stabilisation rings obsolete as a consequence of their negative effect on fan efficiency. Houghton and Day (2010) present a possible way forward for industrial fan designers who are no longer able to utilise stabilisation rings, demonstrating that a compressor's stall resistance may be improved by incorporating a groove into the compressor's casing. The groove was located approximately 50 per cent of blade chord upstream of the blade's leading edge. Incorporating a groove into the compressor casing did not result in reducing compressor efficiency, and consequently, a possible avenue of endeavor for industrial fan designers who are no longer able to apply stabilisation rings because of their negative effect on fan efficiency is to study casing groove application into industrial fan casings.

Passive: air separators

Air separators are able to effectively suppress the onset of stall. Yamaguchi *et al.* (2010) designed an air separator which has radial-vanes with their leading-edges facing the fan rotor blade tips so as to 'scoop' the tip flow, Figure 1.11. The air separator differs from a stabilisation ring in that air separator vanes are radial, in contrast to a stabilisation ring vanes that are axial. Yamaguchi *et al.* (2010) studied the air separator and analysed its stall suppression effects on a low-speed single-stage, lightly loaded axial flow fan. In the air separator's recirculation passage downstream from the inlet cavity, a series of circumferential vanes correct the swirl flow in the axial direction. When the fan approaches stall there is an increase in swirl speed and centrifugal force on stall cells. This causes the stall cells to centrifuge spontaneously into the air separator's inlet. Air separators therefore separate stall cells from the main flow, and as a consequence of requiring no moving parts, constitute a passive stall control method.
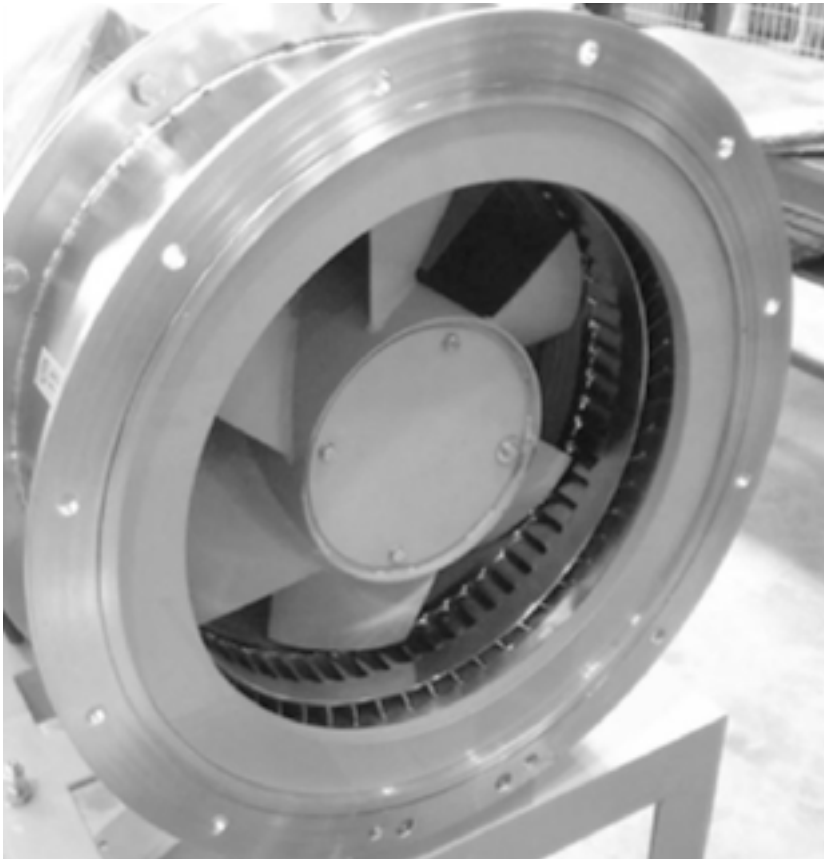
FIGURE 1.11. An axial fan mounted in a casing containing an air separator (Yamaguchi *et al*., 2010).

The four active and two passive stall control techniques, Table 1.2, each represent a valid approach to the control of stall. Researchers have developed and utilised each in different industrial fan or compressor applications where the technique has proven effective. In practice it is stabilisation rings that are the most wide-spread application in industrial fans and bleed valves that are the most wide-spread application in compressors. The other active and passive stall control techniques are the subject of research in an ongoing effort to better understand the flow physics that underpin stall and development in order to improve industrial fan and compressor stability.

Table 1.2. *Matrix of stall control techniques.*

Technique	Classification	How it works	Results
Blade pitch control	Active	Changes the fluid dynamics; changing the pitch angle	Acts after stall detection (Bianchi *et al.*, 2012)
Rotational frequency control	Active	Changes the fluid dynamics; controlling the rotor speed	Acts after stall detection (Bianchi *et al.*, 2010)
Air injection	Active	Rotating stall inception is achieved using full-span distributed jet actuation	The non-ideal injection reduces the stall range's extension by about the same proportion of the effective pressure increase (Vo, 2007)
Bleed valve	Active	Maintain the average flow through the compressor above the critical flow. The air bleeds from the plenum, so as to increase the flow through the compressor	Recirculation alters the compressor operating point. Only use the recirculation or ambient bleeding when stall is imminent (Yeung and Murray, 1997; Prasad *et al.*, 1999)
Stabilisation rings	Passive	Changes the fluid dynamics; provides the stalled flow with a route back into the impeller	Not sure that the stall occurs (Eurovent, 2007)
Air separator	Passive	A series of circumferential vanes correct the swirl flow in the axial direction; the stall cells centrifuge spontaneously into the air separator inlet and separate from the main flow	Air separators are able to effectively suppress the stall zone after the stall cells appear (Yamaguchi *et al.*, 2010)

STALL DETECTION SYSTEMS

Stall control techniques have proven effective in service; however, they are inevitably reactive. Stall control techniques require the fan to be stalling before they have any effect. In many applications it would be more appropriate for the control system to take action to avoid stall before it occurs, as opposed to managing the consequences of stall having occurred. For a control system to take action to avoid stall it is necessary to first predict stall onset. Predicting stall onset is challenging, and is an ongoing research subject in both the industrial fan and compressor community. Despite the challenges of predicting stall onset, it remains an essential precursor to the development of a more effective stall control system.

Stall detection systems that identify stall onset have the potential to form an input into a proactive stall control system theoretically capable of reacting before a fan actually stalls. Researchers recognise that studying stall detection both in industrial fans and compressors as critical to developing a stall management system. To form an effective input into a stall management system, a stall detection system requires as input the output from high frequency response sensors located in the industrial fan or compressor blades' immediate vicinity. Researchers then use the output from high frequency response sensors to identify stall precursors, and when detected, to generate a warning signal that inputs into the stall control system. The stall control system is then able to take remedial action to prevent the identified stall precursors from developing further.

Wadia *et al.* (2006) and Christensen *et al.* (2008) have proposed stall management systems based on instantaneous near-field pressure measurements. They have studied the effectiveness of stall detection systems as part of a stall management system when applied to a multi-stage high-speed compressor test rig. A challenge that both research teams faced was the very short time between the identification of stall precursors and compressor stall. Although stall detection systems have the potential to provide a useful input into compressor stall management systems, those stall management systems must be capable of reacting within a few milliseconds if they are to use an input from a stall detection system effectively.

Two-point spatial correlation

In axial fans instabilities occur primarily as wave-like disturbances around the annulus in the circumferential direction. In the initial state of instability the disturbance amplitude is small, but increases with the evolution of the instability. One may use spatially adjacent fast-response pressure transducers, microphones or hot wire anemometers to identify stall precursors. Researchers associate these pre-cursors with the formation of three-dimensional disturbances of finite amplitude, located in the blade tip region. These are characterised by a spike in the signal which fast response transducers record.

In order to accurately identify the spike in a signal recorded by a fast response transducer as a stall precursor, it is important to characterise the stall inception process dynamics. Only in characterising the stall inception process can one distinguish between spikes that occur with stall inception from background noise. Spike isolation is possible using a windowed two-point spatial correlation which provides spatial and temporal information about rotating features in the flow (Cameron and Morris, 2007). The windowed two-point spatial correlation technique is insensitive to low pass filtering and parameter selection over a wide range of values and is valuable for analysing both pre-stall and stall inception behaviour (Cameron and Morris, 2007).

Stochastic model

The stochastic model for detecting stall precursors utilises an auto-correlation technique. The signals from two circumferentially off-set high frequency response pressure probes mounted in the industrial fan or compressor casing close to the blade tips are auto-correlated. The correlation typically decreases as the compressor or fan approaches its stability limit, and therefore tracking the correlation provides a measure of the industrial fan or compressor's proximity to its stability limit. Dhingra *et al.* (2007) developed the stochastic model. They developed an auto-correlating algorithm and established a minimum threshold correlation value that corresponded to the imminent onset of compressor stall. Although able to demonstrate that the stochastic model could form the basis of a stall detection system, the researchers conducted their reported work in a laboratory and did not include the development of a stall management system that utilised the stochastic model output as an input.

Travelling wave energy analysis

An alternative modelling approach to either the two-point special correlation or stochastic model is travelling wave analysis. Travelling wave analysis involves calculating wave energy, which we define as the difference between positive and negative frequency power spectra. We then compute an 'energy index' for a fixed-time window that must extend to include the spatial Fourier modes within it. Tryfonidis *et al.* (1995) developed the travelling wave analysis as a real time measure of compressor stability. By providing a real timer measure of compressor stability, the analysis technique is useful for providing early warning of spike-type stall inception in high-speed compressors.

Cross-correlation analysis

Cross-correlation analysis is a further analytical approach that cross-correlates a pair of near-field pressure signals. Developed by Park (1994), the analytical

approach is based on the observation that short wavelength disturbances that are recognisably spike-like indications of incipient stall form and decay many rotor revolutions before stall occurs. By cross-correlating the signal from a single high frequency response pressure sensor, we can correlate the presence of spike-like pulses in the pressure signal from one rotor revolution to the next. The analysis produces a similar output to that of the two-point spatial correlation technique, but requires only one sensor and is therefore more practical in real world stall detection system embodiments.

Acoustic stall detection

The symmetrised dot pattern (SDP) stall detection technique is based on an industrial fan or compressor acoustic or unsteady pressure signal's visual waveform analysis (Sheard *et al.*, 2011). One may process an input signal using the symmetrised dot pattern technique to generate distinctly different images at different fan speeds and operating conditions, Figure 1.12. The images which the technique
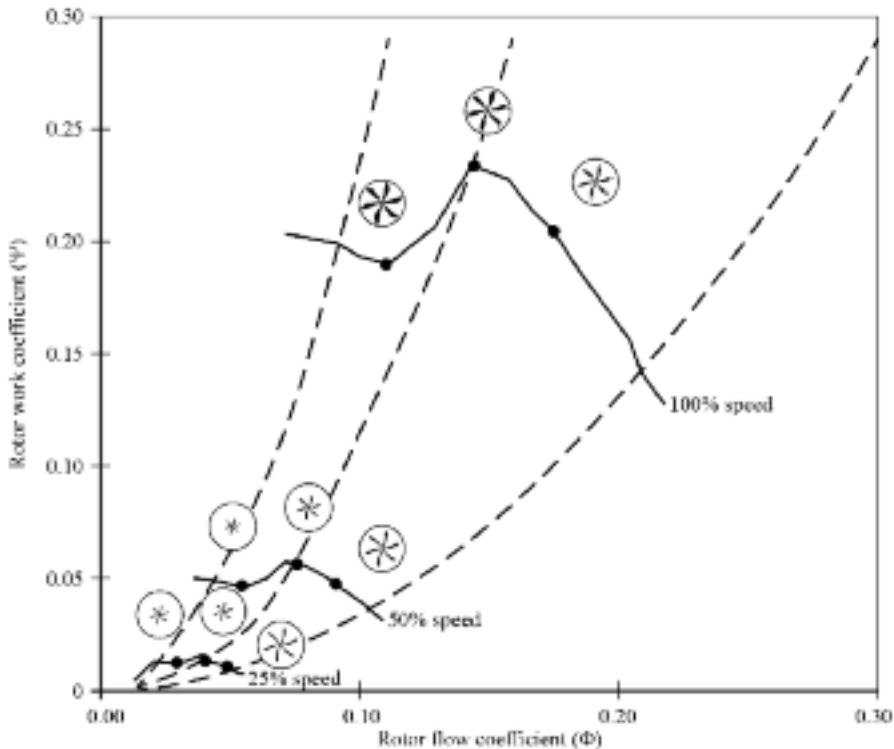
FIGURE 1.12. Unsteady pressure data from a 2.24 metre diameter tunnel ventilation fan at full, half and quarter design speed in stable operation, when stall is incipient and during operation in rotating stall. The authors processed the data using the symmetrised dot pattern (SDP) technique to produce a set of visual images that are distinctly different at each speed and operating condition (Sheard *et al.*, 2011).

produces are distinctly different during stable operation, when stall is incipient and during stalled operation. Sheard *et al.* (2011) first constructed symmetrised dot patterns from the unsteady pressure signal they measured over an industrial fan's blades'. More recently Bianchi *et al.* (2013a) demonstrated the proposed technique's validity by constructing symmetrised dot patterns from the unsteady pressure they measured in an industrial fan's inlet plenum.

An ability to generate images sufficiently different to enable engineers to differentiate between stable operation, incipient stall and rotating stall results in a symmetrised dot pattern technique with the potential to form the basis of a stall detection system. Bianchi *et al.* (2013b) demonstrated that symmetrized dot patterns could be generated using an acoustic signal from a microphone in the fan's far-field. Applying the symmetrised dot pattern technique to acoustic measurements constitutes a significant advance over the two-point spatial correlation, the stochastic model, travelling wave energy analysis or cross-correlation analysis as one can generate the images using a single acoustic signal. The other techniques require mounting a high frequency response pressure transducer in the industrial fan or compressor casing over the blades that are prone to stall. In contrast, one may apply the symmetrised dot pattern technique to acoustic measurement made with a single microphone at any location in close proximity to the industrial fan or compressor. The technique is particularly effective compared to other techniques when the signal of interest is low compared to the background noise. This enables the symmetrised dot pattern technique to provide useful results when the microphone is situated in the acoustic far-field (Bianchi *et al.*, 2013b).

We can differentiate the symmetrised dot pattern technique from other stall detection systems as it can identify a shift from stable operation to incipient stall an order of magnitude more quickly than other techniques. Other stall detection techniques use a Fourier analysis to analyse raw pressure signals which generate the signal's frequency spectrum. They then identify a change in frequency spectrum as a fan moves from stable operation to incipient stall. A weakness associated with using a Fourier analysis is that the minimum sample size needed is relatively large compared to that required by the symmetrised dot pattern technique. Consequently, the other techniques require a longer data acquisition period than is required by the symmetrised dot pattern technique. The shorter the required data acquisition period needed for the signal analysis to be effective, the more likely that the resultant output will be available quickly enough to provide a warning that stall is incipient before a fan transitions into stalled operation.

We may illustrate the effectiveness of the symmetrised dot pattern technique when compared with any of the Fourier transform based stall detection techniques with an example. We present the output from a high frequency pressure transducer located in the far-field for a 20 second period during which the fan operating point moves from stable operation to incipient stall, Figure 1.13. In this context far-field refers to a pressure transducer located in the inlet box of an induced draft fan. The reason for using data from the far-field is that it extends stall detection from the hydrodynamic pressure near-field to the acoustic pressure far-field. In this example, we logged data at 2,000 Hz. From zero to ten seconds the fan is operating in its operat-
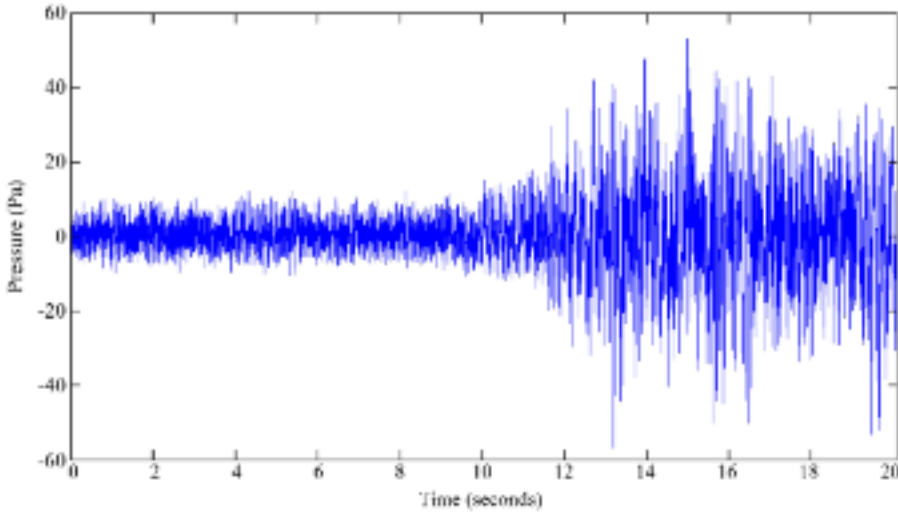
FIGURE 1.13. Data logged at 2,000 Hz from a high frequency response pressure transducer located in the inlet plenum of an induced draft fan. From zero to ten seconds the fan is operating in a stable condition. At ten seconds stall becomes incipient and remains incipient until 11 seconds. From 11 to 20 seconds the fan is operating in rotating stall.

ing characteristic's stable region. At ten seconds stall becomes incipient, and remains incipient for one second. From 11 to 20 seconds the fan is operating in its operating characteristic's unstable region.

A Fourier analysis of ten rotor revolutions of data (0.1 seconds) during stable operation, immediately before ten seconds, Figure 1.13, and ten rotor revolutions of data when stall is incipient, immediately after ten seconds, Figure 1.13, results in distinctly different frequency spectrum, Figure 1.14. This difference between the two frequency spectra below 50 Hz is a consequence of the spike-like pressure pulses associated with incipient stall present in the data from ten to 20 seconds, and absent in the data from zero to ten seconds. We used the difference between the frequency spectrum that we generated using the data from a stable operating condition and an operating condition where stall is incipient as the basis of Fourier transform based stall warning techniques.

The signal processing associated with the symmetrised dot pattern technique does not involve a Fourier transform, instead transforming the data into a set of polar coordinates that one uses to create the symmetrised dot patterns. In the above example, stall becomes incipient at ten seconds, Figure 1.13. One rotor revolution of data (0.01 seconds) during stable operation, immediately before ten seconds, Figure 1.13, and one rotor revolution of data when stall is incipient, immediately after ten seconds, Figure 1.13, results in distinctly different symmetrised dot patterns, Figure 1.15. It is the difference between the generated symmetrised dot pattern using the data from a stable operating condition and an operating condition where stall is incipient that enable one to use the symmetrised dot pattern technique as the basis of a stall warning technique.
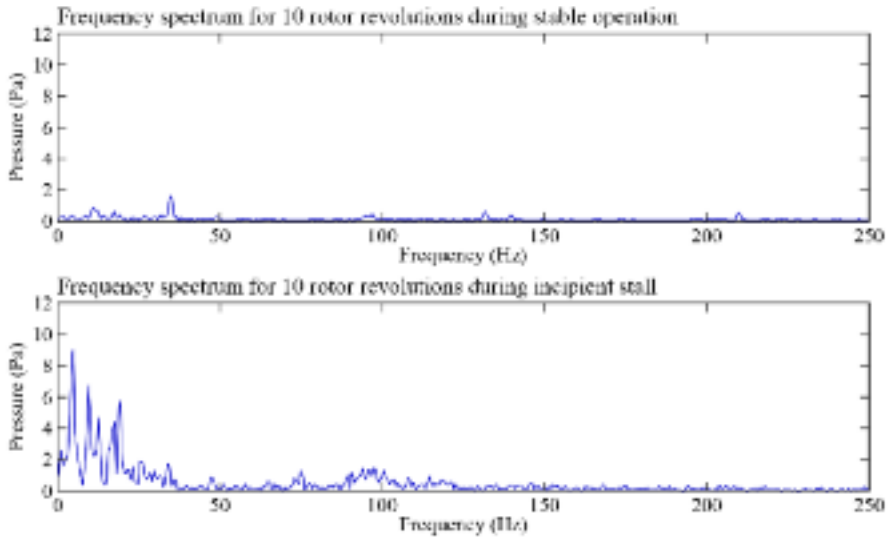
FIGURE 1.14. Frequency spectrum generated using data gathered over ten rotor revolutions during stable fan operation (top) and over ten rotor revolutions when stall is incipient (bottom). The frequency spectrum generated using data when stall is incipient includes features that are associated with the spike-like pressure pulses that occur when stall is incipient. As such, the two frequency spectrums are different enabling one to use them as the basis of a stall detection system.
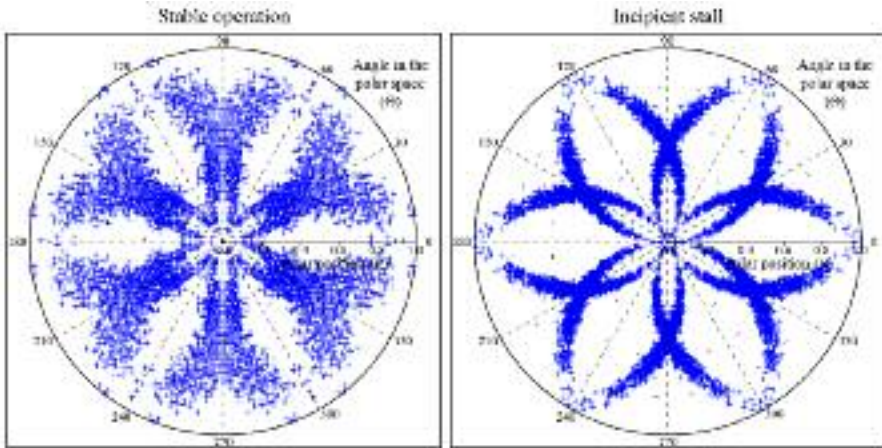
FIGURE 1.15. Symmetrised dot patterns generated using data gathered over one rotor revolution during the fan's stable operation (left) and over one rotor revolution when stall is incipient (right). The two patterns are different enabling one to use them as the basis of a stall detection system.

When one conducts a Fourier analysis using the same one rotor revolution of data to generate each symmetrised dot pattern, the resultant frequency spectrum for the stable operating condition and an operating condition where stall is incipient are similar, Figure 1.16. A consequence of the frequency spectrum being similar is that any of the stall warning techniques based upon the use of a Fourier analysis will not be able to use the frequency spectrum to differentiate between a fan in stable operation and when stall is incipient. In contrast, the symmetrised dot pattern technique is able to generate distinctly different patterns, indicating that the symmetrised dot pattern technique can identify a change from a stable operating condition to one where stall is incipient an order of magnitude more rapid than stall warning techniques based on the use of a Fourier transform based analysis.

The five stall detection techniques, Table 1.3, each represent a valid approach to stall detection. In practice it is the two-point spatial correlation technique that is the most developed stall detection technique in compressor applications and the symmetrised dot pattern technique that is the most wide-spread in industrial fan applications. Stall detection systems well enough developed for in-service applications are still the subject of development in both the industrial fan and compressor communities. Research is ongoing in an effort to better understand the flow physics that occur with incipient stall in order to improve the accuracy and speed with which one can identify incipient stall.
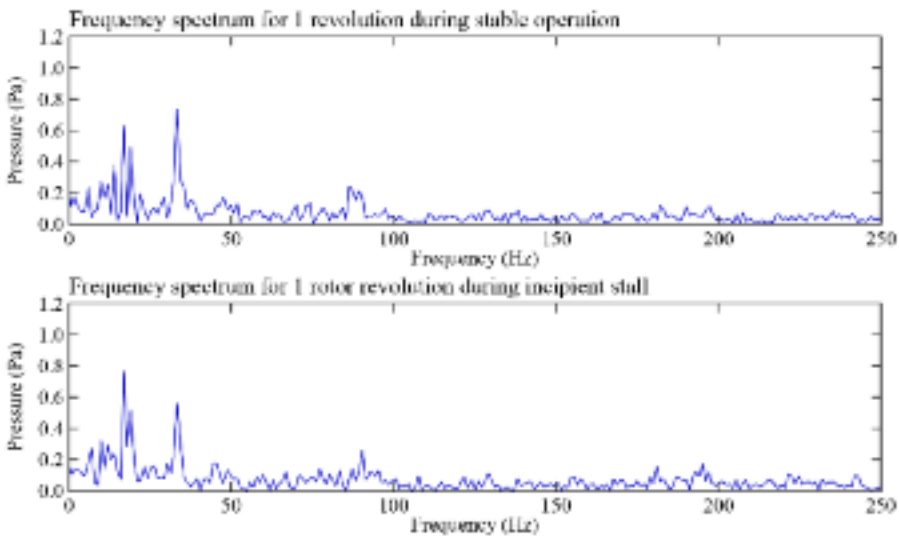
FIGURE 1.16. Frequency spectrum generated using data gathered over one rotor revolution during the fan's stable operation (top) and over one rotor revolution when stall is incipient (bottom). The two frequency spectrums are similar and therefore cannot be used as the basis of a stall detection system.

Table 1.3. *Matrix of stall detection techniques.*

Technique of detection	How it works	Results
Two-point spatial correlation	Finds spikes inception in the signal before the stall happens	Valuable for analysis of pre-stall and stall inception (Cameron and Morris, 2007)
Stochastic model	Correlates the pressure transducers' signals on the casing over the rotor tips. Finds dips in the correlation	Used for stall detection (Dhingra *et al.*, 2007)
Travelling-wave-energy analysis	Uses fan dynamics to introduce the concept of travelling wave energy as a real time measure of compressor stability	Early warning for spikes; good for high-speed compressors (Tryfonidis *et al.*, 1995)
Cross-correlation analysis	Searches for short wavelength disturbances recognisable as spikes that form and decay before the stall	Finds the spike inception, but does not use the instantaneous signal (Park, 1994)
Acoustic stall detection	Transforms the time-series signal's changes in amplitude and frequency into polar coordinates	Discerns from critical and non-critical stall using an easy to understand visual waveform analysis (Sheard *et al.*, 2011)

CONCLUSIONS

This chapter aimed to provide an overview of stall control technologies for industrial fans. These control technologies play an important role in many industrial applications. We have examined the stall phenomenon and paid particular attention to fluid dynamics, stall inception and mechanical failure that may occur when operating industrial fans. We then introduced the technologies that exist today for stall identification and control, distinguishing between active and passive technologies. We can use passive technologies to prevent the worst stall consequence: mechanical failures. Industrial fan manufacturers primarily use passive control technologies in-service.

Although innovation in passive technology is possible, passive technologies generally reduce fan efficiency. Current regulation within the European Union and planned regulation in the USA sets minimum Fan and Motor Efficiency Grades

(FMEGs) for industrial fans. These minimum FMEGs will rise in the European Union on 1 January, 2015, and will continue to rise both within Europe and the USA in an ongoing effort to reduce carbon emissions. As such, it is likely that the efficiency penalty with using passive technologies in industrial fan applications will become progressively less acceptable over the coming decade.

Researchers are focusing on active stall control technologies in an ongoing effort to develop effective stall detection system. Active stall control technologies include technologies that are still the subject of both fundamental research and applied development and therefore, at the time of writing, are still immature. Despite the need for further research and development of active stall control systems, and their associated stall detection systems, they offer the greatest potential for medium term improvement. We can most readily realise the potential for medium term improvement in industrial fan applications, as industrial fans are relatively low-speed machines in comparison to compressors. Consequently, active stall control systems based upon stall detection have the potential for practical application in industrial fans first, with the experience gaining in industrial fan application informing the development of higher speed systems that engineers can then use in compressor applications.

REFERENCES

EN12101-3, 2002, Smoke and Heat Control Systems. Specification for Powered Smoke and Heat Exhaust Ventilators.

ISO 21927-3, 2006, Smoke and Heat Control Systems — Part 3: Specification for Powered Smoke and Heat Exhaust Ventilators.

Bard, H. (1984), "The Stabilisation of Axial Fan Performance", *Proceedings of the Institution of Mechanical Engineers (IMechE) Conference 1984–4 on the Installation Effects in Ducted Fan Systems*, London, UK, 1–2 May, paper no. C120/84, pp. 100–106.

Bianchi, S., Corsini, A., and Sheard, A.G. (2010), "Detection of Stall Regions in a Low-speed Axial Fan, Part 1: Azimuthal Acoustic Measurements", *Proceedings of the 55th American Society of Mechanical Engineers Turbine and Aeroengine Congress*, Glasgow, UK, 14–18 June, paper no. GT2010-22753.

Bianchi, S., Corsini, A., Mazzucco, L., Monteleone, L., and Sheard, A.G. (2012), "Stall Inception, Evolution and Control in a Low Speed Axial Fan with Variable Pitch in Motion", *Transactions of the ASME, Journal of Engineering for Gas Turbines and Power*, vol. 134, paper no. 042602, pp. 1–10.

Bianchi, S., Corsini, A., and Sheard, A.G. (2013a), "Demonstration of a Stall Detection System for Induced-draft Fans", *Proceedings of the IMechE Part A, Journal of Power and Energy*, vol. 227, pp. 272–84.

Bianchi, S., Corsini, A., and Sheard, A.G. (2013b), "Experiments on the Use of Symmetrized Dot Patterns for In-service Stall Detection in Industrial Fans", *Advances in Acoustic and Vibration*, vol. 2013, pp. 1–10.

Bright, M.M., Qammar, H., Vhora, H., and Schaffer, M. (1998), "Rotating Pip Detection and Stall Warning in High-speed Compressors using Structure Function", *Proceedings of GARD RTO AVT Conference*, Toulouse, France, 11–15 May.

Cameron, J., and Morris, S. (2007), "Spatial Correlation Based Stall Inception Analysis", *Proceedings of the 52nd American Society of Mechanical Engineers Gas Turbine and Aeroengine Congress*, Montreal, QC, Canada, 14–17 May, paper no. GT2007-28268.

Camp, T.R., and Day, I.J. (1998), "A Study of Spike and Modal Stall Phenomena in a Low-speed Axial Compressor", *Transactions of the ASME, Journal of Turbomachinery*, vol. 120, pp. 393–401.

Cardillo, L., Corsini, A., Delibra, G., Rispoli, F., and Sheard A.G. (2014), "A Numerical Investigation into the Aerodynamic Effect of Pressure Pulses on a Tunnel Ventilation Fan", *Proceedings of the IMechE Part A, Journal of Power and Energy*, vol. 228, pp. 285–99.

Christensen, D., Cantin, P., Gutz, D., Szucs, P.N., Wadia, A.R., Armor, J., Dhingra, M., Neumeier, Y., and Prasad, J.V. (2008), "Development and Demonstration of a Stability Management System for Gas Turbine Engines", *Transactions of the ASME, Journal of Turbomachinery*, vol. 130(3), paper no. 031011, pp. 1–9.

Copenhaver, W.W., and Okiishi, T.H. (1993), "Rotating Stall Performance and Recoverability of a High-speed 10 Stage Axial Flow Compressor", *Journal of Propulsion and Power*, vol. 9, pp. 281–92.

Corke, T.C., and Post, M.L. (2005), "Overview of Plasma Flow Control: Concepts, Optimization, and Applications", *43rd AIAA Aerospace Sciences Meeting*, Reno, NV, USA, paper no. AIAA 2005–563.

Corsini, A., Delibra, G., Sheard, A.G., and Volponi, D. (2014), "Investigation on Anti-stall Ring Aerodynamic Performance in an Axial Flow Fan", *Proceedings of the 59th American Society of Mechanical Engineers Turbine and Aeroengine Congress*, Dusseldorf, Germany, 16–20 June, paper no. GT2014-25794.

Cumpsty, N.A. (1989), "Part-circumference Casing Treatment and the Effect on Compressor Stall", *Proceedings of the 34th American Society of Mechanical Engineers Gas Turbine and Aeroengine Congress*, Toronto, ON, Canada, 11–14 June, paper no. 89-GT-312.

Day, I.J. (1993), "Stall Inception in Axial Flow Compressors", *Transactions of the ASME, Journal of Turbomachinery*, vol. 115, pp. 1–9.

Day, I.J. (1994), "Axial Compressor Performance During Surge", *Journal of Propulsion and Power*, vol. 10, pp. 329–36.

Day, I.J., and Cumpsty, N.A. (1978), "The Measurement and Interpretation of Flow Within Rotating Stall Cells in Axial Compressors", *Proceedings of the Institution of Mechanical Engineers, Part C, Journal of Mechanical Engineering Science*, vol. 20, pp. 101–14.

de Jager, B. (1995), "Rotating Stall and Surge: a Survey", *Proceedings of the 34th Conference on Decision and Control*, New Orleans, LA, USA.

Deppe, A., Saathoff, H., and Stark, U. (2005), "Spike-type Stall Inception in Axial Flow Compressors*", Proceedings of the 6th Conference on Turbomachinery, Fluid Dynamics and Thermodynamics*, Lille, France, 7–11 March.

Dhingra, M., Neumeier, Y., Prasad, J.V.R., Breeze-Stringfellow, A., Shin, H.W., and Szucs, P.N. (2007), "A Stochastic Model for a Compressor Stability Measure", *Transactions of the ASME, Journal of Engineering for Gas Turbines and Power*, vol. 129, pp. 730–37.

Eisenlohr, G., and Chladek, H. (1994), "Thermal Tip Clearance Control for Centrifugal Compressor of an APU Engine", *Transactions of the ASME, Journal of Turbomachinery*, vol. 116, pp. 629–34.

Emmons, H.W., Pearson, C.E., and Grant, H.P. (1955), "Compressor Surge and Stall Propagation", *Transactions of the ASME*, vol. 77, pp. 455–69.

Epstein, A.H., Ffowcs Williams, J.E., and Greitzer, E.M. (1989), "Active Suppression of Aerodynamic Instabilities in Turbomachines", *Journal of Propulsion and Power*, vol. 5, pp. 204–11.

Eurovent (2007), "Eurovent1/11 – Fans and System Stall: Problems and Solution".

Eveker, K.M., and Nett, C.N. (1991), "Model Development for Active Surge Control/rotating Stall Avoidance in Aircraft Gas Turbine Engines", *Proceedings of the 1991 American Control Conference*, Boston, MA, USA, 26–28 June, vol. 3, pp. 3166–72.

Eveker, K.M., and Nett, C.N. (1993), "Control of Compression System Surge and Rotating Stall: A Laboratory-based 'Hands-on' Introduction", *Proceedings of the 1993 American Control Conference*, vol. 2, pp. 1307–11.

Eveker, K.M., Gysling, D.L., Nett, C.N., and Sharma, O.P. (1995), "Integrated Control of Rotating Stall and Surge in Aeroengines", *Proceedings of the 1995 International Society for Optical Engineering (SPIE) Conference on Sensing, Actuation and Control in Aeropropulsion*, Orlando, FL, USA, 17–18 April, vol. 2494, pp. 21–35.

Ffowcs Williams, J.E., and Huang, X.Y. (1989), "Active Stabilization of Compressor Surge", *Journal of Fluid Mechanics*, vol. 204, pp. 245–62.

Ffowcs Williams, J.E., Harper, M.F.L., and Allwright, D.J. (1993), "Active Stabilization of Compressor Instability and Surge in a Working Engine", *Transactions of the ASME, Journal of Turbomachinery*, vol. 115, pp. 68–75.

Funk, D.A., Cumpsty, N.A., and Greitzer, E.M. (1992), "Surge Dynamics in a Free-spool Centrifugal Compressor System", *Transactions of the ASME, Journal of Turbomachinery*, vol. 114, pp. 321–32.

Gad-el-Hak, M. (2000), *Flow Control: Passive, Active, and Reactive Flow Management*, Cambridge University Press, Cambridge, UK.

Goto, A. (1994), "Suppression of Mixed-flow Pump Instability and Surge by the Active Alteration of Impeller Secondary Flows", *Transactions of the ASME, Journal of Turbomachinery*, vol. 116, pp. 621–8.

Gravdahl, J.T., and Egeland, O. (1999), *Compressor Surge and Rotating Stall: Modeling and Control*, Springer Verlag, London, UK.

Greitzer, E.M. (1980), "Review — Axial Compressor Stall Phenomena", *Transactions of the ASME, Journal of Fluids Engineering*, vol. 102, pp. 134–51.

Greitzer, E.M., and Moore, F.K. (1986), "A Theory of Post-stall Transients in Axial Compression Systems: Part II — Application", *Transactions of the ASME, Journal of Engineering for Gas Turbines and Power*, vol. 108, pp. 231–9.

Gysling, D.L., Dugundji, M., Greitzer, J.E., and Epstein, A.H. (1991), "Dynamic Control of Centrifugal Compressor Surge using Tailored Structures", *Transactions of the ASME, Journal of Turbomachinery*, vol. 113, pp. 710–22.

Houghton, T.O., and Day, I.J. (2010), "Enhancing the Stability of Subsonic Compressors using Casing Grooves", *Transactions of the ASME, Journal of Turbomachinery*, vol. 133, paper no. 021007, pp. 1–11.

Ivanov, S.K. (1965), "Axial Blower", US Patent 3,189,260, 15 June.

Joslin, R.D., Rusell, H.T., and Choudhari, M.M. (2005), "Synergism of Flow and Noise Control Technologies", *Progress in Aerospace Sciences*, vol. 41, pp. 363–417.

Kameier, F., and Neise, W. (1997), "Rotating Blade Flow Instability as a Source of Noise in Axial Turbomachines", *Journal of Sound and Vibration*, vol. 203, pp. 833–53.

Karlsson, S., and Holmkvist, T. (1986), "Guide Vane Ring for a Return Flow Passage in Axial Fans and a Method of Protecting It", US Patent 4,602,410, 29 July.

Kim, K.H., and Fleeter, S. (1994), "Compressor Unsteady Aerodynamic Response to Rotating Stall and Surge Excitations", *Journal of Propulsion and Power*, vol. 10, pp. 698–708.

Lin, F., Tong, Z., Geng, S., Zhang, J., Chen, J., and Nie, C. (2011), "A Summary of Stall Warning and Suppression Research with Micro Tip Injection", *Proceedings of the 56th American Society of Mechanical Engineers Turbine and Aeroengine Congress*, Vancouver, BC, Canada, 6–10 June, paper no. GT2011-46118.

Mongeau, L., Thompson, D.E., and McLaughlin, D.K. (1995), "A Method for Characterizing Aerodynamic Sound Sources in Turbomachines", *Journal of Sound and Vibration*, vol. 181, pp. 369–89.

Moore, F.K. (1984), "A Theory of Rotating Stall of Multistage Compressors, Parts I–III", *Transactions of the ASME, Journal of Engineering for Power*, vol. 106, pp. 313–36.

Nie, C., Xu, G., Cheng, X., and Chen, J. (2002), "Micro Air Injection and its Unsteady Response in a Low-speed Axial Compressor", *Transactions of the ASME, Journal of Turbomachinery*, vol. 124, pp. 572–9.

Okada, K. (1987), "Experiences with Flow-induced Vibration and Low Frequency Noise due to Rotating Stall of Centrifugal Fan", *Journal of Low Frequency Noise and Vibration*, vol. 6, pp. 76–87.

Paduano, J.D., Epstein, A.H., Valavani, L., Longley, J.P., Greitzer, E.M., and Guenette, G.R. (1993a), "Active Control of Rotating Stall in a Low-speed Axial Compressor", *Transactions of the ASME, Journal of Turbomachinery*, vol. 115, pp. 48–57.

Paduano, J.D., Valavani, L., and Epstein, A.H. (1993b), "Parameter Identification of Compressor Dynamics during Closed-loop Operation", *Journal of Dynamic Systems, Measurement, and Control*, vol. 115, pp. 694–703.

Paduano, J.D., Valavani, L., Epstein, A.H., Greitzer, E.M., and Guenette, G.R. (1994), "Modelling for Control of Rotating Stall", *Automatica, a Journal of the International Federation of Automatic Control (IFAC)*, vol. 30, pp. 1357–73.

Park, H.G. (1994), "Unsteady Disturbance Structures in Axial Flow Compressor Stall Inception", MS thesis, Massachusetts Institute of Technology, Cambridge, MA, USA.

Pinsley, J.E., Guenette, G.R., Epstein, A.H., and Greitzer, E.M. (1991), "Active Stabilization of Centrifugal Compressor Surge", *Transactions of the ASME, Journal of Turbomachinery*, vol. 113, pp. 723–32.

Prasad, J.V.R., Neumeier, Y., Lal, M., Bae, S.H., and Meehan, A. (1999), "An Experimental Investigation of Active and Passive Control of Rotating Stall in Axial Compressors", *Proceedings of the IEEE International Conference on Control Applications, held together with the IEEE International Symposium On Computer Aided Control System Design*, Kohala Coast-Island of Hawai'i, Hawai'i, HI, USA, 22–27 August, vol. 2, pp. 985–90.

Rippl, A. (1995), "Experimentelle Untersuchungen Zuminstationaren Betriebsverhahenan der Stabilitarsgrenze Eines Mehrstufigen Transsonischen Verdichters", PhD dissertation, Ruhr-Universitat Bochum.

Rodgers, C. (1991), "Centrifugal Compressor Inlet Guide Vanes for Increased Surge Margin", *Transactions of the ASME, Journal of Turbomachinery*, vol. 113, pp. 696–702.

Sheard, A.G., and Corsini, A. (2011), "The Impact of an Anti-stall Stabilisation Ring on Industrial Fan Performance: Implications for Fan Selection", *Proceedings of the 56th American Society of Mechanical Engineers Turbine and Aeroengine Congress*, Vancouver, BC, Canada, 6–10 June, paper no. GT2011-45187.

Sheard, A.G., and Corsini, A. (2012), "The Mechanical Impact of Aerodynamic Stall on Tunnel Ventilation Fans", *International Journal of Rotating Machinery*, paper no. 402763, pp. 1–12.

Sheard, A.G. and Jones, N.M. (2008), "Approval of High-Temperature Emergency Tunnel-Ventilation Fans: The Impact of ISO 21927-3", *Proceedings of the ITA–AITES World Tunnel Congress and 34th General Assembly*, Agra, India, 19–25 September, pp. 1817–26.

Sheard, A.G., and Jones, N.M. (2012), "Powered Smoke and Heat Exhaust Ventilators: The Impact of EN 12101-3 and ISO 21927-3", *Tunnelling and Underground Space Technology*, vol. 28, pp. 174–82.

Sheard, A.G., Corsini, A. and Bianchi, S. (2011), "Stall Warning in a Low-speed Axial Fan by Visualisation of Sound Signals", *Transactions of the ASME, Journal of Engineering for Gas Turbines and Power*, vol. 133, paper no. 041601, pp. 1–10.

Simon, J.S., and Valavani, L. (1991), "A Lyapunov-based Nonlinear Control Scheme for Stabilizing a Basic Compression System using a Close-coupled Control Valve", *Proceedings of the 1991 American Control Conference*, Boston, MA, USA, 26–28 June, vol. 3, pp. 2398–406.

Simon, J.S., Valavani, L., Epstein, A.H., and Greitzer, E.M. (1993), "Evaluation of Approaches to Active Compressor Surge Stabilization", *Transactions of the ASME, Journal of Turbomachinery*, vol. 115, pp. 57–67.

Suder, K.L., Hathaway, M.D., Thorp, S.A., Strazisar, A.J., and Bright, M.B. (2001), "Compressor Stability Enhancement using Discrete Tip Injection", *Transactions of the ASME, Journal of Turbomachinery*, vol. 123, no. 1, pp.14–23.

Tan, C.S., Day, I., Morris, S., and Wadia, A. (2010), "Spike-type Compressor Stall Inception, Detection, and Control", *Annual Review of Fluid Mechanics*, vol. 42, pp. 275–300.

Tryfonidis, M., Etchevers, O., Paduano, J.D., Epstein, A.H., and Hendricks, G.J. (1995), "Prestall Behaviour of Several High-speed Compressors", *Transactions of the ASME, Journal of Turbomachinery*, vol. 117, pp. 62–80.

Vo, H.D. (2007), "Active Suppression of Rotating Stall Inception with Distributed Jet Actuation", *International Journal of Rotating Machinery*, article ID 56808, pp. 1–15.

Vo, H.D., Tan, C.S., and Greitzer, E.M. (2005), "Criteria for Spike Initiated Rotating Stall", *Proceedings of the 50th American Society of Mechanical Engineers Gas Turbine and Aeroengine Congress*, Reno, NV, USA, 6–9 June, paper no. GT2005-68374.

Vo, H.D., Cameron, J., and Morris, S. (2008), "Control of Short Length-scale Rotating Stall Inception on a High-speed Axial Compressor with Plasma Actuation", *Proceedings of the 53rd American Society of Mechanical Engineers Gas Turbine and Aeroengine Congress*, Berlin, Germany, 9–13 June, paper no. GT2008-50967.

Wadia, A.R., Christensen, D., and Prasad, J.V. (2006), "Compressor Stability Management in Aircraft Engines", *Proceedings of ICAS 2006, the 25th Congress of the International Council of the Aeronautical Sciences (ICAS)*, Hamburg, Germany, 3–8 September, paper no. 759.

Weigl, H.J., Paduano, J.D., Frechette, L.G., Epstein, A.H., Greitzer, E.M., Bright, M.M., and Straziszar, A.J. (1997), "Active Stabilization of Rotating Stall in a Transonic Single Stage Axial Compressor", *Proceedings of the 42nd American Society of Mechanical Engineers Gas Turbine and Aeroengine Congress*, Orlando, FL, USA, 2–5 June, paper no. 97-GT-411.

Wo, A.M., and Bons, J.P. (1994), "Flow Physics Leading to System Instability in a Centrifugal Pump", *Transactions of the ASME, Journal of Turbomachinery*, vol. 116, pp. 612–21.

Yamaguchi, N., Ogata, M., and Kato, Y. (2010), "Improvement of Stalling Characteristics of an Axial-flow Fan by Radial-vaned Air Separators", *Transactions of the ASME, Journal of Turbomachinery*, vol. 132, pp. 1–10.

Yeung, S., and Murray, R.M. (1997), "Reduction of Bleed Valve Rate Requirements for Control of Rotating Stall using Continuous Air Injection", *Proceedings of the 1997 IEEE International Conference on Control Applications*, Hartford, CT, USA, 5–7 October, pp. 683–90.

The Mechanical Impact of Aerodynamic Stall on Tunnel Ventilation Fans

A.G. Sheard and A. Corsini

ABSTRACT

This chapter describes work aimed at establishing the ability of a tunnel ventilation fan to operate without risk of mechanical failure in the event of aerodynamic stall. The research establishes the aerodynamic characteristics of a typical tunnel ventilation fan when operated in both stable and stalled aerodynamic conditions, with and without an anti-stall stabilisation ring, with and without a 'non-stalling' blade angle and at full, half and one-quarter design speed. It also measures the fan's peak stress, thus facilitating an analysis of the implications of the experimental results for mechanical design methodology.

The measured peak stress for a fan with a fitted anti-stall ring during aerodynamic stall resulted in alternating stress increasing, and consequently, the fan blade mechanical safety factor reducing from 2.5 to 1.1. The reduction in mechanical safety factor is significant, as it indicates that although the anti-stall ring provides some mechanical protection in the event of aerodynamic stall, it does not provide complete protection. It is concluded that an assumption of the part of some industrial fan designers that an anti-stall ring does provide complete mechanical protection in the event of aerodynamic stall may have been the root cause of in-service fan blade fatigue failures in tunnel ventilation fan applications where pressure pulses associated with trains passing ventilation shafts are known to routinely drive ventilation fans into aerodynamic stall.

The chapter concludes by presenting three different strategies for tunnel ventilation fan selection in applications where the selected fan will most likely stall. The first strategy selects a fan with a low blade angle that is non-stalling. The second strategy selects a fan with a high pressure developing capability. The third strategy selects a fan with a fitted stabilisation ring. Tunnel ventilation system designers each have their favoured fan selection strategy. However, all three strategies can produce

system designs within which a tunnel ventilation fan performs reliably in service. The chapter considers the advantages and disadvantages of each selection strategy and concludes with a brief assessment of the strengths and weaknesses of each.

NOMENCLATURE

Latin letters

D	fan diameter	m
D_t	tip diameter	mm
g_t	tip gap	mm
H_b	blade height	mm
ℓ_t	blade chord at the tip	mm
P_m	motor power	kW
S	stress level	
s_0	alternating stress level	
s_t	tensile stress	
s_m	mean stress	

Greek letters

γ_t	tip blade angle
η	efficiency
η_{tot}	total efficiency
Σ_t	tip solidity
Φ_{nom}	nominal flow coefficient
Ψ_{nom}	nominal pressure coefficient

INTRODUCTION

The operating maps of fans and compressors are limited by the occurrence of aerodynamic instabilities when throttling the flow rate. Aerodynamic flow instabilities place considerable mechanical stress on the rotors, which can eventually lead to mechanical failure. Rippl (1995) conducted strain gauge measurements on axial compressors, concluding that alternating stress in vanes exceeding stable operation by a factor of five under 'rotating stall' conditions. This leads to rapid fatigue failure of the blades. In contrast, a 'surge' can lead to the heightening magnitude of bending stress enough to cause a mechanical failure during the surge event itself.

Fan designers classically produce a mechanical design that can withstand the alternating loads imposed on the fan blades associated with rotating stall, and therefore mechanical failure during a stall event is not instantaneous. Aluminium is both low cost and light weight, and consequently, the fan designers' preferred choice of blade material. A weakness of aluminium as a structural material is its propensity to fail in fatigue. As such, fan blades that do not typically instantaneously fail during rotating stall, fail in fatigue sometime later. The latter failure occurs as a conse-

quence of a fatigue induced crack initiated in a blade as a consequence of the higher stress during the rotating stall that then goes on to propagate during stable operation.

This chapter studies the impact of rotating stall, generally referred to as 'aerodynamic stall' within the fan industry, on the mechanical performance of a typical tunnel ventilation fan. The chapter starts with a brief literature review relating to fan, blower and compressor aerodynamic stall before moving on to review the anti-stall concepts that other scholars have developed in their attempts to improve axial decelerating turbomachinery aerodynamic stability. Placing strain gauges in the location of the fan blades' peak stress, we were able to establish the mechanical impact of aerodynamic stall with and without an anti-stall stabilisation ring, with and without a 'non-stalling' blade angle and at full, half and one-quarter design speed.

The chosen test matrix incorporated those fan configurations typically utilised in tunnel ventilation applications. The purpose is to establish the increase in peak blade stress associated with transition from stable and stalled aerodynamic conditions. The objective of establishing the increase is to facilitate an analysis of its mechanical consequence. The outcome of the reported research is the identification of change in mechanical safety factors associated with a fan being driven into aerodynamic stall. To the best of our knowledge the results presented in this chapter are the first time the effectiveness of an anti-stall ring has been reported in the literature. The reported research has established that an anti-stall ring provides some mechanical protection in the event of aerodynamic stall, but not complete protection. The reported research demonstrates the error in the wide-spread assumption amongst industrial fan designers that anti-stall rings provide complete mechanical protection in the event of aerodynamic stall.

The chapter concludes with an analysis of the significance of the results for fan design praxis, recommendations on fan selection strategy and mechanical design methodology for those tunnel ventilation fans applied in selected applications where the fan will most likely stall.

AERODYNAMIC STALL

Scholars have examined the detection and analysis of different forms of aerodynamic instability since the 1950s. According to Gravdahl and Egeland (1999), two main types of aerodynamic flow instability exist in compressors: (i) 'rotating stall' in which regions of reversed flow occur locally; and (ii) 'surge' which is characterised by periodic backflow over the entire annulus involving violent oscillations in the compression system.

The first of these, 'rotating stall', is a mechanism by which the rotor adapts to a reduction in flow rate, which results in circumferentially non-uniform flow patterns rotating in the annulus. Researchers have studied the problem of rotating stall in axial flow compressors in multi-stage machines (Day and Cumpsty, 1978; Greitzer, 1980; Moore, 1984). The earlier work of Emmons *et al*. (1955) was one of the first attempts to describe the mechanism underlying the propagation of rotating stall. In reviewing the evolution of rotating stall, Cumpsty (1989) noted that a drop in overall

performance can occur as either a 'progressive stall' or an 'abrupt stall'. Engineers usually associate the former with a part-span stall which results in a small performance reduction; whereas, they associate the later with a full-span stall and a large reduction in performance. Notably, the part-span rotating stall typically occurs in single blade rows (Cumpsty, 1989) and usually leads to more complex disturbances in single-rotor or single-stage machines than in multi-stage compressors (Moore, 1984).

The fan under scrutiny in the reported research is a typical example from a family of tunnel ventilation fans, and has been the subject of recent experimental investigation (Bianchi *et al*., 2010; Sheard *et al*., 2010, 2011). The investigation focused on the stall modes, identifying a rotating stall inception mechanism driven by circumferentially localised pressure disturbances confined to the blade passage's tip region. Localisation of the disturbances in the blade tip region supports the hypothesis of a causal link between tip clearance flow and stall inception.

Some scholars have focused on the physics underlying the tip clearance flow related mechanisms that can lead to the formation of pressure disturbances. Among them, Koch and Smith (1976) and Saathoff and Stark (2000) have observed experimentally that a fan reaches the limit of its pressure developing capability when the interface between the incoming flow and tip clearance vortex region lined-up with the leading edge plane at the blade tip. Numerical simulation has revealed two more mechanisms related to the onset of tip blockage growth (Khalid *et al*., 1999; Vo *et al*., 2005), namely: (i) the backflow of tip clearance fluid at the trailing edge impinging on the blade pressure side of adjacent blades and (ii) the spillage of tip clearance fluid ahead of the blade leading edge below the blade tip into the next blade passage.

Scholars who have studied aerodynamic instability in fans and compressors have suggested that some features of the tip flow of both are directly responsible for the generation of short wave-length disturbances (also called 'spikes' or 'pips') that cause the inception of localised part-span stall cells (Bright *et al*., 1998; Camp and Day, 1998; Deppe *et al*., 2005).

HISTORICAL OVERVIEW OF ANTI-STALL CONCEPTS

Given the potentially catastrophic consequences of a stall event, there is an incentive for developing technologies that can extend the stable operating range of axially decelerating turbomachinery without undue performance degradation. Previously, Hathaway (2007) systematically reviewed techniques and design concepts to improve the stall-free operating margin or to suppress a stall event.

Hathaway noted the earliest proposed techniques from the 1950s that had successfully extended the axial compressor's stable operating range: Wilde (1950), on behalf of Rolls-Royce Ltd, and Turner (1955) on behalf of Power Jets Ltd, filed patents. These concepts were both based on the treatment of the casing end-walls motivated by a desire to control the boundary layer development by combining rear air bleeding and front re-injection (Wilde, 1950) or the use of holes and slots as a method of promoting turbulence, and in so doing, energising the end-wall flow (Turner, 1955).

Griffin and Smith (1966) conducted the first systematic experimental campaign on so-called 'porous end-walls' in compressor rotors during the 1960s at NASA. Their work demonstrated improved stall margins in cascade tunnels irrespective to the air blowing/bleeding. In a similar vein, scholars studied casing treatments, specifically holes, slots and grooves with and without plena in the 1970s (Bailey and Voit, 1970; Prince *et al.*, 1974; Wisler and Hilvers, 1974). They found their effectiveness primarily associated with delaying the onset of stall in tip-limited blade rows.

Takata and Tsukuda (1977) conducted detailed measurements within casing slots, and found that they achieved their anti-stall effect as a consequence of periodic pumping of the flow within the slots into the main stream. Moreover, Greitzer *et al.*'s (1979) investigations demonstrated that the end-wall treatments were effective mostly in high-solidity blade rows prone to wall-stall, but not in low-solidity rotors affected by blade-stall.

In the 1990s, researchers proposed concepts to exploit the potential benefits of flow bleeding (from the stalled region) and blowing (into the clean inflow), and in so doing, revisited earlier stall inception concepts. Most notably, Koff *et al.* (1994), Khalid (1996), Nolcheff (1996) and Gelmedov *et al.* (1998) patented different variants of recirculating casing treatment. A common theme with the different recirculating casing treatments was the provision of a path through the casing for low momentum fluid recirculating upstream from the blade tip leading edge.

More recently, Hathaway (2007) observed that the most significant advances in anti-stall devices have resulted as a consequence of insight into the flow mechanism that researchers associate with three specific technologies: first, circumferential grooves; second, tip injection control technology; and third, stage recirculation devices. Fan and blower designers most favour the stage recirculation devices.

PASSIVE CONTROL BY STABILISATION RINGS

Since the early 1960s, scholars have endeavoured to develop stage recirculation devices tailored to the pressure rise and volume flow rate ranges typical of industrial fans. Ivanov (1965) received the first patent. The concept is of an annular 'slit' in the casing upstream of the blades that stabilises fan performance as it approaches stall, Figure 2.1.

The annual slit enabled air to recirculate through the slit formed between the cylindrical mouth and ferrule. A set of guide vanes then redirected the recirculating flow in an axial direction as it turns back and reenters the fan blades. As the fan approaches stall, the slit and guide vanes provide a path for low momentum flow to recirculate. In practice, this stabilises fan performance.

Karlsson and Holmkvist (1986) filed a patent application on 15 March, 1984, developing and enhancing Ivanov's (1965) patent by incorporating guide vanes into the casing. Then, Bard (1984) named the guide vanes embedded within the fan casing a 'stabilisation ring'. Miyake *et al.* (1987) further developed and patented the original concept proposing the use of air-separators based on an open circumferential cavity facing the rotor-blade tips, which Yamaguchi *et al.* (2010) further
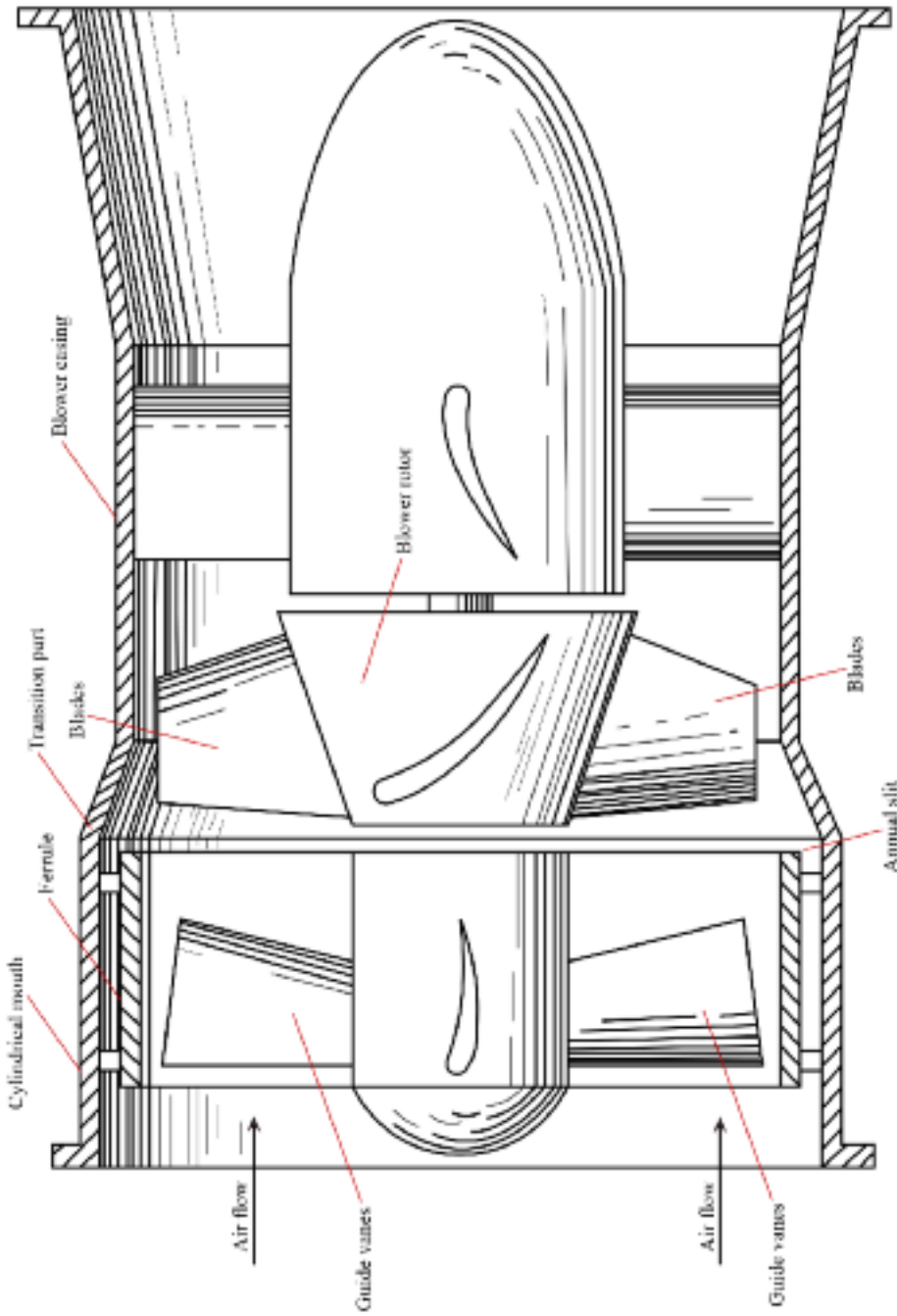
FIGURE 2.1. The proposed 'blower arrangement' (Ivanov, 1965).

developed. Similarly, Kang *et al*. (1995) optimised casing recess geometries and their relative position to the blade rows.

Despite subsequent developments to the concept, the fan community has mostly adopted Karlsson and Holmkvist's (1986) configuration. In practice the concept has proven highly effective as the stabilisation ring guide vanes remove the momentum component both radially and circumferentially and reinject the flow in the axial direction. The flow through the stabilisation ring vanes is turned such that it exits the vanes upstream from the impeller, reenergised and flowing in an axial direction.

The effect of the stabilisation ring on the fan characteristic is to eliminate the sharp drop in its pressure developing capability, which engineers classically associate with fan stall. The primary characteristic of a tunnel ventilation fan fitted with a stabilisation ring is continuously rising pressure back to zero flow. It was this modification in the fan characteristic that led to tunnel ventilation fan designers widely embracing the use of stabilisation rings.

A continuously rising characteristic facilitates multiple fan operation in parallel. As a fans speed falls, its pressure developing capability also falls. During a fan's starting and stopping transient, its pressure developing capability will be below what other fans generate when operating in parallel. As a consequence, a fan in parallel operation will inevitably drive transiently into stall each time it starts or stops. During the 1980s, variable speed drives were not widely available. Therefore, varying the speed of all fans in a parallel installation was not practical, making it inevitable that individual fans would have to start and stop, whilst others ran at full speed. The ability of the stabilisation ring to facilitate the starting and stopping of individual fans when in parallel operation was critically important. Application of the stabilisation ring largely eliminated in-service mechanical failure in fan parallel operation.

A particular feature of the environment within which tunnel ventilation fans operate is the pressure pulses associated with the movement of a train through a tunnel. Pressure pulses can be up to ±50 per cent of the overall work coefficient. With a fan in supply mode such pressure pulses drive the fan first up, and then down, its characteristic operating range, Figure 2.2. To ensure that the tunnel ventilation fan continues to operate in an aerodynamically stable manner during this pressure transient, aerodynamic design of the fan requires the incorporation of sufficient margin to ensure that the fan does not stall due to high positive or negative inlet flow angle.

This propensity to stall under large pressure fluctuations is complicated in off-design conditions when a tunnel ventilation fan operates at partial speeds. When a fan operates at reduced speed, its flow and pressure-developing capability also reduces. Because the pressure pulse of a passing train remains constant, there will be a critical speed when the fan is close to stall, but has not actually stalled. Below that critical speed, the fan stalls in positive incidence as the train approaches, and then stalls in negative incidence as the train departs, Figure 2.2. This combination of positive-incidence aerodynamic stall and negative-incidence aerodynamic stall causes a significant increase in the unsteady forces applied to the fan blades.
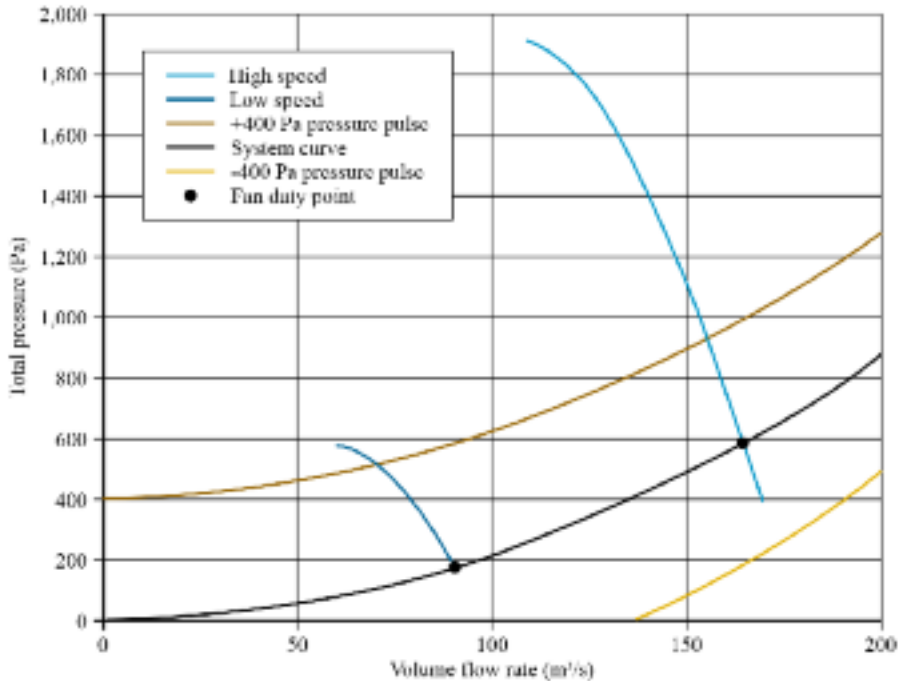
FIGURE 2.2. Fan performance under a pressure pulse at full- and part-speed.

TECHNOLOGY DESCRIPTION

In order to establish the likelihood of mechanical failure of tunnel ventilation fans in applications where aerodynamic stall is likely due to the presence of pressure pulses, we selected a fan typical of tunnel ventilation applications, Table 2.1.

The chosen fan was from a family of tunnel ventilation fans. Although each fan within the family is physically different, all are designed using the same mechanical design methodology. We chose the fan configurations for experimental testing as a consequence of the application into which manufacturers supply tunnel ventilation fans. Tunnel ventilation fans are typically subjected to pressure pulses. Therefore, we tested the fan:

- with a stalling blade angle, without a fitted stabilisation ring at design speed;
- with a stalling blade angle, with a fitted stabilisation ring at design speed;
- with a non-stalling blade angle and no stabilisation ring at design speed;
- with a stalling blade angle and no stabilisation ring at half design speed; and
- with a stalling blade angle and no stabilisation ring at quarter design speed.

Table 2.1. *Fan geometry and operating point data.*

Design speed	980 rpm
Tip speed	115 m/s
Design pressure coefficient, Ψ_{nom}	0.189
Design flow coefficient, Φ_{nom}	0.220
Design point efficiency, η_{tot}	0.69
Tip diameter, D_t	2,240 mm
Blade height, H_b	720 mm
Blade chord at the tip, ℓ_t	163 mm
Tip blade angle, γ_t	70°
Tip gap, g_t (per cent of fan diameter)	0.45%
Blade count	16
Tip solidity, Σ_t	0.37

We installed the fan in a ducted test system and measured the fan performance according to the International Standard ISO 5801:2007 (2007). By throttling flow downstream from the fan, we induced the aerodynamic instabilities of interest. During the flow/pressure throttling, the fan remained in rotating stall without going into surge, irrespective of the fan speed. The aerodynamic load and the plenum geometry ensured that the system could not develop a counter-pressure high enough to induce a surge.

We developed a solid model of the test fan's blade using a computer aided design package, and used a finite element analysis programme for structural analysis. We applied centrifugal force and bending moments (due to the design radial work distribution) using Sheard *et al*.'s (2009) original method using nodal forces in the finite element analysis boundary conditions in order to calculate blade stress. We applied strain gauges to three blades in the three locations that the finite element analysis predicted as the blades' high stress regions.

Stain gauges were applied using the method of Boyes (2003: 77). After chemical cleaning of the blades to be instrumented, foil gauges were applied. Foil gauges were chosen as there flatness makes adhesion easier and improves heat dissipation. The instrumentation system utilised was an adaption of that originally developed by Wasserbauer *et al.* (1995) who reported the design of a low-speed axial compressor test facility at what was then named NASA Lewis. Strain gauge leads are routed from the rotating to static frame of reference through a four channel electrical slip ring to a set of strain gauge amplifiers. The output of the strain gauge amplifiers was then logged using a personal computer based data acquisition system running the software package LabView.

EXPERIMENTAL RESULTS

Application of multiple strain gauges to separate blades enabled us to experimentally determine the actual highest stress location, as well as the impact of manu-

facturing tolerances from blade to blade. The variation in strain gauge output from blade to blade at nominally the same location on different blades was two to three per cent. This variation constitutes a combination of errors associated with gauge calibration, uncertainty in gauge location, plus blade to blade variation of blade geometry.

Using data from a typical strain gauge located at the highest stress position on one blade, we established fan performance with and without a fitted stabilisation ring, Figure 2.3. When throttling the fan without a fitted stabilisation ring, pressure rises until it reaches a peak, and then falls as the fan stalls. This is the classical fan characteristic. In the study, the blade's peak alternating stress increased from 2.27 MPa (Point A, Figure 2.3) to 3.53 MPa as we throttled the fan. As the fan stalled, peak alternating stress increased to 16.00 MPa (Point B, Figure 2.3).

When we throttled the fan with a stabilisation ring, pressure rose continuously with no evidence of a reduction in pressure developing capability as the fan passed through the point at which it stalled without a stabilisation ring, Figure 2.3. The fan characteristic is remarkable in that the pressure rises so smoothly that it is barely possible to identify the onset of stall from the fan's flow/pressure characteristic. However, in studying the strain gauge data, it is apparent that the initial alternating stress level is 2.13 MPa (Point C, Figure 2.3), and remains lower then a fan without a stabilisation ring until the onset of stall. As the fan fitted with a stabilisation ring approaches stall, there is a single point (at 60 m^3/s) where the data from the fan with-
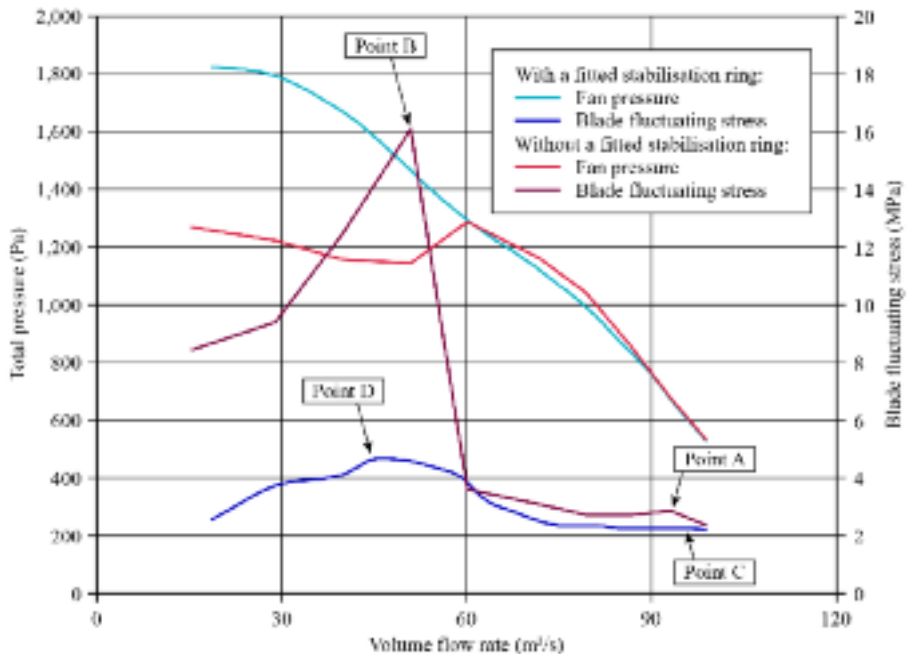
FIGURE 2.3. Stall characteristics of the studied fan with a stalling blade angle, with and without a fitted stabilisation ring.

out a stabilisation ring measures lower stress than the fan with a stabilisation ring. Alternating stress in the fan with a stabilisation ring goes on to peak at 4.60 MPa (Point D, Figure 2.3).

Using data from a typical strain gauge located at the highest stress position on one blade, we established fan performance with a non-stalling blade angle, and no fitted stabilisation ring. We compared data with data for a stalling blade angle with a fitted stabilisation ring, Figure 2.4. We compared the two data sets as a non-stalling blade angle without a stabilisation ring or stalling blade angle with the stabilisation ring representing the two available choices to tunnel system designers who wish to specify a 'stall tolerant fan'.

The change in blade angle from stalling to a non-stalling reduces the fan pressure developing capability by approximately 25 per cent, Figure 2.4. We tested the fan with the stalling blade angle and fitted stabilisation ring under stable and stalled aerodynamic conditions. The alternating stress increased from the initial alternating stress level of 2.13 MPa (Point C, Figure 2.4), going on to peak at 4.60 MPa (Point D, Figure 2.4). In contrast, a non-stalling blade angle without a stabilisation ring, increased from an initial 2.19 MPa (Point E, Figure 2.4), going on to peak at 3.68 MPa (Point F, Figure 2.4).

The peak alternating stress with the non-stalling blade angle and no fitted stabilisation ring was 20 per cent lower than a stalling blade angle and fitted stabilisation
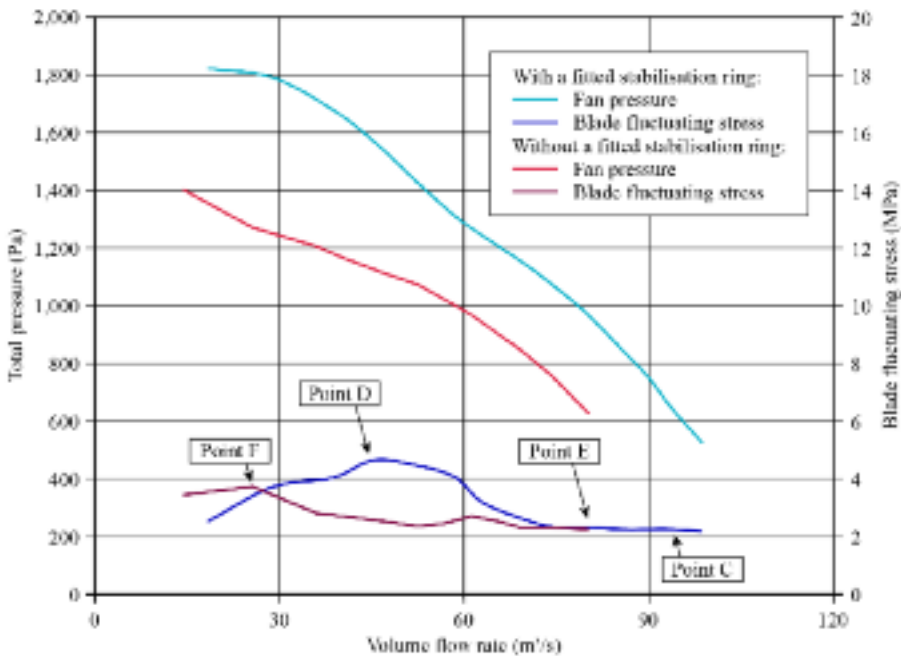
FIGURE 2.4. Stall characteristics of the studied fan with a stalling blade angle and a fitted stabilisation ring plus a non-stalling blade angle without a fitted stabilisation ring.

ring. We considered the uncertainty of the measurement approximately two per cent, and consequently, a 20 per cent reduction in peak alternating stress is an order of magnitude greater then the uncertainty of the measurement. The above result indicates that a fan with a non-stalling blade angle and no fitted stabilisation ring will be subject to lower peak alternating stress during aerodynamic stall then the same fan with a stalling blade angle and a fitted stabilisation ring.

Using data from a typical strain gauge located at the highest stress position on one blade, we established fan performance with a stalling blade angle, and no stabilisation rig fitted at full, half and quarter design speed. The availability of variable speed drives has resulted in tunnel ventilation fans routinely operating at part-speed. We compared the data at full design speed with data at half design speed, Figure 2.5. We compared the two data sets, as tunnel ventilation fans selected to not stall in the presence of a pressure pulse at full design speed, routinely stall in the presence of the same pressure pulse at half design speed.

The same alternating stress data for a fan with stalling blade angle and no fitted stabilisation ring is plotted, with alternating stress increasing from the initial alternating stress level of 2.27 MPa (Point A, Figure 2.5), going on to peak at 16.00 MPa (Point B, Figure 2.5). In contrast, the same fan running at half design speed had an initial alternating stress of 0.57 MPa (Point G, Figure 2.5), going on to peak at 4.00 MPa (Point H, Figure 2.5). As this chapter previously mentioned, at full speed the
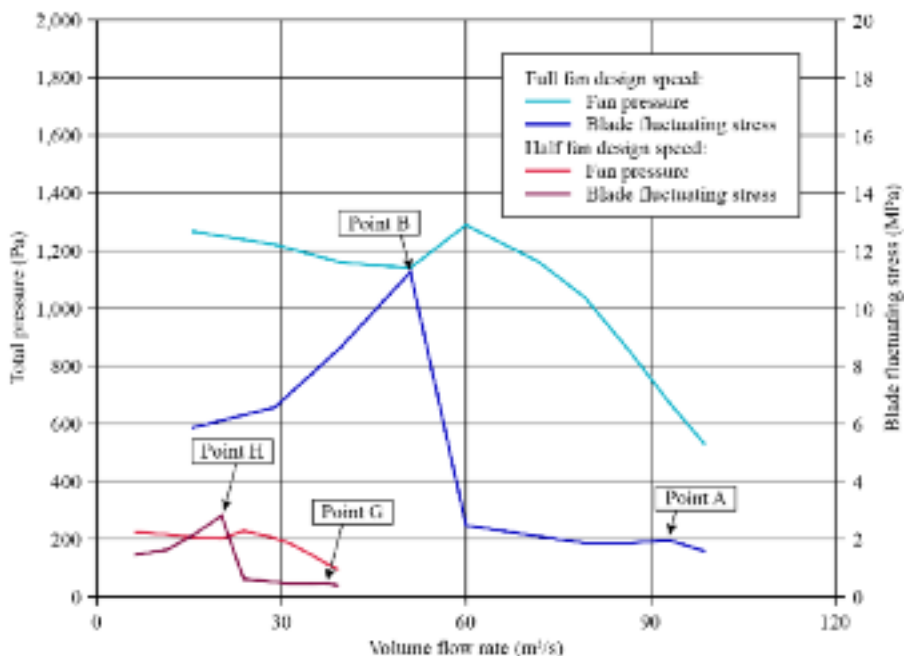
FIGURE 2.5. Stall characteristics of the studied fan with a stalling blade and without a fitted stabilisation ring at full and half design speed.

alternating stress increased to 3.53 MPa immediately prior to aerodynamic stall. As such a fan running at a speed of 100 per cent (with no aerodynamic stall in the event of a pressure pulse) would see a maximum alternating stress of 3.53 MPa. The same fan running at half design speed has a reduced pressure developing capability and so would in all probability stall in the presence of the same pressure pulse, and in doing so, be exposed to a peak alternating stress of 4.00 MPa.

In some metro tunnel ventilation systems, it is customary to operate tunnel ventilation fans at quarter design speed. The same alternating stress data for a fan with stalling blade angle and no fitted stabilisation ring is plotted for the fan running at half design speed, with alternating stress increasing from the initial alternating stress level of 0.57 MPa (Point G, Figure 2.6), going on to peak at 4.00 MPa (Point H, Figure 2.6). In contrast, the same fan running at quarter design speed had an initial alternating stress of 0.14 MPa (Point I, Figure 2.6), going on to peak at 1.00 MPa (Point J, Figure 2.5). The alternating stress level during aerodynamic stall at quarter design speed (1.00 MPa) is significantly lower then the alternating stress level during stable operation at full design speed (3.53 MPa) and, therefore, we concluded that it posed no risk to the fan's mechanical integrity.
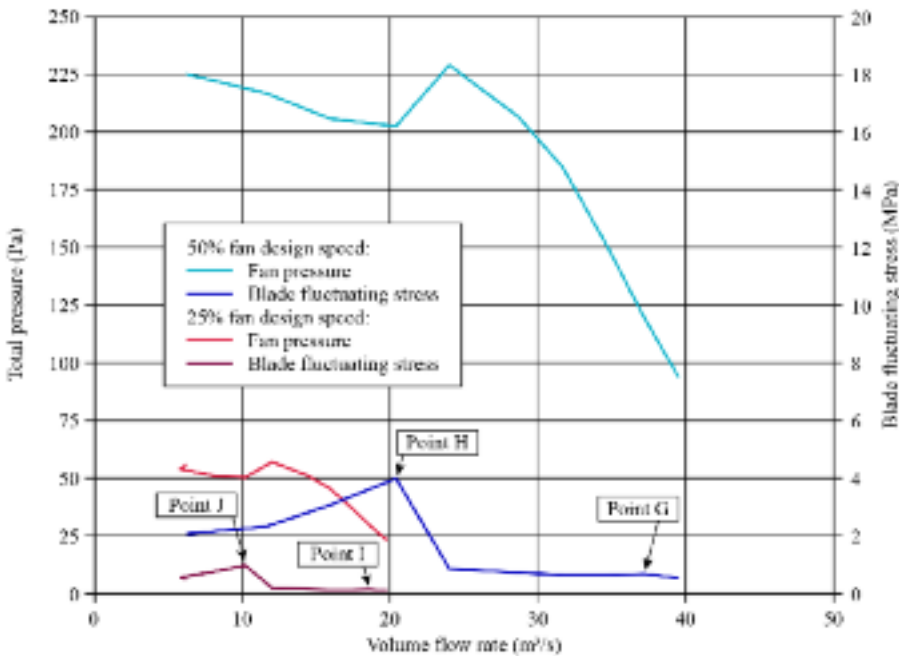
FIGURE 2.6. Stall characteristics of the studied fan with a stalling blade and without a fitted stabilisation ring at half and quarter design speed.

STRUCTURAL ANALYSIS

The term 'fatigue' refers to the phenomenon whereby virtually all materials will break under numerous stress repetitions that are not sufficient to produce an immediate rupture in the first instance. In this regard, fan blades are subject to fatigue stress induced by: (i) the mean force arising from rotation and aerodynamic loading and (ii) the alternating force produced by variations in lift as the fan rotates. The combination of mean and alternating blade forces result in mean and alternating blade stress. This makes the blades inherently susceptible to fatigue.

The endurance limit corresponding to any given range of stress variation has been the subject of extensive study, reviewed by amongst others Young (1989), as has the ability of a wide range of materials to withstand different combinations of mean and alternating stress. Manufacturers usually produce tunnel ventilation fan blades from aluminium and the ability of aluminium to resist fatigue for a fixed alternating stress reduces as mean stress increases. When researchers study material test data for various levels of mean and alternating stress, they derive a relationship known as the Gerber Line, Figure 2.7.

Gerber (1874) himself derived this line and proposed a parabolic relationship between alternating stress and mean stress in iron structures. The maximum alternating stress level(s) for any mean stress in the material, up to the tensile strength of the material, is given by the expression:

FIGURE 2.7. The curve of best fit through the limiting combination of alternating and mean stress is the Gerber Line (Gerber, 1874). Any combination of mean and alternating stress that falls outside the Gerber Line will result in a fatigue failure.

$$\pm s = \pm s_0 \left\{ 1 - \left(\frac{s_m}{s_t} \right)^2 \right\}$$

s_0 = Alternating stress level that constitutes the fatigue limit of the material with zero mean stress.

s_t = Tensile strength of the material.

s_m = Mean stress in the material.

The ability of a given aluminium alloy to resist the effect of mean and alternating stress is dependent on the maximum defect size in the material samples. The larger the defect, the lower the level of mean and alternating stress required to induce fatigue failure. Tunnel ventilation fan manufacturers, therefore, first experimentally establish the relationship between mean and alternating stress for a given defect size, and then undertake X-ray examination of all rotating components to ensure that the maximum defect size is below that on which they established the Gerber Line.

If the peak mean, alternating stress point is below the Gerber Line, the fan blade should not fail due to fatigue. However, in practice, there is some uncertainty about the location of all Gerber Lines as they are derived from experimental data. Additionally, the ability to calculate mean and alternating stress levels is imperfect as a consequence of assumptions during the modelling process. Therefore, in practice, tunnel ventilation fan designers classically choose to design fans with a safety factor of two. In this context, we define a safety factor of two as an alternating stress half that of the Gerber Line at a given value of direct stress.

We assessed the significance of the measured alternating stress results. The manufacturers designed the family of fans that we used in the reported research with direct and alternating stress levels that would fall on a Gerber Line calculated with a safety factor of two. We combined predicted direct and measured alternating stress levels for the fan operating on a stable part of its characteristic, with no fitted stabilisation ring and a stalling blade angle to give a safety factor of 2.3, Table 2.2. The experimentally derived safety factor was greater than two, giving confidence in the conservative nature of the manufacturers mechanical design methodology.

Throttling the fan until stall without a stabilisation ring resulted in increasing alternating stress. The resultant combination of direct and alternating stress is significantly beyond the Gerber Line, giving a safety factor of 0.3, Table 2.2. From this we may conclude that if this fan operated in the stalled condition for an extended period of time, it would suffer a fatigue related failure.

We measured direct and alternating stress levels during stable and stall conditions for the test fan with a stalling blade angle and a fitted stabilisation ring, Table 2.2. The reduction in alternating stress during stable operation resulted in the fan operating with a slightly higher safety factor of 2.5. In stalled operation, the alternating stress increased and, in so doing, reduced the safety factor to 1.1. As a safety factor of 1.1 is greater than one, the mechanical design of the tested fan can tolerate the increase in alternating stress. However, the uncertainty of the Gerber Line location is significant enough for a conservative tunnel ventilation fan designer to consider it low.

Table 2.2. *Safety factor derived from strain gauge data for a fan at full speed with a stalling blade angle, with and without a fitted stabilisation ring and with a non-stalling blade angle, without a fitted stabilisation ring.*

Fan type	Per cent design speed	Stable operation safety factor	Stalled operation safety factor
Plane casing, stalling blade angle	100	2.3	0.3
Anti-stall casing, stalling blade angle	100	2.5	1.1
Plane casing, non-stalling blade angle	100	2.4	1.5

We measured direct and alternating stress levels during normal and stall conditions for the test fan with a non-stalling blade angle and no stabilisation ring, Table 2.2. The increase in alternating stress compared to the same fan with stalling blade angle and a fitted stabilisation ring during stable operation resulted in the fan operating with a slightly lower safety factor of 2.4. In stalled operation the alternating stress increased and, in so doing, reduced the safety factor to 1.5. As a safety factor of 1.5 is greater than one, the mechanical design of the tested fan can tolerate the increase in alternating stress, and therefore, the risk of a fatigue induced mechanical fan failure is low.

Operating the fan at full, half and quarter design speed in both stable and stalled operation facilitated in the calculation of six safety factors, Table 2.3. This study reports a tunnel ventilation fan safety factor during stable operation at full design speed of 2.3, 0.3 higher than the desirable minimum. In a stalled condition, we reduced the safety factor to 0.3, which is significantly lower than 1.0. This indicates that if the fan continued to operate in stall at full design speed, the blades would suffer fatigue failure.

During normal operation, safety increased from 2.3 at full design speed to 10.0 at half design speed, a factor of approximately four. Mean stress in a fan blade reduces with the square of speed, therefore reducing speed by half would be expected to increase the safety factor by four. When we operated the fan at half design speed during stalled operation, the safety factor was 2.5, Table 2.3, an increase of more than six compared to the same fan operating in stall at full design speed. The increase in the safety factor is a consequence of the aerodynamically induced alternating stresses (when operating the fan in stall) falling more rapidly then the mean stress falls when we reduced fan speed from full to half design speed.

Table 2.3. *Safety factors derived from strain gauge data for a fan at full, half and quarter design speed without a fitted stabilisation ring.*

Fan type	Per cent design speed	Stable operation safety factor	Stalled operation safety factor
Plane casing, stalling blade angle	100	2.3	0.3
Anti-stall casing, stalling blade angle	50	10.0	2.5
Plane casing, non-stalling blade angle	25	106.0	7.3

The safety factor at half design speed when operating in stall (2.5) was slightly higher than the safety factor at full design speed in stable operation (2.3). As the safety factor at half design speed when operating in stall is higher then the safety factor of the same fan at full design speed in stable operation, we observed that the fan was less likely to fail mechanically at half design speed when operating in stall then when at full design speed in stable operation.

The above result is significant because tunnel ventilation fans in metro applications routinely operate at both half and quarter design speeds. As a consequence of the reduced pressure-developing capability of the fans at reduced speed, fans in railway tunnel and metropolitan metro applications are routinely driven into stall. The calculated safety factors at quarter design speed are so high during both stable and stalled operation that we can conclude that aerodynamic stall poses no threat to the mechanical integrity of the tunnel ventilation fan.

The above results indicate that the tested fan may operate at full design speed in the stable part of its characteristic, with a mechanical safety factor of 2.3. The same fan can operate also at half design speed in aerodynamic stall with a mechanical safety factor of 2.5. When we scale the fan characteristic to 90 per cent speed, the pressure developing capability reduced to the point where a 500 Pa pressure pulse would take the fan within five per cent of the fan's peak pressure developing capability.

Next, we scaled the direct stress from 50 to 55 per cent design speed, and recalculated the associated mechanical safety factor with operation in an aerodynamically stalled condition. The mechanical safety factor reduced from 2.5 at half design speed to 2.0 at 55 per cent design speed. From the above, we concluded that the tested fan could operate at up to 55 per cent design speed in aerodynamic stall, and down to 90 per cent design speed without stalling. As such, we observed that if tunnel ventilation system operators fitted this particular fan with a variable speed drive (VFD), the 'forbidden' speed range should be 55 to 90 per cent speed for the tested design point, assuming a 500 Pa pressure pulse.

STRATEGY FOR FAN SELECTION

The demand for new mass-transit systems generally, and metro systems in urban areas specifically, has increased rapidly over the last two decades and continues today. However, recent changes in market requirements for tunnel ventilation fans present fan designers with a challenge. The proposed tunnels for the next generation of mass transit systems are longer than the historic norm, and the trains that run in them are to run faster. These two factors result in mass transit systems requiring higher pressure ventilation fans (as the tunnels are longer) with the capability of operating under the influence of larger pressure pulses (as the trains are running faster).

An additional factor increasing the magnitude of pressure pulses in metro systems is the trend towards the use of platform screen doors. Platform screen doors at metro stations screen the platform from the train. They are a relatively new addition to metro systems, and are today in wide use in Asia and Europe. Passenger safety is

driving the adoption of platform screen doors. By separating the platform from the train, platform screen doors prevent the travelling public either accidentally or deliberately falling into the path of oncoming trains. Additionally, metros designed to use driver-less trains are only considered safe if platform screen doors are included in the design. Consequentially it is likely that an increasing proportion of new and refurbished metro stations will include platform screen doors.

Historically, a pressure of 1,200 Pa with pressure pulses of 300 Pa has been typical in tunnel ventilation system application. Today, a pressure of 1,500 Pa with pressure pulses of 500 Pa is typical. Increasing pressure and pressure pulse size increase the importance of tunnel ventilation fan selections that either avoid or manage the effect of fan stall.

A modern mass transit system in a busy urban area can have 500 trains a day passing each tunnel ventilation shaft. Consequently, the fans in those ventilation shafts are subjected to 500 pressure pulses a day, and therefore are potentially driven into stall each time. With a typical in-service life of 20 years, the probability of incorrectly selected fans for the application suffering a fatigue induced mechanical failure becomes high.

Tunnel ventilation fan designers have classically utilised one of three approaches during the selection of tunnel ventilation fans that must operate in the presence of pressure pulses:

- select a fan with a non-stalling blade angle, such that as the fan is driven out of its normal operating range, mechanical stress increases within manageable limits;
- select a fan with a high enough pressure developing capability to operate with a pressure pulse without stalling; and
- select a fan with a stabilisation ring, such that as the fan is driven out of its normal operating range, mechanical stress increases within the limit of the mechanical design.

All three fan selection strategies are valid, and tunnel ventilation system designers have used each for tunnel ventilation system design. The first strategy, a fan with a non-stalling blade angle is the most conservative selection strategy. One may select the fan close to its optimum operating point, without having to compromise the selection to accommodate a pressure pulse within the stable operating range.

The second strategy, a fan with a high enough pressure developing capability to operate with a pressure pulse without stalling, works well with smaller pressure pulses. However, as the size of the pressure pulse increases, the fan's operating point moves further from the optimum resulting in a less efficient fan selection. Despite the reservation about fan efficiency, this strategy avoids the fan stalling completely in the event of foreseen events. Tunnel ventilation system designers who are confident in their ability to predict the conditions under which the fans will operate during all tunnel ventilation system scenarios favour this second strategy.

The third strategy, a fan with a fitted stabilisation ring, works well with larger pressure pulses, allowing fan selection close to its peak aerodynamic efficiency, and

then effectively managing the mechanical consequences of driving into stall under the influence of pressure pulses. Tunnel ventilation system designers who favour this strategy argue that it is not possible to guarantee that the fan will never drive into stall; therefore, a stabilisation ring that provides mechanical protection in the event of aerodynamic stall is prudent. The tunnel ventilation system designers who favour this approach cite the possibility that occasionally two trains might pass close to a ventilation shaft, effectively doubling the size of the pressure pulse. To facilitate comparison of the three strategies, we have made assumptions typical of a present day urban area metro system, Table 2.4.

When considering the required pressure, flow and size of the pressure pulse, the first strategy, a fan with a non-stalling blade angle, results in a fan of 2.5 metre diameter with a design point efficiency of 71 per cent, Figure 2.8. The second strategy, a fan that can accommodate the pressure pulse, results in a fan of 1.8 metre diameter with a design point efficiency of 66 per cent, Figure 2.9. The third strategy, use of a stabilisation ring, results in a fan of 2.24 metre diameter with a design point efficiency of 69 per cent, Figure 2.10.

We can combine the capital cost of each fan selection strategy with the Table 2.4 assumptions to calculate through-life cost of each strategy, Table 2.5. We define the initial capital cost in Table 2.5 as the initial cost of purchasing and installing the ventilation fan. Table 2.5 defines operating cost as the cost of fan purchase and installation plus electricity costs over ten years, based on Table 2.4 assumptions. To facilitate a direct comparison between initial capital cost and operating cost, Table 2.5 presents the net present value of operating costs.

As previously mentioned, different tunnel ventilation system designers favour different fan selection strategies. However, all three strategies have reliable in-service records. In this example, the largest fan (Strategy One) has the lowest operating cost over ten years, Table 2.5, despite not having the highest initial cost, making this selection strategy attractive to those seeking the lowest cost of ownership.

In this example, the smallest fan (Strategy Two) has the highest operating cost over ten years, Table 2.5, despite having the lowest initial cost, making this selection strategy apparently unattractive to those seeking lowest cost of ownership. However, if one accounts for the cost of excavating an underground plant room, the cost of building a plant room for a 2.5 metre diameter fan (Strategy One) may be signifi-

Table 2.4. *Factors impacting on fan capital and through life cost.*

Design point pressure	1,500 Pa
Pressure pulse	500 Pa
Design point flow	85 m^3/s
Fan type	Reversible, 300°C for 2 hours
Running hours per year	4,400 (12 hours a day)
Cost of electricity	0.04 £ per kW/hour
Cost of capital	8%
Period of assessment	10 years

Table 2.5. *Capital cost and ten year through life cost of each selection strategy.*

	Diameter, D (m)	Efficiency, η	Fan investment cost (£)	Power, P_m (kW)	Electricity cost/year (£)	Electricity cost (10 yrs) (£)	Total fan and running costs (£)	Running cost as a percentage of total cost
Strategy 1	2.5	71%	28,500	185	32,412	217,488	245,988	88%
Strategy 2	1.8	66%	23,000	214	37,493	251,582	274,982	92%
Strategy 3	2.24	69%	32,000	190	33,288	223,366	255,366	87%
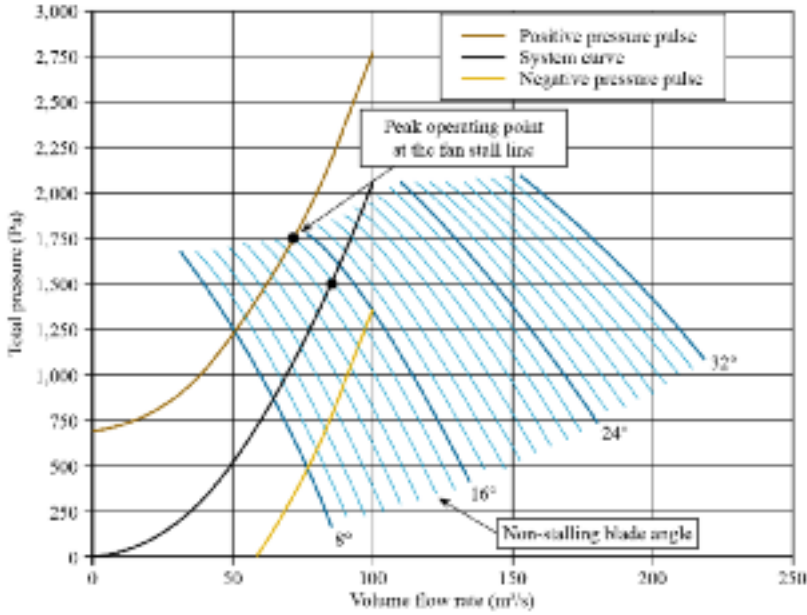
FIGURE 2.8. Optimum fan selections for a common duty point, fan selection Strategy One: non-stalling blade angle.
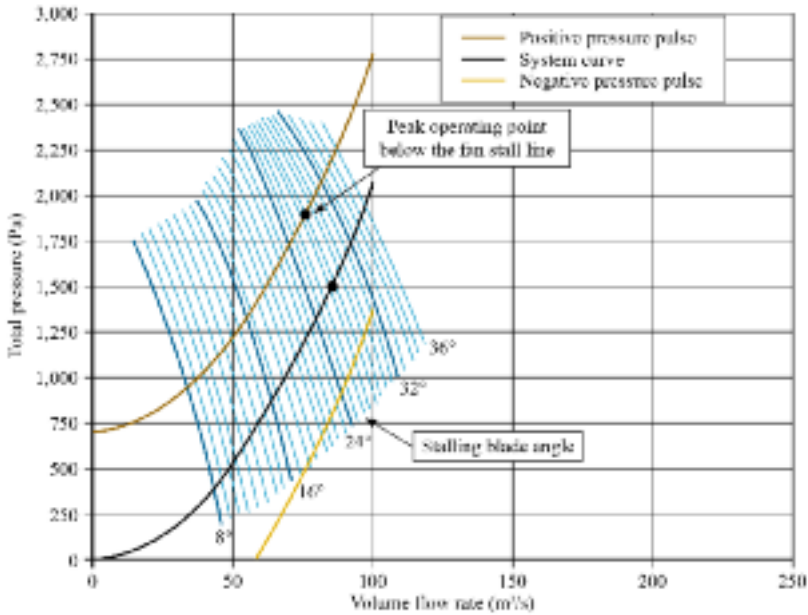
FIGURE 2.9. Optimum fan selections for a common duty point, fan selection Strategy Two: high pressure capability.
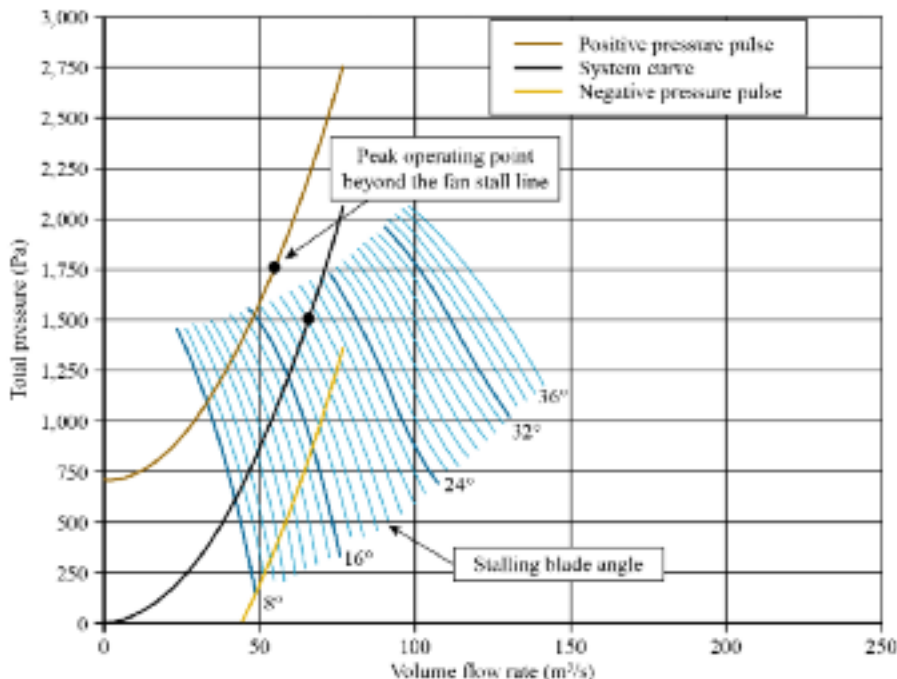
FIGURE 2.10. Optimum fan selections for a common duty point, fan selection Strategy Three: stabilisation ring.

cantly higher than the cost of building a plant room for a 1.8 metre diameter fan (Strategy Two), therefore making the second selection strategy attractive.

In this example, the medium size fan (Strategy Three) has the highest initial cost, Table 2.5, reflecting the manufacturer's cost of a fan casing with a stabilisation ring. Operating costs fall between costs for Strategies One and Two, reflecting the efficiency of the medium sized fan that is between those of the largest and smallest.

Stabilisation rings can reduce the fan's efficiency, due to the recirculating flow in the blade tip region (Corsini *et al.*, 2014). For fans intended for use at ambient temperature only, the reduction in efficiency can be up to five per cent. In this study, we have assumed that the fans associated with each strategy are designed in accordance with the requirements of EN 12101-3 (2002) and ISO 21927-3 (2006) for once-only emergency operation at 300°C. The use of aluminium blade results in the blades expanding more rapidly then the steel casing as temperature rises. Consequently, the blade tip-to-casing clearance has to increase at ambient temperature to prevent it closing at high temperature. The increase in blade tip-to-casing gap from typically 0.25 per cent of fan diameter (for ambient duty only) to 0.45 per cent (for once-only 300°C emergency duty) reduces fan efficiency. In practice, the stabilisation ring would typically reduce efficiency by between two and three per cent when a fan has a large tip gap to facilitate high temperature operation. Consequently, the fan that we used in this study confirms the general rule of thumb that larger fans are more efficient for a fixed duty point.

SUMMARY AND CONCLUSIONS

The experimental results presented in this chapter are significant in that they provide insight into a likely reason for tunnel ventilation fans' in-service failure. In this study, the alternating stress level with fan operation in aerodynamic stall with a fitted stabilisation ring resulted in alternating stress increasing, and consequently, the mechanical safety factor reducing from 2.5 to 1.1. This increase is significant within the context of a smoothly rising fan characteristic that provided little indication that alternating stress had increased.

The smoothly rising fan characteristic resulted in Bard (1984) claiming that 'unstable performance due to stalling is completely eliminated'. As Bard conducted a purely aerodynamic programme, making no measurement of steady or alternating stress, we may assume that when Bard referred to 'unstable performance' he was referring to unstable aerodynamic performance. However, the claim may have resulted in some fan designers assuming that mechanical stress would also remain stable.

A tunnel ventilation fan with a non-stalling blade angle classically exhibits a continually rising characteristic. In effect, the fan blade aerodynamic loading is light enough that the fan does not suffer a classical aerodynamic stall. Alternating stress in a fan blade with a non-stalling blade angle when operated in the unstable region of the fan characteristic does increase compared to the same fan operating in the stable region. Mechanical safety factor reduces from 2.4 to 1.5, and although any reduction in safety factor is undesirable, a safety factor of 1.5 is, nevertheless, high enough to make stalled operation possible, without suffering a fatigue related mechanical failure.

The experimental results for both the stalling blade angle with fitted stabilisation ring and non-stalling blade angle with no stabilisation ring both result in mechanical safety factors that are less then the industry norm of 2.0. As such, we can regard both a stabilisation ring and non-stalling blade angle as methods to mechanically protect a tunnel ventilation fan in the event of an unforeseen stall event. If the fan application is one in which the fan will routinely drive into stall, then the prudent fan designer would increase the mechanical safety factor during stable operation to ensure that it did not fall below 2.0 during stalled operation.

The practice of selecting tunnel ventilation fans to accommodate pressure pulses within the stable part of the fan characteristic avoids the associated mechanical risk with operating tunnel ventilation fans in the stalled condition. However, this approach requires the tunnel ventilation system designer to foresee how the tunnel will operate for the life of the ventilation system. The current practice of fitting platform screen doors to historic metros when they are refurbished has significantly increased the magnitude of pressure pulses. This increase carries with it the consequent risk that tunnel ventilation fans that the pressure pulse did not previously drive into stall will now be driven into stall.

Additionally, fans that are correctly selected to operate within the stable part of their characteristic at full design speed will likely drive into stall if operated at half design speed and certainly drive into stall if operated at quarter design speed. In this chapter, we were able to demonstrate that for a tunnel ventilation fan with a stalling blade angle, without a fitted stabilisation ring, the mechanical factor of

safety during stable operation is 2.3. When we operated the same fan at half speed in an aerodynamically stalled condition, the mechanical factor of safety is 2.5. As the mechanical factor of safety at half speed during stalled operation is higher then the mechanical factor of safety at full speed during stable operation, we conclude that users can operate this tunnel ventilation fan at half speed in an aerodynamically stalled condition without risk of a fatigue related mechanical failure. At quarter design speed, mechanical factors of safety in both stable and aerodynamically stalled operation are sufficiently high that there is no risk of a fatigue related mechanical failure.

We conducted the current study on a single fan, and it is therefore not possible to generalise the findings to all fan types. Despite the limitations of the current study, the seven fold increase in alternating stress (from 2.27 MPa to 16 MPa) that we observed in the tested fan with a stalling blade angle and without a fitted stabilisation ring is consistent with the conclusions of Rippl's (1995) research. Despite the difficultly in generalising results of the reported research, it is possible to observe that if the fan is to operate reliably, the mechanical design must account for the increase in alternating stress when the fan stalls. Not doing so could result in the fan's fatigue related mechanical failure.

When accounting for the increase in alternating stress when a fan stalls, and when assessing if that increase is acceptable, the tunnel ventilation fan designer must make an assumption about the maximum defect size in the fan blades and hub. Therefore, responsible fan manufacturers 100 per cent X-ray inspect all fan blades and hubs to verify that they do not exceed the fan designer's assumptions regarding maximum defect size.

Last, we conclude that the three fan selection strategies classically used by tunnel ventilation system designers each have specific advantages and disadvantages. The optimum fan selection strategy in a specific application will, therefore, depend on the impact of fan diameter on plant room cost, and the relative importance of fan initial cost and fan operating cost.

REFERENCES

EN 12101-3, 2002, Smoke and Heat Control Systems. Specification for Powered Smoke and Heat Exhaust Ventilators.

ISO 21927-3, 2006, Smoke and Heat Control Systems — Part 3: Specification for Powered Smoke and Heat Exhaust Ventilators.

ISO 5801:2007, 2007, Industrial Fans — Performance Testing using Standardized Airways.

Bailey, E.E., and Voit, C.H. (1970), "Some Observations of Effects of Porous Casings on Operating Range of a Single Axial-flow Compressor Rotor", Report NASA-TM-X-2120.

Bard, H. (1984), "The Stabilisation of Axial Fan Performance", *Proceedings of the Institution of Mechanical Engineers (IMechE) Conference 1984–4 on the Installation Effects in Ducted Fan Systems*, London, UK, 1–2 May, paper no. C120/84, pp. 100–106.

Bianchi, S., Corsini, A., and Sheard, A.G. (2010), "Detection of Stall Regions in a Low-speed Axial Fan, Part 1: Azimuthal Acoustic Measurements", *Proceedings of the 54th American Society of Mechanical Engineers Turbine and Aeroengine Congress*, Glasgow, Scotland, 14–18 June, paper no. GT2010-22753.

Boyes, W. (Ed.) (2003), *Instrumentation Reference Book*, Butterworth Heinemann, Oxford, UK.

Bright, M.M., Qammar, H., Vhora, H., and Schaffer, M. (1998), "Rotating Pip Detection and Stall Warning in High-speed Compressors Using Structure Function", *Proceedings of AGARD RTO AVT Conference*, Toulouse, France, 11–15 May.

Camp, T.R., and Day, I.J. (1998), "A Study of Spike and Modal Stall Phenomena in a Low-speed Axial Compressor", *Transactions of the ASME, Journal of Turbomachinery*, vol. 120, pp. 393–401.

Corsini, A., Delibra, G., Sheard, A.G., and Volponi, D. (2014), "Investigation on Anti-stall Ring Aerodynamic Performance in an Axial Flow Fan", *Proceedings of the 59th American Society of Mechanical Engineers Turbine and Aeroengine Congress*, Dusseldorf, Germany, 16–20 June, paper no. GT2014-25794.

Cumpsty, N.A. (1989), "Part-circumference Casing Treatment and the Effect on Compressor Stall", *Proceedings of the 34th American Society of Mechanical Engineers Gas Turbine and Aeroengine Congress*, Toronto, ON, Canada, 11–14 June, paper no. 89-GT-312.

Day, I.J., and Cumpsty, N.A. (1978), "The Measurement and Interpretation of Flow Within Rotating Stall Cells in Axial Compressors", *Proceedings of the Institution of Mechanical Engineers, Part C, Journal of Mechanical Engineering Science*, vol. 20, pp. 101–14.

Deppe, A., Saathoff, H., and Stark, U. (2005), "Spike-type Stall Inception in Axial Flow Compressors", *Proceedings of the 6th Conference on Turbomachinery, Fluid Dynamics and Thermodynamics*, Lille, France, 7–11 March.

Emmons, H.W., Pearson, C.E., and Grant, H.P. (1955), "Compressor Surge and Stall Propagation", *Transactions of the ASME*, vol. 77, pp. 455–69.

Gelmedov, F.S., Lokshtanov, E.A., Olstain, L.E-M., and Sidorkin, M.A. (1998), "Anti-stall Tip Treatment Means", US Patent 5,762,470, 9 June.

Gerber, W.Z. (1874), "Calculation of the Allowable Stresses in Iron Structures", *Z. Bayer Architecture and Engineering*, vol. 6, pp. 101–10.

Gravdahl, J.T., and Egeland, O. (1999), *Compressor Surge and Rotating Stall: Modelling and Control*, Springer Verlag, London, UK.

Greitzer, E.M. (1980), "Review — Axial Compressor Stall Phenomena", *Transactions of the ASME, Journal of Fluids Engineering*, vol. 102, pp. 134–51.

Greitzer, E.M., Nikkanen, J.P., Haddad, D.E., Mazzawy, R.S., and Joslyn, H.D. (1979), "A Fundamental Criterion for the Application of Rotor Casing Treatment", *Transactions of the ASME, Journal of Fluids Engineering*, vol. 101, pp. 237–43.

Griffin, R.G., and Smith, L.H., Jr. (1966), "Experimental Evaluation of Outer Case Blowing or Bleeding of a Single Stage Axial Flow Compressor, Part I — Design of Rotor Blowing and Bleeding Configurations", NASA Report CR-54587.

Hathaway, M.D. (2007), "Passive Endwall Treatments for Enhancing Stability", Report NASA/TM-2007-214409.

Ivanov, S.K. (1965), "Axial Blower", US Patent 3,189,260, 15 June.

Karlsson, S., and Holmkvist, T. (1986), "Guide Vane Ring for a Return Flow Passage in Axial Fans and a Method of Protecting It", US Patent 4,602,410, 29 July.

Kang, C.S., McKenzie, A.B., and Elder, R.L. (1995), "Recessed Casing Treatment Effects on Fan Performance and Flow Field", *Proceedings of the 40th American Society of Mechanical Engineers Gas Turbine and Aeroengine Congress*, Houston, TX, USA, 5–8 June, paper no. 95-GT-197.

Khalid, S.A., Khalsa, A.S., Waitz, I.A., Tan, C.S., Greitzer, E.M., Cumpsty, N.A., Adamczyk, J.J., and Marble, F.E. (1999), "Endwall Blockage in Axial Compressors", *Transactions of the ASME, Journal of Turbomachinery*, vol. 121, pp. 499–509.

Khalid, S.J. (1996), "Compressor Endwall Treatment", US Patent 5,520,508, 28 May.

Koch, C.C., and Smith, L.H. (1976), "Loss Sources and Magnitudes in Axial Compressors", *Transactions of the ASME, Journal of Engineering and Power*, vol. 98, pp. 411–24.

Koff, S.G., Mazzawy, R.S., Nikkanen, J.P., and Nolcheff, A. (1994), "Case Treatment for Compressor Blades", US Patent 5,282,718, 1 February.

Miyake, Y., Kata, T., and Inaba, T. (1987), "Improvement of Unstable Characteristics of an Axial Flow Fan by Air-separator Equipment", *Transactions of the ASME, Journal of Fluids Engineering*, vol. 109, pp. 36–40.

Moore, F.K. (1984), "A Theory of Rotating Stall of Multistage Compressors, Parts I–III", *Transactions of the ASME, Journal of Engineering for Power*, vol. 106, pp. 313–36.

Nolcheff, N.A. (1996), "Flow Aligned Plenum Endwall Treatment for Compressor Blades", US Patent 5,586,859, 24 December.

Prince, D.C., Wisler, D.D., and Hilvers, D.E. (1974), "Study of Casing Treatment Stall Margin Improvement Phenomena", NASA Report CR-134552, March.

Rippl, A. (1995), "Experimentelle Untersuchungen zuminstationaren Betriebsverhahen an der Stabilitarsgrenze eines mehrstufigen transsonischen Verdichters", PhD dissertation, Ruhr-Universität Bochum.

Saathoff, H., and Stark, U. (2000), "Tip Clearance Flow Induced Endwall Boundary Layer Separation in a Single-stage Axial-flow Low-speed Compressor", *Proceedings of the 45th American Society of Mechanical Engineers Gas Turbine and Aeroengine Congress*, Munich, Germany, 8–11 May, paper no. 2000-GT-501.

Sheard, A.G., Corsini. A., Minotti, S., and Sciulli, F. (2009), "The Role of Computational Methods in the Development of an Aero-acoustic Design Methodology: Application in a Family of Large Industrial Fans", *Proceedings of the 14th International Conference on Modelling Fluid Flow Technologies*, Budapest, Hungary, 9–12 September, pp. 71–9.

Sheard, A.G., Corsini, A., and Bianchi, S. (2010), "Method of Detecting Stall in an Axial Fan", GB Patent 468 571 B, 24 December.

Sheard, A.G., Corsini, A., and Bianchi, S. (2011), "Stall Warning in a Low-speed Axial Fan by Visualisation of Sound Signals", *Transactions of the ASME, Journal of Engineering for Gas Turbines and Power*, vol. 133, paper no. 041601, pp. 1–10.

Takata, H., and Tsukuda, Y. (1977), "Stall Margin Improvement by Casing Treatment — Its Mechanism and Effectiveness", *Transactions of the ASME, Journal of Engineering for Power*, vol. 99, pp. 121–33.

Turner, R.C. (1955), "Improvements in or Relating to Gas Turbines", US Patent 826,669, 18 July.

Vo, H.D., Tan, C.S., and Greitzer, E.M. (2005), "Criteria for Spike Initiated Rotating Stall", *Proceedings of the 50th American Society of Mechanical Engineers Gas Turbine and Aeroengine Congress*, Reno, NV, USA, 6–9 June, paper no. GT2005-68374.

Wasserbauer, C.A., Weaver, H.F., and Senyitko, R.G. (1995), "NASA Low-Speed Axial Compressor for Fundamental Research", NASA Technical Memorandum 4635, July.

Wilde, G.L. (1950), "Improvements in or Relating to Gas Turbines", US Patent 701,576, 28 June.

Wisler, D.C., and Hilvers, D.E. (1974), "Stator Hub Treatment Study", NASA Report CR-134729, December.

Yamaguchi, N., Ogata, M., and Kato, Y. (2010), "Improvement of Stalling Characteristics of an Axial-flow Fan by Radial Vaned Air Separator", *Transactions of the ASME, Journal of Turbomachinery*, vol. 132, 021015, 10 pages.

Young, W.C. (1989), *Roark's Formulas for Stress and Strain*, McGraw-Hill, New York, NY, USA.

Stall Inception, Evolution and Control in a Low-speed Axial Fan with Variable Pitch in Motion

S. Bianchi, A. Corsini, L. Mazzucco,
L. Monteleone, and A.G. Sheard

ABSTRACT

Obtaining the correct blade pitch angle is crucial in ensuring that an industrial fan operates only within the stable region of its operating range. This chapter focuses on the inception and evolution of flow instabilities which drive the transition from the stable to unstable region. We conducted an experimental study to investigate the inception patterns and evolution of rotating stall at different blade pitch angle settings with the aim of characterising the associated physical flow mechanisms. The reported research utilised a variable pitch in motion fan that enabled us to change the blade pitch angle whilst the fan rotated at a constant speed. We drove the fan into stall at the design pitch angle setting and then operated the variable pitch in motion mechanism to recover the fan from unstable back to stable operation. We measured pressure fluctuations in the fan's blade tip region using flush mounted unsteady pressure probes. We studied the measured pressure signals, cross-correlated them and analysed their cross-spectra. Thus, we were able to clarify the impact of pitch angle, end-wall flow and tip-leakage flow on stall inception during the transition from stable to unstable, and then back to stable operation. We observed a rotating instability near the maximum pressure-rise point at both design and low pitch angle settings. We concluded that the stall inception patterns exhibited a spike type form at design pitch angle as a result of an interaction between the incoming flow, tip-leakage flow and end-wall flow.

NOMENCLATURE

Latin letters

BPF	customary blade passing frequency of the fan rotor	Hz
D_t	tip diameter	mm
f	signal frequency	Hz
H_b	blade height	mm
ℓ_t	blade chord at the tip	mm
NR	Nyquist rate	Hz
P	power	kW
p	static pressure	Pa
p_n	nominal design pressure	Pa
Q	volume flow rate	m3/s
Q_n	nominal design flow rate	m3/s
T	temperature	°C
t	absolute time	s
U_{tip}	tip speed	m/s
VPIM	variable pitch in motion	

Greek letters

δ_h	hub pitch angle	
η_{tot}	efficiency based on total pressure rise	
θ	microphone's azimuthal position	
Σ	solidity	
τ	tip gap (% of the blade chord at tip)	

INTRODUCTION

The current trend toward increased pressure rise and blade aerodynamic loading reduces the stable operating range of fans and compressors, both of which are limited by the onset of aerodynamic instabilities when throttling the flow rate. Researchers have studied the detection and analysis of these different forms of aerodynamic instabilities for several decades. Numerous studies have clarified the physical flow mechanisms underlying axial flow compressors' rotating stall (Day and Cumpsty, 1978; Greitzer, 1980; Moore, 1984). Emmons *et al*.'s earlier work (1955) was one of the first attempts to describe the mechanisms underlying the propagation of rotating stall.

According to Gravdahl and Egeland (1999), compressors exhibit two main types of aerodynamic flow instability: (i) 'rotating stall' in which regions of reversed flow occur locally and (ii) 'surge' which is characterised by periodic backflow over the entire annulus involving violent oscillations in the compression system. Rotating stall is a mechanism by which the rotor adapts to a reduction in flow rate. This results in circumferentially non-uniform flow patterns rotating in the annulus. In reviewing the evolution of rotating stall, Cumpsty (1989) noted that the drop in overall perfor-

mance can occur as a so-called 'progressive stall' or an 'abrupt stall.' Engineers usually associated the former with a part-span stall which results in a small performance drop; whereas, they associate the latter with a full-span stall and a large drop in performance. Notably, the part-span rotating stall occurs typically in single blade rows (Cumpsty, 1989) and usually leads to more complex disturbances in single-rotor or single-stage machines than in multi-stage compressors (Moore, 1984).

All of these forms of instability place considerable mechanical stress on the rotors involved, which can eventually lead to mechanical failure. Researchers have reported that strain gauge measurements on axial compressors (Rippl, 1995) and fans (Sheard and Corsini, 2012) have bending stress in vanes exceeding stable operation by a factor of five and seven respectively under 'rotating stall' conditions. This leads to the fan blades' rapid fatigue failure. In contrast, a 'surge' can lead to an increased magnitude of bending stress enough to cause a mechanical failure during the surge event itself.

The mechanical stress on axial-fan blades caused by stalled operation can be higher in the case of industrial fans intended for high-temperature operations such as those used in tunnel ventilation systems (Sheard *et al*., 2009). To ensure reliable operation in the event of a tunnel fire, both the Euro Norm EN 12101-3 (EN 12101-3, 2002) and the international standard ISO 21927-3 (ISO 21927-3, 2006; Sheard and Jones, 2008) require fans to have a larger blade tip-to-casing clearance. An increased blade tip-to-casing clearance has a beneficial effect in facilitating a fan's high-temperature operation in the event of a tunnel fire. However, it also has a detrimental effect on the fan's aerodynamic and aero-acoustic performance during routine operation.

Several studies have suggested that both high-speed compressor and low-speed axial fans' tip flow features are directly responsible for generating short wave-length disturbances (also called 'spikes' or 'pips'). These short wave-length disturbances are associated with the inception of localised part-span stall cells (Camp and Day, 1998; Deppe *et al*., 2005; Vo *et al*., 2005). Cumpsty (1989) correlated this inception mechanism with a change in the fan's acoustic emissions in the blade-tip region. Other scholars have utilised an array of azimuthally distributed probes in an attempt to link centrifugal pump and compressors' measured unsteady pressure in the blade tip region to their acoustic signatures (Mongeau *et al*., 1995; Bright *et al*., 1998). Similarly, Kameier and Neise (1997) established a link between tip-clearance noise and associated blade-tip flow instabilities in axial turbo-machinery by correlating rotating sources and vortex mechanisms with rotating stall cells.

A review of the extant literature suggested that a potential key to stability control and performance improvement in decelerating turbomachinery could come from managing the blade pitch. Active pitch control has the potential to interrupt stall development and facilitate its recovery, and therefore, is worthy of study.

During the early 1970s, General Electric produced a proposal for a variable pitch in motion system for turbofan engines (Gall, 1975). Engineers routinely use this technology in low-speed industrial fan applications in order to improve operating range (Sheard, 2012). Recently, Langston (2009) highlighted how a variable pitch in motion capability will be of interest again for reducing fuel consumption in high by-pass ratio turbofans intended for civil aviation application.

The research in this chapter focuses on elucidating the physical flow mechanisms that occur with the stall precursors responsible for stall inception. This chapter establishes the studied fan's stable and unstable characteristics using flush-mounted microphones placed at two azimuthal positions around the casing. We used the microphones as unsteady pressure probes, measuring unsteady pressure whilst throttling the fan from: (i) stable aerodynamic operation, (ii) incipient stall, and finally (iii) rotating stall. We used the variable pitch in motion system to recover from the stall and then analysed unsteady pressure data in order to qualify the fan behaviour under the three studied fan operating conditions. We established spatial and temporal correlations between rotating instabilities which facilitated an analysis of stall inception and recovery.

EXPERIMENTAL FACILITY

We undertook this research using an 18 blade fan with highly twisted C4 profile blades and equipped with a mechanism for varying the blade pitch angle whilst the fan rotated at its design speed, Table 3.1. The industrial fan community refers to any fan fitted with this mechanism as a variable pitch in motion (VPIM) fan. Design engineers originally developed variable pitch in motion fans in the 1950s for application in coal-fired power boilers. The coal's variable calorific value results in a variation in boiler pressure. Maintaining boiler pressure within safe limits requires a boiler's forced- and induced-draft fans to have the ability to respond rapidly to changing flow-rate demand. The size and, therefore, inertia of these forced- and induced-draft fans was high, thus the fan speed could not change quickly enough to follow demand. Consequently, the engineers developed constant speed variable pitch in motion fans. Despite the mechanical complexity of variable pitch in motion fans, they still find wide-spread application in coal-fired power boilers. The cost of high power variable-speed drives remains high. Consequently fixed-pitch variable speed forced- and induced-draft fans are not favoured.

Table 3.1. *Fan geometry and operating point data.*

Design speed	700 rpm
Tip speed	55.13 m/s
Design pressure, p_n	350–400 Pa
Design flow rate, Q_n	12–14 m^3/s
Efficiency based on total pressure rise, η_{tot}	0.92
Tip diameter, D_t	1,500 mm
Blade height, H_b	450 mm
Blade chord at the tip, ℓ_t	105 mm
Hub pitch angle, δ_h	80°–40°
Tip gap, τ (% of the blade chord at tip)	1.3%
Blade count	18
Solidity, Σ	0.6

The studied fan's blade tip-to-casing clearance ranged between 1.3 per cent and 2.0 per cent of blade-tip chord. The blade tip-to-casing clearance's precise value was dependent on the blade pitch angle. The variable pitch in motion mechanism was housed in the fan's spinner, and consisted of two remotely controllable oil-damped actuators. This pair of actuators was linked to a ring that was connected to each of the 18 fan blades. Changes in the ring's axial position resulted in a change in the blades' pitch angle. The variable pitch in motion mechanism was capable of changing blade pitch angle at up to 1.5 degrees per second.

Test rig facility

We conducted the tests in a test facility designed to comply with the ISO 5801:2007 standard, equivalent to the British Standard BS 848 Part 1 (ISO 5801, 2007). We operated the fan in casings made from cast and machined steel rings. A 270-kW direct coupled-induction 400 Volt (AC), three-phase electric motor drove the studied fan at its design speed, 700 rpm. Here, the blade tip speed was 55.13 metres per second and the associated blade passing frequency was 210 Hz. We used an inverter to bring the fan up to its design speed as the variable pitch in motion system was fragile, and therefore, we could not start the fan direct-on-line.

We utilised a fan test facility equipped to undertake a range of aerodynamic and structural testing, Table 3.2. The studied fan was a scale model of a variable pitch in motion fan typical of a forced- or induced-draft fan used in coal-fired boiler application, reducing the required test facility size to a practical scale, Table 3.3. The fan duct exhausted into the test facility's plenum chamber, equipped with a throttling valve to provide a mechanism for changing the fan pressure rise, Figure 3.1. A convergent-divergent NACA standard nozzle, instrumented for measuring temperature, pressure and air-speed, then discharged the airflow from the throttling valve.

Table 3.2. *Specification of the test rig utilised in the reported research.*

Mode	Length (m)	Power, P (kW)	Diameter, Dt (m)	Speed, n (rpm)	Temperature, T (°C)
Stand-alone	50	350	4	-	-
Thrust	-	350	1.6	-	-
Spin testing	-	810	4	5,000	-
High temperature	6	350	3.6	-	400

Table 3.3. *Specification of the fan test-rig pressure chamber.*

Volume flow rate (m³/s)	Pressure (Pa)	Width (m)	Length (m)	Height (m)
50	50,000	4	4	9
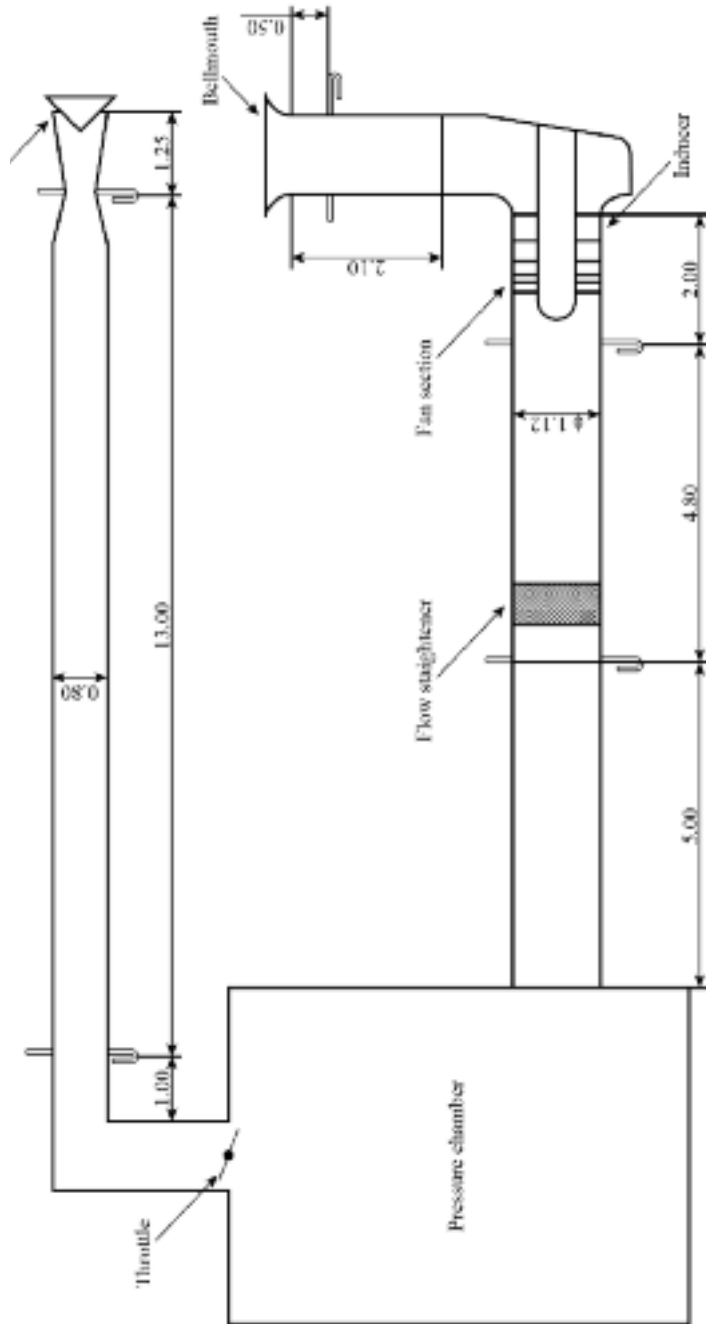
FIGURE 3.1. A schematic layout of the ISO 5801 (2007) standard ducted test rig used to characterise the studied fan.

We measured the fan performance at blade pitch angles of 50, 60 and 70 degrees in accordance with the ISO 5801:2007 standard (2007), Figure 3.2. We measured the pressure to an accuracy of ±0.5 per cent of data for all pressure transducers. By throttling downstream from the fan rotor, we were able to produce the aerodynamic instabilities of interest. During the volume-flow throttling, the fan transitioned from stable to unstable operation, but remained in rotating stall without going into surge. The rotor's aerodynamic load and the downstream plenum geometry ensured that the system could not develop a counter-pressure able to induce a surge. The B parameter's value for the plenum system was 0.15, well below Greitzer's suggested threshold value (1976) for axial compressor rigs.

Instrumentation and data acquisition system

We instrumented the fan rotor casing with two inserts, each containing a 15 mm diameter microphone as high sensitivity unsteady pressure probes. The inserts secured the microphones by reducing the opening over the blades to 10 mm, with the resulting microphone position 1 mm recessed into the insert. The microphone's axial location in each insert positioned it over the blades at 50 per cent blade chord, equidistant from both the blade leading and trailing edge.

Gravdahl and Egeland (1999) concluded that rotating stall is a mechanism by which the rotor adapts to a reduction in flow rate, resulting in circumferentially non-uniform flow patterns rotating in the annulus. In order to study these patterns, we chose to fit two microphones at azimuthal positions 60 degrees off-set, Figure 3.3. We used B&K 4190 microphones with a sensitivity 26.2 dB at 1 Volt per Pascal. Bianchi *et al*. (2010) had previously used this microphone as a high sensitivity unsteady pressure probe which was effective when characterising the physical flow mechanisms at play within the studied fan's blading. We used charge amplifiers to condition the microphones. We logged microphone output using a National Instruments NI Compact Acq. 9172 data acquisition system fitted with NI 9205 analogue input modules.

We calibrated the microphones and data acquisition system in accordance with ISO IEC60651 requirements (1994). We estimated the combined measurement error as 0.1 to 0.2 dB at 1 kHz. Additionally, the flow's high turbulence level over the studied fan's blades contributed to the overall uncertainty of the measurements. Following Corsini and Rispoli's method (2005), we estimated that this turbulence induced error in measured pressure at two per cent of reading.

We sampled each channel at 10 kHz for the 150 second duration of each test where we held the fan at a fixed blade pitch and throttled it to reduce the flow rate until the fan stalled. We then used the fan's variable pitch in motion system to reduce blade angle until the fan returned from stalled to stable operation.
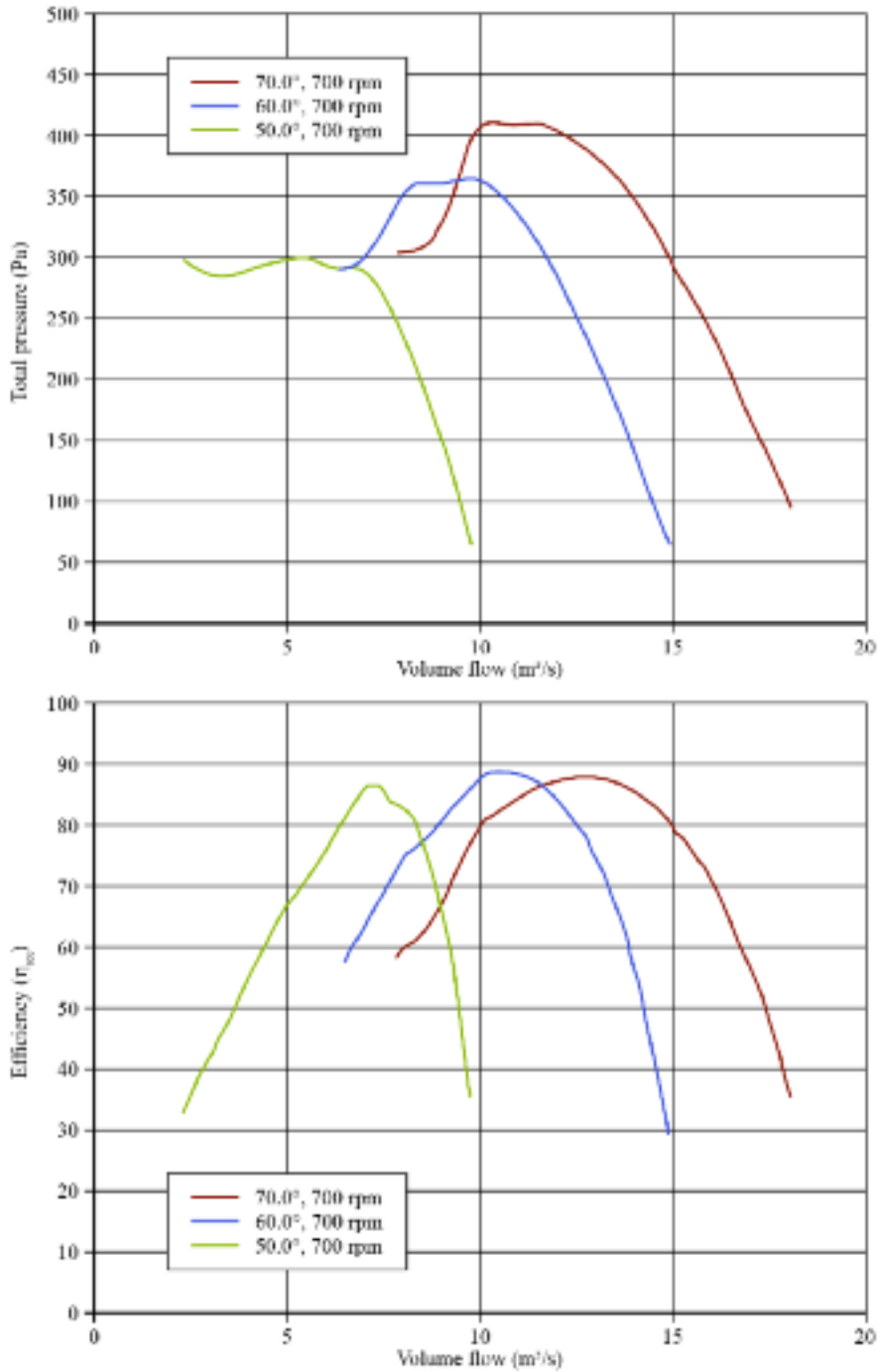
FIGURE 3.2. Measured total pressure rise and efficiency characteristics for the studied fan.
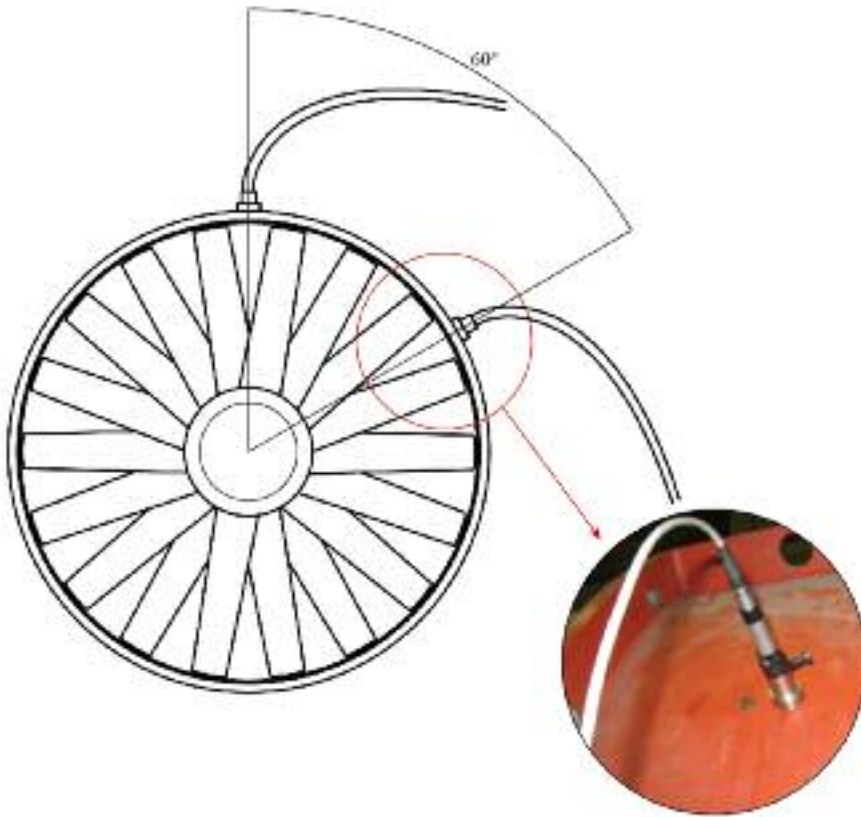
FIGURE 3.3. Sectional view of the studied fan illustrating the azimuthal positions of the two microphones used for making unsteady pressure measurements. The microphones' axial position was at mid-chord, equidistant from the blade leading and trailing edge.

Signal processing technique

We used the microphones purely as pressure transducers to record unsteady casing pressure whilst maintaining good sensitivity. The microphones' lower frequency limit was 2 Hz, below the shaft order frequency of the unsteady features of interest. We took unsteady pressure measurements at a sampling rate of 10 kHz. To avoid signal aliasing, we filtered the unsteady data at 2.5 kHz. The resulting Nyquist rate was 1.25 kHz, with data analysis focused on unsteady features below 200 Hz. The microphones themselves incorporated a cavity between their front face and the microphone diaphragm. We calculated the cavity's resonant frequency at 4,702 Hz, using the Helmholtz equation applied to an equivalent conical cavity. The cavity's behaviour suggested that limiting a signal analysis to unsteady features below 500 Hz would retain the cross-spectrum amplitude near constant and the phase angle shift below

–3 degrees (Boerrigter, 1996). Within the context of an analysis expected to focus on unsteady features with a frequency below 200 Hz, we concluded that a near constant cross-spectrum amplitude and phase shift below –3 degrees was acceptable.

In addition to filtering the unsteady pressure data at 2.5 kHz, we also incorporated a 150 Hz low-pass filter to remove the data's low-frequency content. We selected the 150 Hz cut-off to eliminate the relatively high amplitude blade passing signals, thus simplifying detecting the relatively small magnitude rotating instabilities of interest. We conducted filtering when we post-processed the data using a non-causal digital filter which eliminated phase distortion. We estimated the overall uncertainty that occurred with the unsteady pressure measurements as:

- $\Delta V = 1,000$ mV ± 12 mV (20:3) on the voltage; and
- $\Delta G = 200$ dB ± 2.4 dB (20:3) on the raw signal gain in the considered frequency ranges.

We considered these uncertainties acceptable within the context of the highly unstable physical flow phenomena that were the subject of study (Carbonaro, 2009).

UNSTEADY MEASUREMENTS DURING THE STALL INCEPTION

The objective of our research was two-fold. First, we aimed to characterise the aerodynamic instabilities that occur with incipient stall. Second, we wanted to characterise flow-field features that constitute rotating stall. We chose to characterise both by visually inspecting unsteady pressure data and a cross-correlation of data from the azimuthally offset microphones.

Visual inspection

Visually inspecting unsteady pressure data provides qualitative information about the incipient stall fluid flow mechanisms. We set the blade pitch angle to 70 degrees, and throttled the fan from stable to stalled operation over a 30 second time period, equivalent to 350 rotor revolutions. Unsteady pressure fluctuations approximately 50 times higher than those that characterised stable operation characterised stalled operation. We scaled and offset the unsteady pressure data from the two microphones onto a single figure to facilitate the direct comparison of data from each microphone, Figure 3.4. We defined time zero as the time at which fan throttling commenced, with the transition from stable to stalled operation taking place after 29 seconds.

After 28.5 seconds the unsteady pressure data from the Channel 2 microphone (Figure 3.1) recorded a spike-like pressure instability. The Channel 1 microphone then recorded the same spike-like pressure instability, and it had increased in magnitude. The speed with which the pressure instability moved around the annulus from

FIGURE 3.4. Unsteady pressure data recorded using the two microphones, mounted in the casing over the fan blades as the fan was throttled from stable to stalled operation. The fan rotation speed was 700 rpm, and the blade angle was 70 degrees.

the Channel 2 to Channel 1 microphone resulted in an offset too small to see in Figure 3.4. However, an analysis of the pressure instability's relative position recorded by each microphone indicates that it travelled at 70 per cent of fan speed.

Zhang *et al*. (2005) documented similar spike-like pressure instabilities when studying a NASA37 compressor stage's stall inception mechanisms. Zhang *et al*. (2005) concluded that the spike-like pressure instability resulted in the compressor's immediate transition from stable to stalled operation. Unlike Zhang *et al*. (2005), we observed that at a time between 28.5 and 29 seconds, Figure 3.4, the spike-like pressure instability collapsed, with the fan returning to stable operation for approximately three rotor revolutions as we continued to throttle the fan. The fan finally transitioned from stable to stalled operation after approximately 29 seconds.

A review of the unsteady pressure data, focusing on collected data over a 2.5 second time period facilitates a more detailed analysis, Figure 3.5. The initial spike-like pressure instability at 28.5 seconds (I_1) is followed approximately half a second later by a second spike-like instability (I_2). An analysis of the second pressure instability's relative position recorded by each microphone indicates that it travelled at half design speed. The second pressure instability (I_2) was distinctly different to the first (I_1). The second pressure instability (I_2) persisted for longer than the first. We may regard this as an embryonic rotating stall cell.

Following the second pressure instability (I_2) there is a third (I_3), fourth (I_4) and fifth (I_5) pressure instability that have identifiable characteristics. A review of the unsteady pressure data indicates that the third (I_3) and fifth (I_5) pressure instabilities have the same structure as the second (I_2) pressure instability. A bow-shape pressure rise, followed by multiple narrow peaks characterises each. The time between these peaks for the third (I_3) and fifth (I_5) pressure instability are similar to those of the second. Both travelled at half design speed, the same as the speed with which the second pressure instability (I_2) travelled. In contrast, the fourth (I_4) pressure instability has characteristics similar to those of the first pressure instability (I_1) and travelled at 70 per cent of fan speed, the same as the speed of the first.

A review of the unsteady pressure data indicates that by 31 seconds a new structure emerged, Figure 3.5. We concluded that this structure was the first evidence of a fully developed rotating stall cell, that we named RS6. The unsteady pressure data indicates that the fifth (I_5) pressure instability has a similar form to the fully developed rotating stall cell RS6. We therefore concluded that the fifth (I_5) pressure instability was also a developmental stall cell, that we named RS1. An analysis of the pressure instability's relative position recorded by each microphone indicates that the RS6 rotating stall cell travelled at 40 per cent of fan speed. The RS6 rotating stall
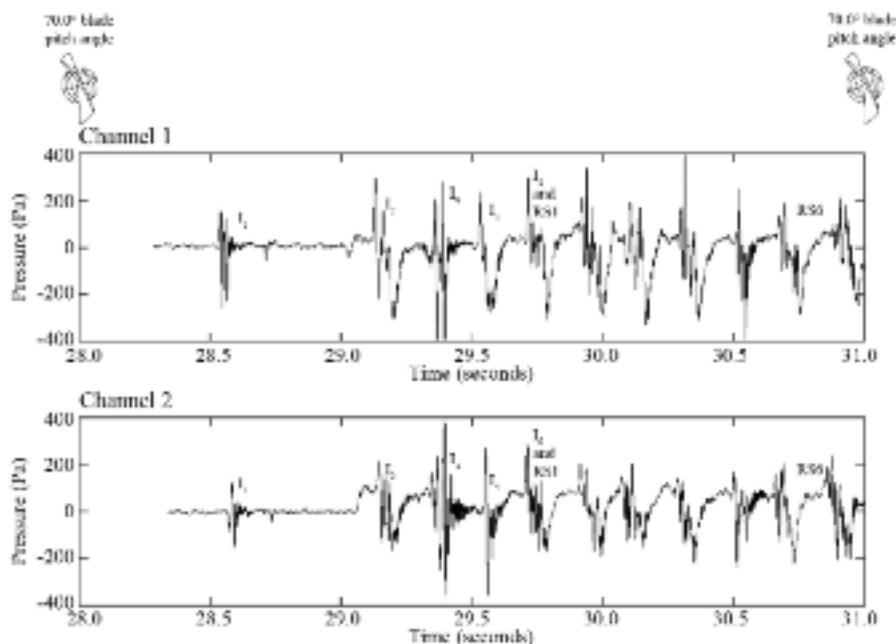
FIGURE 3.5. The pressure instabilities that characterise stall inception and stall precursors during a transition from stable to stalled operation.

cell's speed is similar to that which Day (1993) observed when studying rotating stall in a single-stage compressor. Collectively, the pressure instabilities constitute rotating stall precursors, developmental stall cells and fully developed rotating stall cells. Table 3.4 summarises these.

Day (1993) concluded that an interaction of long and short length-scale structures in the flow-field characterised a compressor's transition from stable to stalled operation. Outa (2005) also studied stall inception in a single-stage compressor, and also concluded that the flow-field features in the blade-tip region were complex. Outa (2005) was able to use the results of a computational analysis to characterise the flow-field features in the blade tip region. Emerging rotating stall cells resulted in a change in compressor inlet incidence angle, compounded by rotating stall cell trailing edge vortices merging with the back-flow that occurred with incipient stall in the blade leading edge region.

Day (1993) and Outa's (2005) conclusions indicate that an interpretation of the pressure instabilities we observed (Figure 3.5 and Table 3.4) are indicative of a separation bubble inducing the spike-like pressure instabilities during rotating stall cell inception. This interpretation would imply that as stall becomes incipient, the spike-

Table 3.4. *Stall precursors and rotating stall cell configurations.*

	Channel 1	Channel 2
Stall inception I_1		
Stall inception I_2		
Stall development I_3		
Stall development I_4		
Rotating stall I_5 and RS1		
Rotating stall RS6		

like pressure instabilities (I_1 and I_4) constitute vortexes that grow and merge into the fully developed rotating stall cell RS6. As such, we may characterise the first (I_1) and fourth (I_4) pressure instabilities as characteristic of the stall inception process. In contrast, we may characterise the second (I_2), third (I_3) and fifth (I_5) pressure instability as rotating stall cell precursors.

Spectral analysis

We complemented the visual inspection of unsteady pressure data with a Fourier analysis of the unsteady pressure data's cross-spectrum from the two microphones. Cross-spectra are useful in that they facilitate an analysis of the frequency components that persist from one microphone location to the next. Thus, the cross-spectrum assists in differentiating between flow features that occur with rotating stall and those that occur with random turbulence.

We calculated the cross-spectrum of unsteady pressure data using a fast Fourier transform over a time window equivalent to approximately 18 rotor revolutions. We calculated cross-spectrum during stable operation, incipient stall and fully developed rotating stall, Figure 3.6. We took the stable operation data from 10 to 11.5 seconds, not shown in Figure 3.4, but similar to the data from 26 to 28 seconds that is shown in Figure 3.4. We took the incipient stall data from 28.5 to 30 seconds, Figure 3.4. We took the fully developed rotating stall data from 50 to 51.5 seconds, not shown in Figure 3.4, but similar to the data from 34 to 36 seconds that is shown in Figure 3.4.

An analysis of the stable operation cross-spectrum indicates the presence of a shaft rotational frequency tone at 11.7 Hz. This is self-consistent with the tone we would expect for a fan rotating at 700 rpm, and dominates the cross-spectra. In contrast, during incipient stall a single very low-frequency peak, indicative of a part-speed rotating stall cell's inception, characterises the cross-spectra. The presence of a part-speed rotating stall cell is consistent with Kameier and Neise (1997) and Bianchi *et al*.'s conclusions (2010). Despite the consistency of our observations with those of other researchers, we did not expect the presence of a part-speed rotating stall cell. The incipient stall cross-spectra exhibited characteristics that we would have expected to observe only if the rotating stall cell were fully developed.

When one studies the incipient stall cross-spectra it is clear that the 11.7 Hz rotating frequency tone is no longer present. We may interpret the loss of this rotating frequency tone as a modulation of the shaft frequency rate that occurs because of the interaction of instabilities rotating at different fan speed fractions (Kameier and Neise, 1997; Bianchi *et al*., 2010). The appearance of tonal components between 30 and 50 Hz characterise the incipient stall cross-spectra. As Bianchi *et al*. (2010) noted, these tonal components may occur because of the interaction of many small 'bubble' cells that later merge to create the fully developed rotating stall cell. These bubble cells are not significant enough to be apparent in the cross-spectra as fundamental tones. However, they do appear as an incremental increase in the broadband over the frequency range where they occur.
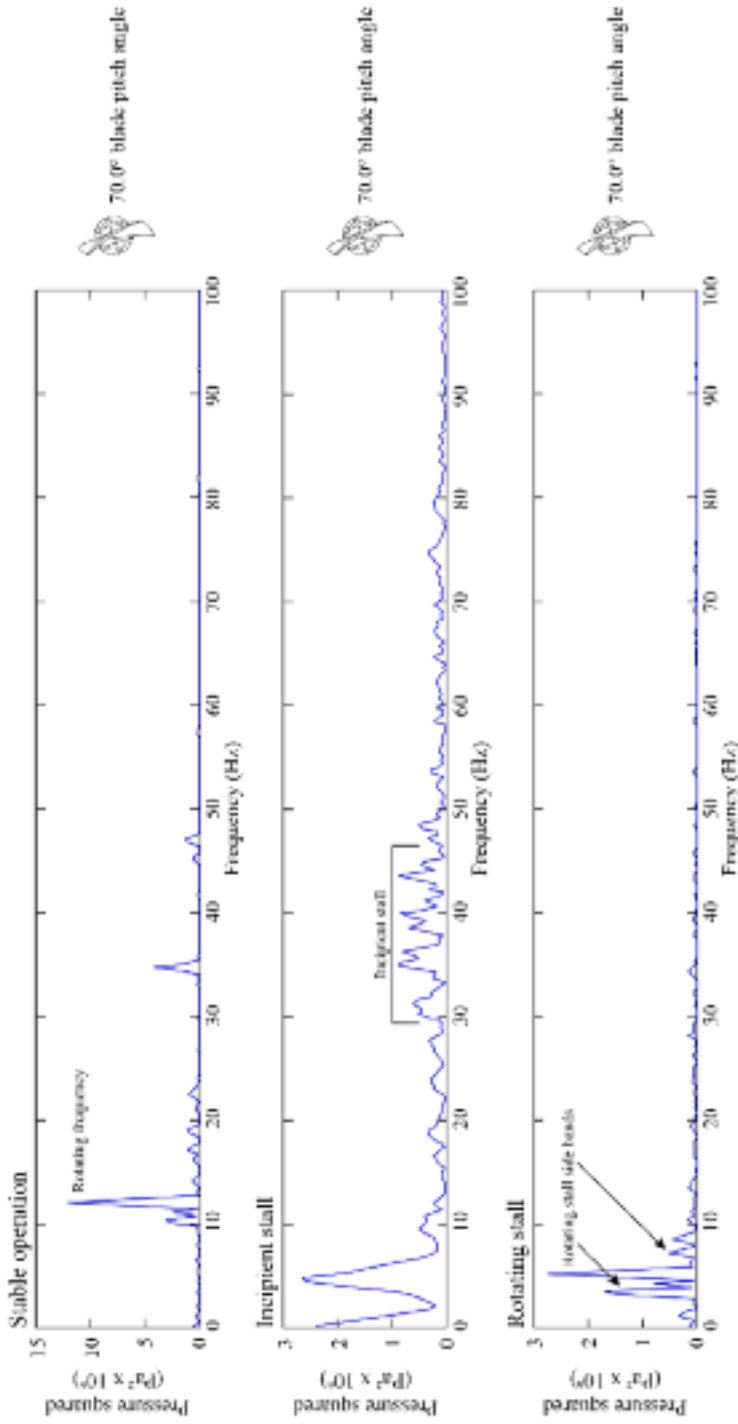
FIGURE 3.6. Cross-correlation spectral amplitude of the two unsteady pressure signals during stable operation, top; incipient stall, middle; and fully developed rotating stall, bottom.

An analysis of the fully developed rotating stall cross-spectrum indicates a shaft rotational frequency tone presence localised at 5 Hz, but split into a series of side bands. These rotating stall side bands occur because of harmonics in the unsteady pressure data from which we calculated the cross-spectra, a feature that Bianchi *et al*. (2010) associated with rotating stall. When considering the difference between the cross-spectra for incipient stall and fully developed rotating stall, it is apparent that the tonal components between 30 and 50 Hz present in the incipient stall cross-spectra are no longer present in the fully developed rotating stall cross-spectra. From this we conclude that the tonal components have developed into larger features, and as they have grown, they have decreased in speed and merged with the 40 per cent speed rotating stall cell. Other researchers have come to similar conclusions when studying instability inception in a compressor (McDougall *et al*., 1990; Leinhos *et al*., 2001).

UNSTEADY MEASUREMENTS
DURING THE STALL RECOVERY

Visually inspecting unsteady pressure data provided qualitative information about the incipient stall fluid flow mechanisms that emerged as we throttled the fan from stable to stalled operation with a constant blade pitch. An analysis of data from when we reduced the fan blade pitch angle to induce a stall recovery complemented this analysis. To the best of our knowledge, this is the first published study on stall recovery through a reduction in blade pitch angle in an industrial fan. The lack of published scholarly work against which to validate any conclusions resulted in us regarding those conclusions we did reach as tentative.

Visual inspections

Visually inspecting unsteady pressure data provides qualitative information about the stall recovery fluid flow mechanisms. We set the blade pitch angle to 70 degrees, throttled the fan from stable to stalled operation and then at a constant throttle position reduced blade pitch angle to 50 degrees at a rate of 1.5 degrees per second. We scaled and offset the unsteady pressure data from the two microphones onto a single figure to facilitate the direct comparison of data from each microphone, Figure 3.7. We defined time zero as the time at which fan throttling commenced, with the variable pitch in motion transition from stalled to stable operation taking place after 88 seconds.

During the variable pitch in motion transition from stalled to stable operation, the unsteady pressure amplitude remained near constant, with two exceptions. The first exception occurred after 80 seconds, Figure 3.7, at a 63 degree blade angle. The unsteady pressure signal exhibited an isolated peak, followed by a shift in the rotating stall cell's phase. The second exception occurred between 83.5 and 84 seconds, at approximately a 58 degree blade angle. An abrupt reduction in pressure that we do
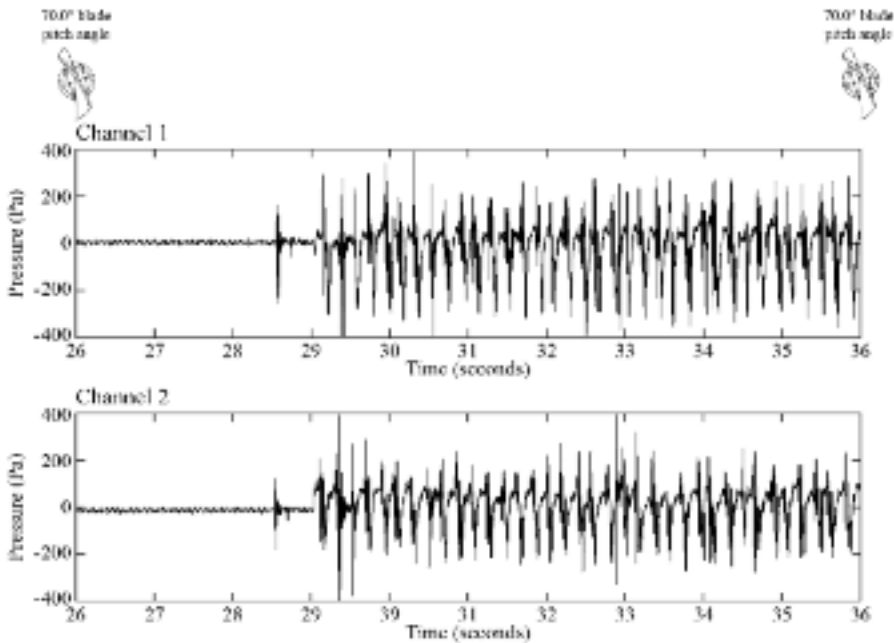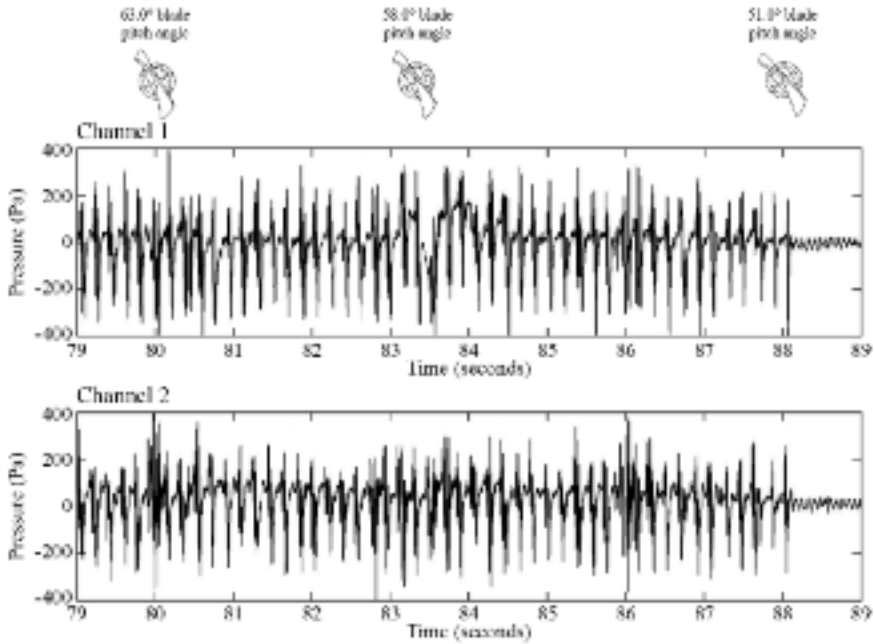
FIGURE 3.7. Unsteady pressure data recorded using the two microphones, mounted in the casing over the fan blades as the variable pitch in motion mechanism was used to reduce blade pitch angle at a constant fan speed of 700 rpm.

not see in the Channel 2 unsteady pressure signal characterises the Channel 1 unsteady pressure signal. The transition from stalled to stable operation occurs after 88 seconds, as the reduction in unsteady pressure levels to those characteristic of the fan before the initial transition from stable to stalled operation indicate.

A review of the unsteady pressure data, focusing on data that we took over a seven second time period facilitates a more detailed analysis, Figure 3.8. The unsteady pressure data between 86 and 88 seconds, immediately before the transition from stalled to stable operation, occurs with the break-down of rotating stall cells. The unsteady pressure data prior to 86 seconds is characteristic of a fully developed rotating stall cell and we may associate it with the presence of a single vortex structure. After 86 seconds the unsteady pressure data is characteristic of a double vortex, and then a triple vortex structure followed by the rotating stall cell's abrupt collapse at 88 seconds as the fan transitions back from stalled to stable operation.

Spectral analysis

We complemented the unsteady pressure data's visual inspection with an analysis of the cross-spectra spectral energy density. Spectral energy density is a useful parameter as it describes how a signal's power distributes itself with frequency. We
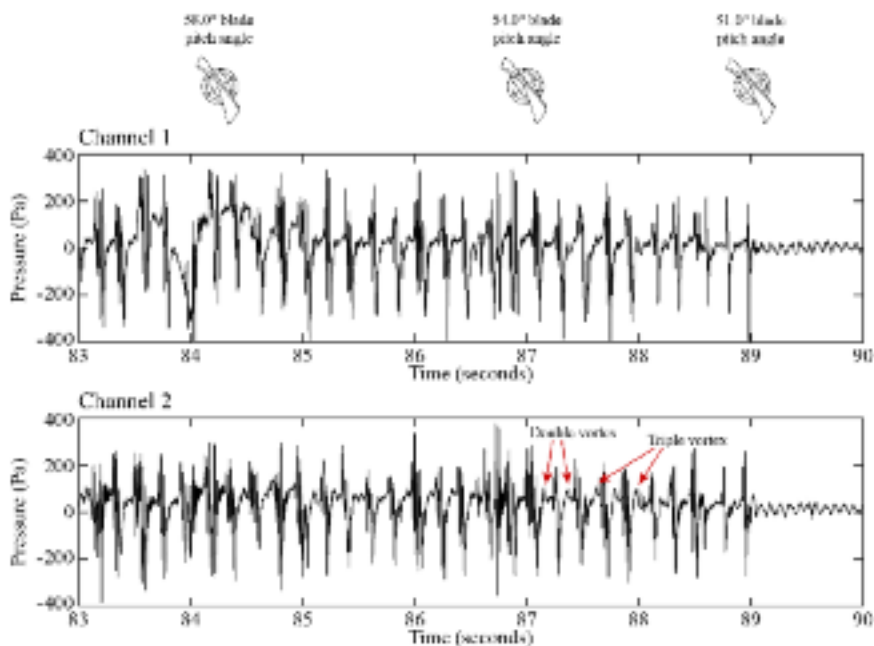
FIGURE 3.8. The pressure instabilities that characterise the transition from stable to stalled operation as the fan's variable pitch in motion mechanism reduces blade pitch angle.

considered this appropriate as visual inspection of unsteady pressure data gave a qualitative indication that the rotating stall cell's frequency content was almost constant during the transition from both stable to stalled, and back to stable operation. We limited the spectra's integration to frequencies below 14 Hz to eliminate the effect of any small-scale, high-speed structures.

We computed the cross-spectra's spectral energy density for a complete 150 second cycle, Figure 3.9. We cycled the fan from stable operation, through stall inception by throttling the fan into stalled operation, and then through stall recovery and back to stable operation through reducing the blade pitch angle. The shift from stable operation to incipient stall as we throttled the fan resulted in a rapid increase in spectral energy density, Figure 3.9. Although an isolated spike-like instability (I_1) initially characterises the stall inception region at 28.5 seconds, Figure 3.5, the spectral energy density rises almost instantly to a level characteristic of fully developed rotating stall, Figure 3.9.

An analysis of the unsteady pressure data, Figure 3.5, indicates that the transition from incipient stall to fully developed rotating stall was complete after less than 31 seconds as the rotating stall cell, RS6, emerged. The calculated spectral energy density indicates that the transition from incipient stall to fully developed rotating stall occurred slightly later at 32 seconds. After transitioning into a fully stalled condition, the spectral energy density varied randomly around a relatively well defined average value up to 75 seconds when we activated the fan's variable pitch in motion
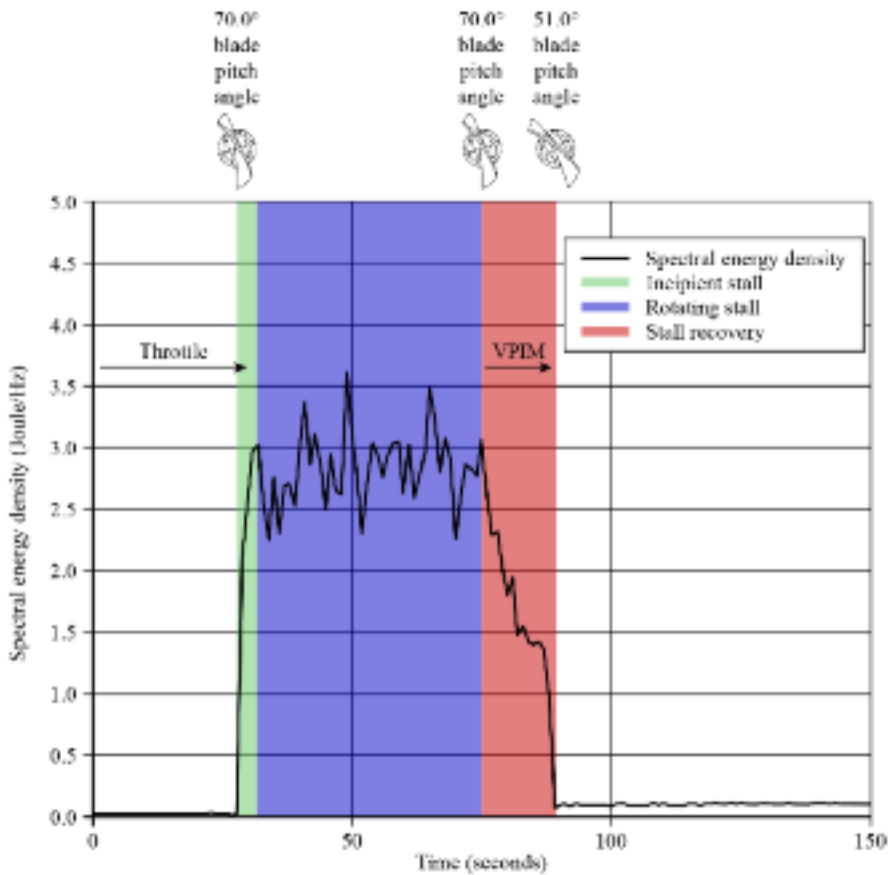
FIGURE 3.9. Spectral energy density for a 150 second cycle from stable operation, into stalled operation and then back to stable operation. The fan transitions from stable into stalled operation by throttling the fan, and then back to stable operation by reducing blade pitch angle.

system. Immediately the blade pitch angle started to reduce, and the spectral energy density began to drop. This reduction in spectral energy density correlates with the reduction in blade pitch until 88 seconds when the rotating stall cells collapse completely and the fan returns to stable operation.

A review of the spectral energy density, focusing on data that we collected over the 50 second time period, facilitates a more detailed analysis, Figure 3.10. The variable pitch in motion transition from stalled to stable operation occurs between 75 and 88 seconds. Within this transition there are three identifiably different spectral energy density regions of decreasing energy content. From 75 to 82 seconds, spectral energy density decreases almost linearly. This reduction in spectral energy density occurred despite no apparent change in the unsteady pressure data. From 82 to 86 seconds there is a plateau in the spectral energy density, despite the blade pitch angle continuing to reduce. From 86 to 88 seconds the spectral energy density drops
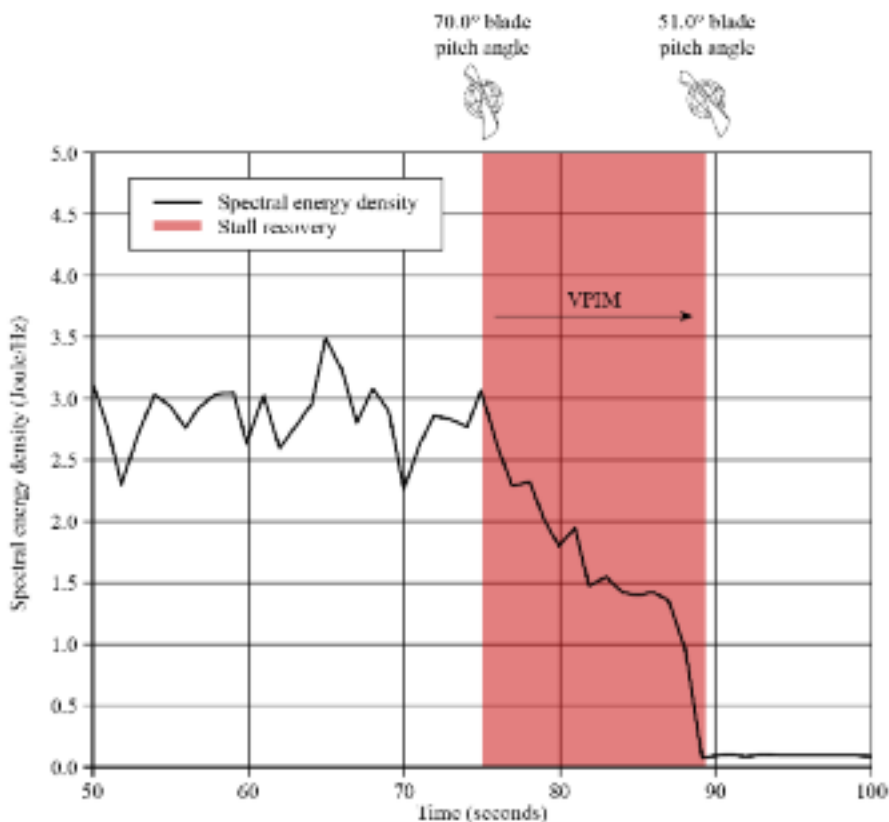
FIGURE 3.10. Spectral energy density for the transition from stalled back to stable operation by reducing blade pitch angle using the studied fan's variable pitch in motion mechanism.

abruptly as the rotating stall cells collapse with the transition back into stable operation. Although it is difficult to speculate the mechanisms underpinning the changes in spectral energy density, we may infer that the changes are indicative of a change in the rotating stall cell configuration from a single to a multiple vortex cell.

The visual inspection of unsteady pressure data and the analysis of spectral energy density are self-consistent with measured fan characteristics. We used the variable pitch in motion mechanism to drive the fan across its performance map, with stall recovery commencing with the start of blade actuation, Figure 3.11. The reduction in blade pitch angle from 70 degrees to 50 degrees resulted in a 28 per cent reduction in fan pressure developing capability and a 16 per cent reduction in flow rate.

CONCLUSIONS

The present study has established an industrial fan's stall characteristic by visually inspecting unsteady pressure data, conducting a Fourier analysis of cross-
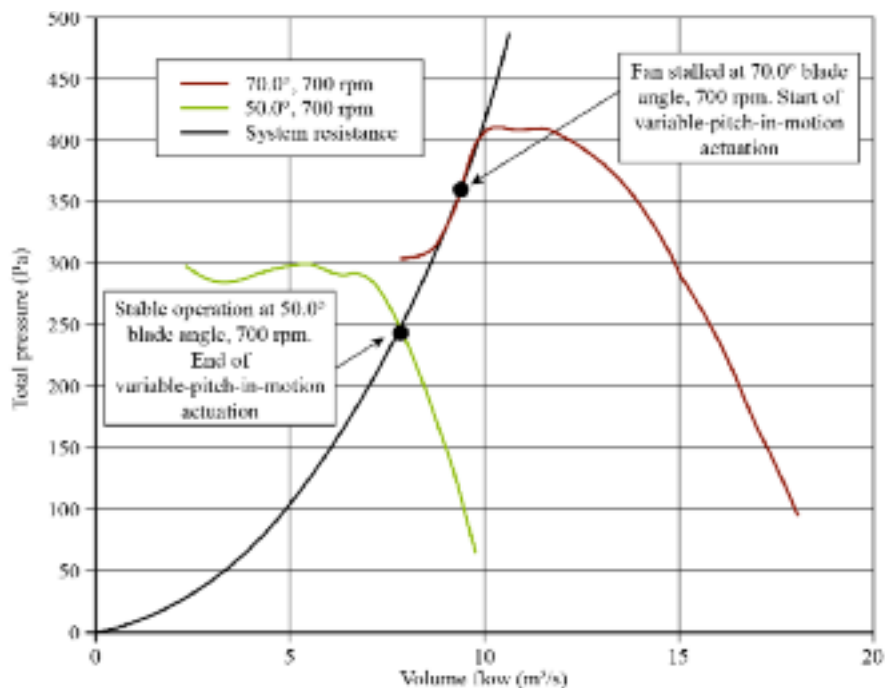
FIGURE 3.11. Fan characteristic at 700 rpm with a 70 degree pitch angle and with a 50 degree pitch angle. The experimental facility system curve illustrates how the stalled and stable operating points are related, with the variation of blade pitch from 70 degrees to 50 degrees shifting the fan from stalled to stable operation.

spectrum and analysing spectral energy density. We have studied both the fan's stall characteristics, and the characteristics that occur with incipient stall. Visually inspecting unsteady pressure data indicates that the transition from stable to stalled operation occurs within a few rotor revolutions after its inception. The stall inception features the interaction of rotating instabilities as different fractions of fan speed. We associated the industrial fan that was the subject of this research with a spike-like pressure pulse that constituted a stall precursor. This spike-like pressure pulse collapsed almost immediately, with the unsteady pressure signal returning to its previous level when the fan operated stably.

The Fourier transformation of cross-correlated unsteady pressure data from two microphones as different azimuthal positions provided more detailed information about the studied fan's stall characteristics. As stall became incipient, a low-frequency tone emerged that we may associate with the rotating stall cells travelling around the annulus at 40 per cent fan speed. The tone band modulation that we observed may be indicative of the interaction of weak rotating instabilities that emerged as stall became incipient. We concluded that by the time rotating stall became fully established, these rotating instabilities had consolidated into a single rotating stall cell that we may regard as characteristic of this class of industrial fan.

The low-frequency tone became established as stall became incipient, and therefore, has the potential to form the basis of a stall warning system that alerts operators to the fact that stall is incipient, but has not yet occurred. Despite this potential, traditional fan and compressor stall-warning systems are unable to utilise the spectrum of measured pressure alone to predict the imminent onset of stall because the required long sampling time precludes its use in practice. As such, an alternative approach to stall warning is required to enable an operator to use stall precursor to identify imminent stall onset.

REFERENCES

EN12101-3, 2002, Smoke and Heat Control Systems. Specification for Powered Smoke and Heat Exhaust Ventilators.

ISO IEC60651, 1994, Specification for Sound Level Meters.

ISO 21927-3, 2006, Smoke and Heat Control Systems — Part 3: Specification for Powered Smoke and Heat Exhaust Ventilators.

ISO 5801, 2007, Industrial Fans — Performance Testing Using Standardized Airways.

Bianchi, S., Corsini, A., and Sheard, A.G. (2010), "Detection of Stall Regions in a Low-speed Axial Fan, Part 1: Azimuthal Acoustic Measurements", *Proceedings of the 55th American Society of Mechanical Engineers Turbine and Aeroengine Congress*, Glasgow, UK, 14–18 June, paper no. GT2010-22753.

Boerrigter, H.L. (1996), "PreMeSys: a Simulation Program to Determine the Frequency and Time Response of a Pressure Measurement System", *VKI Technical Memorandum 53*, von Karman Institute for Fluid Dynamics, Rhode-Saint-Genese, Belgium.

Bright, M.M., Qammar, H., Vhora, H., and Schaffer, M. (1998), "Rotating Pip Detection and Stall Warning in High-speed Compressors using Structure Function", *Proceedings of GARD RTO AVT Conference*, Toulouse, France, 11–15 May.

Camp, T.R., and Day, I.J. (1998), "A Study of Spike and Modal Stall Phenomena in a Low-speed Axial Compressor", *Transactions of the ASME, Journal of Turbomachinery*, vol. 120, pp. 393–401.

Carbonaro, M. (2009), *Measurement Techniques in Fluid Dynamics — An Introduction*, Von Karman Institute for Fluid Dynamics, Rhode-Saint-Genèse, Belgium.

Corsini, A., and Rispoli, F. (2005), "Flow Analyses in a High-pressure Axial Ventilation Fan with a Non-linear Eddy-viscosity Closure", *International Journal of Heat and Fluid Flow*, vol. 26, no. 3, pp. 349–61.

Cumpsty, N.A. (1989), "Part-circumference Casing Treatment and the Effect on Compressor Stall", *Proceedings of the 34th American Society of Mechanical Engineers Gas Turbine and Aeroengine Congress*, Toronto, ON, Canada, 11–14 June, paper no. 89-GT-312.

Day, I.J. (1993), "Stall Inception in Axial Flow Compressors", *Transactions of the ASME, Journal of Turbomachinery*, vol. 115, pp. 1–9.

Day, I.J., and Cumpsty, N.A. (1978), "The Measurement and Interpretation of Flow Within Rotating Stall Cells in Axial Compressors", *Proceedings of the Institution of Mechanical Engineers, Part C, Journal of Mechanical Engineering Science*, vol. 20, pp. 101–14.

Deppe, A., Saathoff, H., and Stark, U. (2005), "Spike-type Stall Inception in Axial Flow Compressors", *Proceedings of the 6th Conference on Turbomachinery, Fluid Dynamics and Thermodynamics*, Lille, France, 7–11 March.

Emmons, H.W., Pearson, C.E., and Grant, H.P. (1955), "Compressor Surge and Stall Propagation", *Transactions of the ASME*, vol. 77, pp. 455–69.

Gall, W. (1975), "Fan with Variable Pitch Blades and Translating Bearing Actuation System", US Patent 3,873,236 A, 25 March.

Gravdahl, J.T., and Egeland, O. (1999), *Compressor Surge and Rotating Stall: Modelling and Control*, Springer-Verlag, London, UK.

Greitzer, E.M. (1976), "Surge and Rotating Stall in Axial Flow Compressors, Part I: Theoretical Compression System Model", *Transactions of the ASME, Journal of Engineering for Gas Turbines and Power*, vol. 98, pp. 190–98.

Greitzer, E.M. (1980), "Review — Axial Compressor Stall Phenomena", *Transactions of the ASME, Journal of Fluids Engineering*, vol. 102, pp. 134–51.

Kameier, F., and Neise W. (1997), "Rotating Blade Flow Instability as a Source of Noise in Axial Turbomachines", *Journal of Sound and Vibration*, vol. 203, pp. 833–53.

Langston, L.S. (2009), "Fitting a Pitch", *ASME Mechanical Engineering Magazine*, vol. 131, no. 12, pp. 38–42.

Leinhos, D.C., Schmid, N.R., and Fottner, L. (2001), "The Influence of Transient Inlet Distortions on the Instability Inception of a Low Pressure Compressor in a Turbofan Engine", *Transactions of the ASME, Journal of Turbomachinery*, vol. 123, pp. 1–8.

McDougall, N.M., Cumpsty, N.A., and Hynes, T.P. (1990), "Stall Inception in Axial Compressors", *Transactions of the ASME, Journal of Turbomachinery*, vol. 112, pp. 116–23.

Mongeau, L., Thompson, D.E., and McLaughlin, D.K. (1995), "A Method for Characterizing Aerodynamic Sound Sources in Turbomachines", *Journal of Sound and Vibration*, vol. 18, no. 3, pp. 369–89.

Moore, F.K. (1984), "A Theory of Rotating Stall of Multistage Compressors, Parts I–III", *Transactions of the ASME, Journal of Engineering for Power*, vol. 106, pp. 313–36.

Outa, E. (2005), "Rotating Stall and Stall-controlled Performance of a Single Stage Subsonic Axial Compressor", *Journal of Thermal Science*, vol. 15, no. 1, pp. 1–13.

Rippl, A. (1995), "Experimentelle Untersuchungen Zuminstationaren Betriebsverhahenan der Stabilitarsgrenze Eines Mehrstufigen Transsonischen Verdichters", PhD dissertation, Ruhr-Universitat Bochum.

Sheard, A.G. (2012), "The Effect of Inlet Box Aerodynamics on the Mechanical Performance of a Variable Pitch in Motion Fan", *Advances in Acoustics and Vibration*, vol. 2012, article ID 278082, pp. 1–10.

Sheard, A.G., and Corsini, A. (2012), "The Mechanical Impact of Aerodynamic Stall on Tunnel Ventilation Fans", *International Journal of Rotating Machinery*, vol. 2012, paper no. 402763, pp. 1–12.

Sheard, A.G., and Jones, N.M. (2008), "Approval of High-temperature Emergency Tunnel-ventilation Fans: The Impact of ISO 21927-3", *Proceedings of the ITA–AITES World Tunnel Congress and 34th General Assembly*, Agra, India, 19–25 September, pp. 1817–26.

Sheard, A.G., Corsini. A., Minotti, S., and Sciulli, F. (2009), "The Role of Computational Methods in the Development of an Aero-acoustic Design Methodology: Application in a Family of Large Industrial Fans", *Proceedings of the 14th International Conference on Modelling Fluid Flow Technologies*, Budapest, Hungary, 9–12 September, pp. 71–9.

Vo, H.D., Tan, C.S., and Greitzer, E.M. (2005), "Criteria for Spike Initiated Rotating Stall", *Proceedings of the 50th American Society of Mechanical Engineers Gas Turbine and Aeroengine Congress*, Reno, NV, USA, 6–9 June, paper no. GT2005-68374.

Zhang, H.W., Deng, X.Y., Lin, F., Chen, J.Y., and Huang, W.G. (2005), "Unsteady Tip Leakage Flow in an Isolated Axial Compressor Rotor", *Journal of Thermal Science*, vol. 14, no. 3, pp. 265–74.

Chapter 4

The Role of Variable Pitch in Motion Blades and Variable Rotational Speed in an Industrial Fan Stall

A.G. Sheard, C. Tortora,
A. Corsini, and S. Bianchi

ABSTRACT

Stall-induced vibration places fundamental limitations on industrial fan performance and remains a persistent problem in developing industrial fans and compressors. In this chapter we present an experimental programme that utilised two strategies to study rotating stall recovery patterns in an industrial fan. The experimental facility incorporated a fan with both variable pitch in motion blades and a variable speed drive. The facility enabled us first, to study the evolution of unsteady pressure signals on the fan casing whilst varying fan blade pitch and then to examine varying fan rotational speed. Consequently, we were able to recover a fan from stall either by varying blade pitch at constant speed, or by varying speed at constant blade pitch. We also studied the physical flow phenomena associated with stall recovery by cross-correlating signals from circumferentially offset high-frequency response pressure transducers and then analysed the cross-spectra. This enabled us to gain insight into the transient fluid flow behaviour associated with stall recovery in the studied industrial fan class.

The transient fluid flow behaviour associated with stall recovery by varying blade pitch was indicative of both a mild and progressive transition. In contrast, stall recovery by varying fan speed occurred more suddenly. In comparison with the variable pitch transition, the variable speed transition was more indicative of recovery from mild surge. From this we may conclude that stall recovery via variable speed resulted in significantly higher unsteady mechanical stress induced in fan rotating components than recovery via variable pitch. Higher bending stresses in the fan blades are more likely to result in mechanical failure, and therefore we may conclude that the studied fan is more 'stall tolerant' when one operates it as a variable pitch fan rather than as a variable speed fan.

NOMENCLATURE

Latin letters

BPF	customary blade passing frequency of the fan rotor	Hz
D_t	tip diameter	mm
f	signal frequency	Hz
H_b	blade height	mm
ℓ_t	blade chord at the tip	mm
n	nominal speed	rpm
n^*	shaft order number (defined as: f/SF)	
NR	Nyquist rate	Hz
P	power	kW
p	static pressure	Pa
p_n	nominal design pressure	Pa
Q	volume flow rate	m^3/s
Q_n	nominal design flow rate	m^3/s
RS	rotating stall cell	
SF	shaft frequency	Hz
t	absolute time	s
U_{tip}	tip speed	m/s

Greek letters

δ_h	hub pitch angle
η_{tot}	efficiency based on total pressure rise
θ	microphone's azimuthal position
Σ	solidity

INTRODUCTION

The current trend toward increased pressure rise and blade aerodynamic loading reduces the stable operating range of industrial fans and compressors. The onset of aerodynamic instability as the flow rate throttles limits the stable operating range. Researchers have studied the detection and analysis of different forms of aerodynamic instability for several decades. Some scholars have studied the phenomenon of rotating stall in both single and multi-stage axial flow compressors (Day and Cumpsty, 1978; Greitzer, 1980; Moore, 1984; Gravdahl and Egeland, 1999). Emmons *et al.*'s earlier work (1955) was one of the first attempts to describe the mechanism underlying rotating stall. Rotating stall is a flow mechanism by which the rotor adapts to a reduction in flow rate and results in a non-uniform flow pattern rotating in the annulus. Part-span rotating stall classically occurs in single blade rows (Cumpsty, 1989) and usually leads to more complex disturbances in single-rotor or stage machines than multi-stage compressors (Moore, 1984).

Rotating stall and stall are purely aerodynamic instability, whilst surge, flutter and their variants constitute aero-elastic instabilities that involve coupled fluid-

structure interaction. The fluid oscillatory frequency associated with stall is classically between 50 and 70 per cent of fan speed. The fluid oscillatory frequency associated with mild surge is classically lower, between 25 and 30 per cent for high-solidity industrial fans. An oscillatory frequency between 25 and 30 per cent of fan speed is low enough to couple with a fan blade's first bending mode, and has the potential to excite aero-elastic modes of vibration. Rotating stall, stall, surge and flutter are all associated with a significant increase in the unsteady mechanical stress which the aerodynamic or aero-elastic instability induces in fan and compressor rotating components.

Strain gauge measurements on axial compressors (Rippl, 1995) and fans (Sheard and Corsini, 2012) have demonstrated that bending stress in blades exceeds those associated with stable operation by a factor of five and seven respectively under 'rotating stall' conditions. This increase in bending stress may lead to initiating a fatigue crack in one or more of the blades, which then propagate and ultimately fail mechanically. In contrast, a 'surge' can lead to bending stresses in the blades increasing to a point at which mechanical blade failure occurs during the surge event itself.

Some researchers have reported studies that suggest that flow-field features in the blade tip region are directly responsible for generating short wave-length disturbances referred to as 'spikes' or 'pips' that are characteristic of the inception of localised part-span stall cells in axial compressors, low- and high-speed fans (Okada, 1987; Camp and Day, 1998; Deppe *et al*., 2005; Vo *et al*., 2005). Some have also correlated this inception mechanism with a noise signal modification in the casing region (Sheard *et al*., 2011), and several studies have attempted to link pump and compressor incipient stall behaviour to their acoustic signatures (Mongeau *et al*., 1995; Kameier and Neise, 1997; Bright *et al*., 1998).

The current state of the art in industrial fan stall control is based on passive techniques intended to modify the flow-field in the blade tip-to-casing region. Passive approaches date back to the 1950s, when researchers first utilised casing treatments in axial compressors. The relatively low cost of passive approaches has resulted in industrial fan manufacturers historically favouring them. The most widely adopted technique is the stabilisation ring (Ivanov, 1965; Karlsson and Holmkvist, 1986) that uses a set of static vanes to redirect the blade tip reverse flow at stall back in an axial direction, and then reintroduce it into the mainstream flow upstream of the blades.

Historically, very large axial industrial fans have incorporated variable pitch in motion blades that enable the blade angle to change whilst the fan operates at a constant speed. The classical application for such fans is in coal fired boilers, where the variable calorific value of coal burnt in the boiler results in a varying pressure in the boiler. In order to avoid inadvertently exploding or imploding the boiler, the forced- and induced-draft fans that drive air in and out of the boiler must be capable to respond to the changing boiler pressure. Researchers have developed variable pitch in motion technology in industrial fan application to a point where one may change the blade angle in a fraction of a second and provide a power plant control system with the necessary responsiveness to operate a boiler safely.

In the early 1970s, General Electric produced a proposal for a variable pitch in motion system for a turbofan's fan (Gall, 1975). This technology is similar to that used in industrial fan applications (Daly, 1985). Recently, Langston (2009) highlighted how variable pitch in motion fans can result in lower turbofan fuel consumption. Although very different technologies, industrial and turbofans share a common attribute. Decreasing the angle of incidence onto the blade will enable both an industrial fan and a turbofan to recover from stall. Consequently, research conducted on a variable pitch in motion industrial fan has the potential to be of interest to both the industrial fan and aerospace fan community.

The research reported in this chapter presents unsteady pressure measurements that we made during stall recovery, with an analysis of the measurements providing insight into the physical mechanisms underpinning stall recovery. The reported research establishes the characteristics of fan recovery using two strategies: variable blade pitch in motion and variable fan speed. We collected pressure data from two positions on the fan casing whilst throttling the fan through three operating regions:

(i)   stalled operation;
(ii)   stall recovery; and
(iii) recovered stable operation.

First, we used the studied fan's variable pitch in motion capability to recover from the stall. Second, we repeated a similar analysis, but this time whilst recovering the fan from stall by varying fan speed. Then we established spatial and temporal correlations between rotating instabilities which we identified in the variable pitch in motion and variable speed data. This facilitated a comparative analysis of the physical flow mechanisms associated with stall recovery.

EXPERIMENTAL FACILITY

We conducted the tests in an experimental facility that complied with ISO 5801:2007 requirements, the International Organization for Standardizations, equivalent to the historic British Standard BS 848 Part 1 (ISO IEC60651, 1994; ISO 5801, 2007), Table 4.1. The experimental facility incorporates a model industrial fan, Table 4.2, equipped with variable pitch in motion blades plus an inverter driven motor. We developed the facility to aid the low Reynolds number aerodynamic characterisation of constant speed, variable pitch in motion industrial fans that in practice may be up to five metres in diameter.

Stall recovery

The experimental facilities fan was equipped with a mechanism for varying the blade pitch as the fan rotated. This variable pitch in motion system consisted of two remotely controlled actuators that were able to change blade pitch at a rate of 1.5

Table 4.1. *Fan test rig and pressure chamber specification.*

Test rig specifications
Test section

Mode	Power, P (kW)	Diameter, D_t (m)	Speed, n (rpm)
Stand-alone	350	1.5	400–700

Ducting

	Inlet length (m)	Outlet length (m)	
	2.1	10.8	

Pressure chamber

Volume flow rate (m₃/s)	Pressure (Pa)	Width (m)	Length (m)	Height (m)
Up to 50	5,000	4	4	9

Table 4.2. *Fan geometry and operating point data.*

Design speed	700 rpm	
Tip speed	55.13 m/s	
Tip diameter, D_t	1,500 mm	
Blade height, H_b	450 mm	
Blade chord at the tip, ℓ_t	105 mm	
Tip gap, τ (% of blade chord at tip)	1.3%	
Blade count	18	
Solidity, Σ	0.6	
Hub pitch angle, δ_h	50.0°	70.0°
Design pressure, p_n	300 Pa	420 Pa
Design flow rate, Q_n	8 m³/s	12 m³/s
Design point efficiency based on total pressure rise, η_{tot}	0.92	0.91

degrees per second. The experimental facility was also equipped with a variable speed drive that could change the fan speed at a rate of one revolution per second. As a consequence of having both a variable pitch in motion and a variable speed drive, we could use the experimental facility to change the studied fans' operating point in two different ways at a known rate of change.

When originally developed, we intended to use the experimental facility for the low Reynolds number characterisation of variable pitch in motion fans. We incorporated the variable speed drive for the secondary purpose of providing a 'soft start' for the fan, as the variable pitch in motion mechanism is relatively fragile and could be

damaged if started 'direct on-line'. As such, the facility was not originally intended for use as a variable speed test facility.

During the initial stage of the research programme, we characterised the studied fan's performance. We selected an operating point that resulted in stalled operation with a fan blade angle of 70.0 degrees and stable operation with a fan blade angle of 50.0 degrees, Figure 4.1. This change in blade angle resulted in the fan pressure developing capability reducing by approximately 28 per cent with an associated volume flow rate reduction of approximately 16 per cent. During the process of identifying an optimum stable operating point we observed that this fan appeared to not obey the fan laws. A fans pressure developing capability should reduce with the square of speed, as should the system's resistance into which the fan is installed. Consequently a fan that stalls at one operating speed should stall at any other speed. We noticed that at reduced speed the studied fan characteristic appeared to change shape. It was not a scaled version of the higher speed characteristic, Figure 4.1. This change in characteristic resulted in the studied fan recovering from stall at reduced speed.

The variable pitch in motion mechanisms fitted in the fan hub utilises counter weights to reduce the necessary forces to change the blade angle. We designed these counter weights so that in the event of a failure of the variable pitch in motion system, the forces on the blades would result in blade angle reducing, and thus protect
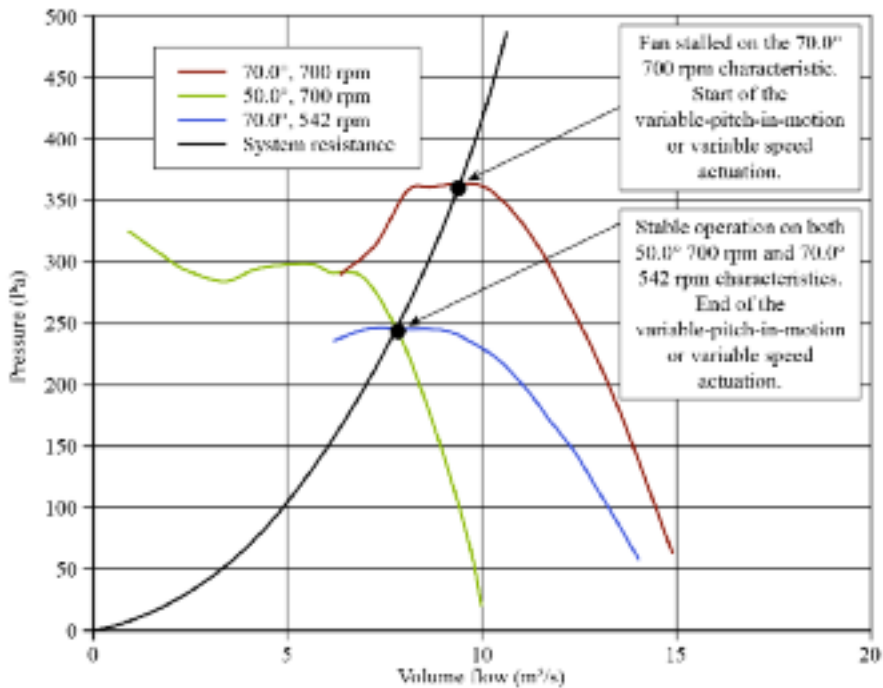
FIGURE 4.1. Fan characteristic at 700 rpm with a 70.0 degree pitch angle, 700 rpm with a 50.0 degree pitch angle and 542 rpm with a 70.0 degree pitch angle. The experimental facility system curve illustrates how the stalled and stable operating points are related.

the fan from mechanical overload. The fan hub's compact size made designing the variable pitch in motion mechanism challenging. The constrained space within the hub resulted in a light-weight variable pitch in motion mechanism. Therefore, the most likely explanation for the fan characteristic not exhibiting kinematic similarity with changing speed is a change in fan geometry with fan speed, and thus the fan laws cannot be perfectly satisfied.

We evaluated the changing fan characteristic with reducing speed. Reducing fan speed from 700 rpm to 542 rpm with a blade angle remaining constant at 70.0 degrees resulted in the fan operating at the same operating point as the fan when we operated it at 700 rpm with a blade angle of 50.0 degrees, Figure 4.1. Crucially, both the reduced speed and the reduced blade angle characteristics were associated with the absence of aerodynamic instabilities. When operated at 700 rpm with a blade angle of 50.0 degrees, the characteristic exhibited a negative slope. Therefore, we expected the fan characteristic to be stable. However, when we operated it at 542 rpm with a blade angle of 70.0 degrees, the characteristic was flat. The absence of aerodynamic instability in the fan characteristic's flat region indicates that the fan had moved from deep stall when operating at 700 rpm with a blade angle of 70.0 degrees to a region of incipient stall when we operated it at 542 rpm with a blade angle of 70.0 degrees.

When we operated the fan at 542 rpm with a blade angle of 70.0 degrees, the fan's characteristic did not exhibit the negative slope that engineers classically associate with stable operation. However, the absence of aerodynamic instabilities indicates this was the highest fan speed when we operated it with a 70.0 degree blade angle at which the fan moved from deep stall to stable operation. Therefore, we considered the 542 rpm with a blade angle of 70.0 degrees operating point to be the operating point of interest. Consequently, we were able to take a fan from stalled operation at 70.0 degrees blade angle and 700 rpm into stable operation either by keeping fan speed constant and reducing the blade angle to 50.0 degrees or by keeping the blade angle constant and reducing the fan speed to 542 rpm.

We recognised that using an experimental facility to study the transition from stalled to stable operating via two independent methods was potentially useful, as we could compare and contrast data on the transition from stalled to stable operation, which we obtained using the two methods. To the best of our knowledge, the work reported in this chapter is the first published study on the comparison of stall recovery by varying methodologies. A comparison of stall recovery by varying methodologies provides a perspective on the fluid flow mechanisms that would not otherwise be possible.

Test conditions and instrumentation

We measured fan performance in accordance with the requirements of ISO 5801:2007. By throttling downstream from the fan, we produced the aerodynamic instabilities of interest. During the volume-flow throttling, the fan remained in rotating stall without going into surge, irrespective of the rotor speed. The rotor's aerody-

namic load and the downstream plenum geometry ensured that the experimental facility could not develop a counter-pressure able to induce a surge. With a nominal fan speed of 700 rpm, the measured blade tip speed was 55.13 m/s. At this tip speed the blade passing frequency was 210 Hz. The duct within which the fan was installed exhausted into a plenum chamber equipped with a throttling valve that provided a mechanism by which fan pressure rise could be changed. A convergent-divergent NACA standard nozzle, fitted with temperature, pressure and air-speed sensors, then discharged the flow from the throttling valve. The duration of each test was approximately 120 seconds, during which time the fan was driven from stable to stalled operation by changing fan pressure rise and then recovered from stall either by varying blade angle or fan speed.

We instrumented the fan casing with two inserts, each containing a microphone which we used in place of unsteady pressure probes. During each test, two microphones (B&K 4190, with sensitivity 50 mV/Pa) monitored the wall pressure at the fan casing. This arrangement of sensors had previously shown to be an effective method for studying an industrial fan's behaviour when transitioning from stable to stalled operation (Bianchi *et al*., 2010). In the present programme of work, we used the method to verify that the fan's tip-leakage flow triggers the inception of rotating stall.

We mounted each microphone on the fan casing a half-chord distance from the blade leading edge with an angular off-set (q) of 60 degrees. The microphones mounted flush with the casing's inner surface with a mechanical support designed to ensure the microphones' stability during each test. Each microphone had a diameter of 15 mm, and was fitted into the fan casing over a 10 mm diameter opening in the casing, reducing the microphones' effective diameter to 10 mm. Charge amplifiers conditioned each microphone, with the resultant signals outputting to a data acquisition system (NI Compact Acq. 9172 with NI 9205 analogical input modules). The uncertainty of the readings was 0.1–0.2 dB at 1 kHz, established in accordance with the requirements of ISO 5801, 2007. We estimated the error in pressure measurements associated with the average turbulence level at the fan inlet flow to be two per cent of reading (Bianchi *et al*., 2011).

Signal processing technique

We used the microphones purely as pressure transducers to record unsteady casing pressure whilst maintaining good sensitivity. The microphones' lower frequency limit was 2 Hz, below the shaft order frequency of the unsteady features of interest. We took unsteady pressure measurements at a sampling rate of 10 kHz. To avoid signal aliasing, we filtered the unsteady data at 2.5 kHz. The resulting Nyquist rate was 1.25 kHz, with analysis of the data focused on unsteady features below 200 Hz. The microphones themselves incorporated a cavity between the front face of the microphone and the microphone diaphragm. We calculated the cavity's resonant frequency at 4,702 Hz, using the Helmholtz equation applied to an equivalent conical cavity (Boerrigter, 1996). The cavity's behaviour suggested that limiting a signal

analysis to an analysis of unsteady features below 500 Hz would retain the cross-spectrum amplitude near constant and the phase angle shift below –3 degrees. Within the context of an analysis expected to focus on unsteady features with a frequency below 200 Hz, we concluded that a near constant cross-spectrum amplitude and phase shift below –3 degrees was acceptable.

In addition to filtering the unsteady data at 2.5 kHz, we also incorporated a 150 Hz low-pass filter to remove the data's low-frequency content. We selected the 150 Hz cut-off to eliminate the relatively high amplitude blade passing signals, and in so doing simplify detecting the relatively small magnitude rotating instabilities of interest. We conducted filtering when we post-processed the data using a non-causal digital filter which eliminated phase distortion. This filtering technique gave an insight into the rotating features within the pressure signals that manifested themselves during stall recovery. We estimated the overall uncertainty associated with the unsteady pressure measurements as:

(i) $\Delta V = 1,000$ mV $\pm$ 12 mV (20:3) on the voltage; and

(ii) $\Delta G = 200$ dB $\pm$ 2.4 dB (20:3) on the raw signal gain in the considered frequency ranges.

We considered these uncertainties acceptable within the context of the highly unstable physical flow phenomena that were the subject of study (Carbonaro, 2009).

Unsteady pressure measurements: variable pitch in motion

The primary objectives of the unsteady pressure measurements were:

(i)   to identify the physical flow phenomena associated with stall recovery for the studied fan when running at full speed; and

(ii) to characterise the studied fans stall recovery pattern in terms of the identified physical flow phenomena.

We measured fan casing unsteady pressure whilst we used the variable pitch in motion mechanism to change blade angle from 70.0 to 50.0 degrees during a transient lasting 30 seconds. We measured unsteady pressure using two microphones offset azimuthally such that the signals from the direction of rotation were top (Channel 1) to bottom (Channel 2), Figure 4.2.

When we visually inspected the Channel 1 fan casing unsteady pressure data that we obtained during a variable pitch in motion transient from stalled to stable operation, it was apparent that the post-stall pressure instabilities collapse after 15.00 seconds, partially recover at 15.20 seconds and then collapse again after 15.90 seconds, Figure 4.3. When we visually inspected the Channel 2 fan casing unsteady pressure data, the same pressure instabilities collapse, partially recover and collapse were present, Figure 4.3. Bianchi *et al.* studied variable pitch in motion fan performance (2011). They concluded that spike-like pressure waves were present during
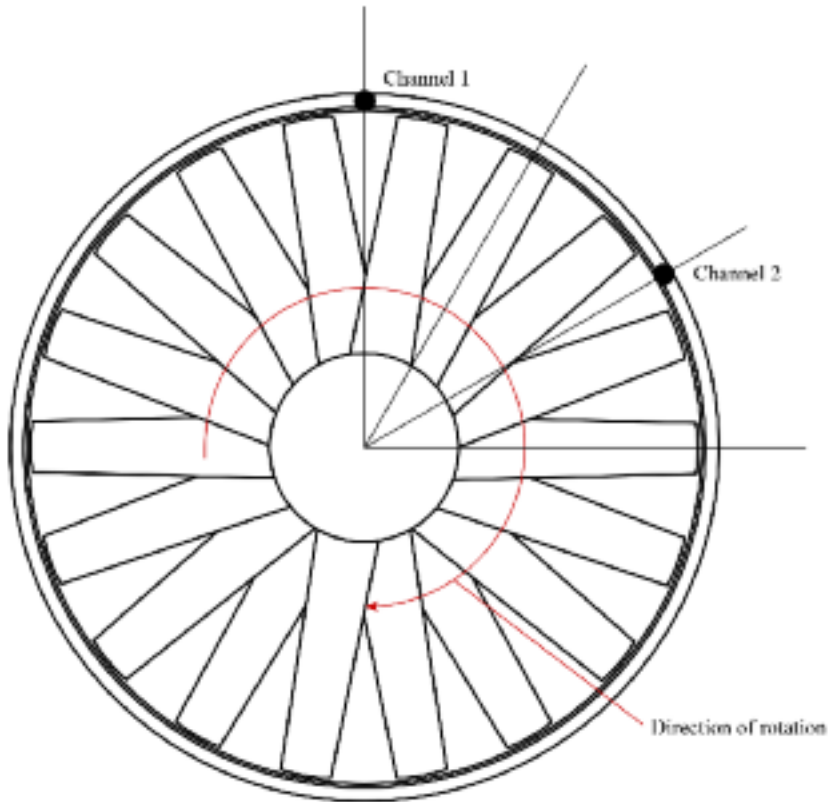
FIGURE 4.2. View looking into the fan inlet, illustrating two microphones 60 degrees azimuthally offset locations around the fan casing and the impeller's rotation direction.

stall inception. The collapse, partial recovery then collapse of the pressure instabilities that we observed is of a similar time scale and magnitude to those which Bianchi *et al.* observed (2011). As such, it is apparent that the occurrence of spike-like pressure instabilities associated with transition from stalled to stable operation also may characterise recovery from stall.

A visual inspection of the pressure instabilities associated with transition from stalled to stable operation indicates that the pressure instabilities have a characteristic bow-shape followed by multiple narrow pressure peaks, Figure 4.3. Outa (2005) observed this characteristic combination when studying rotating stall in a single stage sub-sonic compressor. He characterised this combination as indicative of the presence of a separation bubble. The similarity with data that we recorded during the programme of work reported in this chapter is indicative of the collapse, partial recovery and then final collapse of a separation bubble during the transition from stalled to stable operation.

During the recovery transient we can see a typical bow-shaped pressure instability at a blade angle of 52.5 degrees, Figure 4.3. When the blade angle reduces to

FIGURE 4.3. Detail of the sequence of events during stall recovery via variable pitch in motion. The unsteady pressure data was recorded using two sensors, azimuthally offset by 60 degrees and flush mounted in the fan casing over the blade tips.

51.0 degrees, the pressure signal changes to one with multiple narrow pressure peaks. This evolution of the pressure signal is indicative of initiating a rotating stall cell breakdown, with the rotating stall cell breaking into a series of smaller rotating instabilities. A single rotating stall cell breakdown into a series of smaller rotating instabilities allows for the inlet flow incidence angle's local readjustment. At a blade angle of 50.5 degrees, visually inspecting the pressure signals indicates that the flow stabilises briefly; however, the smaller rotating instabilities re-establish themselves as the blades are still aerodynamically overloaded. Only when the blade angle reduces to 50.0 degrees do the smaller rotating instabilities collapse permanently, with the fan returning to stable operation.

Spectral analysis of the variable pitch in motion data

The visual inspection of Channel 1 and Channel 2 raw pressure signals was complemented by a visual inspection of the cross-correlation spectral amplitude of the Channel 1 and Channel 2 pressure signals, Figure 4.4. A cross-spectrum between

the two circumferentially offset pressure transducers is helpful as it identifies flow features that persist from one circumferential location to another around the fan casing. This allows one to identify rotating flow features, whilst largely eliminating the effect of random turbulence at any given point around the fan casing.

We presented the cross-correlated spectral amplitude against shaft frequency order number n*. Thus, the analysis provides an insight into both the amplitude and frequency of the different pressure instabilities associated with rotating stall, the recovery transient and stable operation. We utilised a Fast Fourier Transform (FFT) using a time window equivalent to 20 rotor revolutions at the four blade angles of interest:

- during the stalled operation, a blade angle of 52.5 degrees, Figure 4.4a;
- across the stall recovery, a blade angle of 51.0 degrees, Figure 4.4b;
- across the stall recovery, a blade angle of 50.5 degrees, Figure 4.4c; and
- during stable operation, a blade angle of 50.0 degrees, Figure 4.4d.

A visual inspection of the stalled operation cross-spectrum (Figure 4.4a) indicates that the shaft frequency peak (n* = 1) was small in comparison to the rotating stall peak that rotates at 50 per cent shaft speed (n* = 0.5). Bianchi *et al.* (2010) observed that the rotating stall cell originates from the interaction of many smaller 'bubble' cells. They observed rotating stall cells that rotate at 50 per cent shaft speed comprises the aggregate effect of the many smaller 'bubble' cells. Individually, these cells do not contain sufficient energy to appear as fundamental tones in the cross-spectrum. However, as the bubble cells rotate at different speeds, they do appear in the cross-spectrum as side-bands to the rotating stall peak, rotating at 30 per cent and 80 per cent shaft speed (n* = 0.3 and n* = 0.8), Figure 4.4a.

As blade angle reduces to 51.0 degrees, it initiates the process of stall recovery as indicated by the change in cross-spectrum, Figure 4.4b. The cross-spectrum reveals a single very low-frequency peak. Other researchers (Kameier and Neise, 1997; Bianchi *et al.*, 2010, 2011) have identified the presence of a very low-frequency peak during stall recovery as indicative of inception of weak rotating instabilities. They characterise this as a 'recovery' bubble. This recovery bubble comprises a series of weak rotating instabilities that aggregate into a series of peaks in the cross-spectrum over a range of zero to 40 per cent shaft speed (n* = 0.0 to n* = 0.4). Therefore, visual inspection of the cross-correlation spectral amplitude at 51.0 degrees (Figure 4.4b) provides clear evidence of post-stall behaviour.

As the blade angle reduces to from 51.0 to 50.5 degrees, the energy within the cross-spectrum reduces by an order of magnitude, as seen in the change in the vertical axis scale of Figure 4.4c when compared with that of Figure 4.4b. A shaft frequency peak replaces low-frequency peaks which disappear at 50.5 degrees in the cross-spectrum, Figure 4.4c. The presence of a dominant shaft frequency peak in the cross-spectrum is indicative of the fan returning to stable operation. There is evidence of side-bands in the cross-spectrum, a feature self-consistent with Kameier and Neise's findings (1997) when studying stall recovery. These researchers concluded
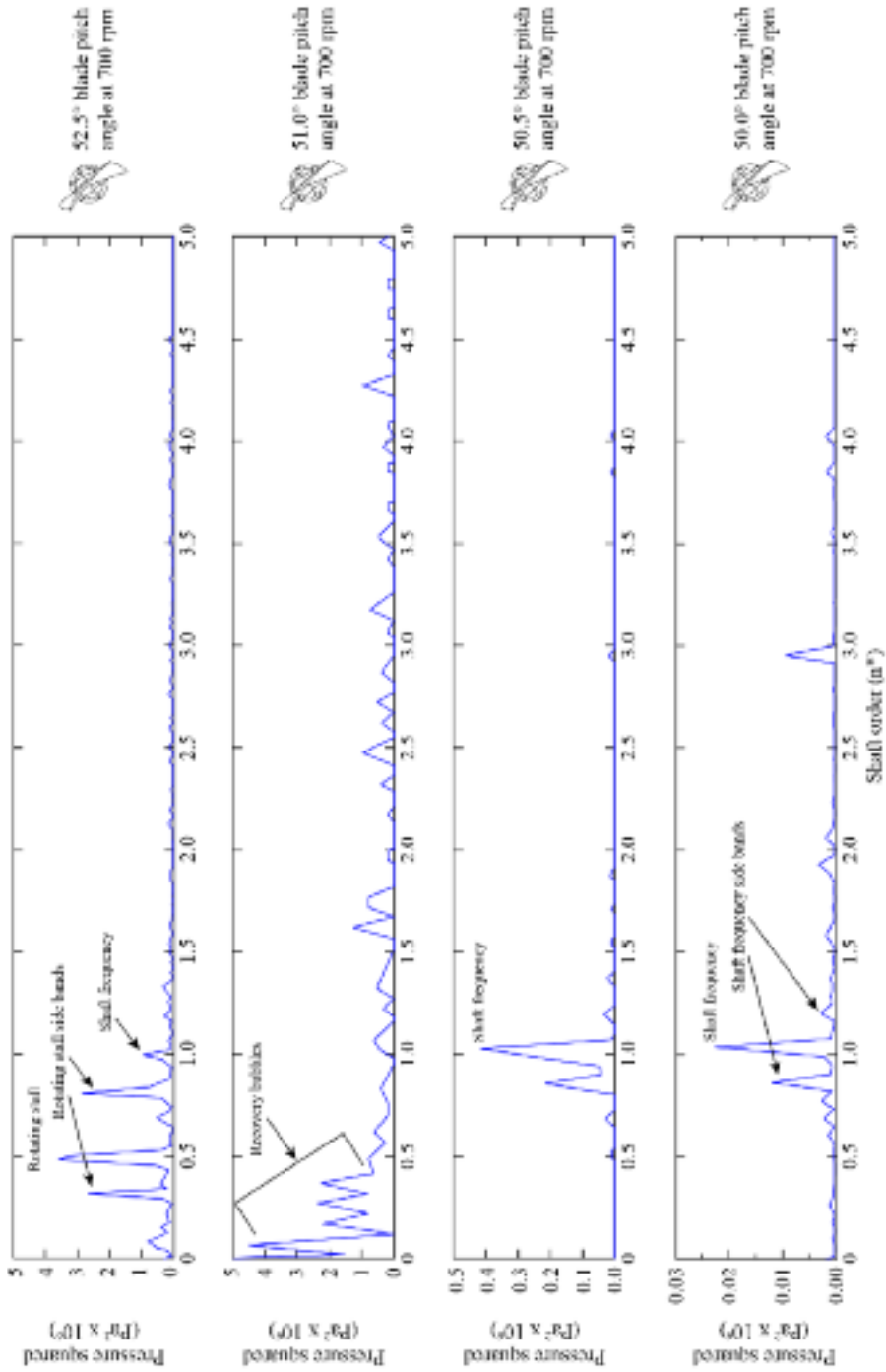
FIGURE 4.4. Cross-correlation spectral amplitude during stall recovery via variable pitch in motion during stalled operation at a blade angle of 52.5 degrees, the start of the stall recovery transient at a blade angle of 51.0 degrees, the end of the stall recovery transients at a blade angle of 50.5 degrees and back to stable operation at a blade angle of 50.0 degrees.

that the studied fan's aerodynamic characteristics resulted in rotating instabilities that occurred over a 30 per cent to 50 per cent characteristic range of shaft speed. During the stall recovery transient these rotating instabilities first emerged, and then collapsed. Other researchers have reported similar findings in a compressor with dynamic inlet flow distortion combined with tip injection (Leinhos *et al.*, 2001) and in low-speed axial fans (McDougall *et al.*, 1990).

As blade angle reduces from 50.5 to 50.0 degrees, the energy contained within the rotating instabilities reduces by an order of magnitude again, as seen in the change in the vertical axis scale of Figure 4.4d when compared with that of Figure 4.4c. This reduction in the energy of rotating instabilities is indicative of the fan returning to stable operation. The shaft frequency peak remains evident in the cross-spectrum, with evidence of very low-power sidebands at 80 per cent and 120 per cent shaft frequency.

Unsteady pressure measurements: variable fan speed

As with the variable pitch in motion unsteady pressure measurements, the primary objectives of the variable speed unsteady pressure measurements were:

(i)   to identify the physical flow phenomena associated with stall recovery for the studied fan when running at full speed; and

(ii) to characterise the studied fans' stall recovery pattern in terms of the identified physical flow phenomena.

We conducted the variable speed tests immediately following the variable pitch in motion tests, and maintained the blade angle at 70.0 degrees with no changes to the experimental facility, fan, instrumentation or data acquisition system. We initiated the transient from stalled to stable operation by driving the fan into stall at 700 rpm, and then reducing fan speed by 1 rpm per second. The fan transitioned from stalled to stable operation at 542 rpm after a 158 rpm speed change. We selected a rate of change of speed of 1 rpm per second as slow enough to facilitate the identification of short time-scale effects associated with specific fan speeds.

As with the variable pitch in motion pressure measurements, Figure 4.5 presents the unsteady pressure measurements, from Channel 1 and Channel 2 (Figure 4.2). As fan speed reduced, the amplitude and frequency of features in the unsteady pressure signals did not change until speed reduced to 547 rpm at a time of 73 seconds, Figure 4.5. Visual inspection of the Channel 2 unsteady pressure signal at 547 rpm indicates that the unsteady pressure signal has changed from the previous bow-shape to a series of isolated pressure spikes. Visual inspection of the Channel 1 unsteady pressure signal indicates the presence of a smaller pressure peak at a speed of 544 rpm which other researchers (Outa, 2005) have identified as typically associated with the recovery transient from stalled to stable operation. As speed reduces to 542 rpm, the multiple spike-like rotating instabilities disappear, indicating that the fan has completed its transition from stalled to stable operation.
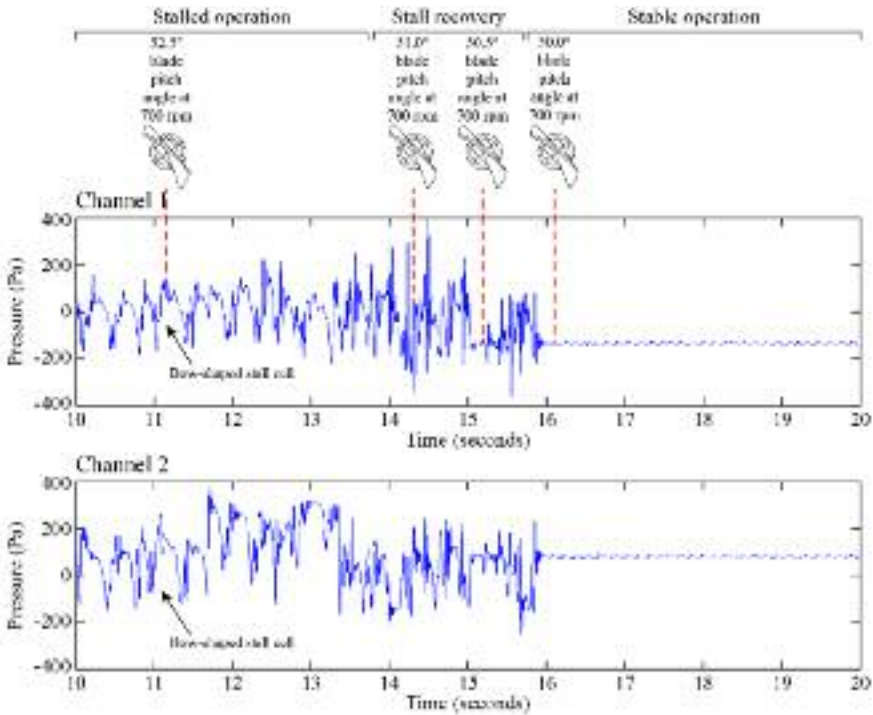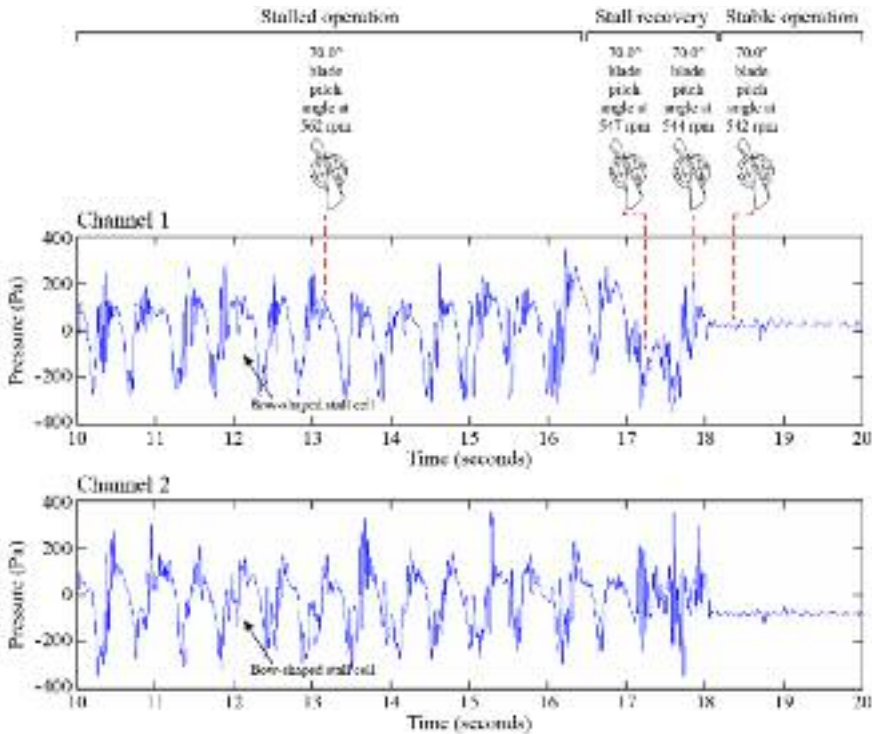
FIGURE 4.5. Detail of the sequence of events during stall recovery via variable speed. The unsteady pressure data was recorded using two sensors, azimuthally offset by 60 degrees and flush mounted in the fan casing over the blade tips.

Spectral analysis of variable fan speed data

The visual inspection of Channel 1 and Channel 2 raw pressure signals was complemented by a visual inspection of the cross-correlation spectral amplitude of the Channel 1 and Channel 2 pressure signals, Figure 4.6. As with the variable pitch in motion pressure signals, a cross-spectrum between the two circumferentially offset pressure transducers is helpful as it identifies flow features that persist from one circumferential location to another around the fan casing. Thus, we may identify rotating flow features induced in the flow as a consequence of varying fan speed, whilst largely eliminating the effect of random turbulence at any given point around the fan casing.

As with the variable pitch in motion analysis, we present the variable speed cross-correlated spectral amplitude against shaft frequency order number n*. This analysis provides an insight into both the amplitude and frequency of the different pressure instabilities associated with rotating stall, the recovery transient and stable operation. We utilised a fast Fourier transform using a time window equivalent to 20 rotor revolutions for four rotational regimes of interest:

(i)   during the stalled operation, a fan speed of 562 rpm, Figure 4.6a;

(ii)   across the stall recovery, a fan speed of 547 rpm, Figure 4.6b;

(iii)   across the stall recovery, a fan speed of 544 rpm, Figure 4.6c; and

(iv)   during stable operation, a fan speed of 542 rpm, Figure 4.6d.

A visual inspection of the stalled operation cross-spectrum (Figure 4.6a) indicates that the shaft frequency peak ($n* = 1$) was very small in comparison to the rotating stall peak that rotates at 30 per cent shaft speed ($n* = 0.3$). However, most noticeable is that the rotating stall peak's magnitude is significantly greater than that which we identified in the variable pitch in motion pressure signal's cross-spectral analysis (Figure 4.4a). The spectral evolution from stalled (Figure 4.6a) to stall recovery (Figure 4.6b) indicates that three low-order spikes rotating at approximately 40, 60 and 75 per cent shaft speed become more prominent whilst the rotating stall peak reduces in amplitude by approximately half. The reduced energy associated with the rotating stall peak and the increase in the energy associated with low-order spikes indicates rotating stall cell collapse and inception of weak rotating instabilities. As was the case with the variable pitch in motion analysis, we may characterise the rotating instabilities that we identified in the variable speed data as a recovery bubble.

As fan speed reduced to from 547 rpm (Figure 4.6b) to 544 rpm (Figure 4.6c) the energy of the rotating stall cell increased. This is in marked contrast to the variable pitch in motion data (Figure 4.4c) which indicates that towards the end of the recovery transient the rotating stall peak collapsed completely. At 544 rpm the rotating instabilities have consolidated into a recovery bubble peak (Figure 4.6c) with four times the amplitude of the low-order peaks associated with the recovery transient at 547 rpm (Figure 4.6b). The difference between the cross-spectrum for the variable pitch in motion data at the end of the recovery transient (Figure 4.4c) and the variable speed data at the end of the recovery transient (Figure 4.6c) is significant. The variable speed recovery transient was associated with peak amplitudes approximately four times those that we observed during the variable pitch transient. From this we may conclude that recovery from stall via variable pitch in motion results in the rotating stall cell breaking up into smaller rotating instabilities more rapidly than during recovery via variable speed. This observation is self-consistent with practitioner experience within the industrial fan community. The industrial fan communityfavoursvariable pitch in motion fans for those applications where stall is likely, and despite the high cost of variable pitch in motion fans when compared to fixed pitch variable speed fans, the community still regards them as less likely to suffer an in-service mechanical failure as a consequence of operating in an application where stalled operation is a possibility.

A comparison of the variable pitch in motion recovery transient (Figures 4.4b and 4.4c) and the variable speed recovery transient (Figures 4.6b and 4.6c) provides an insight into the dynamics of stall recovery. The cross-spectrum at the end of the two recovery transients features both different energy content and distribution. As the variable speed recovery transient commenced, low-order peaks in the cross-spectrum increased in amplitude (Figure 4.6b). This increase in low-order peaks is self-consistent with constant blade loading. It is not possible for blade loading to

remain constant with reducing speed, which indicates that the recovery mechanism via variable speed was associated with rotating stall cells that were able to persist to the end of the recovery transient before collapsing. In contrast, the variable pitch in motion recovery transient was characteristic of reduced blade loading and a corresponding reduction in the rotating stall peak's amplitude.

We must consider the difference between the variable pitch in motion and variable speed recovery transient within the context of the cross-spectrum associated with recovered operation (Figures 4.4d and 4.6d). The shaft frequency peak and side bands have a similar amplitude and distribution for both, indicating that despite the different mechanisms associated with the recovery transient, the fan is behaving in essentially the same way after recovery. As such, the fan was operating at the same initial duty point both before and after the stall recovery (Figure 4.1) with the difference in cross-spectrum associated with approach and transition through the recovery transient. The difference between the variable pitch in motion recovery transient and variable speed recovery transient is significant enough to suggest that the studied fan was exhibiting a form of mild surge during the variable speed recovery transient. If the studied fan induced mild surge during a variable speed recovery transient, but did not during a variable pitch in motion recovery transient, then the aerodynamic forces imposed upon the blades would be significantly lower during a variable pitch in motion recovery transient than during a variable speed recovery transient. This would, in turn, result in lower mechanical forces, and consequently, a lower propensity of the fan to fail mechanically.

Variable pitch in motion and variable speed stall recovery patterns

The evolution of the studied fan's operating point from stalled to stable operation may be via a change in blade angle at constant fan speed, or via a change in fan speed at constant blade angle, Figure 4.1. Notably, the final stable operating condition is near independent of the mechanism by which the fan adapts to stable operation. The final stable operating cross-spectrum indicates shaft frequency peaks and side bands with similar amplitude and distribution for both the variable pitch in motion and variable speed recovery transient. However, the mechanism by which the fan returns to stable operation is different for the variable pitch in motion and variable speed recovery transients.

The spectral analysis showed the differences between a variable pitch in motion and variable speed return to stable operation. Variable pitch in motion results in identifiable 'side bands' and the interaction of many small rotating instabilities that, once the transition from stalled to stable operation starts, will become a 'recovery bubble' at low frequency. We may regard these recovery bubbles as embryonic rotating stall cells that originate from the breakup of the main rotating stall cell. These embryonic rotating stall cells evolve into a primary peak frequency that constitutes a dominant aspect of the transition from stalled back to stable operation.

The variable speed results indicate that the amplitude of unsteady pressure associated with the rotating stall cell is larger than for the variable pitch in motion case and is associated with three lower fan speed order spikes. As the fan approaches
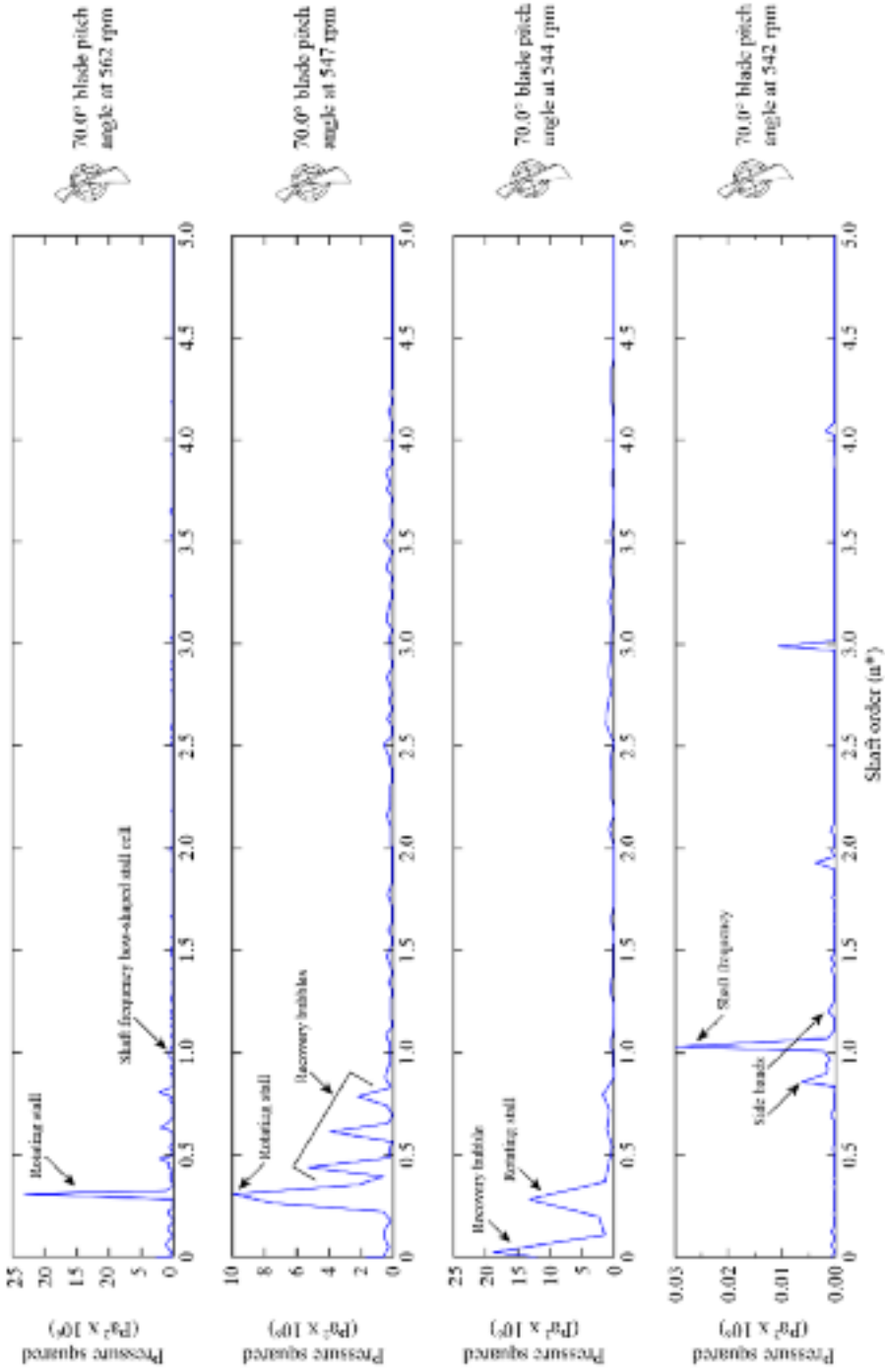
FIGURE 4.6. Cross-correlation spectral amplitude during stall recovery via variable speed during stalled operation at a fan speed of 562 rpm, the start of the stall recovery transient at a fan speed of 547 rpm, the end of the stall recovery transients at a fan speed of 544 rpm and back to stable operation at a fan speed of 542 rpm.

stable operation, but whilst it is still in stalled operation, the rotating stall cell frequency shifts to a lower frequency, but amplitude greater than that associated with variable pitch in motion. From this we may conclude that the transition from stalled to stable operation via variable speed results in a slower transition than that associated with a variable pitch transition as the variable speed recovery appears to influence the stall cell in a way that increases its magnitude during the transition. We may also speculate that the variable pitch in motion results indicate that the studied fan exhibits mild surge during the variable speed recovery transient, whilst remaining in stall during the variable pitch in motion recovery transient.

CONCLUSIONS

The Fourier transformation of cross-correlated pressure signals from two azimuthal positions 60 degrees offset pressure transducers provided unsteady pressure data for the studied fan during the transition from stalled to stable operation for recovery from stall via both varying blade pitch at constant fan speed, and varying fan speed with constant blade pitch. A qualitative inspection of the pressure signals and cross-spectrum for the stall recovery transition via each of the two methods highlighted differences in both the unsteady pressure and cross-spectrum between the variable pitch in motion and variable speed recovery transients.

An analysis of the variable pitch in motion data from the recovery transient from stalled to stable operation indicates that a rotating stall cell breaks down into a series of weak rotating instabilities that constitute a recovery bubble. In contrast, an analysis of the variable speed data from the recovery transient from stalled to stable operation indicates that the rotating stall cell contains more energy and breaks down very late in the stall recovery process. Analysis of the gathered data indicates that reducing fan speed results in a modification of the stall cell's shape from what we name bow-like to multiple spike-like instabilities.

The data that we collected during the recovery transient indicated the presence of a low-frequency tonal component associated with incipient stall recovery. The analysis also identified tone-band modulations in the measured unsteady pressure that we may characterise as harmonics that occur as a consequence of interaction between weak rotating instabilities associated with the stall recovery process.

The primary objective of the research reported in this chapter was characterisation of the physical flow phenomena associated with the transition from stalled to stable operation. The reported research has practical application in that one may use knowledge of the physical flow mechanisms associated with stall recovery in combination with a stall detection system (Sheard *et al.*, 2011). By tuning the stall detection system to the observed physical flow phenomena, one may use the stall detection system as input to a fan control system, with blade angle systematically reduced until the fan transitions from stalled to stable operation. Most significantly, the reported research indicates that the transient fluid flow behaviour associated with stall recovery by varying blade pitch was indicative of both a mild and progressive transition. In contrast, stall recovery by varying fan speed occurred more suddenly.

In comparison with the variable pitch transition, the variable speed transition was more indicative of recovery from mild surge, from which we may conclude that stall recovery via variable speed resulted in significantly higher unsteady mechanical stress induced in fan rotating components then recovery via variable pitch.

<div align="center">

REFERENCES
</div>

ISO IEC60651, 1994, Specification for Sound Level Meters.

ISO 5801, 2007, Industrial Fans — Performance Testing Using Standardized Airways.

Bianchi, S., Sheard, A.G., Corsini, A., and Rispoli, F. (2010), "Detection of Stall Regions in a Low Speed Axial Fan. Part I — Azimuthal Acoustic Measurements", *Proceedings of the 55th American Society of Mechanical Engineers Gas Turbine and Aeroengine Congress*, Glasgow, Scotland, 14–18 June, paper no. GT2010-22753.

Bianchi, S., Sheard, A.G., and Corsini, A. (2011), "Stall Inception Evolution and Control in Low Speed Axial Fan Fitted with Variable Pitch in Motion", *Proceedings of the 56th American Society of Mechanical Engineers Gas Turbine and Aeroengine Congress*, Vancouver, BC, Canada, 6–10 June, paper no. GT2011-45725.

Boerrigter, H.L. (1996), "PreMeSys: a Simulation Program to Determine the Frequency and Time Response of a Pressure Measurement System", *VKI Technical Memorandum 53*, Von Karman Institute for Fluid Dynamics, Rhode-Saint-Genèse, Belgium.

Bright, M.M., Qammar, H., Vhora, H., and Schaffer, M. (1998), "Rotating Pip Detection and Stall Warning in High-speed Compressors using Structure Function", *Proceedings of AGARD RTO AVT Conference,* Toulouse, France, 11–15 May.

Camp, T.R., and Day, I.J. (1998), "A Study of Spike and Modal Stall Phenomena in a Low-speed Axial Compressor", *Transactions of the ASME, Journal of Turbomachinery*, vol. 120, pp. 393–401.

Carbonaro, M. (2009), *Measurement Techniques in Fluid Dynamics — An Introduction*, Von Karman Institute for Fluid Dynamics, Rhode-Saint-Genèse, Belgium.

Cumpsty, N.A. (1989), "Part-circumference Casing Treatment and the Effect on Compressor Stall", *Proceedings of the 34th American Society of Mechanical Engineers Gas Turbine and Aeroengine Congress*, Toronto, ON, Canada, 5–8 June, paper no. 89-GT-312.

Daly, B.B. (1985), *Woods Practical Guide to Fan Engineering*, Woods of Colchester Ltd, Colchester, UK.

Day, I.J., and Cumpsty, N.A. (1978), "The Measurement and Interpretation of Flow Within Rotating Stall Cells in Axial Compressors", *Proceedings of the Institution of Mechanical Engineers, Part C, Journal of Mechanical Engineering Science*, vol. 20, pp. 101–14.

Deppe, A., Saathoff, H., and Stark, U. (2005), "Spike-type Stall Inception in Axial Flow Compressors", *6th Conference on Turbomachinery, Fluid Dynamics and Thermodynamics*, Lille, France, 7–11 March.

Emmons, H.W., Pearson, C.E., and Grant, H.P. (1955), "Compressor Surge and Stall Propagation", *Transactions of the ASME*, vol. 77, pp. 455–69.

Gall, W. (1975), "Fan with Variable Pitch Blades and Translating Bearing Actuation System", US Patent 3,873,236 A, 25 March.

Gravdahl, J.T., and Egeland, O. (1999), *Compressor Surge and Rotating Stall: Modelling and Control*, Springer Verlag, London, UK.

Greitzer, E.M. (1980), "Review — Axial Compressor Stall Phenomena", *Transactions of the ASME, Journal of Fluids Engineering*, vol. 102, pp. 134–51.

Ivanov, S.K. (1965), "Axial Blower", US Patent 3,189,260, 15 June.

Kameier, F., and Neise W. (1997), "Rotating Blade Flow Instability as a Source of Noise in Axial Turbomachines", *Journal of Sound and Vibration*, vol. 203, pp. 833–53.

Karlsson, S., and Holmkvist, T. (1986), "Guide Vane Ring for a Return Flow Passage in Axial Fans and a Method of Protecting It", US Patent 4,602,410, 29 July.

Langston, L.S. (2009), "Fitting a Pitch", *ASME Mechanical Engineering Magazine*, vol. 131, pp. 38–42.

Leinhos, D.C., Schmid, N.R., and Fottner, L. (2001), "The Influence of Transient Inlet Distortions on the Instability Inception of a Low Pressure Compressor in a Turbofan Engine", *Transactions of the ASME, Journal of Turbomachinery*, vol. 123, pp. 1–8.

McDougall, N.M., Cumpsty, N.A., and Hynes, T.P. (1990), "Stall Inception in Axial Compressors", *Transactions of the ASME, Journal of Turbomachinery*, vol. 112, pp. 116–23.

Mongeau, L., Thompson, D.E., and McLaughlin, D.K. (1995), "A Method for Characterizing Aerodynamic Sound Sources in Turbomachines", *Journal of Sound and Vibration*, vol. 18, pp. 369–89.

Moore, F.K. (1984), "A Theory of Rotating Stall of Multistage Compressors, Parts I–III", *Transactions of the ASME, Journal of Engineering for Power*, vol. 106, pp. 313–36.

Okada, K. (1987), "Experiences with Flow-induced Vibration and Low Frequency Noise Due to Rotating Stall of Centrifugal Fan", *Journal of Low Frequency Noise and Vibration*, vol. 6, pp. 76–87.

Outa, E. (2005), "Rotating Stall and Stall-controlled Performance of a Single Stage Subsonic Axial Compressor", *Journal of Thermal Science*, vol. 15, pp. 1–13.

Rippl, A. (1995), "Experimentelle Untersuchungen zuminstationaren Betriebsverhahen an der Stabilitarsgrenze eines mehrstufigen transsonischen Verdichters", PhD dissertation, Ruhr-Universitat Bochum, Germany.

Sheard, A.G., and Corsini, A. (2012), "The Mechanical Impact of Aerodynamic Stall on Tunnel Ventilation Fans", *International Journal of Rotating Machinery*, vol. 2012, article ID 402763, 12 pages, doi:10.1155/2012/402763.

Sheard, A.G., Corsini, A., and Bianchi, S. (2011), "Stall Warning in a Low-speed Axial Fan by Visualisation of Sound Signals", *Transactions of the ASME, Journal of Engineering for Gas Turbines and Power*, vol. 133, paper no. 041601, pp. 1–10.

Vo, H.D., Tan, C.S., and Greitzer, E.M. (2005), "Criteria for Spike Initiated Rotating Stall", *Proceedings of the 50th American Society of Mechanical Engineers Gas Turbine and Aeroengine Congress*, Reno, NV, USA, 6–9 June, paper no. GT2005-68374.

Chapter 5

Stall Warning in a Low-speed Axial Fan by Sound Signal Visualisation

A.G. Sheard, A. Corsini, and S. Bianchi

ABSTRACT

This study describes the development of a novel stall-detection methodology for low-speed axial-flow fans. Because aerodynamic stall is a major potential cause of mechanical failure in axial fans, effective stall-detection techniques have had wide application for many years. However, aerodynamic stall does not always result in mechanical failure. A subsonic fan can sometimes operate at low speeds in an aerodynamically stalled condition without incurring mechanical failure. To differentiate between aerodynamic stall conditions that constitute a mechanical risk and those that do not, the stall-detection methodology in the present study utilises a symmetrised dot pattern (SDP) technique that is capable of differentiating between stall conditions. This chapter describes a stall detection criterion based on a symmetrised dot pattern visual waveform analysis and develops a stall-warning methodology based on that analysis. This study presents an analysis of measured acoustic and structural data across nine aerodynamic operating conditions represented in a three-by-three matrix. The matrix is a combination of: (i) three speeds (full-, half- and quarter-speed) and (ii) three operational states (stable operation, incipient stall and rotating stall). We use the symmetrised dot pattern matrix and structural data to differentiate critical stall conditions (those that will lead to the fan's mechanical failure) from non-critical ones (those that will not result in mechanical failure), thus providing a basis for an intelligent stall-warning methodology.

NOMENCLATURE

Latin letters

BPF	blade passage frequency	Hz
i	number of dots	
D_t	tip diameter	mm
H_b	blade height	mm
ℓ_t	blade chord at the tip	mm
L	time lag	
N	number of the discrete signal	
R	polar position of the dot	
SDP	symmetrised dot pattern	
t	absolute time	s
x*	sampled value of the sound signal	

Greek letters

γ_t	blade tip stagger angle
δ_t	blade tip-pitch angle
Δt	time interval
η_{tot}	total efficiency
Θ^+, Θ^-	two angles of the polar space
ξ	angular gain
σ	input signal amplitude
Σ	solidity
τ	tip gap (% of the blade chord at the tip)
Φ	rotor flow coefficient (based on U_{tip})
Φ_D	design flow coefficient
Ψ	rotor work coefficient (based on U_{tip})
Ψ_D	design work coefficient

INTRODUCTION

The application of industrial fans into metropolitan metro and railway tunnel ventilation systems makes the stalled operation of fan difficult to avoid. Trains generate a pressure pulse as they travel through a tunnel. This pressure pulse drives ventilation fans up and down their characteristic each time a train passes the shaft within which they are situated. When operated at part speed, it is a near inevitability that ventilation fan will be transiently driven into stall (Sheard and Corsini, 2012; Cardillo *et al.*, 2014). In practice, engineers aim to design tunnel ventilation fans that have both (i) an aerodynamic design that will not stall at full speed (in response to the effect of a pressure pulse) and (ii) a mechanical design that is strong enough to enable the fan to run in stall at part speed (without failing). The consequences of a fan's mechanical failure in a tunnel-ventilation system are significant. The fan's primary duty in the event of an underground fire is to remove smoke,

leaving escape routes clear for people trapped. Thus, fan failure has potentially catastrophic consequences.

Although investigators have searched for reliable means of monitoring the approach of the stability limit whilst running both fans and compressors (Ludwig *et al*., 1976; Day *et al*., 1999; Höss *et al*., 2000), at least two questions remain unresolved. First, researchers have identified alert methods for individual test beds (Paduano *et al*., 2001), but reliable warnings of general validity require further research (Bindl *et al*., 2009; Liu *et al*., 2009). Second, researchers have sought techniques for incipient stall detection based on experimental observation of stall pre-cursors to identify their presence as early as possible. Early identification enables an active control system to react and suppress the incipient stall. However, researchers who have studied stall pre-cursors have concluded that an early detection period should last less than two rotor revolutions for axial compressors making detection challenging (Methling *et al*., 2004; Tahara *et al*., 2007). In contrast, the detection period for an industrial fan may be as long as 20 rotor revolutions, making detection a more practical proposition (Bianchi *et al.*, 2013).

Researchers have studied non-model based early-warning techniques in an effort to establish their suitability for real-time control applications. The non-model based techniques use a variety of diagnostic methods, most based on analysis of unsteady pressure measurements in the near-field over the fan blades, or the signals Fourier analyses. For Tryfonidis *et al*. (1995) studied a high-speed compressor's pre-stall behaviour using a technique based on spectral analysis of Fourier harmonics using as input unsteady pressure measured in the near-field over the fan blades. Bright *et al*. (1998) investigated rotating 'pip' detection prior to stall and proposed a method called 'temporal structure function', a statistical approach derived from chaos theory inspired. Christensen *et al*. (2008) developed a full-scale fan and compressor stability-management system by computing a correlation measure from unsteady pressure measured in the near-field over the fan blades. Tahara *et al*. (2007) proposed a stall-warning index, defining the index as the product of pressure fluctuations over two successive rotor revolutions normalised by the corresponding average pressure over the same two rotor revolutions. Tong *et al*. (2009) developed an on-line stall control system using a digital signal processing technique that correlated measured pressures in real time.

Cumpsty (1989) observed that the rotating stall inception mechanism may often correlate with a specific acoustic signature. Therefore researchers can consider noise-related detection techniques as possible solutions to the problem of detecting incipient stall. During the past decade, researchers have proposed diagnostic techniques based on sound-signal visualisation (Shibata *et al*., 2000; Wu and Chuang, 2005). This approach to fault diagnosis in rotating machinery is suitable when an acoustic signal is dominated by discrete and narrow frequency components related to the rotor speed. These conditions arise when the signal-to-noise ratio (or, more precisely, the instability signature-to-background noise ratio) is low, as is the case with industrial fan stall-inception at partial speed. Shibata *et al*. (2000) noted that when analysing acoustic signals, as opposed to unsteady pressure signals the relative probe and blade positions influence the analysis less.

The present study uses a symmetrised dot pattern (SDP) technique to generate images with identifiably different features at different fan operating conditions. This is the first published study in which researchers have applied the symmetrised dot pattern technique to the detection of incipient stall in decelerating axial turbomachinery (Sheard *et al.*, 2010). Researchers first conceived the symmetrised dot pattern technique for the visual characterisation of speech waveforms in automatic human-voice recognition algorithms (Pickover, 1986) and in sound quality evaluation (Schultz, 1978; Sottek and Genuit, 2007). Recently, Bianchi *et al.* (2009) proposed the use of symmetrised dot patterns as a means of characterising far-field acoustic emissions from a low-solidity axial fan. The fan was fitted with tip appendages for passively controlling blade tip-leakage generated noise.

To evaluate effectiveness of the symmetrised dot pattern technique, the study presents an analysis of acoustic and structural data. We consider nine operating conditions represented in a three-by-three matrix combination of (i) three speeds (full-, half- and quarter-speed) and (ii) three operational states (stable aerodynamic operation, incipient stall and rotating stall). The objective in doing so is to establish if identifiable differences exist between the symmetrised dot patterns associated with each of the nine operating conditions. Identifiably different symmetrised dot patterns provide a basis for identifying a fan's real-time operating condition, and therefore the basis of a diagnostic tool.

EXPERIMENTAL METHOD

Fan description

The fan that we used in this study is a scale model typical of those that engineers apply in metro and railway tunnel applications, Table 5.1. The ARA-D blade sections were single-parameter aerofoils that engineers originally designed for propeller applications (Corsini *et al.*, 2010). We used a 27 kW, direct coupled-induction 400 V (ac), three-phase motor to drive the fan rotor at a constant speed of 1480 rpm. The blade tip's speed was 77.5 m/s with an associated blade-passing frequency (BPF) for all the tested configurations of 217 Hz. We installed the fan in a ducted test system four diameters from the duct inlet bell-mouth. We optimised this bell-mouth's shape to give uniform and unseparated flow into the fan.

Casing instrumentation

We instrumented the fan casing with four inserts, each containing a 12 mm diameter GRAS microphone, type 40AG. The microphone specification enabled us to use them as high-frequency response unsteady pressure transducers, Table 5.2. We recessed the microphones from the casing's inner wall, Figure 5.1. The microphones were installed in the casing with an angular offset (θ) of 30 degrees.

Table 5.1. *Fan geometry and operating point data.*

Design speed	1,480 rpm
Tip speed	77.5 m/s
Design work coefficient, Ψ_D	0.21
Design flow coefficient, Φ_D	0.17
Design efficiency, η_{tot}	0.8
Tip diameter, D_t	1,000 mm
Blade height, H_b	375 mm
Blade chord at the tip, ℓ_t	105 mm
Blade tip stagger angle, γ_t	66°
Tip gap, τ (% of the blade chord at tip)	3%
Blade count	9
Solidity, Σ	0.6

Table 5.2. *Specification of the microphone used to make unsteady pressure measurements.*

Microphone	12 mm GRAS microphone, type 40AG
Error	0.1–0.2 dB at 1 kHz
Sampling rate	50 kHz
Calibration	Microphone and acquisition system ISO IEC60651 (1994)

We used a data acquisition system that sampled data over a time interval of 10 seconds. We estimated the uncertainty of the measurements as 0.1 to 0.2 dB at 1 kHz and established the uncertainty by calibrating the microphone and acquisition system in accordance with ISO IEC60651 requirements (1994). We used Corsini and Rispoli's approach (2005) to estimate the error in measured pressure due to turbulence at two per cent of the signal.

Signal processing technique

We utilised a 50 kHz sampling rate giving a Nyquist frequency of 25 kHz. To avoid signal aliasing, we filtered all data at 20 kHz and analysed it in the range of interest below 1 kHz. A range of interest below 1 kHz would require a Nyquist frequency of 2 kHz, and therefore data filtered at 20 kHz was an order or magnitude higher than the minimum required. Consequently, we concluded it to be acceptable in the present study. The microphones themselves incorporated a cavity between their front face and the microphone diaphragm. We calculated the cavity's resonant frequency to be 2,472 Hz, using the Helmholtz equation applied to an equivalent conical cavity. As the frequency range of interest was below 1 kHz, we considered the cavity's resonant frequency acceptable in the present study.

We calculated the system frequency response using the PREMESYS 2.0 MAT-LAB application tool, developed at the von Karman Institute of Fluid Dynamics by Boerrigter (1996). This application tool enabled us to characterise the measurement
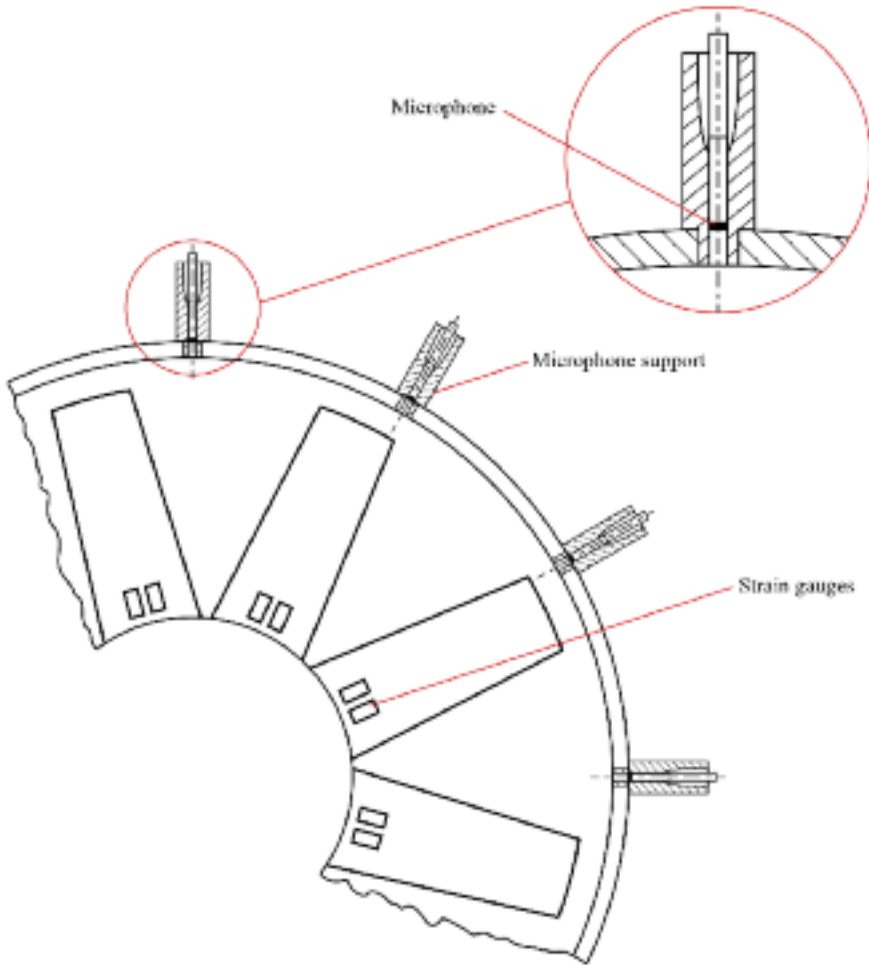
FIGURE 5.1. Sectional view of the impeller with the microphones mounted flush with the casing walls.

system's dynamic response to a step change in input signal, Figure 5.2. The dynamic response indicates that limiting any signal analysis to frequencies below 500 Hz would keep errors in phase angle below –3 degrees, which we considered acceptable in the present study.

We estimated the overall measurement uncertainty as (i) DV=1,000 mV±12 mV (20:3) on voltage and (ii) DG=200 dB±2.4 dB (20:3) on the raw signal gain for frequencies up to 1 kHz. Although the overall uncertainty of the measurement was higher than ideally we would have liked, the flow-field in the blade tip-to-casing region was both turbulent and periodic. We considered the overall uncertainty of the measurement acceptable in the present study as it was self-consistent with Anthoine *et al*.'s recommendations (2009) when taking measurements in unstable flow.
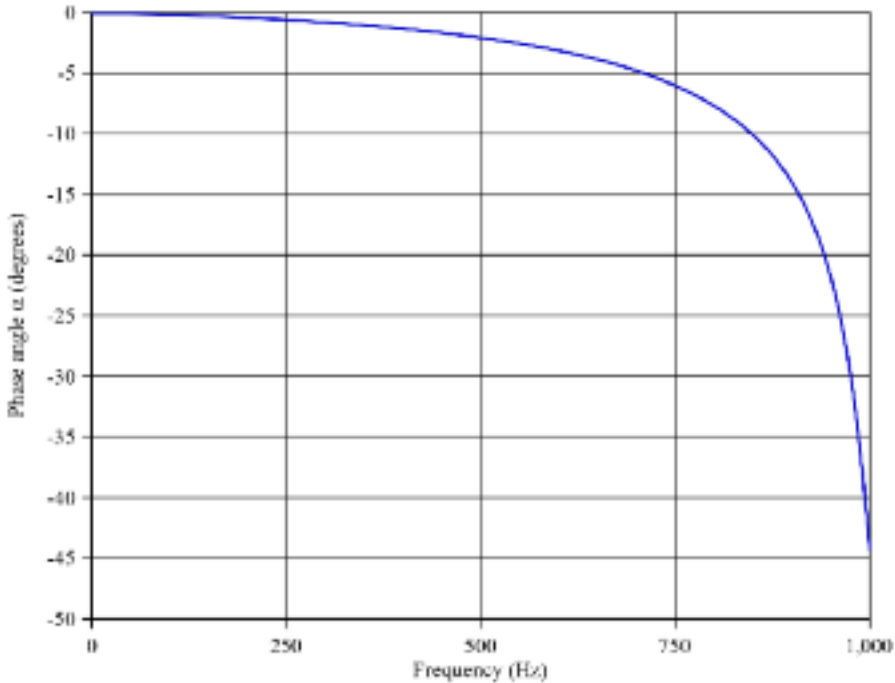
FIGURE 5.2. Characterisation of the measurement systems dynamic frequency response to a step-change in input signal (Boerrigter, 1996).

Test conditions

We measured the studied fan's characteristics at full, half and quarter design speed. At each speed we throttled the flow to establish regions of stable operation, incipient stall and rotating stall, Figure 5.3. We then calculated overall fan pressure rise from the average exit-area total pressure and average inlet-area total pressure. We measured pressure with an accuracy of ±0.5 per cent.

When operated at full, half and quarter design speed, the fan characteristic exhibited a pressure recovery after the transition from incipient stall into rotating stall. Industrial fans classically exhibit a rising characteristic when operated at flow rates below that at which they stall. Additionally, the fan characteristics at both half and quarter design speed are scaled versions of the fan characteristic at full design speed. Both a fan's pressure developing capability and resistance of the system into which it is installed will fall with the square of velocity through the system. As a consequence, one would expect a fan that stalls at one speed to stall at every other speed, and thus the measured fan characteristics were self-consistent with the fan laws.

Strain gauge measurements (Appendix) indicated that unsteady stress levels in the fan blade increased by a factor of approximately six as the fan throttled from stable operation, through incipient stall and into rotating stall. We associated the
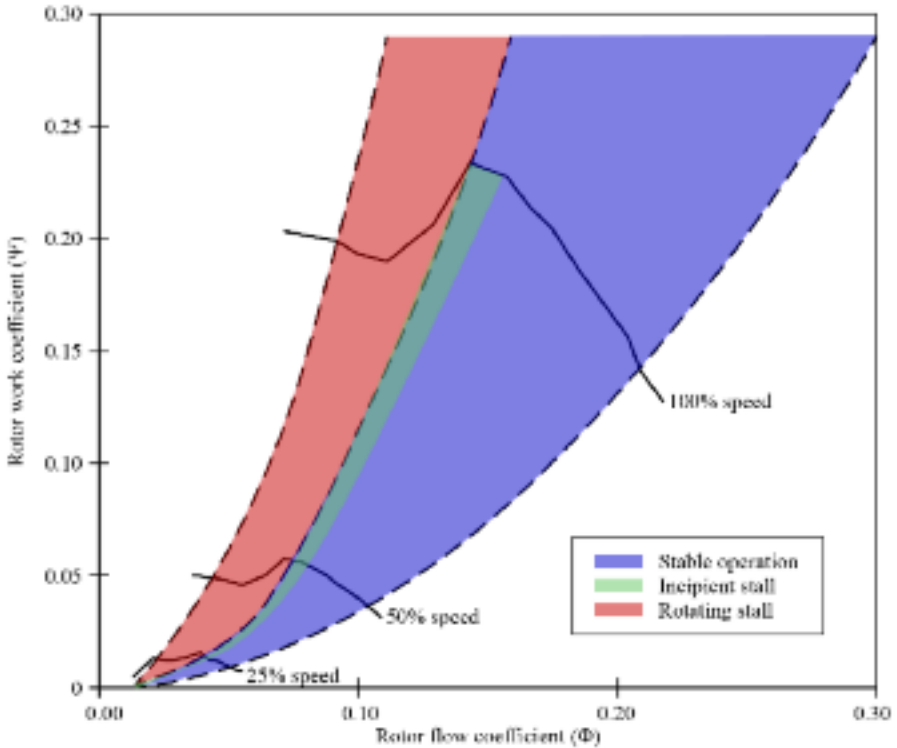
FIGURE 5.3. The studied fan's performance map and operating regions.

six-fold increase in unsteady stress levels with a narrow region of the fan's opera-
tions range, only occurring at flow rates immediately below the fan's peak pressure
developing capability. Flow rates immediately below the fan's peak pressure devel-
oping capability are the transition region from incipient stall to rotating stall.

The increase in the unsteady aerodynamic loads over the fan blades induced the
six-fold increase in unsteady stress level. However, the unsteady pressure that we
measured in the blade-tip region indicated only a small change in unsteady pressure
over the same region of the fan's operating range. The small change in unsteady
pressure at the blade-tip during the transition from incipient to rotating stall provides
an insight into the challenge that occurs with using an unsteady pressure signal as
input for a stall warning system. The absolute unsteady pressure level does not
change sufficiently to indicate that stall has become incipient, or that the transition
has commenced from incipient to rotating stall.

Bianchi *et al.* observed (2013) that a traditional stall warning system relies on
the pressure signal's Fourier transform, followed by an analysis of the measured un-
steady pressure's spectrum. The time taken to perform a Fourier analysis is signifi-
cant within the time-scales of the stall precursors' that indicate that stall has become

incipient. As such, one requires an alternative approach to stall warning to enable one to utilise stall precursors in identifying the onset of stall.

THE SYMMETRISED DOT PATTERN (SDP) TECHNIQUE

Researchers first conceived the symmetrised dot pattern technique for the visual characterisation of speech waveforms in automatic human-voice-recognition algorithms (Pickover, 1986). The symmetrised dot patterns provide a visual representation of the input signal, with pattern features that may be correlated with features of the input signal (Pickover, 1986). Although it may not be apparent which pattern features are associated with specific physical flow phenomena, the symmetrised dot patterns provide a characterisation of them. By linking the patterns' topology and the fan operating condition, the resultant stall detection method shares its foundation with chaos theory (Gleick, 1987).

The symmetrised dot patterns technique's advantage over other approaches is its ability to link pattern features with specific physical flow phenomena. The symmetrised dot pattern technique does not simply measure the overall sound power level produced by an input signal's tonal components. It is able to visually represent more subtle features that would otherwise be difficult to characterise. Therefore, the merit of the symmetrised dot pattern technique is its ability to perceive otherwise 'unquantifiable' differences in sound signals mimicking the way that humans hear (Schultz, 1978; Sottek and Genuit, 2007).

Mathematical framework

We used an algorithm to map a normalised time waveform into a polar coordinate system to produce the symmetrised dot pattern, Figure 5.4. The algorithm maps a point in the time waveform as the polar coordinate's radial component, and the adjacent point in the time waveform as the polar coordinate's angular component. In this way, one may map successive pairs of points from the measured data as single points in a polar coordinate system. Collectively these points comprise the resultant symmetrised dot pattern.

We can formulate the polar transformation $R(i)$ from waveform to symmetrised dot pattern as:

$$R(i) = \frac{\sigma(i) - \sigma_{\min}}{\sigma_{\max} - \sigma_{\min}} \tag{1}$$

$$\Theta^-(i) = \Theta_0 + \frac{\sigma(i+L) - \sigma_{\min}}{\sigma_{\max} - \sigma_{\min}} \xi \tag{2}$$

$$\Theta^-(i) = \Theta_0 - \frac{\sigma(i+L) - \sigma_{\min}}{\sigma_{\max} - \sigma_{\min}} \xi \tag{3}$$
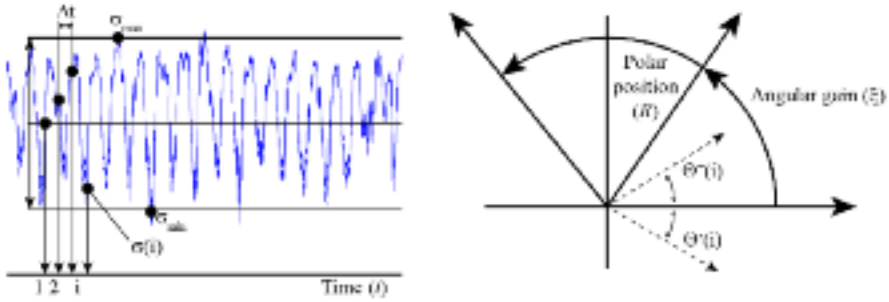
FIGURE 5.4. A schematic illustration of the technique for transforming an input signal into polar coordinates to produce a symmetrised dot pattern.

in which i is the number of dots (i = integer ($t/\Delta t$)), with t the time *abscissa* and Δt the sampling time; L is the time lag coefficient; $\sigma(i)$ is the sampled ith sound signal; σ_{max} and σ_{min} are the highest and the lowest value of the original waveform window; Θ_0 is the rotation of the origin angle of any reference line; ξ is the plot angular gain; and Θ^+ and Θ^- are the two angles of the traditional polar space. The input waveform is first normalised by finding the higher (σ_{max}) and lower values (σ_{min}) for the N data points in the window. Therefore, overall signal amplitude, in general, is not a factor in the characterisation.

The unsteady flow phenomena associated with incipient stall become established and then collapse in less than one rotor revolution (Bianchi *et al*., 2012). In order for a symmetrised dot pattern to visually represent incipient stall, one must take input data over a time that is similar to that of the physical flow phenomena associated with incipient stall. The symmetrised dot pattern quality is less dependent on the total number of data points than the sample rate. Shibata *et al*. (2000) studied the impact of sample rate. They concluded that when using a single-frequency sine wave as an input signal, the higher the sampling rate, the less clear the resultant symmetrised dot pattern. However, if the input signal includes components at multiple frequencies, the resulting symmetrised dot pattern was different from the sum of single frequency symmetrised dot patterns. In contrast, a white noise input signal resulted in a near uniform distribution of dots over the resultant symmetrised dot pattern, irrespective of sampling rate. Thus, Shibata *et al*. (2000) concluded that the combination of features in the input signal resulted in the complexity of the resultant symmetrised dot pattern.

Shibata *et al*. (2000) used different frequency sine waves to generate distinctly different symmetrised dot patterns, Figure 5.5. They concluded that when using a single-frequency sine wave as an input signal the higher the sampling rate the less clear the resultant symmetrised dot pattern. However, if the input signal includes components at multiple frequencies, the resulting symmetrised dot pattern was different from the sum of single frequency symmetrised dot patterns. In contrast, a white noise input signal resulted in a near uniform distribution of dots over the resultant symmetrised dot pattern, irrespective of sampling rate. Shibata *et al*. (2000)
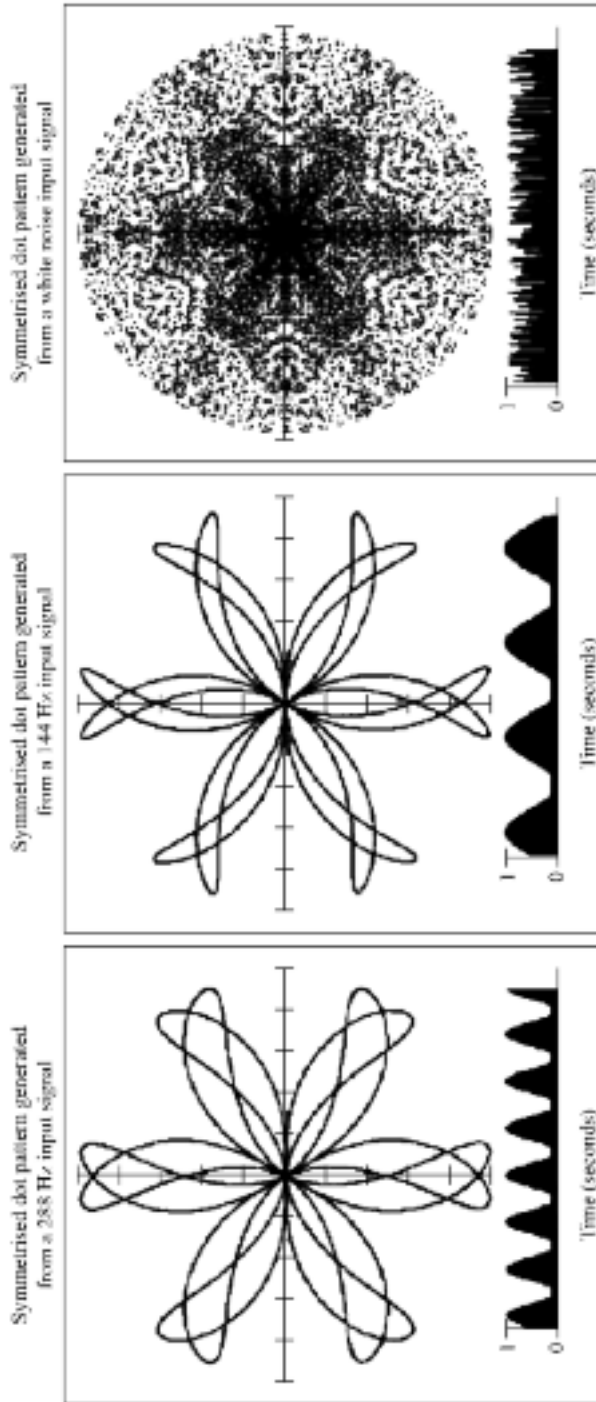
FIGURE 5.5. Symmetrised dot patterns generated from a 288 Hz sine wave, a 144 Hz sine wave and white noise, after Shibata *et al.* (2000).

thus concluded that the combination of features in the input signal resulted in the complexity of the resultant symmetrised dot pattern. Pickover (1986) also used sine wave test signals to illustrate the impact of a signal's frequency content on the resultant symmetrised dot patterns.

Sensitivity analyses

Dot pattern parameters

The transformation of a time waveform into a symmetrised dot pattern is a method for depicting changes in the amplitude and frequency of a time-series signal in a visual representation. As noted above, this involves transforming the pressure signal's time waveform into a set of dots which collectively comprise a snowflake-like pattern. To aid the visual interpretation of the pattern, it is mirrored six-fold to create the symmetrised dot pattern.

The symmetrised dot pattern methodology utilises time lag (L) and the angular gain (ξ) as parameters in the generation of the resultant symmetrised dot pattern. For this reason, the methodology's ability to identify the aerodynamic phenomena of interest depends on the choice of value for time lag and angular gain (De Rosier *et al.*, 1997). In this study we chose a sampling rate (Δt) of 50 kHz, with the total sampling time lasting 240 rotor revolutions. We evaluated the impact of varying time lag and the angular gain, obtaining well-differentiated symmetrised dot patterns with a time lag of 30 and an angular gain of 20, Figure 5.6.

Sampling rate and time

In the research reported in this chapter we aim to detect the aerodynamic instabilities that constitute stall precursors. As a consequence of the short time available to detect aerodynamic instability, it is desirable to sample the input signal at the highest sample rate, to acquire in the minimum time sufficient data points to construct a symmetrised dot pattern. Consequently, establishing the minimum sampling frequency is a key factor in successfully applying the symmetrised dot pattern methodology. We chose to characterise the effect of input signal sample rate with the fan operating at full design speed and at its peak pressure point ($\Phi = 0.13$) when stall is incipient, Figure 5.3. We also chose to use the previously established optimal values of time lag (L) and the angular gain (ξ) of 30 and 20 respectively, Figure 5.6.

We sampled the input signal over 240 rotor revolutions, initially acquiring the input signal first at the data acquisition system's highest sample rate of 50 kHz, Figure 5.7. At 50 kHz, the resultant symmetrised dot pattern dot density is concentrated into a defined pattern with angle in polar space (Θ) increasing more rapidly that the polar position (R). This results in the symmetrised dot pattern's curvature increasing with increasing dot polar position. According to Pickover (1986), a symmetrised dot pattern curvature is indicative of a feature in the input signal and therefore, a sample rate that results in the symmetrised dot pattern's curvature characterises the input signal well.
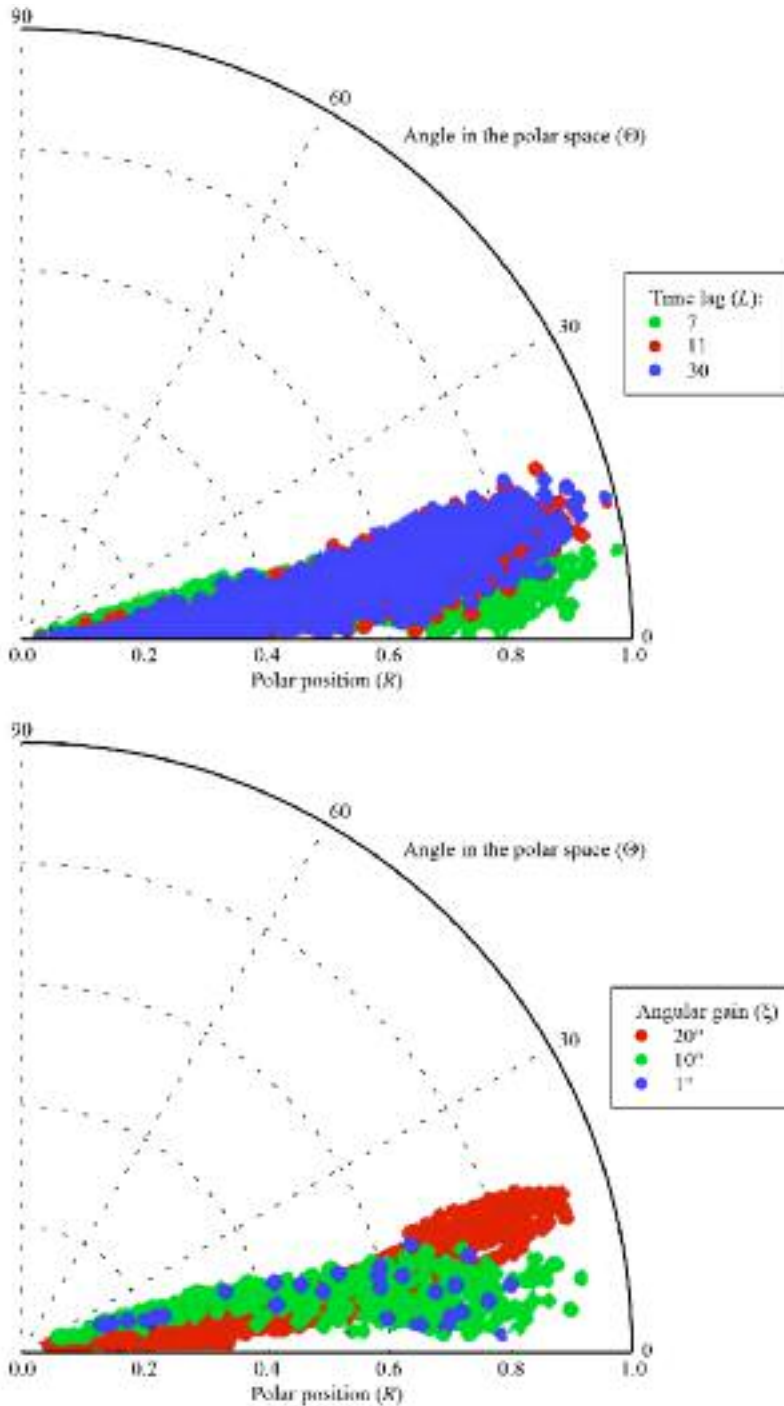
FIGURE 5.6. The impact of time lag (L) and angular gain (ξ) on a symmetrised dot pattern axis segment ($\Theta = 0°$). The authors generated the symmetrised dot patterns from a data set logged at 50 kHz over 240 rotor revolutions.
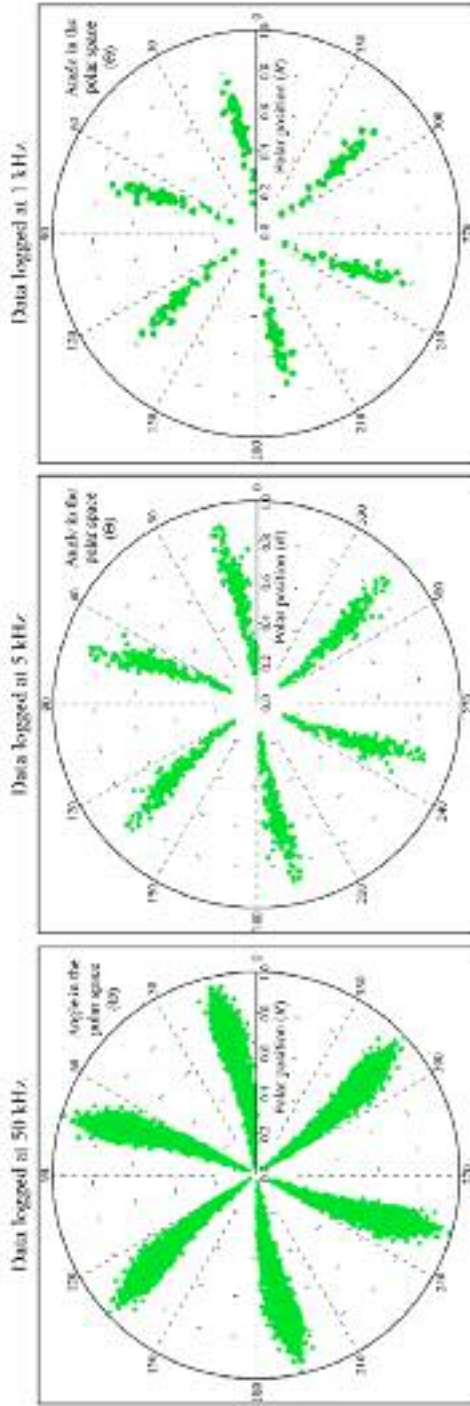
FIGURE 5.7. Symmetrised dot pattern variation with sampling rate. The symmetrised dot patterns were generated with data logged at 50 KHz, 5 kHz and 1 kHz using a time lag (*L*) of 30 and an angular gain (ξ) of 20. Data was logged over 240 rotor revolutions, with the fan running at full design speed at a flow coefficient (Φ) of 0.13 when stall was incipient.

A further study of the symmetrised dot pattern indicates that there is a concentration of dots over a range of polar positions (*R*), from 0.5 to 0.8. Previous researchers have established that a combination of symmetrised dot pattern curvature in combination with a concentration of dots is enough to enable the input signal's characterisation (Pickover, 1986; Shibata *et al*., 2000; Wu and Chuang, 2005).

Next we sampled the input signal over 240 rotor revolutions, now acquiring the input signal at a sample rate of 5 kHz, Figure 5.7. At 5 kHz, the resultant symmetrised dot pattern dot density is still concentrated into a defined pattern. However, angle in polar space (Θ) does not increase more rapidly than the polar position (*R*) and so there is no symmetrised dot pattern curvature with increasing polar position. A study of the symmetrised dot pattern indicates that there is a concentration of dots over a range of polar positions (*R*), from 0.5 to 0.65. Therefore, we may conclude that reducing the sample rate from 50 kHz to 5 kHz reduces the resultant symmetrised dot patterns effectiveness as a means of characterising the input signal.

Finally we reduced sampling rate to 1 kHz, Figure 5.7. At 1 kHz, the resultant symmetrised dot pattern dot density is still concentrated into a defined pattern, with some evidence of dot concentration over a range of polar positions (*R*), from 0.4 to 0.6. However, we concluded that when compared to the symmetrised dot patterns generated at 50 kHz or 5 kHz, the symmetrised dot patterns generated at 1 kHz are ineffective at characterising the input signal. Consequently, we chose to use a sample rate of 50 kHz during the remainder of the research reported in this chapter.

As we previously mentioned, quality of the resultant symmetrised dot patterns is less dependent on the total number of data points than the sample rate. However, the aerodynamic instabilities that constitute stall pre-cursors occur over very short time scales. As such, the shorter the sample time, the more likely a symmetrised dot pattern will include features that we may associate with a stall pre-cursor. In an effort to systematically characterise the impact of sample time, we derived nine symmetrised dot patterns presented in a three-by-three matrix. The matrix is a combination of (i) three speeds (full-, half- and quarter-speed) and (ii) three sample times (3.0, 1.0 and 0.1 rotor revolutions), Figure 5.8. We obtained all data at a sample rate of 50 kHz, using the previously established optimal values of time lag (*L*) and the angular gain (ξ) of 30 and 20 respectively.

A comparison of the symmetrised dot patterns generated with a sample time corresponding to 3.0 and 1.0 rotor revolutions indicates that a reduction in sample time from 3.0 to 1.0 rotor revolution did not result in significant change in the angular distribution of dots in polar space (Θ) with their polar position (*R*). At all three speeds the resultant symmetrised dot patterns generated with a sample time corresponding to 3.0 and 1.0 rotor revolutions were similar. Therefore, we may conclude that reducing sample time from 3.0 to 1.0 revolution does not degrade the quality of the resultant symmetrised dot patterns.

A comparison of the symmetrised dot patterns generated with a sample time corresponding to 1.0 and 0.1 rotor revolutions indicates that the reduction in sample time resulted in significant degradation of symmetrised dot pattern quality. Despite this degradation, it is still possible to infer some of the features evident in the symmetrised dot patterns generated with a sample time corresponding to 1.0 rotor
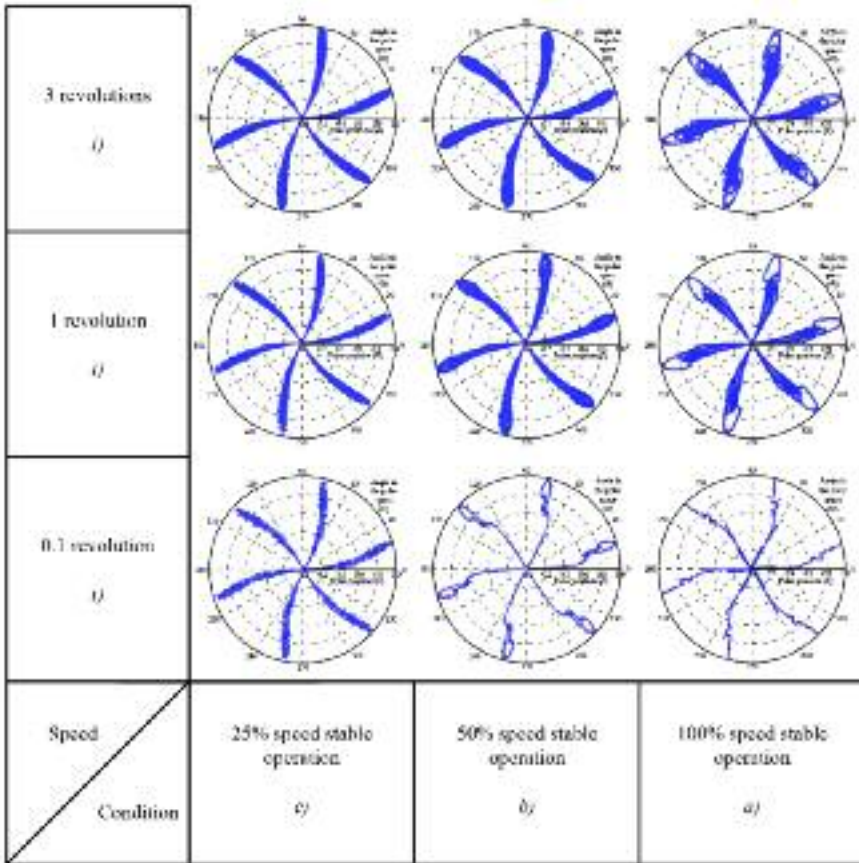
FIGURE 5.8. Symmetrised dot pattern variation with the sampling time and shaft speed. The symmetrised dot patterns were generated with data logged at 50 kHz using a time lag (*L*) of 30 and an angular gain (ξ) of 20.

revolution in the symmetrised dot patterns generated with a sample time corresponding to 0.1 rotor revolutions. Therefore, we may conclude that the symmetrised dot patterns generated with a sample time corresponding to 1.0 rotor revolutions represent the best trade-off between sample time and symmetrised dot pattern quality. However, the symmetrised dot patterns generated with a sample time corresponding to 0.1 rotor revolutions retain the potential to identify very short time-scale aerodynamic instabilities, and therefore may form a useful input to a diagnostic tool.

EXPERIMENTAL RESULTS ON STALL DIAGNOSIS

Bianchi *et al*. (2010) reported the acoustic azimuthal correlations from stall precursors that they observed in subsonic axial fans at full, half and quarter design speed of

the fan's nominal design speed. That spectral analysis identified a low-frequency tone when the studied fan operated in rotating stall, manifesting itself in the harmonic modulation of first and higher order blade passing frequency side-band. Bianchi *et al*. (2010) concluded that symmetric blade passing frequency side-bands were characteristic of rotating stall in the studied fan.

In the research reported in this chapter we continued Bianchi *et al*.'s work (2010), presenting an analysis of measured data across nine operating conditions comprising of (i) three speeds (full-, half- and quarter-speed) and (ii) three states (stable operation, incipient stall and rotating stall), Figure 5.9. We selected the nine operating conditions as they represented the range of conditions to which a fan may be subjected in a metropolitan metro or railway tunnel ventilation system.

We derived symmetrised dot patterns at each of the nine operating conditions with data that we obtained at a sample rate of 50 kHz and a sample time corresponding to 1.0 rotor revolution. We used the previously established optimal values of time lag (*L*) and the angular gain (ξ) of 30 and 20 respectively. The resultant symmetrised dot patterns are represented in a three-by-three matrix. The matrix is a combination of (i) three speeds (full-, half- and quarter-speed) and (ii) three operational states (stable operation, incipient stall and rotating stall), Figure 5.10.
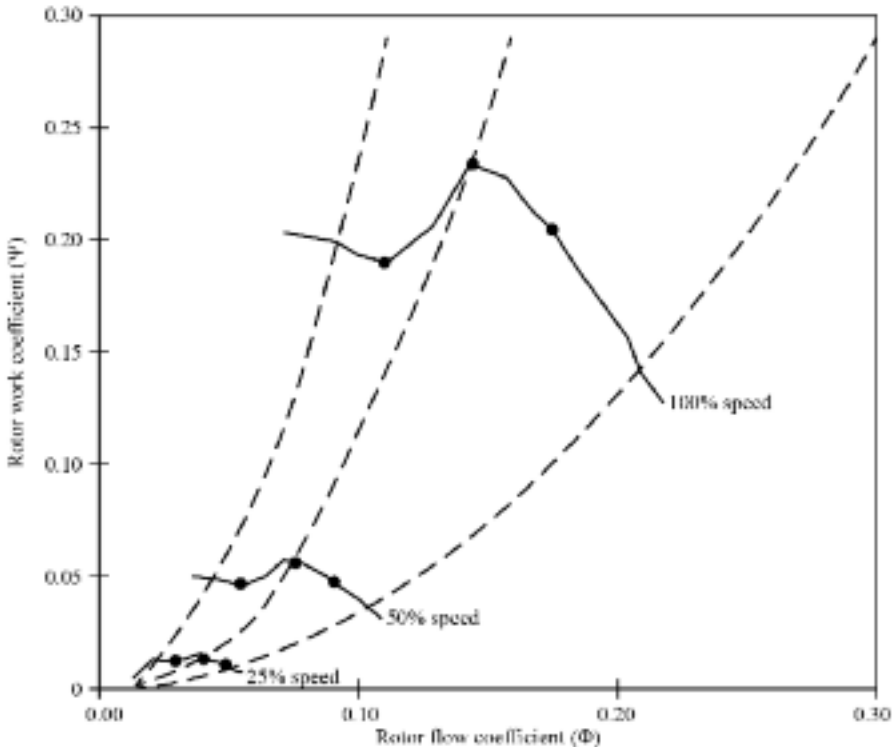
FIGURE 5.9. The nine operating conditions used to characterise the fan during stable operation, incipient stall and rotating stall at full, half and quarter design speed.
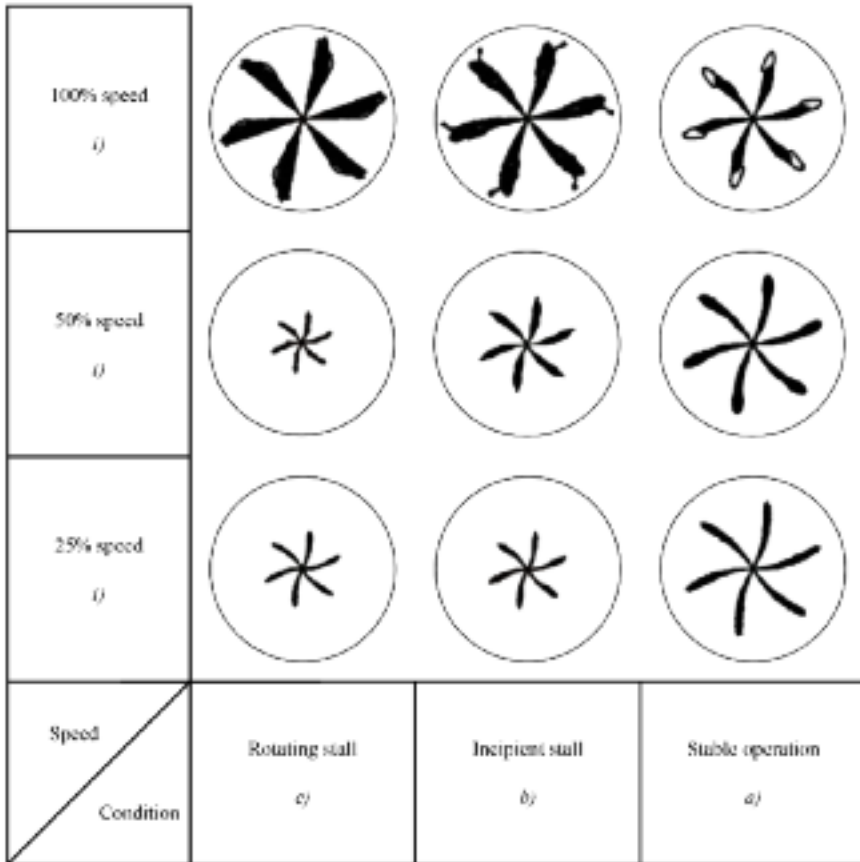
FIGURE 5.10. The nine symmetrised dot patterns used to characterise the fan during stable operation, incipient stall and rotating stall at full, half and quarter design speed. The symmetrised dot patterns were generated with data logged at 50 kHz over one rotor revolution using a time lag (*L*) of 30 and an angular gain (ξ) of 20.

Shibata *et al*. (2000) demonstrated that signals from rotating machinery with a known fault that were apparently indistinguishable from the signal without the fault still resulted in identifiably different symmetrised dot patterns. Therefore, we concluded that a possible basis for a stall-warning system is the generation of symmetrised dot patterns in real time from an input signal, followed by their comparison with symmetrised dot patterns associated with known operating conditions.

We placed the three symmetrised dot patterns associated with stable operation in a databank for template matching. Our logic was that any symmetrised dot pattern generated in real time that did not match a symmetrised dot pattern that occurs with stable operation must occur with either incipient stall or operation in rotating stall. Therefore, the proposed diagnostic tool would generate symmetrised dot patterns in real time, and then compare them with those stored in the databank after each sample interval.

The proposed diagnostic tool relied on identifiably different symmetrised dot patterns at each operating condition. When one studies the symmetrised dot pattern generated at full design speed during stable operation (Figure 5.10 (i) (a)) one notices a distinctive 'ring' at the end of the each 'arm'. This ring was unique to this operating condition and served as a 'benchmark' signature for the fan when operating at its design point. The symmetrised dot pattern's maximum polar position (R) increased as stall became incipient (Figure 5.10 (i) (b)), resulting in an increase in the symmetrised dot pattern's radius. When operated in rotating stall (Figure 5.10 (i) (c)), the area over the symmetrised dot pattern increased. Consequently, at full design speed the three symmetrised dot patterns' operating conditions were identifiably different.

When one studies the symmetrised dot pattern generated at half (Figure 5.10 (ii) (a) (b) (c)) and quarter design speed (Figure 5.10 (iii) (a) (b) (c)), it is apparent that they are identifiably different from the symmetrised dot patterns generated at full design speed (Figure 5.10 (i) (a) (b) (c)). The symmetrised dot patterns generated at half design speed exhibit a reduced radius compared to those generated at full design speed, whilst maintaining a similar overall form. The symmetrised dot patterns generated at quarter design speed are similar to those generated at half design speed, but with the dots comprising the symmetrised dot pattern covering a reduced area. Consequently, at the half and quarter design speed operating conditions symmetrised dot patterns were identifiably different both from each other and from those generated at full design speed. We may illustrate the link between the nine symmetrised dot patterns and the corresponding fan operating condition by placing the symmetrised dot patterns on the studied fan's operating map, Figure 5.11.

Symmetrised dot pattern interpretation

Although it is difficult to see the difference between symmetrised dot patterns when reduced in scale and incorporated onto the studied fan's operating map, it is possible to illustrate the difference. Perhaps the most critical change in symmetrised dot patterns is the change in pattern associated with the shift from stable operation to incipient stall at full design speed. By plotting the symmetrised dot pattern for the incipient stall condition in black, and then over-plotting the symmetrised dot pattern for stable operation in white, the difference between the two is apparent, Figure 5.12. The difference between the symmetrised dot patterns that occur with stable operation and incipient stall is significant enough for them to be regarded as identifiably different.

A study of the individual symmetrised dot patterns provides insight into the change in symmetrised dot pattern geometry with changing operating condition. The full design speed symmetrised dot patterns for the stable and rotating stall operation conditions illustrates the change in pattern geometry with changing operating condition, Figure 5.13. Once can characterise the symmetrised dot pattern's evolution from the stable operation to rotating stall using two parameters. First, the symmetrised dot pattern loses curvature, signifying the predominance of low-frequency components in the signal used to generate the rotating stall symmetrised dot pattern.
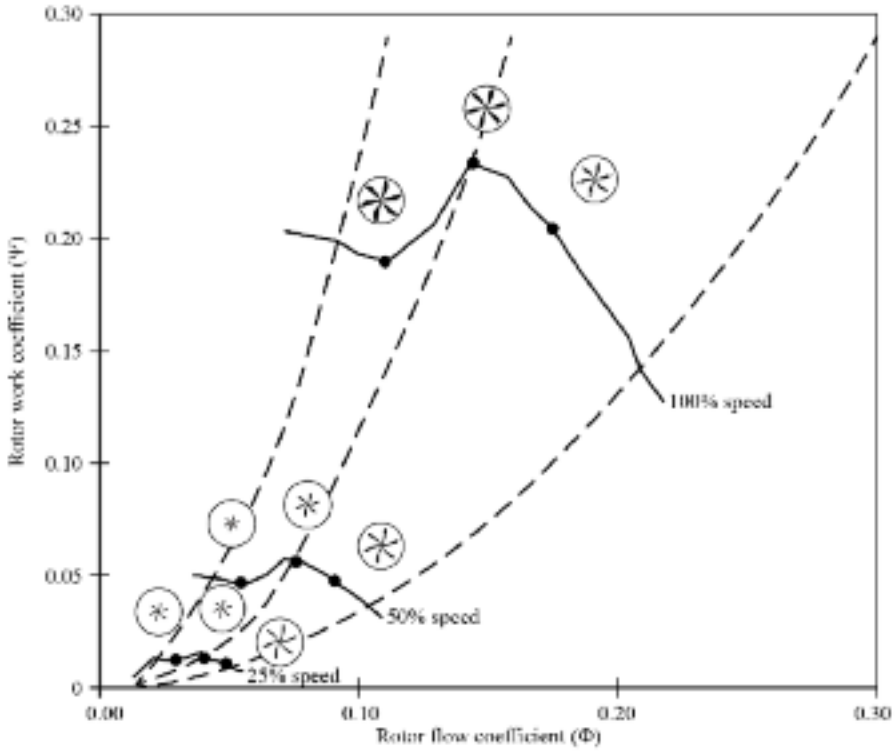
FIGURE 5.11. The generated symmetrised dot patterns at each of the nine studied operating conditions.
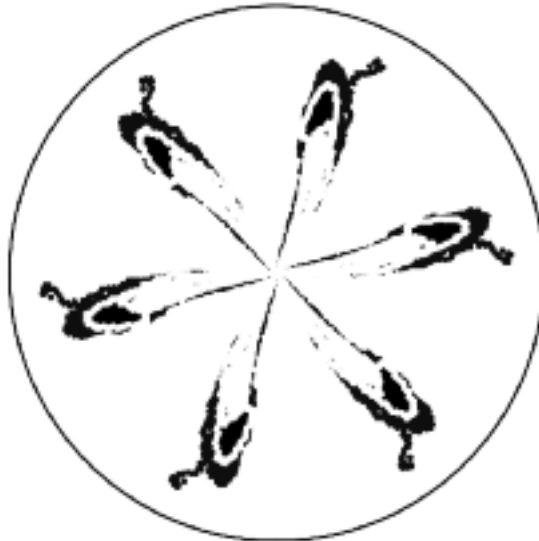
FIGURE 5.12. Superposition of symmetrised dot patterns associated with stable operation and incipient stall at full design speed.
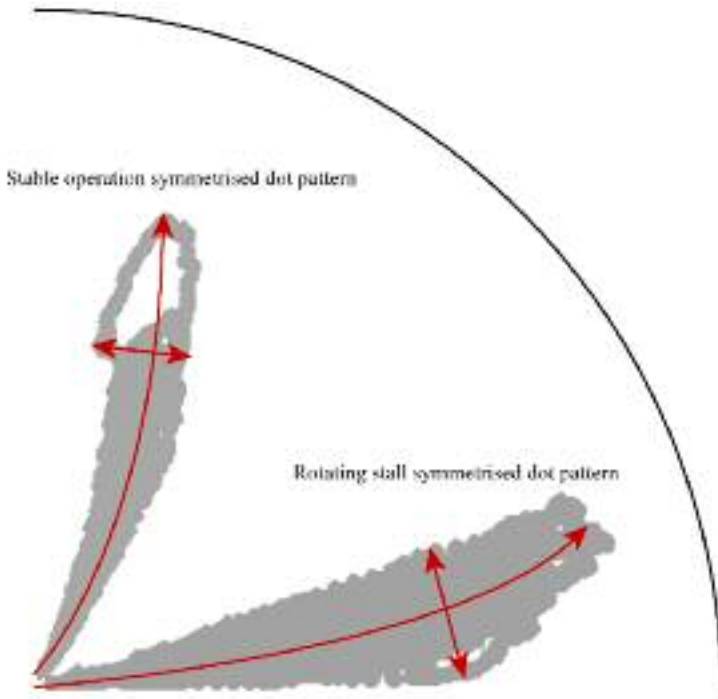
FIGURE 5.13. A comparison of symmetrised dot patterns generated from an input signal with the studied fan operating at full design speed in both stable operation and rotating stall.

An observation that low-frequency components characterising rotating stall is self-consistent with Bianchi *et al*.'s conclusions (2010). Second, the area covered by the symmetrised dot pattern increases with the input signal's increasing instability.

The symmetrised dot patterns generated at half (Figure 5.10 (ii) (a) (b) (c)) and quarter design (Figure 5.10 (iii) (a) (b) (c)) speed exhibit the same tendency to lose curvature with increasing aerodynamic instability. Once again this tendency signifies the increasing dominance of low-frequency components in the input signals that one uses to derive the symmetrised dot patterns. However, at both the half and quarter design speeds it is the reduction in symmetrised dot pattern area that is most apparent. Applying Bianchi *et al*.'s spectral analysis (2010), we can interpret the change in symmetrised dot pattern geometry with reducing speed as evidence of a progressive stall. In contrast, the stall is clearly defined when transitioning at full design speed from incipient stall to rotating stall.

Principle of the symmetrised dot pattern image template matching

It is the difference between symmetrised dot patterns that is the basis of a stall-detection method. Consequently, matching symmetrised dot patterns generated in real time against a library of symmetrised dot pattern has the potential to form the

basis of an incipient stall-detection system, Figure 5.14. In the proposed incipient stall-detection system one uses the data acquisition and processing system to record an input signal as one operates the fan in a series of known operating conditions. One then uses this data to generate a library of symmetrised dot patterns that are stored in a database.

The ability of the incipient stall-detection system to detect a shift from stable operation to incipient stall or rotating stall is its template matching ability, Figure 5.15. Template-matching is a digital image-processing method researchers use to compare image patterns. For the template-matching system, a programmer must convert the symmetrised dot patterns into a standard picture file format. This standardisation ensures that each symmetrised dot pattern is located at the picture centre prior to the match.

For incipient stall diagnosis, the programmer generates a symmetrised dot pattern in real time, using it as input into the template-matching system. One then compares the real-time symmetrised dot pattern against each of the symmetrised dot patterns stored in the database. One then uses the stored symmetrised dot pattern that best matches the real-time symmetrised dot pattern to infer the fan's operating condition. Once one knows the fan's operating condition, one may use the known state as input to a fan control system.
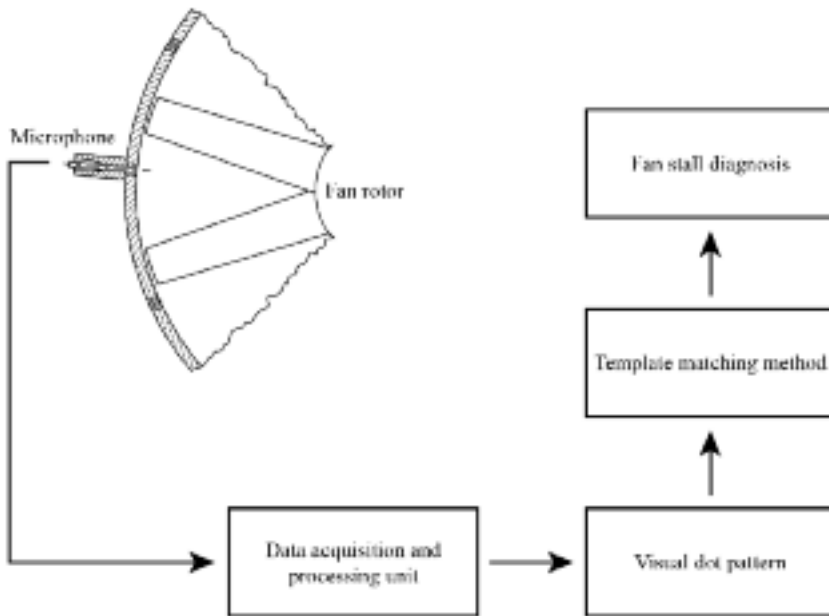
FIGURE 5.14. Schematic layout of a possible 'incipient' stall-diagnostic system based on the use of symmetrised dot patterns.
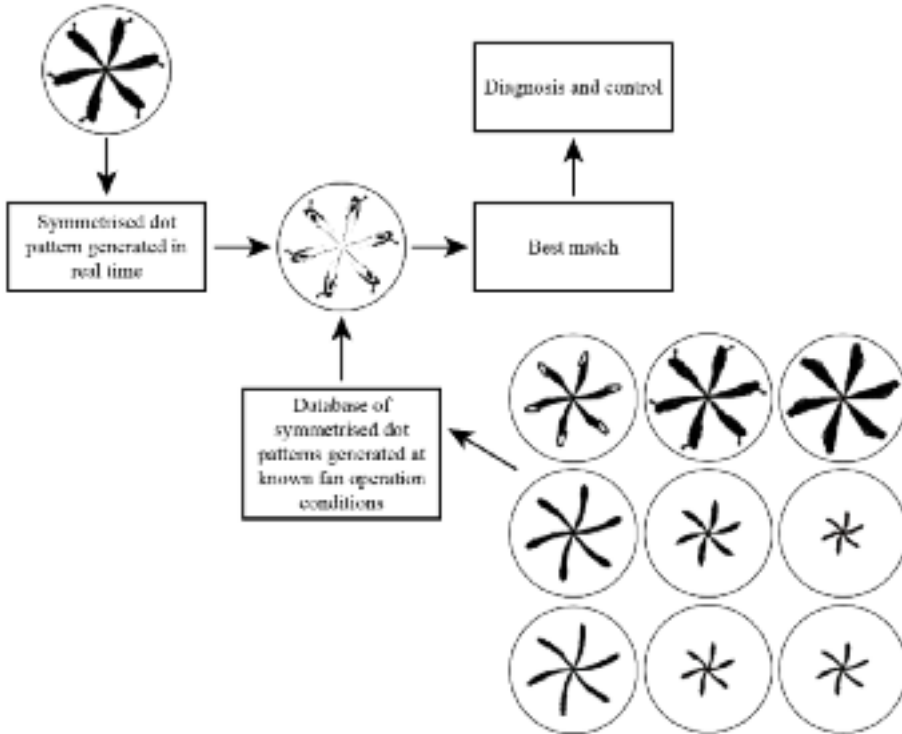
FIGURE 5.15. Template matching of symmetrised dot patterns in a possible 'incipient' stall-diagnostic system.

CONCLUSIONS

The diagnostic approach presented in this chapter detects early aerodynamic instabilities in an axial fan which facilitates the initiation of action to prevent the onset of rotating stall. Researchers have historically based stall-detection methods on an analysis of pressure or vibration signals in either the time or frequency domain. However, the signals researchers associate with stall precursors are often low compared to the background noise. Therefore, they require significant computational effort to extract. This makes conventional methods of stall-detection difficult to apply in active stall control systems.

In this chapter, we proposed a stall-detection method based on an analysis of symmetrised dot patterns. Symmetrised dot patterns represent an input signal on polar coordinates, and thus changes in the input signal frequency content manifest themselves as changes in the resultant symmetrised dot patterns. We have demonstrated that one may generate symmetrised dot patterns with data recorded during one revolution of the studied fan. Stall pre-cursors typically occur over a time scale similar to that of one revolution. Consequently we can generate symmetrised dot patterns fast enough for them to reflect the presence of a stall pre-cursor.

The experimental results presented in this chapter indicate that one can use the generation of symmetrised dot patterns in real time as the basis of an 'incipient' stall detection method that is able to identify stall pre-cursors. Thus, a symmetrised dot pattern technique based stall detection system is able to identify that a fan is likely to stall before it actually has.

In addition to its potential application in an active stall control system, the data in this chapter suggest that the symmetrised dot patterns are significantly differentiated at each of the studied operating condition and speed combinations. By associating each symmetrised dot pattern with mechanical risk (Appendix), one may use the symmetrised dot patterns to differentiate between stall conditions that will lead to the fan's mechanical failure and those that will not. Thus, the symmetrised dot patterns provide the basis of an intelligent stall-warning system that engineers can use to identify if a stall event presents a risk of fan failure. Therefore, the symmetrised dot pattern technique has the potential to not only identify the onset of stall in time for an active stall control system to act, but also to clarify if action is necessary.

APPENDIX: STRUCTURAL ANALYSIS

The term 'fatigue' refers to the phenomenon whereby virtually all materials will break under numerous repetitions of a stress that is not sufficient to produce an immediate rupture in the first instance. In this regard, fan blades are subject to fatigue stress induced by (i) the steady state 'mean' force arising from rotation and aerodynamic loading and (ii) the alternating stress produced by variations in lift as the fan rotates. This combination of mean stress and alternating stress makes fan blades inherently susceptible to fatigue.

The endurance limit for materials is a function of the combination of imposed mean and alternating stress. The ability of a wide range of materials to withstand different combinations of mean and alternating stress has been the subject of extensive study (Young, 1989). Industrial fan blades are usually manufactured from aluminium and as with any other material the ability of aluminium to resist fatigue for a fixed alternating stress reduces as mean stress increases. Gerber (1874) studied material test data for various levels of mean and alternating stress, and derived a relationship known as the Gerber Line, Figure 5.16.

The ability of a given aluminium alloy to resist the effect of mean and alternating stress is dependent on the maximum defect size in the material samples. The larger the defect, the lower the level of mean and alternating stress required to induce fatigue failure. Industrial fan manufacturers, therefore, routinely undertake x-ray examination of all rotating components to ensure that the maximum defect size is below that on which they established the Gerber Line.

Engineers usually analyse a new fan-blade design using a finite element analysis to establish the peak mean and alternating stress location. If the peak mean stress and alternating stress point is below the Gerber Line, the fan should not fail due to fatigue. However, in practice, there is some uncertainty about the Gerber Line's location because researchers derived it from experimental data. Additionally, the ability to calcu-
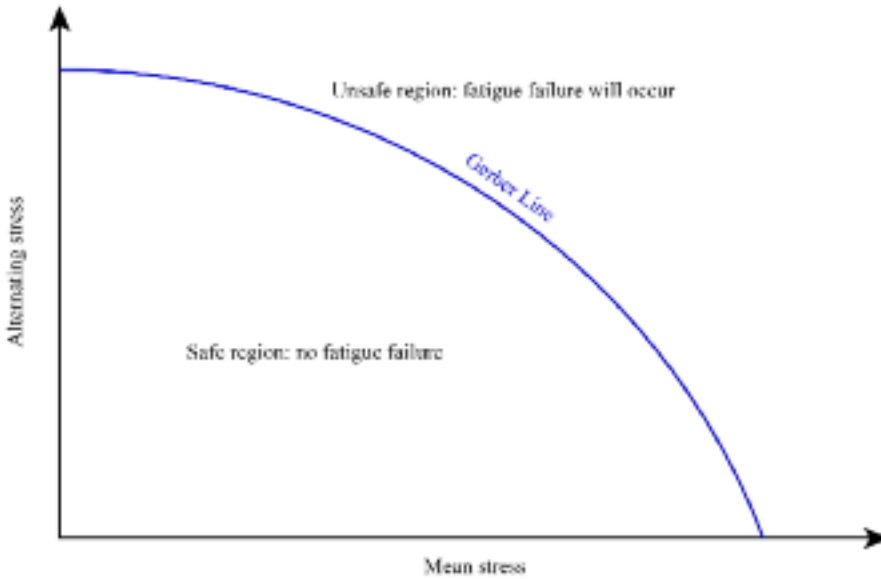
FIGURE 5.16. The curve of best fit through the limiting combination of alternating and mean stress is the Gerber Line (Gerber, 1874). Any combination of mean and alternating stress that falls outside the Gerber Line will result in a fatigue failure.

late mean and alternating stress levels is imperfect as a consequence of the assumptions one makes during the modelling process. In practice, industrial fan manufacturers therefore choose to design fans with a safety factor of two, Figure 5.17.

An industrial fan's ability to resist fatigue in service is satisfactory when designed to fall within a Gerber Line with a safety factor of two during normal operation at full design speed. Industrial fans have traditionally run at a single speed. However, the reduced cost of high-power variable-frequency drives has meant that it is becoming increasingly common to run at reduced speed. At reduced speed, the fan's pressure-developing capability reduces and consequently, a pressure pulse that would not result in the fan stalling at full design speed can result in the same fan stalling at reduced speed.

When a fan stalls, the alternating stress can rise by a factor of between 5 and 10 above normal operation. The actual increase in any given situation is dependent on the fan blade design and the fan application. Sheard and Corsini (2012) studied the mechanical impact of aerodynamic stall on an industrial fan designed for tunnel ventilation application, Table 5.3.

Sheard and Corsini (2012) established alternating stress levels by applying strain gauges to four of 12 fan blades, Figure 5.1. They established the location for the strain gauges through the fan blade's finite-element analysis to identify the peak mean stress region. Strain gauge data indicated that alternating stress would typically rise by less than 10 per cent as the fan approached stall. However, a sharp rise in alternating stress level occurred as the fan actually stalled.
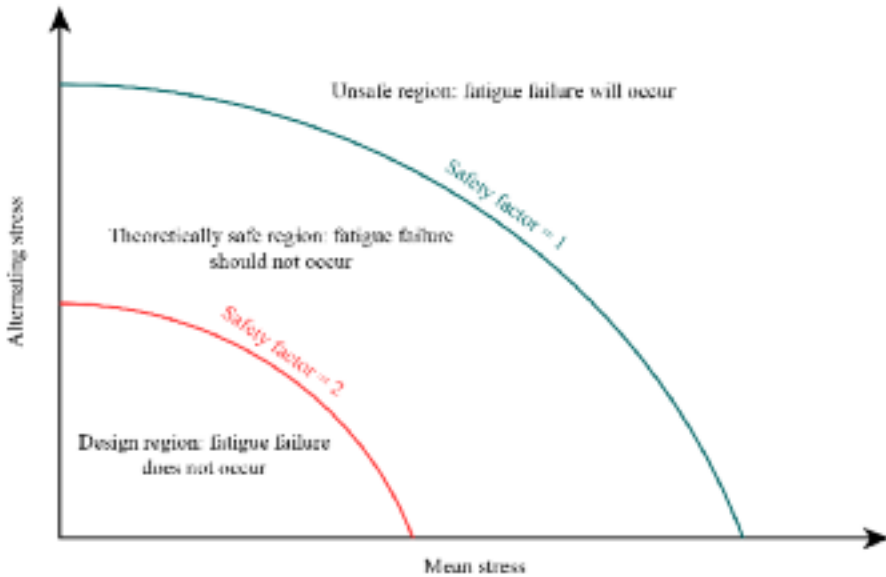
FIGURE 5.17. The Gerber Line associated with material test data, and the Gerber Line with a safety factor of two.

Table 5.3. *Safety factors derived from strain gauge data (Sheard and Corsini, 2012).*

Per cent of full speed	Normal operation safety factor	Stall operation safety factor
100	2.3	0.4
50	10.0	2.5
25	106.0	7.3

Operating the fan at full, half and quarter design speed in both stable operation and in rotating stall resulted in Sheard and Corsini (2012) calculating six separate safety factors. They reported a safety factor during stable operation at full design speed at 2.3, 0.3 higher than the desirable minimum (Table 5.3). When operated in rotating stall, the safety factor reduced to 0.4. As a safety factor of 0.4 is significantly lower than 1.0, this indicates that if the fan continued to operate in rotating stall at full design speed, the blades would suffer fatigue failure.

During stable operation, the safety factor increased from 2.3 at full design speed to 10.0 at half design speed, Table 5.3, a factor of approximately four. Mean stress in a fan blade reduces with the square of speed, therefore one would expect that reducing speed by half would increase the safety factor by four. When Sheard

and Corsini (2012) operated the fan at half design speed in rotating stall, the safety factor was 2.5, an increase of more than six compared with the same fan operating in stall at full design speed. The increase in the safety factor is a consequence of the aerodynamically induced alternating stresses when operating the fan in rotating stall falling more rapidly than the mean stress falls when we reduced fan speed from full to half design speed, Figure 5.18.

The safety factor at half design speed when operating in stall (2.5) was slightly higher than the safety factor Sheard and Corsini (2012) associated with running the fan at full design speed in stable operation (2.3). This result is significant because industrial fans in metropolitan metro and railway tunnel ventilation systems routinely operate at both half and quarter design speeds. As a consequence of the fan's reduced pressure-developing capability at reduced speed they are routinely drive into stall.

We cannot generalise the above results, that a safety factor at half design speed in rotating stall is higher than a safety factor at full design speed during stable operation. Engineers must mechanically validate each fan design to establish the safe maximum speed at which a new fan design can operate in stall without risk of fatigue.
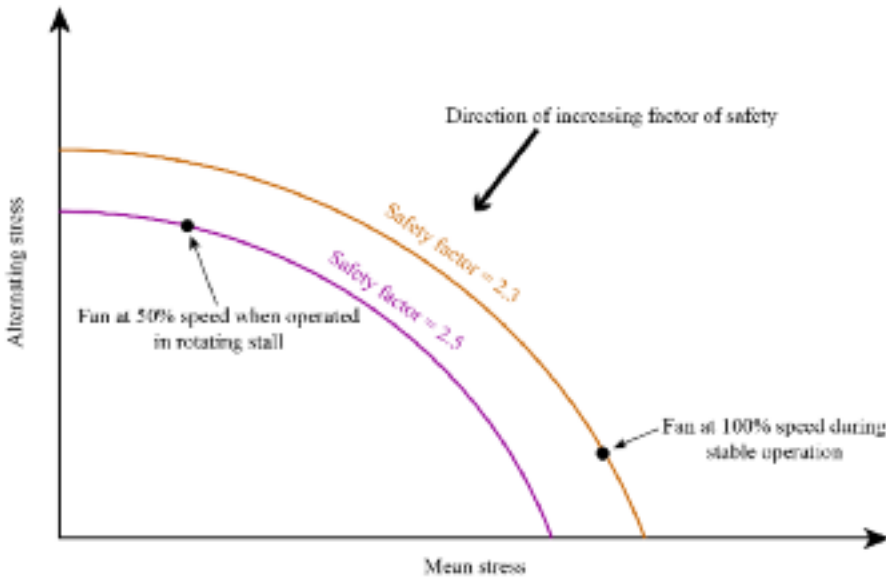

FIGURE 5.18. The Gerber Line associated with full design speed and stable operation plus the Gerber Line associated with half design speed and rotating stall.

REFERENCES

ISO IEC60651, 1994, Specification for Sound Level Meters.

Anthoine, J., Arts, T., Boerrigter, H.L., Buchlin, J.-M., Carbonaro, M., Degrez, G., Dénos, R., Fletcher, D., Olivari, D., Riethmuller, M.L., and Van den Braembussche, R.A. (2009), *Measurement Techniques in Fluid Dynamics — An Introduction*, von Karman Institute for Fluid Dynamics, Rhode-Saint-Genèse, Belgium.

Bianchi, S., Corsini, A., Rispoli, F., and Sheard, A.G. (2009), "Detection of Aerodynamic Noise Sources in Low-speed Axial Fans with Tip End-plates", *Proceedings of the Institution of Mechanical Engineers, Part C: Journal of Mechanical Engineering Science*, vol. 223, pp. 1379–92.

Bianchi, S., Corsini, A., and Sheard, A.G. (2010), "Detection of Stall Regions in a Low-speed Axial Fan, Part 1: Azimuthal Acoustic Measurements", *Proceedings of the 55th American Society of Mechanical Engineers Turbine and Aeroengine Congress*, Glasgow, UK, 14–18 June, paper no. GT2010-22753.

Bianchi, S., Corsini, A., Mazzucco, L., Monteleone, L., and Sheard, A.G. (2012), "Stall Inception, Evolution and Control in a Low Speed Axial Fan with Variable Pitch in Motion", *Transactions of the ASME, Journal of Engineering for Gas Turbines and Power*, vol. 134, paper no. 042602, pp. 1–10.

Bianchi, S., Corsini, A., Sheard, A.G., and Tortora, C. (2013), "A Critical Review of Stall Control Techniques in Industrial Fans", *International Scholarly Research Network, Mechanical Engineering*, vol. 2013, article ID 526192, pp. 1–18.

Bindl, S., Stöel, M., and Niehuis, R. (2009), "Stall Detection within the Low Pressure Compressor of a Twin-spool Turbofan Engine by Tip Flow Analysis", *Proceedings of the 54th American Society of Mechanical Engineers Gas Turbine and Aeroengine Congress*, Orlando, FL, USA, 8–12 June, paper no. GT2009-59032.

Boerrigter, H.L. (1996), "PreMeSys: a Simulation Program to Determine the Frequency and Time Response of a Pressure Measurement System", *VKI Technical Memorandum 53*, von Karman Institute for Fluid Dynamics, Rhode-Saint-Genese, Belgium.

Bright, M.M., Qammar, E., Vhora, H., and Schaffer, M. (1998), "Rotating Pip Detection and Stall Warning in High-speed Compressors Using Structure Function", *Proceedings of the RTO AVT Symposium*, Toulouse, France, 11–15 May.

Cardillo, L., Corsini, A., Delibra, G., Rispoli, F., and Sheard A.G. (2014), "A Numerical Investigation into the Aerodynamic Effect of Pressure Pulses on a Tunnel Ventilation Fan", *Proceedings of the IMechE Part A, Journal of Power and Energy*, vol. 228, pp. 285–99.

Christensen, D., Armor, J., Dhingra, M., Cantin, P., Gutz, D., Neumeier, Y., Prasad, J.V., Szucs, P.N., and Wadia, A.R. (2008), "Development and Demonstration of a Stability Management System for Gas Turbine Engines", *Transactions of the ASME, Journal of Turbomachinery*, vol. 130(3), paper no. 031011, pp. 1–9.

Corsini, A., and Rispoli, F. (2005), "Flow Analyses in a High-pressure Axial Ventilation Fan with a Non-linear Eddy-viscosity Closure", *International Journal of Heat and Fluid Flow*, vol. 26, no. 3, pp. 349–61.

Corsini, A., Rispoli, F., and Sheard, A.G. (2010), "Shaping of Tip End-plate to Control Leakage-vortex Swirl in Axial-flow Fans", *Transactions of the ASME, Journal of Turbomachinery*, vol. 132, paper no. 031005, pp. 1–9.

Cumpsty, N.A. (1989), "Part-circumference Casing Treatment and the Effect on Compressor Stall", *Proceedings of the 34th American Society of Mechanical Engineers Gas Turbine and Aeroengine Congress*, Toronto, ON, Canada, 11–14 June, paper no. 89-GT-312.

Day, I.J., Breuer, T., Escuret, J., Cherrett, M., and Wilson, A. (1999), "Stall Inception and the Prospects for Active Control in Four High-speed Compressors", *Transactions of the ASME, Journal of Turbomachinery*, vol. 121, pp. 18–27.

De Rosier, B., Normand, M.D., and Peleg, M. (1997), "Effect of Lag on the Symmetrised Dot Pattern _SDP_ Displays of the Mechanical Signatures of Crunchy Cereal Foods", *Journal of the Science of Food and Agriculture*, vol. 75, pp. 173–8.

Gerber, W.Z. (1874), 'Calculation of the Allowable Stresses in Iron Structures'. *Z Bayer Architecture and Engineering*, vol. 6, pp. 101–10.

Gleick, J. (1987), *Chaos: Making a New Science*, Vintage Books, New York, NY, USA.

Höss, B., Leinhos, D., and Fottner, L. (2000), "Stall Inception in the Compressor System of a Turbofan Engine", *Transactions of the ASME, Journal of Turbomachinery*, vol. 122, pp. 32–44.

Liu, Y., Dhingra, M., and Prasad, J.V.R. (2009), "Active Compressor Stability Management via a Stall Margin Control Mode", *Proceedings of the 54th American Society of Mechanical Engineers Gas Turbine and Aeroengine Congress*, Orlando, FL, USA, 8–12 June, paper no. GT2009-60140.

Ludwig, G.R., and Nenni, J.P. (1976), "A Rotating Stall Control System for Turbojet Engines", *Proceedings of the 21st American Society of Mechanical Engineers Gas Turbine and Aeroengine Congress*, New Orleans, LA, USA, 12–25 March, paper no. 76-GT-115.

Methling, F.O., Stoff, H., and Grauer, F. (2004), "The Prestall Behavior of a 4-stage Transonic Compressor and Stall Monitoring Based on Artificial Neural Networks", *International Journal of Rotating Machinery*, vol. 10, pp. 387–99.

Paduano, J.D., Greitzer, E.M., and Epstein, A.H. (2001), "Compression System Stability and Active Control", *Annual Review of Fluid Mechanics*, vol. 33, pp. 491–517.

Pickover, C.A. (1986), "On the Use of Symmetrized Dot Patterns for the Visual Characterization of Speech Waveforms and Other Sampled Data", *Journal of the Acoustical Society of America*, vol. 80, pp. 955–60.

Schultz, T.J. (1978), "Synthesis of Social Surveys on Noise Annoyance", *Journal of the Acoustical Society of America*, vol. 64, pp. 377–405.

Sheard, A.G., and Corsini, A. (2012), "The Mechanical Impact of Aerodynamic Stall on Tunnel Ventilation Fans", *International Journal of Rotating Machinery*, vol. 2012, paper no. 402763, pp. 1–12.

Sheard, A.G., Corsini, A., and Bianchi, S. (2010), "A Method of Detecting Stall in an Axial Fan", GB Patent 2 468 571 B, 24 December.

Shibata, K., Takahashi, A., and Shirai, T. (2000), "Fault Diagnosis of Rotating Machinery Through Visualisation of Sound Signals", *Mechanical Systems and Signal Processing*, vol. 14, pp. 229–41.

Sottek, R., and Genuit, K. (2007), "Sound Quality Evaluation of Fan Noise Based on Hearing-related Parameters", *Proceedings of the 3rd International Symposium of Fan Noise*, Lyon, France, 17–19 September.

Tahara, N., Kurosaki, M., Ohta, Y., Outa, E., Nakajima, T., and Nakakita, T. (2007), "Early Stall Warning Technique for Axial-flow Compressors", *Transactions of the ASME, Journal of Turbomachinery*, vol. 129, pp. 448–56.

Tong, Z., Li, L., Nie, C., Lin, B., Cui, Y., and Qi, W. (2009), "On-line Stall Control with the Digital Signal Processing Method in an Axial Compressor", *Proceedings of the 54th American Society of Mechanical Engineers Gas Turbine and Aeroengine Congress*, Orlando, FL, USA, 8–12 June, paper no. GT2009-59509.

Tryfonidis, M., Etchevers, O., Paduano, J.D., Epstein, A.H., and Hendricks, G.J. (1995), "Pre-stall Behaviour of Several High-speed Compressors", *Transactions of the ASME, Journal of Turbomachinery*, vol. 117, pp. 62–80.

Wu, J., and Chuang, C. (2005), "Fault Diagnosis of Internal Combustion Engines Using Visual Dot Patterns of Acoustic and Vibration Signals", *NDT International*, vol. 38, pp. 605–14.

Young, W.C. (1989), *Roark's Formulas for Stress and Strain*, McGraw-Hill, New York, NY, USA.

Demonstration of a Stall Detection System for Induced-draft Fans

S. Bianchi, A. Corsini, and A.G. Sheard

ABSTRACT

Aerodynamic stall is the primary cause of industrial axial fan in-service mechanical failure and consequently, there has been wide-spread application of stall-detection systems. The study reported in this chapter assesses the application of a novel stall-detection system to a class of industrial axial fans for induced-draft service in coal-fired power plants. This class of industrial axial fans operates at constant rotational speed, utilising variable pitch in motion blades to adjust fan duty point. This load modulation system, in combination with blade erosion or fouling, can result in fans becoming prone to stall. Erosion and fouling reduce a fan's pressure developing capability. Consequently, a load modulation system that will increase blade angle to achieve a desired duty point may result in a fan's stall margin gradually reducing with increasing erosion or fouling.

This chapter reports on a novel stall-detection methodology, first proposed for incipient stall detection in low-speed axial-flow fans for tunnel ventilation. The original concept was based on the analysis of near-field pressure as measured via sensors mounted on the casing over fan blades. This chapter demonstrates the potential of processing far-field pressure signals to identify stall pre-cursors. This far-field stall-detection method is characterised in a laboratory environment. We made unsteady pressure measurements with sensors fitted into the fan casing over the fan blades (in the near-field) and simultaneously in the fan's inlet plenum one fan diameter upstream of the fan rotor (in the far-field). We first present an analysis of the physical flow phenomena that characterise the evolution of rotating stall for the studied fan. We then provide the rationale of the stall-detection signal processing technique. Finally, we use a symmetrised dot pattern (SDP) visualisation technique to transform both near- and far-field signals into identifiably different visual images that one can use to identify the studied fan's operating condition.

NOMENCLATURE

Latin letters

D_t	tip diameter	mm
H_b	blade height	mm
i	number of dots	
L	time lag	
ℓ_t	blade chord at the tip	mm
N	number of the discrete signal	
p_n	nominal design pressure	Pa
Q_n	nominal design volume flow rate	m³/s
R	polar position of the dot in the polar map	
SDP	symmetrised dot pattern	
t	absolute time	s
T_{SDP}	sample time	
x*	sampled value of the sound signal	

Greek letters

γt	nominal blade-tip stagger angle
Δt	time interval
δ	blade pitch
η_{tot}	total efficiency
Θ^+, Θ^-	two angles of the polar space
ξ	angular gain
Σ	solidity
σ	input signal amplitude
τ	tip gap (% of the blade chord at the tip)

INTRODUCTION

Engineers select variable pitch in motion axial fans for induced-draft application in steam power plant for two reasons. First, they typically have higher aerodynamic efficiencies, relative to centrifugal blowers, at both design and off-design operating conditions. Second, as one can change the blade pitch, the power plant control system can modulate blade angle in real time. The variable calorific value of the coal burnt in a power plant boiler results in a variation in the volume of combustion products for the coal's fixed flow-rate into the boiler. This variation in the volume of combustion products results in a variation in the boiler pressure. This variation in pressure must be balanced through a corresponding variation in the induced-draft fan duty point that one may achieve by varying blade pitch. A fan for induced-draft application is typically required to operate against a system resistance of 10,000 Pa, with load modulations resulting in a 30 per cent variation (Van Beyer and Bolland, 1998).

Power plant combustion products include erosive particles. The flue-gas treatment upstream of induced-draft fans should remove these erosive particles. In practice some silica and un-burnt carbon passes through the fans, resulting in fan blade erosion. As the blades erode, the blade chord reduces. This destroys the blade leading edge's aerodynamic profile, resulting in the induced-draft fan's reduced pressure developing capability. For a fixed duty point, the power plant control system will increase blade angle to maintain a constant boiler pressure. An induced-draft fan become prone to stall as its pressure developing capability falls and approaches the duty point pressure. If the blades continue to erode the induced-draft fan will move from stable operation to an operating condition where stall is incipient, and finally a rotating stall operating condition.

Rotating stall is a mechanism by which a fan or compressor adapts to a reduced flow, resulting in circumferentially non-uniform flow patterns rotating in the annulus. We may characterise rotating stall according to the nature of the inception mechanism (Gravdahl and Egeland, 1999). Day *et al*. (1999) and Wiechert and Day (2012) studied rotating stall, fitting pressure probes to the compressor's casing upstream of the compressor blade's leading edge. They associated rotating stall with spike-like features in the pressure signals. In reviewing the evolution of rotating stall, Cumpsty (1989) noted that the drop in overall performance can occur as a so-called 'progressive stall' or an 'abrupt stall'. Engineers usually associated the former with a part-span stall which results in a small performance drop; whereas, they associate the latter with a full-span stall and a large drop in performance. Notably, the part-span rotating stall occurs typically in single blade rows (Cumpsty, 1989) and usually leads to more complex disturbances in single-rotor or stage machines than in multi-stage compressors (Moore, 1984).

Strain gauge measurements on axial compressors (Rippl, 1995) and fans (Sheard and Corsini, 2012) have confirmed that bending stress in compressor and fan blades exceed those associated with stable operation by a factor of five and seven, respectively, when operated in rotating stall. Reliable methods of monitoring the stability limit are the subject of ongoing research (Greitzer, 1976; Paduano *et al*., 2001; Liu *et al*., 2009). A need to develop stall-detection systems that operators can apply motivates the research (Bindl *et al*., 2009). Operators need to be able to identify incipient stall in order to alert them that a compressor or fan is about to stall. It is this ability to warn that stall is approaching, but had not yet occurred that is the critical input facilitating development of active control systems that can suppress incipient stall. To be effective, a stall warning system must be able to detect incipient stall in approximately two rotor revolutions for axial compressors (Methling *et al*., 2004), but perhaps ten times longer for industrial fans (Sheard *et al*., 2011).

The industrial fan community currently utilises stall-warning systems that are model-based. They monitor the operating point in real-time and compare it with the fan's known stability limit. However, they are not able to account for the impact of erosion on the fan's pressure developing capability. In an erosive environment model-based stall-warning systems compare the real-time operating point with a stability limit that becomes increasingly irrelevant as blades erode. Researchers have

considered non-model based techniques for real-time control applications. These early warning techniques use diagnostic methods that are mostly based on time or Fourier analyses (Tryfonidis *et al.*, 1995; Christensen *et al.*, 2008; Tong *et al.*, 2009).

In an effort to develop a stall detection method suitable for a real-time control application, Tahara *et al.* (2007) proposed a stall warning index. They calculated this index using the unsteady pressure signal from a sensor mounted in the rotor casing over the blades. The calculation method involved taking a normalised product of unsteady pressure over successive rotor revolutions. Breugelmans *et al.* (1995) studied rotating stall, reconstructing phase-space portraits of measured velocity, static pressure and vibration using Takens's (1981) 'method of delays'. Breugelmans *et al.*'s (1995) research objective was to elucidate the apparently chaotic fluid-flow mechanisms underlying rotating stall. In a similar vein, Bright *et al.* (1998) investigated rotating instabilities prior to stall using a 'temporal structure function' inspired by a statistical approach derived from chaos theory.

The fluid-flow mechanisms underlying rotating stall may contain a chaotic element, but incipient stall is associated with the presence of identifiable flow-field features. The presence of these features results in a change in the fan or compressor's acoustic signature. In an effort to exploit the link between incipient stall and acoustic signature, researchers have proposed diagnostic techniques based on sound-signal visualisation (Shibata *et al.*, 2000; Wu and Chuang, 2005). One can most easily apply this approach to fault diagnosis in rotating machinery when discrete and narrow frequency components dominate an unsteady pressure signal.

Recently, Bianchi *et al.* (2009) used the symmetrised dot pattern (SDP) sound visualisation technique to characterise an industrial fan's performance both with and without fitted blade tip end-plates. Researchers originally conceived the symmetrised dot pattern technique for the visual characterisation of speech waveforms and sound quality evaluation (Schultz, 1978; Pickover, 1986; Sottek and Genuit, 2007). Bianchi *et al.* (2009) were able to associate specific blade-tip end-plate geometries with blade-tip flow features that constituted near-field noise sources. The symmetrised dot patterns technique enabled Bianchi *et al.* (2009) to qualitatively assess the human impact of the change in fan far-field noise.

Sheard *et al.* (2011) first applied the symmetrised dot pattern technique into a stall warning method, using it to differentiate between stable, incipient stall and rotating stall operating conditions in a fixed-pitch axial fan intended to tunnel ventilation applications. Sheard *et al.* (2011) made unsteady pressure measurements in the near-field using a sensor mounted in the studied fan's casing over the blades. They conducted research in a laboratory environment, and therefore, the presence of erosive particles was not a concern. However, an in-service induced-draft fan is subjected to the presence of erosive particles which result in near-field sensors becoming unreliable. Therefore, it is desirable to fit sensors in the far-field in regions where erosive effects are less predominant.

This study extends Sheard *et al.*'s research (2011) from the near-field to the far-field. Using sensors in the far-field is challenging as hydrodynamic pressure decays with the inverse third power of distance. Therefore, this research focuses on demonstrating the capability of the symmetrised dot pattern technique to generate identifi-

ably different symmetrised dot patterns at different operating conditions using low signal-to-noise ratio signals.

EXPERIMENTAL FACILITY

Test rig

Bianchi *et al.* (2012) previously utilised the studied fan and test rig within which it was fitted to study stall inception and control, and so we will only briefly describe it here. The studied fan was a scale model of a single stage variable pitch in motion fan typical of a forced- or induced-draft fan used in coal-fired boiler applications. It was coded PFS, an abbreviation of Pan Fläkt Single were pan and fläkt are respectively the Swedish for boiler and fan. The researchers fitted the studied fan with 18 un-swept C4 free vortex aerofoil blades, Table 6.1. The clearance between blade tips and the casing within which they rotated was 1.3 per cent of chord at the blade tip, a typical value in an induced-draft application.

We conducted the tests in a test facility designed to comply with the ISO 5801:2007 standard, equivalent to the British Standard BS 848 Part 1 (ISO 5801, 2007). We operated the fan in casings made from cast and machined steel rings. A 270 kW direct coupled-induction 400 Volt (AC), three-phase electric motor drove the studied fan at its design speed, 700 rpm. Here, the blade tip speed was 55.13 metres per second and the associated blade passing frequency was 210 Hz. We used an inverter to bring the fan up to its design speed as the variable pitch in motion system was fragile, and therefore, we could not start the fan direct-on-line. The rotor's aerodynamic load and the downstream plenum geometry ensured that the system could not develop a counter-pressure able to induce a surge. As such, the B parameter's value for the plenum system was 0.15, well below Greitzer's suggested threshold value (1976) for axial compressor rigs.

Table 6.1. *Fan geometry and operating condition data.*

Design speed	700 rpm
Tip speed	55.13 m/s
Design pressure, p_n	380 Pa
Design flow rate, Q_n	13 m³/s
Design point efficiency based on total pressure rise, η_{tot}	0.92
Tip diameter, D_t	1,500 mm
Blade height, H_b	450 mm
Blade chord at the tip, ℓ_t	105 mm
Blade pitch, δ	80°–40°
Blade tip stagger angle, γ_t	70º
Tip gap, τ (% of the blade chord at tip)	1.3%
Blade count	18
Solidity, Σ	0.6

Instrumentation

For the near-field measurements we followed Sheard *et al.* (2011), instrumenting the fan casing with a 15 mm diameter GRAS microphone, type 40AG. The microphone specification enabled us to use it as a high-frequency response unsteady pressure transducer. We recessed the microphone 0.5 mm from the casing's inner wall. We installed the microphone in the casing at the axial mid-point between the blade leading and training edge, Figure 6.1. For the far-field measurements, we mounted a microphone one fan diameter from the fan blades' leading edge in the inlet plenum, Figure 6.1.

Charge amplifiers conditioned each microphone, with the resultant signals outputting to a data acquisition system (NI Compact Acq. 9172 with NI 9205 analogical input modules). We logged data at 10 kHz. The uncertainty of the readings was 0.1–0.2 dB at 1 kHz, established in accordance with the requirements of ISO 5801, 2007. We estimated the error in pressure measurements associated with the average turbulence level at the fan inlet flow to be two per cent of reading (Corsini and Rispoli, 2005). By throttling downstream from the fan, we produced the aerodynamic instabilities of interest. During the volume-flow throttling, the fan remained in rotating stall without going into surge.

ROTATING STALL DYNAMICS

We used the test facility to measure the studied fan's characteristics with the fan running at its design speed of 700 rpm and design blade angle of 70 degrees, Figure 6.2. As is customary within the industrial fan community, we measure blade angle in the peripheral direction, which we generally refer to as 'blade pitch angle'. We identified three operating conditions on the fan's characteristic:

- the fan's design operating condition (D);
- the fan's peak pressure operating condition (P); and
- a rotating stall operating condition (S).

We established the performance characteristic by throttling the flow downstream of the fan using the test facility's down-stream damper. We measured unsteady pressure both over the fan blades and in the fan inlet plenum at each operating condition, and then changed the damper position to throttle the fan to a new point on its characteristic following which we measured unsteady pressure again. As the fan reached its peak pressure (P) operating condition, stall became incipient. An increase in the measured unsteady pressure levels indicated incipient stall.

Near-field stall characterisation

Bianchi *et al.* (2012) visually inspected unsteady pressure data from two near-field microphones, concluding that they provided qualitative information about the
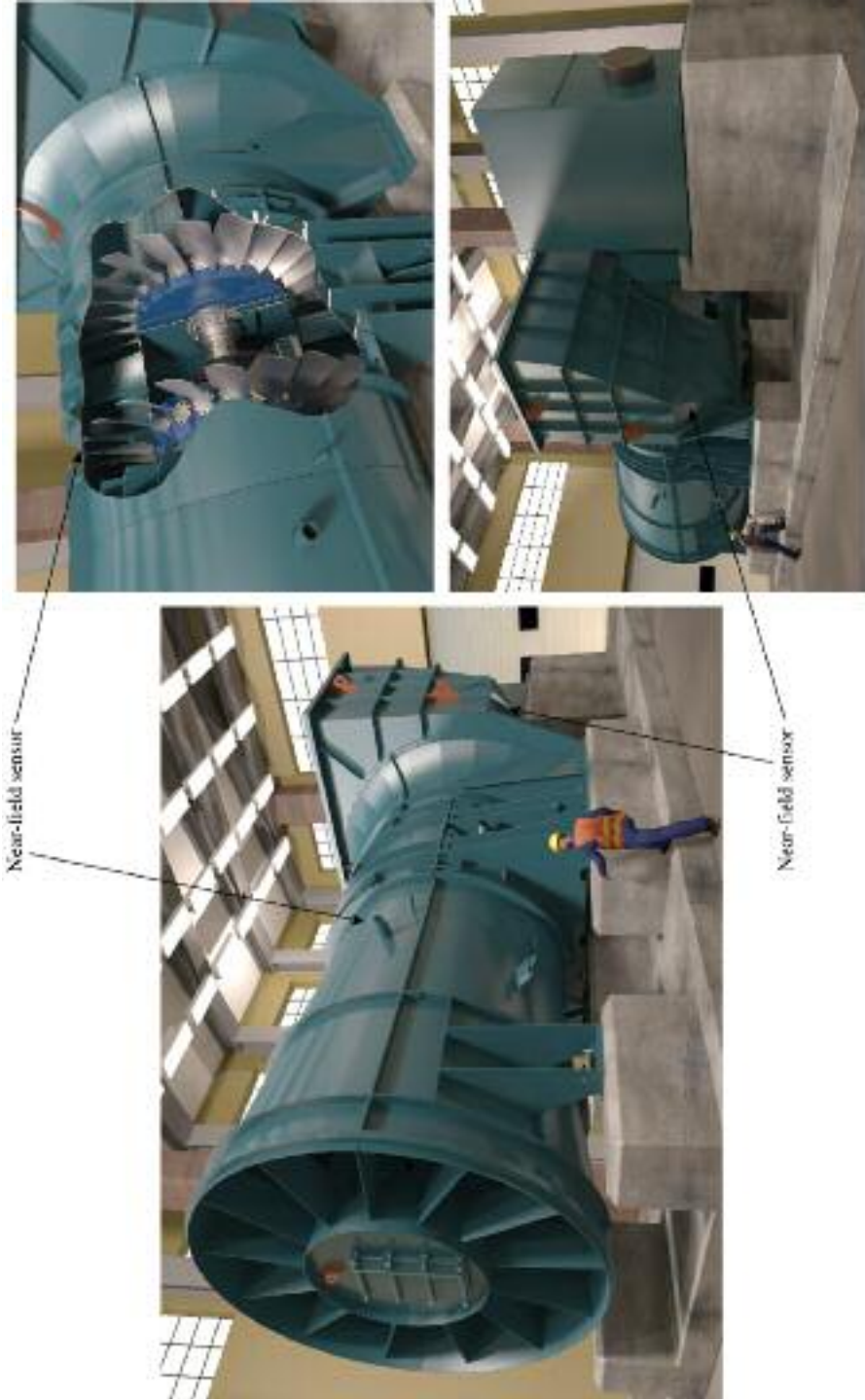
FIGURE 6.1. Position of the near-field microphone mounted in the casing over the fan blades and the far-field microphone mounted in the fan's inlet plenum.
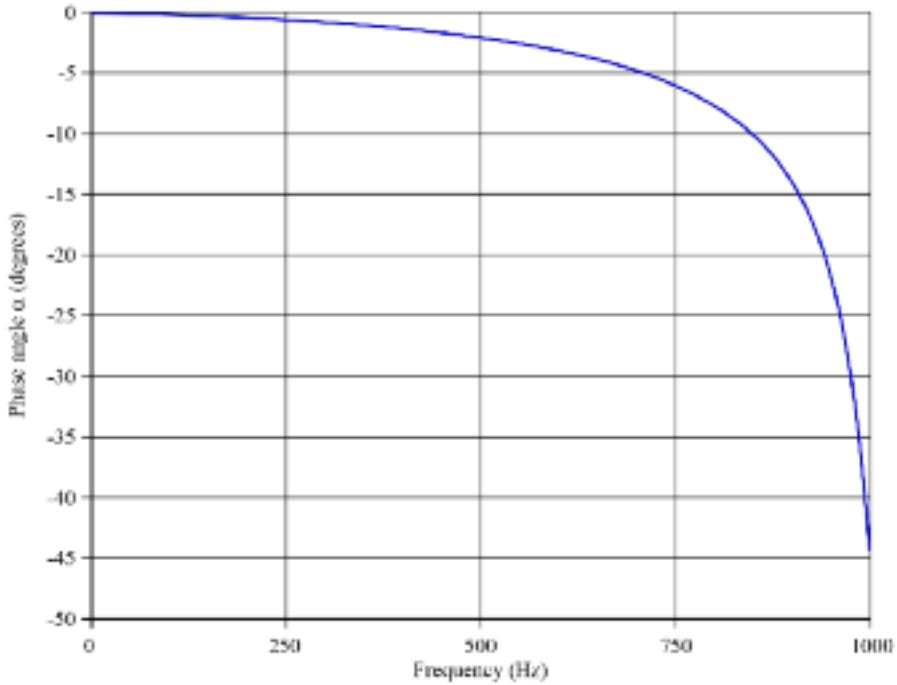
FIGURE 6.2. Fan characteristics at a 700 rpm with a 70 degree pitch angle. The fan operating condition was throttled from design (D), to peak pressure (P) and then finally rotating stall (S).

incipient stall fluid flow mechanisms. In the present study we set the blade pitch angle to 70 degrees, and throttled the fan from stable to stalled operation over a 30 second time period, equivalent to 350 rotor revolutions. We used the near-field microphone to measure unsteady pressure. The measured unsteady pressure fluctuations were approximately 50 times higher than those that characterised stable operation. We defined time zero as the time at which fan throttling commenced, with the first indication of incipient stall occurring after 28.5 seconds, Figure 6.3.

After 28.5 seconds the unsteady pressure data from the near-field microphone recorded a spike-like pressure instability. This spike-like instability occurred as fan throttling resulted in it approaching its peak pressure (P) operating condition. Bianchi *et al.* (2012) observed the same spike-like pressure instability, using circumferentially off-set microphones to deduce that it rotated at 70 per cent of fan speed.

We observed that at a time between 28.5 and 29 seconds, Figure 6.3, the spike-like pressure instability collapsed, with the fan returning to stable operation for approximately three rotor revolutions as we continued to throttle the fan. The fan finally transitioned from stable to stalled operation after approximately 29.1 seconds, Figure 6.3, when a second instability appeared, again self consistent with Bianchi *et al.*'s findings (2012). They concluded that it was an embryonic stall cell rotating at half design speed.
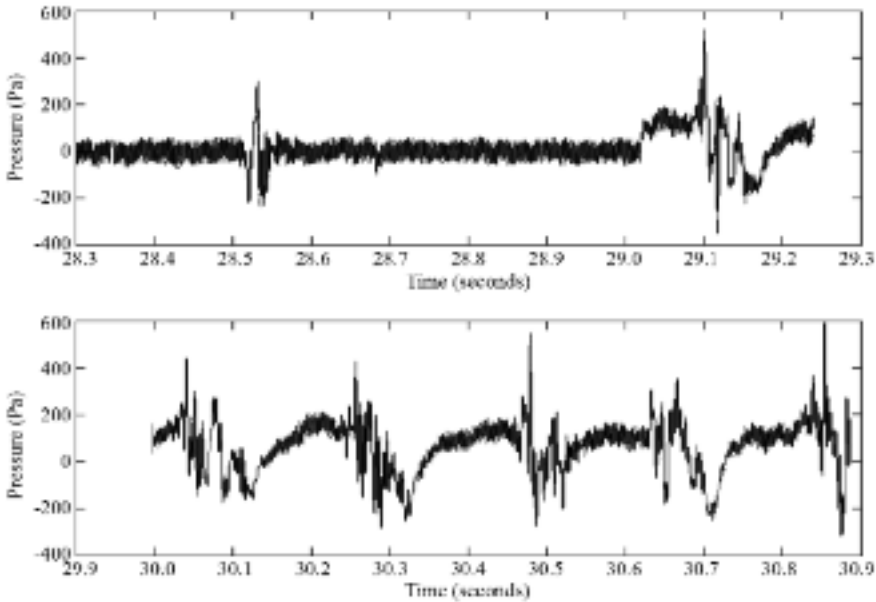
FIGURE 6.3. Unsteady pressure data recorded using a microphone, mounted in the casing over the fan blades as the fan was throttled from the peak pressure (P) to rotation stall (S) operating condition. The fan rotational speed was 700 rpm, and the blade angle was 70 degrees.

The first spike-like pressure instability associated with incipient stall was an isolated event, following which the unsteady pressure level returned to its pre-event level. In contrast, the pressure instability associated with an embryonic stall cell remained chaotic, with the stall cell finally becoming fully established after 30 seconds and then exhibiting a periodic characteristic, Figure 6.3. Bianchi *et al.* (2012) were able to establish that this fully established stall cell rotated at 40 per cent of fan speed.

We complemented the visual inspection with a Fourier analysis of the near-field unsteady pressure data. A Fourier analysis is useful in that it facilitates study of the frequency components within the unsteady data. We calculated the Fourier analysis of near-field unsteady pressure data using a fast Fourier transform over a time window equivalent to approximately 18 rotor revolutions. We calculated the Fourier analysis with the fan operating at both its peak pressure (P) and rotating stall (S) operating conditions. We took the peak pressure operating condition data from 28.5 to 30.0 seconds, Figure 6.3. We took the rotating stall operating condition data from 50.0 to 51.5 seconds, not shown in Figure 6.3, but similar to the data from 30.0 and 30.8 seconds that is shown in Figure 6.3.

An analysis of the peak pressure (P) operating condition frequency spectrum when stall is incipient, Figure 6.4, indicates the presence of a very low-frequency peak. This low-frequency peak is indicative of the inception of a part-speed rotating stall cell which is consistent with Kameier and Neise (1997) and Bianchi *et al.*'s
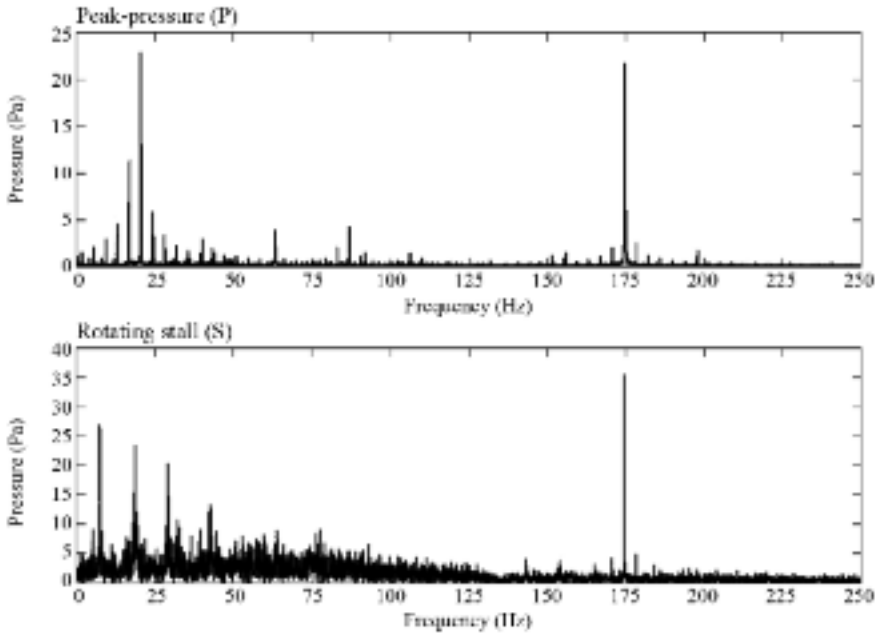
FIGURE 6.4. Frequency spectra of the unsteady pressure data recorded over the fan blades at its peak pressure (P) operating condition and at its rotating stall (S) operating condition.

conclusions (2010). Despite the consistency of our observations with those of other researchers, we did not expect the presence of a part-speed rotating stall cell. The incipient stall frequency spectra exhibited characteristics that we would have expected to observe only if a rotating stall cell were fully developed.

The appearance of tonal components between 30 and 50 Hz characterise the peak pressure (P) operating condition frequency spectra, Figure 6.4. As Bianchi *et al.* (2010) noted, these tonal components may occur because of the interaction of many small 'bubble' cells that later merge to create a fully developed rotating stall cell. These bubble cells are not significant enough to be apparent in the frequency spectra as fundamental tones. However, they do appear as an incremental increase in the broadband over the frequency range where they occur.

An analysis of the rotating stall (S) operating condition frequency spectrum, Figure 6.4, indicates a shaft rotational frequency tone localised at 5 Hz, but split into a series of side bands. These rotating stall side bands occur because of harmonics in the unsteady pressure data from which we calculated the cross-spectra, a feature that Bianchi *et al.* (2010) associated with rotating stall. When considering the difference between the frequency spectra for peak pressure (P) and rotating stall (S) operating conditions, it is apparent that the tonal components between 30 and 50 Hz present in the peak pressure cross-spectra are no longer present in the fully rotating stall operating condition frequency spectra. From this we conclude that the tonal components have developed into larger features, and as they have grown, they have decreased in speed and merged with the 40 per cent fan speed rotating stall cell.

Far-field stall characterisation

The near-field analysis of unsteady pressure data and frequency spectra was able to identify features that characterised both peak pressure (P) and rotating stall (S) operating conditions. However, as we previously mentioned, sensors fitted in the near-field are unreliable when a fan is installed in an erosive environment. Therefore, it is desirable to fit sensors in the fan inlet plenum were velocities are lower and erosive effects are less significant. The studied fan is part of a family of fans intended for induced-draft application in coal-fired power plant. This application requires the fan inlet to incorporate a 90 degree bend, Figure 6.1. When a fan from this family has operated for an extended period of time in an erosive environment, an inspection of the inlet plenum will identify regions that are free from erosive effects. This is true even in the most severely erosive environments, when other components have eroded so badly that the operator must withdraw from service or replace the fan. Consequently, the choice of far-field microphone location is not arbitrary.

A disadvantage of locating a microphone in the far-field is that the microphone's distance from the blade-tip region will attenuate the unsteady pressure data. The signal-to-noise ratio of unsteady pressure data that we recorded in the near-field was approximately 50:1. When we study unsteady pressure data recorded in the far-field, the signal-to-noise ratio is closer to 5:1, Figure 6.5. As with the near-field analysis, we defined time zero as the time at which fan throttling commenced, with the first indication of incipient stall occurring after 30 seconds.

Once again we complemented the visual inspection with a Fourier analysis of the far-field unsteady pressure data. We used a fast Fourier transform over a time window equivalent to approximately 18 rotor revolutions. We calculated the Fourier analysis with the fan operating at both its peak pressure (P) and rotating stall (S) operating conditions, Figure 6.6. We took the peak pressure operating condition data from 28.5 to 30.0 seconds, Figure 6.6. We took the rotating stall operating condition data from 50.0 to 51.5 seconds, not shown in Figure 6.6, but similar to the data from 31.0 and 32.5 seconds that is shown in Figure 6.6.
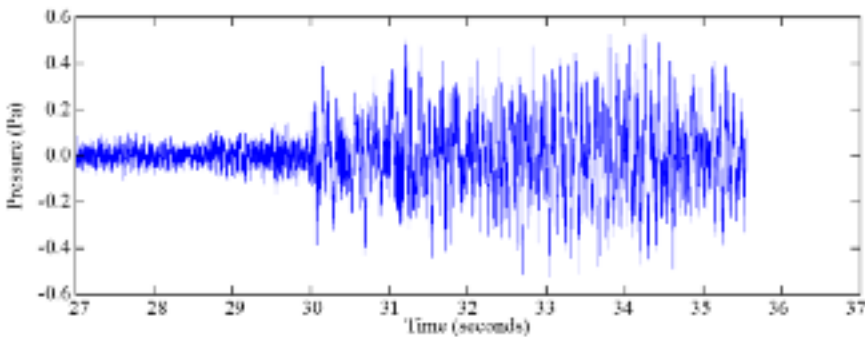

FIGURE 6.5. Unsteady pressure data recorded using a microphone, mounted in the fan inlet plenum as the fan was throttled from the peak pressure (P) to rotating stall (S) operating condition. The fan rotational speed was 700 rpm, and the blade angle was 70 degrees.
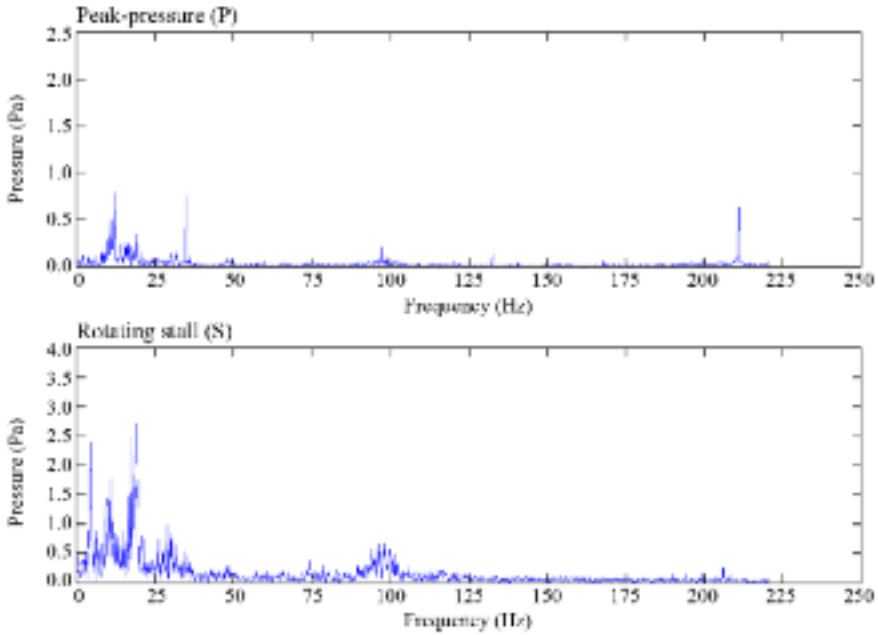
FIGURE 6.6. Frequency spectra of the unsteady pressure data recorded in the fan inlet plenum at the peak pressure (P) operating condition and at its rotating stall (S) operating condition.

An analysis of the peak pressure (P) operating condition frequency spectrum, Figure 6.6, indicates that the low-frequency peaks are still present, but an order of magnitude lower than they were in the near-field frequency spectra, Figure 6.4. An analysis of the rotating stall (S) operating condition frequency spectrum, Figure 6.6, indicates a shaft rotational frequency tone localised at 5 Hz and split into a series of side bands as observed in the near-field frequency spectra, Figure 6.4. The magnitude of observable features in the far-field frequency spectra is similar to what we observe in the near-field spectra. From this we may conclude that there is a significant difference between both the far-field unsteady pressure and frequency spectra at the peak pressure operating condition when stall is incipient and when rotating stall is fully developed at the rotating stall operating condition. Industrial fan manufacturers have not successfully applied traditional stall warning techniques using far-field data. However, the significant difference between the far-field data when stall is incipient and when rotating stall is fully developed indicates that an appropriate signal processing technique may be able to identify that stall is incipient before rotating stall has fully developed.

THE SYMMETRISED DOT PATTERN (SDP) TECHNIQUE

Researchers first conceived the symmetrised dot pattern technique for the visual characterisation of speech waveforms in automatic human-voice-recognition algo-

rithms (Pickover, 1986). The symmetrised dot patterns provide a visual representation of the input signal, with pattern features that may be correlated with features of the input signal (Pickover, 1986). Although it may not be apparent which pattern features are associated with specific physical flow phenomena, the symmetrised dot patterns provide a characterisation of them. By linking the patterns' topology and the fan operating condition, the resultant stall detection method shares its foundation with chaos theory (Gleick, 1987).

The symmetrised dot patterns technique's advantage over other approaches is its ability to link pattern features with specific physical flow phenomena. The symmetrised dot pattern technique does not simply measure the overall sound power level produced by an input signal's tonal components. It is able to visually represent more subtle features that would otherwise be difficult to characterise. Therefore, the merit of the symmetrised dot pattern technique is its ability to perceive otherwise 'unquantifiable' differences in sound signals mimicking the way that humans hear (Schultz, 1978; Sottek and Genuit, 2007).

Mathematical framework and polar pattern construction

We used an algorithm to map a normalised time waveform into a polar coordinate system to produce the symmetrised dot pattern, Figure 6.7. The algorithm maps a point in the input signal as the polar coordinate's radial component, and the adjacent point as the polar coordinate's angular component. In this way, one may map successive pairs of points from the input signal as single points in a polar coordinate system. Collectively, these points comprise the resultant symmetrised dot pattern.

We can formulate the polar transformation $R(i)$ from waveform to symmetrised dot pattern as:

$$R(i) = \frac{\sigma(i) - \sigma_{min}}{\sigma_{max} - \sigma_{min}} \tag{1}$$
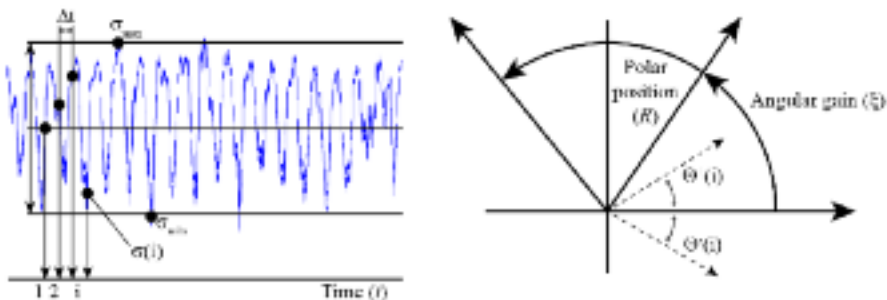

FIGURE 6.7. A schematic illustration of the technique for transforming an input signal into polar coordinates to produce a symmetrised dot pattern.

$$\Theta^-(i) = \Theta_0 + \frac{\sigma(i+L) - \sigma_{\min}}{\sigma_{\max} - \sigma_{\min}} \xi \qquad\qquad (2)$$

$$\Theta^-(i) = \Theta_0 - \frac{\sigma(i+L) - \sigma_{\min}}{\sigma_{\max} - \sigma_{\min}} \xi \qquad\qquad (3)$$

in which i is the number of dots (i = integer (t/Δt)), with t the time *abscissa* and Δt the sampling time; L is the time lag coefficient; $\sigma(i)$ is the sampled ith sound signal; $\sigma_{\max}$ and $\sigma_{\min}$ are the highest and the lowest value of the original waveform window; Θ_0 is the rotation of the origin angle of any reference line; ξ is the plot angular gain; and Θ^+ and Θ^- are the two angles of the traditional polar space. The input waveform is first normalised by finding the higher ($\sigma_{\max}$) and lower values ($\sigma_{\min}$) for the N data points in the window. Therefore, overall signal amplitude, in general, is not a factor in the characterisation.

The unsteady flow phenomena associated with incipient stall become established and then collapse in less than one rotor revolution (Bianchi *et al.*, 2012). In order for a symmetrised dot pattern to visually represent incipient stall, one must take input data over a time that is similar to that of the physical flow phenomena associated with incipient stall. The symmetrised dot pattern quality is less dependent on the total number of data points than the sample rate. Shibata *et al.* (2000) studied the impact of sample rate. They concluded that when using a single-frequency sine wave as an input signal, the higher the sampling rate, the less clear the resultant symmetrised dot pattern. However, if the input signal includes components at multiple frequencies, the resulting symmetrised dot pattern was different from the sum of single frequency symmetrised dot patterns. In contrast, a white noise input signal resulted in a near uniform distribution of dots over the resultant symmetrised dot pattern, irrespective of sampling rate. Thus, Shibata *et al.* (2000) concluded that the combination of features in the input signal resulted in the complexity of the resultant symmetrised dot pattern.

Sheard *et al.* (2011) first studied the application of the symmetrised dot pattern technique to detect incipient stall, concluding that the technique was effective. Sheard *et al.* (2011) generated symmetrised dot patterns with the studied fan in stable, incipient stall and rotating stall operating conditions, with input data collected over 3.0, 1.0 and 0.1 rotor revolutions. The symmetrised dot patterns generated with input data taken over 3.0 and 1.0 rotor revolutions were distinctly different at each operating condition. A comparison of the symmetrised dot patterns generated with a sample time corresponding to 1.0 and 0.1 rotor revolutions indicated that the reduction in sample time resulted in significant degradation of symmetrised dot pattern quality. Despite this degradation, Sheard *et al.* (2011) concluded that it was still possible to infer some of the features evident in the 1.0 rotor revolution symmetrised dot patterns in the 0.1 rotor revolution patterns.

Sheard *et al.* (2011) concluded that the symmetrised dot patterns generated with a sample time corresponding to 1.0 rotor revolutions represent the best trade-off between sample time and pattern quality. In the research reported in this chapter, we

chose to log data for 0.1 seconds, equivalent to 1.5 rotor revolutions. The studied fan was a relatively low-speed fan, and therefore, we judged that logging data for 1.5 rotor revolutions gave the best trade-off between sample time and number of data points in each logged data set.

Signal processing technique

We made acoustic measurements in the studied fan's near- and far-field using GRAS microphones, type 40AG (Sheard *et al.*, 2011). We utilised a 10 kHz sampling rate giving a Nyquist frequency of 5 kHz. To avoid signal aliasing, we filtered all data at 2.5 kHz and analysed it in the range of interest below 200 Hz. Although flush mounted, a small cavity was present in front of both the near- and far-field microphones' diaphragm. We calculated the cavities' resonance frequency at 4702 Hz, using the Helmholtz equation applied to an equivalent conical cavity. As the frequency range of interest was below 200 Hz, we considered the cavity's resonant frequency acceptable in the present study.

Following Sheard *et al.*'s method (2011), we calculated the system frequency response using Boerrigter's (1996) PREMESYS 2.0 MATLAB application tool, which he developed at the von Karman Institute of Fluid Dynamics. This application tool enabled us to characterise the measurement system's dynamic response to a steep change in input signal. The dynamic response indicated that limiting any signal analysis to frequencies below 500 Hz would keep errors in phase angle below –3 degrees, which we considered acceptable in the present study. We estimated the overall measurement uncertainty as (i) $\Delta V = 1,000$ mV $\pm$ 12 mV (20:3) on the voltage and (ii) $\Delta G = 200$ dB $\pm$ 2.4 dB (20:3) on the raw signal gain for frequencies up to 1 kHz. We accepted the estimated uncertainties as they are self-consistent with Arts *et al.*'s uncertainties (1994), which they consider typical when making pressure measurements in an unstable flow-field.

The impact of probe position

Sheard *et al.*'s initial symmetrised dot pattern technique application (2011) characterised the studied fan's operating condition using unsteady pressure measurements in the near-field. The unsteady pressure signals in the near-field invariably include acoustic effects that do not transmit to the far-field. Laurendeau *et al.* (2007) noted that the near-field spectrum consisted of a combination of a low-frequency range, dominated by the hydrodynamic signature, and a high-frequency range, influenced by acoustic pressure fluctuations. Sheard *et al.*'s research (2011) inevitably constituted a characterisation of all near-field effects. By placing the far-field microphone in a region of the inlet plenum associated with low velocities, we aimed to attenuate the hydrodynamic pressure fluctuations' coupling with the far-field. Our objective was to characterise the symmetrised dot pattern technique using far-field data comprising primarily acoustic pressure fluctuations.

RESULTS

We analysed the near- and far-field pressure data at the studied fan's design (D) and rotating stall (S) operating conditions, Figure 6.8. Compiling the near- and far-field pressure data with the studied fan's characteristic clarifies the change in pressure data with the changing fan operating condition. The far-field data's low signal-to-noise ratio is particularly apparent when compared with the near-field data.

When generating symmetrised dot patterns, the methodology requires a choice of values for time lag (L) and the angular gain (ξ). These influence the resulting pattern's topology and consequently, its ability to differentiate between fan operating conditions. In the present study we characterised the impact of time lag (L) and the angular gain (ξ) over a matrix of values on the generated symmetrised dot patterns using both near- and far-field data, Table 6.2.

The matrix of values in Table 6.2 translates into a series of 12 symmetrised dot patterns, Figure 6.9. For the sake of clarity, the illustration shows only one axis of the patterns, highlighting the difference between patterns generated from near- and far-field input signals. It is apparent that low values of time lag (L) do not result in identifiably different design (D) and rotating stall (S) operating condition symmetrised dot patterns. With a time lag (L) of 1, the generated symmetrised dot patterns do not show a change in curvature using a near-field input signal taken at the design and rotating stall operating conditions. If we now consider the generated symmetrised dot patterns using a far-field input signal, it is apparent that low values of time lag (L) also do not result in identifiably different design and rotating stall operating condition symmetrised dot patterns.

The difference between symmetrised dot patterns generated using a near-field input signal is most pronounced with a time lag (L) of 40. The difference between symmetrised dot patterns generated using a far-field input signal is most pronounced with a time lag (L) of 20. We also conducted a similar analysis for angular gain (ξ).

Table 6.2. *Sensitivity test matrix used to establish the optimum values of time lag* (L) *and angular gain* (ξ) *when generating near- and far-field symmetrised dot patterns.*

| Test	Constants	Parameters
Near-field sensitivity to time lag (L)	$\xi = 20°$ $T_{SDP} = 5$ revs = 0.5 s	$L = 1, 20, 40$
Near-field sensitivity to sample time (T_{SDP})	$\xi = 30°$ $L = 40$	$T_{SDP} = 0.5, 1.0$ and 5.0 rotor revolutions $T_{SDP} = 0.05, 0.10$ and 0.50 seconds
Far-field sensitivity to time lag (L)	$\xi = 30°$ $T_{SDP} = 5$ revs = 0.5 s	$L = 1, 20, 40$
Far-field sensitivity to sample time (T_{SDP})	$\xi = 50°$ $L = 20$	$T_{SDP} = 0.5, 1.0$ and 5.0 rotor revolutions $T_{SDP} = 0.05, 0.10$ and 0.50 seconds
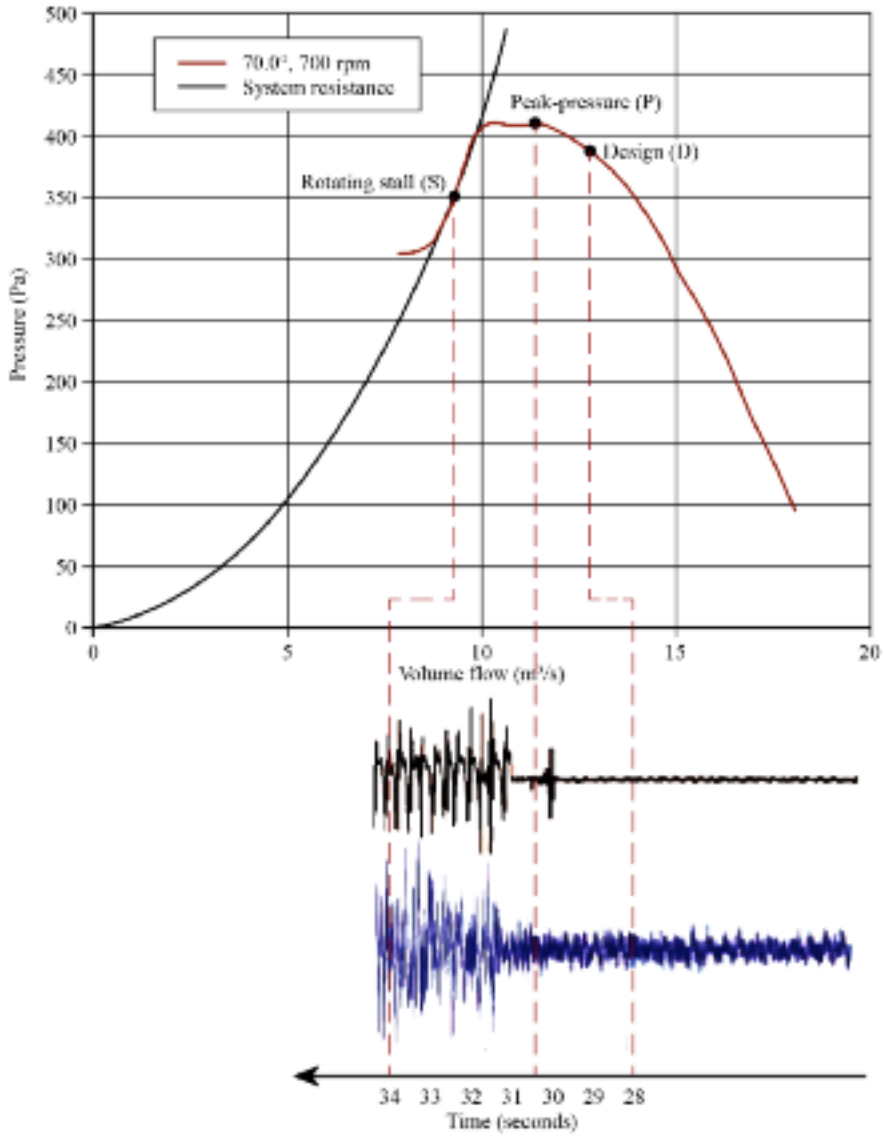
FIGURE 6.8. The studied fan's performance characteristics and unsteady pressure measured both in the near-field over the over the fan blades and in the far-field in the fan's inlet plenum. Unsteady pressure data is shown as the fan was throttled from its design (D) operating condition through to the rotating stall (S) operating condition.
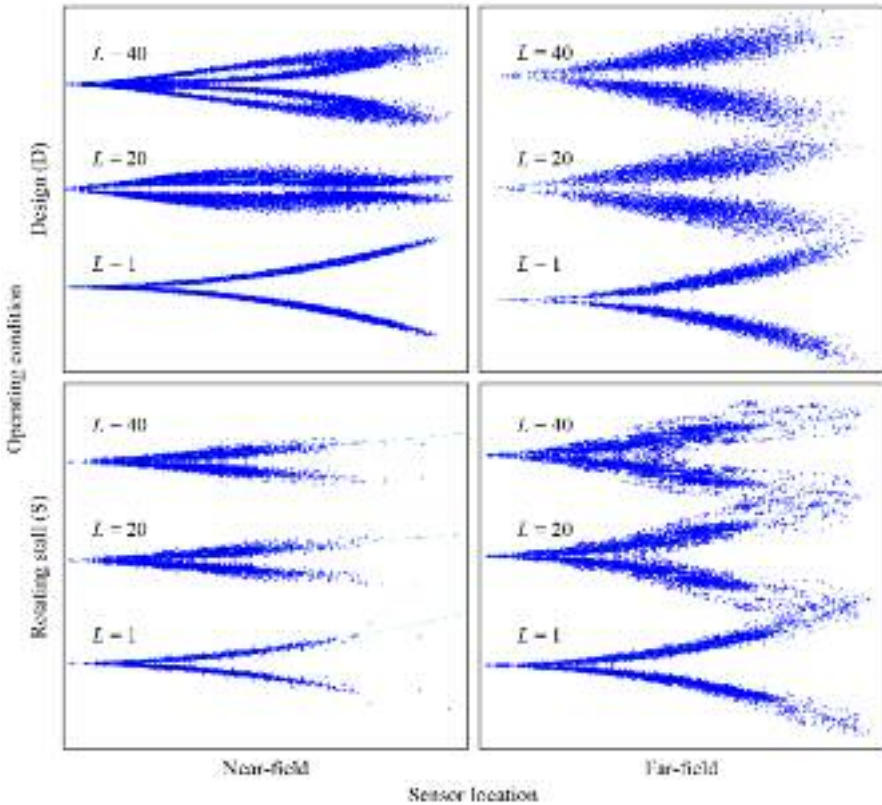
FIGURE 6.9. Sensitivity of the symmetrised dot pattern technique to time lag (*L*). These symmetrised dot patterns were generated from unsteady pressure data recorded at 10 kHz for 0.5 seconds, equivalent to five rotor revolutions. The near-field symmetrised dot patterns were generated using an angular gain (ξ) of 20 degrees. The far-field symmetrised dot patterns were generated using an angular gain (ξ) of 30 degrees.

The difference between symmetrised dot patterns generated using a near-field input signal is most pronounced with an angular gain (ξ) of 20. The difference between symmetrised dot patterns generated using a far-field input signal is most pronounced with an angular gain (ξ) of 30. We conducted the characterisation of time lag (*L*) and angular gain (ξ) using data recorded at 10 kHz for 0.5 seconds, equivalent to five rotor revolutions.

In this chapter, we aim to detect aerodynamic instability as stall precursors. As a consequence of the short time available to detect aerodynamic instability, it is desirable to sample the input signal at the highest sample rate, to acquire in the minimum time sufficient data points to construct a symmetrised dot pattern. Consequently, establishing the minimum sampling time is a key factor in successfully applying the symmetrised dot pattern methodology. We chose to characterise the effect of input signal sample time with the fan operating at design (D) and rotating stall (S) operating conditions, Figure 6.10. We generated symmetrised dot patterns using
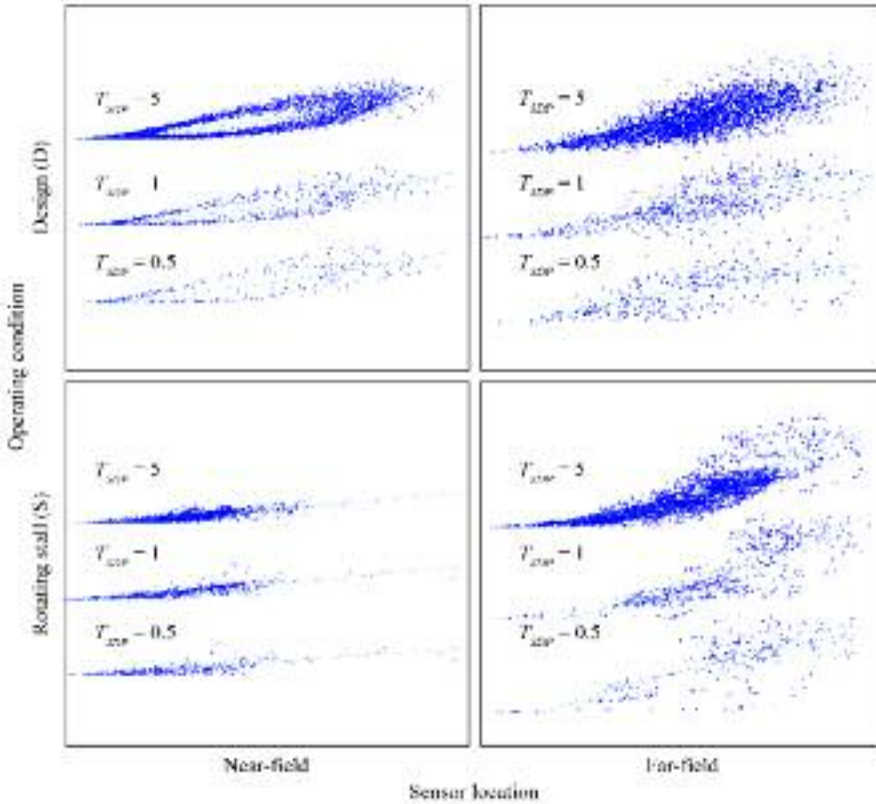
FIGURE 6.10. Sensitivity of the symmetrised dot pattern technique to sample time (T_{SDP}), with all data recorded at 10 kHz. The near-field symmetrised dot patterns were generated using a time lag (L) of 40 and an angular gain (ξ) of 20 degrees. The far-field symmetrised dot patterns were generated using a time lag (L) of 20 and an angular gain (ξ) of 30 degrees.

both near- and far-field input signals using data that we recorded over 5.0, 1.0 and 0.5 rotor revolutions that respectively corresponded to sample times of 0.50, 0.10 and 0.05 seconds. When generating the symmetrised dot patterns we used the previously established optimum values of time lag (L) and angular gain (ξ).

The symmetrised dot patterns generated using a near-field input signal is unaffected by sample time, Figure 6.10. The density of dots within the symmetrised dot patterns did reduce with reducing sample time, but the shape did not change significantly. Critically, the difference was clearly evident at all three sample times. The symmetrised dot patterns generated using a far-field input signal is also unaffected by sample time, Figure 6.10. The difference between the areas of symmetrised dot patterns generated with a far-field input signal was less pronounced then when using a near-field input signal. However, the far-field symmetrised dot patterns at all three sample times indicated a clear difference between pattern curvature when generated using data from the design (D) and rotating stall (S) operating conditions.

The ability of the symmetrised dot pattern technique to generate identifiably different symmetrised dot patterns at different fan operating conditions is the first factor that determines the technique's suitability for use in a stall-detection system. Stall precursors develop and collapse in a fraction of a rotor revolution. Consequently, the technique's ability to generate meaningful different symmetrised dot patterns with data taken over a short sample time is a second factor in determining the technique's suitability for use in a stall-detection system. Preparing a symmetrised dot pattern matrix, Figure 6.11, complements the sensitivity analysis presented in Figures 6.9 and 6.10. Here we see symmetrised dot patterns generated using data from both the near- and far-field input signals, with sample times equivalent to 5.0 and 0.5 rotor revolutions. However, the four resultant symmetrised dot patterns are a hybrid. Each comprises two arms generated using data recorded at the fan's design (D), two arms generated using data recorded at the fan's peak pressure
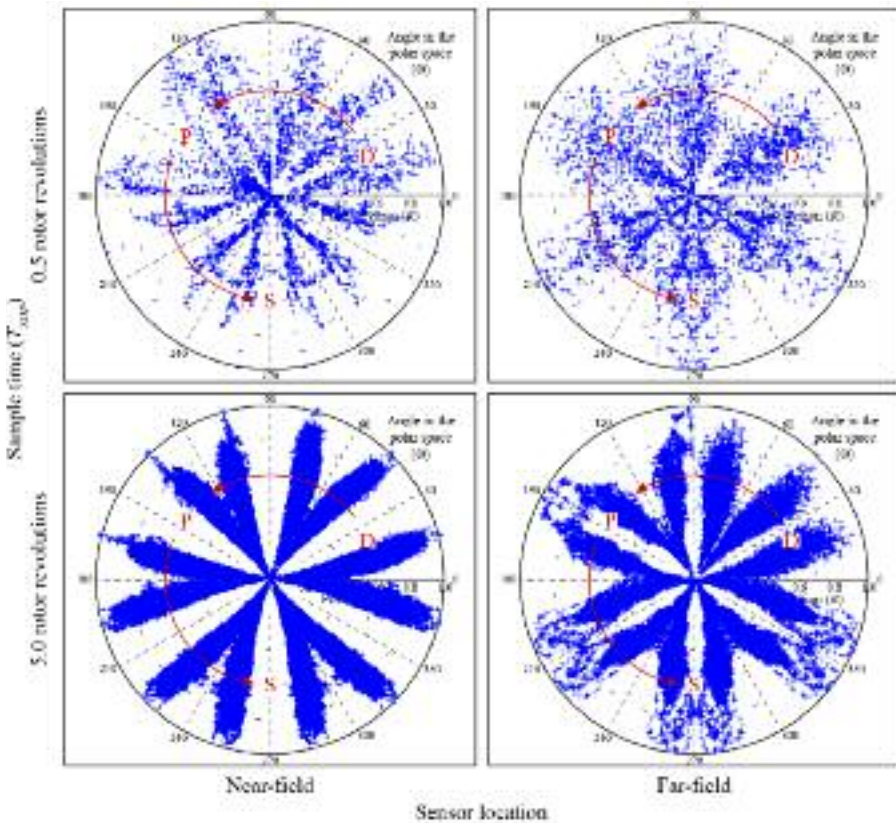
FIGURE 6.11. The evolution of symmetrised dot patterns from the studied fan's design (D), peak pressure (P) and finally rotating stall (S) operating condition. Each symmetrised dot pattern is a hybrid, with two arms from each of the three operating conditions.

(P) and two arms generated using data recorded at the fan's rotating stall (S) operating condition.

If we consider the symmetrised dot patterns generated using a near-field input signal, we see two identifiable differences during the progression from the design (D) to rotating stall (S) operating condition. First, the symmetrised dot pattern arms gradually lose their curvature. This signifies the predominance of low-frequency components at the rotating stall operating condition (Sheard *et al.*, 2011). Second, the area in the symmetrised dot pattern map increases.

If we consider the symmetrised dot patterns generated using a far-field input signal, we still see an identifiable progression from the design (D) to rotating stall (S) operating condition. The symmetrised dot pattern arms also lose curvature, as they did when constructed using a near-field input signal. A reduction in the symmetrised dot pattern arm's radial extension accompanies this curvature loss. We may correlate a loss of radial extension with symmetrised dot pattern topology that is similar to Shibata *et al.* (2000). They associated it with generating symmetrised dot patterns using white noise as an input signal.

Implementation issues

The primary objective of the research reported in this chapter was to establish if the symmetrised dot pattern technique could generate identifiably different symmetrised dot patterns at different fan operating conditions using an input signal from a sensor mounted in the far-field. Sensors mounted in the far-field have a significantly better in-service record of reliability when the fan is operating in an erosive application.

The symmetrised dot patterns generated with data that we collected over a sample time equivalent to 5.0 rotor revolutions were identifiably different at the fan design (D) and rotating stall (S) operating condition. Reducing sample time to 0.5 rotor revolutions still resulted in differentiated symmetrised dot patterns. We may therefore conclude that in this application data that we collected over a sample time equivalent to 5.0 rotor revolutions would form a viable basis for a stall-detection system. Further, in applications with a fan operating at a higher speed it may still be possible to apply the technique with data gathered over a shorter time scale, equivalent to that associated with 0.5 rotor revolutions in this programme of work.

Sheard *et al.* (2010) fully reported the practicality of incorporating the symmetrised dot pattern technique into a method of detection stall and therefore, we will only briefly summarise it here. Sheard *et al.* (2010) monitored the signal from a sensor, and generated the symmetrised dot patterns in real-time. A template matching system then compares the real-time symmetrised dot patterns with a library of symmetrised dot patterns, generated at a series of known fan operating conditions. The template matching system is derived from that used in speech recognition system digital processors. Then, one is able to determine the best match between the real-time symmetrised dot patterns and those stored in the library. Researchers can then use this match to identify the fan's operating condition, which is output from the stall-detection system and used as an input to the fan's control system.

CONCLUSIONS

This chapter assesses the viability of using data from a sensor mounted in a fan's far-field as input to a stall-detection system based upon the symmetrised dot patterns technique. Sensors mounted in the far-field are significantly more reliable in service than sensors mounted in the near-field when one applies the fan to which they are fitted into an erosive environment.

The approach links symmetrised dot pattern topology to different fan operating conditions, providing a method for differentiating between operating conditions. The symmetrised dot pattern technique enables one to create visual representations of the input signal by mapping it onto polar coordinates. The technique's primary strength is its ability to characterise apparently chaotic input signals. We conclude that this characterisation is possible using collected data from both the near- and far-field.

The experimental study focused on the evolution of both near- and far-field input signals as the studied fan progressed from its design to peak pressure and finally a rotating stall operating condition. An analysis of the gathered data demonstrated that the symmetrised dot pattern technique is able to produce symmetrised dot patterns that are identifiably different as different fan operating conditions. The analysis also demonstrates that it is possible to produce identifiably different symmetrised dot patterns using data recorded over a time scale equivalent to 0.5 rotor revolutions. An ability to generate identifiably different symmetrised dot patterns using both input signals from a sensor in the far-field and over short time scales makes the symmetrised dot pattern technique a suitable basis for a stall-detection system.

REFERENCES

ISO 5801, 2007, Industrial Fans — Performance Testing Using Standardized Airways.

Arts, T., Boerrigter, H., Carbonaro, M., Charbonnier, J.M., Degrez, G., Olivari, D., Riethmuller, M.L., and Van den Braembussche, R.A. (1994), *Measurement Techniques in Fluid Dynamics — An Introduction*, von Karman Institute for Fluid Dynamics, Rhode-Saint-Genèse, Belgium.

Bianchi, S., Corsini, A., Rispoli, F., and Sheard, A.G. (2009), "Detection of Aerodynamic Noise Sources in Low-speed Axial Fans with Tip End-plates", *Proceedings of the IMechE Part C, Journal of Mechanical Engineering Science*, vol. 223, pp. 1379–92.

Bianchi, S., Corsini, A., and Sheard, A.G. (2010), "Detection of Stall Regions in a Low-speed Axial Fan, Part 1: Azimuthal Acoustic Measurements", *Proceedings of the 55th American Society of Mechanical Engineers Turbine and Aeroengine Congress*, Glasgow, UK, 14–18 June, paper no. GT2010-22753.

Bianchi, S., Corsini, A., Mazzucco, L., Monteleone, L., and Sheard, A.G. (2012), "Stall Inception, Evolution and Control in a Low Speed Axial Fan with Variable Pitch in Motion", *Transactions of the ASME, Journal of Engineering for Gas Turbines and Power*, vol. 134, paper no. 042602, pp. 1–10.

Bindl, S., Stöbel, M., and Niehuis, R. (2009), "Stall Detection within the Low Pressure Compressor of a Twin-spool Turbofan Engine by Tip Flow Analysis", *Proceedings of the 54th*

American Society of Mechanical Engineers Gas Turbine and Aeroengine Congress, Orlando, FL, USA, 8–12 June, paper no. GT2009-59032.

Boerrigter, H.L. (1996), "PreMeSys: a Simulation Program to Determine the Frequency and Time Response of a Pressure Measurement System", *VKI Technical Memorandum 53*, von Karman Institute for Fluid Dynamics, Rhode-Saint-Genese, Belgium.

Breugelmans, F.A.E., Palomba, C., and Funk, T. (1995), "Application of Strange Attractors to the Problem of Rotating Stall", in Tanida, Y., and Namba, M. (Eds), *Unsteady Aerodynamics and Aeroelasticity in Turbomachinery*, Elsevier Science, Amsterdam, The Netherlands.

Bright, M.M., Qammar, E., Vhora, H., and Schaffer, M. (1998), "Rotating Pip Detection and Stall Warning in High-speed Compressors Using StructureFunction*", Proceedings of the RTO AVT Symposium*, Toulouse, France, 11–15 May.

Christensen, D., Armor, J., Dhingra, M., Cantin, P., Gutz, D., Neumeier, Y., Prasad, J.V., Szucs, P.N., and Wadia, A.R. (2008), "Development and Demonstration of a Stability Management System for Gas Turbine Engines", *Transactions of the ASME, Journal of Turbomachinery*, vol. 130(3), paper 031011, pp. 1–9.

Corsini, A., and Rispoli, F. (2005), "Flow Analyses in a High-pressure Axial Ventilation Fan with a Non-linear Eddy-viscosity Closure", *International Journal of Heat and Fluid Flow,* vol. 26, pp. 349–61.

Cumpsty, N.A. (1989), "Part-circumference Casing Treatment and the Effect on Compressor Stall", *Proceedings of the 34th American Society of Mechanical Engineers Gas Turbine and Aeroengine Congress*, Toronto, ON, Canada, 11–14 June, paper no. 89-GT-312.

Day, I.J., Breuer, T., Escuret, J., Cherrett, M., and Wilson, A. (1999), "Stall Inception and the Prospects for Active Control in Four High-speed Compressors", *Transactions of the ASME, Journal of Turbomachinery*, vol. 121, pp. 18–27.

Gleick, J. (1987), *Chaos: Making a New Science*, Vintage Books, New York, NY, USA.

Gravdahl, J.T., and Egeland, O. (1999), *Compressor Surge and Rotating Stall: Modelling and Control*, Springer Verlag, London, UK.

Greitzer, E.M. (1976), "Surge and Rotating Stall in Axial Flow Compressors, Part I: Theoretical Compression System Model", *Transactions of the ASME, Journal of Engineering and Power,* vol. 98, pp. 190–98.

Kameier, F., and Neise, W. (1997), "Rotating Blade Flow Instability as a Source of Noise in Axial Turbomachines", *Journal of Sound and Vibration,* vol. 203, pp. 833–53.

Laurendeau, E., Jordan, P., Delville, J., and Bonnet, J.P. (2007), "Nearfield-farfield Correlations in Subsonic Jets: What Can They Tell Us?", *Proceedings of the 13th AIAA/CEAS Aeroacoustics Conference* (*28th AIAA Aeroacoustics Conference*), Rome, Italy, 21–23 May, paper no. AIAA 2007-3614.

Liu, Y., Dhingra, M., and Prasad, J.V.R. (2009), "Active Compressor Stability Management via a Stall Margin Control Mode", *Proceedings of the 54th American Society of Mechanical Engineers Gas Turbine and Aeroengine Congress*, Orlando, FL, USA, 8–12 June, paper no. GT2009-60140.

Methling, F.O., Stoff, H., and Grauer, F. (2004), "The Pre-stall Behaviour of a 4-stage Transonic Compressor and Stall Monitoring Based on Artificial Neural Networks", *International Journal of Rotating Machinery*, vol. 10, pp. 387–99.

Moore, F.K. (1984), "A Theory of Rotating Stall of Multistage Compressors, Parts I–III", *Transactions of the ASME, Journal of Engineering for Power*, vol. 106, pp. 313–36.

Paduano, J.D., Greitzer, E.M., and Epstein, A.H. (2001), "Compression System Stability and Active Control", *Annual Review of Fluid Mechanics,* vol. 33, pp. 491–517.

Pickover, C.A. (1986), "On the Use of Symmetrized Dot Patterns for the Visual Characterization of Speech Waveforms and Other Sampled Data", *Journal of the Acoustical Society of America,* vol. 80, pp. 955–60.

Rippl, A. (1995), "Experimentelle untersuchungen zuminstationaren betriebsverhahen an der stabilitarsgrenze eines mehrstufigen trans-sonischen Verdichters", PhD thesis, Ruhr-Universitat Bochum, Germany.

Schultz, T.J. (1978), "Synthesis of Social Surveys on Noise Annoyance", *Journal of the Acoustical Society of America,* vol. 64, pp. 377–405.

Sheard, A.G., and Corsini, A. (2012), "The Mechanical Impact of Aerodynamic Stall on Tunnel Ventilation Fans", *International Journal of Rotating Machinery*, vol. 2012, pp. 1–12.

Sheard, A.G., Corsini, A., and Bianchi, S. (2010), "A Method of Detecting Stall in an Axial Fan", GB Patent 2 468 571 B, 24 December.

Sheard, A.G., Corsini, A., and Bianchi, S. (2011), "Stall Warning in a Low-speed Axial Fan by Visualisation of Sound Signals", *Transactions of the ASME, Journal of Engineering for Gas Turbines and Power*, vol. 133, paper no. 041601, pp. 1–10.

Shibata, K., Takahashi, A., and Shirai, T. (2000), "Fault Diagnosis of Rotating Machinery through Visualisation of Sound Signals", *Mechanical Systems and Signal Processing*, vol. 14, pp. 229–41.

Sottek, R., and Genuit, K. (2007), "Sound Quality Evaluation of Fan Noise Based on Hearing-related Parameters", *Proceedings of the 3rd International Symposium of Fan Noise*, Lyon, France, 17–19 September.

Tahara, N., Kurosaki, M., Ohta, Y., Nakajima, T., Nakakita, T., and Outa, E. (2007), "Early Stall Warning Technique for Axial-flow Compressors", *Transactions of the ASME, Journal of Turbomachinery*, vol. 129(3), pp. 448–56.

Takens, F. (1981), "Detecting Strange Attractors in Turbulence", in Rand, D.A., and Young, L.S. (Eds), *Lecture Notes in Mathematics*, Springer, Berlin, Germany.

Tong, Z., Li, L., Nie, C., Nie, C., Lin, B. Cui, Y., and Qi, W. (2009), "Online Stall Control with the Digital Signal Processing Method in an Axial Compressor", *Proceedings of the 54th American Society of Mechanical Engineers Gas Turbine and Aeroengine Congress*, Orlando, FL, USA, 8–12 June, paper no. GT2009-59509.

Tryfonidis, M., Etchevers, O., Paduano, J.D., Epstein, A.H., and Hendricks, G.J. (1995), "Pre-stall Behaviour of Several High-speed Compressors", *Transactions of the ASME, Journal of Turbomachinery*, vol. 117, pp. 62–80.

Van Beyer, R., and Bolland, O. (1998), "Coal Power Compendium", Department of Thermal Energy and Hydropower, NTNU, Trondheim, Norway.

Wiechert, S., and Day, I.J. (2012), "Detailed Measurements of Spike Formation in an Axial Compressor", *Proceedings of the 57th American Society of Mechanical Engineers Gas Turbine and Aeroengine Congress*, Copenhagen, Denmark, 11–15 June, paper no. GT2012-68627.

Wu, J., and Chuang, C. (2005), "Fault Diagnosis of Internal Combustion Engines using Visual Dot Patterns of Acoustic and Vibration Signals", *NDT&E International*, vol. 38, pp. 605–14.

Experiments on the Use of Signal Visualisation Technique for In-service Stall Detection in Industrial Fans

S. Bianchi, A. Corsini, and A.G. Sheard

ABSTRACT

The chapter describes a stall-detection methodology based on the use of a symmetrised dot pattern (SDP) visual waveform analysis and the stall-warning method based on the developed methodology. The experimental study explores the capability of the symmetrised dot pattern technique to detect the presence of incipient stall, and the evolution of aerodynamic instabilities using low signal-to-noise ratio signals. It is the ability of the symmetrised dot pattern technique to produce identifiably different symmetrised dot patterns using low signal-to-noise ratio signals that enables the stall-warning method to function in a noisy working environment. The research reported in this chapter presents a systematic analysis of the probe position's influence on the ability of the symmetrised dot pattern technique to detect the aerodynamic instabilities of interest. We conclude that one may use the symmetrised dot pattern technique, in combination with acoustic measurements in the fan's near vicinity, as the basis of a stall detection system. The technique does not require fitting a sensor in the fan casing. A microphone in the fan's near vicinity or the duct system within which it is installed is sufficient to provide an input signal from which one may create distinctly different symmetrised dot patterns at different fan operating conditions.

NOMENCLATURE

Latin letters

D_h	hub diameter	mm
D_t	tip diameter	mm
i	number of dots	
L	time lag	
ℓ	blade chord	mm
N	number of the discrete signal	
R	polar position of the dot	
SDP	symmetrised dot pattern	
t	absolute time	s
x*	sampled value of the sound signal	
T_{SDP}	sample time	

Greek letters

γ_t	blade tip stagger angle
δ	blade pitch angle
δ_t	blade tip pitch angle
Δt	time interval
Θ^+, Θ^-	two angles of the polar space
ξ	plot angular gain
σ	input signal amplitude
Σ	solidity
Φ	blade camber angle
χ	rotor tip clearance (% of blade span)

INTRODUCTION

Aerodynamic instability arises when flow rate throttling constrains the operational envelope of fans, blowers and compressors. To avoid instability, aerodynamicists must provide adequate stability (stall) margin to accommodate inlet distortions, degradation due to wear, throttle transients and other factors that reduce fan, blower and compressor stability from the original design baseline. Because aerodynamic stall results in increased alternating aerodynamic loads, it is a major potential cause of mechanical failure in axial fans. Consequently, stall detection techniques have had wide application for many years.

Researchers have studied the detection and analysis of the different forms of aerodynamic instability for several decades (Ludwig and Nenni, 1976; Day *et al.*, 1999; Höss *et al.*, 2000; Bianchi *et al.*, 2012). The standard classification of aerodynamic stalls in axial fans and compressors (Gravdahl and Egeland, 1999) distinguishes between rotating stall in which reversed flow regions occur locally and surge which is characterised by periodic backflow over the entire annulus. The latter is unusual in fan applications due to the system's insufficient counter-pressure. Rotating

stall is typically associated with industrial axial fans. It is a mechanism by which the rotor adapts to a reduced flow rate. This results in circumferentially non-uniform flow patterns rotating in the annulus.

In reviewing the evolution of rotating stall, Cumpsty (1989) noted that the drop in overall performance can occur as a so-called 'progressive stall' or an 'abrupt stall'. Engineers usually associated the former with a part-span stall which results in a small performance drop; whereas, they associate the latter with a full-span stall and a large drop in performance. Notably, the part-span stall occurs typically in single blade rows (Cumpsty, 1989) and usually leads to more complex disturbances in single-rotor or single-stage machines than in multi-stage compressors (Moore, 1984).

The likelihood of an industrial axial fan shifting from stable operation into rotating stall will increase when the fan operates in an erosive environment. This results in the fan blades' leading edge wearing away, reducing the blade chord and destroying the leading edge's aerodynamic profile. Increasing the blade pitch angle may recover the fan's pressure developing capability, but this has the secondary effect of reducing the fan's stall-free operating margin. Irrespective of whether the blade pitch angle increases, continued blade erosion will result in the fan pressure developing capability reducing with an associated risk that it may transition from stable operation to incipient stall and finally rotating stall.

Strain gauge measurements on axial compressors (Rippl, 1995) and fans (Sheard and Corsini, 2011) have confirmed that bending stress in compressor and fan blades exceed those associated with stable operation by a factor of five and seven, respectively, when operated in rotating stall. Reliable methods of monitoring the stability limit are the subject of ongoing research (Greitzer, 1976; Paduano *et al*., 2001; Liu *et al*., 2009). A need to develop stall-warning systems that operators can apply motivates the research (Bindl *et al*., 2009). Operators need to be able to identify incipient stall in order to alert them that a compressor or fan is about to stall. It is this ability to warn that stall is approaching, but had not yet occurred that is the critical input facilitating development of active control systems that can suppress incipient stall. To be effective, a stall warning system must be able to detect incipient stall in approximately two rotor revolutions for axial compressors (Methling *et al*., 2004), but perhaps ten times longer for industrial fans (Sheard *et al*., 2011).

Prior stall detection methods have had drawbacks. They are unable to detect incipient stall and consequently, are not able to initiate a sufficiently rapid response to the onset of stall to avoid damage. Researchers have identified incipient stall detection methods for individual test beds, but reliable detection methods of general validity require further research. Existing techniques for the detection of incipient stall are based on experimental observation of pre-stall behaviours. They have sought to identify pre-stall behaviour as early as possible to enable an active control system to react and suppress the incipient stall. Existing detection techniques all rely on the use of on-board probes able to sense the unsteady pressure in the vicinity of the blade rows. When applied into real-time control applications, they typically utilise a time or Fourier analyses (Tryfonidis *et al*., 1995; Christensen *et al*., 2008; Tong *et al*., 2009).

In an effort to develop a stall detection method suitable for a real-time control application, Tahara *et al*. (2007) proposed a stall warning index. They calculated this

index using the unsteady pressure signal from a sensor mounted in the rotor casing over the blades. The calculation method involved taking a normalised product of unsteady pressure over successive rotor revolutions. Breugelmans *et al.* (1995) studied rotating stall, reconstructing phase-space portraits of measured velocity, static pressure and vibration using Takens's (1981) 'method of delays'. Breugelmans *et al.*'s (1995) research objective was to elucidate the apparently chaotic fluid-flow mechanisms underlying rotating stall. In a similar vein, Bright *et al.* (1998) investigated rotating instabilities prior to stall using a 'temporal structure function' inspired by a statistical approach derived from chaos theory.

The fluid-flow mechanisms underlying rotating stall may contain a chaotic element, but incipient stall is associated with the presence of identifiable flow-field features. The presence of these features results in a change in the fan or compressor's acoustic signature. In an effort to exploit the link between incipient stall and acoustic signature, researchers have proposed diagnostic techniques based on sound-signal visualisation (Shibata *et al.*, 2000; Wu and Chuang, 2005). One can most easily apply this approach to fault diagnosis in rotating machinery when discrete and narrow frequency components dominate an unsteady pressure signal. Recently, Sheard *et al.* (2010) used a sound visualisation technique to assess the improvement in acoustic performance of a low-solidity axial fan when fitted with a blade tip treatment intended to minimise blade tip-to-casing leakage flow generated noise. Successively, Bianchi *et al.* (2009) refined the sound visualisation technique and applied it as a stall warning tool in axial industrial fans.

The present study explores using a symmetrised dot pattern (SDP) technique to generate a visual representation of an acoustic input signal, and then using their identifiable features to characterise incipient stall. Bianchi *et al.* (2009) generated symmetrised dot patterns from the unsteady pressure they measured using a sensor mounted in the fan's casing. In contrast, the present study generates symmetrised dot patterns from acoustic signals measured using a microphone in the fan's near vicinity. This extension of the technique facilitates using acoustic measurements taken at different locations in the fan's acoustic far-field, avoiding the need to mount a sensor in the fan casing.

Researchers originally conceived the symmetrised dot pattern technique for the visual characterisation of speech waveforms and sound quality evaluation (Schultz, 1978; Pickover, 1986; Sottek and Genuit, 2007). Sheard *et al.* (2011) first applied the technique into an industrial fan, using it to differentiate between stable, incipient stall and rotating stall operating conditions. Sheard *et al.*'s (2011) key conclusion was that the symmetrised dot pattern technique could produce an identifiably different pattern using data collected over a time period lasting from 0.1 to as little as 0.004 seconds. This ability to identify incipient stall using data taken over a time period similar to the time scales associated with incipient stall makes the technique a potential basis for a stall detection system.

The reported research establishes the symmetrised dot pattern techniques ability to detect incipient stall using low signal-to-noise ratio acoustic measurements. Specifically, we took the acoustic measurements with a microphone in the working environment around the studied fan, not using sensors fitted to, or in the fan casing.

We investigated the influence of microphone position on the technique's effectiveness. We concluded that although some microphone locations result in a better signal-to-noise ratio than others, the symmetrised dot pattern technique is able to generate identifiably different patterns in any location in the fan's general vicinity. Consequently, the symmetrised dot pattern technique, in combination with an acoustic signal from a microphone in the fan's far-field, is able to identify incipient stall and therefore form the basis of a stall detection system.

EXPERIMENTAL METHODOLOGY

We conducted the reported research on a family of commercially available cooling fans. The studied fan configuration, coded AC90/6, incorporates a six-blade un-swept rotor, with modified ARA-D profile aerofoils blade, Table 7.1. One may set the blade-pitch angle during final assembly to customise the fan to a desired duty point.

Investigated flow conditions

The AC90/6 fan features a peak pressure rise of approximately 208 Pa with a design operating condition pressure rise of 125 Pa. We measured the fan's characteristic in accordance with ISO 5801 requirements (2007), Figure 7.1. The selected blade angle for the fan was 28 degrees, measured as is customary in the industrial fan industry in the peripheral direction. We selected a 28 degree blade angle to ensure that the fan blades were highly loaded. Highly loaded blades suffer more severe

Table 7.1. *The fan AC90/6 specification and geometry.*

Blade geometry	AC90/6 fans	
	Hub	Tip
Blade pitch angle, δ	36°	28°
Blade camber, ϕ	46°	41°
Solidity, Σ	1.24	0.3

Fan rotor	
Blade number	6
Blade tip pitch angle, δ_t	28°
Blade tip stagger angle, γ_t	62°
Hub diameter to casing diameter ratio, D_h/D	0.22
Tip diameter, D_t	900 mm
Rotor tip clearance, χ (% of blade span)	1.0%
Design speed	935−950 rpm
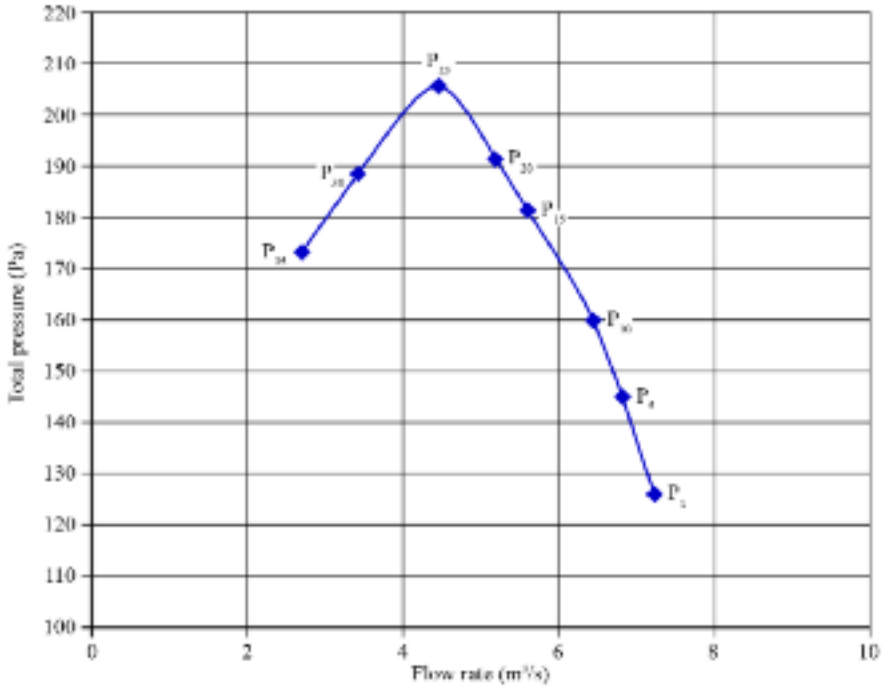
FIGURE 7.1. The fan's performance characteristic, and eight of the 35 points where we took acoustic measurements. We analysed acoustic measurements at the fan's design (P_1), peak pressure (P_{25}) and a rotating stall (P_{35}) operating condition.

degradation of both aerodynamic and acoustic performance because of the blade tip-leakage vortex's intensity. We used the experimental facility within which we fitted the fan to throttle it from stable operation at its design to peak pressure operating condition, where stall was incipient and then into rotating stall. During the throttle transient we measured fan far-field noise in accordance with ISO IEC60651 requirements (1994).

Experimental setup

We conducted the experimental measurements in the Latina-Borgo Isonzo Laboratory of the University of Roma, Sapienza (Italy). The fan impeller was balanced to ensure vibration below 4 mm/s, a balance quality typically of industrial fans. We operated the fan in a custom-built casing made from rings of cast and machined steel. Clearance between the blade tips and the casing was constant at one per cent of blade span. We used a 2.5 kW direct-coupled induction 400 Volt (AC), three-phase CM29 motor to drive the rotor at a constant speed of 940 rpm, resulting in a 44.34 m/s blade tip speed and a blade-passing frequency (BPF) in the 93.75–96.88 Hz range.

We made acoustic measurements at the duct inlet (A), the duct exhaust (B) and in two positions along the duct within which the fan was fitted: next to the fan (C) and mid-way along the inlet duct (D), Figure 7.2. We made measurements at location A, B, C and D with a microphone positioned two metres from the test system duct work. Charge amplifiers conditioned the microphone, with the resultant signals outputting to a data acquisition system (NI Compact Acq. 9172 with NI 9205 analogical input modules). The uncertainty of the readings was 0.1–0.2 dB at 1 kHz, established in accordance with ISO 5801 requirements (2007).

STALL WARNING TECHNIQUE

The symmetrised dot pattern technique transforms an input signal into polar coordinates, and thus generates a visual representation of the input signal. For application in a stall detection system, one uses the symmetrised dot pattern technique to generate visual representations at known fan operating conditions. Although it may not be apparent which symmetrised dot pattern features are associated with specific physical flow phenomena, the symmetrised dot patterns provide a characterisation of them. By linking topology of symmetrised dot patterns and fan operating condition, the resultant stall detection method shares its foundation with chaos theory (Gleick, 1987).

The symmetrised dot pattern techniques advantage over other approaches is its ability to link features with specific physical flow phenomena. The symmetrised dot pattern technique does not simply provide a measure of the overall sound power level produced by an input signal's tonal components. It is able to visually represent more subtle features that would otherwise be difficult to characterise. Therefore, the merit of the symmetrised dot pattern technique is its ability to perceive otherwise 'unquantifiable' differences in an input signal, mimicking the way that humans hear (Schultz, 1978; Sottek and Genuit, 2007).

Mathematical framework and polar pattern construction

We used an algorithm to map a normalised input signal into a polar coordinate system to produce the symmetrised dot pattern, Figure 7.3. The algorithm maps a point in the input signal as the polar coordinate's radial component, and the adjacent point in the input signal as the polar coordinate's angular component. In this way, one may map successive pairs of points from the input signal as single points in a polar coordinate system. Collectively these points comprise the resultant symmetrised dot pattern.

We can formulate the polar transformation $R(i)$ from input signal to symmetrised dot pattern as:

$$R(i) = \frac{\sigma(i) - \sigma_{\min}}{\sigma_{\max} - \sigma_{\min}} \tag{1}$$
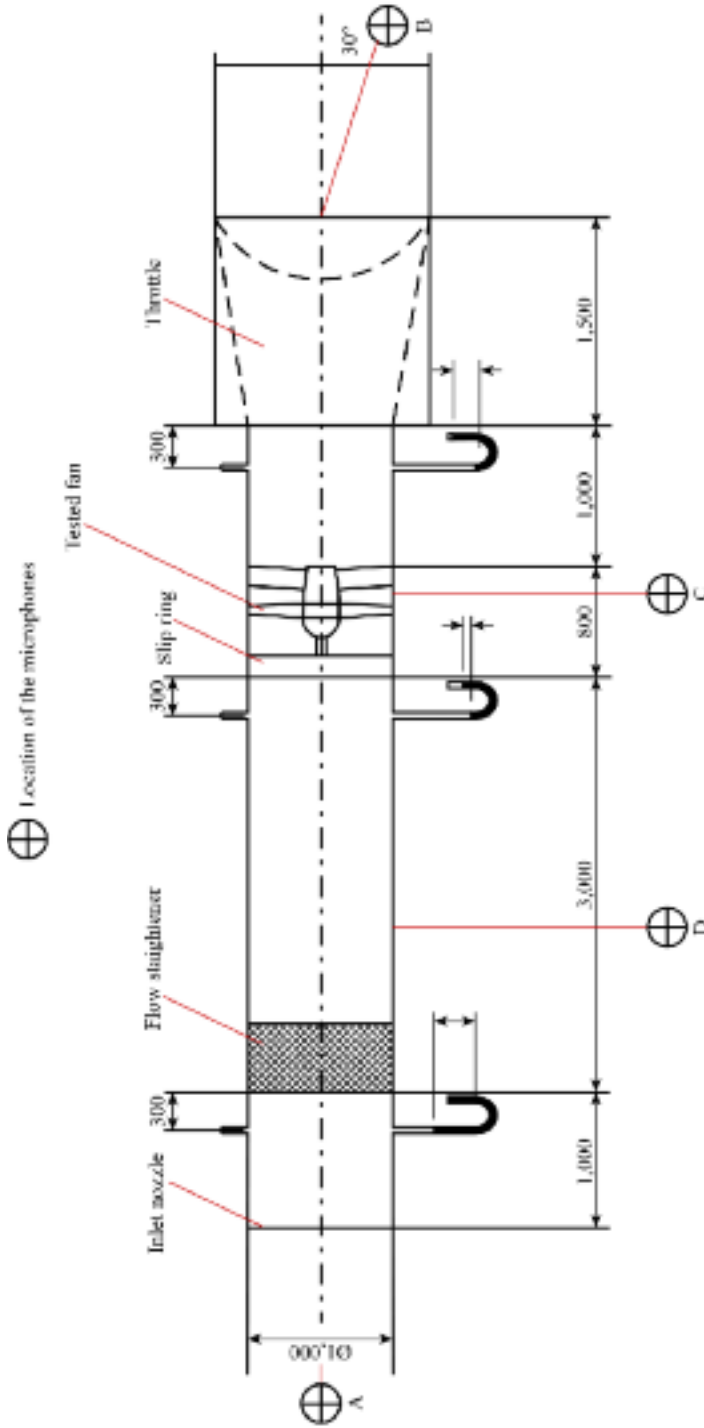
FIGURE 7.2. A side view of the ISO 5801 (2007) standard ducted test rig, identifying the four locations at which we took acoustic measurements. The first location is the duct inlet (location A). The second is the duct exhaust (location B). The third is next to the fan (location C). The fourth is mid-way along the inlet duct (location D).

FIGURE 7.3. A schematic illustration of the technique for transforming an input signal into polar coordinates to produce a symmetrised dot pattern.

$$\Theta^{-}(i) = \Theta_0 + \frac{\sigma(i+L) - \sigma_{min}}{\sigma_{max} - \sigma_{min}} \xi \tag{2}$$

$$\Theta^{-}(i) = \Theta_0 - \frac{\sigma(i+L) - \sigma_{min}}{\sigma_{max} - \sigma_{min}} \xi \tag{3}$$

in which i is the number of dots (i = integer ($t/\Delta t$)), with t the time *abscissa* and Δt the sampling time; L is the time lag coefficient; $\sigma(i)$ is the sampled ith input signal; σ_{max} and σ_{min} are the highest and the lowest value of the original input signal window; Θ_0 is the rotation of the origin angle of any reference line; ξ is the angular gain; and Θ^+ and Θ^- are the two angles of the traditional polar space. The input signal is first normalised in the range (0, 1) by finding the higher (σ_{max}) and lower values (σ_{min}) for the N data points in the window. Therefore, overall signal amplitude, in general, is not a factor in the characterisation.

The unsteady flow phenomena associated with incipient stall in an axial industrial fan become established and then collapse in less than one rotor revolution (Bianchi *et al*., 2012). In order for a symmetrised dot pattern to visually represent incipient stall, one must take input data over a time that is similar to that of the physical flow phenomena associated with incipient stall. The symmetrised dot pattern quality is less dependent on the total number of data points than the sample rate. Shibata *et al*. (2000) studied the impact of sample rate. They concluded that when using a single-frequency sine wave as an input signal, the higher the sampling rate and the less clear the resultant symmetrised dot pattern. However, if the input signal includes components at multiple frequencies, the resulting symmetrised dot pattern was different from the sum of single frequency symmetrised dot patterns. In contrast, a white noise input signal resulted in a near uniform distribution of dots over the resultant symmetrised dot pattern, irrespective of sampling rate. Thus, Shibata *et al*. (2000) concluded that the combination of features in the input signal resulted in the complexity of the resultant symmetrised dot pattern.

Sheard *et al*. (2011) first studied the application of the symmetrised dot pattern technique to detect incipient stall. They concluded that the technique was effective.

Sheard *et al*. (2011) generated symmetrised dot patterns with the studied fan in stable, incipient stall and rotating stall operating conditions, with input data collected over 3.0, 1.0 and 0.1 rotor revolutions. The symmetrised dot patterns generated with input data taken over 3.0 and 1.0 rotor revolutions were distinctly different at each operating condition. A comparison of the symmetrised dot patterns generated with a sample time corresponding to 1.0 and 0.1 rotor revolutions indicated that the reduction in sample time resulted in significant degradation of symmetrised dot pattern quality. Despite this degradation, Sheard *et al*. (2011) concluded that it was still possible to infer some of the features evident in the symmetrised dot patterns generated with a sample time corresponding to 1.0 rotor revolution in the symmetrised dot patterns generated with a sample time corresponding to 0.1 rotor revolutions.

Sheard *et al*. (2011) concluded that the symmetrised dot patterns generated with a sample time corresponding to 1.0 rotor revolutions represent the best trade-off between sample time and symmetrised dot pattern quality. In the research reported in this chapter, we chose to log data for 0.1 seconds, equivalent to 1.5 rotor revolutions. The studied fan was a relatively low-speed fan, and therefore, we judged that logging data for 1.5 rotor revolutions gave the best trade-off between sample time and number of data points in each logged data set.

Signal characterisation

We made acoustic measurements in the studied fan's far-field using a GRAS microphone, type 40AG (Sheard *et al*., 2011). We utilised a 10 kHz sampling rate giving a Nyquist frequency of 5 kHz. To avoid signal aliasing, we filtered all data at 4 kHz and analysed it in the range of interest below 1 kHz. Following Sheard *et al*.'s method (2011), we calculated the system frequency response using the PREMESYS 2.0 MATLAB application tool, developed at the von Karman Institute of Fluid Dynamics by Boerrigter (1996). This application tool enabled us to characterise the measurement system's dynamic response to a step change in input signal. The dynamic response indicated that limiting any signal analysis to frequencies below 500 Hz would keep errors in phase angle below –3 degrees, which we considered acceptable in the present study. We estimated the overall measurement uncertainty as (i) $\Delta V=1,000$ mV $\pm$ 12 mV (20:3) on the voltage and (ii) $\Delta G=200$ dB $\pm$ 2.4 dB (20:3) on the raw signal gain for frequencies up to 1 kHz.

RESULTS

We throttled the studied fan from its design (P_1) to a rotating stall (P_{35}) operating condition, whilst logging acoustic data, Figure 7.4. We positioned the microphone at the duct inlet, location A, Figure 7.2. A visual inspection of the acoustic data indicates that incipient stall becomes established at P_{20}, prior to the peak pressure (P_{25}) operating condition, an observation that is consistent with Arts *et al*.'s conclusions (1994).
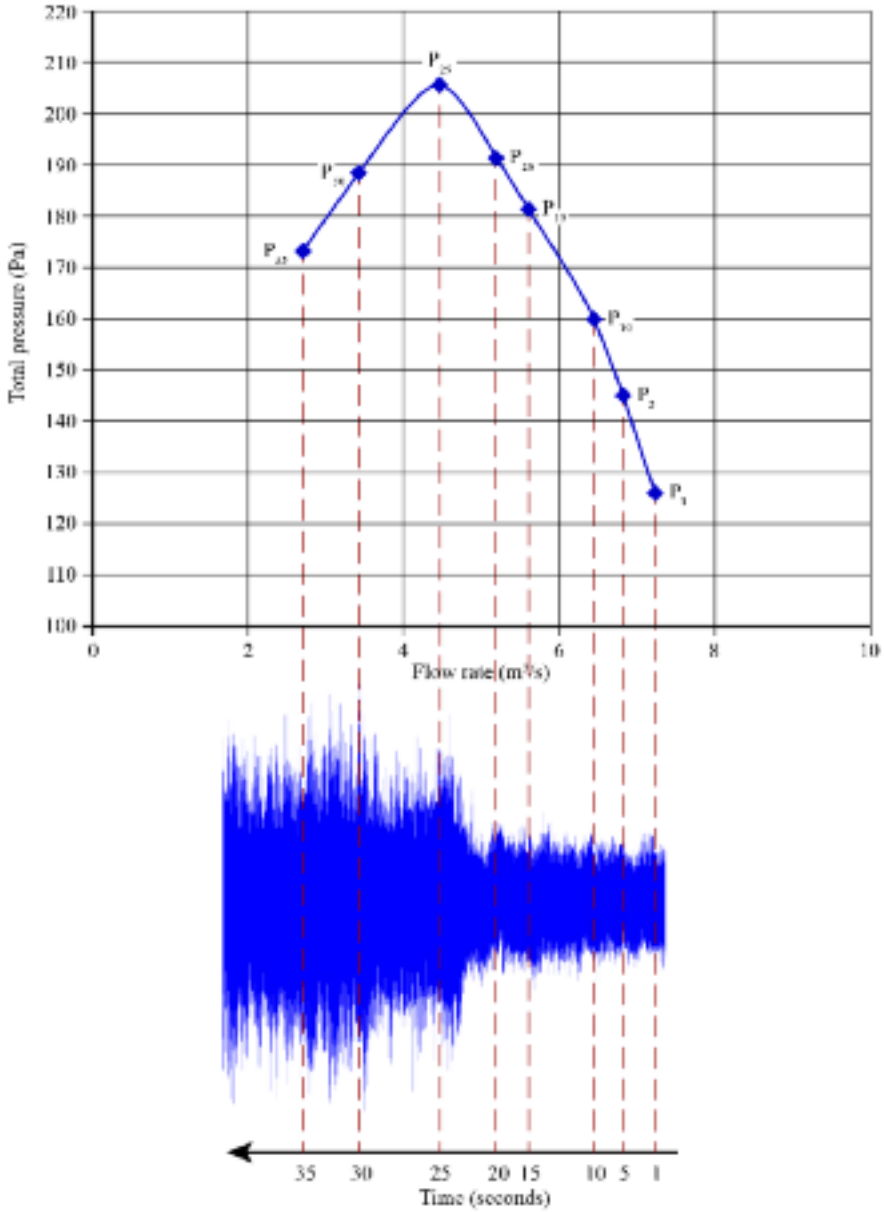
FIGURE 7.4. The fan's performance characteristic and acoustic data measured at the duct inlet (location A) as the fan was throttled from its design (P_1) through to a rotating stall (P_{35}) operating condition.

Sensitivity analysis

We used acoustic data logged at the studied fan's design (P_1) and a rotating stall (P_{35}) operating conditions with the microphone at the duct inlet (location A) to generate symmetrised dot patterns over a matrix of time lag (L) and angular gain (ξ), Table 7.2. We logged all data at a sampling frequency of 10 kHz for 0.1 seconds. Our objective was to establish the impact of time lag (L) and angular gain (ξ) on the resultant symmetrised dot pattern topology.

The symmetrised dot patterns generated from acoustic data logged at both the fan design (P_1) and a rotating stall (P_{35}) operating condition indicate that a low value of time lag (L) results in the resultant symmetrised dot pattern's curvature, Figures 7.5 and 7.6. As the value of time lag (L) increases, the resultant symmetrised dot patterns becomes progressively more rectangular in shape which we interpreted as a reduction in quality of the symmetrised dot pattern topology. In contrast, increasing angular gain (ξ) increased the size of the resultant symmetrised dot pattern, Figure 7.5. We interpreted this as an improvement in the quality of the symmetrised dot pattern topology. Our interpretations of symmetrised dot pattern quality were consistent with those of De-Rosier *et al*. (1997). Following the analysis of impact of time lag (L) and angular gain (ξ), we chose a time lag of 10 and an angular gain of 50 when generating subsequent symmetrised dot patterns.

Detection of the stall incipience

Using a time lag (L) of 10 and angular gain (ξ) of 50, we generated symmetrised dot patterns at eight points on the studied fan's characteristic, with the microphone at location A, B, C and D, Figure 7.7. The studied fan's design point (P_1) is a stable operating condition, with stall becoming incipient at P_{20} and fully developed by P_{30}. In order for the symmetrised dot pattern technique to form the basis of a stall detection system, the symmetrised dot patterns at each operating condition must be identifiably different (Sheard *et al.*, 2010).

When we study the symmetrised dot patterns, we see two identifiable features of the topology change as the fan throttles from its design (P_1) to incipient stall (P_{20}) operating condition. First, the symmetrised dot pattern arms progressively become

Table 7.2. *Sensitivity test matrix used to establish the optimum values of time lag (L) and angular gain (ξ) when generating symmetrised dot patterns.*

Type of test	Constants	Parameters
Sensitivity to angular gain (ξ)	$L = 1$ $T_{SDP} = 0.1$ seconds	$\xi = 1, 30, 50$
Sensitivity to time lag	$(L)\,\xi = 10$ $T_{SDP} = 0.1$ seconds	$L = 1, 10, 50$
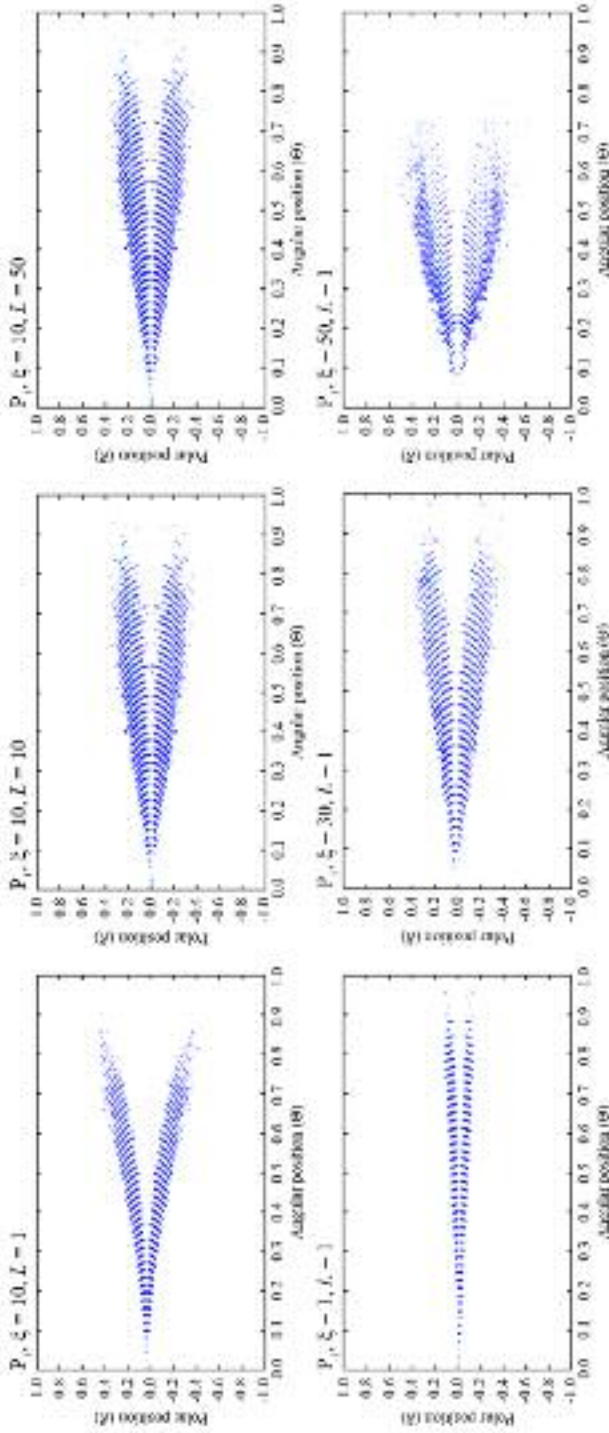
FIGURE 7.5. Sensitivity of the symmetrised dot pattern technique to time lag (L) and angular gain (ξ), with data recorded at the duct inlet (location A) with the fan operating at its design (P_1) operating condition.
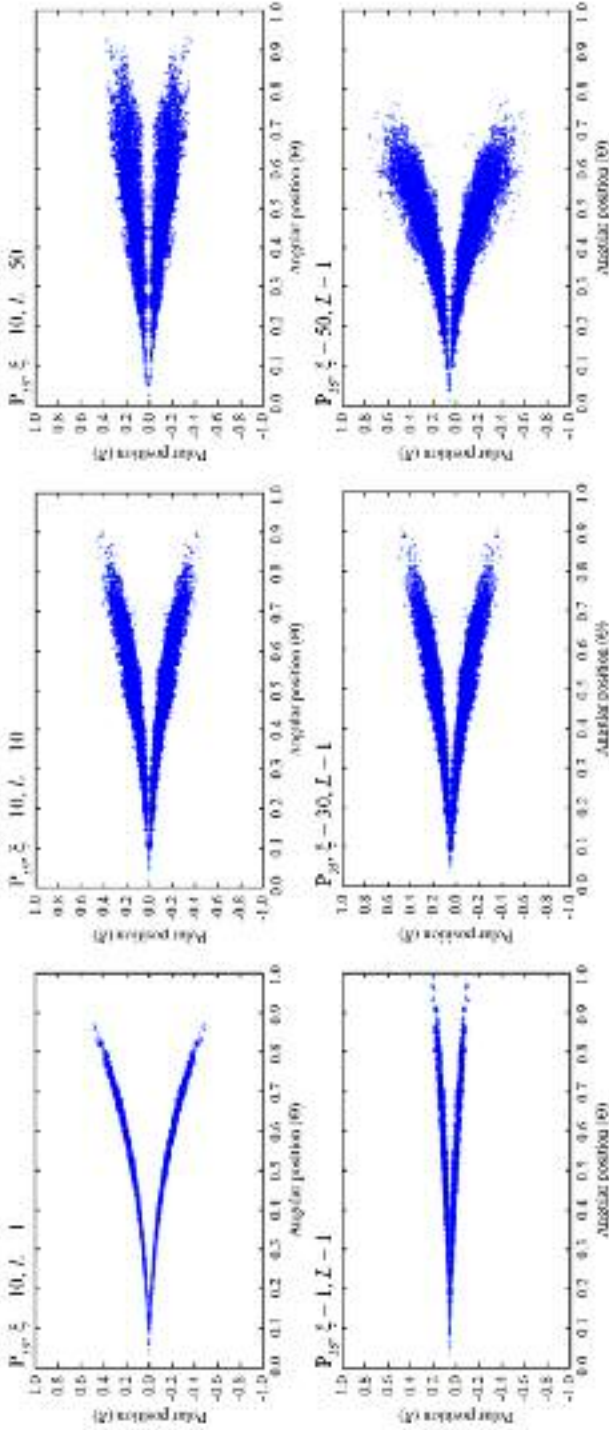
FIGURE 7.6. Sensitivity of the symmetrised dot pattern technique to time lag (*L*) and angular gain (ξ), with data recorded at the duct inlet (location A) with the fan operating at a rotating stall (P_{35}) operating condition.
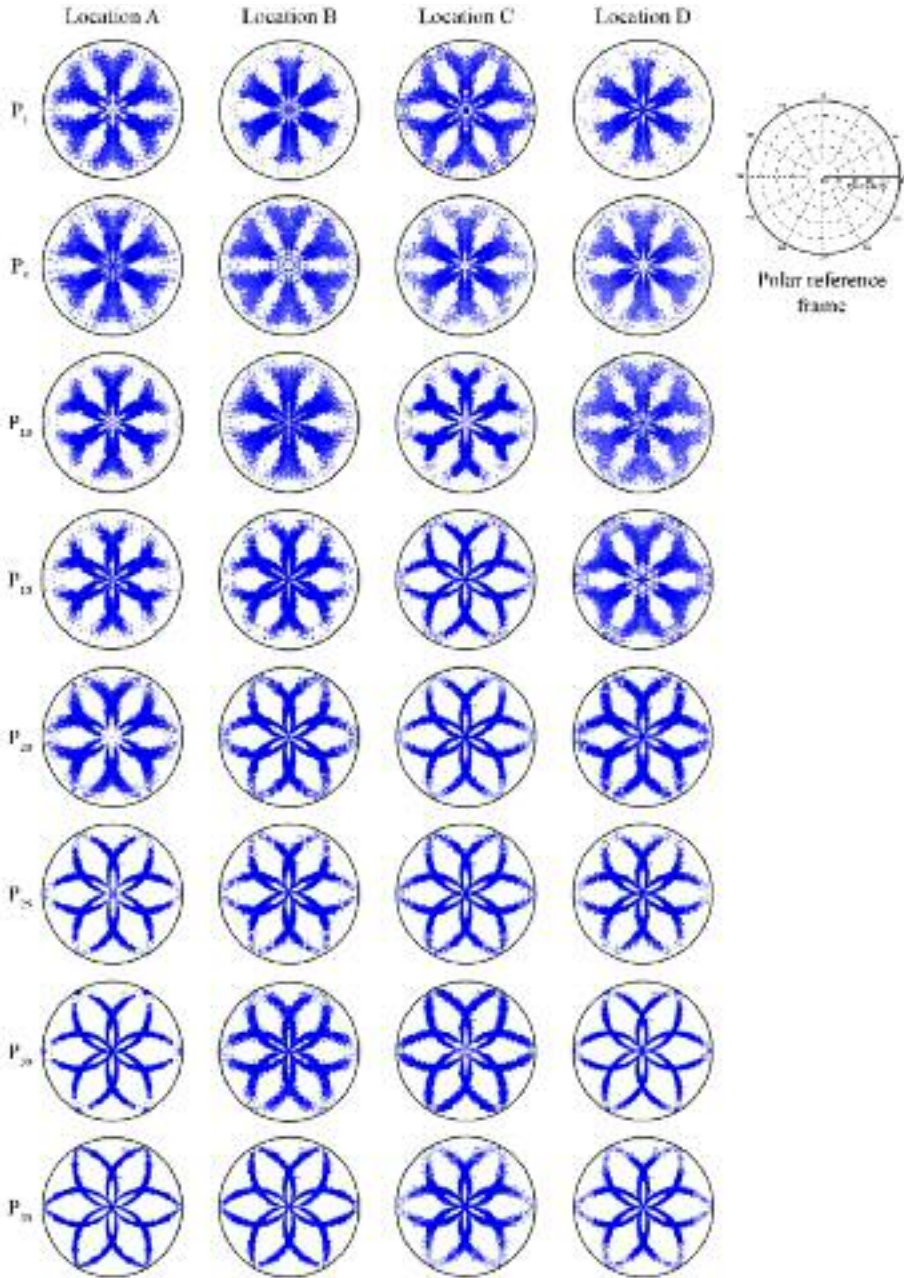
FIGURE 7.7. Symmetrised dot pattern evolution from the fan's design (P_1) to a rotating stall(P_{35}) operating condition, generated using input data from four microphone locations located at the duct inlet (location A), the duct exhaust (location B), next to the fan (location C) and mid-way along the inlet duct (location D).

more highly curved. An increase in curvature is indicative of an increase in the low-frequency tonal components of the input signal that we used to generate the symmetrised dot patterns (Sheard *et al*., 2011). Second, the area covered by the symmetrised dot patterns reduces. This is indicative of an increased modulation of the input signal's low-frequency components that we used to generate the symmetrised dot patterns (Sheard *et al*., 2011).

THE IMPACT OF MICROPHONE LOCATION

When we study the symmetrised dot patterns, we see that the change in topology with changing operating condition remains evident as we move the microphone from one location to another, Figure 7.7. The symmetrised dot patterns generated with stall becoming incipient (P_{20}) at each microphone location were all identifiably different to the symmetrised dot patterns generated at the fan's peak pressure (P_{25}) operating condition and after rotating stall had become fully established (P_{30}). Perhaps not surprisingly, the microphone positioned next to the fan (location C) produced data that was able to detect incipient stall first. The symmetrised dot pattern generated at location C, operating condition P_{15}, is identifiably different to the symmetrised dot pattern generated at location C, operating condition P_{10}. As such, we may conclude that although the microphone should be located opposite the fan if possible. However, microphone location did not affect the symmetrised dot pattern technique's ability to identify incipient stall.

We may evaluate the impact of microphone location by considering the symmetrised dot patterns generated at the duct inlet (location A) and mid-way along the inlet duct (location D), Figure 7.8. We consider the symmetrised dot patterns generated at each location at the studied fan's design (P_1), prior to incipient stall (P_{15}) and peak pressure (P_{25}) operating conditions. Although the symmetrised dot patterns generated using data from location A and D are identifiably different at operating conditions P_1, P_{15} and P_{25}, there is a chaotic aspect to them which we can characterise using chaos theory (Takens, 1981; Fraser and Swinney, 1986; Pickover, 1990; Perugini *et al*., 2003). Those scholars who have studied chaos theory stress that the fractal of a random time series is usually clustered in sub-triangular regions and does not define any particular structure. In contrast, in a chaotic time series the points are dispersed along hyperbolic curves that intersect each other, indicating a clear and well-recognisable structure in the time series. Therefore, we may characterise the symmetrised dot patterns as typical of those associated with well structured, but chaotic input data.

When we consider the symmetrised dot patterns generated at location A and D for operating conditions P_1, P_{15} and P_{25}, we may conclude that their features are not random. The chaotic overlay on the symmetrised dot pattern structure is indicative of a mix of features in the input data. This combination of deterministic and chaos in the symmetrised dot patterns is indicative of aerodynamic and thermodynamic phenomena (Takens, 1981). We may speculate that the physical flow phenomena that characterise incipient stall are inherently chaotic. Therefore, as the studied fan's op-
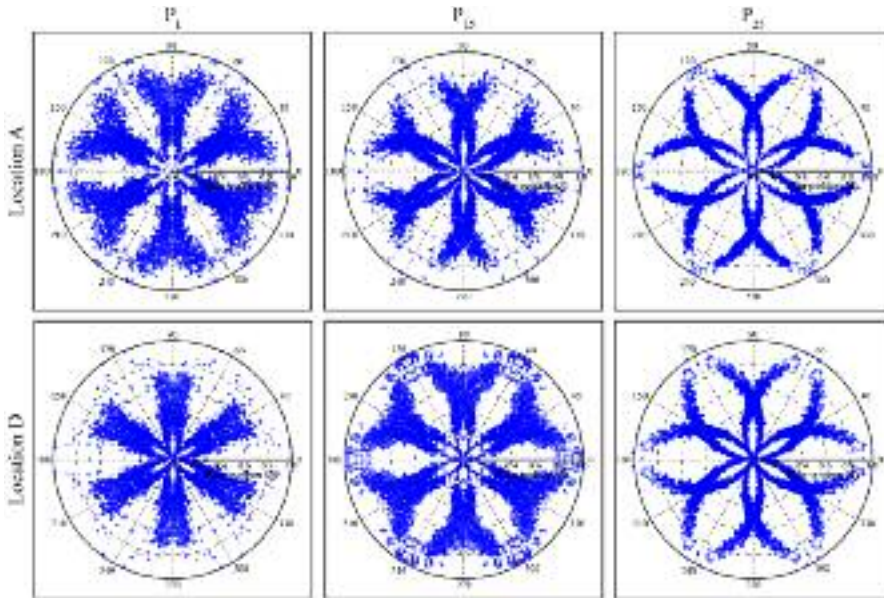
FIGURE 7.8. Symmetrised dot pattern evolution from the fan's design (P_1), prior to incipient stall (P_{15}) and peak pressure (P_{25}) operating condition. The symmetrised dot patterns were generated using input data from microphones located at the duct inlet (location A) and mid-way along the inlet duct (location D).

erating condition moves from its design (P_1) towards incipient stall (P_{15}) and on to peak pressure (P_{25}), the chaotic contribution to the originally deterministic input data will increase.

A consideration of the impact of changing microphone position from location A to location D for operating conditions P_1, P_{15} and P_{25} provides an insight into the impact of incipient stall on the resultant symmetrised dot patterns. Location D is associated with symmetrised dot patterns at the studied fan's design (P_1) and approaching incipient stall (P_{15}) operating conditions that we may characterise as deterministic. In contrast, the symmetrised dot pattern generated with the microphone positioned at location A when approaching incipient stall (P_{15}) is more chaotic. Location A is at the duct inlet, and location D is mid-way along the inlet duct upstream of the fan, Figure 7.2. Consequently, location A will be most sensitive to the radial modes that reflect from the duct walls and so are less pronounced at location D. In contrast, location D will be most sensitive to transverse modes that radiate from the duct system.

As the fan approaches its peak pressure (P_{25}) operating condition, we may characterise the symmetrised dot patterns generated with input data from both location A and D as chaotic. This indicates that as the fan reaches its peak pressure operating condition and is on the verge of stalling, the chaotic characteristics of the input data dominate the resultant symmetrised dot patterns and therefore, microphone location becomes less significant.

Any stall detection system that can operate with a sensor mounted remote from a fan is easier to implement than a system that requires a sensor mounted either on or in the fan's casing. The ability of the symmetrised dot pattern technique to generate identifiably different symmetrised dot patterns at different fan operating conditions using only a microphone located in the far-field constitutes a distinct advantage. The symmetrised dot pattern technique's ability to identify incipient stall is a particular advantage. The combination of far-field acoustic measurement and the identification of incipient stall constitute the essential pre-requisites for a stall detection system suitable for application with industrial fans. The far-field acoustic measurements require no special adaptation of the fan. An identification of incipient stall, as opposed to rotating stall provides an operator with the information on fan condition that one needs to take action before rotating stall has become established, and therefore, before any mechanical damage has occurred.

CONCLUSIONS

The reported research presents a novel diagnostic method for detecting incipient stall. The approach links the topology of symmetrised dot patterns to different fan operating conditions, providing a method for differentiating between operating conditions. The symmetrised dot pattern technique enables the creation of visual representations of the input signal by mapping it onto polar coordinates. The technique's primary strength is its ability to characterise apparently chaotic input signals. This characterisation is possible using data gathered over a time period equivalent to those of the physical flow phenomena associated with incipient stall.

Scholars who have previously studied the symmetrised dot pattern technique have concluded that a symmetrised dot pattern generated from random input data has no structure. In contrast, chaotic input data results in a symmetrised dot pattern with points dispersed along intersecting hyperbolic curves. In the reported research the symmetrised dot patterns generated at different fan operating conditions were characteristic of input data that was chaotic, but with a clear structure. This structure indicated that the input data was not random, with the resultant symmetrised dot patterns reflecting features in the input signal. Specifically, as stall becomes incipient the chaotic content of the input signal increased with the resultant symmetrised dot patterns reflecting the increased chaos. It was this change in the symmetrised dot patterns with the changing fan operating condition that enabled the two to be linked.

An analysis of the impact of microphone location concluded that a microphone at any location in the near vicinity of the fan resulted in identifiably different symmetrised dot patterns at different fan operating conditions. There was some difference in the symmetrised dot patterns generated from input signals measured along the fan duct and at the duct inlet. We concluded that the duct system's vibration modes within which the fan was installed may have resulted in the amplification of some acoustic tones. However, at the fan's peak pressure operating condition, when stall is incipient, the symmetrised dot patterns were essentially similar irrespective of microphone location.

The reported research demonstrated that the symmetrised dot pattern technique has the potential to identify incipient stall using an input signal from a microphone located in the fan far-field. We took data over 0.1 seconds, equivalent to 1.5 rotor revolutions. Despite the noisy working environment in the fan's near vicinity, the resultant symmetrised dot patterns were identifiably different at different fan operating conditions. This demonstrates that the symmetrised dot pattern technique can form the basis of a stall detection system that is able to identify incipient stall, providing an operator with a warning that a fan is about to stall, but has not yet done so. Because operation in a rotating stall condition results in mechanical damage, a stall detection system that can detect incipient stall can assist operators in avoiding damage.

REFERENCES

ISO IEC60651, 1994, Specification for Sound Level Meters.

ISO 5801, 2007, Industrial Fans — Performance Testing Using Standardized Airways.

Arts, T., Boerrigter, H., Carbonaro, M., Charbonnier, J.M., Degrez, G., Olivari, D., Riethmuller, M.L., and Van den Braembussche, R.A. (1994), *Measurement Techniques in Fluid Dynamics — An Introduction*, von Karman Institute for Fluid Dynamics, Rhode-Saint-Genèse, Belgium.

Bianchi, S., Corsini, A., Rispoli, F., and Sheard, A.G. (2009), "Detection of Aerodynamic Noise Sources in Low-speed Axial Fans with Tip Endplates", *Proceedings of the Institution of Mechanical Engineers, Part C: Journal of Mechanical Engineering Science*, vol. 223(6), pp. 1379–92.

Bianchi, S., Corsini, A., and Sheard, A.G. (2012), "Stall Inception, Evolution, and Control in a Low-speed Axial Fan with Variable Pitch in Motion", *Journal of Engineering for Gas Turbines and Power*, vol. 134, article ID 042602, 10 pages.

Bindl, S., Stößel, M., and Niehuis, R. (2009), "Stall Detection within the Low Pressure Compressor of a Twin-spool Turbofan Engine by Tip Flow Analysis", *Proceedings of the 54th American Society of Mechanical Engineers Gas Turbine and Aeroengine Congress*, Orlando, FL, USA, 8–12 June, paper no. GT2009-59032.

Boerrigter, H.L. (1996), "PreMeSys: a Simulation Program to Determine the Frequency and Time Response of a Pressure Measurement System", *VKI Technical Memorandum 53*, von Karman Institute for Fluid Dynamics, Rhode-Saint-Genèse, Belgium.

Breugelmans. F.A.E., Palomba, C., and Funk, T. (1995), "Application of Strange Attractors to the Problem of Rotating Stall", in Tanida, Y., and Namba, M. (Eds), *Unsteady Aerodynamics and Aeroelasticity in Turbomachinery*, Elsevier, New York, NY, USA.

Bright, M.M., Qammar, H., Vhora, H., and Schaffer, M. (1998), "Rotating Pip Detection and Stall Warning in High-speed Compressors using Structure Function", *Proceedings of GARD RTO AVT Conference*, Toulouse, France, 11–15 May.

Christensen, D., Armor, J., Dhingra, M., Cantin, P., Gutz, D., Neumeier, Y., Prasad, J.V., Szucs, P.N., and Wadia, A.R. (2008), "Development and Demonstration of a Stability Management System for Gas Turbine Engines", *Transactions of the ASME, Journal of Turbomachinery*, vol. 130(3), paper 031011, pp. 1–9.

Cumpsty, N.A. (1989), "Part-circumference Casing Treatment and the Effect on Compressor Stall", *Proceedings of the 34th American Society of Mechanical Engineers Gas Turbine and Aeroengine Congress*, Toronto, ON, Canada, 11–14 June, paper no. 89-GT-312.

Day, I.J. Breuer, T., Escuret, J., Cherrett, M., and Wilson, A. (1999), "Stall Inception and the Prospects for Active Control in Four High Speed Compressors", *Transactions of the ASME, Journal of Turbomachinery*, vol. 121(1), pp. 18–27.

De-Rosier, B., Normand, M.D., and Peleg, M. (1997), "Effect of Lag on the Symmetrised Dot Pattern (SDP) Displays of the Mechanical Signatures of Crunchy Cereal Foods", *Science of Food and Agriculture*, vol. 75, pp. 173–8.

Fraser, A.M., and Swinney, H.L. (1986), "Independent Coordinates for Strange Attractors from Mutual Information", *Physical Review A*, vol. 33(2), pp. 1134–40.

Gleick, J. (1987), *Chaos: Making a New Science*, Vintage Books, London, UK.

Gravdahl, J.T., and Egeland, O. (1999), *Compressor Surge and Rotating Stall: Modelling and Control*, Springer, London, UK.

Greitzer, E.M. (1976), "Surge and Rotating Stall in Axial Flow Compressors, Part I: Theoretical Compression System Model", *Transactions of the ASME, Journal of Engineering for Power*, vol. 98, pp. 190–98.

Höss, B., Leinhos, D., and Fottner, L. (2000), "Stall Inception in the Compressor System of a Turbofan Engine", *Transactions of the ASME, Journal of Turbomachinery*, vol. 122(1), pp. 32–44.

Liu, Y., Dhingra, M., and Prasad, J.V.R. (2009), "Active Compressor Stability Management via a Stall Margin Control Mode", *Proceedings of the 54th American Society of Mechanical Engineers Gas Turbine and Aeroengine Congress*, Orlando, FL, USA, 8–12 June, paper no. GT2009-60140.

Ludwig, G.R., and Nenni, J.P. (1976), "A Rotating Stall Control System for Turbojet Engines", *Proceedings of the 21st American Society of Mechanical Engineers Gas Turbine and Aeroengine Congress*, New Orleans, LA, USA, 12–25 March, paper no. 76-GT-115.

Methling, F.O., Stoff, H., and Grauer, F. (2004), "The Pre-stall Behaviour of a 4-stage Transonic Compressor and Stall Monitoring Based on Artificial Neural Networks", *International Journal of Rotating Machinery*, vol. 10, pp. 387–99.

Moore, F.K. (1984), "A Theory of Rotating Stall of Multistage Compressors, Parts I–III", *Transactions of the ASME, Journal of Engineering for Power*, vol. 106, pp. 313–36.

Paduano, J.D., Greitzer, E.M., and Epstein, A.H. (2001), "Compression System Stability and Active Control", *Annual Review of Fluid Mechanics*, vol. 33, pp. 491–517.

Perugini, D., Busà, T., Poli, G., and Nazzareni, S. (2003), "The Role of Chaotic Dynamics and Flow Fields in the Development of Disequilibrium Textures in Volcanic Rocks", *Journal of Petrology*, vol. 44(4), pp. 733–56.

Pickover, C.A. (1986), "On the Use of Symmetrized Dot Patterns for the Visual Characterization of Speech Waveforms and Other Sampled Data", *Journal of the Acoustical Society of America*, vol. 80(3), pp. 955–60.

Pickover, C.A. (1990), *Computers, Pattern, Chaos and Beauty*, St Martin's Press, New York, NY, USA.

Rippl, A. (1995), "Experimentelle Untersuchungen zuminstationaren Betriebsverhahen an der Stabilitarsgrenze eines mehrstufigen trans-sonischen Verdichters", PhD thesis, Ruhr-Universitat Bochum, Germany.

Schultz, T.J. (1978), "Synthesis of Social Surveys on Noise Annoyance", *Journal of the Acoustical Society of America*, vol. 64, pp. 377–405.

Sheard, A.G., and Corsini, A. (2011), "The Impact of an Anti-stall Stabilisation Ring on Industrial Fan Performance: Implications for Fan Selection", *Proceedings of the 55th American Society of Mechanical Engineers Turbine and Aeroengine Congress*, Vancouver, BC, Canada, June, paper no. GT2011-45187.

Sheard, A.G., Corsini, A., and Bianchi, S. (2010), "A Method of Detecting Stall in an Axial Fan", GB Patent 2,468,571 B, 24 December.

Sheard, A.G., Corsini, A., and Bianchi, S. (2011), "Stall Warning in a Low-speed Axial Fan by Visualisation of Sound Signals", *Transactions of the ASME, Journal of Engineering for Gas Turbines and Power*, vol. 133(4), paper no. 041601, pp. 1–10.

Shibata, K., Takahashi, A., and Shirai, T. (2000), "Fault Diagnosis of Rotating Machinery through Visualisation of Sound Signals", *Mechanical Systems and Signal Processing*, vol. 14, pp. 229–41.

Sottek, R., and Genuit, K. (2007), "Sound Quality Evaluation of Fan Noise Based on Hearing-related Parameters", *Proceedings of the 3rd International Symposium of Fan Noise*, Lyon, France, 17–19 September.

Tahara, N., Kurosaki, M., Ohta, Y., Outa, E., Nakajima, T., and Nakakita, T. (2007), "Early Stall Warning Technique for Axial-flow Compressors", *Transactions of the ASME, Journal of Turbomachinery*, vol. 129(3), pp. 448–56.

Takens, F. (1981), "Detecting Strange Attractors in Turbulence", in Rand, D.A., and Young, L.S. (Eds), *Lecture Notes in Mathematics*, vol. 898, pp. 366–81.

Tong, Z., Li, L., Nie, C., Lin, B., Cui, Y., and Qi, W. (2009), "On-line Stall Control with the Digital Signal Processing Method in an Axial Compressor", *Proceedings of the 54th American Society of Mechanical Engineers Gas Turbine and Aeroengine Congress*, Orlando, FL, USA, 8–12 June, paper no. GT2009-59509.

Tryfonidis, M., Etchevers, O., Paduano, J.D., Epstein, A.H., and Hendricks, G.J. (1995), "Pre-stall Behavior of Several High-speed Compressors", *Transactions of the ASME, Journal of Turbomachinery*, vol. 117(1), pp. 62–80.

Wu, J., and Chuang, C. (2005), "Fault Diagnosis of Internal Combustion Engines using Visual Dot Patterns of Acoustic and Vibration Signals", *NDT&E International*, vol. 38, pp. 605–14.

Chapter 8

Using Sweep to Extend Stall-free Operational Range in Axial Fan Rotors

A. Corsini and F. Rispoli

ABSTRACT

The chapter discusses the use of sweep as a remedial strategy to control the onset of aerodynamic instabilities in low-speed axial fan rotors. The reported research contributes to an understanding of the effect of blade lean on fan stall margin. We report results of a numerical investigation of the flow-field through two highly loaded fans of forced-vortex design. The studied fans had a pressure coefficient-typical of an industrial axial fan. They had identical nominal design parameters and, respectively, 35 degrees forward-swept blades and un-swept blades. We used an in-house developed multi-level parallel finite element Reynolds-averaged Navier–Stokes (RANS) solver, with non-isotropic two-equation turbulence closure. We assessed the pay-off associated with incorporating blade sweep in terms of the resultant improvement in fan operating range. We analysed the flow structure that developed through the blade passages and downstream of the fans, as well as loss distributions at design and near-peak pressure operating conditions. An analysis of the three-dimensional flow structure indicated that forward blade sweep attenuates the forced-vortex span-wise secondary flows, thus delaying the onset of stall. The forward-swept blade design features a reduced sensitivity to leakage flow effects and consequently, it operated more efficiently as it approached its stability limit.

NOMENCLATURE

Latin letters

AR	fan blade aspect ratio
C_p	static pressure coefficient
D_h	hub diameter
D_t	tip diameter
DF	diffusion factor
H	shape factor
K_B	blockage factor
k	turbulent kinetic energy
k_ε	turbulent dissipation rate
ℓ	blade chord
LE	leading edge
n	direction normal to the wall
PS	pressure side
p	static pressure
$\bar{r}$	dimensionless radius $\bar{r} = r/r_c$
r	radius
SS	suction side
TE	trailing edge
U_c	casing relative peripheral velocity
v, w	absolute and relative velocities
x, y, z	Cartesian coordinates

Greek letters

β	incidence angle
γ	blade angle
δ	blade pitch
δ^*	displacements thickness
ζ	total pressure loss coefficient
θ^*	momentum thickness
λ	sweep angle
v	fan hub diameter to blade tip diameter ratio
ρ	air density
Σ	solidity
Φ_D	design flow coefficient
φ	camber angle
φ_p	radial velocity coefficient
$\bar{\varphi}_3$	swirl coefficient at rotor inlet
ψ_D	design work coefficient
ψ	power function
χ	tip gap (% of blade span)

Subscripts and superscripts

0	total flow properties
1, 3	inlet and outlet measuring axial planes
a, p, r	axial, peripheral and radial
c	casing wall
D	design point
e	boundary layer edge
h	hub wall

INTRODUCTION

Over the years, researchers have demonstrated that the use of sweep in decelerating axial turbomachinery is a change in blade geometry that improves operational characteristics. Early attempts to apply sweep to compressor blades started in the 1950s. These include Goodwin's (1957) experimental work on low-speed compressors and Smith and Yeh's (1963) analytical studies. The aim of this early research was to characterise the effect of sweep, with the objective of defining a swept blade design concept. Although the early researchers were able to demonstrate that swept blades performed well, development of design methodologies that incorporated sweep as a parameter in the design process proved challenging. It was not until the mid-1980s that researchers were able to incorporate sweep into the design of gas turbine low aspect ratio transonic compressor blades. The improvement in compressor efficiency facilitated by these swept blade designs was significant enough for the effect of sweep on the blade-to-blade flow-field to become a focus for researchers through the 1990s (Wennerstrom, 1984; Hah and Wennerstrom, 1991; Rabe *et al.*, 1991; Copenhaver *et al.*, 1996; Wadia *et al.*, 1997).

The extant literature on low-speed fans and compressors includes reports that favourably characterise the effects of blade sweep. Blade sweep is particularly effective in fans designed with a span-wise gradient of circulation. This is true both if the gradient of circulation occurs as a consequence of the design concept (Vad and Bencze, 1998) or from running at an off-design operating point. Mohammed and Prithvi Raj (1977) first characterised the improvement associated with the application of forward sweep in the performance characteristics in axial fan impellers. Yamaguchi *et al.*'s experiments (1991) identified that forward-swept blades resulted in an increased efficiency. Wright and Simmons' studies (1990) exploited the higher peak total pressure rise and shift of stall margin towards lower flow rate after applying forward sweep. Corsini and Vad's experimental and numerical investigation (2002) focused on low aspect ratio industrial axial fans, identifying that forward sweep significantly improved both fan efficiency and stall margin.

Building on the research of other scholars, this chapter aims to provide additional insight into the influence that a forward swept stacking line exerts on the blade-to-blade flow-field. We characterise the impact of a forward-swept stacking line on end-wall losses, with a specific focus on their reduction when operating at an off-design operating point. We have carried out comparative numerical investigations on two fan blade designs with different stacking lines. Corsini *et al.* (2001) originally proposed these blade designs. The first is an un-swept forced-vortex design with straight blades. The second is a forward-swept forced-vortex blade, with a design adapted from the first.

Corsini *et al.*'s forward-swept blade design (2001) features a complex blade-to-blade flow-field. The flow-field features develop as a consequence of interaction between the vorticity induced by the non-uniform span-wise work distribution and the three-dimensional effects induced in the flow-field by the blades' forward-swept stacking line. Smith and Yeh (1963) first reported the complexity of the blade-to-blade flow-field associated with a forward-swept stacking line. Their research

focused on compressors intended for aerospace application. In this chapter we aim to characterise Corsini *et al.*'s blade designs (2001), and therefore the research is focused on fans intended for industrial application.

Corsini *et al.*'s blade designs (2001) are relatively low aspect ratio designs when compared to the historic norm within the industrial fan community. Corsini *et al.*'s (2001) choice of aspect ratio was a consequence of the trend within the industrial fan community towards more highly aerodynamically loaded blades. The blade-to-blade flow-field's three-dimensionality within low aspect ratio blading can result in boundary layer fluid forming complex secondary flow features that are prone to separate. Even if boundary layers do remain attached at the design point, there is an increased probability that they will separate at off-design conditions. When boundary layers are likely to separate, numerical simulation of the blade-to-blade flow-field becomes challenging. The approach to turbulence modelling must characterise the flow-field physics appropriately.

In the programme of work in this chapter we simulated the blade-to-blade flow-field with a Reynolds-averaged Navier–Stokes (RANS) model based non-linear code, with two-equation closure (Craft *et al.*, 1996). The two-equation closure was able to cope with non-isotropic and non-equilibrium turbulence effects without a significant increase in the required computational effort. The code utilised a parallel multi-grid (MG) numerical scheme, developed for an in-house finite element method (FEM) code which Borello *et al*. (2003) first proposed. The finite element method formulation is based on a stabilised Petrov-Galerkin (PG) method modified for application to three-dimensional equal- and mixed-order spaces of approximation.

Using Borello *et al*.'s computational code (2003), we predicted the blade-to-blade flow-field for both the un-swept and the forward-swept blade designs at both their design point, and a near-peak pressure operating point. We used the predictions to characterise loss distributions for both blade designs. We then related the change in blade-to-blade flow-field from the un-swept to the forward-swept blade design to the extension of the forward-swept blade design's stall-free operating range. Relating the forward-swept blade design's stall-free operating range extension to changes in the blade-to-blade flow-field enabled us to characterise the effect of incorporating a forward-swept blade stacking line on the fan's performance.

TEST ROTORS

Corsini *et al.*'s (2001) research purpose was to improve an un-swept blade design's performance by using a forward-swept blade stacking line. The un-swept blade was designed to operate at a relatively high flow rate and pressure rise compared to the norm within the industrial fan community. They were able to further increase aerodynamic blade loading by designing the fan into which the un-swept blade was incorporated with a moderate diameter, minimum speed and blade number. Consequently, the un-swept blade design was aerodynamically highly loaded, with Corsini *et al.* (2001) studying the impact of a forward-swept blade stacking line within the context of a highly loaded design.

Corsini *et al.* (2001) designed the forward-swept blade using Vad and Bencze's (1998) design concept. The forward-swept blade pressure rise was prescribed in the span-wise direction from the blade hub to tip using a power function $\bar{\psi}(\bar{r}) = \bar{\psi}(\bar{v})$ $(\bar{r}/\bar{v})^n$ with $n = 1.4$. The span-wise change in blade circulation induced three-dimensionality into the blade-to-blade flow-field. Corsini *et al.* (2001) calculated the sweep angle using Mohammed and Prithvi Raj's method (1977), defining sweep angle relative to the forward-swept blade section centres' locus. They designed both the un-swept and forward-swept blades assuming incompressible flow, utilised the non-uniform axial inlet conditions Vad and Bencze (1998) experimentally measured and assumed a zero inlet swirl distribution.

Corsini *et al.* (2001) implemented forward sweep using Vad's (2001) optimisation methodology. This methodology involved the systematic incorporation of blade sweep into the un-swept design. After each change in blade sweep they conducted a computational analysis of the resulting blade geometry, followed by a review of the blade-to-blade flow-field and a further incremental change in blade sweep. Corsini *et al.* (2001) designed both the original un-swept and newly optimised forward-swept blade around the same design point, Table 8.1. Vad's (2001) methodology for incorporating forward sweep resulted in a variation in blade chord, and consequently fan solidity. The final forward-swept blade geometry reflects an optimised span-wise distribution of non-dimensional leading edge position (x_{LE}) and blade solidity (Σ), Figure 8.1.

Both the un-swept and forward-swept blades have circular arc camber lines with a thin profile of uniform thickness, Figure 8.2. This facilitates manufacturing

Table 8.1. *Forward-swept and un-swept fan blade design parameters.*

	Un-swept blade			Forward-swept blade		
Blade number	12			12		
Fan hub to tip diameter ratio, $\bar{v}$	0.676			0.676		
Fan blade aspect ratio, AR	0.58			0.54		
Tip gap, χ (% of blade span)	2.5			2.5		
Design flow coefficient, Φ_D	0.5			0.5		
Design work coefficient, ψ_D	0.7			0.7		
Design speed	1,100 rpm			1,100 rpm		
	Hub	Mid-span	Tip	Hub	Mid-span	Tip
Solidity, Σ	1.53	1.24	1.05	1.79	1.23	1.13
Sweep angle, λ	0.0°	0.0°	0.0°	35.0°	35.0°	35.0°
Blade angle, γ	47.9°	42.2°	38.3°	56.3°	43.1°	37.4°
Camber angle, ϕ	27.4°	23.1°	19.9°	35.4°	25.4°	20.3°
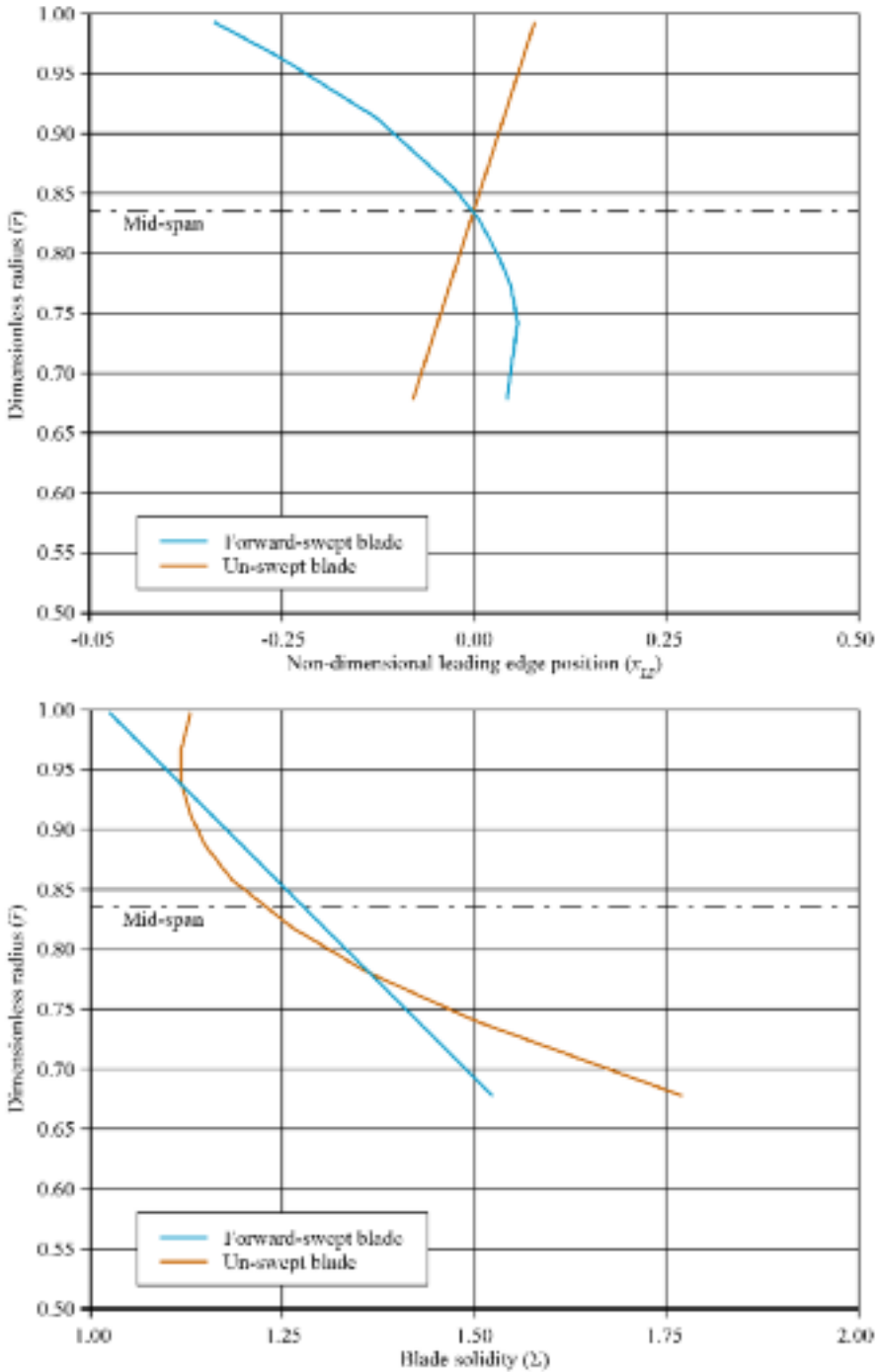
FIGURE 8.1. The forward-swept and un-swept blade geometry. The variation in non-dimensional leading edge position (x_{LE}) from the mid-span and the span-wise distributions of blade solidity (Σ) for both blade designs are shown top and bottom respectively.
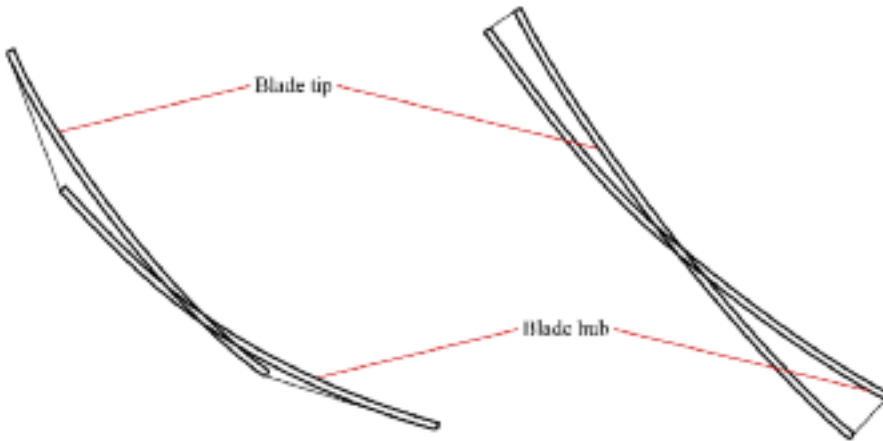
FIGURE 8.2. The forward-swept (left) and un-swept (right) blade configuration, illustrating the use of flat-plate, not aerofoil sections to form the blades. Using flat-plate to minimise manufacturing cost is common practice within the industrial fan community.

them from sheet steel. Despite this limitation, the small leading edge radius produces large local flow accelerations and a suction surface boundary layer that remains attached at the fan's design point. When operated off-design the suction surface boundary layer has a tendency to separate. Therefore, off-design performance will be relatively poor compared to the same fan with aerofoil blade sections. Despite the compromised off-design performance, the low cost of uniform thickness sheet steel blades makes their use common practice within the industrial fan community

Corsini and Vad (2002) measured the un-swept and forward-swept blade performance in an experimental facility, Figure 8.3. The un-swept and forward-swept blade tip-to-casing clearance was 2.5 and 4.0 per cent of blade span respectively. Corsini and Vad (2002) demonstrated that the forward-swept blade features a stable operating range down to a lower flow rate than possible with the un-swept blade. The forward-swept blade design was also able to generate a higher pressure rise at its peak pressure operating point with no reduction in efficiency.

NUMERICAL METHOD

When conducting the research in this chapter we solved the averaged Navier-Stokes equations using an original parallel multi-grid finite element method scheme, originally developed by Borello *et al*. (2001). We modelled the flow within the blade-to-blade passage in the rotating frame of reference using a non-linear k–ε turbulence model with a high Reynolds number wall treatment first developed by Craft *et al*. (1996). Previously, researchers have successfully applied this combination of turbulence model and wall treatment. Corsini and Rispoli (2002) used it to predict a compressor cascade's performance. Borello *et al*. (2003) used it when predicting the
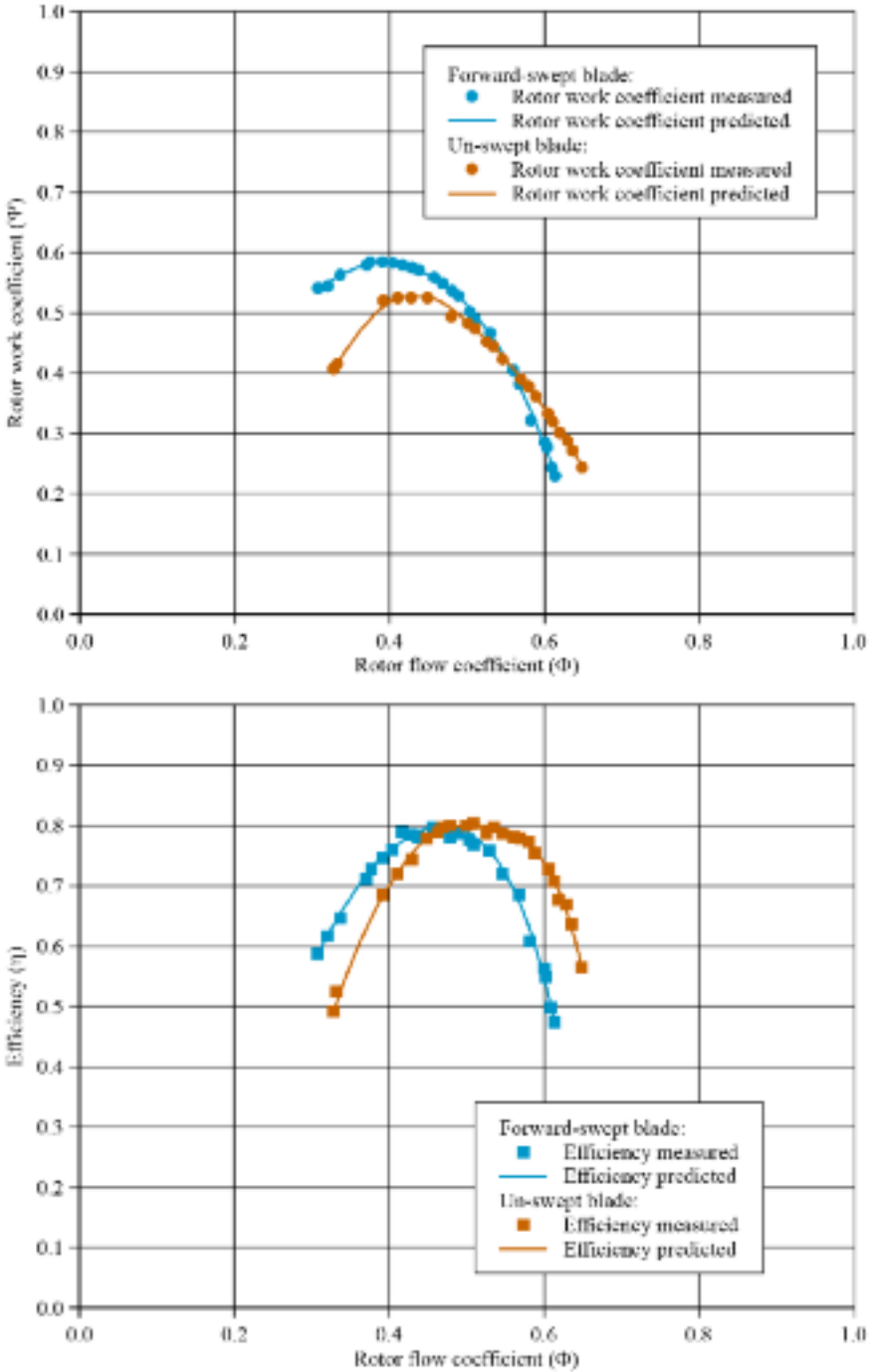
FIGURE 8.3. Measured and predicted characteristics for the forward-swept and un-swept blade designs, from Corsini *et al.* (2001).

performance of a highly loaded axial fan. Borello *et al*. (1997) used it when studying the flow-field through a radial water turbine. In each case the combination of turbulence model and wall treatment was able to model the physical flow phenomena of interest, thus predicting performance well.

We developed and applied a stabilised Petrov-Galerkin (PG) scheme to control the instability that affects the advective-diffusive incompressible flow, and the momentum's reaction and turbulent scale equations. The turbulent scale equations relate to Coriolis acceleration (Corsini *et al*., 2003). We used equal-order Q1-Q1 and mixed-order Q2-Q1 interpolation for primary turbulent scale equations and constrained secondary variables, implicitly eliminating the undesirable pressure-checker boarding effects. We performed the computational analysis using the hybrid full linear multi-grid accelerator running on an overlapping parallel solver (Borello *et al*., 2001).

We parallelised an iterative Krylov method when smoothing and solving using the adopted multi-grid finite element method scheme with an original additive domain decomposition algorithm. This algorithm managed the message passing operations using the Message Passing Interface (MPI) libraries, a standardised message-passing system. We used the preconditioned GMRes(5) and GMRes(50) algorithms respectively as a smoother and as the core solver. We adopted standard boundary conditions which researchers have previously used when undertaking un-swept and forward-swept blade numerical simulation. Corsini and Rispoli (1999) and Corsini *et al*. (2001) have utilised this approach. They were able to predict well both the un-swept and forward-swept blade performance.

Rotor modelling and computed flow conditions

The approach we adopted when constructing a computational mesh utilised a non-orthogonal body fitted coordinate system. We used three discretisation levels for the numerical simulations. The coarse-density mesh has 59×21×31 nodes, respectively in the axial, pitch and span-wise directions. The mid-density mesh has 81×31×41 nodes. The fine-density mesh has 117×41×61 nodes. There are five coarse-density mesh plus 11 mid- and fine-density mesh grid nodes across the blade tip-to-casing gap. All three mesh density regions maintain an adequate computational cell aspect ratio toward solid boundaries. The computational grid developed for the forward-swept blade illustrates how mesh density increased in the solid wall's near vicinity, Figure 8.4.

We studied the impact of the adopted approach to mesh refinement effect by comparing the casing wall boundary layer integral properties at rotor exit, 0.047 blade chord downstream of the blade trailing edge in the hub region. We considered the following boundary layer parameters:

- displacement thickness, $\delta^*_{a\,z}$;
- momentum thickness, $\theta^*_{a\,z}$;
- shape factor, H_{a3}; and
- blockage factor, K_{B3}.
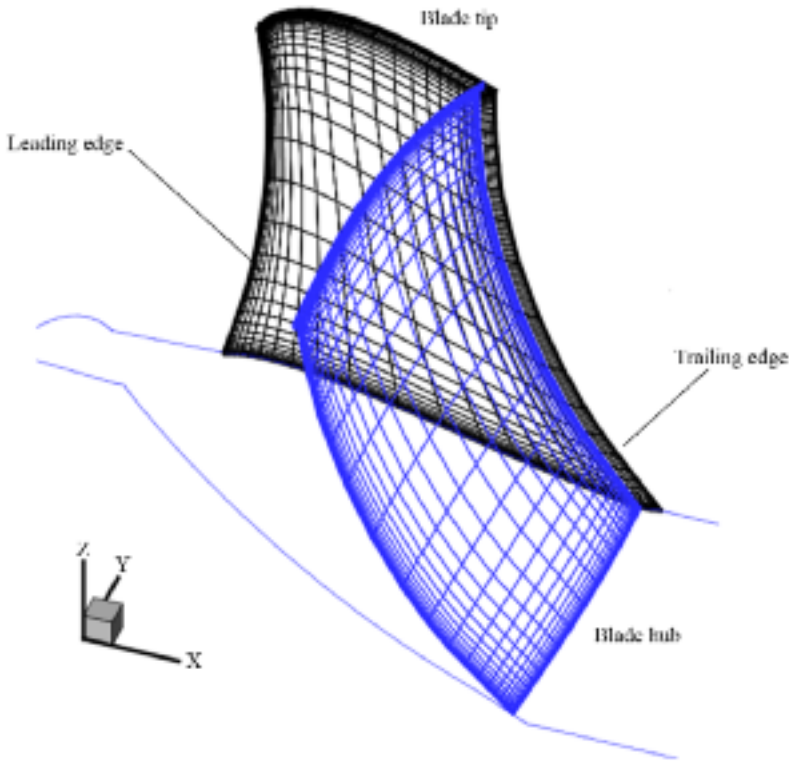
FIGURE 8.4. The forward-swept blade computational grid, shown on the blade suction surface and across the blade-to-blade passage as the trailing edge.

We calculated the boundary layer parameters for three computational meshes. The first was a course-density mesh. The second was a course-density mesh with mid-density regions in the solid wall's near vicinity. The third was a course-density mesh with a mid-density mesh progressing to a fine-density mesh in the solid wall's near vicinity. We used our three meshes in conjunction with our adopted computational approach to predict the boundary layer parameters for the forward-swept blade at its design operating condition. We then compared our computed values with Vad and Bencze's (1998) experimentally measured values, Table 8.2.

The computed boundary layer parameters were in good agreement with the experimentally measured values for both the course-density mesh and those with mid- and fine-density mesh in the solid wall's near vicinity. Although the course-density mesh and mesh with mid-density in the near solid wall's vicinity were in good agreement with measured values, the fine-density mesh gave the best overall result. Specifically, the fine-density mesh was able to predict the boundary layer blockage factor (K_{B3}) more accurately than either the course- or mid-density mesh. Consequently, we chose to use the fine-density mesh for the numerical simulation that we report in this chapter.

Table 8.2. *Results of a grid-dependency study for the un-swept blade. We conducted the numerical simulation at the design operating condition, with casing wall boundary layer parameters given 0.047 blade chords downstream from the blade trailing edge.*

Boundary layer parameters	Measured values (Vad and Bencze, 1998)	Predicted values (course-density mesh)	Predicted values (mid-density mesh)	Predicted values (fine-density mesh)
Displacement thickness, $\delta^*_{a\,z}$ (mm)	2.7	3.29	2.91	2.79
Momentum thickness, $\theta^*_{a\,z}$ mm	2.1	2.29	1.97	2.07
Shape factor, H_{a3}	1.3	1.27	1.48	1.35
Blockage factor, K_{B3}	0.95	0.92	0.921	0.937

DATA ANALYSES

Corsini and Vad's experimental study (2002) demonstrated that the forward-swept blade performance characteristic operated down to a lower flow rate that the un-swept blade, Figure 8.3. Additionally, the forward-swept blade had a significantly high peak pressure rise. The research in this chapter complements Corsini and Vad's work (2002).They present an experimental analysis of both the un-swept and forward-swept blade performance. In contrast our objective was to identify the impact of a forward-swept blade stacking line on the resultant blade-to-blade flow-field, and thus provide an insight into the physical flow mechanisms that result in improving overall fan performance.

Averaged flow properties

Before considering the flow structure within the blade-to-blade passage, we will first review the impact of our decision to use a non-linear eddy viscosity turbulence model on predicted swirl flow coefficient. We present pitch-wise averaged swirl flow coefficient at the blade outlet, and calculate it at a plane 0.05 mid-span blade chord downstream of the blade trailing edge, Figure 8.5. We show the computed values with experimentally measured values from Vad and Bencze (1998) who utilised a laser Doppler anemometer technique to measure exit swirl.

Borello *et al.* (2003) and Corsini and Rispoli (2002) previously assessed the effectiveness of the non-linear eddy viscosity turbulence model when applied to the un-swept blade. These researchers concluded that the non-linear eddy viscosity turbulence model resulted in a more accurate prediction of blade outlet swirl than the linear eddy viscosity turbulence model. When we study the results of the computational analysis for the un-swept blade, we see that both the linear and non-linear eddy viscosity turbulence models capture the over-turning in the blade's hub region.
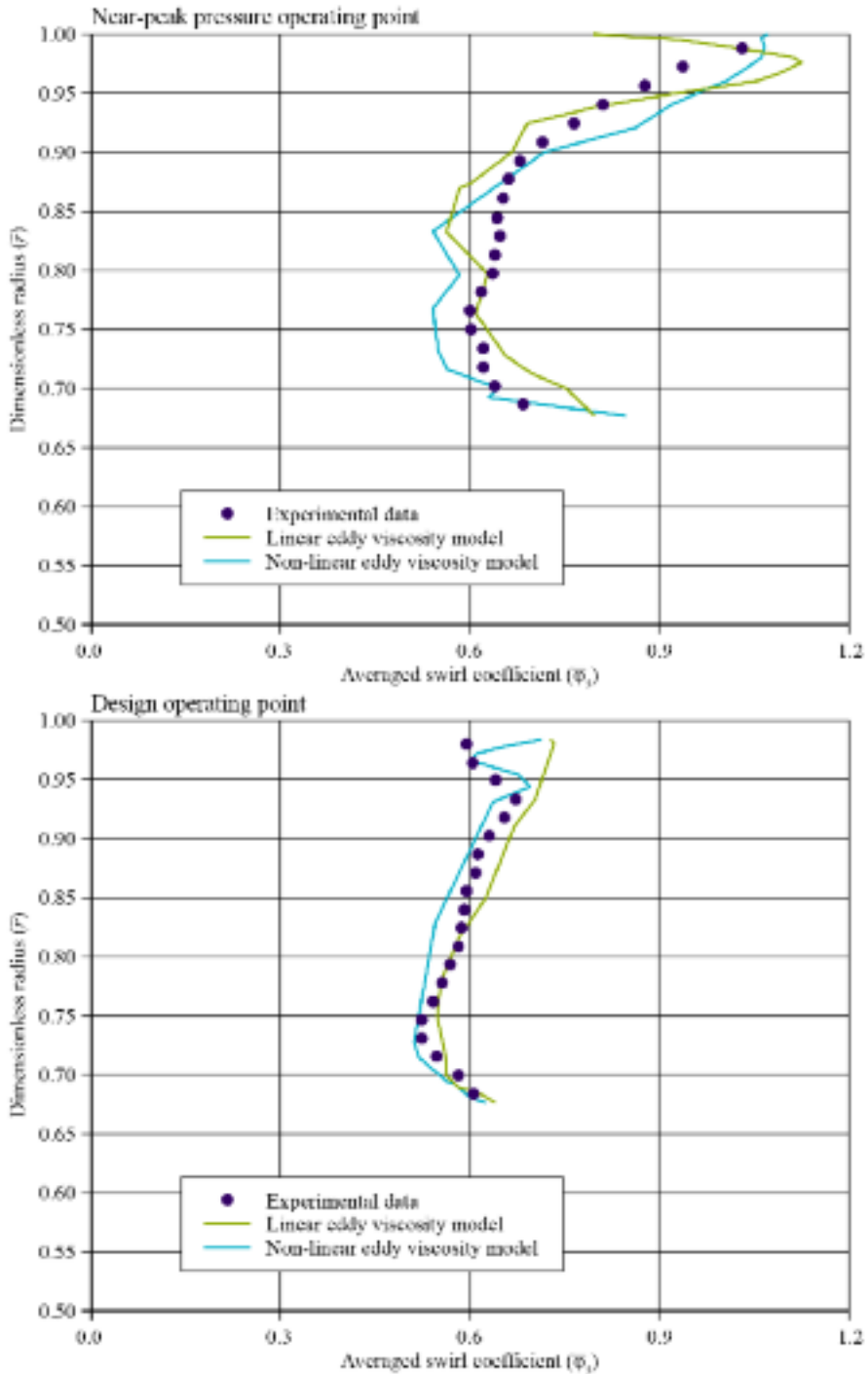
FIGURE 8.5. Distributions of pitch-wise averaged swirl coefficient at rotor inlet ($\bar{\varphi}_3$) for the un-swept blades at both the design and near-peak pressure operating points.

This over-turning occurs at both the near-peak pressure and design operating points as a consequence of the impact the passage vortex has on the hub boundary layer.

As we move from the hub towards the blade tip, the measured outlet swirl decreases despite a work distribution that increases towards the blade tip. This decrease in outlet swirl occurs as a consequence of the combined effect of under turning the flow in the blade tip region and the blade tip-leakage flow. We can predict well the radial variation of outlet swirl with the non-linear eddy viscosity turbulence model. The linear eddy viscosity turbulence model is less able to predict the outlet swirl's radial distribution as it is less able to model the flow-field features in the blade tip region. We associate the near-peak pressure operating point with the most developed blade tip-to-casing leakage vortex, and therefore, it is the most difficult operating point to model. The non-linear eddy viscosity turbulence model is able to capture flow over-turning in the blade tip region reasonably well, and certainly better than the linear eddy viscosity turbulence model.

Having established that the non-linear eddy viscosity turbulence model results in a reasonable prediction of outlet swirl, we will now consider predicted diffusion factors for both the un-swept and forward-swept blade, Figure 8.6. We calculated the diffusion factor's (*DF*) span-wise variation using Lieblein's method (1965). He defined the diffusion factor's limiting value as 0.5. Above a diffusion factor of 0.5, boundary layers become prone to separation, and therefore, aerodynamic losses increase.

Corsini *et al.* (2001) designed the un-swept blade with a mid-span diffusion factor of 0.5 at both the design and peak pressure operating points, Figure 8.6. In contrast, the forward-swept blade diffusion factor changes its diffusion factor span-wise distribution as the operating point shifts from the design to peak pressure operating point. Most significant is the increase in diffusion factor in the mid-span region at the near-peak pressure operating point. This increase in mid-span diffusion factor indicates that the forward-swept blade is operating closer to the limit of its load capability than the un-swept blade. This conclusion is self-consistent with Wadia *et al.*'s conclusions (1997).

Flow structure within the blade-to-blade passage

Let us now study the evolution of the flow-field within the blade-to-blade passage. We may gain an insight into the flow-field with both the un-swept and forward-swept blade-to-blade passage by considering the static pressure coefficient distribution and streamlines over the blade suction surface, Figure 8.7. It is the blade suction surfaces where blade sweep induced effects have their primary impact on vorticity and static pressure. Therefore, we consider static pressure coefficient distribution and streamlines over blade suction surfaces at both the design and near-peak pressure operating points.

Consider the design operating point static pressure coefficient distribution and streamlines for the un-swept blade. The primary flow feature is characteristic of a corner-stall, but without evidence of reverse flow. A study of the un-swept blade
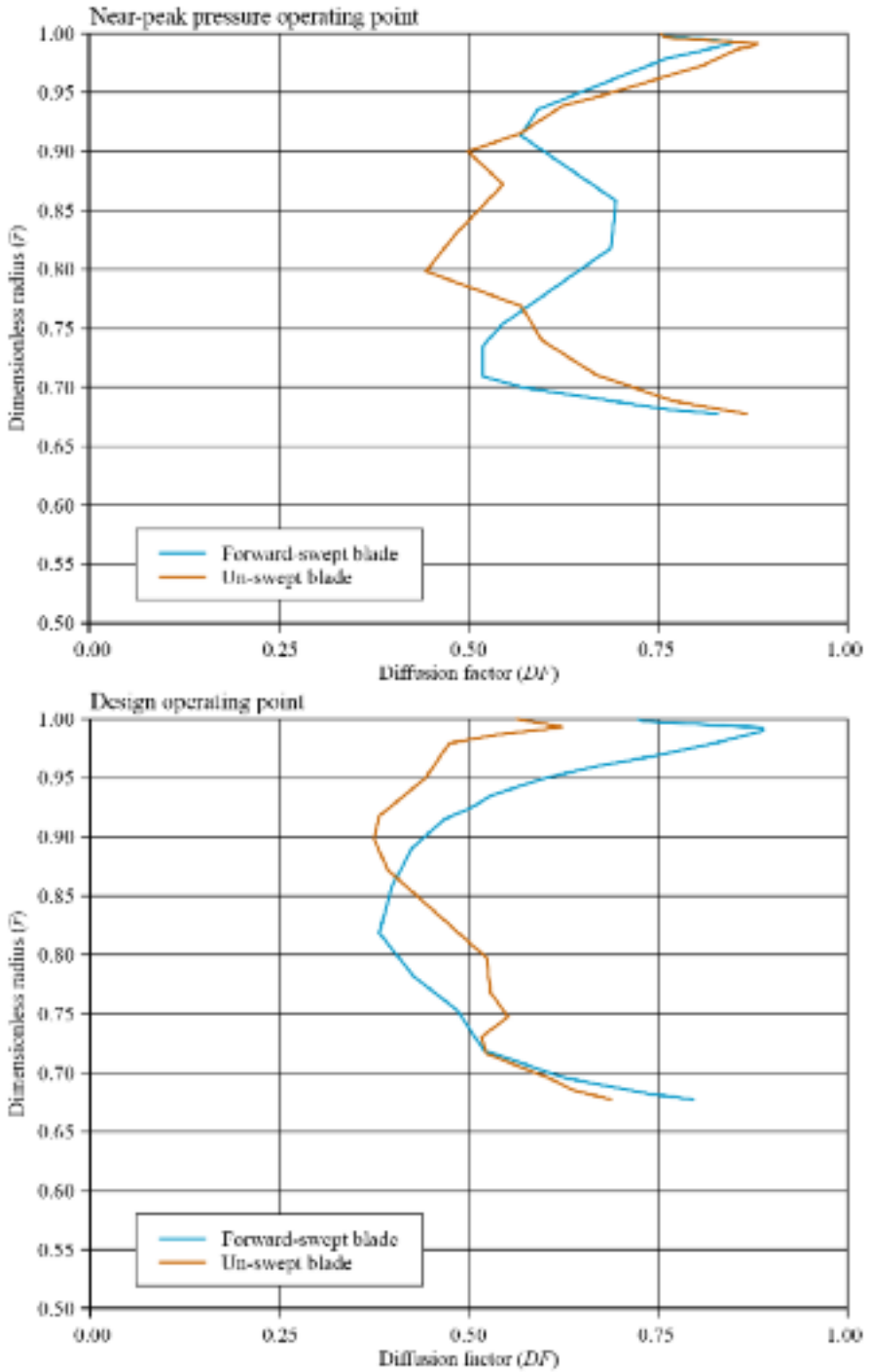
FIGURE 8.6. Comparison of the span-wise distributions of diffusion factor (*DF*) for the forward-swept and un-swept blades at both the design and near-peak pressure operating points.
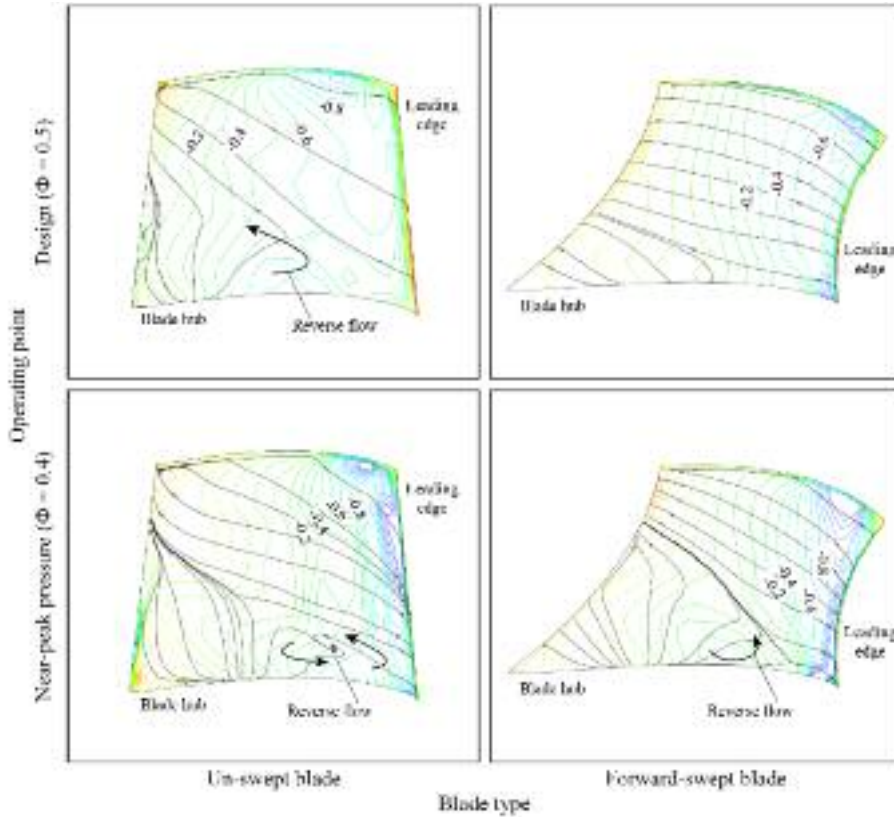
FIGURE 8.7. Static pressure coefficient (*Cp*) distribution and streamlines over the forward-swept and un-swept blade suction surfaces at both the design and near-peak pressure operating points.

streamlines along the blade chord indicates that there is a separation just after the mid-chord point. This corner-stall develops as a consequence of the passage vortex that drives the suction surface boundary layer radially outward and is induced by the un-swept blade geometry.

Consider the design operating point static pressure coefficient distribution and streamlines for the forward-swept blade. In contrast to the un-swept blade, there is no evidence of a corner-stall. The forward-swept blade sweep-induced vorticity in the blade-to-blade passage appears to counteract the passage vortex's effect, and is consistent with Corsini *et al.* (2001) and Smith and Yeh's (1963) conclusions. The static pressure coefficient distribution in the forward-swept blade leading edges' vicinity is similar to that of the un-swept blade. From about 30 per cent blade chord down-stream of the blade leading edge the forward-swept blade static pressure coefficient distribution isobars are almost parallel with the blade stacking line. The isobars following the stacking line determine the suction surface peak pressure zone, an observation that is self-consistent with the conclusions of Mohammed and Prithvi Raj (1977), Yamaguchi *et al.* (1991) and Beiler and Carolus (1999).

Now consider the aerodynamic mechanisms at play in the blade tip region of the forward-swept blade. The forward-swept blade static pressure coefficient distribution and streamlines indicate the presence of a flow feature approximately 10 per cent chord down-stream of the blade leading edge. Next consider the aerodynamic mechanisms at play in the blade tip region of the un-swept blade. The un-swept blade static pressure coefficient distribution and streamlines indicate the presence of a flow feature approximately 20 per cent chord down-stream of the blade leading edge. We may characterise the flow feature as a blade tip-to-casing leakage vortex. The static pressure coefficient distribution indicates that it exerts less influence on the forward-swept than the un-swept blade near-surface fluid.

We may conclude that an effect of shifting the blade's peak pressure point towards the leading edge is to attenuate the mechanism that drives the intensity of the blade tip leakage vortex. This conclusion is self-consistent with Storer and Cumpsty's (1991) conclusions. Shifting the blade peak pressure point towards the leading edge is an effect of introducing sweep into the blade design. Reducing the peak velocity is responsible for reducing the blade tip leakage vortex's intensity, a phenomenon that Mohammed and Prithvi Raj demonstrated experimentally (1977).

Consider the near-peak pressure operating point static pressure coefficient distribution and streamlines for both the un-swept and forward-swept blades. Throttling the un-swept blade from its design to near-peak pressure operating point increases the intensity of the corner-stall, with the hub region now stalled from approximately 20 per cent chord down-stream of the leading edge. Reattaching the separated flow does not take place at the blade trailing edge until it has been driven approximately 75 per cent up the trailing edge from the hub towards the tip.

In contrast to the un-swept blade, the forward-swept blade corner-stall originates further down-stream of the blade leading edge, with reverse flow establishing itself at approximately mid-chord. Therefore, we may conclude that an effect of sweep is to delay development of the corner-stall. This will help minimise the extent of any separated flow region, as the relatively smooth forward-swept blade reattachment line indicates. Reducing the intensity of the corner-stall may contribute to improving the forward-swept blade operating range.

We may gain additional insight into the flow-field within both the un-swept and forward-swept blade-to-blade passage by considering radial velocity coefficient (φ_p) distribution. Figure 8.8 presents radial velocity coefficients over a plane 0.03 mid-span blade chord downstream of the blade trailing edge. Radial velocity coefficients over this downstream plane provide an insight into the nature and extent of secondary flow features leaving the blade-to-blade passage, and therefore, into the impact of a forward swept stacking line.

Consider the design operating point radial velocity coefficient distribution for both the un-swept and forward-swept blades. The radial velocity coefficient's contours indicate that the un-swept blade is associated with radial velocities that are significantly higher than those associated with the forward-swept blade. The radial velocity coefficient streamlines are tightly packed at the leading edge, and are inclined towards the suction surface at both the blade hub and tip. We may attribute this to the un-swept blade's forced vortex design. In contrast, the forward-swept
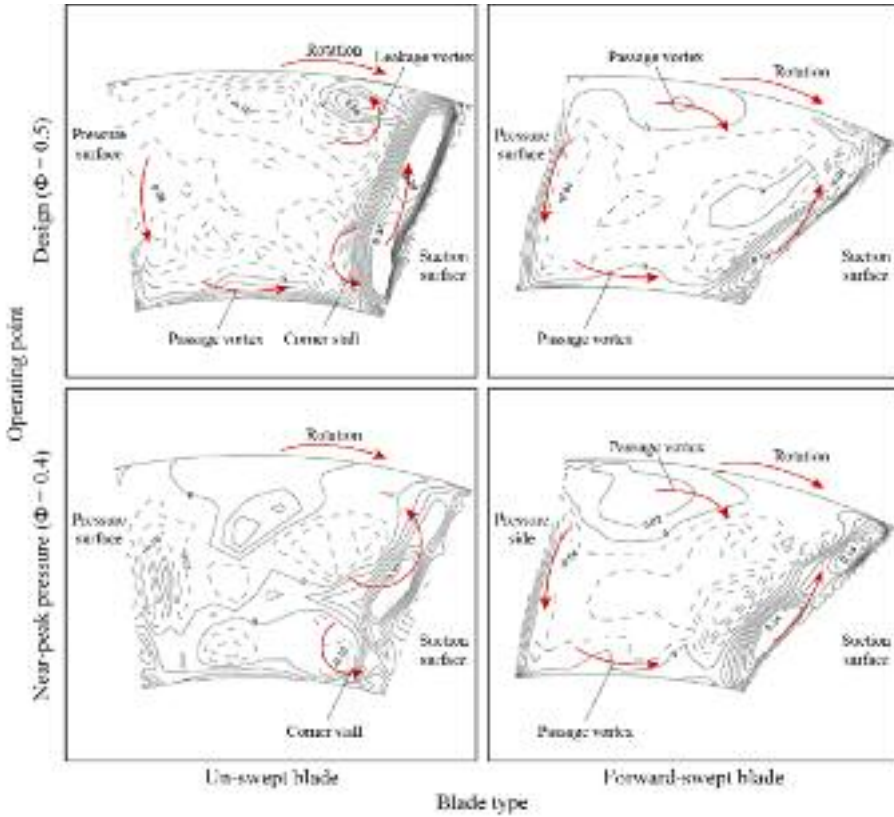
FIGURE 8.8. Radial velocity coefficient (ϕ_p) distributions computed on inclined planes 0.03 mid-span blade chord downstream from the blade trailing edges for the forward-swept and un-swept blade at both the design and near-peak pressure operating points.

blade radial velocity coefficient streamlines are less tightly packed. This indicates a generally lower level of secondary flow feature intensity than we associate with the un-swept blade.

A generally lower level of secondary flow feature intensity indicates that the sweep induced blade-to-blade static pressure field exerts an inward force in the blade suction side's vicinity. This force is able to partly offset the centrifugal forces and fluid motion driven by the forced-vortex design's work distribution. Partially offsetting the radially outward forces inherent in a forced-vortex blade design reduces the magnitude of the forces that drive the creation of secondary flow features through the blade-to-blade passage. Minimising the magnitude of secondary flow features is particularly significant in the vicinity of the blade hub and tip. At the blade tip, forward sweep reduces low-energy fluid accumulations. When one studies the radial velocity coefficient distributions for the un-swept blade, it is evident that the blade-to-blade passage is characterised by the presence of a clearly defined leakage vortex. It is also

evident that the blade-to-blade passage is characterised by the presence of a corner-stall. In contrast, a leakage vortex at the blade tip or a corner-stall at the blade hub does not characterise the forward-swept blade-to-blade passage.

Consider the near-peak pressure operating point radial velocity coefficient distribution for both the un-swept and forward-swept blades. The magnitude of the un-swept blade corner-stall indicates that the hub region is now operating in a stalled condition. A shift from the design to near-peak pressure operating point also results in the leakage vortex disappearing at the blade tip. In contrast, the forward-swept blade radial velocity coefficient distribution is similar at the near-peak operating point to that observed at the design operating point. This indicates that the forward sweep mitigates the growth of secondary flow features in the blade-to-blade passage as it throttles towards a stalled operating point.

Flow structure in the tip-to-casing gap

We may gain further insight into the impact of forward sweep by studying the static pressure (p) distribution in the blade tip region. Figure 8.9 presents the static pressure distribution for both the un-swept and forward swept blades across a blade-to-blade plane at 99.4 per cent blade span. Static pressure distributions in the blade tip region clarify the nature and extent of blade tip-to-casing leakage flow, and therefore, into the impact of a forward swept stacking line.

Consider the design operating point static pressure distribution for both the un-swept and forward-swept blades. The un-swept blade static pressure distributions indicate that the blade tip-to-casing leakage flow affects the blade-to-blade flow-field from approximately 10 per cent chord distance from the leading edge back to the trailing edge. In contrast, the forward-swept blade static pressure distributions indicate that the blade tip-to-casing leakage flow affects the blade-to-blade flow-field back to approximately 30 per cent blade chord from the blade leading edge.

Consider the near-peak pressure operating point static pressure distribution for both the un-swept and forward-swept blades. The un-swept blade static pressure distributions indicate that the blade tip-to-casing leakage flow trajectory is highly skewed. The blade tip-to-casing leakage flow appears to have resulted in a detached leakage vortex, with a resulting static pressure distribution that is significantly different to that associated with the design operating point. In contrast, the forward-swept blade features a static pressure field that is relatively similar at both the design and near-peak pressure operating points. The similarity between the static pressure field at both the design and near-peak pressure operating points indicates that sweep can reduce the extent of blade tip-to-casing leakage flow. This reduction is primarily a consequence of sweep reducing the peak pressure difference across the blade tip and so it is an inherently invicid mechanism.

Studying blade tip-to-casing leakage flow streamlines can complement the analysis of static pressure distributions in the blade tip region. This is facilitated by considering their trajectory within the context of turbulence level over blade-to-blade planes at 10 and 98 per cent blade chord, Figure 8.10. Leakage flow streamline
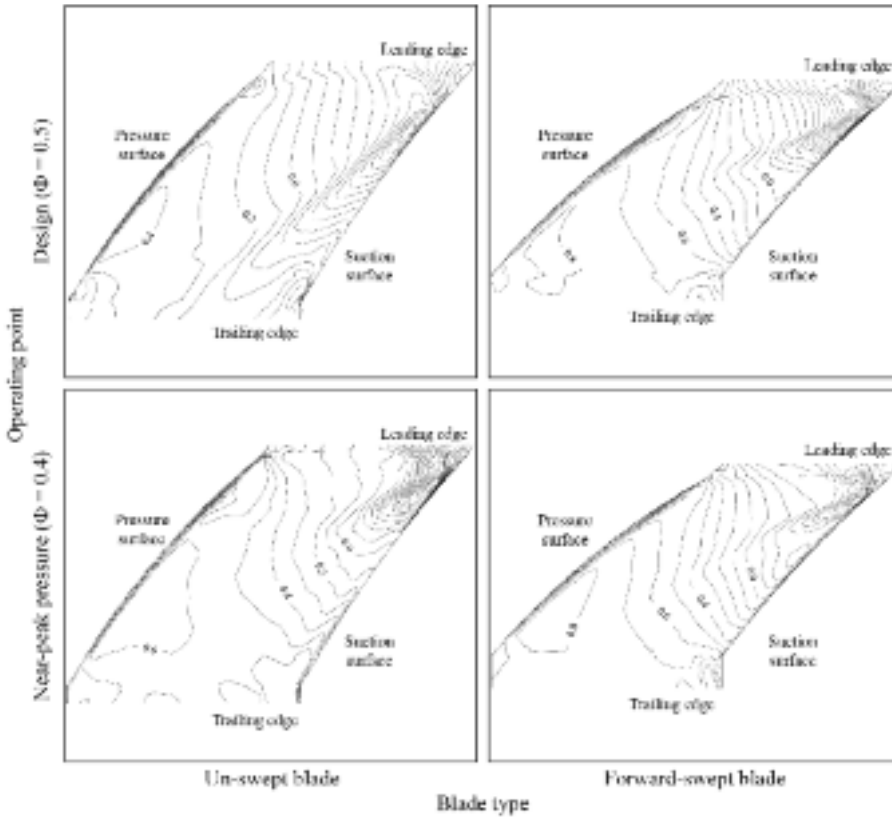
FIGURE 8.9. Static pressure (p) distributions at 99.4 per cent blade span ($r = 0.994$) for the forward-swept and un-swept blade at both the design and near-peak pressure operating points.

trajectory provides an insight into the development of the tip leakage vortex, and therefore, into the impact of a forward swept stacking line.

Consider the design operating point leakage flow streamlines for both the un-swept and forward-swept blades. The un-swept blade tip-to-casing leakage flow streamlines indicate a tip leakage vortex presence that we associate with a low turbulence core. There is an interaction between the tip leakage vortex and blade suction surface boundary layer. This interaction results in a peak turbulence level of approximately 20 per cent near the suction surface that rapidly decays as the fluid rolls into the tip leakage vortex. In contrast, the blade tip-to-casing leakage flow over the forward-swept blade does not develop a vortex structure.

Consider the near-peak pressure operating point leakage flow streamlines for both the un-swept and forward-swept blades. The un-swept blade tip-to-casing leakage flow streamlines emphasise the flow's migration up the blade suction surface from the blade hub to tip. There is evidence of low-energy fluid accumulating over the suction surface in the blade tip region, driven by the forced-vortex blade design
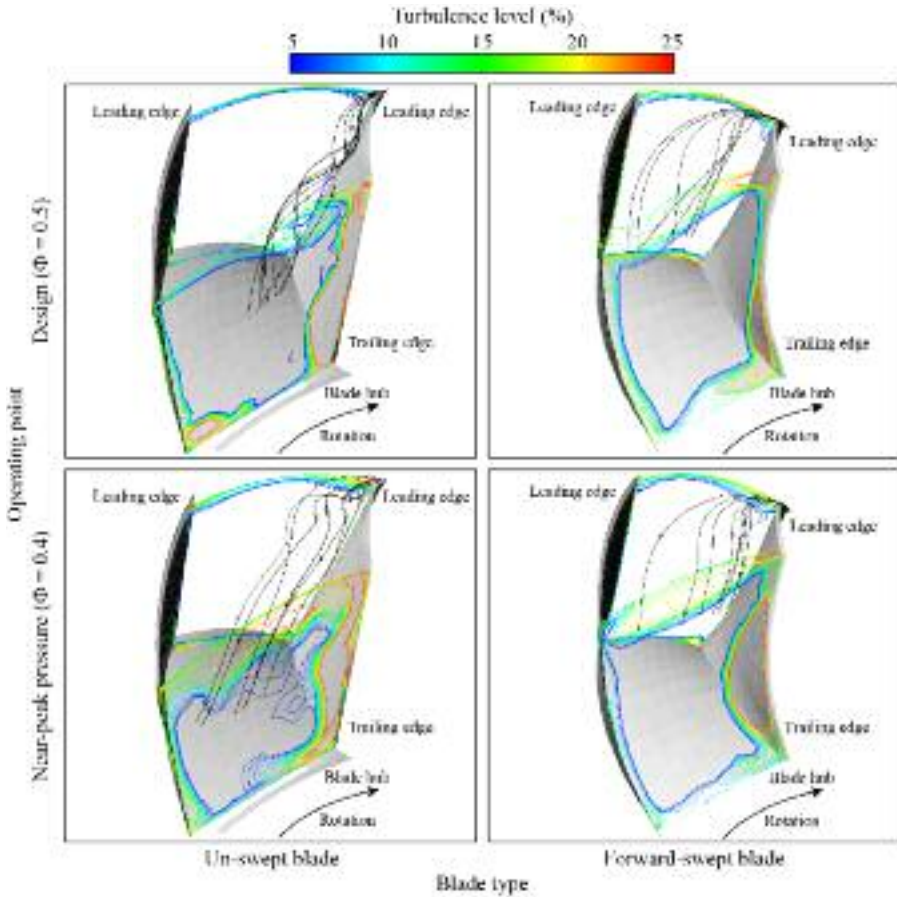
FIGURE 8.10. Evolution of leakage streamlines through the blade-to-blade passage, plus turbulence level (%) across blade-to-blade passage at 10 per cent and 98 per cent of blade chord.

concept. A consequence of the low-energy fluid accumulation appears to be the suppression of the tip leakage vortex at the blade leading edge. In contrast to the unswept blade leakage flow streamlines' highly three-dimensional behaviour, the forward-swept blade leakage flow streamlines appear almost two-dimensional in comparison. Although there is some change in the leakage flow streamlines from the design to near-peak pressure operating point, the forward-swept blade is relatively insensitive to operating condition.

Rotor loss

Finally, we discuss the evolution of losses within the blade-to-blade passage. We may gain an insight into the flow-field within both the un-swept and forward-swept blade-to-blade passage by considering the evolution of total pressure loss co-

efficient (ζ). We define total pressure loss as $\zeta = \bar{p}_{01} - \dfrac{p_0}{0.5\rho \bar{w}_1^2}$, where p_0 is the local total pressure and p_{01} and $0.5\rho \bar{w}_1^2$ are the respective reference pitch-averaged relative total and dynamic pressures at the blade passage inlet's mid-span. To complement the previous analysis of the blade tip-to-casing leakage flow streamlines, Figure 8.11 presents total pressure loss coefficients over blade-to-blade planes at 10 and 98 per cent blade chord.

Consider the design operating point total pressure loss coefficient distribution for the un-swept blade. The evolution of total pressure loss coefficients from leading to trailing edge clearly indicates that the suction surface boundary layer thickens, and that secondary flow features develop in both the blade hub and tip region. Yamaguchi *et al.* (1991) observed a similar evolution of total pressure loss coefficient distribution when studying the development of losses through a low-speed compressor.
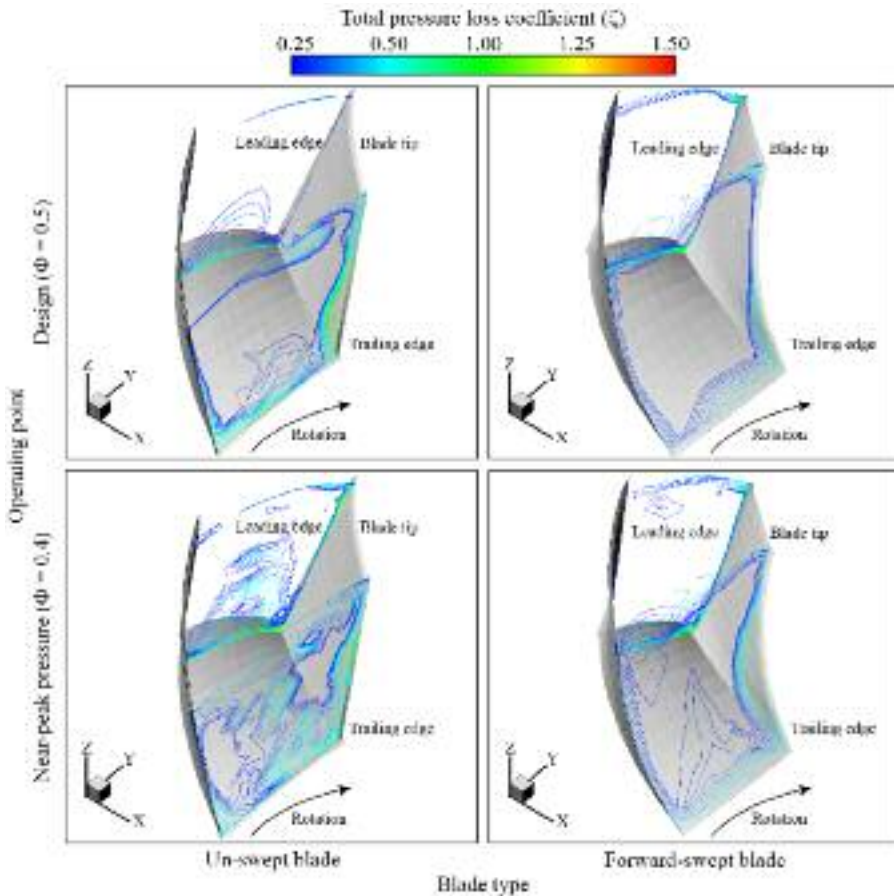
FIGURE 8.11. Evolution of total pressure loss coefficient (ζ) distributions inside the blade passage, at 10 per cent and 98 per cent of blade chord for the forward-swept and un-swept blade at both the design and near-peak pressure operating points.

Consider the design operating point total pressure loss coefficient distribution for the forward-swept blade. The distribution of total pressure loss coefficient across the 10 per cent blade chord blade-to-blade passage indicates that the losses are concentrated on the annulus' walls. This is in contrast to the un-swept blade that featured loss cores that we may consider characteristic of a classical turbomachinery secondary flow structure. Across the 98 per cent blade chord blade-to-blade passage, there is a smaller loss core in the hub region. This indicates that the passage vortex has been suppressed. It is only at the mid-span that the un-swept and forward-swept blades have comparable losses. A reduced loss core close to the suction surface characterises the forward-swept blade in the blade tip region. This reduced loss core is a consequence of the reduced quantity of low-energy fluid centrifuged up the blade. Further, a small loss core close to the blade pressure surface in the tip region characterises the forward-swept blade. This indicates that the forward-swept blade is associated with higher diffusion than the un-swept blade in the tip region.

Consider the near-peak pressure operating point total pressure loss coefficient distribution for both the un-swept and forward-swept blades. The analysis for the design operating point remains valid at the near-peak pressure operating point. The forward-swept blade total pressure loss coefficient distribution across the 98 per cent blade chord blade-to-blade passage indicates that there is significantly less radial rearrangement of the near-suction surface flow. This indicates that forward sweep induced vorticity has substantially reduced the development of secondary flow features through the blade-to-blade passage.

CONCLUSIONS

The research in this chapter presents blade-to-blade flow-field numerical simulation results through both an un-swept and forward-swept blade. Corsini *et al.* (2001) designed each blade to operate at the same nominal design point. We undertook the numerical simulations using an in-house developed parallel multi-level finite element Navier-Stokes solver, utilising non-isotropic turbulence closure. We predicted the three-dimensional flow-field for both the un-swept and forward-swept blade, comparing the results with experimental measurements. The former experimental study had identified that the forward-swept blade had a wider stall-free operating range than the un-swept blade and a higher pressure rise capability. An analysis of the numerical simulation results has enabled us to reach the following conclusions:

- The forward swept stacking line induces a vorticity component in the blade-to-blade passage's leading edge region. This vorticity component is in opposition to that induced in the flow-field by the blade's forced-vortex design concept. Therefore, a forward-swept stacking line results in reduced turning of the incoming hub end-wall boundary layer.
- Forward sweep attenuates span-wise secondary flow features as a consequence of the induced vorticity component being in opposition to that induced by the blade's forced-vortex design. The reduced intensity of span-wise secondary flow features minimises rearrangement of the forward-swept blade velocity profile.

- Minimising the forward-swept blade velocity profile's rearrangement occurs as a consequence of reducing the near-surface boundary layer fluid's centrifugal migration over the forward-swept blade suction surface. Minimising this reduces low-energy fluid accumulation in the blade tip region. Thus, the onset of stall is delayed as the blade throttles towards lower flow rates.
- In the blade tip region the net effect of sweep is to reduce the leading edge velocity peak which in turn attenuates the pressure difference across the blade tip-to-casing gap. Optimising the extent of forward sweep incorporated into a blade design minimises the blade tip leakage vortex's intensity, and thus delays the onset of stall as the blade throttles towards lower flow rates.
- A primary contribution of sweep to extend the forward-swept blade operating range was the impact of the flow's reduced radial rearrangement on the suction surface corner-stall. Corner-stall inception was delayed, and occurred further downstream from the blade leading edge as its intensity reduced. As a direct consequence, less low-energy fluid migrated to the blade tip, and consequently, the stall-free operating range was extended.

REFERENCES

Beiler, M.G., and Carolus, T.H. (1999), "Computation and Measurement of the Flow in Axial Flow Fans with Skewed Blades", *Transactions of the ASME, Journal of Turbomachinery*, vol. 121, pp. 59–66.

Borello, D., Corsini, A., and Rispoli, F. (1997), "Prediction of Francis Turbine Runner Performance using a 3D Finite Element Technique with Unassembled Stiffness Matrix Treatment", *Proceedings of the 2nd European Conference on Turbomachinery*, Antwerp, Belgium, 5–7 March.

Borello, D., Borrelli, P., Quagliata, E., and Rispoli, F. (2001), "A Multi-grid Additive and Distributive Parallel Algorithm for FEM Turbomachinery CFD", *Proceedings of the European Congress on Computational Methods in Applied Sciences (ECCOMAS CFD 2001)*, Swansea, UK, 4–7 September.

Borello, D., Corsini, A., and Rispoli, F. (2003), "A Finite Element Overlapping Scheme for Turbomachinery Flows on Parallel Platforms", *Computers and Fluids*, vol. 32(7), pp. 1017–47.

Copenhaver, W.W., Mayhew, E.R., Hah, C., and Wadia, A.R. (1996), "The Effect of Tip Clearance on a Swept Transonic Compressor Rotor", *Transactions of the ASME, Journal of Turbomachinery*, vol. 118, pp. 230–39.

Corsini, A., and Rispoli, F. (1999), "Numerical Simulation of Three-dimensional Viscous Flow in an Isolated Axial Rotor", *Polish Academy of Sciences, Archive of Mechanical Engineering (Archiwum budowy maszyn)*, vol. XLVI(4), pp. 369–92.

Corsini, A., and Rispoli, F. (2002), "Anisotropic Turbulence Modelling of Near Wall Effects Pertinent to Turbomachinery Flows", *Proceedings of the FEDSM-02, the 2002 ASME-European Engineering Summer Conference*, Montreal, QC, Canada, 14–18 July, paper no. FEDSM02-31206.

Corsini, A., and Vad, J. (2002), "Application of Forward Blade Sweep to Axial Flow Industrial Fans of High Specific Performance", *Proceedings of the 9th International Symposium on Transport Phenomena and Dynamics of Rotating Machinery (ISROMAC9)*, Honolulu, HI, USA, 10–14 February.

Corsini, A., Rispoli, F., Bencze, F., and Vad, J. (2001), "Effects of Blade Sweep in a High Performance Axial Flow Rotor", *Proceedings of the 4th European Conference on Turbomachinery*, Florence, Italy, 20–23 March.

Corsini, A., Rispoli, F., and Santoriello, A. (2003), "A High Order Petrov-Galerkin Stabilized Finite Element Method for Incompressible RANS in Presence of Strong Reaction Effects", *Proceedings of CMFF-03, the Conference on Modelling Fluid Flow*, Budapest, Hungary, 3–6 September.

Craft, T.J., Launder, B.E., and Suga, K. (1996), "Development and Application of a Cubic Eddy-viscosity Model of Turbulence", *International Journal of Heat and Fluid Flow*, vol. 17, pp. 108–55.

Goodwin, W.R. (1957), "Effect of Sweep on Performance of Compressor Blade Sections as Indicated by Swept-blade Rotor, Unswept-blade Rotor, and Cascade Tests", National Advisory Committee for Aeronautics (NACA) Technical Note 4062.

Hah, C., and Wennerstrom, A.J. (1991), "Three-dimensional Flow Fields Inside a Transonic Compressor with Swept Blades", *Transactions of the ASME, Journal of Turbomachinery*, vol. 113(2), pp. 241–51.

Lieblein, S. (1965), "Experimental Flow in Two-dimensional Cascades", in Johnsen, I.A., and Bullock, R.O. (Eds), *Aerodynamic Design of Axial-Flow Compressors*, National Aeronautics and Space Administration Report No. NASA SP-36, pp. 183–226.

Mohammed, K.P., and Prithvi Raj, D. (1977), "Investigations on Axial Flow Fan Impellers with Forward Swept Blades", *Transactions of the ASME, Journal of Fluids Engineering*, vol. 99, pp. 543–7.

Rabe, D., Hoying, D., and Koff, S. (1991), "Application of Sweep to Improve Efficiency of a Transonic Fan: Part II. Performance and Laser Test Results", *Proceedings of the AIAA/SAE/ASME 27th Joint Propulsion Conference*, Sacramento, CA, USA, 24–26 June, paper no. AIAA 91-2544.

Smith, L.H., and Yeh, H. (1963), "Sweep and Dihedral Effects in Axial-flow Turbomachinery", *Transactions of the ASME, Journal of Basic Engineering*, vol. 85(3), pp. 401–16.

Storer, J.A., and Cumpsty, N.A. (1991), "Tip Leakage Flow in Axial Compressors", *Transactions of the ASME, Journal of Turbomachinery*, vol. 113(2), pp. 252–9.

Vad, J. (2001), "Incorporation of Forward Blade Sweep in Non-free Vortex Design Methods of Axial Flow Turbomachinery Rotors", *Periodica Polytechnica*, vol. 45(2), pp. 217–38.

Vad, J., and Bencze, F. (1998), "Three-dimensional Flow in Axial Flow Fans of Non-free Vortex Design", *International Journal of Heat and Fluid Flow*, vol. 19, pp. 601–7.

Wadia, A.R., Szucs, P.N., and Crall, D.W. (1997), "Inner Working of Aerodynamic Sweep", *Proceedings of the 42nd American Society of Mechanical Engineers Gas Turbine and Aeroengine Congress*, Orlando, FL, USA, 2–5 June, paper no. 97-GT-401.

Wennerstrom, A.J. (1984), "Experimental Study of a High-through Flow Transonic Axial Compressor Stage", *Transactions of the ASME, Journal of Engineering for Gas Turbines and Power*, vol. 106(3), pp. 552–60.

Wright, T., and Simmons, W.E. (1990), "Blade Sweep for Low-speed Axial Fans", *Transactions of the ASME, Journal of Turbomachinery*, vol. 112, pp. 151–8.

Yamaguchi, N., Tominaga, T., Hattori, S., and Mitsuhashi, T. (1991), "Secondary-loss Reduction by Forward-skewing of Axial Compressor Rotor Blading", *Proceedings of the Yokohama International Gas Turbine Congress*, Yokohama, Japan, 27 October–1 November.

On the Role of Leading Edge Bumps in the Control of Stall Onset in Axial Fan Blades

A. Corsini, G. Delibra, and A.G. Sheard

ABSTRACT

Humpback whale pectoral fins are characterised by a series of tubercules that result in a sinusoidal-like leading edge. Taking its inspiration from the humpback whale, this chapter reports the results of a three-dimensional numerical study into the effect of a sinusoidal leading edge on both symmetrical and cambered aerofoil performance. Using the open source solver OpenFOAM, we computed turbulent flow around the aerofoils with and without a sinusoidal leading edge at different angles of attack. The reported research focused on the effects of the modified leading edge on lift-to-drag performance and the influence of camber on lift and drag.

The research was primarily concerned with elucidating the fluid flow mechanisms associated with the presence of a sinusoidal leading edge, and the impact of those mechanisms on profile performance. We found that a sinusoidal leading edge influenced aerofoil lift. It exhibited an early recovery post-stall for the symmetric profile and both an early recovery post-stall and a gain in lift post-stall for the cambered profiles.

We concluded that the increase in cambered profile post-stall lift induced by the sinusoidal leading edge's presence occurs because the leading edge geometry impacts the profile's velocity and vorticity fields. A sinusoidal leading edge introduces peaks and troughs along a profile's leading edge that induce vortex pairs. These vortices migrate from leading to trailing edge and supress suction side separated flow regions that develop at the trailing edge as a profile approaches stall. The separated flow is suppressed because it is confined to trailing edge regions down-stream of a leading edge trough. By confining the separated flow at the trailing edge, a sinusoidal leading edge is able to minimise the extent of separated flow regions and thus improve profile post-stall lift.

NOMENCLATURE

Latin letters

c	chord
d	distance from the suction side surface (see inserts in Figures 9.12 or 9.13)
C_L	lift coefficient
C_D	drag coefficient
C_p	$p - p_0$ = pressure coefficient
k	turbulent kinetic energy
p	pressure
p_0	average pressure value on the inflow of the computational domain
RANS	Reynolds-averaged Navier–Stokes
Re	Reynolds number
U,V,W	stream, pitch and span-wise components of the velocity field
U_∞	free-stream velocity
x, y, z	stream, pitch and span-wise directions
Z	normalised span-wise coordinate $Z = \mathbf{z}/\mu$

Greek letters

α	angle of attack
μ	sinusoid leading edge wavelength
ν_t	turbulent viscosity
ω	vorticity

INTRODUCTION

Researchers in both academia and industry continue to study the fluid flow mechanisms at play within turbomachinery blading in an ongoing effort to increase blade loading. Despite increasing insight into the blade-to-blade flow-field physics, the operating range of both fans and compressors remains constrained. The rise of aerodynamic instabilities on a blade's surface as blade loading increases inevitably imposes operational limits (Gravdahl and Egeland, 1999).

These aerodynamic instabilities are linked to the inception of rotating stall that occurs at a critical air inlet incidence angle (Weichert and Day, 2012). Rotating stall is a fluid flow mechanism that enables a rotor to adapt to a reducing flow rate, resulting in circumferentially non-uniform flow patterns rotating in the annulus at 50 to 70 per cent of the fan speed (Sheard *et al*., 2011). For an industrial fan the classical mechanical consequence of rotating stall is a fatigue crack in one or more blade. This fatigue crack then propagates, and ultimately results in an in-service mechanical failure (Sheard and Corsini, 2012).

Rotating stall results in mechanical failure because it increases the magnitude of unsteady aerodynamic forces to which fan blades' are subjected by a factor of seven (Sheard and Corsini, 2012). Industrial fan, aerospace fan and compressor design engineers therefore regard controlling aerodynamic instabilities as a key tech-

nology. This facilitates the development of higher pressure fans and compressors that have the potential to either achieve a given duty point at a higher efficiency, or the same duty point efficiency at a lower cost.

In an effort to extend the stable operating range of fans and compressors, researchers within the aerospace community have explored a range of strategies. Langston (2009) recently revisited the use of variable pitch in motion blades for application in a high-bypass ratio gas turbine fan intended for civil aviation application. Variable pitch in motion blades are a standard industrial fan component in induced draft boiler application (Bianchi *et al.*, 2012). Sheard *et al.*'s recent research (2014) concluded that when a fan transitions from stalled to stable operation by varying the blade pitch, the unsteady aerodynamic forces were up to an order of magnitude lower than when the same fan transitioned by varying fan speed. We may therefore conclude that a variable pitch in motion fan is intrinsically more stall-tolerant than a variable speed fan.

Variable pitch in motion fans may be intrinsically more stall tolerant than variable speed fans, but they are expensive in comparison to variable speed fixed pitch fans. In practice, industrial fan designers typically attempt to avoid stall using one of three strategies. They select a fan with a non-stalling blade angle, avoid stall completely by selecting a fan with a high pressure developing capability or select a fan with an anti-stall 'stabilisation ring' (Sheard and Corsini, 2012). In practice, a fan selected with a non-stalling blade angle tends to be relatively large and therefore expensive. A fan selection incorporating an anti-stall ring tends to be relatively low efficiency. As such, designers typically favour fan selections with a high pressure developing capability, and consequently, high blade loading. In an effort to increase blade loading, Corsini and Rispoli (2004) optimised using sweep and lean in blade design and Kroger *et al.* (2011) studied the impact of non-axisymmetric end-wall contouring. Blade design optimisation is a more practical strategy in most applications then either a shift from variable speed to variable pitch, a non-stalling blade angle or anti-stall ring.

Aerospace fan and compressor operating limits have substantially increased over the last decade by applying stall control methodologies (Paduano *et al.*, 2001; Liu *et al.*, 2009). Despite this progress, interest in extending stable operating range is as strong as ever. This interest has resulted in researchers looking at a broader range of aerodynamic applications than traditional fan and compressor blading in their efforts to develop new stall-tolerant solutions (Rusak and Morris, 2011). When considering a broader range of applications one possible source of inspiration comes from biomimicry. Biomimicry is the study of nature, its models and processes, with insight providing the inspiration for man-made applications of that which occurs naturally in nature.

The evolutionary process has given *animalia* and *plantae* millennia to adapt, with the best surviving and developing further. Studying the natural world can provide an insight into the flow-field physics underpinning the associated fluid dynamics (White and Miller, 2010). Within the context of turbomachinery blade design, natural flyers and swimmers provide a wide range of elegant aerodynamic and hydrodynamic solutions. Some of these solutions are difficult, if not impossible to

replicate. Try to imagine the difficulties in building a mechanical bat. It would be necessary to replicate the ten different mobile junctions needed to reproduce its wing motion when in flight (Shyy *et al*., 2008). However, despite the difficulty inherent in biomimicry, the insight it provides is a source of inspiration.

A hydrodynamic biomimicry pioneer is Professor Frank Fish who analysed the efficiency with which mammals swim. He highlighted the drag reduction mechanisms that developed with the evolutionary process (Fish, 1993). Continuing his research, Professor Fish went on to study passive and active flow control mechanisms in natural swimmers (Fish *et al*., 2008). Hua *et al*. (2010) carried out an aerodynamic study of a seagull wing with the objective of establishing the wing's stability limit, and specifically the role of the wing's natural camber. Hua *et al*. (2010) were able to use a numerical simulation to demonstrate the advantages of a naturally cambered wing by comparing its lift-to-drag ratio against a NACA four digit aerofoil.

The biomimicry based research reported in the extant literature provides a fascinating insight into the aerodynamic and hydrodynamic solutions that exist in the natural world. Despite this promise, industrial fan designers cannot exploit directly the ideas and concepts as the evolutionary process is associated with a range of Reynolds numbers that is simply too low for turbomachinery applications. An exception is the Reynolds number range associated with the humpback whale's pectoral fins. The humpback whale (*megaptera novaeangliae)* may move relatively slowly due to its large size, but the Reynolds numbers it produces over its pectoral fins are similar to those that occur with an industrial fan blade.

The humpback whale is of interest to industrial fan designers as it is able to perform sharp rolls and loops under water whilst hunting. Marine biologists attribute this capability to the shape of its pectoral fins, which are characterised by a wing-like aspect ratio and a leading edge with typically ten or eleven tubercles, Figure 9.1. Fish and Battle (1995) studied humpback whale pectoral fins, observing that the inter-tubercle distance is constant and the first tubercle is placed at about 30 per cent of the pectoral fin's span, Figure 9.2. The pectoral fin's profile is essentially un-cambered with a cross-section that is constant irrespective of the span-wise position and reduces towards the tip. Fish and Battle (1995) concluded that the humpback whale's ability to perform sharp rolls and loops is linked to the geometry of its pectoral fin.

Miklosovic *et al*. (2004) studied the application of a sinusoidal blade leading edge that mimics humpback whale pectoral fin geometry. Miklosovic *et al*. (2004) concluded that the sinusoidal leading edge 'serves to delay stall by providing higher lift at higher incidence angles, and to ameliorate the post-stall characteristics by maintaining higher lift with lower drag'. Miklosovic *et al*. (2007) went on to compare the effects of a finite-span sinusoidal leading edge pectoral fin with the same pectoral fin section in infinite cascade. They concluded that lift and drag were affected by three-dimensional effects associated with the finite-span pectoral fin. Post-stall the finite-span pectoral fin exhibited reduced drag and increased lift, leading Miklosovic *et al*. (2007) to conclude that flattening the post-stall lift curve for the finite-span pectoral fin could be beneficial when operating in a near-stall condition under the influence of an unsteady incoming flow-field. Therefore, the humpback whale pectoral fin tubercles act as a stall-control system.

FIGURE 9.1. A humpback whale (left) and detail of the whale's pectoral fin leading edge tubercles (right).
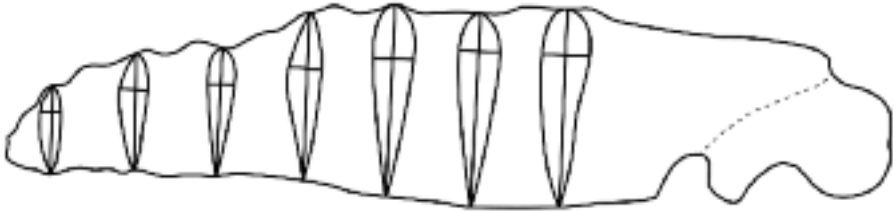
FIGURE 9.2. A plan view and sections through a humpback whale pectoral fin, from Fish and Battle (1995).

Pedro and Kobayashi (2008) performed a numerical study of a finite-span blade modelled on a humpback whale pectoral fin's actual morphology. They concluded that the improved aerodynamic performance post-stall was associated with the pectoral fin's 'wavy' leading edge. This improvement was a consequence of stream-wise vortices originating from the tubercles. Dewar *et al.* (2009) went on to commercially exploit Pedro and Kobayashi's work (2008). They applied a series of tubercles to a ceiling fan's leading edge. Thus, Dewar *et al.* (2009) delayed the onset of fan stall, and increased the peak flow through the fan.

Among the hydrodynamic studies reported in the literature, van Nierop *et al.* (2008) studied the mechanism that the tubercle's presence induced on a two-dimensional model. They modelled the tubercles as a sinusoidal leading edge, reaching two primary conclusions. First, increasing sinusoid amplitude flattens the lift curve. Second, the stall-delay effect was insensitive to sinusoid wavelength.

Johari *et al*. (2007) investigated experimentally the sinusoidal leading edge's impact on a nominally two-dimensional bluff body. They measured lift, drag and pitching moment on a NACA 63$_4$-021 profile with and without a sinusoidal leading edge over a range of inlet flow angles of attack from 6 to 30 degrees. The studied sinusoid amplitudes ranged from 2.5 per cent to 12 per cent of the chord. Johari *et al*. (2007) concluded that at angles of attack lower than those occurring with stall without a sinusoidal leading edge, a sinusoidal leading edge presence increased drag and decreased lift. However, at angles of attack greater than those occurring with stall without a sinusoidal leading edge, a sinusoidal leading edge presence increased lift by approximately 50 per cent compared to the baseline profile with little negative impact on drag. Johari *et al*. (2007) concluded that the sinusoid's wavelength was not an influential parameter on aerofoil performance. In contrast, the sinusoid's amplitude has a distinct effect on aerofoil lift.

The reported research in this chapter extends work from the extant literature. We present the results of a numerical investigation of a sinusoidal leading edge's effects when fitted to NACA 0015 and NACA 4415 profiles. Accepting Johari *et al*.'s conclusion (2007) that sinusoid wavelength is not an influential parameter on aerofoil performance, the reported research focuses on combining a sinusoidal leading edge with aerofoil camber. A humpback whale's pectoral fin profile has an un-cambered profile, and consequently, it is necessary to establish the combined effect of a sinusoidal leading edge and aerofoil camber. We present the numerical method that we utilised, then present the results of the numerical study. We advocate the use of a numerical method with an anisotropy resolving turbulence closure as we found that the approach accurately modelled the flow-field around an aerofoil with a sinusoidal leading edge. The results provide an insight into the impact of a sinusoidal leading edge and camber, with aerofoil lift and drag performance characterising both.

NUMERICAL METHOD

We carried out our numerical study using an unstructured open-source finite volume solver, OpenFOAM (Jasak, 2010). We used it to solve the steady state incompressible Reynolds-averaged Navier–Stokes (RANS) equations using a non-linear eddy viscosity k-ε model (Lien and Leschziner, 1994). Although the RANS approach is unable to reproduce stall hysteresis, the chosen turbulence closure is able to resolve the boundary layer development when subjected to the adverse pressure gradient associated with aerofoil camber. The cubic stress-strain relationship utilised by the non-linear eddy viscosity k-ε turbulence model partially accounts for the Reynolds stresses' anisotropy. Thus, the model reproduces the effect of impingement and curvature more accurately than linear k-ε turbulence models such as that of Launder and Sharma (1974).

We carried out the numerical simulations using OpenFOAM's built-in version of the *simple*FOAM solver. Following Corsini *et al*.'s recommendation (2013), we chose a low-Reynolds formulation for wall treatment. We selected a second order QUICK divergence scheme and a GAMG linear solver for the SIMPLE subset of equations. For all other equations we utilised *smooth*Solver, setting a convergence tolerance to $10{\times}10^{-8}$ for all the computed quantities. We performed the numerical

simulations on the computer clusters MATRIX at the CASPUR HPC facility (Rome) and PLX cluster at the CINECA HPC facility (Bologna).

We selected two NACA four-digit profiles for study: the NACA 0015 symmetric un-cambered aerofoil and the NACA 4415 cambered aerofoil. These two aerofoils constituted the un-cambered and cambered baseline aerofoils to which we then added sinusoidal leading edges, Table 9.1. Following Johari *et al.*'s recommendations (2007), we selected a 2.5 per cent sinusoid amplitude of aerofoil chord. We did not study wavelength effects as van Nierop *et al.*'s (2008) and Johari *et al.*'s studies (2007) concluded that wavelength did not influence the aerofoil performance.

The computational domain was discretised with approximately 2.5×10^6 hexahedral cells in order to keep the y^+ parameter equal to approximately unity on the aerofoil surface, Figure 9.3. We carried out a grid sensitivity assessment on three two-dimensional meshes, solving the flow around the NACA 0015 profile at different angles of attack. The three meshes comprised approximately 8,000, 30,000 and 60,000 cells, respectively. A study of the computed lift coefficients indicated that the intermediate mesh was sufficiently dense to achieve a grid-independent solution.

Following the results of the two-dimensional mesh dependency study, we extruded the mesh in a span-wise direction using 80 equally spaced cells. We defined the computational domain's stream-wise extension downstream of the trailing edge following Corsini *et al.*'s recommendations (2013) to ensure that we accurately computed the aerofoil wake structure. Both span-wise and pitch-wise periodic boundaries help reduce the extent of the computational domain, whilst partially accounting for the effect of adjacent aerofoils as in a linear cascade, Table 9.2. The average computational time for each numerical simulation at each angle of attack was 200 hours.

Table 9.1. *Details of the computational model.*

Aerofoil profiles	NACA0015 and NACA4415
Leading edge lines	Straight and sinusoidal
Mean normalised chord length	c = 1.0
Sinusoid amplitude of the leading edge	2.5% of chord
Wavelength of the sinusoid	0.25 of chord
Computational domain extent	1.3 chord upstream of the blade leading edge
	9.3 chord downstream of the blade trailing edge
	0.5 chord in span-wise direction (two sinusoids)
	1.0 chord in pitch-wise direction
Reynolds number	Re = c × U_∞/ν = 183,000

Table 9.2. *Computational model boundary conditions.*

Inlet	Steady velocity profile (velocity magnitude = 1.0 and different angles of attack)
	Turbulence intensity = 1.5%
	$\nu_T/\nu = 30$
Outlet	Convective boundary conditions
Blade	No-slip conditions
Pitch- and span-wise directions	Periodicity
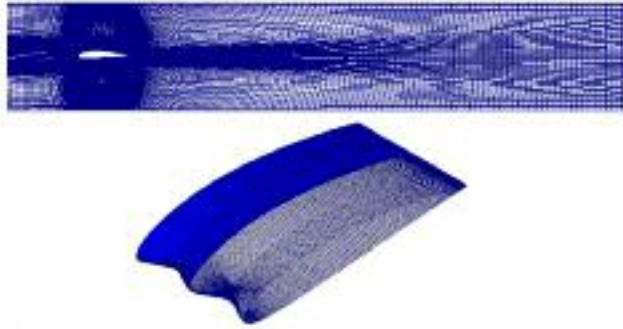
FIGURE 9.3. The computational domain used in the OpenFOAM numerical simulations (top) and details of the grid over the WHALE 4415 profile, one of the studied profiles (bottom).

RESULTS

Lift and drag performance

Sheldahl and Klimas (1981) studied the aerofoil NACA 0015 and computed the profile lift coefficient over a range of angles of attack at a Reynolds number of 183,000. They then compared the computed results with available experimental data that they measured at a Reynolds number of 360,000, Figure 9.4. The agreement between the computed and measured data pre-stall was good. Post-stall the computed lift coefficients were typically nine per cent higher than the measured values. We may associate the discrepancy with the higher Reynolds number from Sheldahl and Klimas' (1981) experimental measurements or their numerical simulation assumptions. The periodic boundary conditions that Sheldahl and Klimas (1981) imposed may not have accurately replicated the experimental boundary conditions associated with a two-dimensional cascade of aerofoils.

In an effort to ensure consistent assumptions, we chose to compute a reference numerical solution for the NACA 0015 and NACA 4415 profiles. We computed the reference solution using XFoil, a quasi three-dimensional viscous analysis public domain solver based on a boundary element method (BEM). Engineers originally developed the XFoil solver for simulating the performance of isolated sub-sonic aerofoils (Drela, 1989). The XFoil computational predictions for the NACA 0015 and NACA 4415 profile lift and drag agreed well with the OpenFOAM predictions, Figures 9.5 and 9.6. The XFoil and OpenFOAM predictions of both lift and drag for the symmetrical NACA 0015 profile were within one per cent, which we considered to be excellent. The XFoil and OpenFOAM predictions of both lift and drag for the cambered NACA 4415 profile were within five per cent. We may associate this discrepancy with the impact of grid distortion around the blade in the OpenFOAM numerical model, and the lateral blade interaction that occurs with imposed pitch-wise periodicity. Although a five per cent discrepancy is larger than we would have considered ideal, it is still small enough for any conclusions drawn from the results to be valid and therefore, we accepted it.
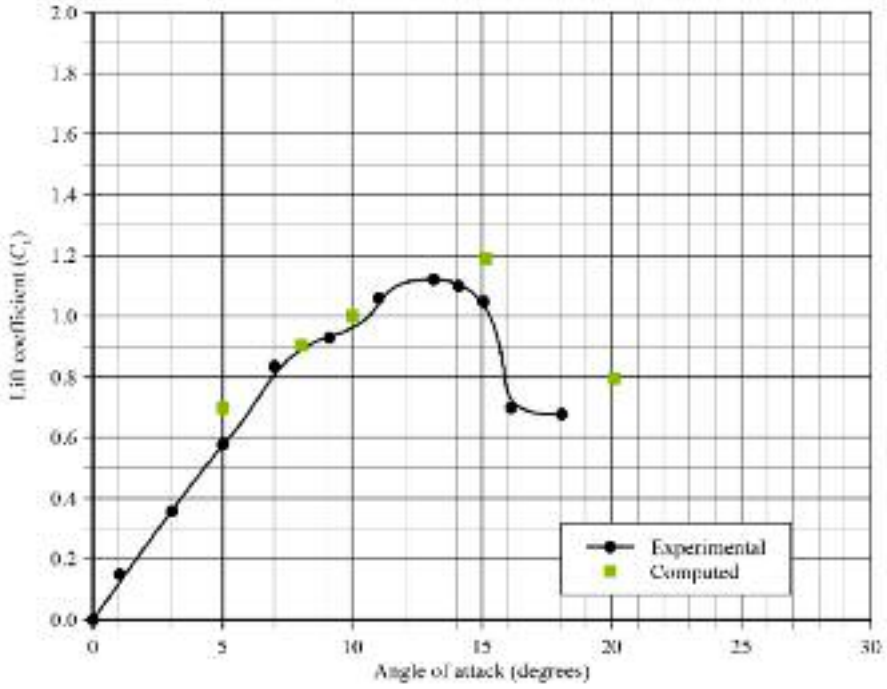
FIGURE 9.4. Lift coefficient versus angle of attack for a NACA 0015 aerofoil, from Sheldahl and Klimas (1981).
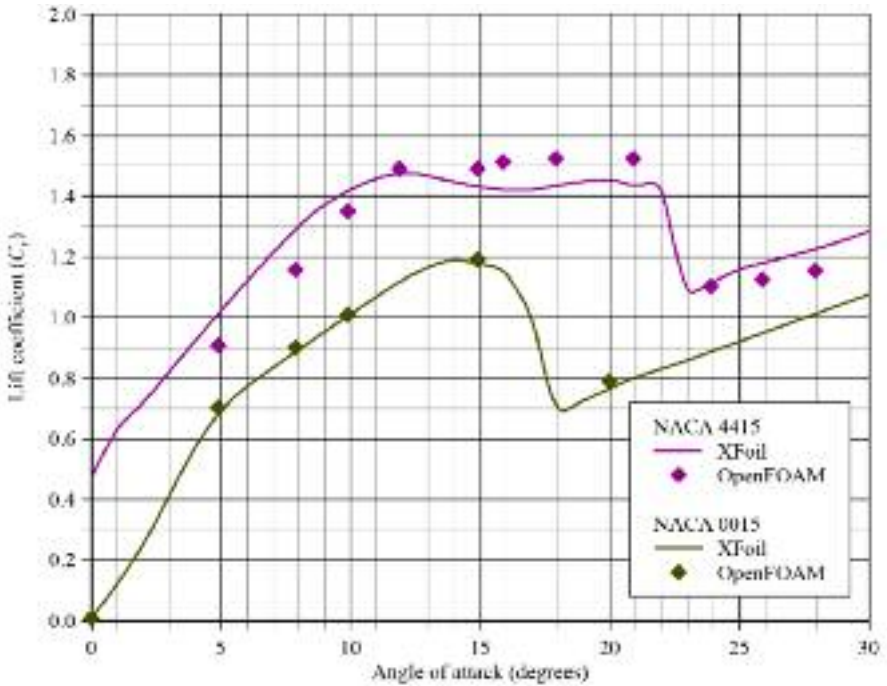
FIGURE 9.5. Lift coefficients computed using the XFoil and OpenFOAM solvers for the NACA 0015 and NACA 4415 profiles.
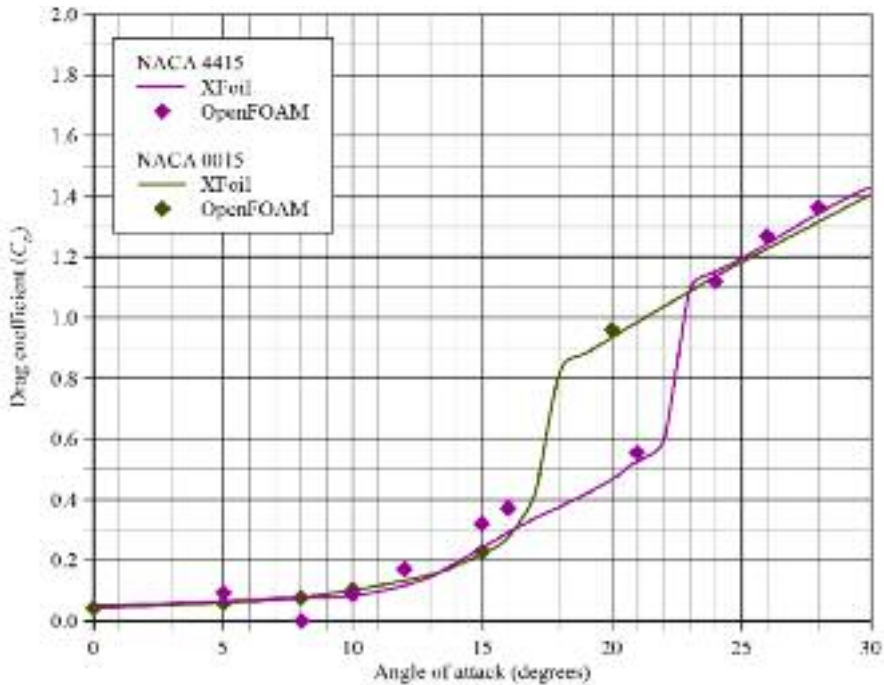
FIGURE 9.6. Drag coefficients computed using the XFoil and OpenFOAM solvers for the NACA 0015 and NACA 4415 profiles.

The agreement between XFoil and OpenFOAM predictions for the NACA 0015 and NACA 4415 performance gave confidence in the computational models that we utilised in the OpenFOAM predictions. We then adapted the NACA 0015 and NACA 4415 profiles and included a sinusoidal leading edge of 2.5 per cent chord amplitude to create 'whale fan' versions of the profiles that we respectively named WHALE 0015 and WHALE 4415. We adapted the NACA 0015 and NACA 4415 OpenFOAM computational grids to create WHALE 0015 and WHALE 4415 computational grids. Figures 9.7 and 9.8 illustrate computed lift and drag for the WHALE 0015 and WHALE 4415 profiles.

When we compare the NACA 0015 and WHALE 0015 OpenFOAM computed lift coefficients, we see that the WHALE 0015 results are lower than the NACA 0015 results below 15 degrees angle of attack and higher after 15 degrees. The shape of the lift coefficient's distribution makes it apparent that the profile stalls at 15 degrees, Figure 9.7. Post-stall at a 21 degree angle of attack for the WHALE 0015 profile, lift coefficient is 20 per cent higher than the NACA 0015 profile. By 24 degrees the WHALE 0015 profile is 40 per cent higher than the NACA 0015 profile. When we compare NACA 0015 and WHALE 0015 drag coefficients post-stall, Figure 9.8, they remain similar. This is an observation that is self-consistent with Johari *et al*.'s results (2007).

When we compare the NACA 4415 and WHALE 4415 OpenFOAM computed lift coefficients, we see that the WHALE 4415 results are higher than the NACA
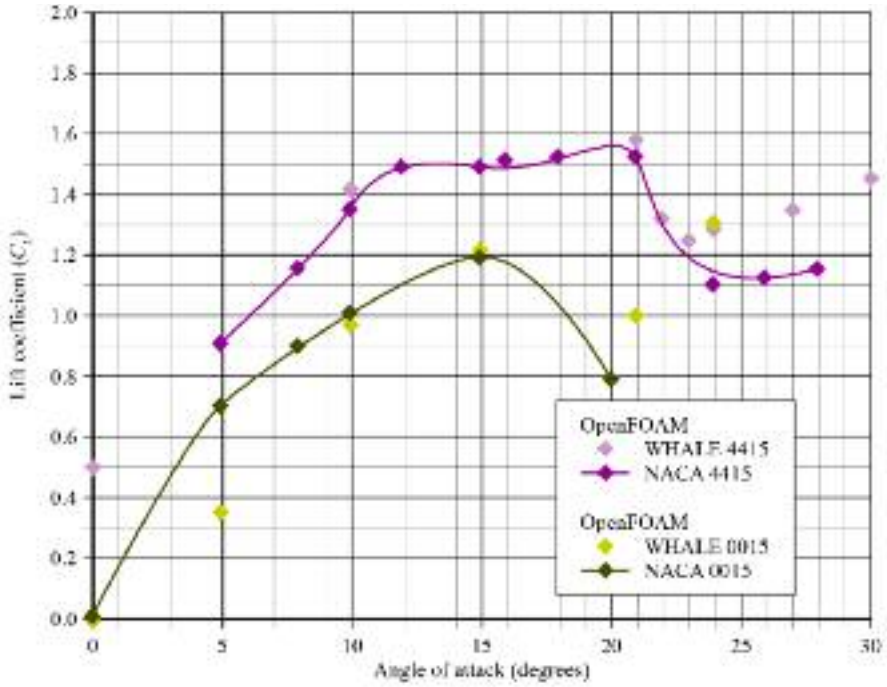
FIGURE 9.7. Lift coefficients computed using the OpenFOAM solvers for the NACA 0015, NACA 4415, WHALE 0015 and NACA 4415 profiles.
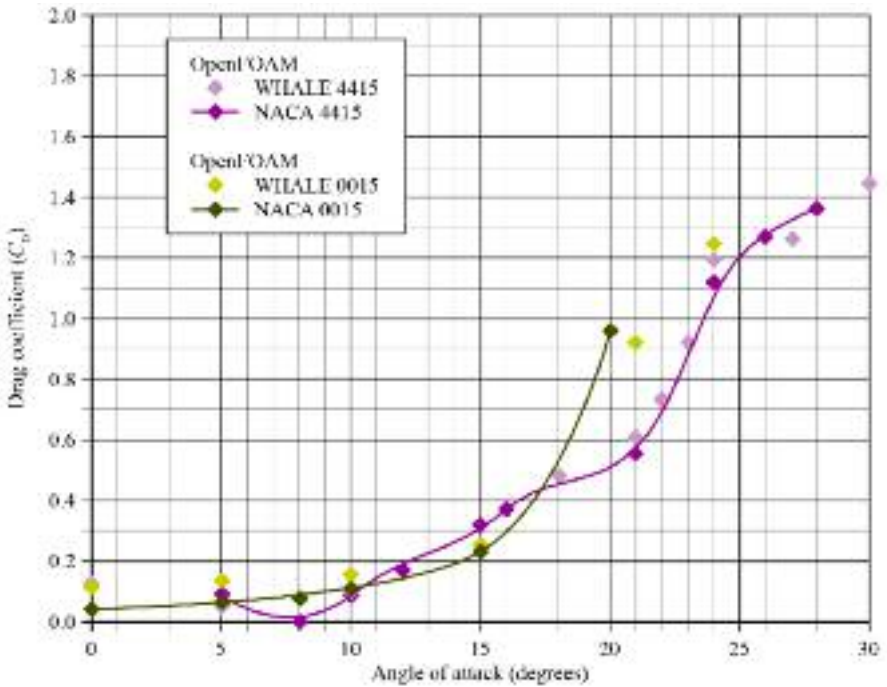
FIGURE 9.8. Drag coefficients computed using the OpenFOAM solvers for the NACA 0015, NACA 4415, WHALE 0015 and NACA 4415 profiles.

4415 results both below and above a 23 degree angle of attack. From the lift coefficient distribution's shape it is apparent that the profile stalls at 23 degrees, Figure 9.7. Post-stall the WHALE 4415 profile recovers its working capability more rapidly than the NACA 4415 profile, indicated by the WHALE 4415 slope increasing 30 per cent more rapidly with increasing angle of attack. When we compared NACA 4415 and WHALE 4415 drag coefficients post-stall, Figure 9.8, they once again remain similar both pre-and post-stall.

We may use the computed lift and drag coefficients to provide an insight into the combined effect of camber and a sinusoidal leading edge on profile performance. Consider the computed lift coefficients for the WHALE 0015 profile and NACA 0015 profiles at a pre-stall angle of attack of five degrees, Figure 9.7. A sinusoidal leading edge reduces the lift coefficient by 50 per cent, a result that is consistent with Johari *et al*.'s conclusions (2007). Now consider the computed lift coefficients for the WHALE 4415 profile and NACA 4415 profiles at a pre-stall angle of attack of five degrees, Figure 9.7. The sinusoidal leading edge reduces the lift coefficient by 10 per cent. In the post-stall region above an angle of attack of 23 degrees the sinusoidal leading edge resulted in a WHALE 4415 profile lift coefficient that is 20 per cent higher than that of the NACA 4415 profile.

As we have mentioned previously, the WHALE 4415 profile's computed post-stall drag coefficients are similar to those of the NACA 4415 profile. In contrast, the WHALE 0015 profile's post stall lift coefficients are slightly higher than those of the NACA 0015 profile, Figure 9.8. The lift-to-drag ratio provides further insight into the effect of a sinusoidal leading edge, Table 9.3. For the NACA 4415 and WHALE 4415 profiles stall is incipient at a 21 degree angle of attack and is fully developed at a 24 degree angle of attack. The WHALE 4415 profile lift-to-drag ratio at both 21 and 24 degrees is higher than that of the NACA 4415 profile.

Sinusoidal leading edge fluid-flow mechanisms

The presence of a sinusoidal leading edge has an impact on both the profile velocity and vorticity fields. Before considering the numerical simulation's results,

Table 9.3. *Lift-to-drag coefficients at selected angles of attack for the studied aerofoils.*

Profile	21 degrees	24 degrees
OpenFOAM: NACA 0015	3.25[1]	3.20[1]
OpenFOAM: WHALE 0015	4.35	4.21
XFoil: NACA 0015	3.28	3.14
OpenFOAM: NACA 4415	11.01	3.94
OpenFOAM: WHALE 4415	10.40	4.29
XFoil: NACA 4415	10.83	3.90

[1]Values are interpolated

we must first consider the applicability of the chosen computation modelling approach to resolve this velocity and vorticity field. The linear k-ε turbulence model is based on a simple gradient diffusion hypothesis. As a consequence, Reynolds stresses within the momentum equation are modelled as a linear function of the velocity gradients (Launder and Sharma, 1974). In contrast, the cubic k-ε turbulence model incorporates second- and third-order terms based on velocity gradient.

These higher-order terms enable the cubic k-ε turbulence model to better reproduce the flow-field's turbulent kinetic energy in impingement zones, and to partially account for the profile's curvature (Lien and Leschziner, 1994). Accounting for curvature is a key capability when attempting to accurately predict the impact of a sinusoidal leading edge on the flow-field around the peaks and troughs associated with the leading edge geometry (Durbin, 2011).

We evaluated the impact of the selected turbulence model, predicting the flow-field around the WHALE 4415 profile when stall was incipient, Figure 9.9. Launder and Sharma's (1974) linear k-ε turbulence model results in a significantly different predicted flow field when compared to Lien and Leschziner's (1994) cubic k-ε turbulence model. In comparison to the cubic k-ε turbulence model, the linear k-ε turbulence model significantly under predicts the extent of separated flow regions at the trailing edge. Both turbulence models predict separation of the trailing edge flow down-stream of a leading edge trough, with the flow remaining attached downstream of a leading edge peak. As such, the numerical simulations that we undertook with both a linear and cubic k-ε turbulence model predict the separated flow regions. However, the difference in the size of predicted separated flow regions is significant enough to result in substantial differences between the computed lift and drag coefficients. Assessing the accuracy with which the cubic k-ε turbulence model predicts the extent of separated flow regions around the WHLAE 4415 is challenging. In the reported research we chose to utilise the cubic k-ε turbulence model, following Corsini *et al.*'s recommendations (2013), and thus, we have confidence that any errors are at least minimised.

We may illustrate the impact of a sinusoidal leading edge through studying profile pressure distributions. In Figures 9.10 and 9.11, we have plotted the pressure distribution around a peak, trough and the middle of a leading edge sinusoid for both
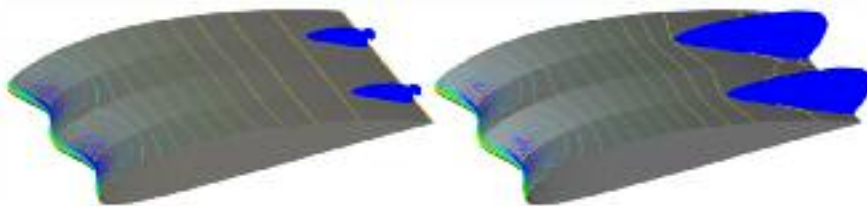
FIGURE 9.9. Recirculation zones in the WHALE 4415 profile's trailing edge region at a 21 degree angle of attack. The authors computed the flow-field using (left) Launder Sharma's (1974) linear k-ε turbulence model and (right) Lien and Leschziner's (1994) cubic k-ε turbulence model.
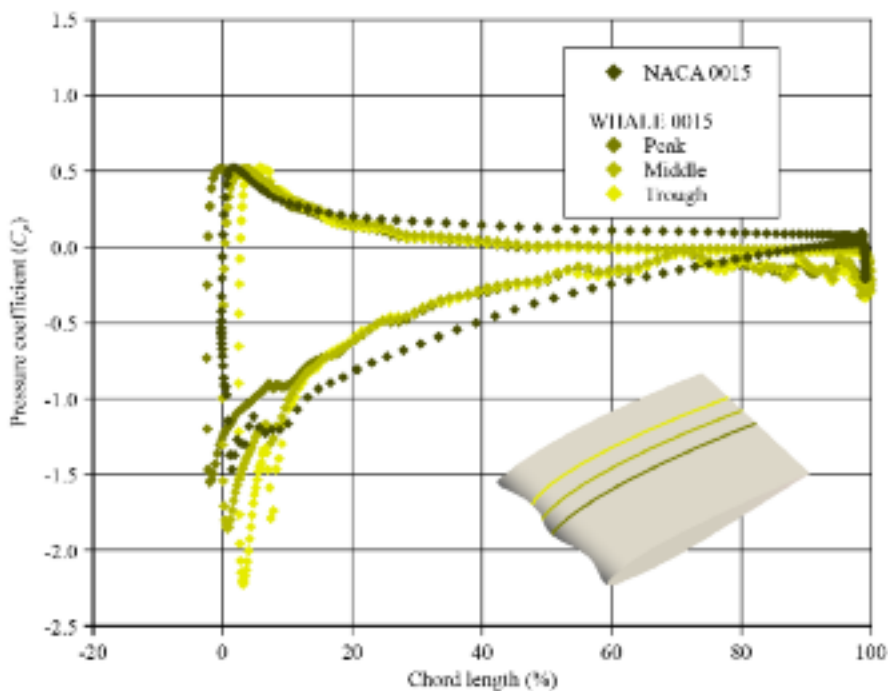
FIGURE 9.10. Pressure coefficient distribution at different span-wise positions for the WHALE 0015 profile at a 21 degree angle of attack. Refer to provided NACA 0015 profile data for comparison

the WHALE 0015 and WHALE 4415 profiles. We also show the profile pressure distributions for the NACA 0015 and NACA 4415 profiles for comparative purposes. As would reasonably be expected, the sinusoidal leading edge's primary impact on profile pressure distribution is at the leading edge. The pressure distribution profile at the sinusoid's middle for the WHALE 0015 profile is similar to that of the NACA 0015 profile, Figure 9.10. In contrast, the peak and trough pressure distribution profiles respectively reduce and increase. The difference between peak and trough pressure distribution profiles is more pronounced for the WHALE 4415 profile, Figure 9.11. The WHALE 4415 profile is unique in that at the sinusoid's peak there is no peak in the leading edge pressure profile distribution.

We may elucidate the fluid-flow mechanisms at play around the studied profiles through analysing pressure iso-lines over the WHALE 0015 and WHALE 4415 profiles, Figures 9.12 and 9.13 respectively. Both the WHALE 0015 and the WHALE 4415 profile iso-lines of pressure indicate that as angle of attack increases, a low-pressure core develops in the sinusoid troughs. The creation of this low-pressure core is driven by velocity field distortion that occurs with the leading edge sinusoids' presence, Figure 9.14. As flow impinges on a leading edge sinusoid peak, the low-pressure core in the trough draws fluid into the core from the pressure surface. Fluid draws into the core in a span-wise direction from either side of the sinusoid peak.
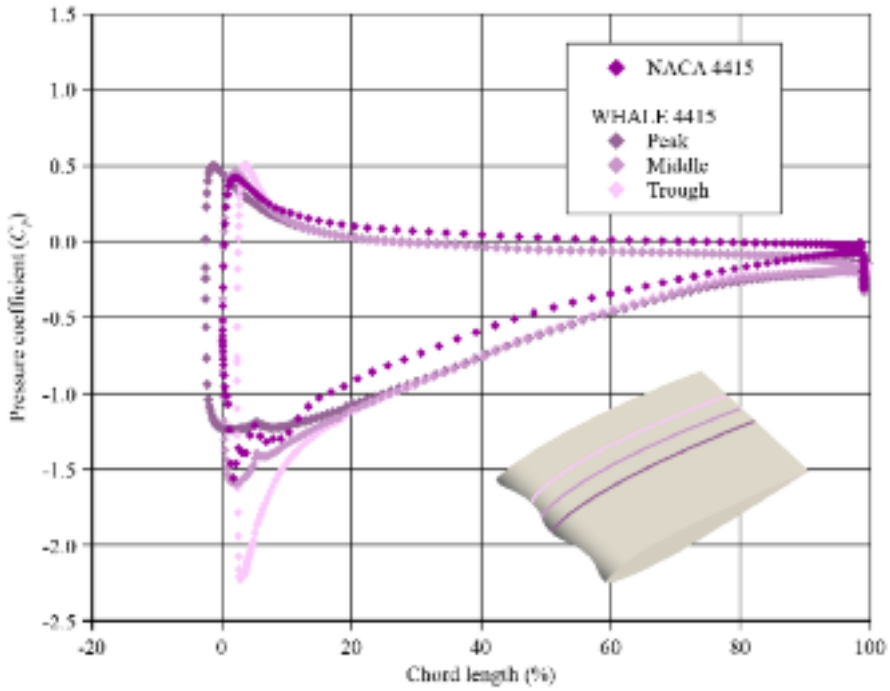
FIGURE 9.11. Pressure coefficient distribution at different span positions for the WHALE 4415 profile at a 21 degree angle of attack. Refer to provided NACA 4415 profile data for comparison.
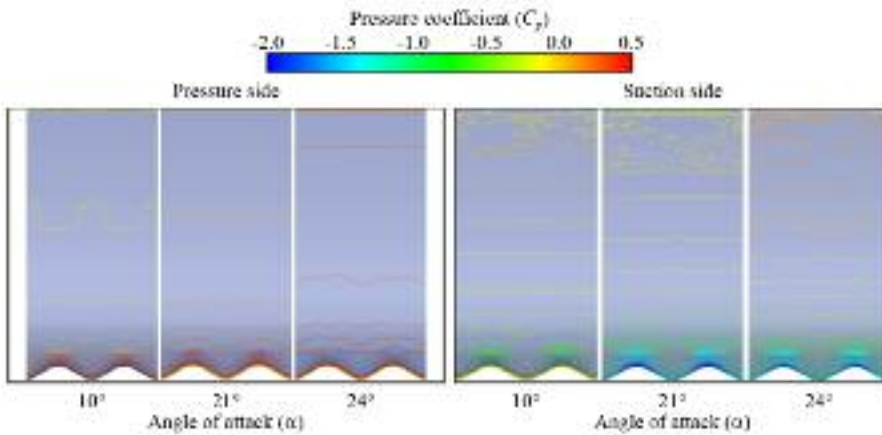
FIGURE 9.12. Pressure coefficient distributions at three angles of attack over the pressure side (left) and suction side (right) of the profile WHALE 0015.
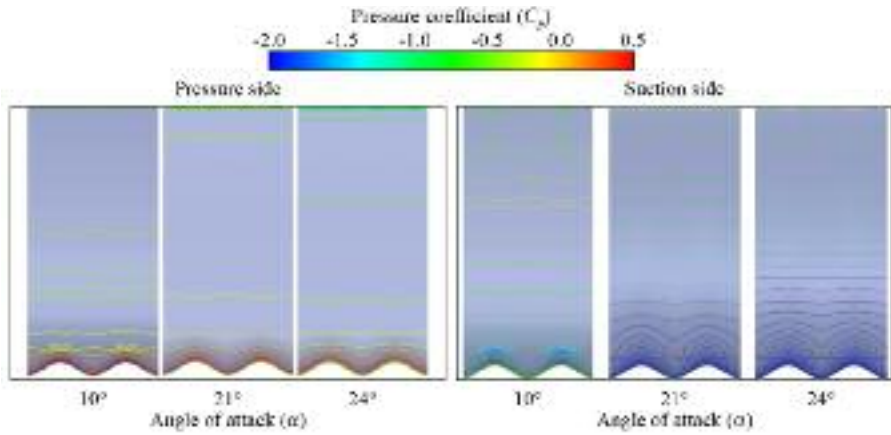
FIGURE 9.13. Pressure coefficient distributions at three angles of attack over the pressure side (left) and suction side (right) of the profile WHALE 4415.
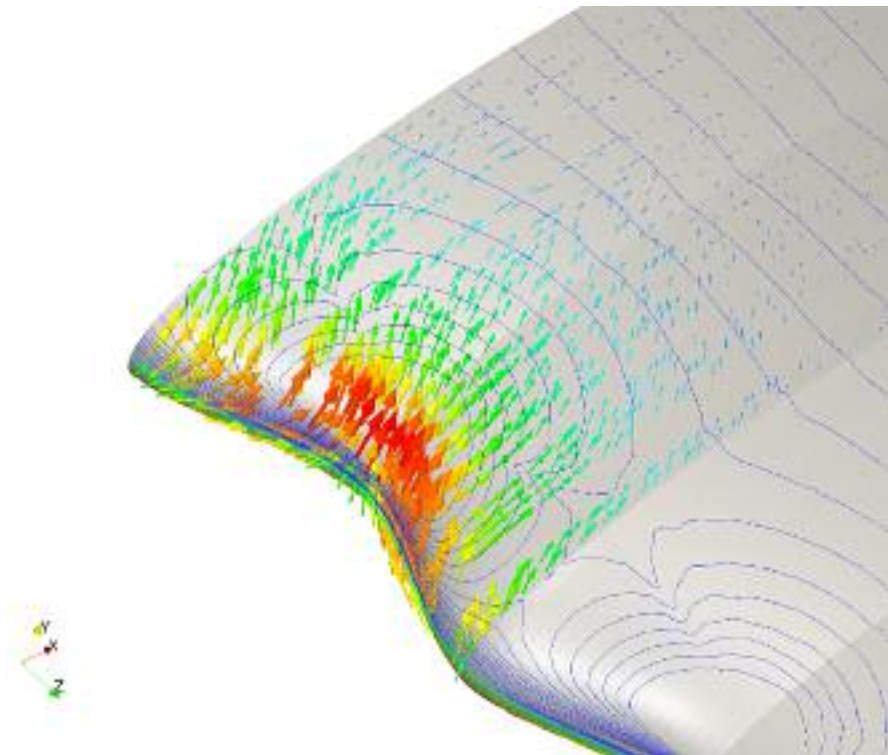
FIGURE 9.14. The WHALE 4415 profile at a 21 degree angle of attack. The two-dimensional velocity vectors are constructed from span- and pitch-wise velocity components.

The result is that a pair of counter-rotating vortex become established on either side of a leading edge sinusoid, and then migrate from the profile's leading to trailing edge. These vortex pairs constrain the extent of trailing edge separated flow regions that develop as the angle of attack increases and stall becomes incipient, Figure 9.15.

We may provide further insight into a sinusoidal leading edge's impact on the trailing edge flow-field of the WHALE 4415 profile by studying profile velocity fields, Figure 9.16. Here we see the stream-, pitch- and span-wise variation of velocity at 90 per cent blade chord at distances of 5, 10 and 15 per cent above the suction surface. The leading edge sinusoids impact stream-, pitch- and span-wise velocity. Although the stream- and pitch-wise variations in velocity reduce with increasing distance from the suction surface, the span-wise variation is relatively insensitive to distance from the suction surface.

We also may elucidate a sinusoidal leading edge's impact on the trailing edge flow-field through studying profile vorticity, Figure 9.17. Once again, we see the stream-, pitch- and span-wise variations at 90 per cent blade chord at distances of 5, 10 and 15 per cent above the suction surface. As one might reasonably expect, vorticity magnitude reduces with increasing distance from the suction surface for stream-, pitch- and span-wise components of vorticity. Additionally, stream- and pitch-wise variations in vorticity shift by half a wavelength of the leading edge
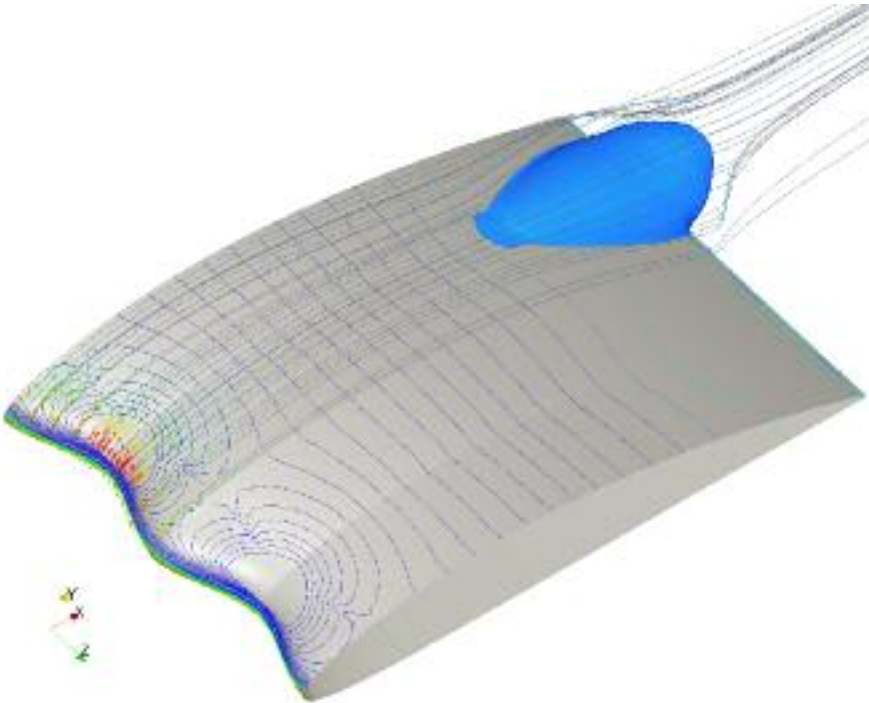
FIGURE 9.15. The WHALE 4415 profile at a 21 degree angle of attack. The isometric view provides an insight on the velocity field's distortion generated by the sinusoidal leading edge.
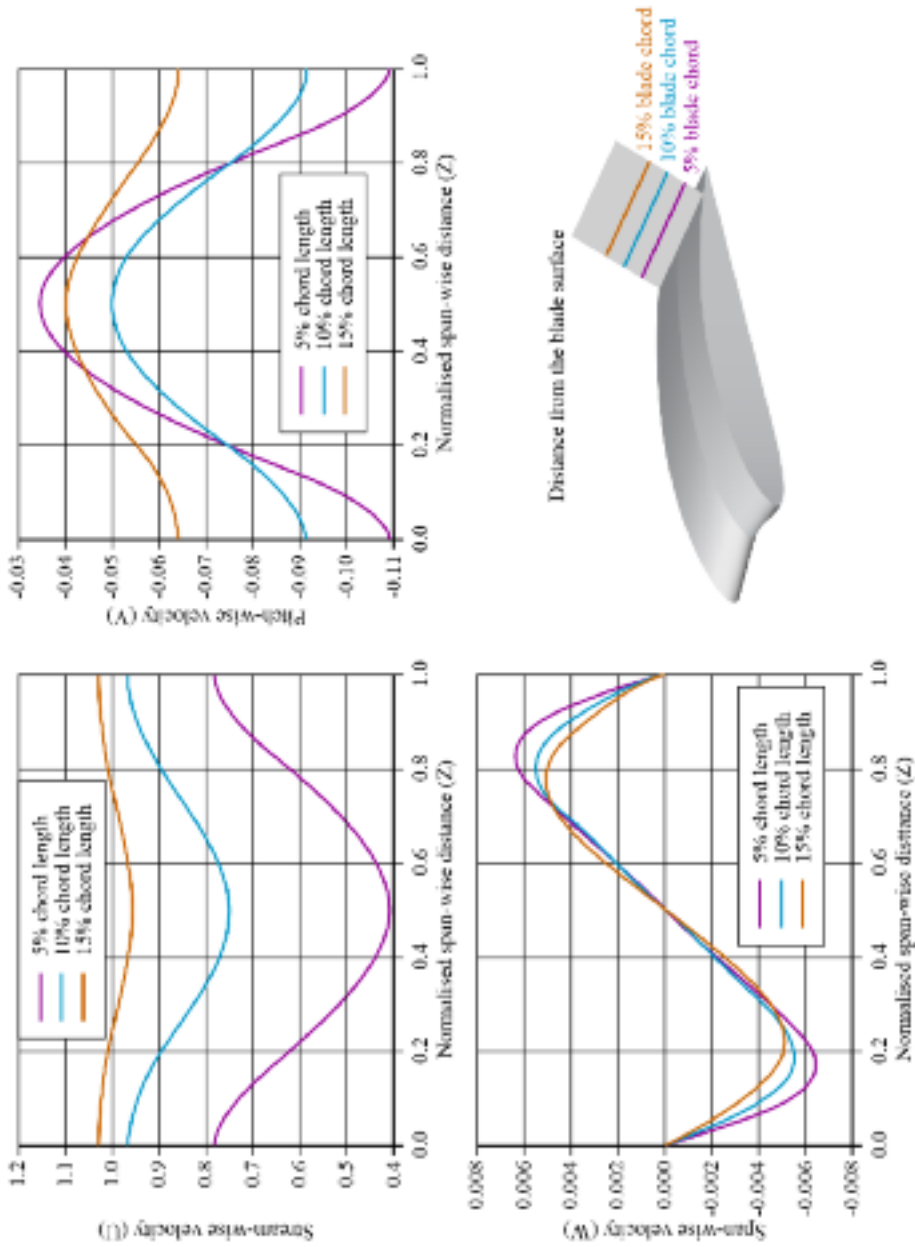
FIGURE 9.16. WHALE 4415 velocity profiles at 90 per cent of the chord, 5 per cent, 10 per cent and 15 per cent blade chord from the blade surface.
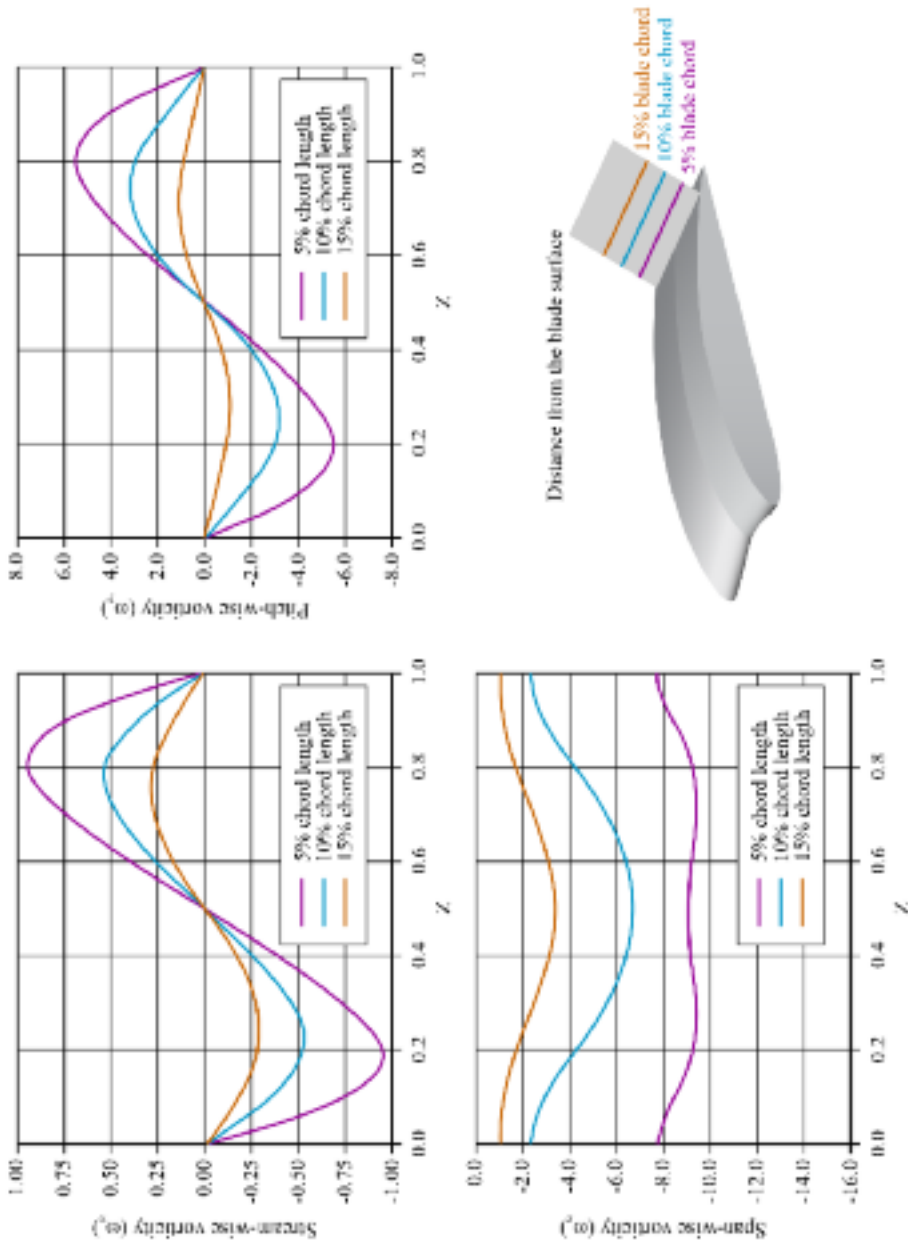
FIGURE 9.17. WHALE 4415 vorticity profiles at 90 per cent of the chord, 5 per cent, 10 per cent and 15 per cent blade chord from the blade surface.

sinusoids. In contrast, the vorticity's span-wise components frequency doubles 5 per cent from the suction surface, a feature that has diffused 10 per cent from the suction surface. The change in span-wise vorticity with distance from the suction surface is indicative of a non-uniform flow-field at the WHALE 4415 profile's trailing edge.

We may provide a final insight into the flow-field topology induced by a sinusoidal leading edge presence through studying enstrophy iso-surfaces for the WHALE 0015 and WHALE 4415 profile suction and pressure surfaces, Figures 9.18 and 9.19 respectively. Studying suction surface enstrophy iso-surfaces indicates that the two low-pressure cores associated with each leading edge sinusoid release a vortex pair that migrates from the leading to trailing edge. When applied to a symmetrical profile, WHALE 0015, the leading edge sinusoids result in a thin structure pre-stall at low angles of attack that detaches from the profile surface and consequently, does not impact on the flow-field down-stream of the leading edge. At higher angles of attack this structure that was detached remains attached post-stall. This attached structure results in high stream-wise vorticity inside the boundary layer, ultimately resulting in the flow separating from the profile at the trailing edge.

A study of enstrophy iso-surfaces for the WHALE 4415 suction surface indicates that the fluid-flow structures that develop as a consequence of the leading edge sinusoids remain attached at both pre- and post-stall angles of attack, Figure 9.18. The fluid-flow structure remaining attached pre-stall results in a higher level of stream-wise vorticity that results in the structure being better able to remain attached with increasing angle of attack. For the WHALE 4415 profile, the leading edge sinusoids' presence results in elongating fluid-flow structures at low angles of attack pre-stall. As stall first becomes incipient, and then occurs, the fluid-flow structures become increasingly stretched, with increasing stretch correlated with reducing lift.

Finally, the enstrophy iso-surfaces for the WHALE 4415 pressure surface indicate that the fluid-flow structures that develop because of the leading edge sinusoids remain attached at both pre- and post-stall angles of attack, Figure 9.19. We would expect the fluid-flow structures to remain attached on the pressure surface because of the pressure field's effect. The distribution of stream-wise vorticity indicates that the profile camber has a stabilising effect on the flow-field structures. High-vorticity regions are confined to the WHALE 4415 profile leading edge. In contrast, we associated the WHALE 0015 profile with regions of high stream-wise vorticity that extend towards the trailing edge that then results in boundary layer disturbance over the entire pressure surface. Therefore, we may conclude that the leading edge sinusoids' stabilising effect on the flow-field around a cambered profile indicates that a sinusoidal leading edge has a more positive impact on cambered than un-cambered profiles.
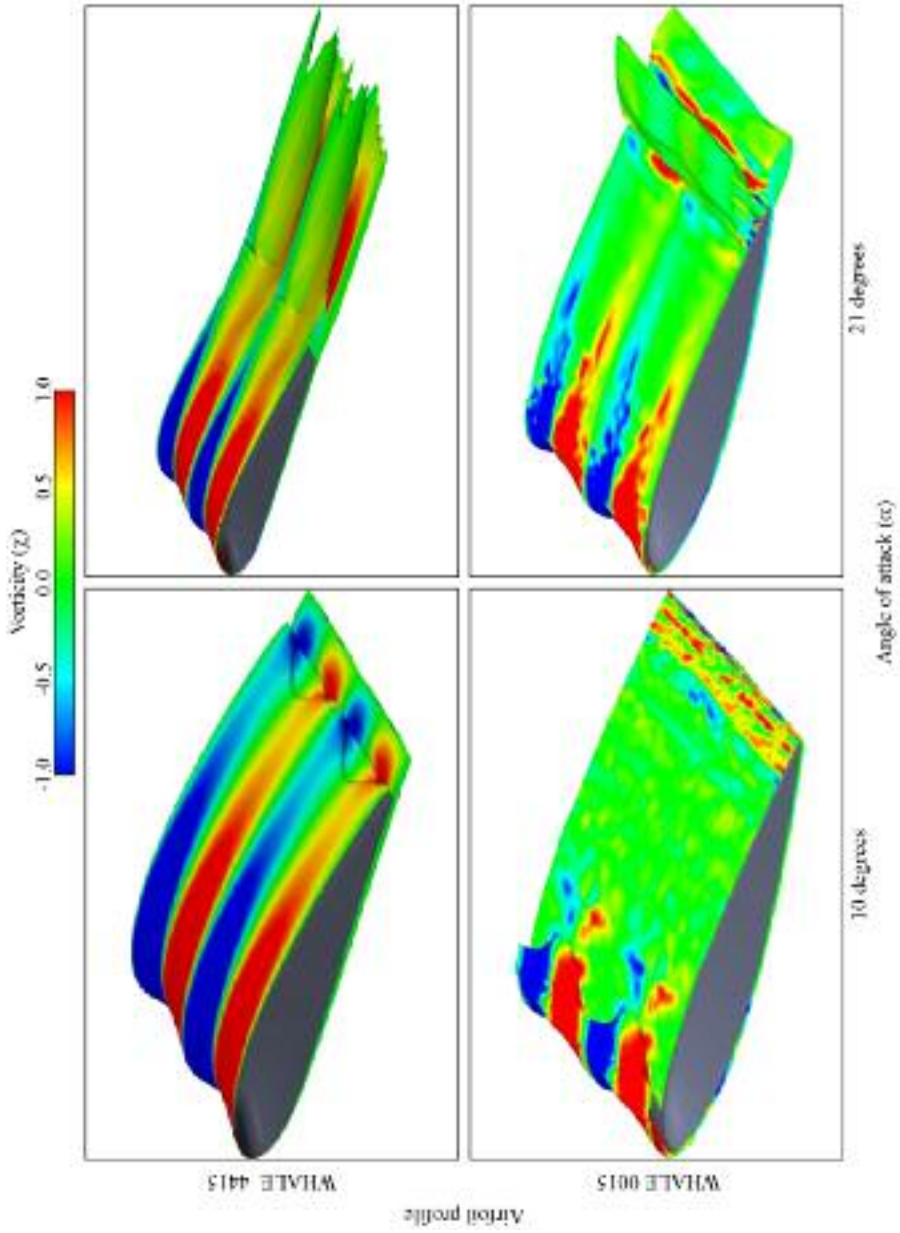
FIGURE 9.18. An isometric view of the blade suction side with enstrophy iso-surfaces at an angle of attack 10 degrees (left) and 21 degrees (right) for WHALE 4415 (top) and WHALE 0015 (bottom) profiles.
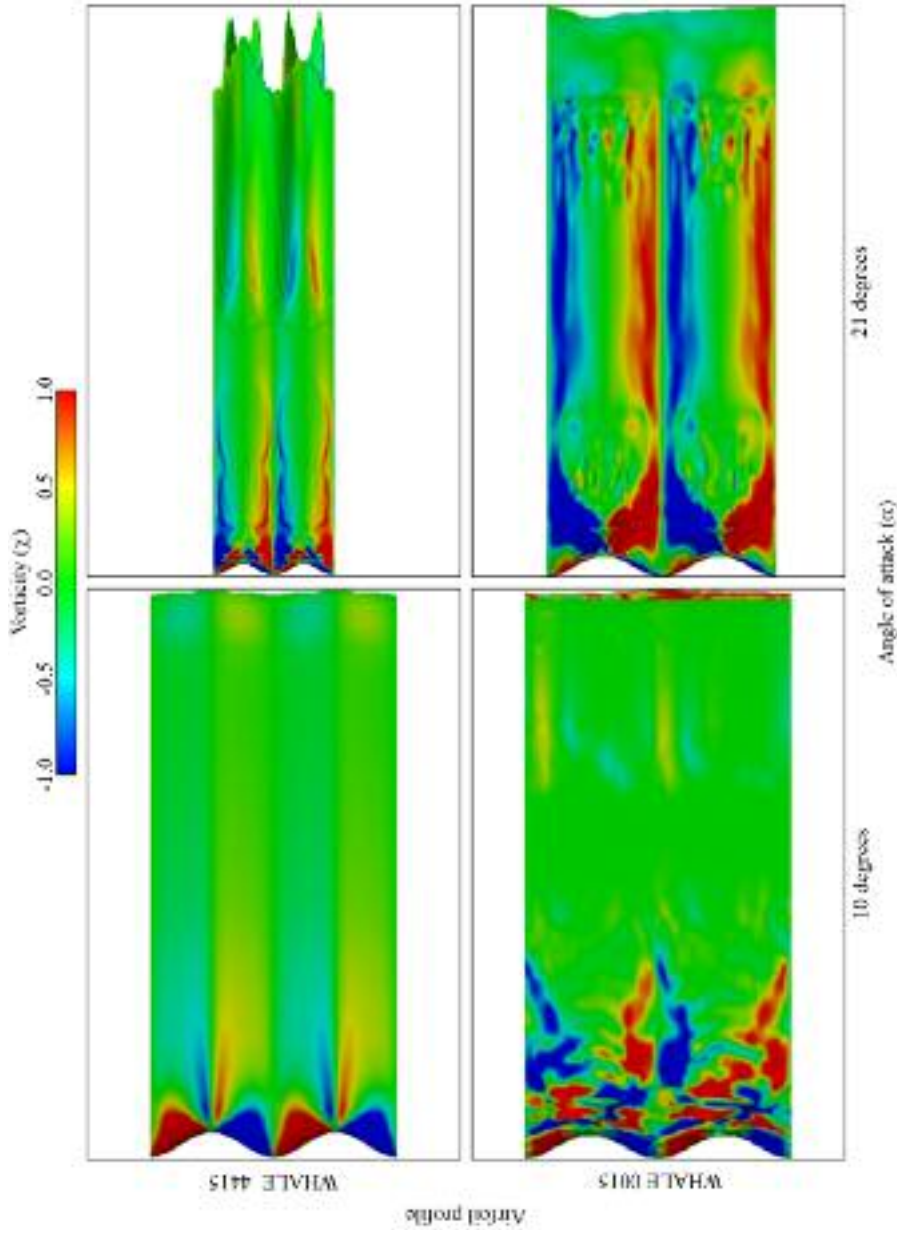
FIGURE 9.19. A plan view of pressure side with enstrophy iso-surfaces at an angle of attack 10 degrees (left) and 21 degrees (right) for WHALE 4415 (top) and WHALE 0015 (bottom) profiles.

CONCLUSIONS

This chapter presented a three-dimensional numerical study on sinusoidal leading edges' impact on cambered aerofoil profiles. We carried out the numerical study with the open source solver OpenFOAM using a cubic implementation of the k-ε turbulence model. The study provides insight into the influence of profile leading edge geometry at different operating conditions both pre- to post-stall.

We calculated the lift and drag of both cambered and un-cambered aerofoils. We also calculated the lift and drag of the same cambered and un-cambered aerofoils with a sinusoidal leading edge. Both cambered and un-cambered aerofoil lift coefficients changed as a consequence of introducing a sinusoidal leading edge. The cambered profile WHALE 4415 with a sinusoidal leading edge exhibited a 30 per cent increase in post-stall life compared to the same profile without a sinusoidal leading edge.

The increase in post-stall lift induced by a sinusoidal leading edge's presence occurs as a consequence of the leading edge geometry impacting the profile's velocity and vorticity fields. Peak and trough presence along the profile's leading edge induces vortex pairs at the leading edge that migrate from leading to trailing edge. These pairs suppress suction side separation at the trailing edge by confining the separation to trailing edge regions down-stream of a leading edge trough. By confining the separated flow at the trailing edge, the sinusoidal leading edge is able to minimise the extent of separated flow regions and thus improve profile post-stall lift.

REFERENCES

Bianchi, S., Corsini, A., Mazzucco, L., Monteleone, L., and Sheard, A.G. (2012), "Stall Inception, Evolution and Control in a Low Speed Axial Fan with Variable Pitch in Motion", *Transactions of the ASME, Journal of Engineering for Gas Turbines and Power*, vol. 134, paper no. 042602, pp. 1–10.

Corsini, A., and Rispoli, F. (2004), "Using Sweep to Extend the Stall-free Operational Range in Axial Fan Rotors", *Proceedings of the IMechE Part A, Journal of Power and Energy*, vol. 218, pp. 129–39.

Corsini, A., Delibra, G., and Sheard, A.G. (2013), "A Critical Review of Computational Methods and Their Application in Industrial Fan Design", *International Scholarly Research Network, Mechanical Engineering*, vol. 2013, article ID 625175, 20 pages.

Dewar, S.W., Watts, P., and Fish, F.E. (2009), "Turbine and Compressor Employing Tubercle Leading Edge Rotor Design", US Patent No. 20,090,074,578 A1, 19 March.

Drela, M. (1989), "XFoil: an Analysis and Design System for Low Reynolds Number Airfoils", *Lecture Notes in Engineering*, vol. 54, pp. 1–12.

Durbin, B. (2011), "Review: Adapting Scalar Turbulence Closure Models for Rotation and Curvature", *Transactions of the ASME, Journal of Fluids Engineering*, vol. 133(6), paper no. 061205, pp. 1–8.

Fish, F.E. (1993), "Influence of Hydrodynamic Design and Propulsive Mode on Mammalian Swimming Energetics", *Australian Journal of Zoology*, vol. 42, pp. 79–101.

Fish, F.E., and Battle, J.M. (1995), "Hydrodynamic Design of the Humpback Whale Flipper", *Journal of Morphology*, vol. 225, pp. 51–60.

Fish, F.E., Howle, L.E., and Murray, M.M. (2008), "Hydrodynamic Flow Control in Marine Mammals", *Integrative and Comparative Biology*, vol. 48(6), pp. 788–800.

Gravdahl, J.T., and Egeland, O. (1999), *Compressor Surge and Rotating Stall: Modelling and Control*, Springer, London, UK.

Hua, X., Gu, R., Jin, J., Liu, Y., Ma, Y., Cong, Q., and Zheng, Y. (2010), "Numerical Simulation and Aerodynamic Performance Comparison Between Seagull Aerofoil and NACA 4412 Aerofoil Under Low-Reynolds", *Advances in Natural Science*, vol. 3(2), pp. 244–50.

Jasak, H. (2010), "OpenFOAM: a Year in Review", *Proceedings of the Fifth OpenFOAM Workshop*, Gothenburg, Sweden, 21–24 June.

Johari, H., Henoch, C.W., Custodio, D., and Levshin, A. (2007), "Effects of Leading-edge Protuberances on Airfoil Performance", *AIAA Journal*, vol. 45(11), pp. 2634–42.

Kroger, G., Vob, C., Nicke, E., and Cornelius, C. (2011), "Theory and Application of Axisymmetric End-wall Contouring for Compressors", *Proceedings of the 56th American Society of Mechanical Engineers Gas Turbine and Aeroengine Congress*, Vancouver, BC, Canada, 6–10 June, paper no. GT2011-45624.

Langston, L.S. (2009), "Fitting a Pitch", *ASME Mechanical Engineering Magazine*, vol. 131(12), pp.38–42.

Launder, B.E., and Sharma, B.R. (1974), "Application of the Energy-dissipation Model of Turbulence to the Calculation of Flow Near a Spinning Disc", *Letters in Heat and Mass Transfer*, vol. 1, pp. 131–8.

Lien, F.S., and Leschziner, M.A. (1994), "Assessment of Turbulence-transport Models Including Non-linear RNG Eddy-viscosity Formulation and Second-moment Closure for Flow Over a Backward-facing Step", *Computational Fluids*, vol. 23,pp. 983–1004.

Liu, Y., Dhingra, M., and Prasad, J.V.R. (2009), "Active Compressor Stability Management via a Stall Margin Control Mode", *Proceedings of the 54th American Society of Mechanical Engineers Gas Turbine and Aeroengine Congress*, Orlando, FL, USA, 8–12 June, paper no. GT2009-60140.

Miklosovic, D.S., Murray, M.M., Howle, L.E., and Fish, F.E. (2004), "Leading-edge Tubercles Delay Stall on Humpback Whale (*Megaptera novaeangliae*) Flippers", *Physics of Fluids*, vol. 16(5), pp. L39–L42.

Miklosovic, D.S., Murray, M.M., and Howle, L.E. (2007), "Experimental Evaluation of Sinusoidal Leading Edges", *Journal of Aircraft*, vol. 44, pp. 1404–8.

Paduano, J.D., Greitzer, E.M., and Epstein, A.H. (2001), "Compression System Stability and Active Control", *Annual Review of Fluid Mechanics*, vol. 33, pp. 491–517.

Pedro, H.T.C., and Kobayashi, M.H. (2008), "Numerical Study of Stall Delay on Humpback Whale Flippers", *46th AIAA Aerospace Sciences Meeting and Exhibit*, Reno, NV, USA, 7–10 January.

Rusak, Z., and Morris, W.J. (2011), "Stall Onset on Airfoils at Moderately High Reynolds Number Flows", *Transactions of the ASME, Journal of Fluids Engineering*, vol. 133(11), paper no. 111104, pp. 1–12.

Sheard, A.G., and Corsini, A. (2012), "The Mechanical Impact of Aerodynamic Stall on Tunnel Ventilation Fans", *International Journal of Rotating Machinery*, vol. 2012, paper no. 402763, pp. 1–12.

Sheard, A.G., Corsini, A., and Bianchi, S. (2011), "Stall Warning in a Low-speed Axial Fan by Visualisation of Sound Signals", *Transactions of the ASME, Journal of Engineering for Gas Turbines and Power*, vol. 133, paper no. 041601, pp. 1–10.

Sheard, A.G., Tortora, C., Corsini, A., and Bianchi, S. (2014), "The Role of Variable Pitch in Motion Blades and Variable Rotational Speed in an Industrial Fan Stall", *Proceedings of the IMechE Part A, Journal of Power and Energy*, vol. 228, pp. 272–84.

Sheldahl, R.E., and Klimas, P.C. (1981), "Aerodynamic Characteristics of Seven Symmetrical Airfoil Sections Through 180-degrees Angle of Attack for Use in Aerodynamic Analysis of Vertical Axis Wind Turbines", Sandia National Laboratories Energy Report SAND80-2114, Sandia National Laboratories, Albuquerque, NM, USA.

Shyy, W., Lian, Y., Tang, J., Viieru, D., and Liu, H. (2008), *Aerodynamics of Low Reynolds Number Flyers*, Cambridge University Press, Cambridge, UK.

van Nierop, E.A., Alben, S., and Brenner, M.P. (2008), "How Bumps on the Whale Flippers Delay Stall: an Aerodynamic Model", *Physical Review Letters*, vol. 100, p. 054502.

Weichert, S., and Day, I. (2012), "Detailed Measurements of Spike Formation in an Axial Compressor", *Proceedings of the 57th American Society of Mechanical Engineers Gas Turbine and Aeroengine Congress*, Copenhagen, Denmark, 11–15 June, paper no. GT2012-68627.

White, E.R., and Miller, T.F. (2010), "A Serendipitous Application of Super cavitation Theory to the Water-running Basilisk Lizard", *Transactions of the ASME, Journal of Fluids Engineering*, vol. 132(5), paper no. 054501, pp. 1–7.

The Application of Sinusoidal Blade Leading Edges in a Fan Design Methodology to Improve Stall Resistance

A. Corsini, G. Delibra, and A.G. Sheard

ABSTRACT

Taking inspiration from previous biomimetic studies on the performance of humpback pectoral fins, this chapter reports a programme of work to design a 'whale-fan' that incorporates a sinusoidal leading edge blade profile that mimics the tubercles on humpback whales pectoral fins. Previous researchers have used two-dimensional cascades of aerofoils to study the effects of a sinusoidal profile on aerofoil lift and drag performance. The research was primarily concerned with elucidating the fluid-flow mechanisms induced by the sinusoidal profile, and the impact of those mechanisms on aerofoil performance. The results indicate that a sinusoidal leading edge profile has improved lift recovery post-stall, and thus, is inherently more aerodynamically resistant to the effect of stall.

The reported research focuses on the application of previous research conducted with infinite span cascades of aerofoils to the design and optimisation of a finite span aerofoil. The chapter presents the assumptions when developing a three-dimensional aerofoil design methodology that correlates the blade leading edge's sinusoidal profile with the desired vorticity distribution at the trailing edge. We apply the developed methodology to the design of a fan blade's tip region to control separation at the trailing edge. The chapter presents numerically derived whale-fan performance characteristics, and compares them with both the baseline fan's numerically and experimentally derived performance characteristics.

NOMENCLATURE

Latin letters

c	chord	mm
C_p	static pressure coefficient	
D_t	tip diameter	mm
DF	diffusion factor	
k	turbulent kinetic energy	
ℓ	blade chord	mm
Ma	Mach number	
p	static pressure	Pa
p_{tot}	total pressure	Pa
Q	volume flow rate	m³/s
QUICK	Quadratic Upwind Interpolation Convection Kinematics scheme	
RANS	Reynolds-averaged Navier–Stokes	mm
r_c	casing radius	
Re	Reynolds number, $Re = V_{tip}D_t/n$	
V	local velocity	
V_{tip}	tip velocity	
V^{tg}	tangential velocity	
V^{tg}_{in}	tangential velocity at the inflow	
V^*	normalised velocity	
V^*_{ax}	normalised axial velocity	
V^*_{rad}	normalised radial velocity	
w	relative velocity	
y^+	non-dimensional wall distance	

Greek letters

γ	blade angle
Δp	static pressure rise
Δp_{tot}	total pressure rise
ζ	total pressure loss coefficient
η	efficiency
ν_t	turbulent viscosity
ν	kinematic viscosity
Σ	blade solidity
χ	tip clearance
ω	vorticity

INTRODUCTION

Industrial fan design intended for application in mass transit systems is made challenging by an increasingly demanding regulatory framework. The European Norm EN 12101-3 (2002) and international standard ISO 21927-3 (2006) require in-

dependent testing of tunnel ventilation fans which must have the capability to clear smoke at elevated temperatures in the event of a tunnel fire (Sheard and Jones, 2008, 2012). A requirement to operate at elevated temperatures results in a more conservative fan mechanical design. This consequently lowers aerodynamic efficiency.

Tunnel ventilation fans are typically 'dual use' intended for both emergency operation to clear smoke in the event of a fire and routine operation to ventilate a tunnel system on a day-to-day basis. A legal requirement to comply with EN 12101-3 does not release industrial fan designers from an obligation to also comply with the European Union Regulation 327. This sets minimum Fan and Motor Efficiency Grades (FMEGs) for industrial fans and is intended to reduce tunnel ventilation systems' carbon footprints.

An unintended consequence of EN 12101-3 and ISO 21927-3 requirements is to reduce fan efficiency during routine operation. This is in direct conflict with Regulation 327. This conflict is within the context of a trend toward railway tunnels and metro systems that are both longer and deeper, therefore requiring ventilation fans capable of developing a higher pressure for a given flow rate. A shift towards higher speed trains in railway tunnels and the use of platform screen doors in metro systems further compounds the situation. Both result in a significant increase in the magnitude of pressure pulses imposed upon ventilation fans as a train first approaches and then moves away from the ventilation shaft within which they are situated. The combined effect of higher pressure and increased magnitude of pressure pulses is to increase the risk that a tunnel ventilation fan will be driven into aerodynamic stall (Borello *et al.*, 2013a). Aerodynamic stall results in increased unsteady aerodynamic loads on rotating mechanical components that produce increased mechanical stress and therefore a consequential risk of mechanical failure.

Tunnel ventilation fans have historically incorporated blade designs that are aerodynamically lightly loaded. Aerodynamically lightly loaded blade designs exhibit a continually rising characteristic back to zero flow. They do not suffer from the limiting phenomena that researchers classically associate with aerodynamic stall of more heavily loaded fans and compressors. When a lightly loaded tunnel ventilation fan is subjected to a large pressure pulse, there is almost no excitation and unsteady aerodynamic forces on fan blades remain almost constant. Consequently, unsteady mechanical forces on the blades also remain almost constant and there is low risk of mechanical blade failure. The market trend towards higher pressures at a given flow rate requires a shift to blade designs that are aerodynamically more heavily loaded, and therefore are prone to aerodynamic stall. Further, the market trend towards larger pressure pulses increases the risk that a fan will be transiently driven into stall during each pressure pulse.

Within the industrial fan community, tunnel ventilation fan blades are typically based on 1950s NACA designed aerofoil profiles. These profiles classically exhibit increased loss with increased loading, and consequently, more heavily loaded tunnel ventilation fans typically have a lower aerodynamic efficiency than more lightly loaded designs. The industrial fan community is in the process of adopting the computational methods used within the aerospace fan community that facilitate the design of both heavily loaded and high-efficiency fans (Corsini *et al.*, 2013a). The new

regulatory requirement for improved fan and motor efficiency is primarily driving this adoption. Therefore, the new regulatory and market environment places two separate but linked demands on industrial fan designers:

(i)   Design aerodynamically more heavily loaded blades than has been the historic norm that result in a tunnel ventilation fan with high enough pressure developing capability to meet market requirements whilst reaching the minimum efficiency required by Regulation 327, with a mechanical design that enables the fan to operate at an elevated temperature in accord with EN 12101-3 and ISO 21927-3.

(ii)   As aerodynamically more highly loaded blades are prone to aerodynamic stall, ensure that the resulting fan design avoids in-service mechanical failure as a consequence of inadvertently operating the fan in or transiently driving it into aerodynamic stall.

We focus on the second of these demands in this chapter. The industrial fan community has an interest in design methodologies that facilitate tunnel ventilation fan design that is intrinsically stall tolerant. Within the context of industrial fan design the term 'stall tolerant' refers to an aerodynamic design that will induce lower alternating mechanical stresses in fan rotating components during stalled operation.

Researchers have studied the evolution of rotating stall (Cumpsty, 2004; Weichert and Day, 2012). They do not fully understand it despite some success in developing new stall detection techniques derived from understanding the physical flow mechanisms associated with stall inception (Gravdahl and Egeland, 1999; Sheard *et al.*, 2011). For industrial fan designers, stall control is critical to developing intrinsically stall tolerant design methodologies.

Fan designers have historically utilised both active and passive stall control techniques, with the most widely adopted within the industrial fan community being the 'anti-stall' stabilisation ring (Bianchi *et al.*, 2013). The stabilisation ring comprises a ring of guide vanes fitted in the fan casing immediately upstream of the fan blade leading edge. The stabilisation ring's effect is to stabilise a fan's characteristic, such that it rises continuously back to zero flow. A disadvantage of the stabilisation ring is that it typically reduces fan efficiency by three per cent. The advent of the more stringent Regulation 327 fan and motor efficiency grades within Europe from 1 January, 2015, is expected to render the stabilisation ring obsolete as a consequence of its negative impact on fan efficiency.

Designers have also used variable pitch in motion blades when developing fans for aerospace application (Langston, 2009) and also in industrial fan applications with a constant pressure element (Bianchi *et al.*, 2012). In such applications a fixed pitch, variable speed fan will inevitably stall during each starting and stopping transient and is therefore likely to suffer an in-service mechanical failure (Sheard and Corsini, 2012).

The industrial fan community has utilised widely passive stall control techniques. Researchers have focused on the development of three-dimensional blade concepts (Corsini and Rispoli, 2004), and end-wall contouring (Kröger *et al.*, 2011).

Some researchers have used biomimicry as the basis of a novel stall control blade design methodology, with the objective of producing aerofoil designs that are inherently 'stall tolerant'. Although many of the stall tolerant examples of natural flyers are associated with Reynolds numbers that are too low to be of use in turbomachinery applications (Shyy *et al.*, 2007), a possible source of inspiration is the humpback whale (Fish, 1993). The humpback whale is able to perform sharp turns whilst hunting, with researchers associating this ability with the presence of approximately ten tubercles along the leading edge of the humpback whale's pectoral fins (Fish and Battle, 1995; Fish *et al.*, 2008).

A number of scholars have studied the lift and drag performance of aerofoils with sinusoidal leading edge profiles developed to mimic the shape of tubercles (Miklosovic *et al.*, 2004, 2007; Johari *et al.*, 2007; Pedro and Kobayashi, 2008; van Nierop *et al.*, 2008). These researches have focused their work on sinusoidal profiles as applied to symmetrical un-cambered aerofoils with an infinite span. The reported research elucidates the improvement in lift and drag performance associated with the presence of the studied sinusoidal profiles. Specifically, the sinusoidal leading edge geometry increases lift recovery after stall, and consequently, the transition from stable to stalled operation is less abrupt. The sinusoidal profile's wavelength has a second order effect on lift and drag, but the amplitude of sinusoids directly affects aerofoil lift, drag and the blade angle at which an aerofoil stalls (van Nierop *et al.*, 2008).

Miklosovic *et al.* (2007) studied the performance of finite span aircraft wing aerofoils with a sinusoidal leading edge wing profile. They concluded that the result was a wing with better post-stall lift recovery than that achieved by the same profile when studied as an infinite span profile. Corsini *et al.* (2013b) studied an infinite span industrial fan blade profile's performance with sinusoidal leading edge blade profile. They conducted their research on a cambered blade profile, with the combined effect of a sinusoidal leading edge and camber resulting in a superior lift and drag performance to that reported by previous researchers who had studied infinite span un-cambered profiles.

Corsini *et al.*'s research (2013b) demonstrated that the beneficial effects of a sinusoidal leading edge blade profile increase when applied to a cambered aerofoil. Corsini *et al.* (2013b) observed that the primary aerodynamic mechanism, driven by a sinusoidal leading edge blade profile's presence, was a low-pressure core formation on the blade suction surface at each sinusoid's trough. This trough draws fluid from the aerofoil pressure surface, and induces span-wise vorticity that results in the creation of counter-rotating vortices as the flow travels from the aerofoil suction surface's leading to trailing edge. The impact of these counter-rotating vortices is to assist the trailing edge flow to remain attached in those span-wise sections that correspond to a leading edge sinusoid's peak. By assisting the flow to remain attached, the separated flow associated with stalled operation is confined to the trailing edge regions that correspond with a sinusoid trough. By confining trailing edge separated flow to a sinusoid trough, the aerofoil is able to operate at a higher blade angle before stalling and suffers a less severe reduction in lift during stall.

Building on Corsini *et al.*'s work (2013b), the research in this chapter focuses on developing a design methodology that incorporates a sinusoidal leading edge

blade profile in a three-dimensional fan blade (Sheard *et al.*, 2012). The following sections first describe the fan that we used as a baseline for the present study. We then present the design process associated with applying a sinusoidal leading edge blade profile and describe the adopted computational methodology. We present numerically derived whale-fan performance characteristics and compare them with the baseline fan's numerically and experimentally derived performance characteristics. The chapter concludes with a summary of the impact of the sinusoidal leading edge blade profile on fan performance and implications for tunnel ventilation fan design praxis.

DESCRIPTION OF THE TEST CASE

We conducted the reported research on an axial fan, named JFM, developed for application in metropolitan metro and railway tunnel ventilation systems, Table 10.1. Tunnel ventilation system fans are typically between 1.6 metres and 2.8 metres in diameter, with 1.8 and 2.0 metre diameter fans running at 1,500 revolutions per minute the most common size and speed selections. The studied fan is 2.24 metres in diameter, running at 1,500 revolutions per minute and therefore has a blade tip speed of 175 metres per second. Sheard and Daneshkhah (2012) considered the practicality of developing a 2.5 metre diameter tunnel ventilation fan operating at 1,500 revolutions per minute, and therefore having a blade tip speed of 196 metres per second. They evaluated the potential of three new tunnel ventilation fan concepts and rejected a 2.5 metre diameter fan running at 1,500 revolutions per second because of the high noise level that occurs with the increase in blade tip speed. Consequently, the studied fan's

Table 10.1. *Fan range geometry and operating point data.*

	Hub	Tip
Performance standard	ISO 5801	
Volume flow rate, Q	10–$300 \ m^3/s$	
Total pressure rise, Δp_{tot}	500–3,000 Pa	
Rotational speed	1,500 rpm	
Reynolds number, Re (based on tip diameter)	26×10^6	
Mach number, Ma (at the blade tip)	0.55	
High-temperature certification	400°C	
Blade section	ARA-D	
Tip diameter, D_t	2,240 mm	
Blade count	16	
Hub-to-tip ratio	0.5	
tip gap, χ	6.5% of the blade span	
	Hub	*Tip*
Chord, c	143 mm	92.5 mm
Solidity, Σ	0.64	0.21
Blade angle, γ	48°	24°

blade tip speed may be a practical limit for fans intended for application in mass transit ventilation systems.

In the programme of work reported in this chapter, we established the JFM fan's performance experimentally at four blade angle settings, 8, 16, 24 and 32 degrees. We conducted the tests in accordance with the ISO 5801 standard (equivalent to BS 848 Part 1) (ISO 5801:2007, 2007) for a fully ducted configuration and installation type D, Figure 10.1. The JFM fan has characteristics typical of those intended for application in mass transit ventilation systems. With a blade angle of 8 degrees, the fan exhibits a continuously rising characteristic back to near zero flow, Figure 10.1. This 'non-stalling' characteristic is typical of lightly loaded tunnel ventilation fans, and some tunnel ventilation applications still use fans with a non-stalling blade angle where the ventilation system designers are particularly conservative. When one increases the blade angle to 16 degrees the fan characteristic flattens as flow reduces. The blade loading is now just high enough to result in a fan characteristic that shows signs of aerodynamic stall. At blade angles of both 24 and 32 degrees, the fan characteristic reaches a peak, and then falls with reducing flow rate, indicating that the blade loading is now high enough to result in aerodynamic stall.

When one studies the JFM's power characteristics, it is evident that fan efficiency with a blade angle of 32 degrees is significantly lower than at a blade angle of 24 degrees, Figure 10.1. The JFM fan's peak pressure developing capability is approximately the same with both a 24 and 32 degree blade angle, indicating a blade angle of 24 degrees gives the maximum pressure rise with optimum efficiency. We therefore conducted the computational analysis with a blade angle of 24 degrees and selected four operating points:

(i) design point flow, 150 m³/s;
(ii) near-peak pressure flow, 130 m³/s;
(iii) peak pressure flow, 110 m³/s; and
(iv) stalled flow, 95 m³/s.

Sinusoidal leading edge profile design

The term biomimicry refers to the practice of taking concepts from nature and applying them to solve technical problems. Corsini *et al.* (2013b) were the first within the industrial fan community to apply the concept of tubercles on humpback whales pectoral fins to blade profiles. They studied blade performance in a two-dimensional infinite span cascade. Corsini *et al.* (2013b) demonstrated that the presence of the tubercles on the blade leading edge improved lift recovery post-stall, which resulted in a blade that was inherently more aerodynamically resistant to the effect of stall.

The combination of high blade tip speed and compromised blade aerodynamic design results in the JFM fan suffering a particularly dramatic loss of aerodynamic lift post-stall when the blade angle is 24 or 32 degrees, Figure 10.1. This loss post-stall makes the JFM fan a suitable candidate for the application of tubercles as they
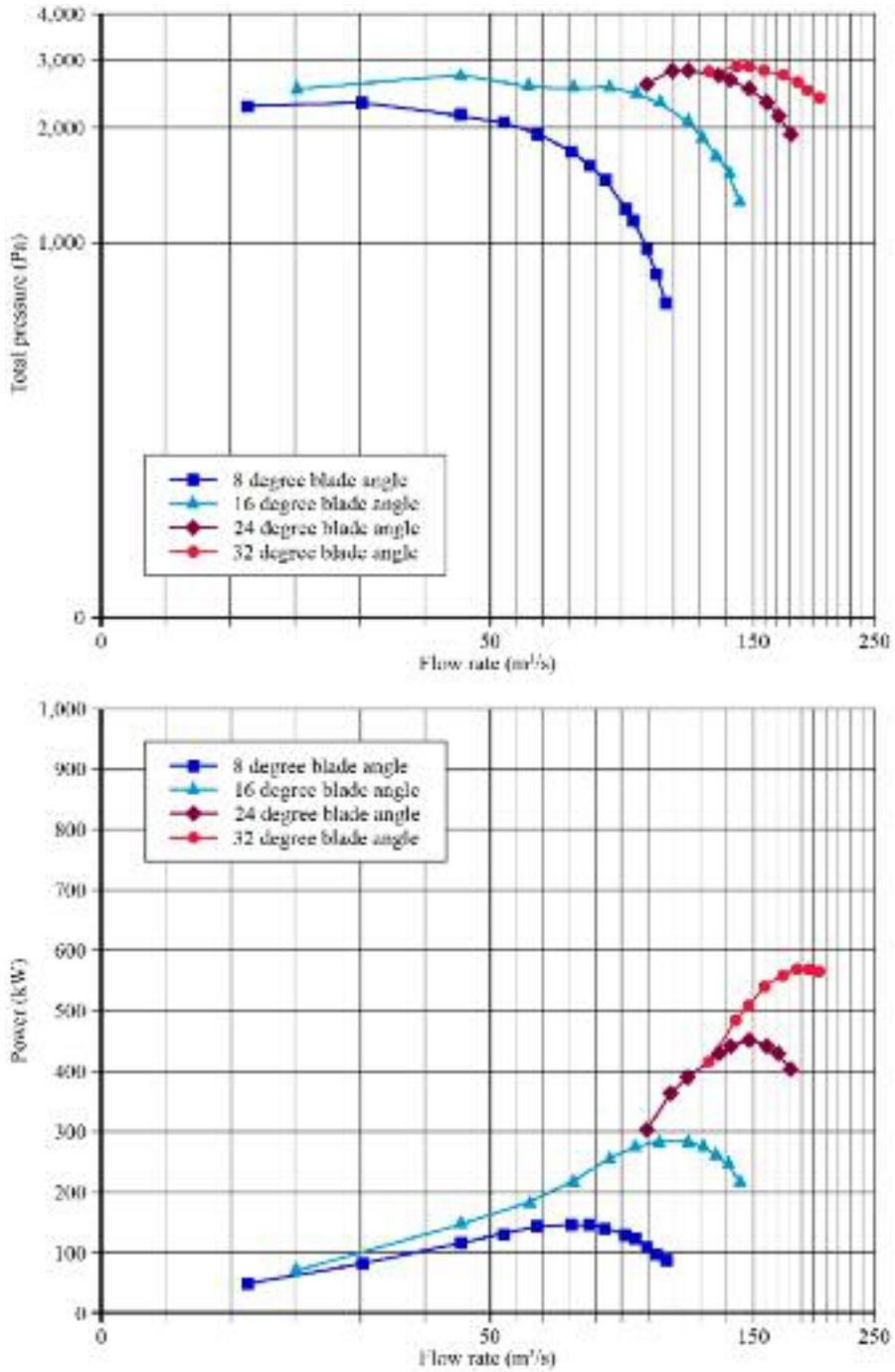
FIGURE 10.1. The experimentally measured performance of the JFM fan. The studied blade angle is 24 degrees.

improve lift recovery post-stall and should therefore reduce the stall's severity. When considering how to extend Corsini *et al.*'s work (2013b) from a two-dimensional infinite span cascade study to a three-dimensional finite span aerofoil design methodology, we made the following assumptions:

- applying a sinusoidal leading edge blade profile enhances the existing blade design methodology, and therefore we applied it to the already existing JFM fan blade; and
- the JFM fan blade is 'tip limited' with rotating stall initiating in the blade's tip region. Therefore we confined applying a sinusoidal leading edge blade profile to the blade tip region.

The first assumption results in an unaltered fan blade profile, camber, twist distributions and span-wise work distribution. The second assumption results in the design methodology being applicable to tip limited blade designs only.

The above assumptions constitute a way to constrain the variables associated with the transition from a two-dimensional infinite span cascade study to a three-dimensional finite span aerofoil design methodology. The assumptions are not ideal as the role of the blade hub region during fan stall is effectively ignored. However, a preliminary study of the practicality associated with adding a sinusoidal leading edge blade profile in the blade root region indicated that it would be challenging. The blade root region is associated with high mechanical stress levels, with a sinusoidal leading edge blade profile introducing mechanical features with associated stress concentration factors that would go on to result in in-service fatigue issues. We therefore accepted the above assumptions as the basis for the reported research.

We accomplished control of separation at the blade tip by following Johari *et al.*'s (2007) and Corsini *et al.*'s (2013b) approach of applying a sinusoidal leading edge blade profile by scaling, but not modifying aerofoil geometry. Therefore, we can characterise the resultant design process as a sinusoidal leading edge design process based around the variation of three parameters:

- the number of sinusoids, starting from the blade tip;
- the sinusoid wavelength as a percentage of blade span; and
- the sinusoid amplitude as a percentage of blade chord.

We developed the reported sinusoidal blade leading edge design methodology by utilising the results of a large eddy simulation conducted on the JFM fan by Borello *et al.* (2013b). We used Borello *et al.*'s (2013b) results to assist in defining the number of sinusoids, the sinusoid wavelength and amplitude. First, we used Borello *et al.*'s (2013b) results to calculate the JFM fan's diffusion factor (*DF*) based on Lieblein's definition, but unlike Lieblein, we used local quantities. By defining diffusion factor based on local quantities, we were able derive information about the mixing process downstream of the JFM fan. We define local diffusion factor (*DF*) as:

$$DF = 1 - \frac{V}{V_{in}} + \frac{V^{tg} - V_{in}^{tg}}{2\Sigma V_{in}}$$

where Σ is the fan's solidity, V is the local velocity, V^{tg} is the tangential velocity and the '*in*' subscript refers to average values at the inflow. Contours of diffusion factor at the 110 m^3/s peak pressure operating point 20 per cent blade chord downstream of the blade trailing edge identify the blade tip leakage vortex as a high diffusion core at approximately 90 per cent blade span, Figure 10.2. Diffusion factor falls close to zero over the outer 20 per cent of the blade span, indicating that the blade is close to stall.

If one accepts that when stall is incipient blade aerodynamic performance is influenced over the outer 20 per cent of blade span, then it is also reasonable to accept that one should apply the sinusoidal leading edge blade profile to the outer 20 per cent of the blade. Having fixed the blade span over which one would apply the sinusoidal leading edge at 20 per cent, we generated the leading edge geometry with three, four and five sinusoids. The resultant geometry with four or five sinusoids was close to what Corsini *et al.* (2013b) considered optimum, and therefore we abandoned the geometry with three sinusoids.

A decision to start the sinusoid with a peak or a trough at the blade tip drove the final choice of number of sinusoids. In the reported research we chose to start with a sinusoid peak at the blade tip as this avoided reducing chord at the blade tip. By choosing to start the sinusoid with a peak, the number of sinusoids over the outer 20 per cent of blade span increased by half, and therefore the number of sinusoids that we chose was four and a half as it was between four and five, the optimum number which Corsini *et al.* (2013b) identified. The resultant sinusoidal wavelength was five per cent of blade span.

We chose the sinusoids' amplitude via a consideration of the JFM fan flow-field's relative velocity magnitude 20 and 40 per cent blade chord upstream of the blade trailing edge as calculated by Borello *et al.* (2013b), Figure 10.3. The sinusoids' amplitude influences the intensity of the counter-rotating vortex's induced in the flow by the sinusoids' presence. Corsini *et al.* (2013b) studied the impact of sinusoid amplitude and evaluated its effect on pre-stall drag and post-stall lift recovery. Given the JFM fan's relative velocity magnitude, application of Corsini *et al.*'s (2013b) method indicates that a three per cent blade chord sinusoidal amplitude will optimise post-stall lift recovery, whilst minimising the pre-stall increase in drag.

The final blade geometry comprised four and a half sinusoids over the outer 20 per cent of the blade span, with a resultant sinusoidal wavelength of five per cent blade span and sinusoidal amplitude of three per cent blade chord. The final realisation of the sinusoidal leading edge blade profile incorporated minor variations in the twist of each sinusoidal blade section to maintain the same blade twist as the JFM fan blade with varying span-wise chord. We named the JFM fan when incorporating the sinusoidal leading edge blade JWFM, Figure 10.4.

NUMERICAL TECHNIQUE

We undertook the computational analysis of the JFM and JWFM fans using the open source finite volume Computational Fluid Dynamics (CFD) code OpenFOAM 2.1.x written in C++ (Weller *et al.*, 1998). The code solves the Reynolds-averaged
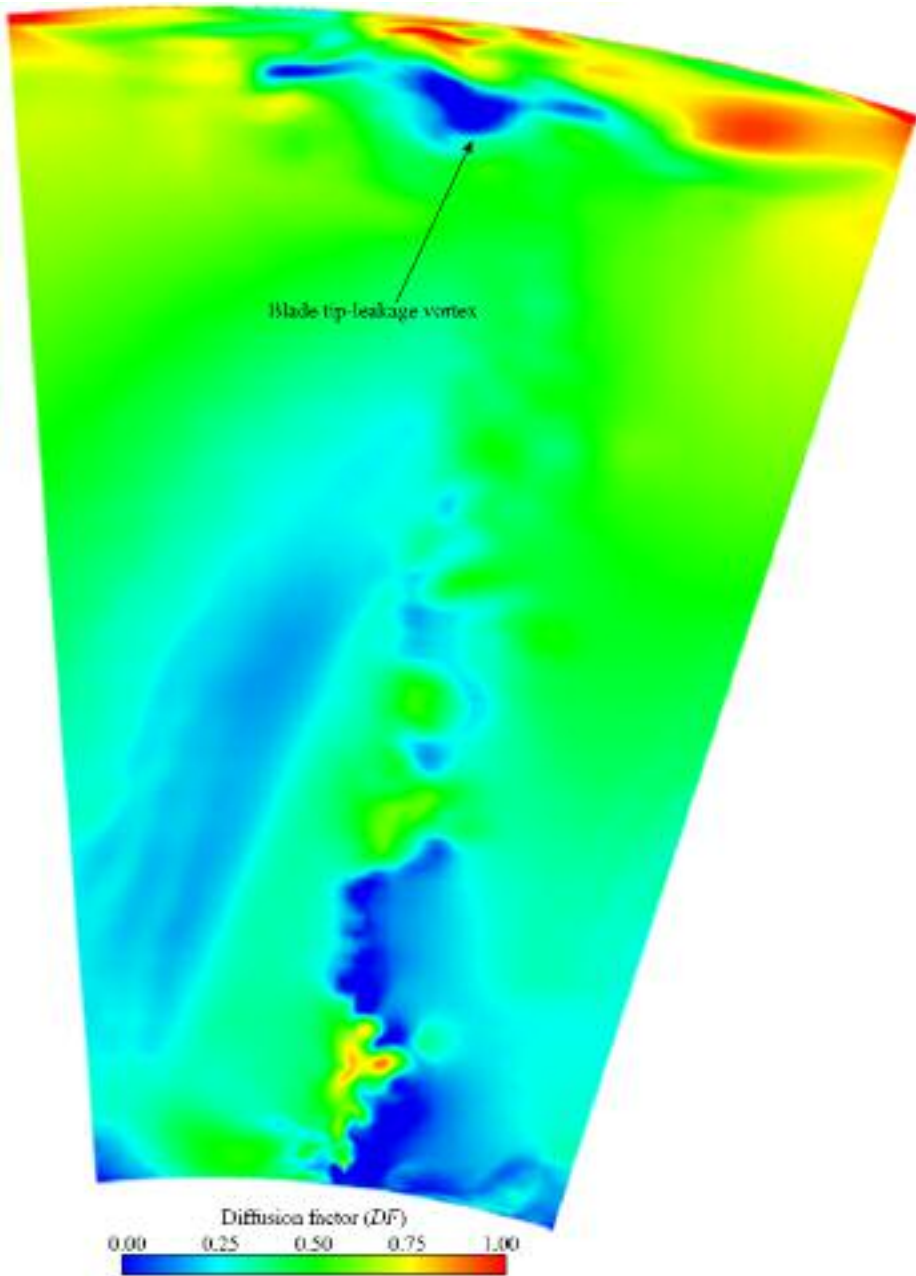
FIGURE 10.2. Contours of local diffusion factor (*DF*) for the JFM fan, 20 per cent blade chord downstream of the blade trailing edge at the 110 m^3/s peak pressure operating point, from Borello *et al.* (2013b). Diffusion factor falls close to zero over the outer 20 per cent of the blade span.
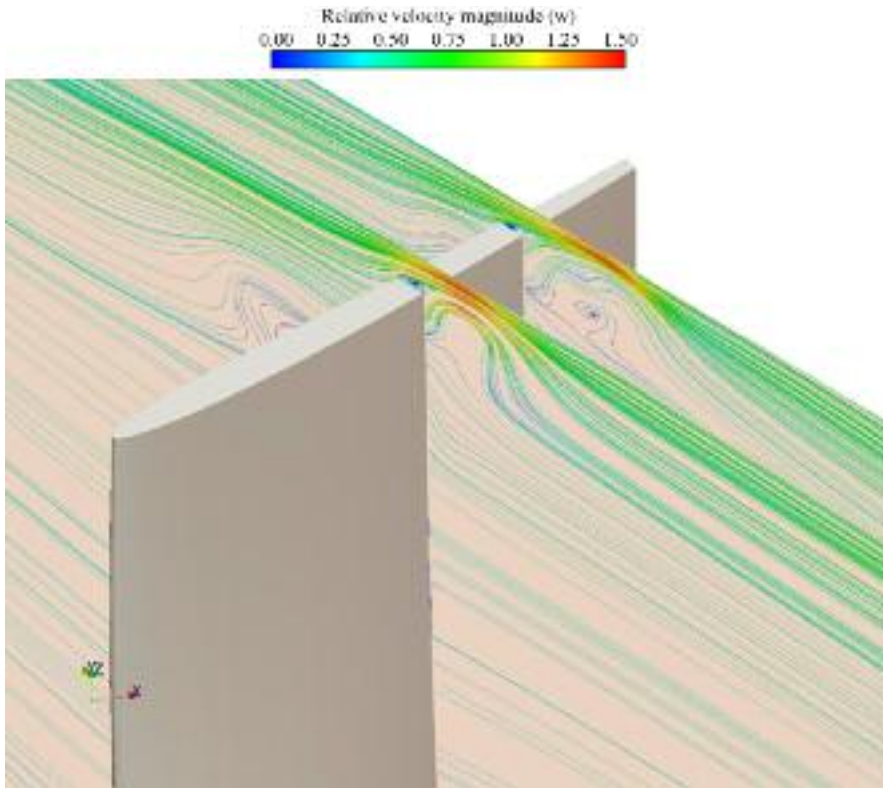
FIGURE 10.3. Contours of relative velocity magnitude (w) for the JFM fan 20 and 40 per cent blade chord upstream from the blade trailing edge, from Borello *et al.* (2013b). The relative velocity magnitude contours illustrate the evolution of the tip leakage vortex.

Navier–Stokes (RANS) incompressible equations in the rotating frame of reference, taking into account Coriolis and centrifugal terms in the momentum equations. We used an incompressible solver despite local Mach number at the blade tip exceeding 0.5. The rationale for using an incompressible solver was that the pressure-rise through the fan was no more than 3,000 Pa, low enough to avoid variations in density significant enough to affect the blade-to-blade velocity field.

The turbulence closure that we used in the simulation was the non-linear k-e model in its cubic formulation with a low Reynolds number wall treatment (Lien and Leschziner, 1994). We used a cubic eddy viscosity turbulence model to partially account for the anisotropy of the Reynolds stresses, thus giving better performance in impingement and recirculating regions and additionally, partially accounting for streamline curvature over surfaces.

Other scholars have established the robustness of the adopted approach when analysing an industrial fan's blade-to-blade flow-field with similar Reynolds and Mach numbers. They have conducted both benchmarking exercises (Lien and Leschziner, 1994; Durbin, 2011) and also applied the approach in fully three-dimensional blade
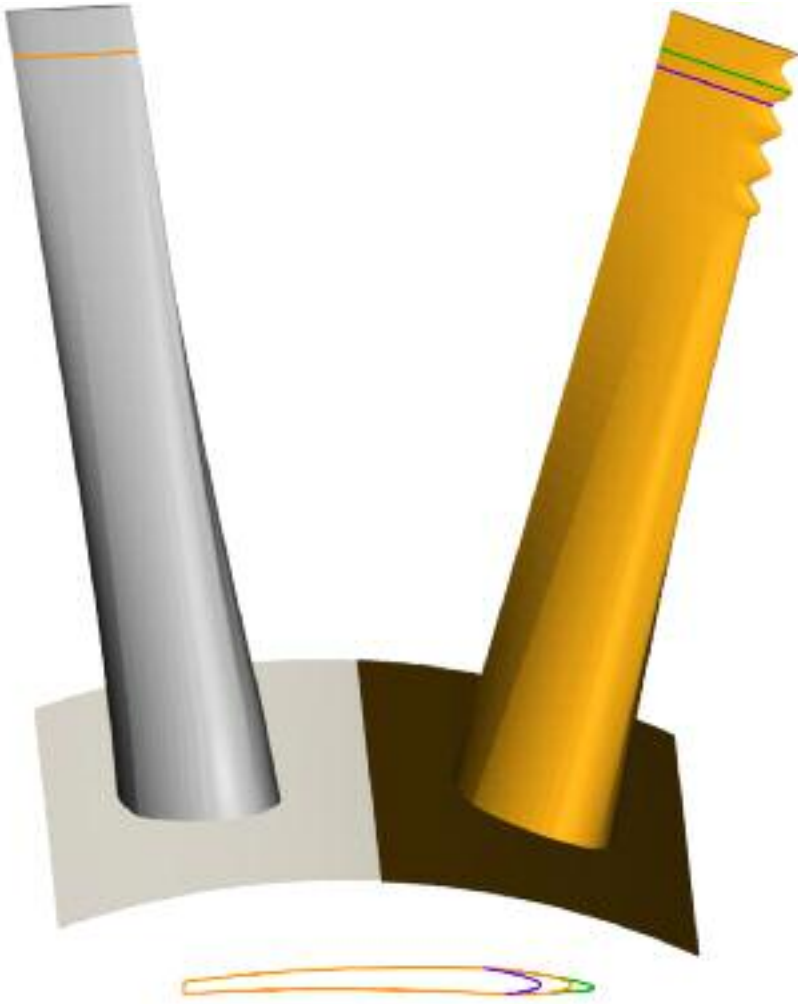
FIGURE 10.4. Three-dimensional computer aided design models of the JFM fan blade (left) and the JWFM fan blade (right). Below the models is an illustration of the JFM blade's tip cross-section and the JWFM blade peak and trough cross-sections.

design applications (Corsini and Rispoli, 2005). A common conclusion was that the approach reproduces three-dimensional flow structures well, and is therefore inherently suitable for predicting the flow-field features induced by the presence of a sinusoidal leading edge blade profile.

Corsini *et al.* (2013b) specifically considered the suitability of the chosen numerical approach. They observed that the formulation models eddy viscosity as a third order function of the rate of strain. Thus, the modelling approach overcomes the classical limits of the k-e turbulence model, minimising the tendency for over-production of k in impingement zones and separation flow regions (Lien and

Leschziner, 1994). Corsini *et al.* (2006) provide a more complete review of the modelling approach. Another article (Durbin, 2011) offers a more complete analysis of cubic and linear eddy viscosity models for turbomachinery applications.

The numerical solution is based on the use of a central difference scheme to discretise the convective terms into momentum equations. For the k and e equations we selected a quadratic upstream interpolation for a convective kinetics (QUICK) scheme as it is a higher order differencing scheme which considers a three point upstream weighted quadratic interpolation when calculating cell values. We solved the non-linear algebraic equations using a geometric agglomerated algebraic multi-grid solver for pressure, with a tolerance threshold of 10^{-10} and conjugate gradient for all the other computed quantities to the same tolerance.

Computational grid and boundary conditions

The computational analysis simulated the flow-field around a single blade, with periodic boundary conditions imposed at mid-pitch. We analysed only a single blade as the reported research focus was the effect of the sinusoidal leading edge blade profile. The computational domain extended one blade chord upstream of the blade leading edge and two blade chords downstream of the blade trailing edge. The computational grid that we used for both the JFM fan and JWFM fan computational analysis contained 2.0 million hexahedra and 2.1 million tetrahedral degrees of freedom. We divided the blade chord using 200 cells and divided the blade span using 250 cells, Figure 10.5. The blade aerofoil was enveloped in 80 layers of hexahedra cells. We modelled the blade tip-to-casing gap using 31 cells in the radial and 40 cells in the pitch-wise direction. The mesh refinement is such that the average values of the normalised wall distance y+ are 1.2 on the blade surfaces and 1.9 on the endwalls. Table 10.2 provides further details regarding the mesh.
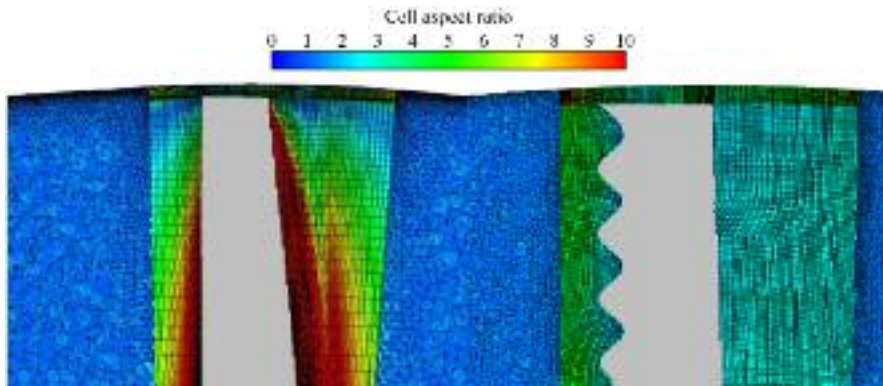
FIGURE 10.5. The computational mesh used when predicting the JFM fan's (left) and the JWFM fan's (right) blade-to-blade flow-field.

Following Launder and Sharma's method (1974), we derived the in-flow pitch-averaged profiles of both axial and radial velocity by numerically simulating the flow-field in the fan's inlet spinner cone region, Figure 10.6. We also derived the turbulent kinetic energy's pitch-wise profile, and then used it to calculate the radial distribution of dissipation based on a dissipation length scale of ten per cent of mid-span blade chord, Figure 10.6. This method of generating boundary conditions enabled the numerical simulation to take into account the effect of sharp reductions of the flow area and the wake generated by struts used to support the spinner. The need to certify the JFM fan in accordance with Euro Norm EN 12101-3 requirements for operation at 400 centigrade for two hours resulted in a need for a static spinner, mounted using five struts to the fan casing. It is the five struts that generate wakes. Table 10.3 summarises the boundary conditions on each sub-set of boundary surface.

RESULTS

We calculated the JFM fan's overall pressure rise and efficiency and compared the computational results with the experimental results, Figure 10.7. The agreement between computational and experimental results was good, particularly for the 110 m^3/s and 95 m^3/s operating points that are associated with incipient stall and stalled operation. However, there was a discrepancy of up to 2.2 per cent between the experimental and computational results. This discrepancy was within the context of a 0.5 per cent error in pressure when making experimental measurements. One may attribute the remainder of the error to the computational analysis that we conducted.

Table 10.2. *Details of the computational mesh.*

Number of cells	2M hexahedra + 2.1M tetrahedra		
	Minimum	*Average*	*Maximum*
Aspect ratio	1	12	40
Minimum include angle	18	42	89
Volume ratio	1	1.3	2.8
Skewness	0.01	0.4	0.6
y^+ (blade)	0.31	0.61	1.2
y^+ (hub)	0.42	0.62	1.85
y^+ (shroud)	0.41	0.65	1.90

Table 10.3. *Computational model boundary conditions.*

Inflow	Velocity, k and e profiles (Corsini *et al*., 2006)
Outflow	Convective
Hub and blade	No-slip condition with zero relative velocity
Casing	No-slip condition with relative velocity $w = -\omega R_c$
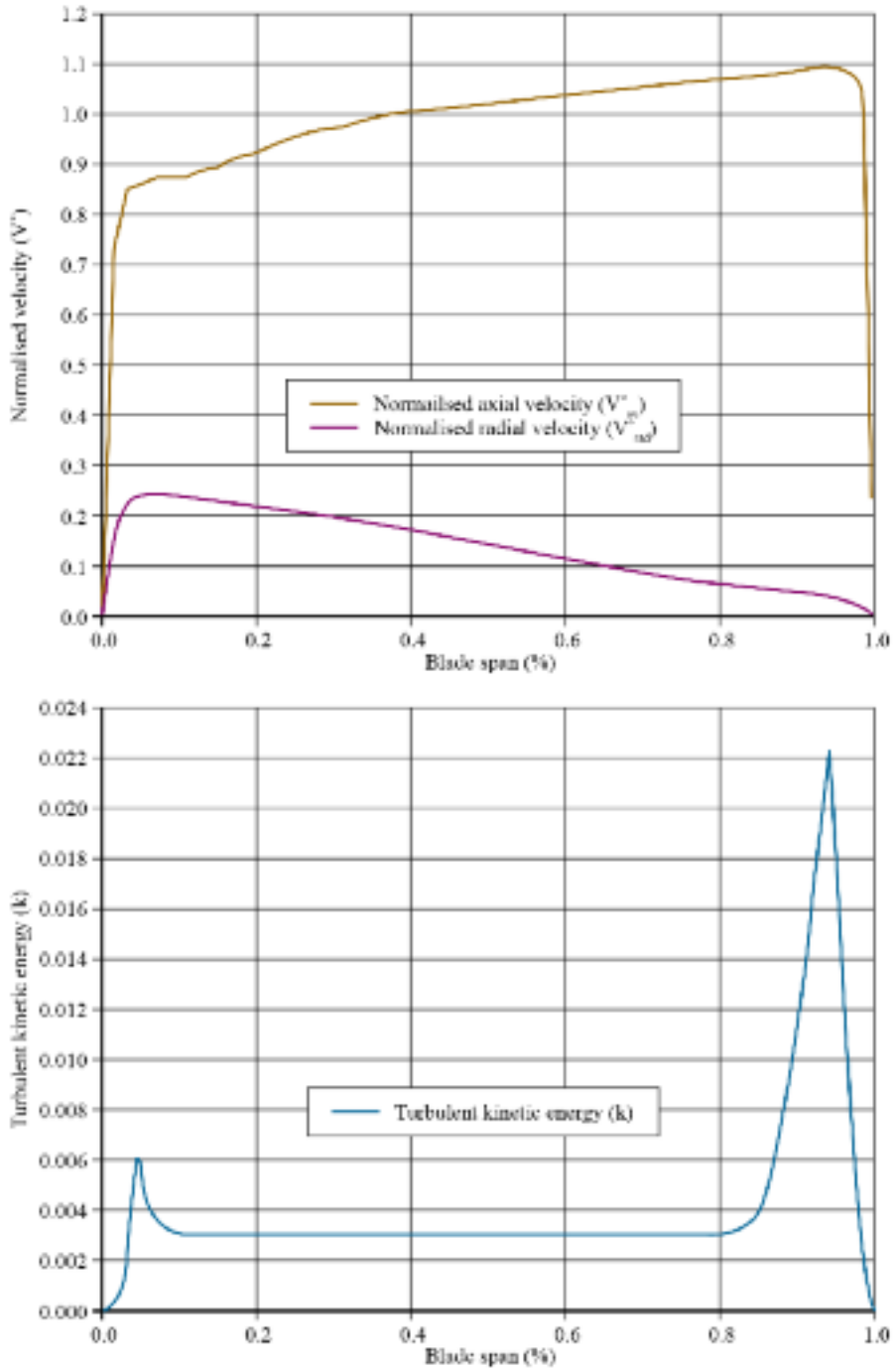
FIGURE 10.6. Axial and radial velocity plus turbulent kinetic energy inflow conditions for the computational model. Axial and radial components of absolute velocity are normalised with bulk velocity.
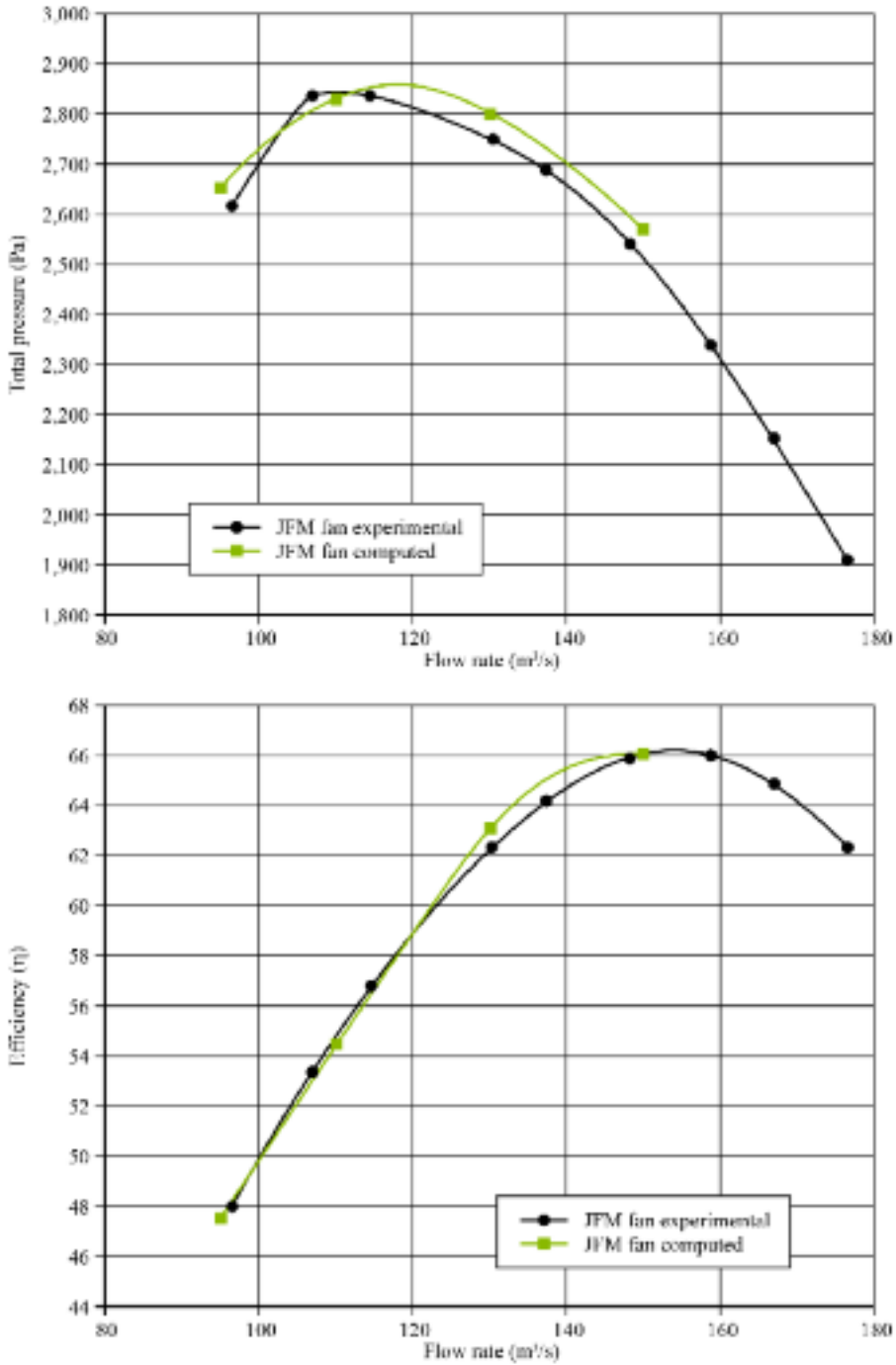
FIGURE 10.7. Experimentally measured and computed total pressure rise against flow rate (top) and efficiency (bottom) for the JFM fan with a 24 degree blade angle.

First, we neglected local compressibility effects and second, modelled the rotor only, with a correction applied to account for the effect of the stator. Therefore, we may consider that neglecting compressibility effects and correcting for the stator's effect to introduce an error of up to 1.7 per cent. Although undesirable, this error should not undermine conclusions when comparing computational results for the JFM and JWFM fans.

We calculated and compared the JWFM fan's overall pressure rise and efficiency with the calculated data for the JFM fan, Figure 10.8. The sinusoidal leading edge blade profile results in a JWFM's pressure rise that is approximately three per cent lower for the 150 m³/s, 130 m³/s and 110 m³/s operating points associated with the fan's stable operating range. Using the fan laws to scale the calculated JWFM's characteristic indicated that restaggering the JFWM blade angle from 24 to 28 degrees results in the JWFM fan having the same pressure rise capability as the JFM fan. The JWFM fan's 95 m³/s post-stall pressure rise is approximately one per cent higher than that of the JFM fan. The impact of the sinusoidal leading edge blade profile is therefore to flatten the characteristic, and hence we may conclude that the sinusoidal leading edge blade profile improves stall performance at the expense of pressure rise. The most noticeable difference between the JFM and the JWFM fan characteristics is the difference between the 110 m³/s and 95 m³/s operating points, with the JWFM fan exhibiting a significantly less abrupt transition from stable (110 m³/s) to stalled (95 m³/s) operation. This result is self-consistent with Corsini *et al.*'s findings (2013b).

Flow topology

One may assess the effectiveness of the chosen computational approach in predicting the flow-field associated with a sinusoidal leading edge blade profile by considering normalised turbulent viscosity (n_t/n). Normalised turbulent viscosity distributions at 10 per cent and 90 per cent blade chord for the JFM fan indicate a regular distribution that is self-consistent with the expected boundary layer state, given the local blade loading, Figures 10.9 and 10.10. In contrast, a more complex distribution at both 10 per cent and 90 per cent blade chord characterises the JWFM fan normalised turbulent viscosity. The more complex distribution is expected as it reflects the three-dimensionality of the sinusoidal leading edge blade profile.

When modelling a more complex three-dimensional flow-field the use of a non-linear eddy viscosity closure results in a better representation of the anisotropy of the Reynolds stresses and consequently, a more accurate reproduction of the flow-field. The effectiveness of the chosen computational approach in predicting the JFM fan normalised turbulent viscosity distributions, combined with a computational approach that includes non-linear eddy viscosity closure, gives confidence that the JWFM fan flow-field is adequately predicted and is therefore valid.

Having established that the computational approach that we utilised predicted both the JFM fan and JWFM fan overall performance and flow-field adequately, one may use the computational results to provide an insight into the flow features induced in the flow-field by a sinusoidal leading edge blade profile. A way in which a
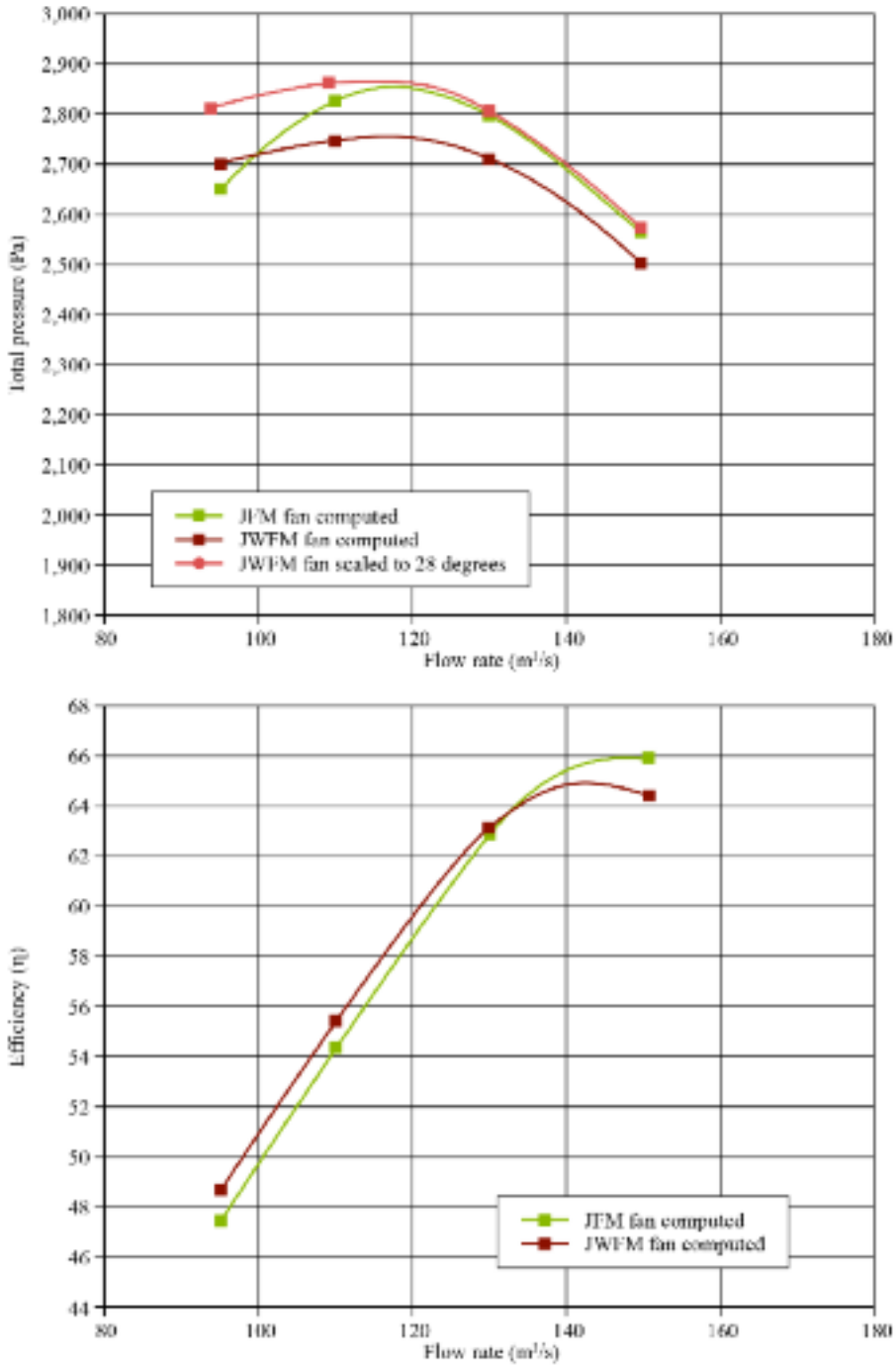
FIGURE 10.8. Computed total pressure rise against flow rate (top) and efficiency (bottom) for the JFM fan and JWFM fan, both with a 24 degree blade angle. Additionally, the JWFM fan characteristic has been scaled to 28 degrees.
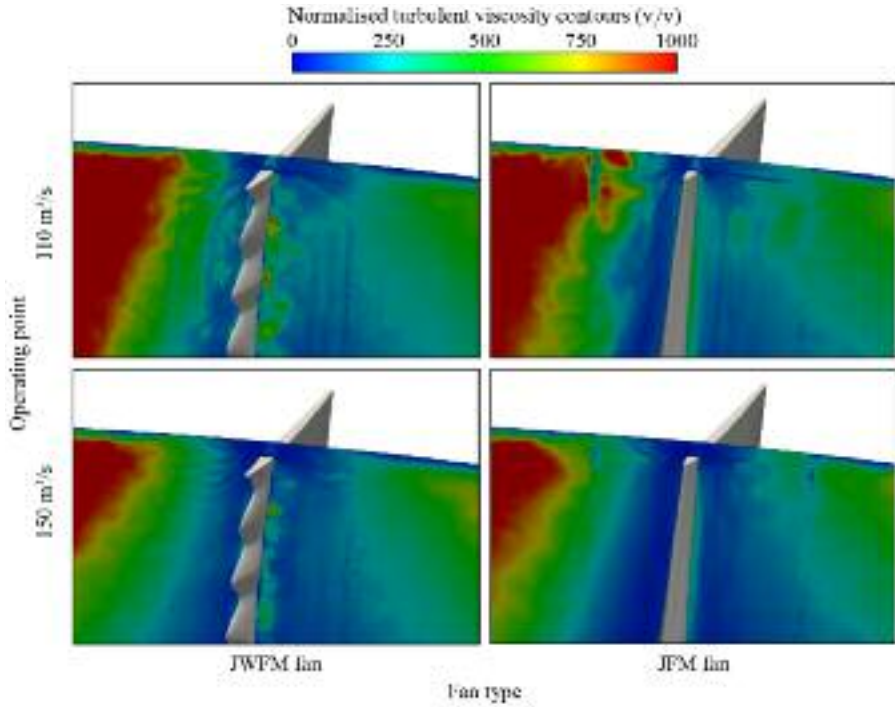
FIGURE 10.9. Normalised turbulent viscosity contours at 10 per cent blade chord for both the JFM fan blade and the JWFM fan blade leading edge.
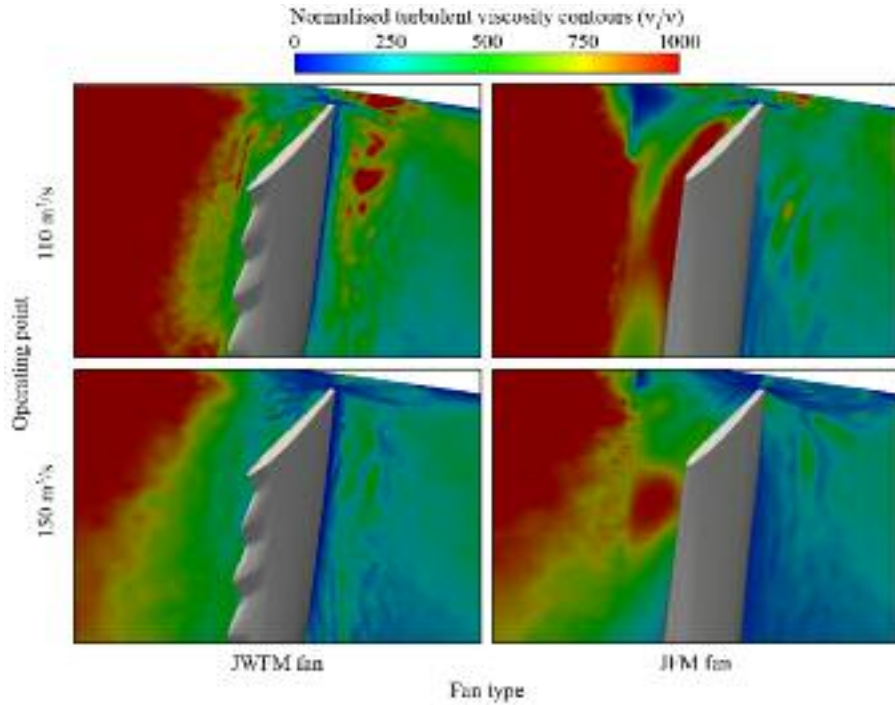
FIGURE 10.10. Normalised turbulent viscosity contours at 90 per cent blade chord from both the JFM and JWFM fan blade's leading edge.

sinusoidal leading edge blade profile influences the blade-to-blade flow-field is by influencing the generation of vortical structures. An analysis of vorticity magnitude (w) is therefore useful as it provides an insight into how the JWFM fan flow-field's vortical structure differs from that of the JFM fan, Figure 10.11.

At both the 150 m^3/s and 110 m^3/s operating points the flow-field around the JFM blade is not associated with any large-scale structures. The only significant region of swirling flow is in the blade tip region, associated with the tip leakage vortex, Figure 10.11. As the JFM fan moves from the 150 m^3/s to the 110 m^3/s operating point, a region of separated flow develops in the blade tip region. This region of separated flow combines with the tip leakage vortex and is indicative of incipient stall. In contrast, the JWFM blade is less affected by the movement for the 150 m^3/s to the 110 m^3/s operating point. The sinusoidal leading edge blade profile generates pairs of counter-rotating vortices, and in the blade tip region a vortex induced by the outer most sinusoid counter-rotates with respect to the tip leakage vortex. Interaction between the sinusoid induced vortex and the tip leakage vortex results in reattachment of the JWFM fan blade suction surface flow. Thus, the sinusoidal leading edge blade profile has induced a flow feature that reduces the JWFM fan's propensity to stall.
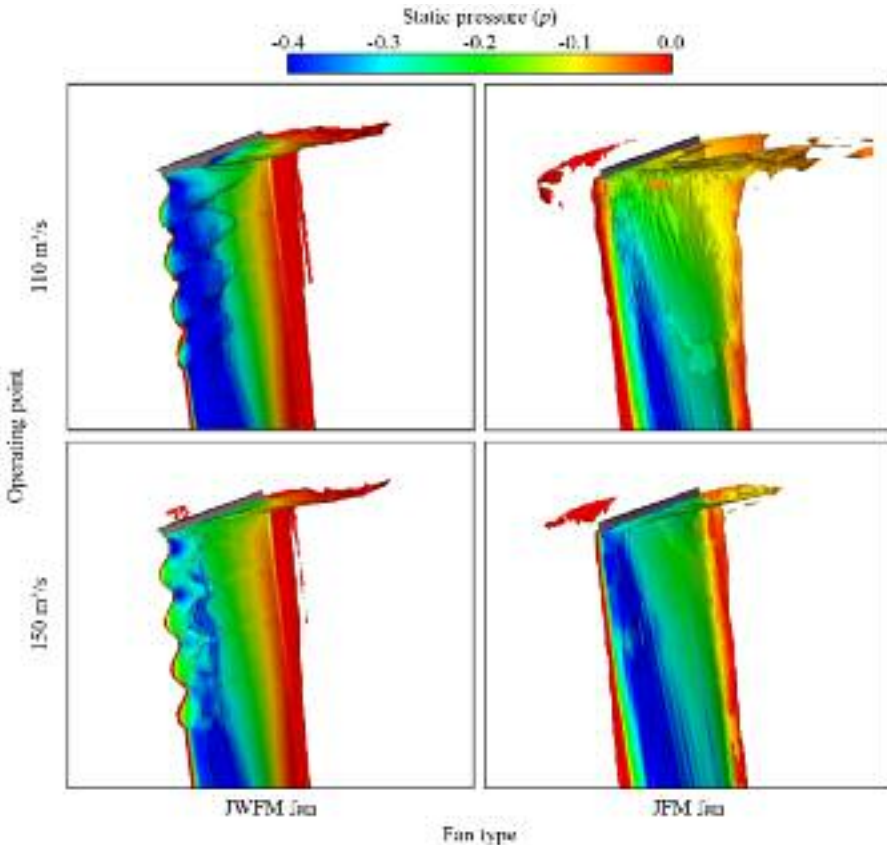
FIGURE 10.11. Vortical structures stemming from the JFM and JWFM fan blade's leading edge, visualised using an iso-surface of vorticity magnitude (w=70).

We can verify the ability of a sinusoidal leading edge blade profile to induce a flow feature that reduces the blade's propensity to stall through a study of the flow streamlines in the blade tip region. At the 150 m^3/s operating point the JWFM fan tip leakage vortex is more intense than the JFM fan tip leakage vortex, Figure 10.12. This increase in intensity results from the vorticity induced in the flow-field by the sinusoidal leading edge blade profile that induces a low-pressure region on the blade suction surface.

The 95 m^3/s operating point is associated with aerodynamic stall, Figure 10.12. When one studies the JFM fan flow streamlines for the 95 m^3/s operating point, it is evident that the tip leakage vortex has broken away from the blade tip completely, and could be indicative of a blade that has stalled, Figure 10.12. In contrast, we associate the JWFM fan with a tip vortex that remains attached at the 95 m^3/s operating point. Again, the sinusoidal leading edge blade profile induced flow features have reduced the JWFM fan's propensity to stall.
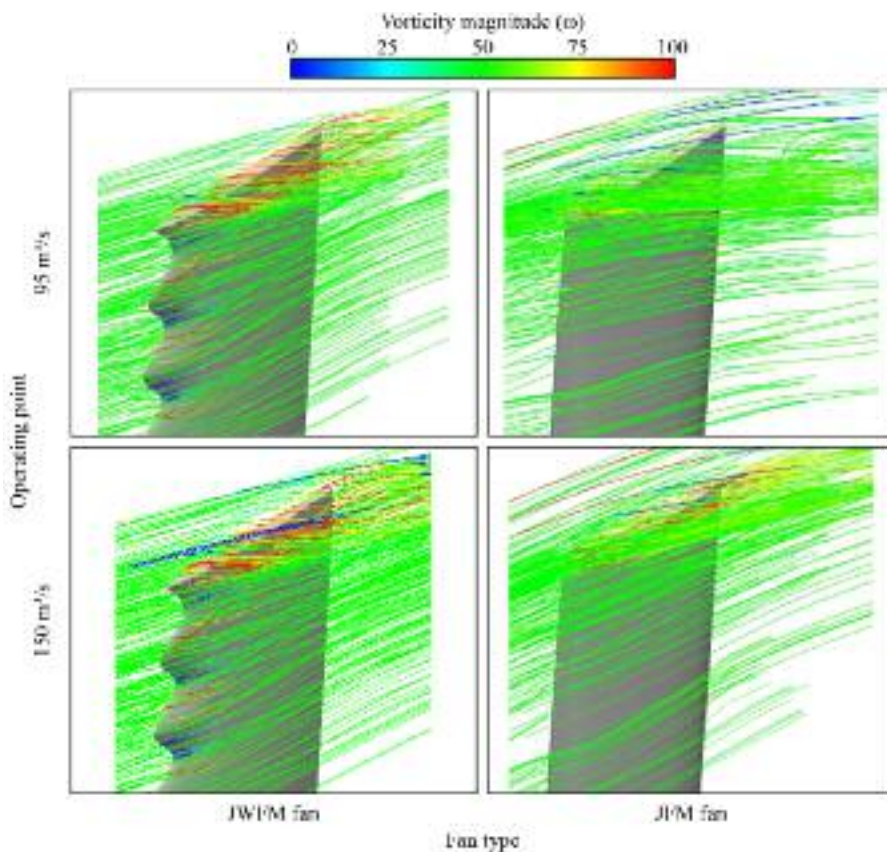
FIGURE 10.12. Flow streamlines at the JFM and JWFM fan blade's tip, illustrating vortex separation at the JFM fan blade's tip at the 95 m^3/s operating point.

Blade pressure field

The presence of a sinusoidal leading edge blade profile affects the fluid flow over a blade and it is through insight into how the fluid flow is affected that we can better understand the JWFM fan's pre- and post-stall behaviour. A consideration of static pressure coefficient (C_p) iso-lines for both the JFM and the JWFM fans over the outer 20 per cent of blade span at the 110 m³/s and 150 m³/s operating points provides an initial insight into the impact of a sinusoidal leading edge blade profile, Figure 10.13. For the JFM fan, irrespective of the operating point, the iso-lines are vertical and aligned with the blade leading edge. The only exception is very close to the blade tip where fluid leakage from pressure to suction surface alters the pressure distribution. When we study the iso-lines for the JWFM fan, it is apparent that they are also vertical on the pressure surface. However, when we study the iso-lines for the JWFM suction surface, there is evidence of low-pressure regions generated by
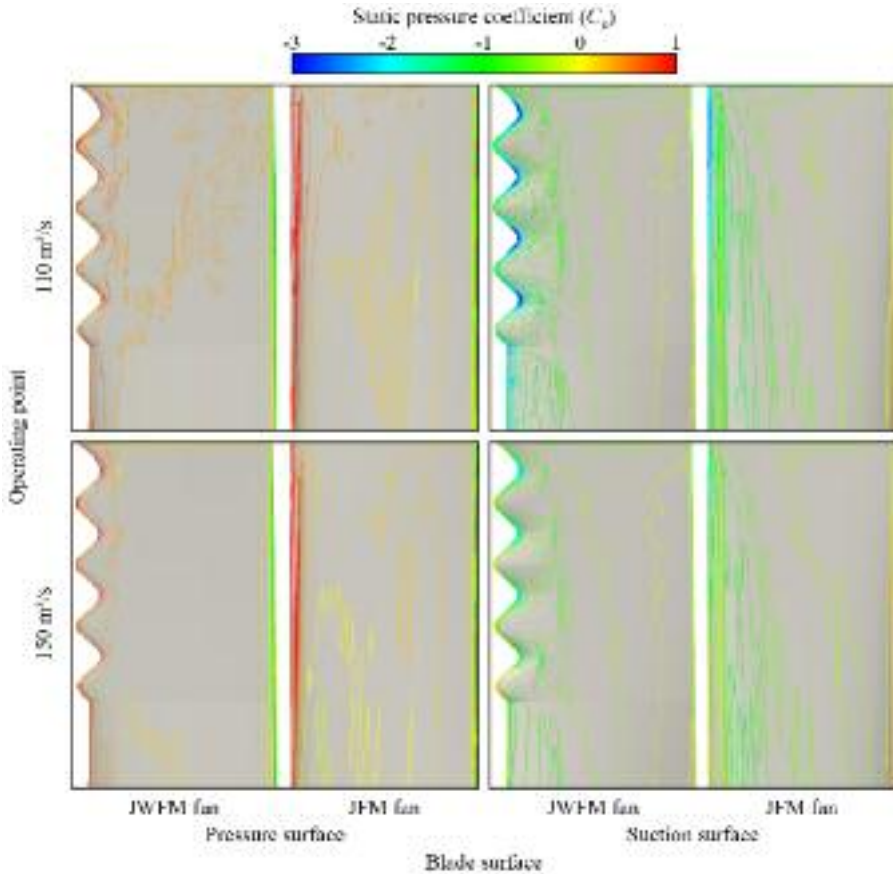
FIGURE 10.13. Static pressure iso-line distribution over the outer 25 per cent of the JFM and JWFM fan blades' span.

the sinusoid troughs. The presence of low-pressure regions generated by the sinusoid troughs is consistent with Corsini *et al.*'s findings (2013b).

We may assess the effectiveness of a sinusoidal leading edge blade profile by considering its impact on the evolution of static pressure coefficient (C_p), Figure 10.14. When one studies the JFM fan blade pressure coefficient at the 150 m³/s
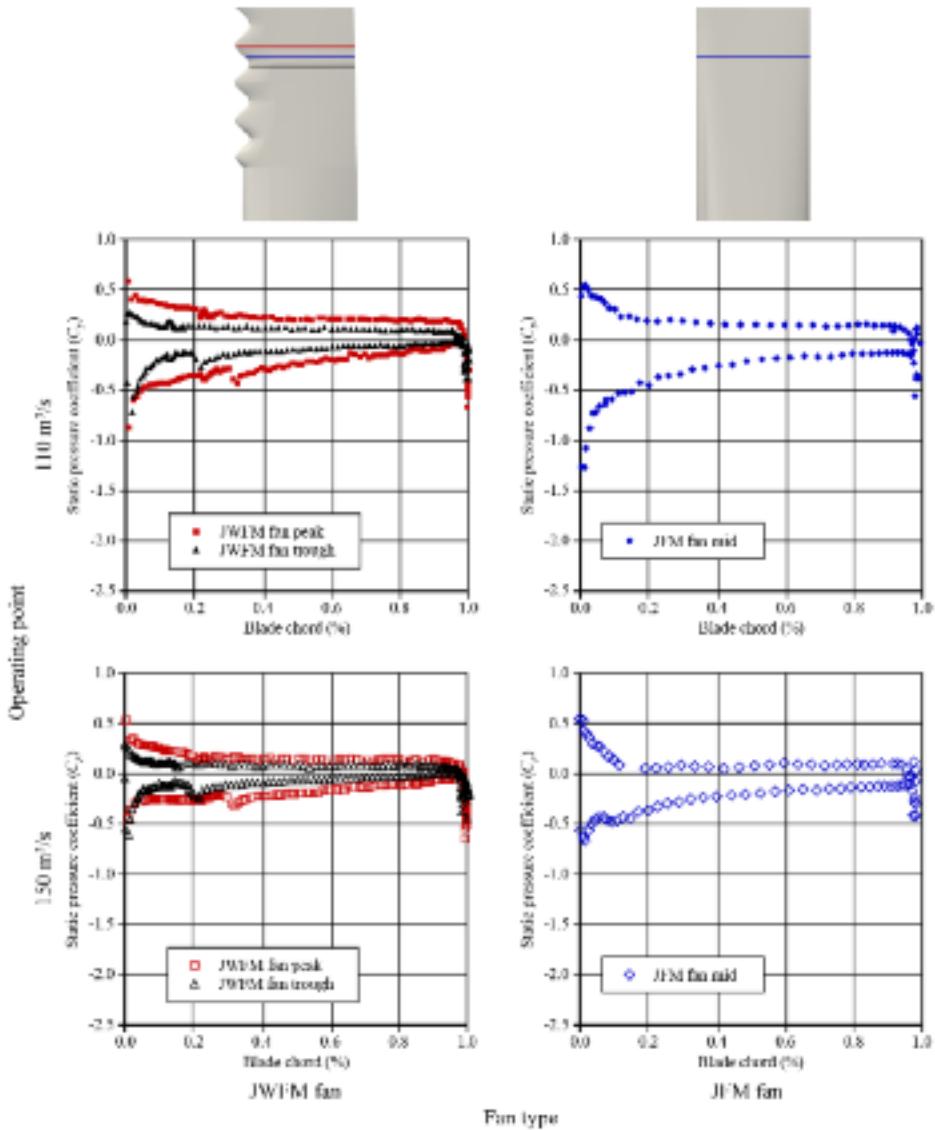
FIGURE 10.14. The JFM and JWFM fan blades' pressure and suctions surface static pressure coefficient distributions.

operating point there is evidence of a leading edge separation bubble at approximately 10 per cent chord. At the 110 m^3/s operating point this separation bubble is no longer evident. The evolution of the JWFM fan blade pressure coefficient is plotted at two blade cross-sections, the first corresponding to a sinusoid peak and the second to a sinusoid trough, Figure 10.14. When one studies the JWFM fan blade pressure coefficient at both the 150 m^3/s and 110 m^3/s operating points it is apparent that unlike the JFM fan blade, the change in operating point has little effect on pressure coefficient distribution. The pressure coefficient distribution indicates that at both 150 m^3/s and 110 m^3/s operating points there is no separated flow developing as the flow rate reduces. The relative stability of the JWFM fan static pressure coefficient distribution compared to the JFM fan static pressure coefficient distribution with reducing flow rate indicates that the JWFM fan is more stable at the 110 m^3/s operating point that then JFM fan, and consequently, the JWFM fan's sinusoidal leading edge blade profile is effective.

Losses at the blade tip

Insight into the flow features induced in the flow-field by a sinusoidal leading edge blade profile clarifies why the JWFM fan is less susceptible to stall than the JFM fan. However, one must consider any reduction in susceptibility to aerodynamic stall within the context of the impact that reduction has on fan efficiency. It is therefore helpful to consider the evolution of aerodynamic losses associated with a sinusoidal leading edge blade profile. We presented contours of total pressure loss coefficient (ζ) for the JFM fan blade and JWFM fan blade from three cylindrical surfaces:

- R1 at 95.6 per cent blade span, corresponding to a sinusoid trough, Figure 10.15;
- R2 at 96.8 per cent blade span, corresponding to the outer sinusoid peak, Figure 10.16; and
- R3 at 98.0 per cent blade span, corresponding to the outer sinusoid trough, Figure 10.17.

We present contours of total pressure loss coefficient for both the JFM fan and the JWFM fan at the same cylindrical surface radius, to allow a direct comparison between the two. If we first consider the contours of total pressure loss coefficient at the 150 m^3/s operating point for both the JFM fan blade and the JWFM fan blade, the topology is similar for the two blades at all three cylindrical surface radii. There is a slight difference between the JFM fan blade and JWFM fan blade contours of total pressure loss coefficient at radii R3 in the leading edge region. This difference is due to a local increase in angle of attack induced in the flow by the sinusoidal leading edge blade profile, but we may regard it as a minor change in the overall topology of losses. We may therefore conclude that at the 150 m^3/s operating point the sinusoidal leading edge blade profile has a second order impact on total pressure losses.
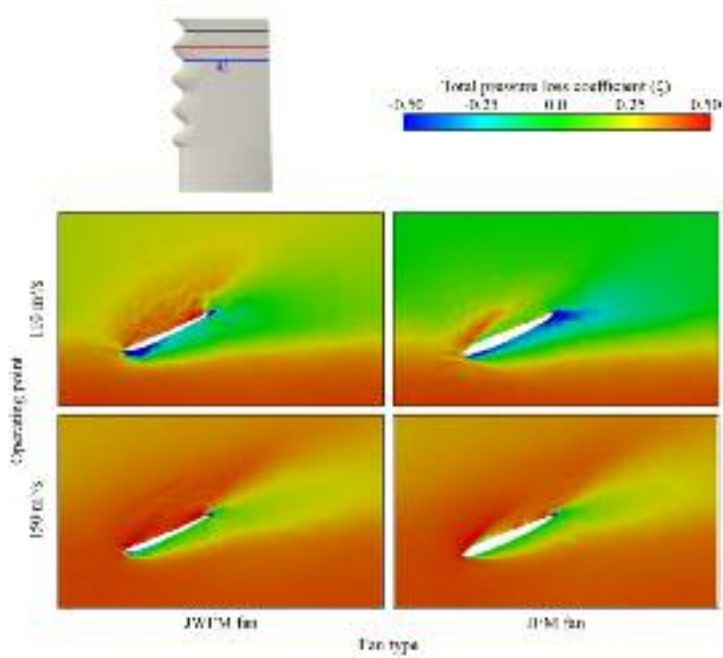
FIGURE 10.15. Contours of total pressure loss coefficient (ζ) on the cylindrical surface R1 for both the JFM and JWFM fan at the 150 m³/s and 110 m³/s operating points.

Moving on to consider contours of total pressure loss coefficient at the 110 m³/s operating point, there is a significant difference between the JFM fan blade and JWFM fan blade topology. At radii R1 the JFM fan blade has significantly deeper losses in the wake region. At radii R2 the JFM fan blade suction surface boundary layer is now separated, forming a thick wake. At radii R3 the JFM fan blade topology indicates that the tip leakage vortex and suction surface boundary layer have now formed a deep loss core, a feature of the topology that is indicative of incipient stall.

The JWFM fan blade topology at radii R3 indicates that the suction surface boundary layer is associated with significantly larger losses than it was at radii R1 or R2; however, the wake remains defined. A defined wake indicates that one consequence of the tip separation control associated with a sinusoidal leading edge blade profile is to confine losses to a region close to the blade suction surface. We may therefore conclude that the fluid structures induced in the flow by the sinusoidal leading edge blade profile result in better control of separation at the trailing edge. As a direct result, the JWFM fan is inherently more aerodynamically resistant to the effect of stall than the JFM fan.
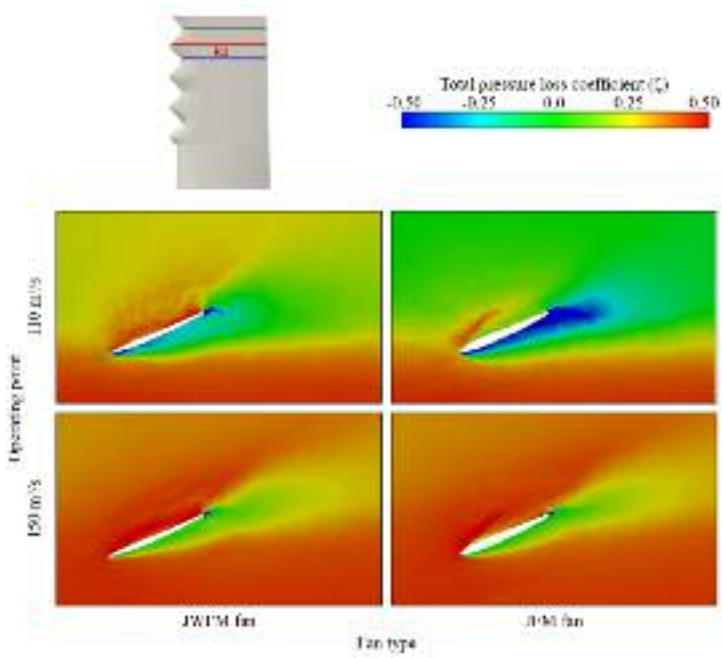
FIGURE 10.16. Contours of total pressure loss coefficient (ζ) on the cylindrical surface R2 for both the JFM and JWFM fan at the 150 m^3/s and 110 m^3/s operating points.
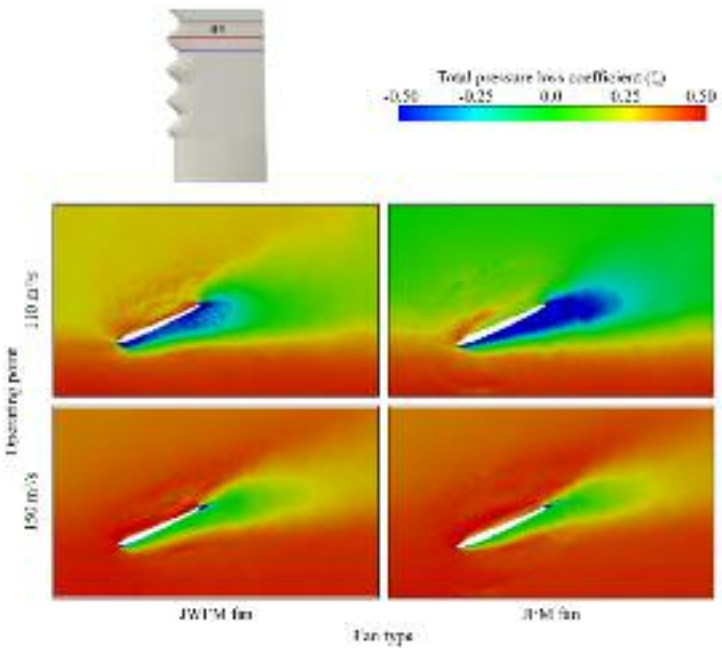
FIGURE 10.17. Contours of total pressure loss coefficient (ζ) on the cylindrical surface R3 for both the JFM and JWFM fan at the 150 m^3/s and 110 m^3/s operating points.

CONCLUSIONS

The reported research presents a design methodology for applying sinusoidal leading edge blade profiles to finite span aerofoils intended for application in axial fans used in metropolitan metro and railway tunnel ventilation systems. The research takes its inspiration from the pectoral fins of humpback whales that have tubercles along their leading edge. Previous researchers have shown that the presence of the tubercles, when studied in infinite cascades, improve the post-stall lift recovery of aerofoils utilised by the industrial fan community.

The research reported in this chapter shows that when applied to a three-dimensional blade, the presence of a sinusoidal leading edge also improved the blades stall resistance. The addition of a sinusoidal leading edge reduced blade pressure developing capability by three per cent, requiring the blade to be restaggered from 24 to 28 degrees. At the peak pressure condition the presence of a sinusoidal leading edge resulted in a small improvement in fan efficiency.

The reported research focuses on assumptions when developing the design methodology. The design methodology objective was to optimise the sinusoidal leading edge blade profile in order to induce the desired vorticity distribution at the blade trailing edge. We identified three variables:

(i)   number of sinusoids from the blade tip;
(ii)   sinusoid wavelength in the span-wise direction; and
(iii)   sinusoid amplitude in the chord-wise direction.

We utilised the developed methodology to optimise the three variables, adapting a blade from a baseline fan named JFM to create a 'whale-fan' we named JWFM. The JWFM fan has a blade with a sinusoidal leading edge profile with three per cent blade chord amplitude, five per cent blade span wavelength and four and a half sinusoids from the blade tip.

We carried out numerical computations on both the JFM fan and the JWFM fan. The numerical computations for the JFM fan were within the combined uncertainty of experimental measurements and assumptions when accounting for the effect of compressibility and the fan stator. The agreement between the two gave confidence in the computational results. We then compared the numerical computations for the JFM fan quantitatively with those for the JWFM fan. We analysed and compared the difference between the two sets of results with those of previous researchers. The analysis confirmed that the choice of amplitude, wavelength and number of sinusoids resulted in similar flow-field features to those that had resulted in an improvement in the post stall lift recovery of infinite span aerofoils.

We then studied the blade tip flow features for the JFM fan blade and the JWFM fan blade with the objective of identifying the fluid dynamic mechanisms induced in the flow by the sinusoidal leading edge blade profile. We verified the presence of pairs of counter rotating vortices associated with each sinusoid, and confirmed the ability of the optimised sinusoidal leading edge blade profile to maintain attached flow at the blade trailing edge. Thus, we concluded that the sinusoidal leading edge

blade profile resulted in a JWFM fan that is inherently more aerodynamically resistant to the effect of stall than the baseline JFM fan.

REFERENCES

EN 12101-3, 2002, Smoke and Heat Control Systems. Specification for Powered Smoke and Heat Exhaust Ventilators.

ISO 21927-3, 2006, Smoke and Heat Control Systems — Part 3: Specification for Powered Smoke and Heat Exhaust Ventilators.

ISO 5801:2007, 2007, Industrial fans — performance testing using standardized airways.

Bianchi, S., Corsini, A., Mazzucco, L., Monteleone, L., and Sheard, A.G. (2012), "Stall Inception, Evolution and Control in a Low Speed Axial Fan with Variable Pitch in Motion", *Transactions of the ASME, Journal of Engineering for Gas Turbines and Power*, vol. 134, paper no. 042602, pp. 1–10.

Bianchi, S., Corsini, A., Sheard, A.G., and Tortora, C. (2013), "A Critical Review of Stall Control Techniques in Industrial Fans", *International Scholarly Research Network, Mechanical Engineering*, vol. 2013, article ID 526192, pp. 1–18.

Borello, D., Corsini, A., Delibra, G., and Sheard, A.G. (2013a), "Numerical Investigation of Detrimental Aerodynamic Effect of Pressure Pulses on a Metro Tunnel Fan", *Proceedings of the 10th European Turbomachinery Conference*, Lappeenranta, Finland, 15–19 April, pp. 573–82.

Borello, D., Corsini, A., Delibra, G., Fiorito, M., and Sheard, A.G. (2013b), "Large-eddy Simulation of a Tunnel Ventilation Fan", *Transactions of the ASME, Journal of Fluids Engineering*, vol. 135(7), paper no. 071102, pp. 1–9.

Corsini, A., and Rispoli, F. (2004), "Using Sweep to Extend Stall-free Operational Range in Axial Fan Rotors", *Proceedings of the IMechE Part A, Journal of Power and Energy*, vol. 218, pp. 129–39.

Corsini, A., and Rispoli, F. (2005), "Flow Analyses in a High-pressure Axial Ventilation Fan with a Non-linear Eddy Viscosity Closure", *International Journal of Heat and Fluid Flow*, vol. 17, pp. 108–55.

Corsini, A., Rispoli, F., Santoriello, A., and Tezduyar, T.E. (2006), "Improved Discontinuity-capturing Finite Element Techniques for Reaction Effects in Turbulence Computation", *Computational Mechanics*, vol. 38, pp. 356–64.

Corsini, A., Delibra, G., and Sheard, A.G. (2013a), "A Critical Review of Computational Methods and Their Application in Industrial Fan Design", *International Scholarly Research Network, Mechanical Engineering*, vol. 2013, article ID 625175, pp. 1–20.

Corsini, A., Delibra, G., and Sheard, A.G. (2013b), "On the Role of Leading Edge Bumps in the Control of Stall Onset in Axial Fan Blades", *Transactions of the ASME, Journal of Fluids Engineering*, vol. 135, paper no. 081104, pp. 1–9.

Cumpsty, N.A. (2004), *Compressor Aerodynamics*, Krieger Publishing Company, Malabar, FL, USA.

Durbin, B. (2011), "Review: Adapting Scalar Turbulence Closure Models for Rotation and Curvature", *Transactions of the ASME, Journal of Fluids Engineering*, vol. 133, paper no. 061205, pp. 1–8.

Fish, F.E. (1993), "Influence of Hydrodynamic Design and Propulsive Mode on Mammalian Swimming Energetics", *Australian Journal of Zoology*, vol. 42, pp. 79–101.

Fish, F.E., and Battle, J.M. (1995), "Hydrodynamic Design of the Humpback Whale Flipper", *Journal of Morphology*, vol. 225, pp. 51–60.

Fish, F.E., Howle, L.E., and Murray, M.M. (2008), "Hydrodynamic Flow Control in Marine Mammals", *Integrative and Comparative Biology*, vol. 48, pp. 788–800.

Gravdahl, J.T., and Egeland, O. (1999), *Compressor Surge and Rotating Stall: Modelling and Control,* Springer Verlag, London, UK.

Johari, H., Henoch, C.W., Custodio, D., and Levshin, A. (2007), "Effects of Leading-edge Protuberances on Airfoil Performance", *AIAA Journal*, vol. 45(11), pp. 2634–2642.

Kröger, G., Vo, C., Nicke, E., and Cornelius, C. (2011), "Theory and Application of Axisymmetric End-wall Contouring for Compressors", *Proceedings of the 56th American Society of Mechanical Engineers Turbine and Aeroengine Congress*, Vancouver, BC, Canada, 6–10 June, paper no. GT2011-45624.

Langston, L.S. (2009), "Fitting a Pitch", *ASME Mechanical Engineering Magazine*, vol. 131(12), pp. 38–42.

Launder, B.E., and Sharma, B.R. (1974), "Application of the Energy-dissipation Model of Turbulence to the Calculation of Flow Near a Spinning Disc", *Letters in Heat and Mass Transfer*, vol. 1, pp. 131–8.

Lien, F.S., and Leschziner, M.A. (1994), "Assessment of Turbulence-transport Models Including Non-linear RNG Eddy-viscosity Formulation and Second-moment Closure for Flow Over a Backward-facing Step", *Computational Fluids*, vol. 23, pp. 983–1004.

Miklosovic, D.S., Murray, M.M., Howle, L.E., and Fish, F.E. (2004), "Leading-edge Tubercles Delay Stall on Humpback Whale (*Megaptera Novaeangliae*) Flippers", *Physics of Fluids*, vol. 16, pp. L39–L42.

Miklosovic, D.S., Murray, M.M., and Howle, L.E. (2007), "Experimental Evaluation of Sinusoidal Leading Edges", *Journal of Aircraft*, vol. 44, pp. 1404–8.

Pedro, H.T.C., and Kobayashi, M.H. (2008), "Numerical Study of Stall Delay on Humpback Whale Flippers", *Proceedings of the 46th AIAA Aerospace Sciences Meeting and Exhibit*, Reno, NV, USA, 7–10 January, paper no. 2008-0584.

Sheard, A.G., and Corsini, C. (2012), "The Mechanical Impact of Aerodynamic Stall on Tunnel Ventilation Fans", *International Journal of Rotating Machinery*, vol. 2012, paper no. 402763, pp. 1–12.

Sheard, A.G., and Daneshkhah, K. (2012), "The Conceptual Design of High Pressure Reversible Axial Tunnel Ventilation Fans", *Advances in Acoustics and Vibration*, vol. 2012, article ID 562309, pp. 1–11.

Sheard, A.G., and Jones, N.M. (2008), "Approval of High-temperature Emergency Tunnel-ventilation Fans: The Impact of ISO 21927-3", *Proceedings of the ITA–AITES World Tunnel Congress and 34th General Assembly*, Agra, India, 19–25 September, pp. 1817–26.

Sheard, A.G., and Jones, N.M. (2012), "Powered Smoke and Heat Exhaust Ventilators: The Impact of EN 12101-3 and ISO 21927-3", *Tunneling and Underground Space Technology*, vol. 28, pp. 174–82.

Sheard, A.G., Corsini, A., and Bianchi, S. (2011), "Stall Warning in a Low-speed Axial Fan by

Visualisation of Sound Signals", *Transactions of the ASME, Journal of Engineering for Gas Turbines and Power*, vol. 133, paper no. 041601, pp. 1–10.

Sheard, A.G., Delibra, G., and Corsini, A. (2012), "Air Movement Fans", GB Patent Application 1219502.0, 30 October.

Shyy, W., Lian, Y., Tang, J., Viieru, D., and Liu, H. (2007), *Aerodynamics of Low Reynolds Number Flyers,* Cambridge University Press, Cambridge, UK.

van Nierop, E.A., Alben, S., and Brenner, M.P. (2008), "How Bumps on the Whale Flippers Delay Stall: an Aerodynamic Model", *Physical Review Letters*, vol. 100, paper no. 054502, pp. 1–4.

Weichert, S., and Day, I. (2012), "Detailed Measurements of Spike Formation in an Axial Compressor", *Proceedings of the 57th American Society of Mechanical Engineers Turbine and Aeroengine Congress*, Copenhagen, Denmark, 11–15 June, paper no. GT2012-68627.

Weller, H.G., Tabor, G., and Jasak, H. (1998), "A Tensorial Approach to Continuum Mechanics Using Object-oriented Techniques", *Computational Physics*, vol. 12, pp. 620–31.

Investigation on Anti-stall Ring Aerodynamic Performance in an Axial Flow Fan

A. Corsini, G. Delibra, F. Rispoli,
A.G. Sheard, and D. Volponi

ABSTRACT

Metropolitan metro and railway tunnel ventilation fans are subjected to positive and negative pressure pulses. As a train travels along a tunnel it drives air down the tunnel. This creates a 'piston effect' that results in positive and negative pressure pulses. A pressure pulse transiently drives a ventilation fan to a higher pressure operating point. If the operating point is beyond the fan's pressure developing capability, there is a risk it may stall. Tunnel ventilation fan designers classically utilise a stabilisation ring to stabilise the fan's characteristic and thus mitigate the mechanical consequences of driving a fan into stall.

A stabilisation ring consists of an annular chamber that is incorporated into the fan casing over the fan blade's leading edge. As a tip-limited axial fan approaches stall, boundary layer fluid centrifuges up the blade. The fan stalls at the point when flow inside the annulus reverses direction in the blade tip region. The stabilisation ring provides an annular chamber into which this fluid may flow. It incorporates a set of vanes that redirect the reverse flow into an axial direction, and then reintroduces it into the main-stream flow up-stream of the fan blade leading edge. Although effective in stabilising the fan's characteristic, stabilisation rings typically reduce fan efficiency by three per cent, and consequently, are becoming progressively less acceptable as required minimum fan efficiencies increase.

The reported research combines experimental measurements of overall fan performance with and without a fitted stabilisation ring, and a numerical analysis of the flow-field within the stabilisation ring. Visualisation of the flow-field provides an insight into the physical flow mechanisms that enable the stabilisation ring to stabilise the fan's characteristic. A conclusion of the research is that at the fan's peak efficiency operating point, flow through the stabilisation ring separated from the

stabilisation ring vanes. Therefore, redesigning the vanes to avoid separated flow offers the potential to eliminate this aerodynamic loss mechanism, thus reducing the efficiency loss classically associated with applying a stabilisation ring.

NOMENCLATURE

Latin letters

B	exit area	m^2
D_t	tip diameter	m
h	stabilisation ring height	m
I	stabilisation ring inlet area	m
k	turbulent kinetic energy	m^2/s^2
ℓ	blade chord	mm
L_t	turbulence length scale	m
P	power	W
p	static pressure	Pa
p^*	normalised static pressure; $p^* = 2p / [\rho(v_{tip})^2]$	
Q	volume flow rate	m^3/s
Re	Reynolds number; $Re = v_{tip}D_t/n = 5.16 \times 10^6$	
S	stabilisation ring shroud area	m^2
v, w, u	absolute, relative and rotation velocity	m/s
V^*	normalised velocity; $V^* = v/v_{tip}$	m/s
u_t	friction velocity	m/s
y^+	non-dimensional wall distance $= y_n u_t / v$	
y_n	wall distance	m
z	axial coordinate	m

Greek letters

δ	blade pitch angle	
Σ	fan solidity	
Δp_{tot}	total pressure rise	Pa
Δp_{stat}	averaged static pressure difference	Pa
η	efficiency $\eta = \Delta p \times Q/P$	%
Θ^*	flow rate entering the stabilisation ring normalised with Q	
v	kinematic viscosity	m^2/s
Π^*	flow rate entering the stabilisation ring normalised with its peak efficiency value	
ϕ^*_{ax}	axial flow coefficient; $\phi^*_{ax} = v_{ax}/u_{bulk}$	
ϕ^*_r	radial flow coefficient; $\phi^*_r = v_q/u_{bulk}$	
χ	rotor tip clearance (% of blade span)	
ω_a	angular velocity	1/s

Acronyms, subscripts and superscripts

ax	axial component of a vector
DS	deep stall
LE	leading edge
PE	peak efficiency
PP	peak pressure
QUICK	Quadratic Upwind Interpolation Convection Kinematics scheme
RANS	Reynolds-averaged Navier–Stokes
TE	trailing edge
θ	peripheral component of a vector, tangential direction

INTRODUCTION

The axial fans utilised in tunnel ventilation systems have a good in-service record of reliability. However, over the past decade there have been an increasing number of in-service mechanical failures of tunnel ventilation fans. There has also been a trend towards higher train speeds in railway tunnels and the use of platform screen doors in metropolitan metro systems. These trends have resulted in an increase in pressure pulse magnitude to which tunnel ventilation fans are subjected from typically no more than ±300 Pa ten years ago to as high as ±1,000 Pa today (Sheard and Corsini, 2012). Borello *et al.* (2013) conducted an analysis of the aerodynamic effects of a ±1,000 Pa pressure pulse on a tunnel ventilation fan, concluding that larger pressure pulses can result in fan blade unsteady mechanical loads increasing by a factor of two. This increase occurred despite a fan pressure developing capability high enough to operate without stalling when subjected to the pressure pulse. Therefore, larger pressure pulses may be driving the tunnel ventilation fans beyond their design limit, resulting in in-service fatigue induced mechanical failure.

In axial flow fan applications where the fan may operate in aerodynamic stall, industrial fan designers have historically favoured using a stabilisation ring. Sheard and Corsini (2012) observed that a stabilisation ring does not offer a fan complete protection from the mechanical consequences of aerodynamic stall. However, a stabilisation ring can reduce by 80 per cent the increase in unsteady mechanical load which aerodynamic stall induces in fan blades. Therefore, a stabilisation ring minimises the mechanical consequences of aerodynamic stall, and thus reduces the probability that a fan will fail mechanically if one operates it in an aerodynamically stalled condition.

A negative consequence of fitting a stabilisation ring is that fan efficiency typically reduces by three per cent. On 1 January 2013, EU Commission Regulation No. 327/2011 (2011) came into effect within the European Union, mandating minimum Fan and Motor Efficiency Grades (FMEGs). For applicable fans the 2013 minimum FMEGs have resulted in approximately 33 per cent of those fans sold before 1 January, 2013, now deemed illegal within Europe (Hauer and Brooks, 2012). On 1 January, 2015, the Regulation 327 minimum FMEGs will increase again (Hauer and Brooks, 2012).

Corsini *et al.* (2013a) observed that it is not only the European Union that aims to eliminate inefficient fans from the market. In the USA, the US Department of Energy has been monitoring activity within the European Union. On 1 February, 2013, the US federal government published a framework document in the Federal Register, outlining the approach to fan efficiency regulation within the USA (US Department of Energy, 2013). The framework reflected a desire to be consistent with many elements of the European approach in Regulation 327. With both Europe and the USA now regulating or declaring intent to do so, it is likely that Asian countries will introduce regulations setting minimum fan or fan and motor efficiencies. Currently, Malaysia, Korea and Taiwan have considered adopting fan efficiency requirements based on the Air Movement and Control Association (AMCA) Standard 205 Energy Efficiency Classification for Fans, as a mandatory requirement for government and private-sector projects (Gho, 2013).

Members within the industrial fan community widely believe that the minimum 2015 FMEGs are high enough to effectively exclude using stabilisation rings as a consequence of the efficiency penalty associated with their application. Further, within the European Union, minimum FMEGs most likely will continue to increase, and the same regulation pattern followed by a stepped increase in minimum fan or fan and motor efficiency will play out in both the USA and Asia.

Despite the regulatory challenge, tunnel ventilation fan designers are faced with an ongoing trend towards larger pressure pulses and therefore, an increasing likelihood that tunnel ventilation fans will be transiently driven beyond their mechanical design limits. Tunnel ventilation fan designers have historically utilised one of three approaches when selecting fans to operate in applications where aerodynamic stall is likely. The first is to select a fan with a non-stalling blade angle. A non-stalling blade angle is a blade angle at which a fan's characteristic rises continuously back to zero flow. In effect, the fan is aerodynamically so lightly loaded that it does not stall. The second is to select a fan with a high enough pressure developing capability to operate in the presence of a pressure pulse without stalling. The third is to fit a stabilisation ring to manage the mechanical consequences of aerodynamic stall.

The first approach results in relatively large and low speed fan selections. Sheard *et al.* (2013) observed that the cost of underground plant rooms is proportional to the diameter of the fans they must accommodate. As the cost of an underground plant room can be many times the cost of the tunnel ventilation fans installed in it, the first approach, whilst attractive to tunnel ventilation fan designers, is unattractive to tunnel designers. Practitioners have increasingly discredited the second approach as a consequence of its inability to prevent tunnel ventilation fan in-service mechanical failures. As we previously noted, Borello *et al.* (2013) concluded that a difference between small and large pressure pulses is that a large pressure pulse that does not result in aerodynamic stall may still double the unsteady mechanical forces to which fan blades are subjected. This doubling of unsteady mechanical forces may explain why the second approach is becoming increasingly less effective as the magnitude of pressure pulses increases.

A market requirement for smaller tunnel ventilation fans, to minimise plant room construction cost, combined with a trend towards larger pressure pulses, has

made the first and second approach less attractive when selecting fans to operate in applications where aerodynamic stall is likely. Consequently, we must consider the alternative approaches to stall control. Members of the aerospace community have studied fan and compressor stall control extensively. Bianchi *et al*. (2013) reported that active stall control concepts include:

- variable pitch in motion blades (Bianchi *et al*., 2012);
- bleed valves (Vo, 2007); and
- air injection (Suder *et al*., 2001; Nie *et al*., 2002).

Members of the industrial and aerospace fan communities have also studied passive stall control. Bianchi *et al*. (2013) reported that passive stall control concepts include:

- air separators (Yamaguchi *et al*., 2010);
- sinusoidal blade leading edges (Corsini *et al*., 2014); and
- stabilisation rings (Ivanov, 1965; Karlsson and Holmkvist, 1986).

Sheard and Corsini (2012) studied the mechanical impact of aerodynamic stall. They observed that since the early 1960s, scholars have tried to develop stage recirculation devices tailored to the pressure rise and volume flow rate ranges typical of industrial fans. Ivanov (1965) received the first patent in 1965. The concept is of an annular 'slit' in the casing upstream of the blades that stabilises fan performance as it approaches stall. Karlsson and Holmkvist (1986) patented a more practical embodiment of Ivanov's concept. They incorporated static vanes into an annular chamber positioned immediately upstream of the fan blade's leading edge. It was Karlsson and Holmkvist's concept that Bard (1984) named a 'stabilisation ring', Figure 11.1. Despite subsequent developments to the concept (Hill *et al*., 1988), tunnel ventilation fan designers have almost exclusively adopted Karlsson and Holmkvist's (1986) configuration. We may consider the stabilisation ring to be a part of the wider family of casing treatments that include grooves and slots (Takata and Tsukuda, 1977; Smith and Cumpsty, 1984) and stepped tip gaps (Thompson *et al*., 1998). Engineers originally developed casing treatments for application in axial compressors to improve their stable operation range.

Stabilisation ring vanes are classically constructed from curved plate, with a shroud to separate stabilisation ring inlet and exit, Figure 11.2. The stabilisation ring has historically proven highly effective as the vanes remove the momentum component circumferentially and re-inject the flow in the axial direction. The flow through the vanes is turned such that it exits the vanes upstream from the fan blade's leading edge, re-energised and flowing in an axial direction. The stabilisation ring's effect on the fan characteristic eliminates the sharp drop in its pressure developing capability, which engineers classically associate with fan stall. The primary characteristic of a fan fitted with a stabilisation ring is continuously rising pressure back to zero flow. It was this modification in the fan characteristic that led to tunnel ventilation fan designers widely embracing stabilisation ring.
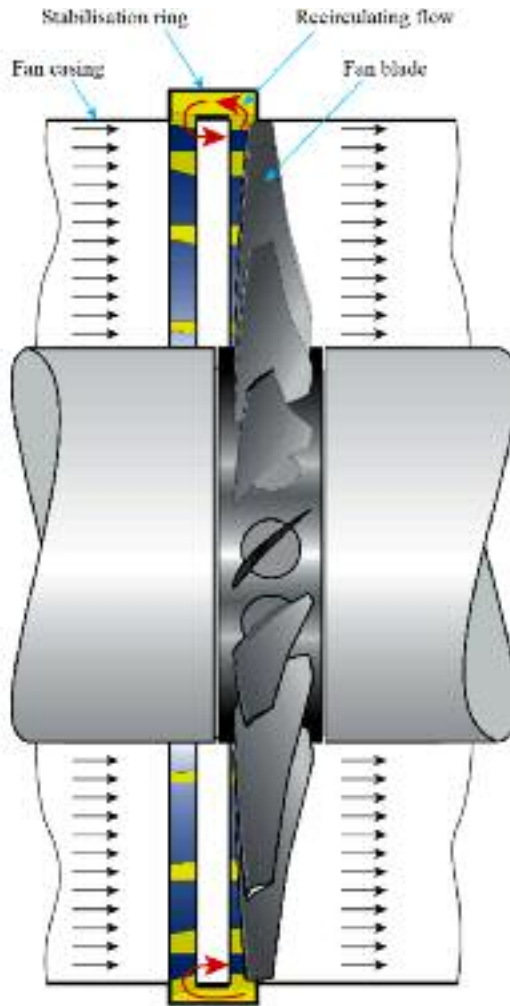
FIGURE 11.1. An example of an axial fan with a stabilisation ring over the blade tip (Eurovent, 2007). As the fan stalls, blade boundary layer fluid reverses direction at the blade tip, enters the stabilisation ring and is redirected in an axial direction. The recirculating flow then reintroduces itself into the main-stream flow upstream of the blade leading edge.

Within the extant literature there are experimental studies into the impact of stabilisation ring geometry on a fan's characteristic. Azimian *et al*. (1987) and Ziabasharhagh *et al*. (1992) studied the effect of varying height (h), Figure 11.2. Miyake *et al*. (1987) studied the effects of varying inlet area (I). Kang *et al*. (1995) and Azimian *et al*. (1987) studied the effect of varying shroud area (S). Yamaguchi *et al*. (2010) studied the effect of varying chord exposure (Ce). Azimian *et al*. (1987) and Miyake *et al*. (1987) both studied the effect of varying vane position, number and inlet angle within a stabilisation ring. Their twin objective was to optimise the
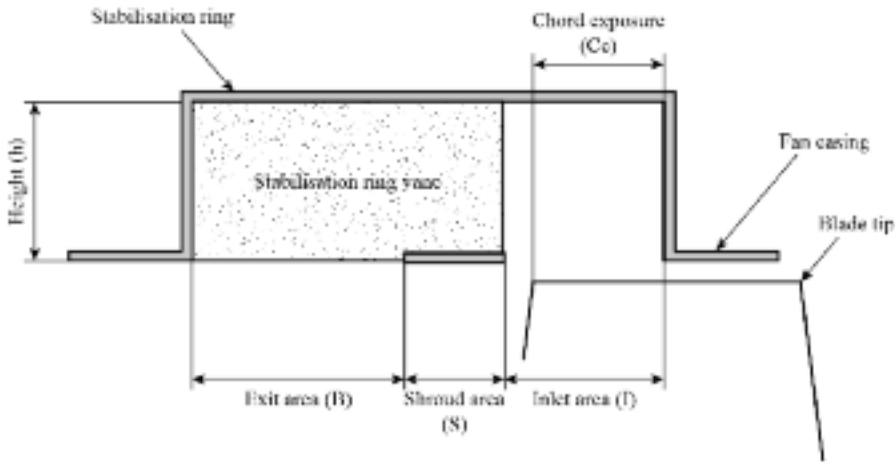
FIGURE 11.2. Location of the stabilisation ring casing relative to the fan blades, and the parameters used to define stabilisation ring geometry.

vane inlet angle and minimise blockage into the stabilisation ring. These scholars were successful in there endeavours to identify the impact of a stabilisation ring's geometry on a fan's characteristic. Thus, they were able to optimise geometry to produce the most stable fan characteristic. However, they were unable to identify why a stabilisation ring reduced fan efficiency.

The research reported in this chapter combines both an experimental assessment of overall fan performance with and without a fitted stabilisation ring and a numerical analysis of the flow-field within the stabilisation ring. A review of the experimental and numerical results facilitates the elucidation of physical flow mechanisms at play within the stabilisation ring. The chapter then discusses the impact of stabilisation ring geometry on fan efficiency at different fan operating points. It concludes with an assessment of a possible reason why stabilisation rings reduce fan efficiency, and how one might avoid that reduction.

DESCRIPTION OF THE TEST CASE

Tunnel ventilation fans, classically, must have the ability to both supply and extract air from a tunnel system, with the operator's choice dependent on the tunnel ventilation system's operating mode most appropriate at any given point in time. Consequently, tunnel ventilation fans must incorporate a reversible aerodynamic design. Sheard and Daneshkhah (2012) considered the conceptual design of reversible axial tunnel ventilation fans. They observed that the reversibility requirement results in the necessity for symmetrical fan blade aerofoil sections. Also, the fan designer must reduce the guide vanes to flow-straighteners if the fan is to produce the same flow and pressure in both directions. It is necessary for tunnel ventilation fans to produce the same flow and pressure in both supply and extract modes to enable the

tunnel ventilation system to accommodate the varied requirements for routine venti-
lation and to keep escape routes clear in the event of a fire. The reported research
utilised a one metre axial fan, incorporating reversible blades with a hub-to-tip di-
ameter ratio of 0.4, close to the optimum for an axial fan and standard in fans in-
tended for tunnel ventilation application, Table 11.1.

EXPERIMENTAL TEST RIG

We conducted measurements in an experimental facility that complied with
ISO 5801:2007 requirements, the International Organization for Standardizations
equivalent to the historic British Standard BS 848 Part 1 (2007). During experimen-
tal tests of the studied fan, both with and without a fitted stabilisation ring, we mea-
sured static pressure upstream and downstream of the fan. We varied the flow rate
using a throttle in the test facilities pressure chamber, Figure 11.3. We derived fan
power by measuring motor torque and speed. We interpolated the fan characteristics
at each studied blade angle from 20 flow, pressure and power measurement points.
The measurements were intentionally clustered in the near-stall region. Each pres-
sure measurement is an average value of pressure, derived from an unsteady mea-
surement of pressure. In the fan characteristic's stable region, we measured unsteady
pressure for 60 seconds and then averaged it. In the fan characteristic's near-stall and
unstable regions, we measured unsteady pressure for 160 seconds and then averaged
it. The accuracy of pressure measurements was ±0.5 per cent of measured data. The
accuracy of power measurements was ± 0.5 per cent of measured data.

Table 11.1. *Fan geometry and operating point data.*

Performance standard	ISO 5801	
Volume flow rate, Q	5–20 m^3/s	
Total pressure rise, Δp_{tot}	200–750 Pa	
Rotational speed	1,490 rpm	
High temperature certification	300°C / 2h	
Blade section	Reversible	
Tip diameter, D_t	1,000 mm	
Blade count	9	
Hub-to-tip ratio	0.4	
Tip clearance, χ	1.2 % of the blade span	
Blade pitch angle, δ	20°, 25°, 30°	
	Hub	Tip
Blade chord, ℓ	148 mm	170 mm
Fan solidity, Σ	1.22	0.43
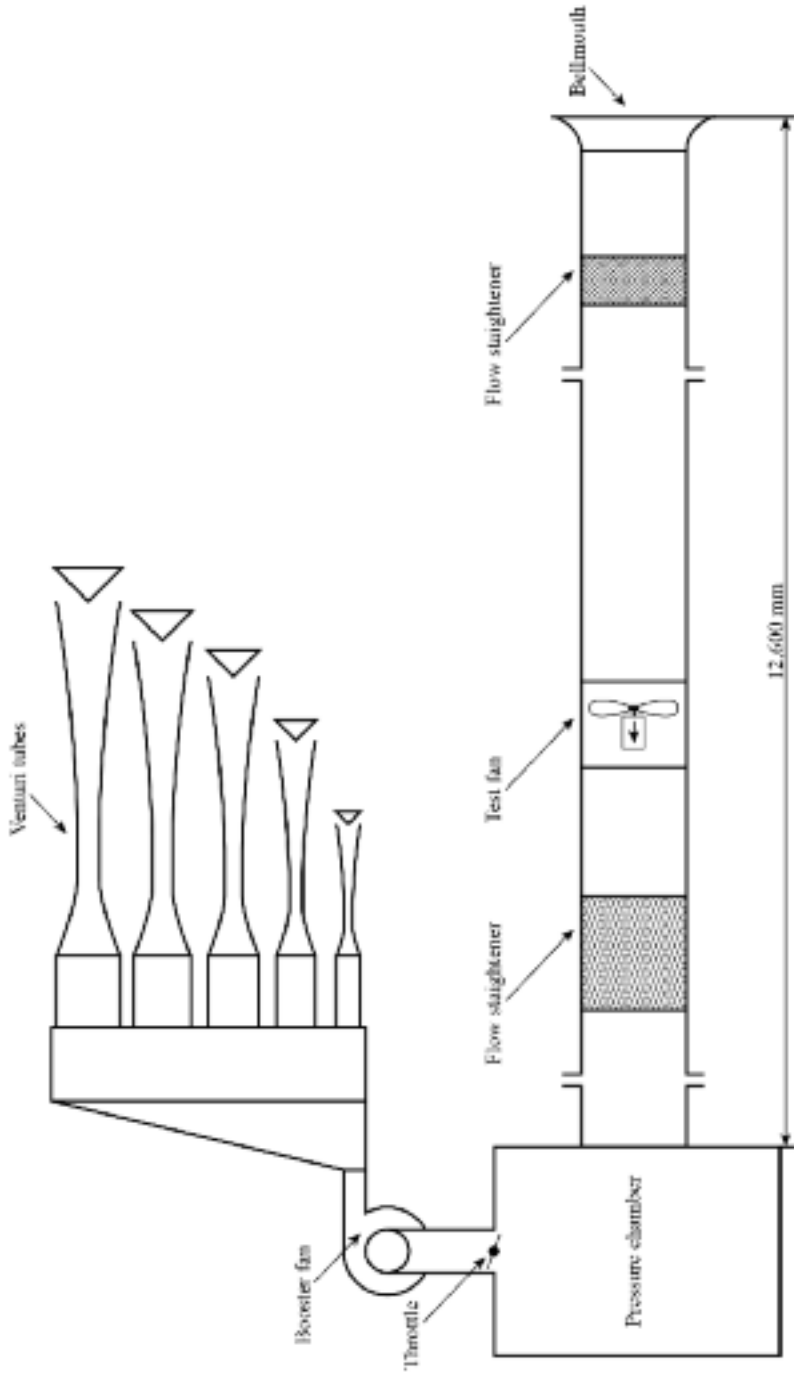
FIGURE 11.3. A schematic view of the ISO 5801:2007 (2007) standard ducted test rig used to characterise the studied fan both with and without a fitted stabilisation ring.

NUMERICAL TECHNIQUE

We carried out the numerical analysis using OpenFOAM 2.2.x (Weller *et al.*, 1998), an open source finite volume computational fluid dynamic code. When modelling the studied fan without a fitted stabilisation ring the least complex configuration that one can model is the rotor alone because if one neglects static components then one can carry out the computations in the rotating frame of reference. Consequently, there is no requirement to account for the computational mesh's movement. We applied periodic boundary conditions at mid-pitch in order to compute the flow-field through a single blade passage, Table 11.2. A disadvantage that occurs with applying periodic boundary conditions is that they can fail to model accurately turbulent structures if one associates those structures with long wavelengths or length-scales. The limitations that occur with applying periodic boundary conditions is not an issue with a Reynolds-averaged Navier–Stokes (RANS) approach as the approach itself does not model the turbulent structures that periodic boundary conditions fail to model. Consequently, the use of periodic boundary conditions does not degrade the RANS simulation's accuracy. In this case, we carried out computations with the *SRFSimpleFoam* solver fromOpenFOAM's library.

When modelling the studied fan with a fitted stabilisation ring, a rotor alone approach was not appropriate as the modelling needed to account for the vanes within the stabilisation ring. The modelling approach that we selected was the frozen rotor approach, as the blade-to-vane coupling did not require a moving mesh. The relative position of the blades and vanes is fixed in time, with relative motion managed using different frames of reference and adding Coriolis and centrifugal forces to the momentum equation in the rotating frame of reference. The frozen rotor approach is able to account for a non-uniform circumferential distribution of velocity and pressure at the interface between the computational domain's rotating and static regions. However, it fails at fully reproducing the full mixing of the wakes released by the fan blades inside the stabalisation ring, partially limiting the accuracy of the computations (Horlock and Denton, 2005). Despite this ultimate limitation, the frozen rotor approach offers a good trade-off between accuracy and computational effort.

We were able to reduce the computational effort further as the fan blades and the stabilisation ring vanes are not adjacent, but indirectly coupled through the stabilisation ring. Consequently the impact of the vane-to-vane flow-field on the blade-to-blade flow-field may be neglected. The geometry of the stabilisation ring resulted in three vane-to-vane passages for each fan blade-to-blade passage. We therefore computed the blade-to-blade flow-field in just one fan blade-to-blade passage and

Table 11.2. *Computational model boundary conditions.*

Inflow	Velocity and *k* profile (Sheard *et al.*, 2009); L_t=0.1c
Outflow	Zero gradient
Mid-pitch	Periodicity
Hub and rotor	ωR
Shroud, vanes, stabilisation ring surfaces	No-slip conditions

three stabilisation ring vane-to-vane passages. In this case, we carried out computations with the solver *MRFSimpleFoam*, with the rotating and static regions coupled using an Arbitrary Mesh Interface (AMI) technique (Farrell and Maddison, 2011).

Corsini *et al.* (2013a) observed that a limiting factor with a RANS approach is the definition of eddy viscosity used in most of the basic turbulence models. Modelling eddy viscosity using a Boussinesq approximation results in the Reynolds stress tensor aligning with the velocity's gradient. The Reynolds stress tensor is not aligned with the velocity's gradient in regions of separated flow or impingement, and therefore, the modelling approach for eddy viscosity does not accurately model the flow-field physics. A method to improve the accuracy with which one models the flow-field physics without increasing the required computational effort is to use a non-linear eddy viscosity turbulence model. The formulation is better able to account for the production of turbulent kinetic energy in impingement regions as it constitutes a more realistic anisotropic reproduction of Reynolds stresses with respect to linear eddy viscosity.

The studied fan's computational simulations both with and without a fitted stabilisation ring utilised a cubic low-Reynolds number formulation of the k-e eddy viscosity turbulence model (Lien and Leschziner, 1994). Other researchers have demonstrated that this formulation partially recovers the anisotropy of Reynolds stresses, and is able to correctly reproduce flow-field features typically associated with turbomachinery flow (Corsini and Rispoli, 2005; Corsini *et al.*, 2006, 2013b, 2014; Corsini and Sheard, 2007; Durbin, 2011). All computational simulations utilised a second order quadratic upstream interpolation for a convective kinetics (QUICK) divergence scheme, with a convergence tolerance of 10^{-7} for all computed quantities. We carried out the simulations on the Cineca Fermi HPC system over 264 processors, with each computed operating point requiring approximately three hours of computational time.

Numerical grid

When considering the required number of cells to achieve a grid independent solution, it is noteworthy that not all parts of the computational domain are equally important. For example, we associate the blade tip-to-casing region with a tip-leakage vortex, and in order to model this flow feature, it requires a relatively high grid density. However, we must associate this cell clustering in regions of known flow-field features with a smooth transition from regions of low to high cell density. We must avoid cells with a large aspect ratio or those that are heavily distorted. Despite this caveat, we can minimise the required number of cells to achieve a grid independent solution through a grid refinement process.

In the reported research, we undertook a grid sensitivity analysis using fan pressure, blade lift and drag as convergence parameters with grids of 1.2, 4.0 and 7.5 million cells. The final grid for the numerical analysis without fitted stabilisation ring comprised 2.0 million hexahedra and 4.5 million tetrahedral, Table 11.3 and Figure 11.4. The final grid for the numerical analysis with a fitted stabilisation ring included an additional 1.0 million hexahedra, Figure 11.5.

Table 11.3. *Details of the numerical mesh used for the peak efficiency operating point numerical analysis without a fitted stabilisation ring.*

Number of cells	3M hexahedra + 4.5M tetrahedra		
	Minimum	*Average*	*Maximum*
Aspect ratio	1.0	12	32
Minimum included angle	18	42	89
Volume ratio	1.0	1.3	2.8
Skewness	0.01	0.50	0.65
y^+ (blade)	0.70	0.81	1.21
y^+ (hub)	0.42	0.62	1.23
y^+ (shroud)	0.41	0.65	1.21
y^+ (vanes)	0.30	0.52	1.40
y^+ (stabilisation ring)	0.33	0.54	1.35
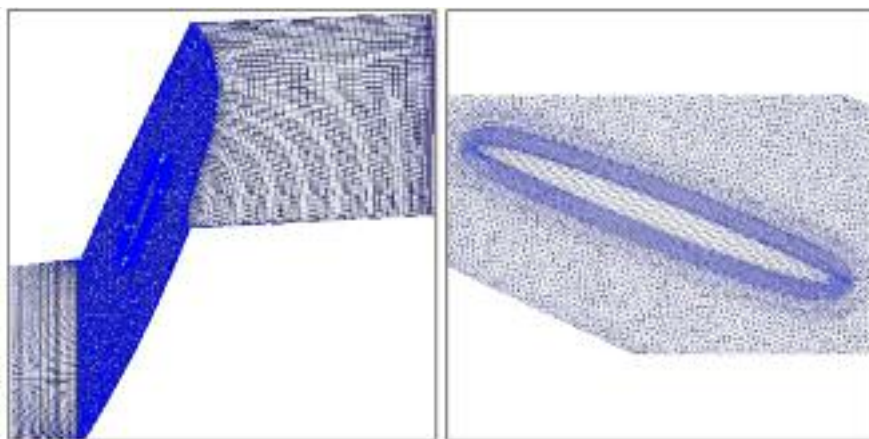
FIGURE 11.4. The fan blade computational mesh in the blade tip region. The aerofoil section is symmetrical as fans for tunnel ventilation application are required to provide the same flow in both forward and reverse.

EXPERIMENTALLY MEASURED FAN PERFORMANCE

The studied fan's measured performance without a fitted stabilisation ring is typical of an axial fan, with pressure rising with reducing flow rate followed by a drop in pressure that one classically associates with fan stall, Figure 11.6. The fan that we utilised in the reported research incorporated a casing manufactured in sections, a feature that allows one to change a plane casing section to a casing section incorporating a stabilisation ring. Thus, the casing design enabled us to experimentally establish fan performance with and without a fitted stabilisation ring, Figure 11.7. Critically, we could change the plane casing to a casing incorporating a stabilisation ring without removing or adjusting the fan impeller. This feature ensured that fan geometry did not change as we changed the plane casing section to a casing section incorporating a stabilisation ring.
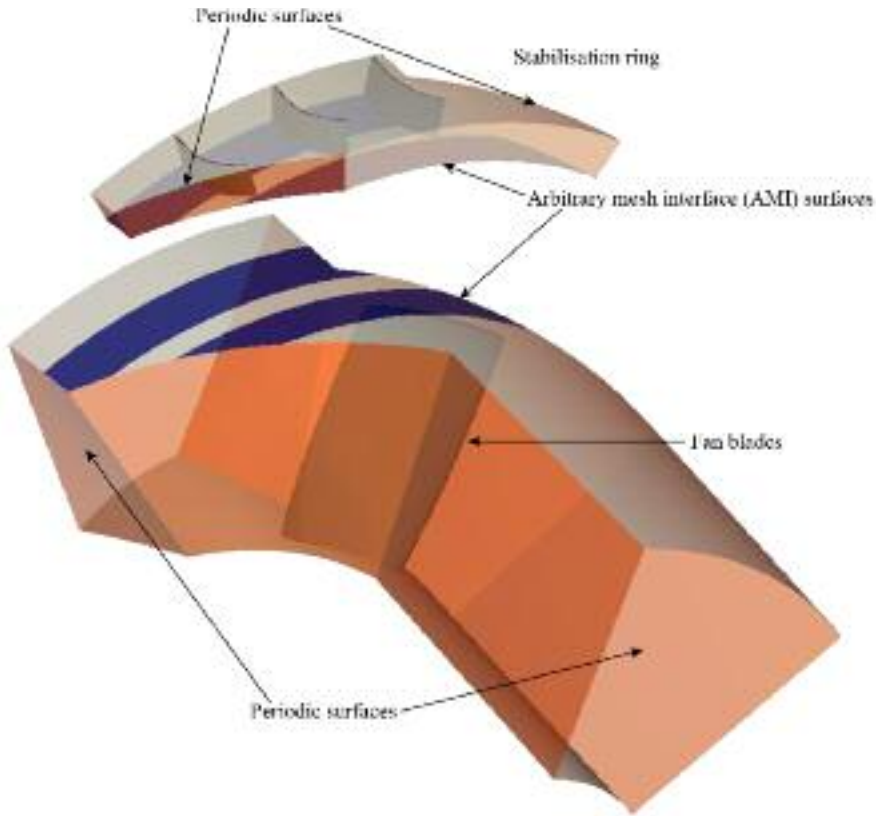
FIGURE 11.5. Computational domain with periodic surfaces, shaded orange and arbitrary mesh interface (AMI) surfaces, shaded blue. The fan blade-to-blade and stabilisation ring vane-to-vane domains are separated for the sake of clarify. In actuality the arbitrary mesh interface surfaces are coincident.

When we study the measured performance data, the stabilisation ring's impact is apparent. At peak pressure the stabilisation ring has almost no impact on either fan pressure rise or efficiency, Figure 11.7. As flow reduces and the fan stalls, the stabilisation ring's effect is to eliminate the drop in pressure, with continuously rising pressure back to zero flow. The stabilisation ring increases both the fan's pressure developing capability and efficiency at lower flow rates that would occur with stall if there were no fitted stabilisation ring. We should not interpret continuously rising pressure and improved fan efficiency as an indication that it is prudent to operate a fan with a stabilisation ring at low flow-rates that would occur with stall if there were no fitted stabilisation ring. Sheard and Corsini (2012) observed that the stabilisation ring does not provide complete mechanical protection from the effects of stall. If one fits a stabilisation ring, one should not select a fan to operate at a pressure higher than its peak pressure operating point without a fitted stabilisation ring.

In practical tunnel ventilation system applications, one must select the fans to operate at a pressure below their maximum pressure developing capability as a
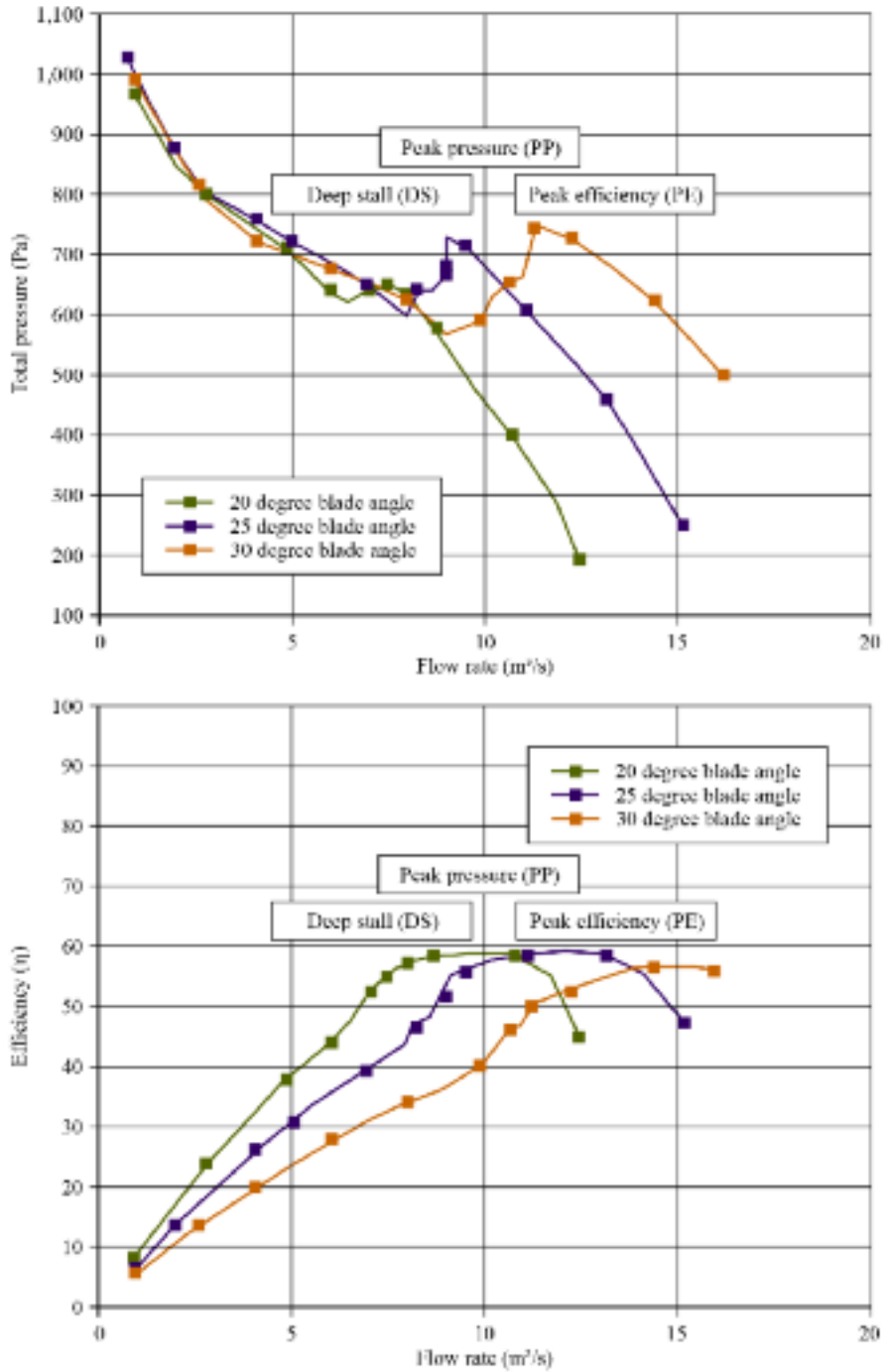
FIGURE 11.6. The experimentally measured performance of the fan, without a fitted stabilisation ring.
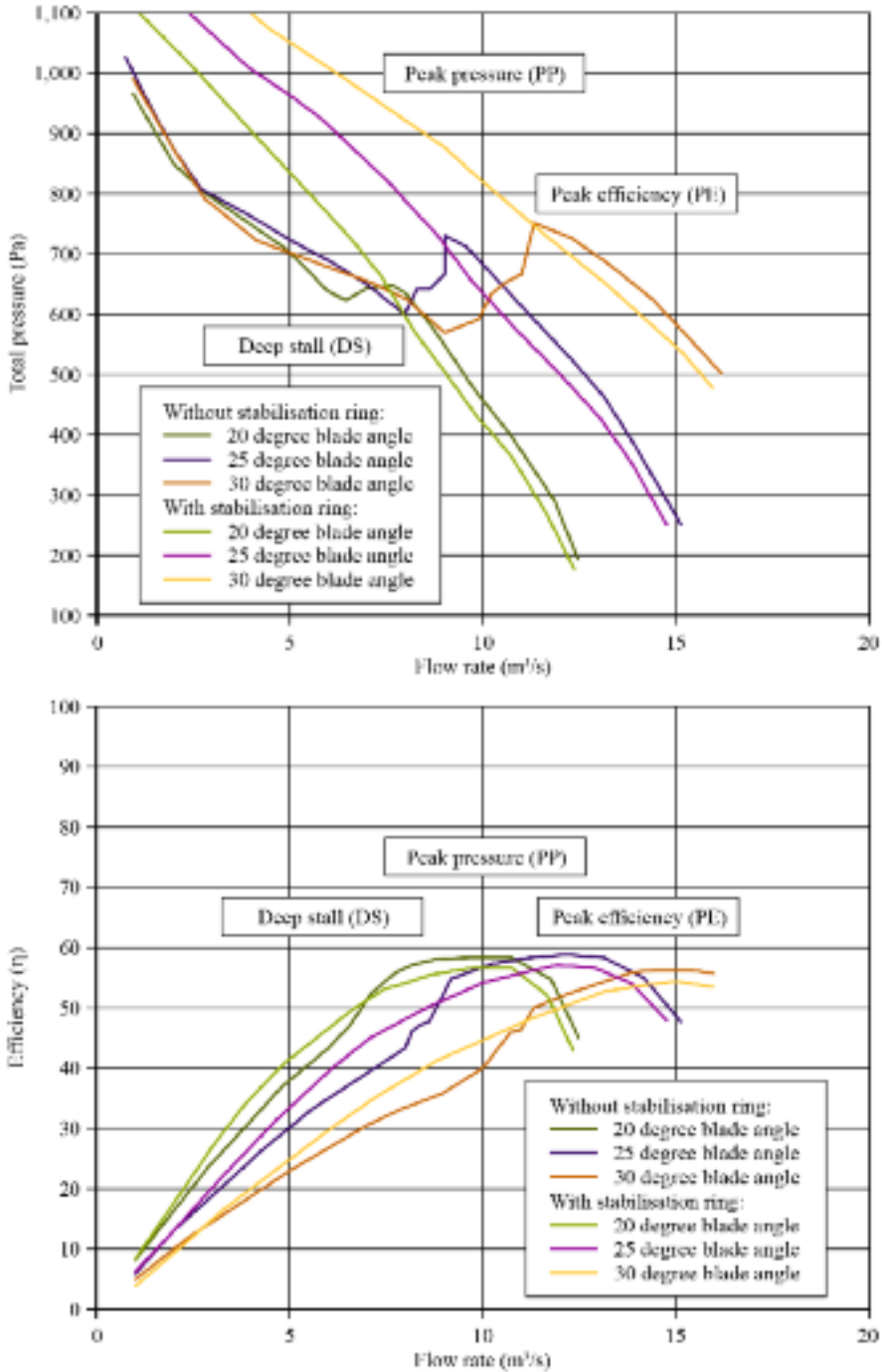
FIGURE 11.7. The experimentally measured performance of the fan, with and without a fitted stabilisation ring. Individual measurement points are not shown for the sake of clarity.

consequence of the pressure pulses to which they are subjected. In practice, one typically selects tunnel ventilation fans close to their peak efficiency operating point, both to minimise operating cost and to ensure that a pressure pulse does not drive the fan into stall. When one studies the measured performance data, it is apparent that at flow rates above that associated with peak pressure, the impact of a stabilisation ring is to reduce the fan's pressure developing capability, Figure 11.7. This reduction in pressure developing capability represents a fan efficiency loss at flow-rates above the peak pressure flow-rate. The loss in efficiency at the fans peak efficiency operating point is 2.4 per cent, Table 11.4. The industrial fan community generally assumes that fitting a stabilisation ring results in a three per cent reduction in fan efficiency, and so the experimentally measured reduction of 2.4 per cent is self-consistent with the experience of industrial fan designers.

When one studies the experimentally measured fan performance at the fan's peak pressure operating point, it is apparent that the stabilisation ring reduces fan performance by 0.6 per cent, Table 11.4. A reduction is fan efficiency of 0.6 per cent, whilst undesirable, is preferable to a reduction of 2.4 per cent and indicates that fitting a stabilisation ring can result in reduced fan efficiency of no more than 0.6 per cent. However, at the peak efficiency operating point where one invariably selects tunnel ventilation fans, the 2.4 per cent reduction suggests that the stabilisation ring is not performing to its full potential. In the reported research we used a numerical analysis to study the physical flow mechanisms in both the fan blade-to-blade and stabilisation ring vane-to-vane flow-field. The objective was to establish why the stabilisation ring was not performing to its full potential at flow rates above that of the peak pressure point on the fan's characteristic.

NUMERICAL ANALYSIS

The measured performance with and without a fitted stabilisation ring illustrates the stabilisation ring's effectiveness, Figure 11.7. At all three blade angles the stabilisation ring's presence results in a continuously rising characteristic. The measured performance without a fitted stabilisation ring, with 25 and 30 degree blade angles both show a sharp drop in pressure, Figure 11.7. The measured performance with a 20 degree blade angle shows a drop in pressure, but in comparison to the drop

Table 11.4. *The effect of a stabilisation ring on fan pressure and efficiency, with fan blade angle set at 20 degrees.*

| Operating point | Pressure (Pa) | | | Efficieny (η) | | |
| | Stabilisation ring? | | | Stabilisation ring? | | |
	No	Yes	Difference	No	Yes	Difference
Deep stall	623	730	17.2%	46.9	49.4	2.5%
Peak pressure	646	651	0.8%	54.6	53.2	−0.6%
Peak efficiency	595	548	−7.9%	57.8	55.4	−2.4%

measured at 25 and 30 degrees, it is a relatively shallow drop. This correlates with a relatively mild stall. Industrial fan designers classically utilise stabilisation rings in applications where the pressure drop associated with stall is sharp. One associates a shallow pressure drop with a less well defined change in aerodynamic conditions in the blade tip region. This presents a stabilisation ring with a greater challenge. We may therefore assume that a stabilisation ring that can operate effectively with a 20 degree blade angle will operate effectively at 25 and 30 degrees. For that reason we conducted the numerical analysis, both with and without a fitted stabilisation ring with a 20 degree blade angle.

We conducted the numerical analysis with and without a fitted stabilisation ring at three operating points. The first was at the fan's peak efficiency (PE) operating point. The second was at the fan's peak pressure (PP) operating point. The third was at a deep stall (DS) operating point:

- peak efficiency (PE), Δp_{tot} = 595 Pa, Q = 8.5 m^3/s;
- peak pressure (PP), Δp_{tot} = 646 Pa, Q = 7.5 m^3/s; and
- deep stall (DS), Δp_{tot} = 623 Pa, Q = 6.5 m^3/s.

Results of the numerical analysis for the three operating points, both with and without a fitted stabilisation ring, were in good agreement with the experimentally measured fan performance, Figure 11.8. The difference between both predicted and measured pressure and efficiency was typically no more than one per cent, Table 11.5. The uncertainty of the measured pressure and efficiency was of the same order, and therefore the agreement was good enough to give confidence in the ability of the numerical analysis to predict both the fan blade-to-blade and stabilisation ring vane-to-vane flow-field.

Table 11.5. *Experimentally measured (EXP) and numerically predicted (CFD) pressure and efficiency with and without a fitted stabilisation ring, with fan blade angle set at 20 degrees.*

Operating point	Stabilisation ring fitted?	Pressure (Pa)			Efficiency (η)		
		EXP	CFD	$\Delta\%$	EXP	CFD	$\Delta\%$
Deep stall	Yes	623	617	0.9	46.9	45.8	1.1
	No	730	740	1.3	49.4	50.2	0.8
Peak pressure	Yes	646	639	1.0	54.6	55.1	0.5
	No	651	643	1.2	53.2	53.7	0.5
Peak efficiency	Yes	595	591	1.0	57.8	57.2	0.6
	No	548	539	1.6	55.4	54.9	−0.5
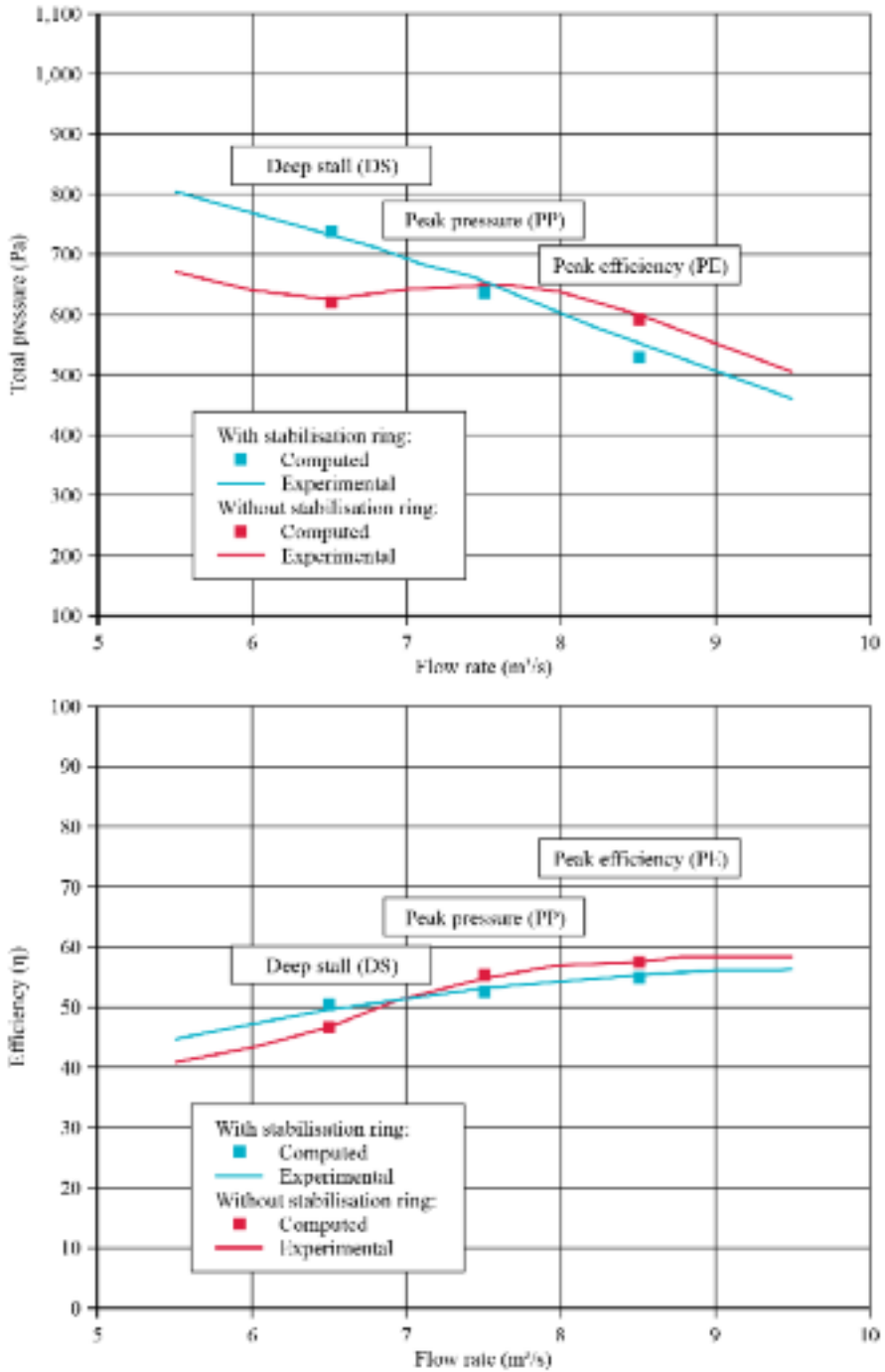
FIGURE 11.8. Comparison between the experimentally measured and numerically predicted fan performance for the studied fan, with and without a fitted stabilisation ring at a blade angle of 20 degrees.

BLADE-TO-BLADE NUMERICAL RESULTS

One may study the fan blade-to-blade flow-field through a consideration of normalised pressure (p*) contours on the blade pressure surface, Figure 11.9. For the studied fan without a fitted stabilisation ring, a shift from the peak efficiency to peak pressure operating point results in an increase in the pressure over the blade pressure surface. The blade tip stagnation region moves to the blade pressure side with a shift from the peak pressure to deep stall operating point. Perhaps most significantly, the blade boundary layer separates at the hub, partially blocking the blade passage as a consequence of operating in deep stall.

For the studied fan with a fitted stabilisation ring, a shift from the peak efficiency to peak pressure operating point results in an increase in the pressure over the blade pressure surface. The shift from the peak pressure to deep stall operating point continues the trend that we have seen with the shift from the peak efficiency to the peak pressure operating point, with pressure continuing to rise over the blade surface. We no longer associate the deep stall operating point with the blade boundary layer separating at the hub. Although there is some evidence of an over developed wake at the blade trailing edge in the hub region, the large scale separation that was evident with no stabilisation ring is now eliminated. The absence of the hub separation indicates that the stabilisation ring has affected blade loading over the entire blade span.

Normalised pressure contours over the blade pressure surface with and without a fitted stabilisation ring provide an insight into the span-wise flow-field. A stabilisation ring fitted over the blade tip leading edge eliminates a separation at the blade hub trailing edge. Reasonably, we might expect a stabilisation ring fitted over the blade tip to have a primary impact on the blade-to-blade flow-field in the blade tip region. However, when one studies cylindrical surfaces at 99 per cent blade span, contours of normalised pressure for the studied fan are similar with and without a fitted stabilisation ring at each of the studied operating points, Figure 11.10. At the peak efficiency operating point the normalised pressure contours over the blade suction surface indicate that a stabilisation ring presence results in a small reduction in a negative pressure core's magnitude at the blade leading edge. We may associate this reduction with the flow that diverts into the stabilisation ring.

At the peak pressure operating point the stabilisation ring's presence results in the suction surface negative pressure core moving upstream, Figure 11.10. Along the suction surface the low pressure core has extended from the blade leading edge over approximately 60 per cent of the blade chord. We also associate the first 20 per cent of the pressure surface with the presence of a high pressure core. Although changes in the cylindrical blade-to-blade flow-field are modest compared to the changes in the span-wise blade-to-blade flow-field, they indicate that the stabilisation ring's presence does affect boundary layer development in the blade tip region.

At the deep stall operating point the trends that we observed with the move from the peak efficiency to the peak pressure operating point continue. Both suction surface negative pressure and pressure surface high pressure cores are clearly defined along the blade chord, indicating that the control of boundary layer fluid has
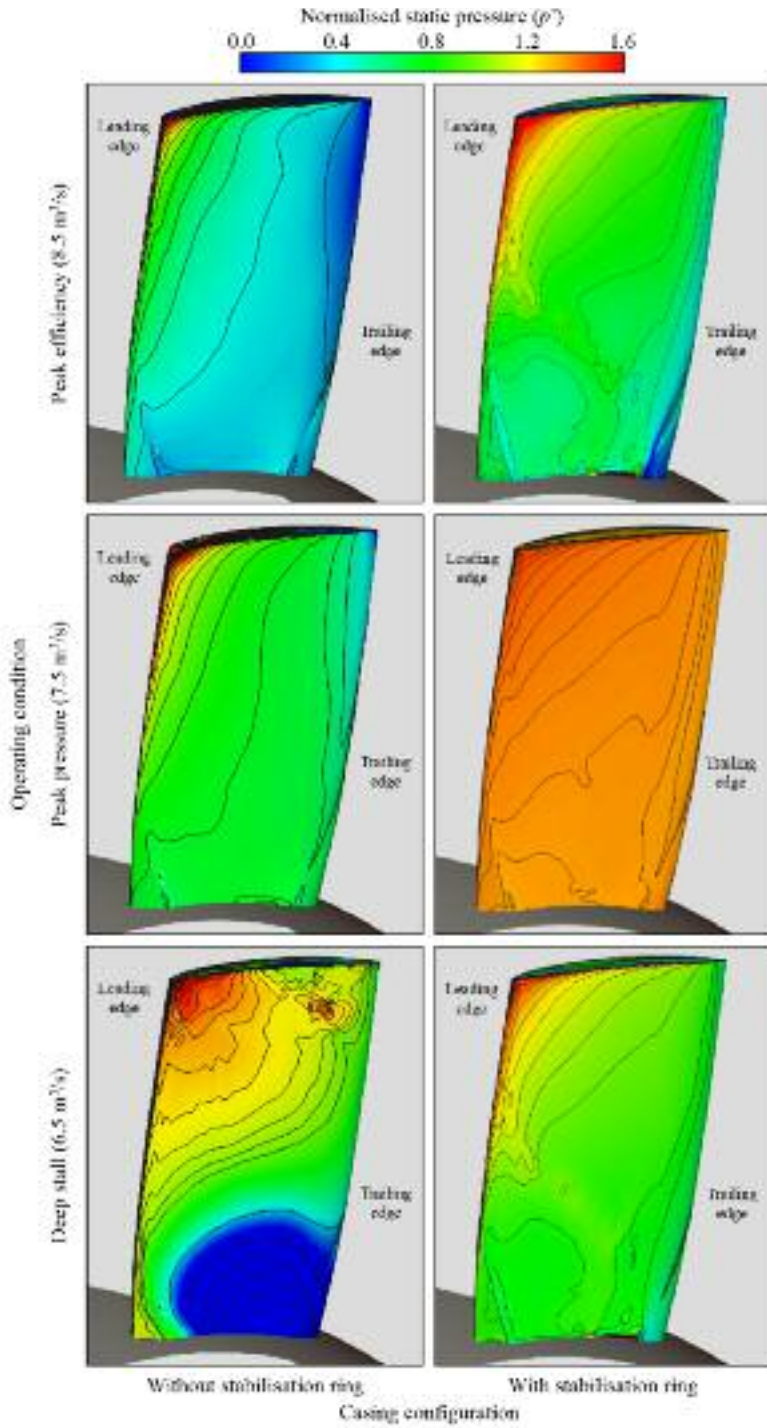
FIGURE 11.9. Normalised pressure (p*) contours over the blade pressure surface at the peak efficiency, peak pressure and deep stall operating points both with and without a fitted stabilisation ring.
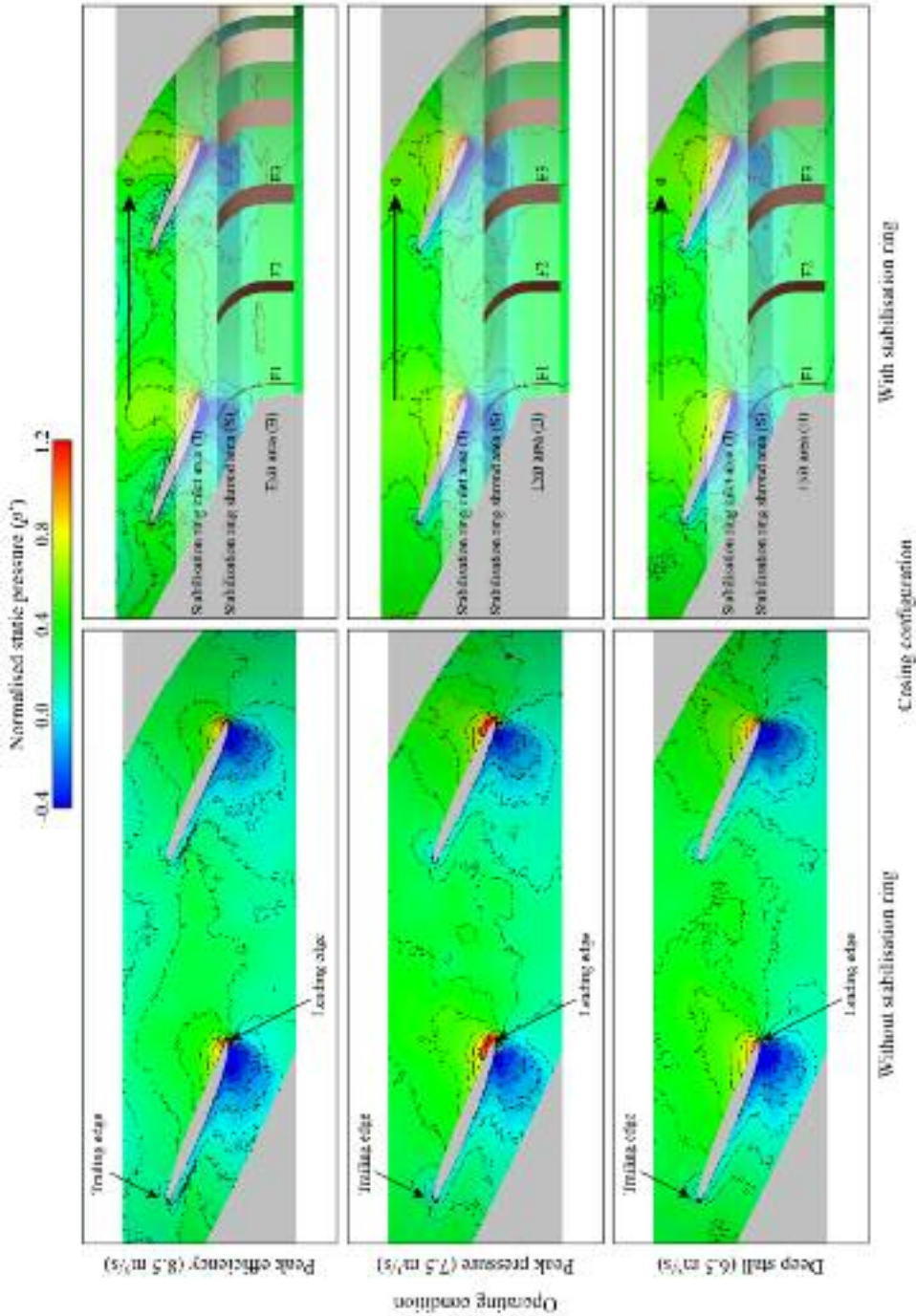
FIGURE 11.10. Normalised pressure (p*) contours over a cylindrical surface at 99 per cent blade span at the peak efficiency, peak pressure and deep stall operating points with a fitted stabilisation ring.

now become more fully established. The implication is that at the deep stall operating point the stabilisation ring's presence has resulted in a blade-to-blade flow-field that feeds boundary layer fluid into the stabilisation ring. We may verify this assertion by analysing the flow-field within the stabilisation ring.

STABILISATION RING NUMERICAL RESULTS

We conducted a numerical analysis of the flow-field through the stabilisation ring at three operating points: peak efficiency, peak pressure and deep stall, Table 11.6. We defined normalised volume flow rate in two ways to aid interpretation. First, we divided the volume flow rate through the stabilisation ring by the volume flow rate through the stabilisation ring when operating at the peak efficiency operating point, Θ^*. Second, for each operating point we divided the volume flow rate through the stabilisation ring by the volume flow rate through the fan, Π^*. The normalised volume flow rates illustrate that at the peak efficiency operating point, 2.3 per cent of the flow through the fan passes through the stabilisation ring, Table 11.6. As the fan moves to its peak pressure and then deep stall operating point, the flow increases to 6.1 and then 9.2 per cent respectively of the flow through the fan.

The flow passing through the stabilisation ring at the peak efficiency operating point is a small enough proportion of the flow passing through the fan to reasonably expect a relatively minor impact on the blade-to-blade flow-field. The flow passing through the stabilisation ring at the deep stall operating point is a large enough proportion of the flow passing through the fan to reasonably expect a relatively major impact on the blade-to-blade flow-field. This subjective observation is self-consistent with the span-wise blade-to-blade flow-field over the blade pressure surface that indicates that at the deep stall operating point a hub separation has been eliminated. We may conclude that a reason why the stabilisation ring is effective at the deep stall operating point is that almost ten per cent of the flow through the fan recirculates through the stabilisation ring. The analysis of normalised pressure over span-wise and cylindrical surfaces is self-consistent with the overall analysis of normalised flow through the stabilisation ring. However, the analysis provides no insight into why fan efficiency reduces by 2.4 per cent at the peak efficiency operating point with a fitted stabilisation ring. With a relatively minor 2.3 per cent of the flow through the

Table 11.6. *Numerically predicted flow-rate through the stabilisation ring normalised by the flow through the fan (Θ^*) and flow through the stabilisation ring normalised by the flow through the stabilisation ring at the peak efficiency operating point (Π^*), with fan blade angle set at 20 degrees.*

Operating point	Θ^*	Π^*
Deep stall	3.0	9.2%
Peak pressure	2.3	6.1%
Peak efficiency	1	2.3%

fan passing through the stabilisation ring at the peak efficiency operating point, reasonably, we might expect little or no impact on fan efficiency. To understand why the stabilisation ring has such a negative impact on fan efficiency we must study the stabilisation ring flow-field.

We used a numerical analysis to study the stabilisation ring vane-to-vane flow-field. The starting point for a numerical analysis was to compute the azimuthally averaged static pressure difference across the stabilisation ring's inlet and exit. The static pressure difference is relatively low at both the peak efficiency and peak pressure operating points, but significantly larger at the deep stall operating point, Table 11.7. Within the stabilisation ring, we may study the vane-to-vane flow-field. The vane-to-vane flow-field computed at the deep stall operating point, Figure 11.11, is used to illustrate the location of the three studied vane-to-vane passages; passage F1-F2, passage F2-F3 and passage F3-F1. The change in static pressure across the three vane-to-vane passage is then presented as a function of stabilisation ring flow, Figure 11.11.

The stabilisation ring inlet is positioned over the blade leading edge, resulting in a periodic inlet static pressure field. In contrast, the stabilisation ring exit is far enough up-stream of the blades to be relatively unaffected by potential flow effects associated with the rotating blade-to-blade flow-field. Consequently the pressure difference across stabilisation ring vane-to-vane passages is periodic. Consider the vane-to-vane passage F2-F3. This passage is positioned mid-way between two blades, with static pressure across the stabilisation ring remaining close to zero for the peak efficiency, peak pressure and deep stall operating points, Figure 11.11. Consider the vane-to-vane passage F1-F2. This passage is positioned over a blade pressure surface, with static pressure across the stabilisation ring reaming between 120 and 140 Pa for the peak efficiency, peak pressure and deep stall operating points. Consider the vane-to-vane passage F3-F1. This passage is positioned over a blade suction surface, with static pressure across the stabilisation ring changing from –175 Pa for the peak efficiency to –125 Pa at the peak pressure to –40 Pa at the deep stall operating point. The change in static pressure across the vane-to-vane passage F3-F1with changing operating point results in the change azimuthally averaged static pressure difference across the stabilisation ring's inlet and exit, Table 11.7.

We may study the vane-to-vane flow-field by considering streamlines through the stabilisation ring. We may plot stream lines on a surface midway between vanes (Figure 11.12, left) and also as three-dimensional stream lines (Figure 11.12, right). At the peak efficiency operating point the stream lines on a surface midway between vanes indicate the presence of a secondary flow feature. This suggests that the flow

Table 11.7. *The azimuthally averaged static pressure difference (Δp_{stat}) across the stabilisation ring's inlet and exit, with fan blade angle set at 20 degrees.*

Operating point	Δp_{stat}(Pa)
Deep stall	38
Peak pressure	–2
Peak efficiency	8
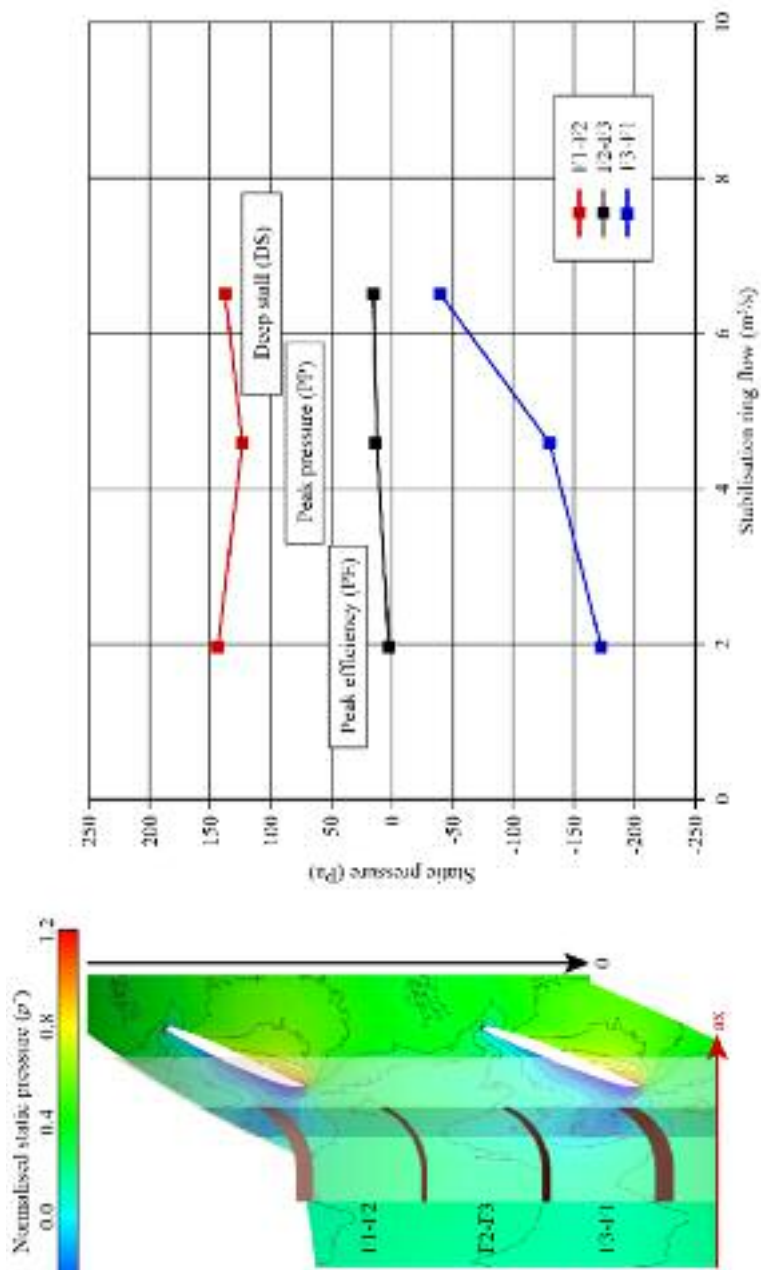
FIGURE 11.11. The vane-to-vane flow-field computed at the deep stall operating point, left, illustrating the location of the three vane-to-vane passages; passage F1-F2, passage F2-F3 and passage F3-F1. The change in static pressure across the three vane-to-vane passage within changing operating point is presented as a function of stabilisation ring flow, right.
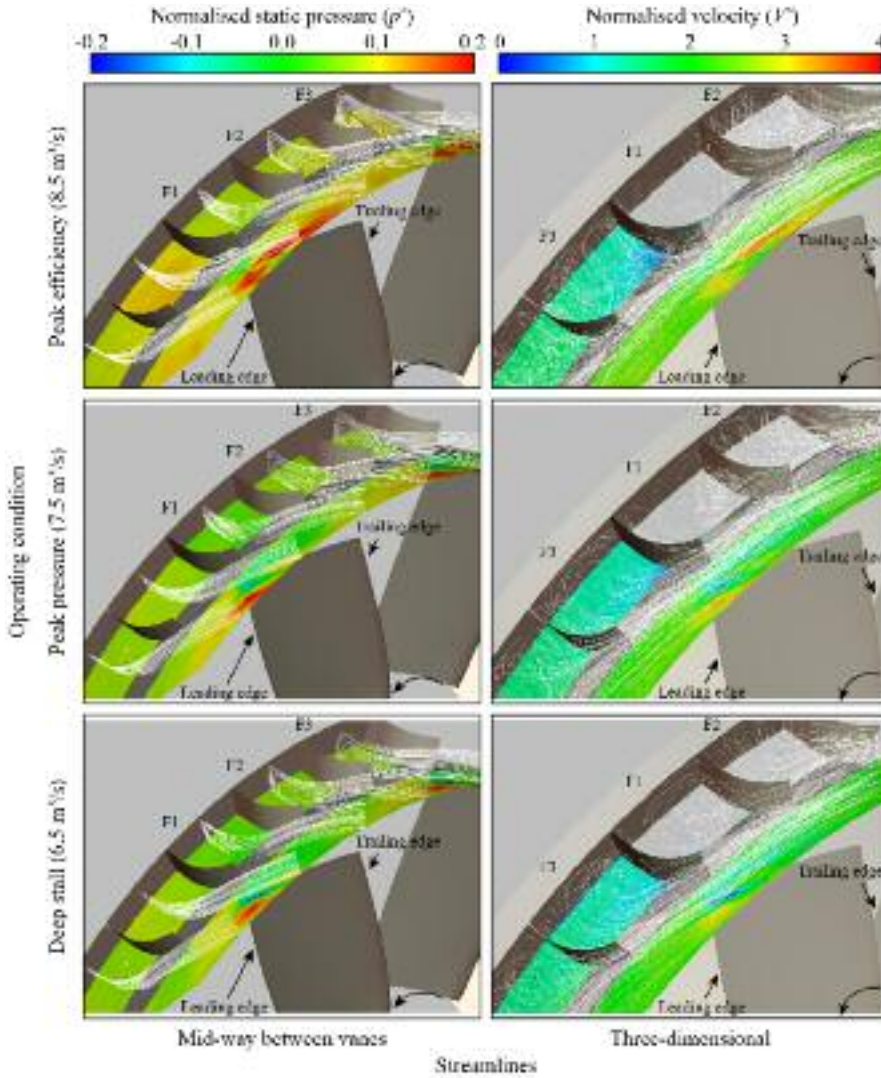
FIGURE 11.12. Streamlines within the stabilisation ring vane-to-vane passages on a surface midway between vanes (left) and as three-dimensional stream lines (right).

through the stabilisation ring is highly separated from the vanes. At the peak pressure and deep stall operating points the secondary flow feature is not evident. This indicates that the flow is attached to the vanes through the stabilisation ring. At the peak pressure operating point the stabilisation ring's presence reduces fan efficiency by 0.6 per cent. At the peak efficiency operating point the stabilisation ring's presence reduces fan efficiency by 2.4 per cent. Therefore, we may conclude that separated flow through the stabilisation ring vanes at the peak efficiency operating point constitutes an aerodynamic loss mechanism that reduces fan efficiency by 1.8 per cent.

We may provide a further insight into the flow-field through the stabilisation ring by considering axial flow coefficient contours, Figure 11.13. The axial flow coefficients' surface extends over three vane-to-vane passages, as the studied stabilisation ring configuration incorporates three vanes for each fan blade. Hence, vane-one and van-three are close to a fan blade, whilst vane-two is midway between blades. The axial flow coefficients' surfaces are augmented with a single black line that denotes zero axial flow, with forward flow and back flow on either side of the black line.

At the peak efficiency operating point, axial flow coefficients between all three vanes indicate back flow over the vane's outer portion. There is a smaller region of black flow for vane-one due to the blade's presence beneath the vane. As the fan throttles towards its peak pressure operating point, the percentage of flow through the stabilisation ring increases, resulting in an increase in the attached flow region's thickness on vane-one and vane-three's suction surface. Vane-two that is midway between fan blades does not show an increase in the suction surface attached flow. The trend that we observed with the shift from the peak efficiency to the peak pressure operating point continues with the shift from the peak pressure to deep stall operating point. The variation in vane-to-vane axial flow coefficients at the peak pressure and deep stall operating points indicates that the flow-field within the stabilisation ring is periodic in nature. The flow-field's periodic nature illustrates that we cannot study the flow-field through the vanes in isolation. We must study it within the context of the fan blades over which the stabilisation ring is fitted.

We may provide a final insight into the vane-to-vane flow-field by considering radial flow coefficient contours, Figure 11.14. Once again, the radial flow coefficients' surface extends over three vane-to-vane passages. The radial flow coefficients' surface are augmented with a single black line that denotes zero radial flow, with flow radially outward and flow radially inward on either side of the black line. At the peak efficiency operating point the vane-to-vane radial flow coefficient contours indicate that the vane-to-vane flow drives up the vane pressure surface and down the vane suction surface. At the peak pressure operating point the vane-one to vane-three passage flow still drives up the vane pressure surface and down the vane suction surface. However, the vane-two to vane-three passage flow uniformly drives inwards across the vane-to-vane passage. At the deep stall operating point the vane-one to vane-two and vane-two to vane-three passage flow uniformly drives inwards across the vane-to-vane passage, with only the vane-three to vane-one passage now exhibiting flow that drives up the vane pressure surface and down the vane suction surface. Once again, the radial flow coefficient contour analysis illustrates that we cannot study the stabilisation ring flow-field in isolation. The potential flow-field generated by the fan blades' passage past the vanes fundamentally affects the flow-field.
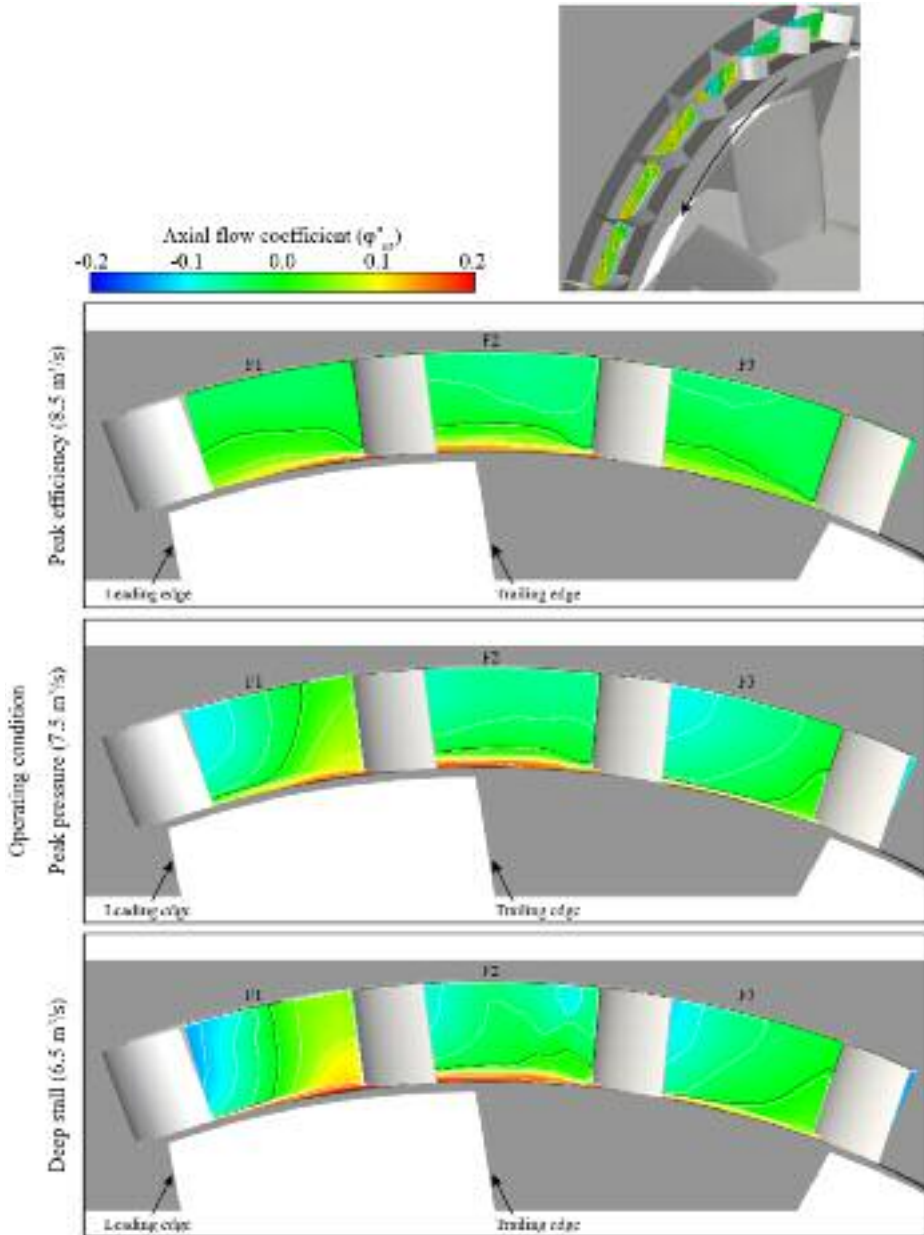
FIGURE 11.13. Axial flow coefficient across the stabilisation ring vane-to-vane passages, see insert top right. The black line ($\phi^*_{ax} = 0$) denotes zero axial flow, with forward flow and back flow on either side of the black line.
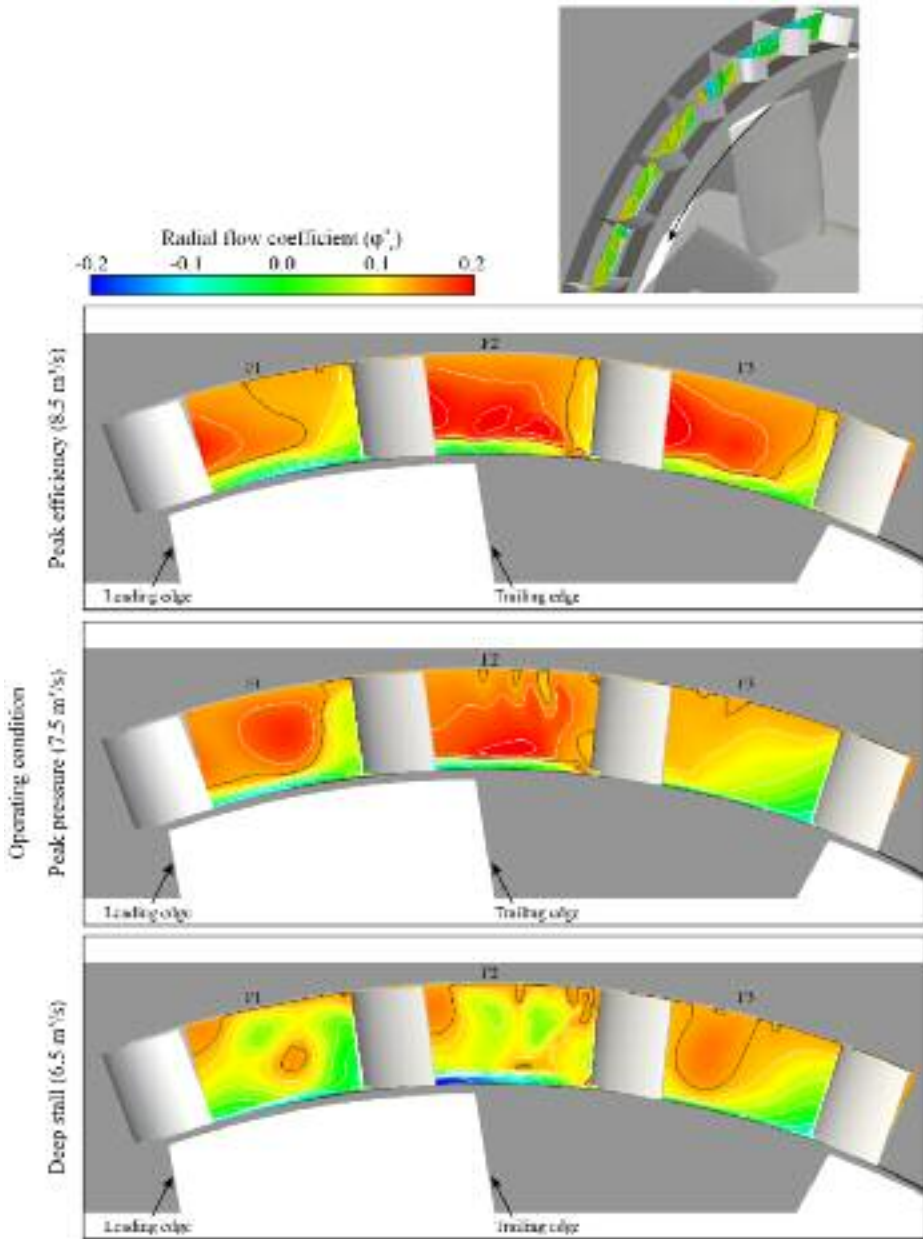
FIGURE 11.14. Radial flow coefficient across the stabilisation ring vane-to-vane passages, see insert top right. The black line ($\phi^*_r = 0$) denotes zero radial flow, with positive vales denoting flow moving radially outward and negative values denoting flow moving radially inward on either side of the black line.

CONCLUSIONS

We have established experimentally a tunnel ventilation fan's overall characteristics, both with and without a fitted stabilisation ring. The stabilisation ring's effect is to stabilise the characteristic, such that it rises continuously back to zero flow. Results from the numerical analysis at peak efficiency, peak pressure and deep stall operating points provide an insight into the stabilisation ring's effect on the fan blade-to-blade flow-field. At the peak efficiency and peak pressure operating points the stabilisation ring's effect is minimal. However, at the deep stall operating point, the stabilisation ring has a significant impact on the blade-to-blade flow-field. Most significantly, the stabilisation ring's presence results in control of a hub separation, indicating that the stabilisation ring affects the blade-to-blade flow-field over the entire blade span.

The experimentally measured fan efficiency with a fitted stabilisation ring at the peak pressure operating point was 0.6 per cent lower than the efficiency when we measured it without a fitted stabilisation ring. The numerical analysis indicated that the flow within the stabilisation ring is attached to the stabilisation ring vanes at the peak pressure operating point. From this we may conclude that when the flow within the stabilisation ring remains attached to the vanes, fitting a stabilisation ring reduces fan efficiency by 0.6 per cent. In contrast, the experimentally measured fan efficiency with a fitted stabilisation ring at the peak efficiency operating point was 2.4 per cent lower than the efficiency we measured without a fitted stabilisation ring. The numerical analysis indicated that the flow within the stabilisation ring is separated from the stabilisation ring vanes at the peak efficiency operating point. From this we may conclude that the separated flow through the stabilisation ring constitutes an aerodynamic loss mechanism that reduces fan efficiency by 1.8 per cent.

Tunnel ventilation fan designers do not specify tunnel ventilation fans at their peak pressure operating point as a consequence of the need to accommodate the pressure pulses to which they are subjected in service. Tunnel ventilation fans must operate at a lower pressure operating point to avoid the fan transiently driving into stall during a positive pressure pulse. Additionally, within the European Union, tunnel ventilation fans are legally required to comply with the 1 January, 2013. EU Commission Regulation No. 327/2011 requirements that specify a minimum allowable fan and motor efficiency. The two requirements result in tunnel ventilation system designers typically selecting tunnel ventilation fans close to their peak efficiency operating point.

The conclusion that at the peak efficiency operating point flow within the stabilisation ring is highly separated provides an insight into how industrial fan designers may improve fan efficiency. The highly separated flow within the stabilisation ring constitutes an aerodynamic loss mechanism that reduces fan efficiency by 1.8 per cent. If one could optimise vane design within the stabilisation ring to eliminate separated flow at the peak efficiency operating point, this would eliminate the loss mechanism and increase fan efficiency.

REFERENCES

ISO 5801:2007, 2007, Industrial Fans — Performance Testing using Standardized Airways.

Azimian, A.R., McKenzie, A.B., and Elder, R.L. (1987), "A Tip Treatment for Axial Flow Fans and Compressors", *Proceedings of the IMechE Seminar on Inducted Fan Aerodynamics*, London, UK, 9 April.

Bard, H. (1984), "The Stabilisation of Axial Fan Performance", *Proceedings of the Institution of Mechanical Engineers (IMechE) Conference 1984–4 on the Installation Effects in Ducted Fan Systems*, London, UK, 1–2 May, paper no. C120/84, pp. 100–106.

Bianchi, S., Corsini, A., Mazzucco, L., Monteleone, L., and Sheard, A.G. (2012), "Stall Inception, Evolution and Control in a Low Speed Axial Fan with Variable Pitch in Motion", *Transactions of the ASME, Journal of Engineering for Gas Turbines and Power*, vol. 134, paper no. 042602, pp. 1–10.

Bianchi, S., Corsini, A., Sheard, A.G., and Tortora, C. (2013), "A Critical Review of Stall Control Techniques in Industrial Fans", *International Scholarly Research Network, Mechanical Engineering*, vol. 2013, article ID 526192, 18 pages, http://dx.doi.org/10.1155/2013/526192.

Borello, D., Corsini, A., Delibra, G., and Sheard, A.G. (2013), "Numerical Investigation of Detrimental Aerodynamic Effect of Pressure Pulses on a Metro Tunnel Fan", *Proceedings of the 10th European Turbomachinery Conference*, Lappeenranta, Finland, 15–19 April, pp. 573–82.

Corsini, A., and Rispoli, F. (2005), "Flow Analyses in a High-pressure Axial Ventilation Fan with a Non-linear Eddy-viscosity Closure", *International Journal of Heat and Fluid Flow*, vol. 26(3), pp. 349–61.

Corsini, A., and Sheard, A.G. (2007), "Tip End-plate Concept Based on Leakage Vortex Rotation Number Control", *Journal of Computational and Applied Mechanics*, vol. 8, pp. 21–37.

Corsini, A., Rispoli, F., Santoriello, A., and Tezduyar, T.E. (2006), "Improved Discontinuity-capturing Finite Element Techniques for Reaction Effects in Turbulence Computation", *Computational Mechanics*, vol. 38, pp. 356–64.

Corsini, A., Delibra, G., and Sheard, A.G. (2013a), "A Critical Review of Computational Methods and Their Application in Industrial Fan Design", *International Scholarly Research Network, Mechanical Engineering*, vol. 2013, article ID 625175, pp. 1–20.

Corsini, A., Delibra, G., and Sheard, A.G. (2013b), "On the Role of Leading-edge Bumps in the Control of Stall Onset in Axial Fan Blades", *Transactions of the ASME, Journal of Fluids Engineering*, vol. 135, paper no. 081104, pp. 1–9.

Corsini, A., Delibra, G., and Sheard, A.G. (2014), "The Application of Sinusoidal Blade Leading Edges in a Fan Design Methodology to Improve Stall Resistance", *Proceedings of the IMechE Part A, Journal of Power and Energy*, vol. 228, pp. 255–71.

Durbin, B. (2011), "Review: Adapting Scalar Turbulence Closure Models for Rotation and Curvature", *Transactions of the ASME, Journal of Fluids Engineering*, vol. 133, paper no. 061205, pp. 1–8.

EU Commission Regulation No. 327/2011 (2011), *Official Journal of the European Union,* 1 June, http://www.amca.org/UserFiles/file/COMMISSION%20REGULATION%20%28EU%29%20No%20327-2011.pdf.

Eurovent (2007), Eurovent1/11 — Fans and System Stall: Problems and Solution.

Farrell, P.E., and Maddison, J.R. (2011), "Conservative Interpolation between Volume Meshes by Local Galerkin Projection", *Computer Methods in Applied Mechanics and Engineering*, vol. 200, pp. 89–100.

Gho, S.L. (2013), "AMCA Grows in Asia", *AMCA inmotion*(3), p. 27.

Hauer, A., and Brooks, J. (2012), "Fan Motor Efficiency Grades in the European Market", *AMCA inmotion*(2), pp. 14–20.

Hill, S.D., Elder, R.L., and McKenzie, A.B. (1998), "Application of Casing Treatment to an Industrial Axial-flow Fan", *Proceedings of the IMechE Part A, Journal of Power and Energy*, vol. 212, pp. 225–33.

Horlock, J.H., and Denton, J. (2005), "A Review of Some Early Design Practice Using Computational Fluid Dynamics and a Current Perspective", *Transactions of the ASME, Journal of Turbomachinery*, vol. 127, pp. 5–13.

Ivanov, S.K. (1965), "Axial Blower", US Patent No. 3,189,260, 15 June.

Kang, C.S., McKenzie, A.B., and Elder, R.L. (1995), "Recessed Casing Treatment Effects of Fan Performance and Flow Field", *Proceedings of the 40th American Society of Mechanical Engineers Gas Turbine and Aeroengine Congress*, Houston, TX, USA, 5–8 June, paper no. 95-GT-197.

Karlsson, S., and Holmkvist, T. (1986), "Guide Vane Ring for a Return Flow Passage in Axial Fans and a Method of Protecting it", US Patent No. 4,602,410, 29 July.

Lien, F.S., and Leschziner, M.A. (1994), "Assessment of Turbulence-transport Models Including Non-linear RNG Eddy-viscosity Formulation and Second-moment Closure for Flow over a Backward-facing Step", *Computers & Fluids*, vol. 23, pp. 983–1004.

Miyake, Y., Kata, T., and Inaba, T. (1987), "Improvement of Unstable Characteristics of an Axial Flow Fan by Air-separator Equipment", *Transactions of the ASME, Journal of Fluids Engineering*, vol. 109(1), pp. 36–40.

Nie, C., Xu, G., Cheng, X., and Chen, J. (2002), "Micro Air Injection and its Unsteady Response in a Low-speed Axial Compressor", *Transactions of the ASME, Journal of Turbomachinery*, vol. 124, pp. 572–9.

Sheard, A.G., and Corsini, A. (2012), "The Mechanical Impact of Aerodynamic Stall on Tunnel Ventilation Fans", *International Journal of Rotating Machinery*, vol. 2012, article ID 402763, pp. 1–12.

Sheard, A.G., and Daneshkhah, K. (2012), "The Conceptual Design of High Pressure Reversible Axial Tunnel Ventilation Fans", *Advances in Acoustics and Vibration*, vol. 2012, article ID 562309, pp. 1–11.

Sheard, A.G., Corsini. A., Minotti, S., and Sciulli, F. (2009), "The Role of Computational Methods in the Development of an Aero-acoustic Design Methodology: Application in a Family of Large Industrial Fans", *Proceedings of the 14th International Conference on Modelling Fluid Flow Technologies*, Budapest, Hungary, 9–12 September, pp. 71–9.

Sheard, A.G., Daneshkhah, K., and Corsini, A. (2013), "Fan Conceptual Design as Applied to the Marmaray Tunnel Ventilation System", *Proceedings of the58th American Society of Mechanical Engineers Gas Turbine and Aeroengine Congress*, San Antonio, TX, USA, 3–7 June, paper no. GT2013-94548.

Smith, G.D.J., and Cumpsty, N.A. (1984), "Flow Phenomena in Compressor Casing Treatment", *Transactions of the ASME, Journal of Engineering for Gas Turbines and Power*, vol. 106(3), pp. 532–41.

Suder, K.L., Hathaway, M.D., Thorp, S.A., Strazisar, A.J., and Bright, M.B. (2001), "Compressor Stability Enhancement Using Discrete Tip Injection", *Transactions of the ASME, Journal of Turbomachinery*, vol. 123, pp. 14–23.

Takata, H., and Tsukuda, Y. (1977), "Stall Margin Improvement by Casing Treatment — its Mechanism and Effectiveness", *Transaction of the ASME, Journal of Engineering for Power*, vol. 99(1), pp. 121–33.

Thompson, D.W., King, P.I., and Rabe, D.C. (1998), "Experimental and Computational Investigation on Stepped Tip Gap Effects on the Flow Field of a Transonic Axial-flow Compressor Rotor", *Transactions of the ASME, Journal of Turbomachinery*, vol. 120, pp. 477–86.

US Department of Energy (2013), "Energy Conservation Standards Rulemaking Framework for Commercial and Industrial Fans and Blowers", US Department of Energy, 1 February.

Vo, H.D. (2007), "Active Suppression of Rotating Stall Inception with Distributed Jet Actuation", *International Journal of Rotating Machinery*, vol. 2007, article ID 56808, pp. 1–15.

Weller, H.G., Tabor, G., Jasak, H., and Fureby, C. (1998), "A Tensorial Approach to Continuum Mechanics using Object-oriented Techniques", *Journal of Computational Physics*, vol. 12(6), pp. 620–31.

Yamaguchi, N., Kato, Y., and Ogata, M. (2010), "Improvement of Stalling Characteristics of an Axial-flow Fan by Radial-vaned Air-separators", *Transactions of the ASME, Journal of Turbomachinery*, vol. 132(2), article ID 021015, pp. 1–10.

Ziabasharhagh, M., McKenzie, A.B., and Elder, R.L. (1992), "Recess Vane Passive Stall Control", *Proceedings of the 37th American Society of Mechanical Engineers Gas Turbine and Aeroengine Congress*, Cologne, Germany, 1–4 June, paper no. 92-GT-36.

A Method of Detecting Stall in an Axial Fan

A.G. Sheard, A. Corsini, and S. Bianchi

ABSTRACT

This appendix is adapted from the patent 'A method of detecting stall in an axial fan'. The adaption aims to present the invention in a more accessible way to the reader, without significantly altering the patent's content.

A need to detect the imminent onset of stall inspired the research that resulted in the intellectual property that forms the basis of the patent. The described stall-detection method involves analysing fan acoustic emissions. It includes measuring the sound that emanates from the flow adjacent to the fan. From this, one can prepare a visual representation of the sound. Then, one can compare visual representations derived from a plurality of tests that are representative of the fan's performance under a range of operating conditions. In selecting the previously derived visual representation that most closely matched a visual representation generated in real time, fan operating condition may be inferred. A control signal may then be derived from the inferred operating condition. The inventors used a symmetrised dot pattern (SDP) technique to generate the visual representations.

NOMENCLATURE

Latin letters

i	number of dots
R	polar position of the dot
SDP	symmetrised dot pattern
t	absolute time

Greek letters

Δt	time interval
Θ^+, Θ^-	two angles of the polar space
ξ	angular gain
σ	input signal amplitude
Φ	rotor flow coefficient
Ψ	rotor work coefficient

INTRODUCTION

The present invention relates to an axial fan stall detection method that uses acoustic input signals. Because of aerodynamic flow instability, stall is a major potential cause of mechanical failure in axial fans. As a result, stall-detection techniques have had wide application for many years. Researchers have studied and analysed different forms of aerodynamic instability for several decades. Two main types of aerodynamic flow instability exist:

(i)   rotating stall in which regions of reversed flow occur locally; and,

(ii) surge which is characterised by periodic backflow over the entire annulus involving violent oscillations in the air flow.

Prior stall-detection methods have had drawbacks in their inability to enable a sufficiently rapid response to stall onset to avoid damage and in their inability to sense the approaching stall. The present invention seeks to develop a stall-detection methodology that is able to differentiate between aerodynamic stall conditions constituting a mechanical risk and those that do not. Therefore, the resulting methodology is capable of differentiating between critical and non-critical stall conditions.

The present invention provides a stall-detection method based on measurements of the sound that emanates from the flow through a fan. It prepares a visual representation of the sound. Then, one can compare the visual representation with fixed visual representations derived from a plurality of tests that are representative of the fan's performance under a range of operating conditions. One may select the fixed visual representation that most closely matches the said sound's visual representation and derive a control signal from the selected fixed visual representation.

In a preferred embodiment, one uses a symmetrised dot pattern (SDP) technique to generate the visual representations. Preferably, one measures the sound over a period of time covering less than ten fan revolutions. One may measure the sound over less than three or even less than one revolution. Preferably, one measures the sound at a point adjacent to the fan's periphery and uses the selected visual representation to infer fan operating condition and then generate a feedback signal to control the fan's operation and speed.

The invention also provides an apparatus for conducting the tests for developing visual representations of sound that emanate from the said fan under a range of operating condition, including a microphone for measuring actual sound emanating from the fan, and means for comparing the actual sound with the various visual representations and selecting and displaying the closest match.

We now describe and provide examples of the present method and apparatus' preferred embodiment. A typical application for the invention would be a multi-bladed axial fan intended for use in the ventilation system within a metropolitan metro or underground railway system, Figure A1.1. The fan's rotating system is mounted in a casing that is then installed in the tunnel ventilation system's ducting.
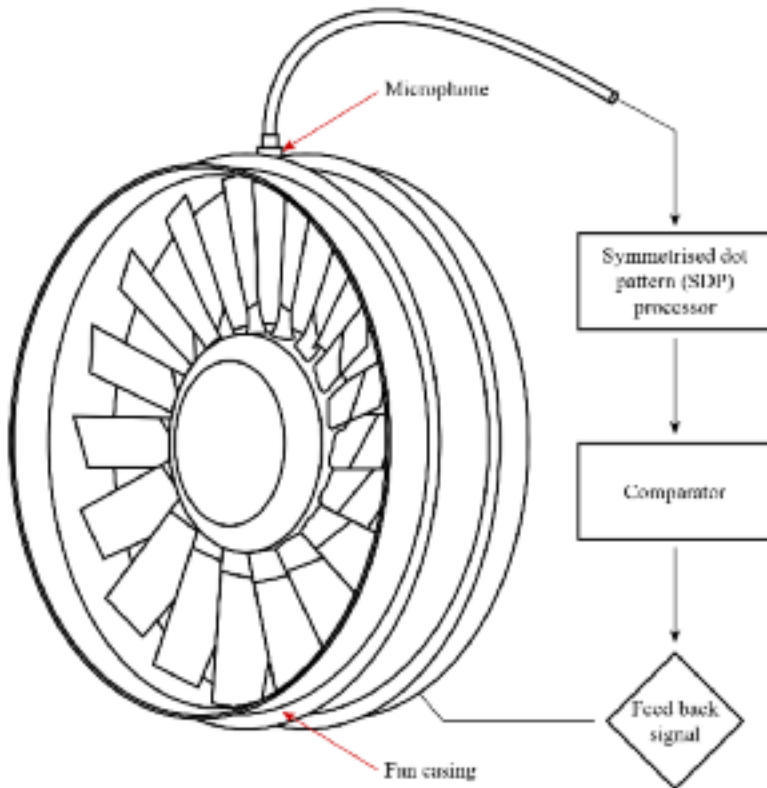
FIGURE A1.1. An isometric view of an axial fan typical of those utilised in metropolitan metro and railway tunnel ventilation systems.

In order to measure the sound emanating from the fan, a high-sensitivity microphone is mounted in the casing adjacent to the fan. In practice, one can place the microphone some distance from the fan with little loss of efficiency in response. It is therefore possible to place the microphone next to the fan casing within which the blades rotate, or if not practical, over another accessible part of the fan casing or ventilation system duct work.

Signals from the microphone transmit at ten second intervals to a symmetrised dot pattern (SDP) processor, which generates a visual image representative of the sound that the air flow through the fan generates. The visual image then transmits to a comparator which contains fixed visual representations which correspond to a plurality of the fan's operating conditions that we obtained in a test rig. One then uses the comparator to match the real-time image with the closest reference image stored in the comparator. This closest reference image then enables the generation of an appropriate control signal that constitutes a feedback signal that one may use to control fan speed.

We derive the reference images from series of fan tests that we conducted in a laboratory environment using a test setup configured in accordance with ISO 5801:2007 (2007) requirements, Figure A1.2. We mounted the fan in a duct with an inlet section that has a length four times the fan's diameter. The inlet contained a flow straightener to provide lamina air flow to the fan. An adjustable throttle is located downstream of the fan. Pressure transducers are located upstream of the fan, between the fan and the throttle, and in the inlet.

We placed a flush-mounted microphone in the fan casing to collect acoustic data from the microphone at full-, half- and quarter-speed, position C in Figure A1.2. We then processed the data to establish, for each speed, regions of:

(i)   stable operation;
(ii)   incipient stall; and
(iii)   rotating stall.

This establishes spatial and temporal correlations between rotating instabilities, which facilitates an analysis to establish the onset of incipient stall. We use a symmetrised dot pattern technique to generate a library of visual representations. The symmetrised dot patterns are different for stable operation, incipient and rotating stall, providing a basis for differentiation. This technique makes it possible to detect the on-set of incipient stall that is the pre-cursor to a transition from stable operation to rotating stall.

There is typically a rapid transition from a stable operation to rotating stall, and prior detection systems typically take up to 240 revolutions to react, by which time rotating stall has fully developed with the associated risk of catastrophic damage already occurring. In contrast, the present invention can detect incipient stall in less than ten revolutions, often less than three or even less than one, with the result that one can take corrective action before rotating stall has developed.

Rotating stall is a type of aerodynamic instability that results in an increase in the unsteady aerodynamic loads imposed on fan blades. An increase in unsteady
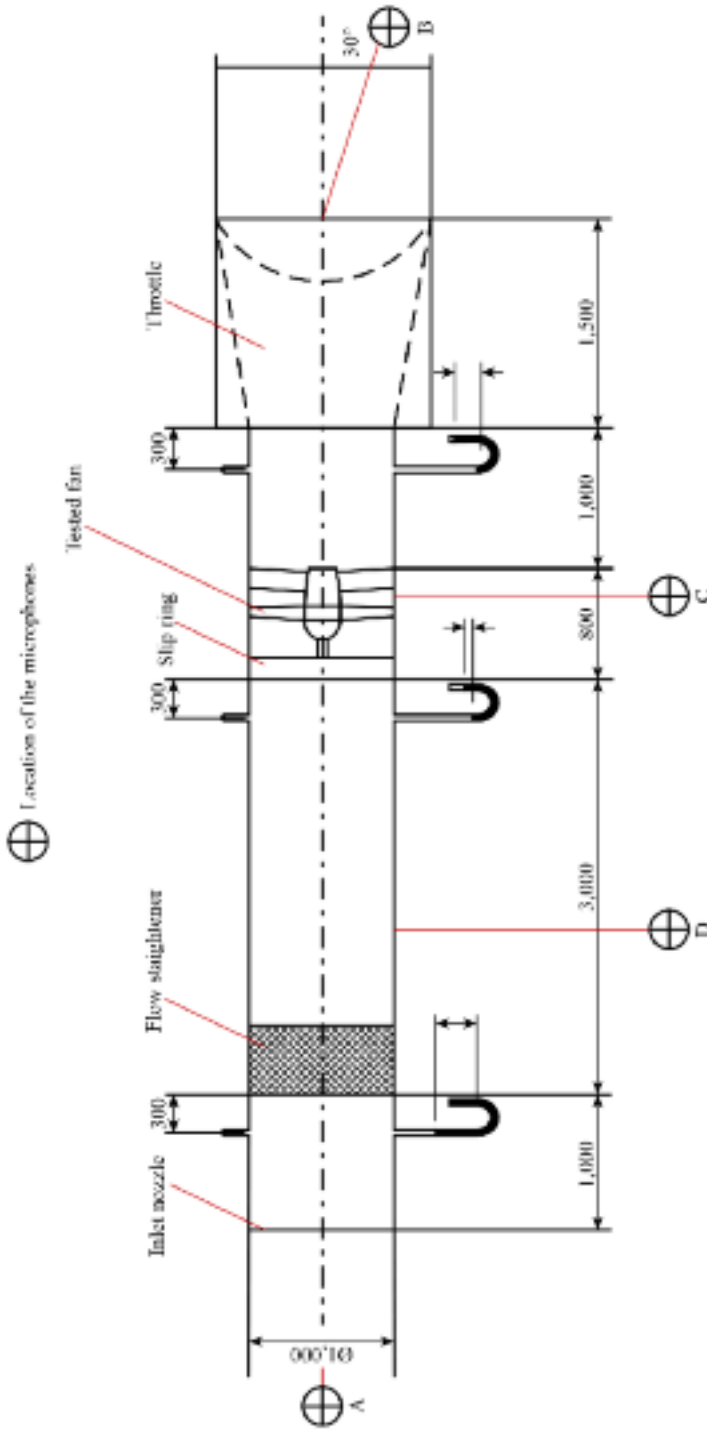
FIGURE A1.2. A side view of the ISO 5801:2007 (2007) standard ducted test rig used to characterise a fan, identifying regions of stable operation, incipient stall and rotating stall.

aerodynamic loads induces an increase in unsteady mechanical loads in the fan blades. Researchers have used strain gauge measurements to establish that when one operates an axial fan in an aerodynamically stalled condition, unsteady bending stress levels exceed those that occur with stable aerodynamic operation by a factor of five. It is this increase in unsteady stress levels that initiates a fatigue crack in one or more fan blades that then goes on to propagate, ultimately resulting in the blade's mechanical failure.

In the case of industrial fans utilised in the ventilation systems for metropolitan metros and underground railways, the Euro Norm EN 12101-3 and International Standard ISO 21927-3 require fans to have a high temperature capability. This poses new challenges to fan manufacturers. For example, to operate a fan at elevated temperatures during a tunnel fire requires that the fan blades have a larger tip-to-casing gap at ambient temperature. This increased tip-to-casing gap prevents the blades from contacting the casing within which they run at an elevated temperature. However, at ambient temperature an increase in tip-to-casing gap reduces the fan's pressure developing capability. The probability that a pressure pulse will transiently drive a fan into stall increases with reducing pressure developing capability.

A particular feature of both metropolitan metro and railway tunnel environments is the pressure pulses that occur with a train's movement through a tunnel. Pressure pulses can be up to ±50 per cent of a ventilation fan's overall work coefficient. The effect of such pressure pulses on a tunnel ventilation fan is to drive the fan first up, and then down its operating characteristic. To ensure that the fan continues to operate in an aerodynamically stable manner during this pressure transient, the fan's aerodynamic design requires incorporating sufficient margin to ensure that the fan does not transiently drive into stall when subjected to pressure pulses.

This propensity for a tunnel ventilation fan to stall when subjected to a pressure pulse is complicated in off-design conditions when one operates a fan at partial speeds. When one reduces a fan's speed from full to half design speed, its flow and pressure developing capability also reduces. Because the pressure pulse that occurs with a passing train remains constant, a fan that would have a high enough pressure developing capability to avoid stall at full design speed will almost certainly stall when subjected to the same pressure at half design speed. Therefore, a direct consequence of operating tunnel ventilation fans at part speed is an increased probability that they will stall transiently under the influence of the pressure pulse which each passing train generates.

The use of a symmetrised dot pattern technique is particularly advantageous in detecting incipient stall. It enables corrective action before stress levels in fan blades rise to dangerous levels. Detecting incipient stall has many practical as well as cost advantages. Taking corrective action to avoid stall extends the fan service life. It also enables one to operate a fan closer to its peak efficiency operating point that is invariably at a lower stall margin than operators historically would have considered acceptable. The reasons for the effectiveness of the symmetrised dot pattern technique are:

(1) The generation of symmetrised dot patterns is quite light on the signal processing requirement, so it is easier to conduct the signal processing in real time, and therefore identify incipient stall, as opposed to stall that has already happened.

(2) The symmetrised dot pattern technique is effective when working with low signal-to-noise ratio signals.

(3) The symmetrised dot pattern technique is effective with signals from a microphone placed in any location. Known techniques for stall-detection need an unsteady pressure measurement over the blade. As such, the symmetrised dot pattern technique, in combination with an acoustic measurement according to the invention, is able to create a visual pattern that one can use to detect stall in any location, not just with the microphone over the blade itself. Furthermore, it is possible to achieve the desired results using one microphone only, in contrast to the known arrangements which use multiple pressure transducers distributed about the fan casing's periphery. The present invention, therefore, offers significant savings in the complexity of the required equipment and the complexity of signal processing.

(4) Because of its low processing power requirement and its speed of processing an input signal, the symmetrised dot pattern technique is able to produce the input signal's visual representation that incorporates features that are linked to the approach of stall.

The advantages of the symmetrised dot pattern technique enable more sophisticated monitoring and control of fan performance. Fan stall does not always result in mechanical failure. A subsonic fan can sometimes operate at low speeds in an aerodynamically stalled condition without risking mechanical failure. Rotating stall at full design speed will typically result in an early fatigue failure. At some lower speed, which can be the half design speed, the direct operating stress on the fan blades caused by fan rotation reduces by a factor of four. This is sufficient to enable tolerating the additional alternating stress that occurs with operation in rotating stall without risking mechanical failure due to fatigue.

To determine the maximum speed at which a fan may safely operate in stall, one must conduct laboratory tests to measure the direct and alternating stresses on the fan under various combinations of operating speed and condition. Once one determines the safe maximum speed at which the fan can operate rotating in stall without risking mechanical failure, then one can define of the various symmetrised dot patterns that occur at this speed with stable aerodynamic operation, incipient stall and rotating stall. This is the critical maximum allowed speed at which the fan can operate in stall without the risk of mechanical failure.

SYMMETRISED DOT PATTERN (SDP) TECHNIQUE

Researchers first conceived the symmetrised dot pattern technique for the visual characterisation of speech waveforms in automatic human-voice recognition

algorithms. Developed to characterise acoustic input signals, the methodology's merit is its ability to perceive otherwise 'unquantifiable' differences in sound. Experiments on psychological perception demonstrate that people perceive noise 'annoyance' not only by the sound power level produced by the sounds tonal components, but also by 'howling' and signal modulation. The symmetrised dot pattern technique provides a visual representation of an acoustic signal that researchers can apply to characterise its significant features.

Mathematical framework

An algorithm that maps an input signal into polar coordinates produces the symmetrised dot patterns, Figure A1.3. Transforming the input signals into polar coordinates result in symmetrised dot patterns that are able to reflect subtle differences in the input signal as identifiable differences in the resultant symmetrised dot patterns. The signal is first normalised by finding highest (σ max) and lowest (σ min) values amongst the measured data point. Normalising the data is an important aspect of the symmetrised dot pattern algorithm as it results in signal amplitude becoming a secondary factor in a signal's characterisation. It is the secondary importance of signal amplitude that enables the algorithm to work effectively with low signal-to-noise level signals.

The inventors characterised the performance of a fan, identifying regions of stable operation, incipient stall and rotating stall, Figure A1.4. As metropolitan metro and railway tunnel ventilation fans frequently operate at part speed, the stable operation, incipient stall and rotating stall regions were characterised at full, half and quarter design speed.

The inventors derived the symmetrised dot patterns after optimising the parameters that they used to derive the symmetrised dot patterns and the sampling time, Figure A1.5. The inventors presented the symmetrised dot patterns as a matrix of operating conditions, with operating condition on the horizontal axis and fan speed on the vertical axis. The three operating conditions are (a) stable operation, (b) incipient stall and (c) rotating stall. The three fan speeds are: (i) full design speed, (ii) half design speed and (iii) quarter design speed. With three operating conditions and three fan speeds, the matrix comprises nine symmetrised dot patterns. The nine symmetrised dot patterns serve as the template images against which the inventors compared symmetrised dot patterns generated in real time during the fan's in-service operation. The comparison of symmetrised dot patterns generated in real time with various template images form the basis of a stall diagnostic system.

At full design speed the symmetrised dot pattern associated with stable operation, Figure A1.5 (i) (a), had a distinctive shape with a ring at the end of each symmetrised dot pattern arm. This shape was exclusive to the full design speed and stable operation condition, and the inventors regarded it as a 'benchmark' signature for the fan when operating at its design operating condition. Incipient stall resulted
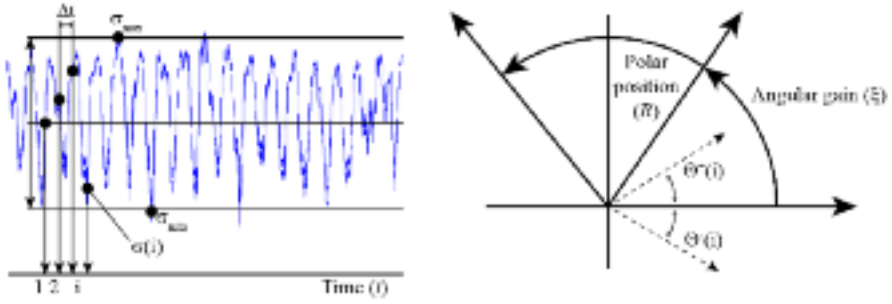
FIGURE A1.3. A schematic illustration of the technique for transforming an input signal into polar coordinates to produce a symmetrised dot pattern.
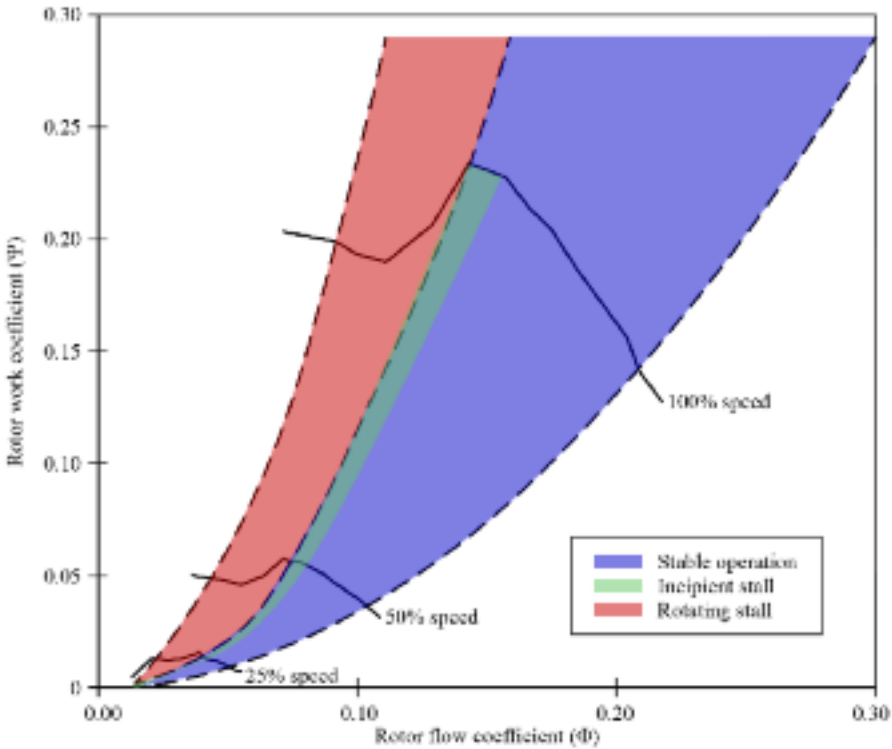
FIGURE A1.4. A characterisation of the studied fan at full, half and quarter design speed, identifying regions of stable operation, incipient stall and rotating stall.
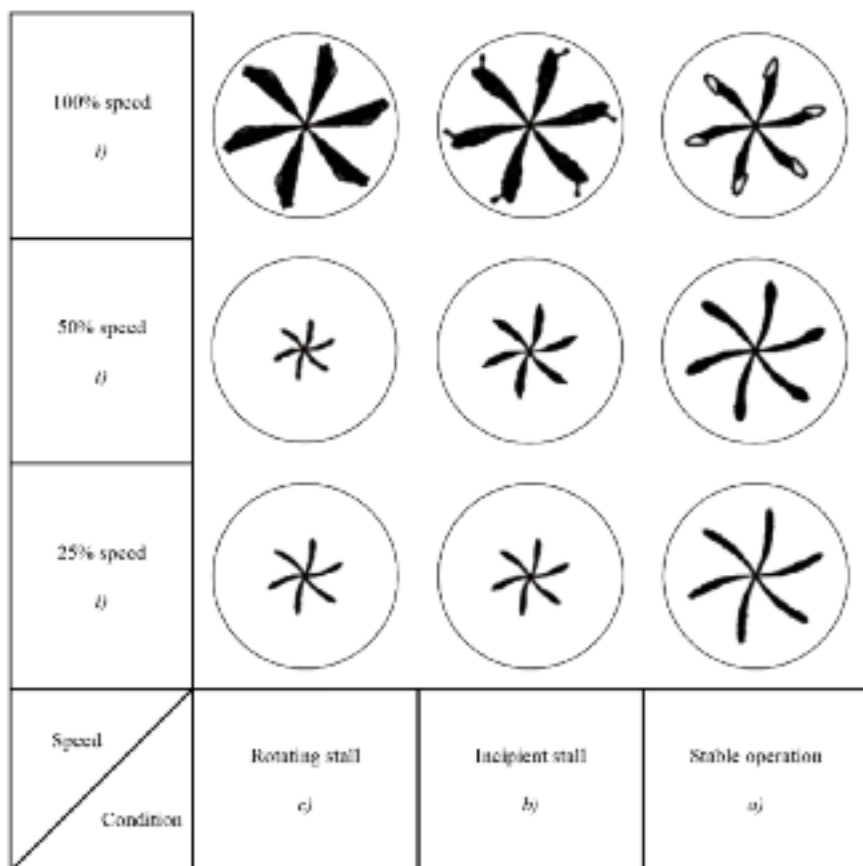
FIGURE A1.5. The symmetrised dot patterns produced from an unsteady pressure input signal for a fan over a range of fan speeds and aerodynamic conditions. Each symmetrised dot pattern is distinctly different, providing a basis for differentiation.

in an increase in the symmetrised dot pattern radius, Figure A1.5 (i) (b). Rotating stall resulted in an increase in the area of the symmetrised dot pattern arms, Figure A1.5 (i) (c). Critically, the symmetrised dot patterns that we generated using an input signal associated with stable operation, incipient stall and rotating stall were different enough to form the basis of a stall-detection system.

The symmetrised dot patterns that we generated using an input signal associated with with half and quarter design speed were distinctly different to those associated with full design speed, Figures A1.5 (ii) (a), (ii) (b) and (ii) (c) and Figures A1.5 (iii) (a), (iii) (b) and (iii) (c). At both half and quarter design speed, the symmetrised dot patterns reduced in radius as the fan moved from stable operation to incipient stall and then rotating stall. As the symmetrised dot patterns' radius reduced, the fan maintained the angular dot distribution. Once again the

symmetrised dot patterns that we generated with stable operation, incipient stall and rotating stall were different enough to form the basis of a stall-detection system. Using the matrix of nine symmetrised dot patterns, a matching template system can then determine:

- that stall has become incipient and therefore that stalled operation is likely; and,
- that the fan's speed is such that if one operates it in a stalled condition, continued operation is either safe or will result in a mechanical failure.

Knowing the above enables one to take the appropriate control action. A symmetrised dot pattern's shape generated in real time during routine operation indicates whether the fan is running at or above its safe maximum speed when operating in a stalled condition. There is therefore no requirement for separately measuring the fan speed.

CLAIMS

(1)   A method of detecting stall in an axial fan through acoustic measurements in the air flow. This includes measuring the sound that emanates from the flow and preparing a visual representation of the sound in real time. This real-time representation is then compared with visual representation derived from a plurality of tests of the fan's performance under a range of operating conditions. The previously prepared visual representation that most closely matches the real-time visual representation is then selected, and used to derive a control signal.

(2)   A method according to Claim 1, wherein the symmetrised dot pattern (SDP) technique is used to generate the visual representations.

(3)   A method according to Claim 1 or 2, wherein one measures the sound over a period of time covering less than the ten revolutions of the fan's impeller.

(4)   A method according to Claim 3, wherein one measures the sound over less than three or less than one revolution.

(5)   A method according to Claim 1, wherein one uses the selected visual representation to generate a feedback signal to control the operation and the fan's speed.

(6)   A method according to Claim 1, wherein the operating conditions include stable operation, incipient stall and rotating stall.

(7)   A method according to Claim 1 or Claim 6, wherein the parameters include different fan operating speeds.

(8)   A method according to Claim 7, wherein the operating speeds are full, half and quarter design speed.

(9)   A method according to any one of the preceding claims, wherein the microphone is adjacent to the fan.

(10) Apparatus for carrying out the method according to any one of the preceding claims, comprising a test system for developing visual representations of the sound emanating from the fan under a range of operating conditions, a microphone for measuring actual sound that emanates from the fan, and a means for comparing the actual sound with the previously derived visual representations and displaying the closest match.

(11) A method of detecting stall in the air flow through an axial fan substantially as described herein with reference to Figures A1.1, A1.2, A1.3, A1.4 and A1.5.

(12) Apparatus for carrying out the method according to any one of Claims 1–9 and 11.

Appendix 2

Axial Air Movement Fans

A.G. Sheard, A.F.E. Godichon, and D. Revillot

ABSTRACT

This appendix is adapted from the patent 'axial air movement fans'. The adaption aims to make the invention presented in the appendix more accessible to the reader, without significantly altering the patent's content.

A need to increase axial fan blade damping inspired the research resulting in the intellectual property that forms the basis of the patent. An axial fan comprises a hub with a plurality of elongated fan blades extending outwardly. Each blade includes at least one damping mass secured to the blade. The mass can oscillate relative to the blade in response to oscillatory flexing and thus damp the flexing. The damping mass may be located within a hollow part of the blade. The mass may be attached to the blade by a supporting wire which is secured at its ends to the blade. The mass may be attached to the blade by a resilient bush or bushes. A resilient plate may be located within the blade, and secured to the blade at one end to form a cantilever. The mass may be attached to the plate, or the plate may itself be the mass. The mass may instead be attached to the outside of the blade.

INTRODUCTION

The present invention relates to axial fans comprising a plurality of elongated blades distributed about a hub so as to extend in a generally radial direction. Each blade therefore constitutes a cantilever secured to the hub and extends outwardly to the blade's outer free end. The blades are typically placed at an angle to the rotating axis' circumferential plane and may have an aerofoil type cross-section. In cross-section, blades have a major and a minor axis. In operation the blades are subject to air pressure and further forces caused by buffeting and air turbulence passing through the fan.

The normal operating forces are exacerbated if the vibratory loads on the blade are generated at the natural frequency of the cantilevered blade. This can cause a permanent oscillation or vibration about the blades' major axis at its root. These forces are transmitted to the hub as a cyclical bending moment through the blade's root and into the hub. Thus, the blades tend to bend about the major axis and the stress concentration at the blade root can lead to cracking and blade failure. The present invention seeks to provide a solution to this problem.

The invention relates to axial fans comprising a hub mounted for rotation about an axis, Figure A2.1. The fan comprises a plurality of elongated fan blades, only one of which is shown as reference, equidistantly disposed about the hub's periphery and secured so as to extend in a generally radial direction. The blade consists of an elongated member extending generally radially and is secured at its root to the hub at a slight angle to the hub's plane of rotation. The fan has in its cross-section a major and a minor axis. It also has a radially extending longitudinal main axis. Each blade
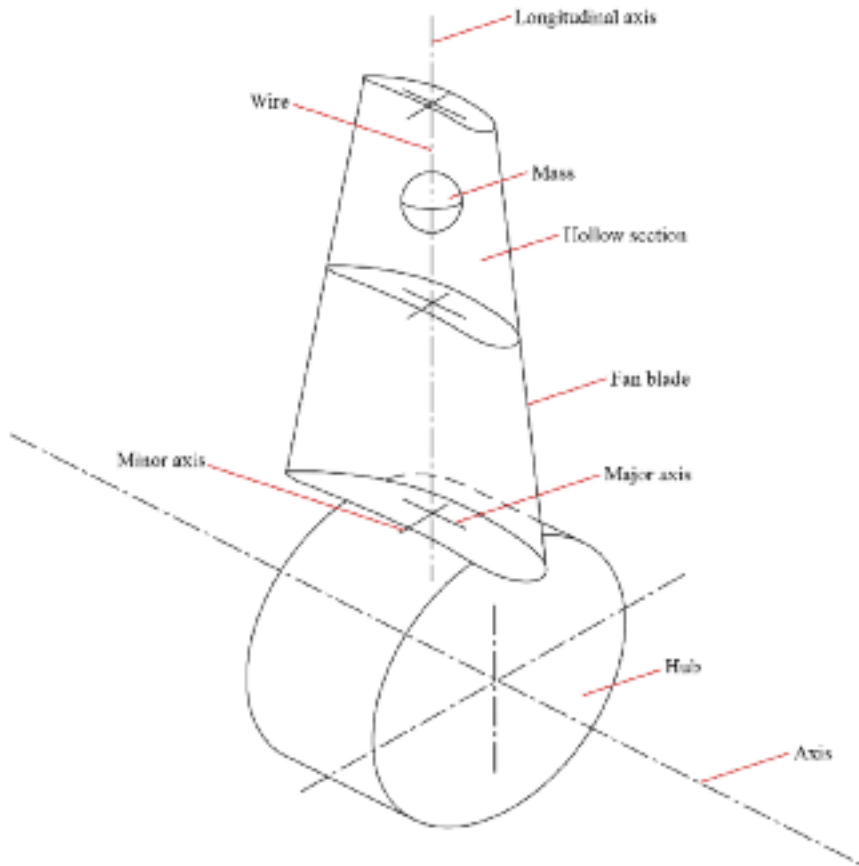
FIGURE A2.1. A schematic view of one axial fan blade, illustrating the mass' location used to increase blade damping.

includes at least one damping mass secured to the fan in such a way as to enable the mass to oscillate relative to the blade in response to the blade's oscillatory flexing, thereby damping the blade's flexing.

It is preferable for each blade to be at least partially hollow and therefore the damping mass may be contained within it, Figure A2.2. The damping mass forms a spring-mass system consisting of a mass, which may be formed of lead, which is suspended using a wire. The wire extends along the blade's longitudinal axis and is secured to the blade at its ends. Thus, the mass is constrained by the wire against movement in the radial direction caused by centrifugal force apart from a slight resilient extension of the wire between the mass and the radially innermost fastening. However, the mass is permitted a degree of lateral movement. It is envisaged that some degree of damping of the masses lateral movement may in turn damp the blade's oscillatory flexing. A rubber bush could facilitate damping of the masses lateral movement.
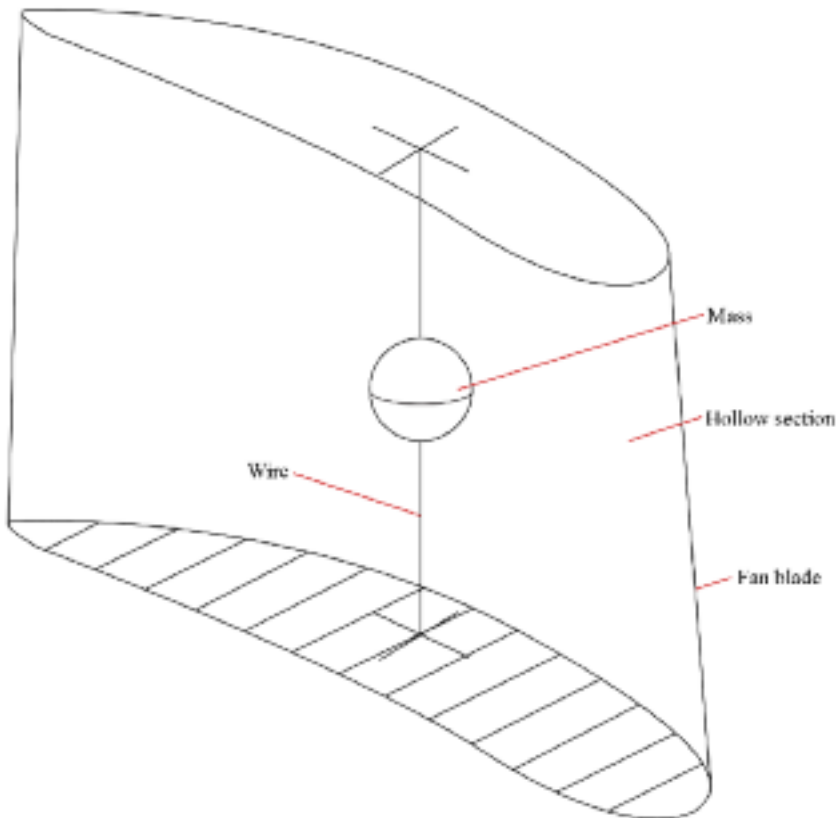
FIGURE A2.2. A schematic cross-sectional view showing the blade's hollow interior, illustrating the damping mass location and its wire support within a blade's hollow section.

One must calculate the mass' weight, the wire's resilience and the initial wire tension to permit the mass to oscillate in response to the blade's oscillatory flexing at its first natural frequency. The blade acts as a cantilever and if an exciting force caused by turbulent airflow over the blade is present at the blade's first natural frequency, permanent oscillation at the natural frequency may occur. This oscillatory flexing is opposed and dampened by the corresponding mass oscillations, which responds to the blade's oscillation and serves to damp out the induced oscillations in the blade. In this way, the stresses in the blade, particularly at its root, which could lead to early blade failure, are substantially reduced.

It is desirable for the mass to be located as far towards the blade's outer tip as possible as this reduces the required mass size. Although depicted as a mass suspended on a wire, it is conceivable to support the mass on a synthetic rubber bushing system designed to restrain the mass against movement in a radial direction, but to move in a controlled resilient manner in a direction normal to the blade's major axis. Although Figures A2.1 and A2.2 show only one mass, two separate masses may be located in the hollow space in the blade and one may tune these two masses to be responsive to different frequencies.

In an alternative embodiment, the damping mass comprises a plate secured at its radially innermost edge to the blade, and its radially outermost end held in a guide device to constrain its movement in a controlled manner when the plate is oscillating. Preferably, the guide device comprises two members between faces of which the outermost end is clamped so it is constrained against lateral movement, but is able to pivot relative to the members. In this case, the faces may be curved so that the contact between the members and the plate is a line contact.

In one form, a resilient damping mass is located between each of the two members and the plate, Figure A2.3. The flexible plate is located in the blade's interior. Bolts secure the radially innermost plate edge in a mounting secured to the blade's main body. At its radially outermost end, the plate is located in a guide device which has a pair of opposing clamping members and between which the plate is located. Bolts fix the locating members to a mounting bracket secured to the blade's main body. The clamping members' surfaces facing and engaging with the plate are curved so that there is only a single line contact between the clamping members and the plate on a line that is a short distance from the plate's outer edge. In this way, the plate's outer part is able to pivot slightly when the plate curves due to oscillatory forces and is also able to accommodate the plate's slight change in length due to the curvature it adopts when deflected.

Additionally, one may position a further guide intermediate at the plate's ends to control the amount of plate movement in this mid-position, Figure A2.3. This further guide device is located approximately one quarter of the way from the plate's fixed end towards the free end, but its position may be varied to give the desired characteristics. Similarly to the first guide device, the further guide device has two clamping members which engage the plate on a line contact. The two clamping members are bolted again to a mount secured to the blade's main body. It is also envisaged that resilient damping means may be disposed between the members' clamping faces and the plate. In this way, when the plate flexes due to oscillatory
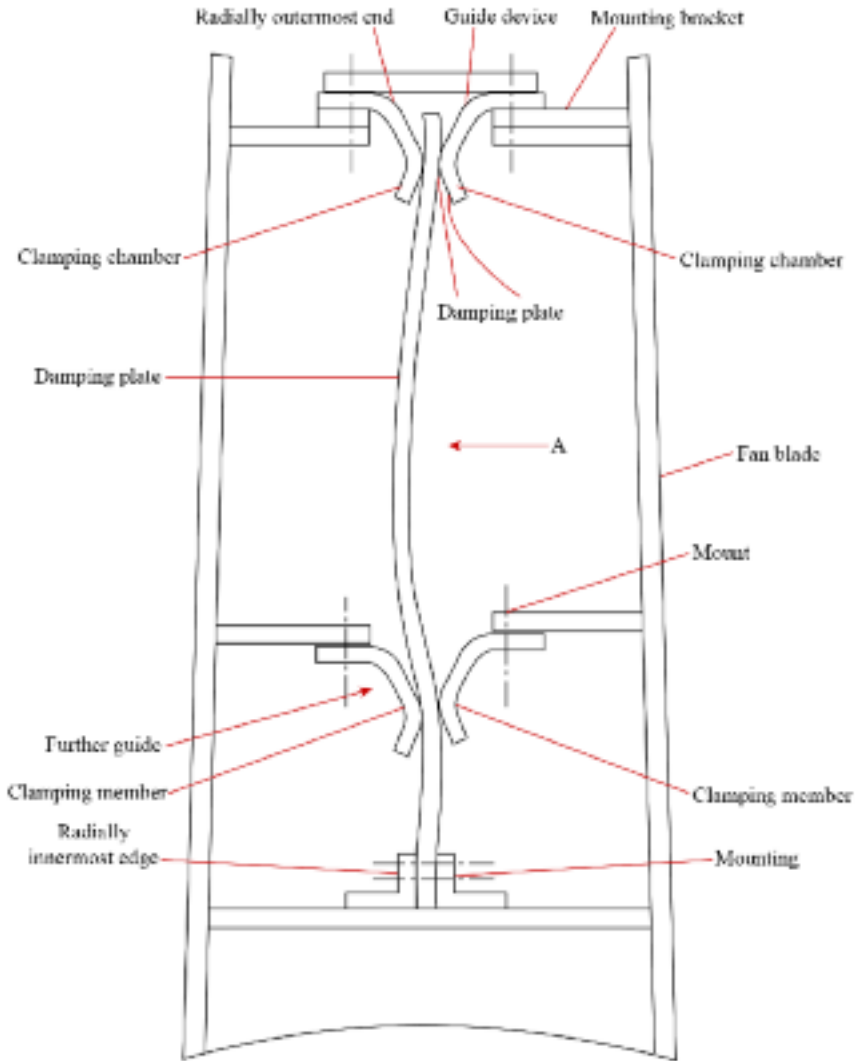
FIGURE A2.3. A schematic arrangement in which a plate forms the damping mass.

forces, it assumes a shallow S shape with the part below the lower guide curving in one direction and the part between the two guides curving in the opposite direction. By appropriately positioning the further guide device, it is possible to tune the frequency and amount by which the plate deflects when subjected to oscillatory forces.

In a preferred embodiment, the plate's cross-sectional area along its length complements the further guide device's positioning. One may vary the plate's cross-sectional area by altering the metal thickness, or its width, Figure A2.4. Varying the plate's cross-sectional area is a second mean by which it is possible to vary the frequency and amount by which the plate deflects when subjected to oscillatory forces.

In an alternative embodiment (not shown), one may position resilient means such as a rubber bushing between the clamping members' surfaces and the plate, with the resilient means having sufficient flexibility to accommodate the required slight movement at the plate's end.

The present invention's practical embodiment comprises a hollow interior containing two damping plates, Figure A2.5. In this embodiment the two damping
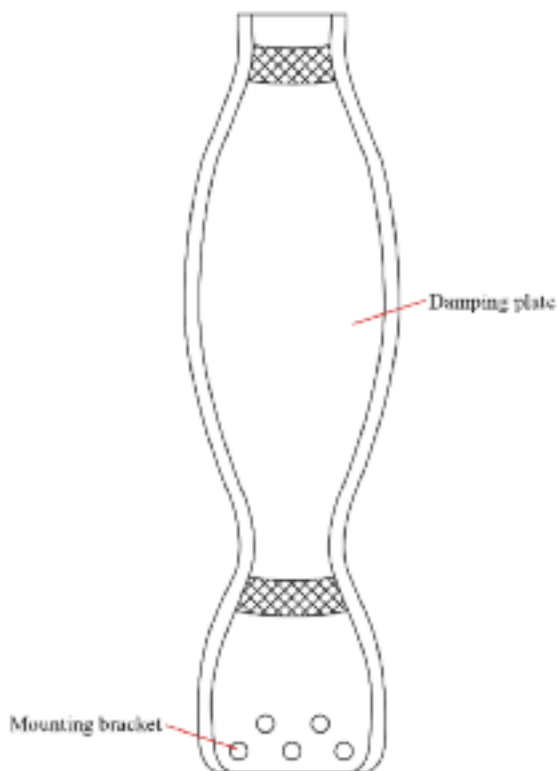
FIGURE A2.4. A schematic arrangement of the plate that forms the damping mass, as seen from the direction of arrow A in Figure A2.3.

plates are identical and we will describe only one for convenience, although note that the two devices may be different sizes, thicknesses and shapes to achieve the required damping characteristics. The plate is secured in a mounting bracket that is in turn secured to the blade's main body. At its radially outermost end, the plate is located in a guide device as described in connection with Figure A2.3. Just radially outwardly of the mounting bracket is a further guide, although, compared to the embodiment (see Figure A2.3), the clamping members are directed in the radially outward direction rather than radially inwardly.

In addition, in this embodiment, a further damping means is located between the guide devices. The damping means consists of brackets secured to the blade's main body and each carry a pair of resilient damping masses formed by rubber bushes, which abut the plate's faces. These are designed to limit and damp the plate's oscillatory movement. Although shown as abutting the plate, note that in certain circumstances one may space these resilient masses from the plate's surface. To increase flexibility, the plate mountings are located in elongated slots in a sub-frame which is secured to the blade. In this way, one can build the whole damping
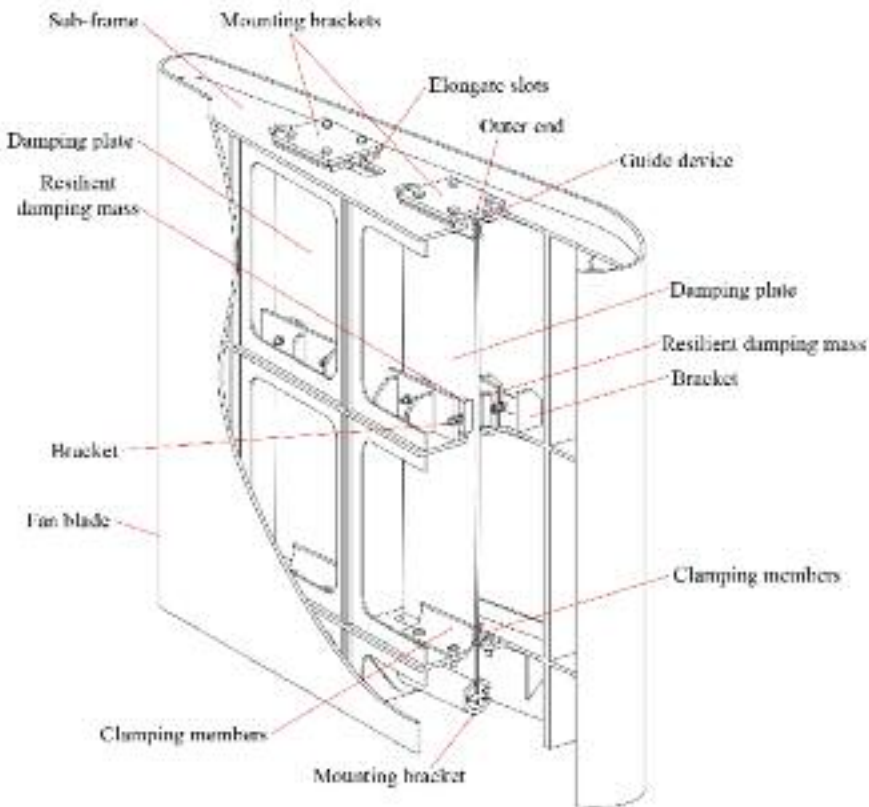
FIGURE A2.5. The damping system's practical embodiment in which the mass comprises two damping plates.

assembly as a subassembly with varying plate widths for easy incorporation into the blade on final assembly.

For relatively small blade sizes, it may not be practical to locate the mass within the blade. In this case, one may suspend the mass on the outside of the blade by securing the wire to limbs extending outwardly from the blade surface. It is possible to provide two masses, one on each side of the blade. It is also possible to secure the mass or masses directly to the blade by using a synthetic rubber bush.

In some installations the blade may generate a higher frequency harmonic causing the blades to oscillate about their longitudinal axis. To counter this, one may secure a smaller mass in the blade's hollow section in such a way that it is constrained against radial movement, but is able to oscillate about the blade's longitudinal axis. In such an arrangement, it may be preferable for the mass to be a disc like structure with its mass concentrated at the periphery. In a further embodiment, an outer skin section bonded to the rest of the blade may form the mass by means of a resilient bushing and have the same profile as the blade so as not to adversely affect the air flow past the blade.

CLAIMS

(1)   An axial fan comprising a hub with a plurality of elongated blades extends generally radially outwardly. Each blade includes at least one damping mass secured to the fan in such a way as to enable the mass to oscillate relative to the blade in response to the blade's oscillatory flexing, thereby damping the blade's flexing.

(2)   A fan as claimed in Claim 1, wherein each blade is at least partially hollow and the damping mass is located within the hollow part.

(3)   A fan as claimed in Claim 1 or 2, wherein the mass is secured to a supporting wire extending in the radial direction and is secured to the blade at its ends, so that the mass is constrained against radial movement caused by centrifugal force. The mass is permitted a degree of lateral movement to enable it to oscillate laterally.

(4)   A fan as claimed in Claim 1, 2 or 3, wherein the mass is secured to the blade through the medium of a resilient bush or bushes.

(5)   A fan as claimed in Claim 1 or 2, wherein a resilient plate is located in the hollow space, one edge of which is secured to the blade to provide a cantilever. The plate provides the mass, or is at least partially formed by a mass on the plate's free end.

(6)   A fan as clamed in Claim 5, wherein the plate is secured to the hollow space's radially outermost face.

(7)   A fan as claimed in Claim 5, wherein the plate is secured at its radially innermost edge to the blade, its radially outermost end remote from said secured end which is held in a guide device to constrain its movement in a controlled manner when the plate is oscillating.

(8)   A fan as claimed in Claim 7 wherein the guide device comprises two members between faces of which said outermost end is clamped so as to be constrained against lateral movement, but is able to pivot relative to the members.

(9)   A fan as claimed in Claim 8 wherein faces are curved so that the contact between the members and the plate is a line contact.

(10)   A fan as claimed in Claim 8 wherein a resilient damping mass is located between each of the two members and the plate.

(11)   A fan according to anyone of Claims 7 to 10 wherein a further guide device is located between the plate's secured inner end and the first guide device.

(12)   A fan according to Claim 11 wherein the further guide device is located closer to the secured end than the outermost end.

(13)   A fan according to Claims 11 or 12 wherein the further guide device comprises two members between faces of which the plate's intermediate part is clamped so as to be constrained against lateral movement, but is able to pivot relative to the members.

(14)   A fan as claimed in Claim 13 wherein faces are curved so that the contact between the members and the plate is a line contact.

(15)   A fan as claimed in Claim 11 or 12 wherein a resilient damping mass is located between each of the two members and the plate.

(16)   A fan as claimed in any one of Claims 7 to 15, wherein the plate's cross-sectional area varies along its length to give a desired form of flexure.

(17)   A fan according to any one of Claims 7 to 16 wherein plate plurality is provided.

(18)   A fan as claimed in Claim 1, wherein the mass is secured on the outside of the fan blade.

(19)   A fan as claimed in anyone of the preceding claims wherein the mass comprises two separate weights.

(20)   A fan as claimed in anyone of the preceding claims, including a further mass adapted to dampen a higher frequency harmonic by oscillatory movement about the blade's longitudinal axis.

(21)   An axial fan substantially described herein with reference to and as illustrated in Figures A2.1, A2.2, A2.3, A2.4 and A2.5.

Bibliography

Page numbers in italics refer to figures or tables

Anthoine, J., Arts, T., Boerrigter, H.L., Buchlin, J.M., Carbonaro, M., Degrez, G., Dénos, R., Fletcher, D., Olivari, D., Riethmuller, M.L., and Van den Braembussche, R.A., *Measurement Techniques in Fluid Dynamics,* 3rd ed., von Karman Institute for Fluid Dynamics, Rhode-Saint-Genèse, Belgium, 2009, 118

Arts, T., Boerrigter, H.L., Carbonaro, M., Charbonnier, J.M., Degrez, G., Olivari, D., Riethmuller , M.L., and Van den Braembussche, R.A., *Measurement Techniques in Fluid Dynamics-An Introduction,* von Karman Institute for Fluid Dynamics, Rhode-Saint-Genèse, Belgium, 1994, 118 157

Azimian, A.R., McKenzie, A.B., and Elder, R.L., "A Tip Treatment for Axial Flow Fans and Compressors," *Proceedings of the IMechE Seminar on Inducted Fan Aerodynamics,* London, UK, 9 April, 1987, 276

Bailey, E.E, and Voit, C.H., "Some Observations of Effects of Porous Casings on Operating Range of a Single Axial-flow Compressor Rotor," Report NASA-TM-X-2120, 1970, 43

Bard, H. (1984), "The Stabilisation of Axial Fan Performance", *Proceedings of the Institution of Mechanical Engineers (IMechE) Conference 1984-4 on the Installation Effects in Ducted Fan Systems*, London, UK, 1–2 May, paper no. C120/84, 1984, 22 43 61 275

Beiler, M.G., and Carolus, T.H., "Computation and Measurement of the Flow in Axial Flow Fans with Skewed Blades," *Transactions of the ASME, Journal of Turbomachinery,* vol. 121(2), 1999, 203

Bianchi, S., Corsini, A., and Sheard, A.G., "Demonstration of a Stall Detection System for Induced-draft Fans," *Proceedings of the IMechE Part A, Journal of Power and Energy,* vol. 227(3), 2013, 28

Bianchi, S., Corsini, A., and Sheard, A.G., "Detection of Stall Regions in a Low-speed Axial Fan, Part 1: Azimuthal Acoustic Measurements," *Proceedings of the 54th American Society of Mechanical Engineers Turbine and Aeroengine Congress,* Glasgow, UK, 14-18 June, paper no. GT2010-22753, 2010, 6 9 17 24 42 73 80 82 98 102 128-9 133 151-2

Bianchi, S., Corsini, A., and Sheard, A.G., "Experiments on the Use of Signal Visualization Technique for In-service Stall Detection in Industrial Fans," *Advances in Acoustics and Vibration,* vol. 2013, Article ID 610407 2013, 28

Bianchi, S., Corsini, A., Mazzucco, L., Monteleone, L., and Sheard, A.G., "Stall Inception, Evolution and Control in a Low Speed Axial Fan with Variable Pitch in Motion," *Transactions of the ASME, Journal of Engineering for Gas Turbines and Power,* vol. 134(4), 2012, paper no. 042602, 2012, 8 14 *15* 24 122 147 148 150 151 156 168 175 215 275

Bianchi, S., Corsini, A., Rispoli, F., and Sheard, A.G., "Detection of Aerodynamic Noise Sources in Low-speed Axial Fans with Tip End-plates," *Proceedings of the Institution of Mechanical Engineers, Part C, Journal of Mechanical Engineering Science,* vol. 223, 2009, 116 146 170

Bianchi, S., Corsini, A., Sheard, A.G.,and Tortora, C., "A Critical Review of Stall Control Techniques in Industrial Fans," *International Scholarly Research Network, Mechanical Engineering,* vol. 2013, article ID 526192, 2013, 115 120 242 275

Bianchi, S., Sheard, A.G., and Corsini, A., "Stall Inception, Evolution and Control in a Low Speed Axial Fan Fitted with Variable Pitch in Motion," *Proceedings of the 56th American Society of Mechanical Engineers Gas Turbine and Aeroengine Congress,* Vancouver, Canada, 6-10 June, paper no. GT2011-45725, 2011, 98 100 102

Bindl, S., Stößel, M., and Niehuis, R., "Stall Detection within the Low Pressure Compressor of a Twin-spool Turbofan Engine by Tip Flow Analysis," *Proceedings of the 54th American Society of Mechanical Engineers Gas Turbine and Aeroengine Congress,* Orlando, FL, USA, 8-12 June, paper no. GT2009-59032, 2009, 115 145 169

Boerrigter, H.L., "PreMeSys: a Simulation Program to Determine the Frequency and Time Response of a Pressure Measurement System," *VKI Technical Memorandum 53,* von Karman Institute for Fluid Dynamics, Rhode-Saint-Genèse, Belgium, 1996, 76 98 117 *119* 157 176

Borello, D., Borelli, P., Quagliata, E., and Rispoli, F., "A Multi-grid Additive and Distributive Parallel Algorithm for FEM Turbomachinery CFD," *Proceedings of the European Congress on Computational Methods in Applied Sciences (ECCOMAS CFD 2001),* Swansea, UK, 4-7 September 2001, 195 197

Borello, D., Corsini, A., and Rispoli, F., "A Finite Element Overlapping Scheme for Turbomachinery Flows on Parallel Platforms," *Computers and Fluids,* vol. 32(7), 2003, 192 195-6 199

Borello, D., Corsini, A., and Rispoli, F., "Prediction of Francis Turbine Runner Performance using a 3D Finite Element Technique with Unassembled Stiffness Matrix Treatment," *Proceedings of the 2nd European Conference on Turbomachinery",* Antwerp, Belgium, 5-7 March, 1997, 197

Borello, D., Corsini, A., Delibra, G., and Sheard, A.G., "Numerical Investigations of Detrimental Aerodynamic Effect of Pressure Pulses on a Metro Tunnel Fan," *Proceedings of the 10th European Turbomachinery Conference,* Lappeenranta, Finland, 15-19 April, 2013, 241 273 274

Borello, D., Corsini, A., Delibra, G., Fiorito, M., and Sheard, A.G., "Large-eddy Simulation of a Tunnel Ventilation Fan," *Transactions of the ASME, Journal of Fluids Engineering,* vol. 135(7), paper no. 071102, 2013, 247 248 *250*

Boyes, W., (Ed.), *Instrumentation Reference Book,* Butterworth Heinemann, Oxford, UK, 2003, 47

Breugelmans, F.A.E., Palomba, C., and Funk, T., "Application of Strange Attractors to the Problem of Rotating Stall," in Tanida, Y., and Namba, M. (Eds), *Unsteady Aerodynamics and Aeroelasticity in Turbomachinery,* Elsevier Science, Amsterdam; Oxford; New York, 1995, 146 170

Bright, M.M., Qammar, H., Vhora, H., and Schaffer, M., "Rotating Pip Detection and Stall Warning in High-speed Compressors using Structure Function," *Proceedings of AGARD RTO AVT Conference,* Toulouse, France, 11-15 May, 1998, 8 42 69 93 115 146 170

Cameron, J., and Morris, S., "Spatial Correlation Based Stall Inception Analysis," *Proceedings of the 52nd American Society of Engineers Gas Turbine and Aeroengine Congress,* Montreal, Canada, 14-17 May, 2007, 26 32

Camp, T.R., and Day, I.J., "A Study of Spike and Modal Stall Phenomena in a Low-speed Axial Compressor," *Transactions of the ASME, Journal of Turbomachinery,* vol.120, 1998, 8 42 69 93

Carbonaro, M., *Measurement Techniques in Fluid Dynamics - An Introduction,* von Karman Institute for Fluid Dynamics, Rhode-Saint-Genèse, Belgium, 2009, 76

Cardillo, L., Corsini, A., Delibra, G., Rispoli, F., and Sheard, A.G., "A Numerical Investigation into the Aerodynamic Effect of Pressure Pulses on a Tunnel Ventilation Fan," *Proceedings of the IMechE Part A, Journal of Power and Energy,* vol. 228, 2014, 11 *12* 13 114

Christensen, D., Cantin, P., Gutz, D.,P., Szucs, P.N., Wadia, A.R., Armor, J., Dhingra, M., Neumeier, Y., and Prasad, J.V., "Development and Demonstration of a Stability Management System for Gas Turbine Engines," *Transactions of the ASME, Journal of Turbomachinery,* vol. 130(3), paper no. 031011, 2008, 25 115 146 169

Copenhaver, W.W., and Okiishi, T.H., "Rotating Stall Performance and Recoverability of a High-speed 10 Stage Axial Flow Compressor," *Journal of Propulsion and Power,* vol. 9, 1993, 5 191

Copenhaver, W.W., Mayhew, E.R., Hah, C., and Wadia, A.R., "The Effect of Tip Clearance on a Swept Transonic Compressor Rotor," *Transactions of the ASME, Journal of Turbomachinery,* vol. 118, 1996, 191

Corke, T.C., and Post, M.L., "Overview of Plasma Flow Control: Concepts, Optimization, and Applications," *43rd AIAA Aerospace Sciences Meeting , Reno,* NV, USA, paper no.AIAA 2005-563, 2005, 19

Corsini, A., and Rispoli, F., "Anisotropic Turbulence Modelling of Near Wall Effects Pertinent to Turbomachinery Flows," *Proceedings of the FEDSM-02, the 2002 ASME-European Engineering Summer Conference,* Montreal, Canada, 14-18 July, paper no. FEDSM02-31206, 2002, 195 199

Corsini, A., and Rispoli, F., "Flow Analyses in a High-pressure Axial Ventilation Fan with a Non-linear Eddy-viscosity Closure," *International Journal of Heat and Fluid Flow,* vol. 26(3), 2005, 73 117 148 251 281

Corsini, A., and Rispoli, F., "Numerical Simulation of Three-dimensional Viscous Flow in an Isolated Axial Rotor," *Polish Academy of Sciences, Archive of Mechanical Engineering (Archiwum budowy maszyn),* vol. XLVI(4), 1999, 197

Corsini, A., and Rispoli, F., "Using Sweep to Extend the Stall-free Operational Range in Axial Fan Rotors, *"Proceedings of the IMechE Part A, Journal Of Power and Energy,* vol. 218, 2004, 215 242

Corsini, A., and Sheard, A.G., "Tip End-plate Concept Based on Leakage Vortex Rotation Number Control," *Journal of Computational and Applied Mechanics,* vol. 8, 2007, 281

Corsini, A., and Vad, J., "Application of Forward Blade Sweep to Axial Flow Industrial Fans of High Specific Performance," *Proceedings of the 9th International Symposium on Transport Phenomena and Dynamics of Rotating Machinery (ISROMAC9),* Honolulu, HI, USA, 10-14 February, 2002, 191 195 199

Corsini, A., Delibra, G., and Sheard, A.G., "A Critical Review of Computational Methods and Their Application in Industrial Fan Design," *International Scholarly Research Network, Mechanical Engineering,* vol. 2013, article ID 625175, 2013, 218 219 225 241 274 281

Corsini, A., Delibra, G., and Sheard, A.G., "On the Role of Leading-edge Bumps in the Control of Stall Onset in Axial Fan Blades," *Transactions of the ASME, Journal of Fluids Engineering,* vol. 135(8), paper no. 081104, 2013, 243 245 247 248 251 256 262 281

Corsini, A., Delibra, G., and Sheard, A.G., "The Application of Sinusoidal Blade Leading Edges in a Fan Design Methodology to Improve Stall Resistance," *Proceedings of the IMechE Part A Journal of Power and Energy,* vol. 228, 2014, 275 281

Corsini, A., Delibra, G., Sheard, A.G., and Volponi, D., "Investigation on Anti-stall Ring Aerodynamic Performance in an Axial Flow Fan," *Proceedings of the 59th American Society of Mechanical Engineers Turbine and Aeroengine Congress,* Dusseldorf, Germany, 16-20 June, 2014, 22 60

Corsini, A., Rispoli, F., and Santoriello, A., "A High Order Petrov-Galerkin Stabilized Finite Element Method for Incompressible RANS in Presence of Strong Reaction Effects," *Proceedings of CMFF-03, the Conference on Modelling Fluid Flow"*, Budapest, Hungary, 3-6 September, 2003, 197

Corsini, A., Rispoli, F., and Sheard, A.G., "Shaping of Tip End-plate to Control Leakage-vortex Swirl in Axial-flow Fans," *Transactions of the ASME, Journal of Turbomachinery,* vol. 132, paper no. 031005, 2010, 116

Corsini, A., Rispoli, F., Bencze, F., and Vad, J., "Effects of Blade Sweep in a High-performance Axial Flow Rotor," *Proceedings of the 4th European Conference on Turbomachinery,* Florence, Italy, 20-23 March, 2001, 191 192-3 *196* 197 201 203 210

Corsini, A., Rispoli, F., Santoriello, A., and Tezduyar, T.E., "Improved Discontinuity-capturing Finite Element Techniques for Reaction Effects in Turbulence Computation," *Computational Mechanics,* vol. 38, 2006, 252 281

Craft, T.J., Launder, B.E. and Suga, K., "Development and Application of a Cubic Eddy-viscosity Model of Turbulence," *International Journal of Heat and Fluid Flow,* vol.7, 1996, 192 195

Cumpsty, N.A., "Part-circumference Casing Treatment and the Effect on Compressor Stall," *Proceedings of the 34th American Society of Mechanical Engineers Gas Turbine and Aeroengine Congress,* Toronto, ON, Canada, 11-14 June, paper no. 89-GT-312, 1989, 9 41-2 68-9 92 115 145 169

Cumpsty, N.A., *Compressor Aerodynamics,* Krieger Publishing Company, Malabar, FL, USA, 2004, 242

Daly, B.B., *Woods Practical Guide to Fan Engineering,* Woods of Colchester Ltd, Colchester, UK, 1985, 94

Day, I.J., "Axial Compressor Performance During Surge," *Journal of Propulsion and Power,* vol. 10, 1994, 5

Day, I.J., "Stall Inception in Axial Flow Compressors," *Transactions of the ASME, Journal of Turbomachinery,* vol. 115, 1993, 5 9 79

Day, I.J., and Cumptsy, N.A., "The Measurement and Interpretation of Flow Within Rotating Stall Cells in Axial Compressors," *Proceedings of the Institution of Mechanical Engineers, Part C, Journal of Mechanical Engineering Science,* vol. 20, 1978, 4 7 41 68 92

Day, I.J., Breuer, T., Escuret, J., Cherrett, M., and Wilson. A., "Stall Inception and the Prospects for Active Control in Four High-speed Compressors," *Transactions of the ASME, Journal of Turbomachiney,* vol. 121(1), 1999, 115 145 168

de Jager, B., "Rotating Stall and Surge: a Survey," *Proceedings of the 34th Conference on Decision and Control,* New Orleans, LA, USA, 1995, 2

De Rosier, B., Normand, M.D., and Peleg, M., "Effect of Lag on the Symmetrised Dot Pattern (SDP) Displays of the Mechanical Signatures of Crunchy Cereal Foods," *Journal of the Science of Food and Agriculture,* vol. 75(2), 1997, 124 178

Deppe, A., Saathoff, H., and Stark, U., "Spike-type Stall Inception in Axial Flow Compressors," *Proceedings of the 6th Conference on Turbomachinery, Fluid Dynamics and Thermodynamics,* Lille, France, 7-11 March, 2005, 8 42 69 93

Dewar, S.W., Watts, P., and Fish, F.E., "Turbine and Compressor Employing Tubercle Leading Edge Rotor Design," US Patent No. 20,090,074,578 A1, 19 March, 2009, 217

Dhingra, M., Neumeier, Y., Prasad, J.V.R., Breeze-Stringfellow, A., Shin, H.W., and Szucs, P.N., "A Stochastic Model for a Compressor Stability Measure"*, Transactions of the ASME, Journal of Engineering for Gas Turbines & Power,* vol. 29, 2007, 26 32

Drela, M., "XFoil: an Analysis and Design System for Low Reynolds Number Airfoils," *Lecture Notes in Engineering,* vol. 54, 1989, 220

Durbin, B., "Review: Adapting Scalar Turbulence Closure Models for Rotation and Curvature," *Transactions of the ASME, Journal of Fluids Engineering,* vol. 133(6), 061205, 2011, 225 250 252 281

Eisenlohr, G., and Chladek, H., "Thermal Tip Clearance Control for Centrifugal Compressor of an APU Engine," *Transactions of the ASME, Journal of Turbomachinery,* vol. 116, 1994, 5

Emmons, H.W., Pearson, C.E., and Grant, H.P., "Compressor Surge and Stall Propagation," *Transactions of the ASME,* vol. 77, 1955, 4 8 41 68 92

EN12101-3, Smoke and Heat Control Systems. Specification for Powered Smoke and Heat Exhaust Ventilators, 2002, 11 60 69 240-1 242 308

Epstein, A.H., Ffowcs Williams, J.E., and Greitzer, E.M., "Active Suppression of Aerodynamic Instabilities in Turbomachines," *Journal of Propulsion and Power,* vol. 5, 1989, 5

EU Commission Regulation No.327/2011, *Official Journal of the European Union,* 1 June, 2011, 273 299

Eurovent, "Eurovent1/11 - Fans and System Stall: Problems and Solution," 2007, *21* 24

Eveker, K.M., and Nett, C.N., "Control of Compression System Surge and Rotating Stall: A Laboratory-based 'Hands-on' Introduction," *Proceedings of the 1993 American Control Conference,* vol. 2, 1993, 5

Eveker, K.M., and Nett, C.N., "Model Development for Active Surge Control/rotating Stall Avoidance in Aircraft Gas Turbine Engines," *Proceedings of the 1991 American Control Conference,* Boston, Massachusetts, 26-28 June, vol. 3, 1991, 5

Eveker, K.M., Gysling, D.L., Nett, C.N., and Sharma, O.P., "Integrated Control of Rotating Stall and Surge in Aeroengines," Proceedings of the 1995 International Society for Optical Engineering (SPIE) Conference on Sensing, Actuation and Control in Aeropropulsion, Orlando, Florida, 17-18 April, vol. 2494, 1995., 5

Farrell, P.E., and Maddison, J.R., "Conservative Interpolation between Volume Meshes by Local Galerkin Projection," *Computer Methods in Applied Mechanics and Engineering,* vol. 200, 2011, 281

Ffowcs Williams, J.E., and Huang, X.Y., "Active Stabilization of Compressor Surge," *Journal of Fluid Mechanics,* vol. 204, 1989, 5

Ffowcs Williams, J.E., Harper, M.F.L., and Allwright, D.J., "Active Stabilization of Compressor Instability and Surge in A Working Engine," *Transactions of the ASME, Journal of Turbomachinery,* vol. 115, 1993, 5

Fish, F.E., "Influence of Hydrodynamic Design and Propulsive Mode on Mammalian Swimming Energetics," *Australian Journal of Zoology,* vol. 42, 1993, 216 243

Fish, F.E., and Battle, J.M., "Hydrodynamic Design of the Humpback Whale Flipper," *Journal of Morphology,* vol. 225, 1995, 216 243

Fish, F.E., Howle, L.E., and Murray, M.M., "Hydrodynamic Flow Control in Marine Mammals," *Integrative and Comparative Biology,* vol. 48(6), 2008, 216 243

Fraser, A.M., and Swinney, H.L., "Independent Coordinates for Strange Attractors from Mutual Information," *Physical Review A,* vol. 33(2), 1986, 182

Funk, D.A., Cumpsty, N.A., and Greitzer, E.M., "Surge Dynamics in a Free-spool Centrifugal Compressor System," *Transactions of the ASME, Journal of Turbomachinery,* vol.114, 1992, 4 5

Gad-el-Hak, M., *Flow Control: Passive, Active, and Reactive Flow Management,* Cambridge, UK: Cambridge University Press, 2000, 13

Gall, W., "Fan with Variable Pitch Blades and Translating Bearing Actuation System," US Patent 3, 873,236 A, 25 March, 1975, 69 94

Gelmedov, F.S., Lokshtanov, E.A., Olstain, L.E-M., and Sidorkin, M.A., "Anti-stall Tip Treatment Means," US Patent 5,762,470, 9 June 1998, 43

Gerber, W.Z., "Calculation of the Allowable Stresses in Iron Structures," *Z. Bayer Architecture and Engineering,* vol.6, 1874, *52* 136-7

Gho, S.L., "AMCA Grows in Asia, *AMCA inmotion*(3), 2013, 274

Gleick, J., *Chaos: Making a New Science,* Vintage Books, New York, NY, USA, 1987, 121 155 173

Goodwin, W.R., "Effect of Sweep on Performance of Compressor Blade Sections as Indicated by Swept-blade Rotor, Unswept-blade Rotor, and Cascade Tests," National Advisory Committee for Aeronautics (NACA) Technical Note 4062, 1957, 191

Goto, A., "Suppression of Mixed-flow Pump Instability and Surge by the Active Alteration of Impeller Secondary Flows," *Transactions of the ASME, Journal of Turbomachinery,* vol. 116, 1994, 5

Gravdahl, J.T., and Egeland, O., *Compressor Surge and Rotating Stall: Modeling and Control,* Springer-Verlag, London, UK, 1999, 4 41 68 73 92 145 168 214 242

Greitzer, E.M., "Review - Axial Compressor Stall Phenomena," *Transactions of the ASME, Journal of Fluids Engineering,* vol. 102, 1980, 4 41 68 92 169

Greitzer, E.M., "Surge and Rotating Stall in Axial Flow Compressors, Part 1: Theoretical Compression System Model"*, Transactions of the ASME, Journal of Engineering for Gas Turbines and Power,* vol.98, 1976, 73 145 147

Greitzer, E.M., and Moore, F.K., "A Theory of Post-stall Transients in Axial Compression Systems," *Transactions of the ASME, Journal of Engineering for Gas Turbines and Power,* vol. 108, 1986, 5

Greitzer, E.M., Nikkanen, J.P., Haddad, D.E., Mazzawy, R.S., and Joslyn, H.D., "A Fundamental Criterion for the Application of Rotor Casing Treatment," *Transactions of the ASME, Journal of Fluids Engineering,* vol. 101, 1979, 43

Griffin, R.G., and Smith, L.H., Jr., "Experimental Evaluation of Outer Case Blowing or Bleeding of a Single Stage Axial Flow Compressor, Part I-Design of Rotor Blowing and Bleeding Configurations," NASA Report CR-54587, 1966, 43

Gysling, D.L., Dugundji, M., Greitzer, E.M., and Epstein, A.H., "Dynamic Control of Centrifugal Compressor Surge using Tailored Structures," *Transactions of the ASME, Journal of Turbomachinery,* vol. 113, 1991, 5

Hah, C., and Wennerstrom, A.J., "Three-dimensional Flow Fields Inside a Transonic Compressor with Swept Blades," *Transactions of the ASME, Journal of Turbomachinery,* vol. 113(2), 1991, 191

Hathaway, M.D., "Passive Endwall Treatments for Enhancing Stability," Report NASA /TM-2007-214409, 2007, 42 43

Hauer, A., and Brooks, J., "Fan Motor Efficiency Grades in the European Market," *AMCA inmotion*(2), 2012, 273

Hill, S.D., Elder, R.L., and McKenzie, A.B., "Application of Casing Treatment to an Industrial Axial Flow Fan," *Proceedings of the IMechE Part A, Journal of Power and Energy,* vol. 212, 1998, 275

Horlock, J.H., and Denton, J., "A Review of Some Early Design Practice Using Computational Fluid Dynamics and a Current Perspective," *Transactions of the ASME, Journal of Turbomachinery,* vol. 127, 2005, 280

Höss, B., Leinhos, D., and Fottner, L., "Stall Inception in the Compressor System of a Turbofan Engine," *Transactions of the ASME, Journal of Turbomachinery,* vol.122(1), 2000, 115 168

Houghton, T.O., and Day, I.J., "Enhancing the Stability of Subsonic Compressors using Casing Grooves, *"Transactions of the ASME, Journal of Turbomachinery,* vol.113, 2010, 22

Hua, X., Gu, R., Jin, J., Liu, Y., Ma, Y., Cong, Q., and Zheng, Y., "Numerical Simulation and Aerodynamic Performance Comparison Between Seagull Aerofoil and NACA 4412Aerofoil Under Low-Reynolds," *Advances in Natural Science,* vol. 3(2), 2010, 216

ISO 21927-3, Smoke and Heat Control Systems - Part 3: Specification for Powered Smoke and Heat Exhaust Ventilators, 2006, 11 60 69 240-1 242 308

ISO 5801:2007, Industrial Fans-Performance Testing Using Standardized Airways, 2007, 47 *72* 73 94 97-8 147 171 173 245 278-9 306-*7*

ISO/IEC 60651, Specification for Sound Level Meters, 1994, 73 94 117 172

Ivanov, S.K., "Axial Blower," US Patent 3,189, 260, 15 June 1965, 22 43 *44* 93 275

Jasak, H., "OpenFOAM: a Year in Review," *Proceedings of the Fifth OpenFOAM Workshop,* Gothenburg, Sweden, 21-24 June, 2010, 218

Johari, H., Henoch, C.W., Custodio, D., and Levshin, A., "Effects of Leading-edge Protuber-ances on Airfoil Performance," *AIAA Journal,* vol. 45(11), 2007, 218 219 220 224 243 247

Joslin, R.D., Russell, H.T., and Choudhari, M.M., "Synergism of , Flow and Noise Control Technologies," *Progress in Aerospace Sciences,* vol. 41, 2005, 13

Kameier, F. and Neise, W., "Rotating Blade Flow Instability as a Source of Noise in Axial Tur-bomachines," *Journal of Sound and Vibration,* vol. 203, 1997, 9 69 80 93 102-3 151-2

Kang, C.S., McKenzie, A.B., and Elder, R.L., "Recessed Casing Treatment Effects on Fan Performance and Flow Field," *Proceedings of the 40th American Society of Mechanical Engineers Gas Turbine and Aeroengine Congress,* Houston, TX, USA, 5-8 June, paper no. 95-GT-197, 1995, 45 276

Karlsson, S., and Holmkvist, T., "Guide Vane Ring for a Return Flow Passage in Axial Fans and a Method of Protecting it," US Patent 4,602, 410, 29 July 1986, 22 43 45 93 275

Khalid, S.J., "Compressor Endwall Treatment," US Patent 5,520, 508, 28 May 1996, 43

Khalid, S.J., Khalsa, A.S., Waitz, , I.A., Tan, C.S., Greitzer, E.M., Cumptsy, N.A., Adamczyk, J.J., and Marble, F.E., "Endwall Blockage in Axial Compressors," *Transactions of the ASME, Journal of Turbomachinery,* vol. 121, 1999, 42

Kim, K.H., and Fleeter, S, "Compressor Unsteady Aerodynamic Response to Rotating Stall and Surge Excitations," *Journal of Propulsion and Power,* vol. 10, 1994, 5

Koch, C.C., and Smith, L.H., "Loss Sources and Magnitudes in Axial Compressors," *Transactions of the ASME, Journal of Engineering and Power,* vol. 98, 1976, 42

Koff, S.G., Mazzawy, R.S., Nikkanen,J.P., and Nolcheff, A., "Case Treatment for Compressor Blades," US Patent 5,282, 718, 1 February, 1994, 43

Kröger, G., Vob, C., Nicke, E., and Cornelius, C., "Theory and Application of Axisymmetric End-wall Contouring for Compressors," *Proceedings of the 56th American Society of Engineers Gas Turbine and Aeroengine Congress,* Vancouver, Canada, 6-10 June, paper no. GT2011-45624, 2011, 215 242

Langston L.S., "Fitting a Pitch," *ASME Mechanical Engineering Magazine,* vol. 131(12), 2009, 69 94 215 242

Launder, B.E., and Sharma, B.R., "Application of the Energy-dissipation Model of Turbulence to the Calculation of Flow Near a Spinning Disc," *Letters in Heat and Mass Transfer,* vol. 1, 1974, 218 225 253

Laurendeau, E., Jordan, P., Delville, J., and Bonnet, J.P., "Nearfield-farfield Correlations in Subsonic Jets: What Can They Tell Us?", *Proceedings of the 13th AIAA/CEAS Aeroacoustics Conference (28th AIAA Aeroacoustics Conference),* Rome, Italy, 21-23 May, paper no. AIAA 2007-3614, 2007, 157

Leinhos, D.C., Schmid, N.R., and Fottner, L., "The Influence of Transient Inlet Distortions on the Instability Inception of a Low Pressure Compressor in a Turbofan Engine," *Transactions of the ASME, Journal of Turbomachinery,* vol. 112, 2001, 82 104

Lieblin, S., "Experimental Flow in Two-dimensional Cascades," in Johnson, I.A., and Bullock, R.O. (Eds), A*erodynamic Design of Axial-flow Compressors,* National Aeronautics and Space Administration Report No. NASA SP-36, 1965, 201

Lien, F.S., and Leschziner, M.A., "Assessment of Turbulence-transport Models Including Non-linear RNG Eddy-viscosity Formulation and Second-moment Closure for Flow Over a Backward-facing Step," *Computational Fluids,* vol.23, 1994, 218 225 250 251-2 281

Lin, F., Tong, Z., Geng, S., Zhang, J., Chen, J., and Nie, C., "A Summary of Stall Warning and Suppression Research with Micro Tip Injection," *Proceedings of the 56th American Society of Engineers Turbine and Aeroengine Congress,* Vancouver, BC, Canada, 6-10 June, paper no. GT2011-46118, 2011, 18

Liu, Y., Dhingra, M., and Prasad, J.V.R., "Active Compressor Stability Management via a Stall Margin Control Mode," *Proceedings of the 54th American Society of Mechanical Engineers Gas Turbine and Aeroengine Congress,* Orlando, FL, USA, 8-12 June, paper no. GT2009-60140, 2009, 115 145 169 215

Ludwig, G.R., and Nenni, J.P., "A Rotating Stall Control System for Turbojet Engines," *Proceedings of the 21st American Society of Mechanical Engineers Gas Turbine and Aeroengine Congress,* New Orleans, LA, USA, 12-25 March, paper no. 76-GT-115, 1976, 115 168

McDougall, N.M., Cumpsty, N.A., and Hynes, T.P., "Stall Inception in Axial Compressors," *Transactions of the ASME, Journal of Turbomachinery,* vol.112, 1990, 82 104

Methling, F.O., Stoff, H., and Grauer, F., "The Prestall Behaviour of a 4-stage Transonic Compressor and Stall Monitoring Based on Artificial Neural Networks," *International Journal of Rotating Machinery,* vol. 10, 2004, 115 145 169

Miklosovic, D.S., Murray, M.M., and Howle, L.E., "Experimental Evaluation of Sinusoidal Leading Edges," *Journal of Aircraft,* vol. 44, 2007, 216 243

Miklosovic, D.S., Murray, M.M., Howle, L.E., and Fish, F.E., "Leading Edge Tubercles Delay Stall on Humpback Whale *(Megaptera Novaeangliae)*", *Physics of Fluids,* vol. 16, 2004, 216 243

Miyake, Y., Kata, T., and Inaba, T., "Improvement of Unstable Characteristics of an Axial Flow Fan by Air-separator Equipment, *Transactions of the ASME, Journal of Fluids Engineering,* vol. 109(1), 1987, 43 276-7

Mohammed, K.P., and Prithvi Raj, D., "Investigations on Axial Flow Fan Impellers with Forward Swept Blades," *Transactions of the ASME, Journal of Fluids Engineering,* vol. 99, 1977, 191 193 203 204

Mongeau, L., Thompson, D.E., and McLaughlin, D.K., "A Method for Characterizing Aerodynamic Sound Sources in Turbomachines," *Journal of Sound and Vibration,* vol. 181, no. 3, 1995, 9 69 93

Moore, F.K., "A Theory of Rotating Stall of Multistage Compressors, Parts I-III," *Transactions of the ASME, Journal of Engineering for Gas Turbines and Power,* vol. 106, 1984, 4 9 41 42 68 69 92 145 169

Nie, C., Xu, G., Cheng, X., and Chen, J., "Micro Air Injection and its Unsteady Response in a Low-speed Axial Compressor," *Transactions of the ASME, Journal of Turbomachinery,* vol.124, 2002, 18 275

Nolcheff, N.A., "Flow Aligned Plenum Endwall Treatment Compressor Blades," US Patent 5,586,859, 24 December 1996, 43

Okada, K., "Experiences with Flow-induced Vibration and Low Frequency Noise due to Rotating Stall of Centrifugal Fan," *Journal of Low Frequency Noise and Vibration,* vol. 6, 1987, 9

Okada, K., "Experiences with Flow-induced Vibration and Low Frequency Noise due to Rotating Stall of Centrifugal Fan," *Journal of Low Frequency Noise and Vibration,* vol. 6, 1987, 93

Out, E., "Rotating Stall and Stall-controlled Performance of a Single Stage Subsonic Axial Compressor," *Journal of Thermal Science,* vol. 15, no. 1, 2006, 79 104

Paduano, J.D., Epstein, A.H., Galvani, L., Longley, J.P., Greater, E.M., and Genets, G.R., "Active Control of a Rotating Stall in a Low-speed Axial Compressor," *Transactions of the ASME, Journal of Turbo machinery,* vol.115, 1993, 5

Paduano, J.D., Greater, E.M., and Epstein, A.H., "Compression System Stability and Active Control," *Annual Review of Fluid Mechanics,* vol. 33, 2001, 115 145 215

Paduano, J.D., Galvani, L., and Epstein, A.H., "Parameter Identification of Compressor Dynamics during Closed-loop Operation," *Journal of Dynamic Systems, Measurement, and Control,* vol. 115, 1993, 5

Paduano, J.D., Galvani, L., Epstein, A.H., Greater, E.M., and Genets, G.R.,"Modelling for Control of Rotating Stall," *Automatica, a Journal of the International Federation of Automatic Control (IFAC),* vol. 30, 1994, 5

Park, H.G., "Unsteady Disturbance Structures in Axial Flow Compressor Stall Inception," MS Thesis, Massachusetts Institute of Technology, Cambridge, MA, USA, 1994, 26-7 32

Pedro, H.T.C., and Kobayashi, M.H., "Numerical Study of Stall Delay on Humpback Whale Flippers," *46th AIAA Aerospace Sciences Meeting and Exhibit,* Reno, NV, USA.7-10 January, paper no. 2008-0584, 2008, 217 243

Perugini, D., Busà, T., Poli, G., and Nazzereni, S., "The Role of Chaotic Dynamics and Flow Fields in the Development of Disequilibrium Textures in Volcanic Rocks," *Journal of Petrology,* vol. 44(4), 2003, 182 2003

Pickover, C.A., "On the Use of Symmetrized Dot Patterns for the Visual Characterization of Speech Waveforms and Other Sampled Data," *Journal of the Acoustical Society of America.* vol. 80. 1986, 116 121 124 127 146 155 170

Pickover, C.A., *Computers, Pattern, Chaos and Beauty,* St. Martin's Press, New York, NY, USA, 1990, 116 182

Pinsley, J.E., Guenette, G.R., Epstein, A.H., and Greitzer, E.M., "Active Stabilization of Centrifugal Compressor Surge," *Transactions of the ASME, Journal of Turbomachinery,* vol. 113, 1991, 5

Prasad, J.V.R, Neumeier, Y., Lal, M., Bae, S.H., and Meehan, A., "An Experimental Investigation of Active and Passive Control of Rotating Stall in Axial Compressors," *Proceedings of the IEEE International Conference on Control Applications, held together with the IEEEE International Symposium On Computer Aided Control System Design,* Kohala Coast-Island of Hawai'i, Hawai'i, HI, USA, 22-27 August, vol.2, 1999, 20 24

Prince, D.C., Wisler, D.D., and Hilvers, D.E., "Study of Casing Treatment Stall Margin Improvement Phenomena," NASA Report CR-134552, March 1974, 43

Rabe, D., Hoying, D., and Koff, S., "Application of Sweep to Improve Efficiency of a Transonic Fan: Part II, Performance and Laser Test Results," *Proceedings of the AIAA/SAE/ASME 27th Joint Propulsion Conference,* Sacramento, CA, USA, 24-26 June, paper no. AIAA 91-2544, 1991, 191

Rippl, A., "Experimentelle Untersuchungen Zuminstationaren Betriebsverhahenan der Stabilitarsgrenze Eines Mehrstufigen Trans-sonischen Verdichters," PhD dissertation, Ruhr-Universität Bochum, 1995, 9 40 62 69 93 145 169

Rodgers, C., "Centrifugal Compressor Inlet Guide Vanes for Increased Surge Margin," *Transactions of the ASME, Journal of Turbomachinery,* vol.113, 1991, 5

Rusak, Z., and Morris, W.J., "Stall Onset on Airfoils at Moderately High Reynolds Number Flows," *Transactions of the ASME, Journal of Fluids Engineering,* vol. 133(11), 2011, 215

Saathoff, H., and Stark, U., "Tip Clearance Flow Induced Endwall Boundary Layer Separation in a Single-stage Axial-flow Low-speed Compressor," *Proceedings of the 45th American Society of Mechanical Engineers Gas Turbine and Aeroengine Congress,* Munich, Germany, 8-11 May, paper no. 2000-GT-501, 2000, 42

Schultz, T.J., "Synthesis of Social Surveys on Noise Annoyance," *Journal of the Acoustical Society of America,* vol. 64, 1978, 116 121 146 155 170 173

Sheard, A.G., "The Effect of Inlet Box Aerodynamics on the Mechanical Performance of a Variable Pitch In Motion Fan," *Advances in Acoustics and Vibration,* vol. 2012, article ID 278082, 2012, 69

Sheard, A.G., and Corsini, A., "The Impact of an Anti-stall stabilisation Ring on Industrial Fan Performance: Implications for Fan Selection," *Proceedings of the 55th American Society of Mechanical Engineers Turbine and Aeroengine Congress,* Vancouver, Canada, June, paper no. GT2011-45187, 2011, *10* 11 22 169

Sheard, A.G., and Corsini, A., "The Mechanical Impact of Aerodynamic Stall on Tunnel Ventilation Fans," *International Journal of Rotating Machinery,* vol. 2012, paper no. 402763, 2012, 4 16 *17* 69 93 114 137 138-9 145 214 215 242 273 275 283

Sheard, A.G., and Daneshkhah, K., "The Conceptual Design of High Pressure Reversible Axial Tunnel Ventilation Fans," *Advances in Acoustics and Vibration,* vol. 2012, article ID 562309, 2012, 244 277

Sheard, A.G., and Jones, N.M., "Approval of High-temperature Emergency Tunnel-ventilation Fans: The Impact of ISO 21927-3," *Proceedings of the ITA-AITES World Tunnel Congress and 34th General Assembly,* Agra, India, 19-25 September, 2008, 11 69 241

Sheard, A.G., and Jones, N.M., "Powered Smoke and Heat Exhaust Ventilators: The Impact of EN 12101-3 and ISO 21927-3," *Tunnelling and Underground Space Technology,* vol. 28, 2012, 11

Sheard, A.G., Corsini, A., and Bianchi, S.,"A Method of Detecting Stall in an Axial Fan," GB Patent 2 468 571 B, 24 December, 2010, 42 115 163 170 178

Sheard, A.G., Corsini, A., and Bianchi, S.,"Stall Warning in a Low-speed Axial Fan by Visualisation of Sound Signals," *Transactions of the ASME, Journal of Engineering for Gas Turbines & Power,* vol. 133(4), paper no. 041601, 2011, 6 9 *27* 28 32 42 93 109 145 146 148 156 157 163 169 170 175-6 176 182 214 242

Sheard, A.G., Corsini, A., Minotti, S., and Sciulli, F., "The Role of Computational Methods in the Development of an Aero-acoustic Design Methodology: Application in a Family of Large Industrial Fans," *Proceedings of the 14th International Conference on Modelling Fluid Flow Technologies,* Budapest, Hungary, 9-12 September, 2009, 47 69

Sheard, A.G., Daneshkhah, K., and Corsini, A., "Fan Conceptual Design as Applied to The Marmaray Tunnel Ventilation System." *Proceedings of the 58th American Society of Me-*

chanical Engineers Gas Turbine and Aeroengine Congress, San Antonio, TX, USA, 3-7 June, paper no. GT2013-94548, 2013, 274

Sheard, A.G., Delibra, G., and Corsini, A., "Air Movement Fans," GB Patent Application 1219502.0, 30 October, 2012, 244

Sheard, A.G., Tortora, C., Corsini, A., and Bianchi, S., "The Role of Variable Pitch in Motion Blades and Variable Rotational Speed in an Industrial Fan Stall," *Proceedings of the IMechE Part A, Journal of Power & Energy,* vol. 228, 2014, 215

Sheldahl, R.E., and Klimas, P.C., "Aerodynamic Characteristics of Seven Symmetrical Airfoil Sections Through 180-degree Angle of Attack for Use in Aerodynamic Analysis of Vertical Axis Wind Turbines," Sandia National Laboratories Energy Report SAND80-2114, Sandia National Laboratories, Albuquerque, New Mexico, USA, 1981, 220

Shibata, K., Takahashi, A., and Shirai, T., "Fault Diagnosis of Rotating Machinery through Visualisation of Sound Signals," *Mechanical Systems and Signal Processing,* vol. 14, 2000, 115 122-*3* 127 130 146 156 163 170 175

Shyy, W., Lian, Y., Tang, J., Viieru, D., and Liu, H., *Aerodynamics of Low Reynolds Number Flyers,* Cambridge University Press, Cambridge, UK, 2007, 243

Simon, J.S., and Valavani, L., "A Lyapunov-based Nonlinear Control Scheme for Stabilizing a Basic Compression System using a Close-coupled Control Valve," *Proceedings of the 1991 American Control Conference,* Boston, Massachusetts, 26-28 June, vol., 3, 1991, 5

Simon, J.S., Valavani, L., Epstein, A.H., and Greitzer, E.M., "Evaluation of Approaches to Active Compressor Surge Stabilization," *Transactions of the ASME, Journal of Turbomachinery,* vol. 115, 1993

Smith, G.D.J., and Cumpsty, N.A., "Flow Phenomena in Compressor Casing Treatment," *Transactions of the ASME, Journal of Engineering for Gas Turbines and Power,* vol. 106(3), 1984, 275

Smith, L.H., and Yeh, H., "Sweep and Dihedral Effects in Axial-flow Turbomachinery," *Transactions of the ASME, Journal of Basic Engineering,* vol. 85(3), 1963, 191 203

Sottek, R., and Genuit, K., "Sound Quality Evaluation of Fan Noise Based on Hearing-related Parameters," *Proceedings of the 3rd International Symposium of Fan Noise,* Lyon, France, 17-19 September, 2007, 116 121 146 155 170 173

Storer, J.A. and Cumpsty, N.A., "Tip Leakage Flow in Axial Compressors," *Transactions of the ASME, Journal of Turbomachinery,* vol, 113(2), 1991, 204

Suder, K.L., Hathaway, M.D., Thorp, S.A., Strazisar, A.J., and Bright, M.B., "Compressor Stability Enhancement using Discrete Tip Injection," *Transactions of the ASME, Journal of Turbomachinery,* vol. 123, 2001, 18 275

Tahara, N., Kurosaki, M., Ohta, Y., Outa, E., Nakajima, T., and Nakakita, T., "Early Stall Warning Technique for Axial-flow Compressors," *Transactions of the ASME, Journal of Turbomachinery,* vol. 129(3), 2007, 115 146 169-70

Takata, H., and Tsukuda, Y., "Stall Margin Improvement by Casing Treatment-Its Mechanism and Effectiveness," *Transactions of the ASME, Journal of Engineering for Power,* vol. 99(1), 1977, 43 275

Takens, F., "Detecting Strange Attractors in Turbulence" in Rand, D.A., and Young, L.S. (Eds), *Lecture Notes in Mathematics,* Springer, Berlin, Germany, 1981, 146 170 182

Tan, C.S., Day, I., Morris, S., and Wadia, A., "Spike-type Compressor Stall Inception, Detection, and Control," *Annual Review of Fluid Mechanics,* vol. 42, 2010, 20

Thompson, D.W., King, P.L., and Rabe, D.C., "Experimental and Computational Investigation on Stepped Tip Gap Effects on the Flow Field of a Transonic Axial-flow Compressor Rotor," *Transactions of the ASME, Journal of Turbomachinery,* vol. 120, 1998, 275

Tong, Z., Li, L., Nie, C., Lin, B., Cui, Y., and Qi, W., "On-line Stall Control with the Digital Signal Processing Method in an Axial Compressor," *Proceedings of the 54th American Society of Mechanical Engineers Gas Turbine and Aeroengine Congress,* Orlando, FL, USA, 8-12 June, paper no. GT2009 59509, 2009, 115 146 169

Tryfonidis, M., Etchevers, O., Paduano, J.D., Epstein, A.H., and Hendricks, G.J., "Pre-stall Behaviour of Several High-speed Compressors," *Transactions of the ASME, Journal of Turbomachinery,* vol. 117(1), 1995, 26 32 115 146 169

Turner, R.C., "Improvements in or Relating to Gas Turbines," US Patent 826, 669, 18 July 1955, 42

US Department of Energy, "Energy Conservation Standards Rulemaking Framework for Commercial and Industrial Fans and Blowers," 28 January, 2013, 274

Vad. J., "Incorporation of Forward Blade Sweep in Non-free Vortex Design Methods of Axial Flow Turbomachinery Rotors," *Periodica Polytechnica,* vol.45(2), 2001, 193

Vad. J., and Bencze, F., "Three-dimensional Flow in Axial Flow Fans in a Non-free Vortex Design, *International Journal of Heat and Fluid Flow,* vol. 19, 1998, 191 198 199

Van Beyer, R., and Bolland, O., "Coal Power Compendium," Department of Thermal Energy and Hydropower, NTNU, Trondheim, Norway, 1998, 144

Van Nierop, E.A., Alben, S., and Brenner, M.P., "How Bumps on the Whale Flippers Delay Stall: an Aerodynamic Model," *Physical Review Letters,* vol. 100, paper no. 054502, 2008, 217 219 243

Vo, H.D., "Active Suppression of Rotating Stall Inception with Distributed Jet Actuation," *International Journal of Rotating Machinery,* vol. 2007, article ID 56808, 2007, 19 24 275

Vo, H.D., Cameron, J., and Morris, C.S., "Control of Short Length-scale Rotating Stall Inception on a High-speed Axial Compressor with Plasma Actuation," *Proceedings of the 53rd American Society of Mechanical Engineers Gas Turbine and Aero engine Congress,* Berlin, Germany, 9-13 June, paper no. GT2008-50967, 2008, 19

Vo, H.D., Tan, C.S., and Greater, E.M., "Criteria for Spike Initiated Rotating Stall," *Proceedings of the 50th American Society of Mechanical Engineers Gas Turbine and Aero engine Congress,* Reno, NV, USA, 6-9 June, paper no. GT2005-68374, 2005, 8 42 69

Wada, A.R., Christensen, D., and Prasad, J.V., "Compressor Stability Management in Aircraft Engines," *Proceedings of ICAS 2006, the 25th Congress of the International Council of the Aeronautical Sciences (ICAS),* Hamburg, Germany, 3-8 September, paper no. 759, 2006, 25

Wada, A.R., Sauces, P.N., and Call, D.W., "Inner Workings of Aerodynamic Sweep," *Proceedings of the 42nd American Society of Mechanical Engineers, Gas Turbine and Aero-engine Congress,* Orlando, FL,USA, 2-5 June, paper no. 97-GT-401, 1997, 191 201

Wasserbauer, C.A., Weaver, H.F., and Senyitko. R.G., "NASA Low-speed Axial Compressor for Fundamental Research" NASA Technical Memorandum 4635, July, 1995, 47

Weichert, S., and Day, I.J., "Detailed Measurements of Spike Formation in an Axial Compressor," *Proceedings of the 57th American Society of Mechanical Engineers Gas Turbine and Aeroengine Congress,* Copenhagen, Denmark, 11-15 June, paper no. GT2012-68627, 2012, 145 214 242

Weigel, H.J., Paduano, J.D., Frechette, L.G., Epstein, A.H., Greitzer, E.M., Bright, M.M., and Strazisar, A.J., "Active Stabilization of Rotating Stall in a Transonic Single Stage Axial Compressor," *Proceedings of the 42nd American Society of Mechanical Engineers Gas*

Turbine and Aeroengine Congress, Orlando, FL, USA, 2-5 June paper no. 97-GT-411, 1997, 18

Weller, H.G., Tabor, G., Jasak, H., and Fureby, C., "A Tensorial Approach to Continuum Mechanics Using Object-oriented Techniques," *Computational Physics,* vol. 12, 1998, 248 280

Wennerstrom, A.J., "Experimental Study of a High-through Flow Transonic Axial Compressor Stage," *Transactions of the ASME, Journal of Engineering for Gas Turbines and Power,* vol. 106(3), 1984, 191

White, E.R., and Miller, T.F., "A Serendipitous Application of Super Cavitation Theory to the Water-running Basilisk Lizard," *Transactions of the ASME, Journal of Fluids Engineering,* vol. 132(5), paper no. 054501, 2010, 215

Wilde, G.L., "Improvements in or Relating to Gas Turbines," US Patent 701, 576, 28 June 1950, 42

Wisler, D.C., and Hilvers, D.E., "Stator Hub Treatment Study," NASA Report CR-134729, December, 1974, 43

Wo, A.M., and Bons, J.P., "Flow Physics Leading to System Instability in a Centrifugal Pump," *Transactions of the ASME, Journal of Turbomachinery,* vol. 116, 1994, 4

Wright, T., and Simmons, W.E., "Blade Sweep for Low-speed Axial Fans," *Transactions of the ASME, Journal of Turbomachinery,* vol. 112, 1990, 191

Wu, J. and Chuang, C., "Fault Diagnosis of Internal Combustion Engines Using Visual Dot Patterns of Acoustic and Vibration Signals," *NDT&E International,* vol. 38, 2005, 115 127 146 170

Yamaguchi, N., Ogata, M., and Kato, Y., "Improvement of Stalling Characteristics of an Axial-flow Fan by Radial-vaned Air-separators," *Transactions of the ASME,, Journal of Turbomachinery,* vol. 132(2), 2010, *23* 24 43 45 275 276

Yamaguchi, N., Tominaga, T., Hattori, S., and Mitsuhashi, T., "Secondary-loss Reduction by Forward-skewing of Axial Compressor Rotor Blading," *Proceedings of the Yokohama International Gas Turbine Congress,* Yokohama, Japan, 27 October-1 November, 1991, 191 203 209

Yeung, S., and Murray, R.M., "Reduction of Bleed Valve Rate Requirements for Control of Rotating Stall using Continuous Air Injection," *Proceedings of the 1997 IEEE International Conference on Control Applications,* Hartford, CT, USA, 5-7 October, 1997, 20 24

Young, W.C., *Roark's Formulas for Stress and Strain,* McGraw-Hill, New York, NY, USA, 1989, 136

Zhang, H.W., Deng, X.Y., Lin, F., Chen, J.Y., and Huang, W. G., "Unsteady Tip Leakage Flow in an Isolated Axial Compressor Rotor," *Journal of Thermal Science,* vol. 14, no. 3, 2005, 77

Ziabasharhagh, M., McKenzie, A.B., and Elder, R.L., "Recess Vane Passive Stall Control," *Proceedings of the 37th American Society of Mechanical Engineers gas Turbine and Aeroengine Congress,* Cologne, Germany, 1-4 June, paper no. 92-GT-36, 1992, 276

Author Index

Subject Index

Page numbers in italics refer to figures or tables